Response Modification of Bridges

(MAE Center Project ST-12)

Reginald DesRoches, PI

Roberto T. Leon, Co-PI

Shirley Dyke, Co-PI

TABLE OF CONTENTS

Page

CHAPTER

1 INTRODUCTION 1

1.1 Problem Description 1

1.2 Objectives of Research 2

1.3 Outline of Report 3

2 SUMMARY OF PREVIOUS STUDIES ON BRIDGES IN MID-AMERICA REGION 5

2.1 Seismic Performance of Bridges 5

2.2 Seismic Retrofit of Bridges 9

3 SEISMIC HAZARDS AND GROUND MOTIONS IN MID-AMERICA 13

3.1 Historical Earthquakes and Seismic Hazards in Mid-America 13

3.2 New Madrid Seismic Zone 15

3.3 Comparing Seismic Hazards for Mid-America and the West Coast 18

3.4 Ground Motions in Mid-America 21

3.4.1 Characteristics of Ground Motions 23

4 TYPICAL BRIDGES AND ANALYTICAL MODELS IN MID-AMERICA 31
4.1 Inventory of Bridges and Typical Bridges in Mid-America 31
4.1.1 Multi-Span Simply Supported (MSSS) Bridge 35
4.1.2 Multi-Span Continuous (MSC) Bridge 38
4.1.3 Single Span (SS) Bridge 41
4.2 Bearings Found in Typical Bridges 43
4.3 Analytical Models of Typical Bridges 46
4.4 Analytical Models of Bridge Components 49
4.4.1 Steel Bearings 49
4.4.1.1 Overview of Steel Bearings 49
4.4.1.2 Analytical Models of Steel Bearings 53
4.4.2 Elastomeric Pads and Dowels 64
4.4.2.1 Overview of Elastomeric Pads and Dowels 64
4.4.2.2 Analytical Models of Elastomeric Pads and Dowels 64
4.4.3 Abutments 69
4.4.3.1 Overview of Abutments 69
4.4.3.2 Analytical Models of Abutments 70
4.4.4 Analytical Model of Impact Element 77
4.4.5 Multi-Column Bents 78
4.4.5.1 Overview of Multi-Column Bents 78
4.4.5.2 Material Models of Columns 78
4.4.5.3 Cross Section Behavior of Columns 82
4.4.6 Pile Foundations 85
4.4.6.1 Overview of Pile Foundations 85
4.4.6.2 Analytical Model of Pile Foundations 88
4.5 Capacity Estimation of Bridge Components 94
4.5.1 Fixed Steel Bearing Capacity 94
4.5.2 Expansion Steel Bearing Capacity 95

4.5.3 Capacity of Columns 96
4.5.4 Foundation Capacity 103
4.5.5 Abutment Capacity 105

5 DETERMINISTIC SEISMIC RESPONSE ANALYSIS OF TYPICAL BRIDGES 107
5.1 Modal Analysis 107
5.2 Seismic Response Analysis of Typical Bridges 113
5.3 Statistical Analysis of Typical Bridges Subjected to Ground Motions 135
5.3.1 Performance of MSSS Steel Bridge 135
5.3.2 Performance of MSSS Concrete Bridge 139
5.3.3 Performance of MSC Steel Bridge 143
5.3.4 Performance of MSC Concrete Bridge 146
5.3.5 Performance of SS Steel Bridge 150
5.3.6 Performance of SS Concrete Bridge 152
5.4 Summary 154

6 PARAMERIC AND SENSITIVITY STUDY OF TYPICAL BRIDGES 155
6.1 Description of Parameters 155
6.2 Results of MSSS Steel Bridge 158
6.2.1 Frictional Coefficient of Expansion Bearings 158
6.2.2 Mass of Decks 159
6.2.3 Gap between Deck and Abutment 159
6.2.4 Gap between Decks 161
6.2.5 Rotational Stiffness of Pile Foundations 161
6.2.6 Summary 161
6.3 Results of MSC Steel Bridge 165
6.3.1 Frictional Coefficient of Expansion Bearings 165
6.3.2 Mass of Decks 165

6.3.3 Gap between Deck and Abutment 166
6.3.4 Rotational Stiffness of Pile Foundations 166
6.3.5 Summary 167
6.4 Sensitivity of Parameters 170

7 EXPERIMENTAL TESTS 173
7.1 Experimental Setup 176
7.1.1 General Overview 176
7.1.2 Testing Facility 180
7.1.3 Bridge Substructure 182
7.1.3.1 Piers 182
7.1.3.2 Concrete Pedestals 184
7.1.3.3 Elastomeric Bearing Assemblies 186
7.1.4 Bridge Superstructure 188
7.1.5 Bridge Assemblies 190
7.1.6 Bracing Frames 194
7.1.7 Cable Restrainer Retrofits 196
7.1.7.1 Restrainer Cable 196
7.1.7.2 Restrainer Connections 199
7.2 Description of Tests and Results 202
7.2.1 Instrumentation 202
7.2.2 Loading Equipment 206
7.2.3 Elastomeric Bearing Tests 207
7.2.3.1 Description of Elastomeric Bearing Tests 207
7.2.3.2 Elastomeric Bearing Tests Results 210
7.2.4 Cable Restrainer Tests 219
7.2.4.1 Des. and Results of Cable Restrainer Tests 220
7.2.4.1.1 Current DOT Practice 221
7.2.4.1.2 Retrofit Modification 1 226

7.2.4.1.3 Retrofit Modification 2 230
7.2.4.1.4 Retrofit Modification 3 234
7.2.4.1.5 Retrofit Modification 4 238
7.2.4.1.6 Retrofit Modification 5 242
7.2.4.1.7 Retrofit Modification 6 247
7.2.4.2 Summary of Cable Restrainer Test Results 251
7.3 Analysis of Retrofitted Bridge 254
7.3.1 Bridge Used in Analysis 254
7.3.1.1 MSSS Steel Girder Bridge 255
7.3.1.2 Continuous Steel Girder Bridge 256
7.3.2 Analytical Bridge Models 257
7.3.3 Restrainer Elements in Analysis 259
7.3.4 Ground Motions 261
7.3.5 Results of Analysis 263
7.3.5.1 MSSS Steel Girder Bridge Results 264
7.3.5.2 Continuous Steel Girder Bridge Results 265
7.3.6 Summary of Analytical Results 266

8 RETROFIT MEASURES FOR TYPICAL BRIDGES 268
8.1 Elastomeric Bearings 269
8.1.1 Overview of Elastomeric Bearings 269
8.1.2 Analytical Model of Elastomeric Bearings 271
8.2 Lead-Rubber Bearings 274
8.2.1 Overview of Lead-Rubber Bearings 274
8.2.2 Analytical Model of Lead-Rubber Bearings 276
8.3 Restrainer Cables 281
8.3.1 Overview of Restrainer Cables 281
8.3.2 Analytical Model of Restrainer Cables 286
8.4 Performance of Retrofit Measures 286

8.4.1 Performance of Retrofitted MSSS Bridges 288
8.4.2 Performance of Retrofitted MSC Bridges 292
8.4.3 Performance of Retrofitted SS Bridges 296
8.5 Summary 299

9 SUMMARY, CONCLUSIONS, AND IMPACT OF RESEARCH 300
9.1 Summary and Conclusions 300
9.2 Impact of Research 356

APPENDIX A FORMULATION FOR EXPANSION STEEL BEARINGS' CAPACITY 357
APPENDIX B RESULTS OF STATISTICAL ANALYSIS FOR TYPICAL BRIDGES 361
APPENDIX C STRUCTRUAL PERIODS OF TYPICAL BRIDGES 372
APPENDIX D PROBABILISTIC SEISMIC DEMAND MODELS FOR SIMULATED BRIDGES 380
APPENDIX E EQUIPMENT SPECIFICATIONS 403
APPENDIX F ELASTOMERIC BEARING TEST RESULTS 409
REFERENCES 428

LIST OF TABLES

Table		Page
3.1	Ten Largest Earthquakes in United States	14
3.2	Mean Values of Ground Motion Parameter for Suite of Synthetic Ground Motion for Mid-America	24
3.3	Characteristics of Synthetic Ground Motion Records	30
4.1	Inventory of Bridges in Mid-America According to Structural Type	32
4.2	Inventory of Bridges in Mid-America According to Material Type of Superstructure	33
4.3	Inventory of Bridges in Mid-America According to Superstructure Type	34
4.4	Superstructure Section Properties for Typical Bridges	48
4.5	Properties of Abutment in Passive and Active Action	76
4.6	Stiffness of Pile Foundations	93
4.7	Maximum Allowable Displacement of Expansion Steel Bearings	95
4.8	Shear Capacity of Columns	100
4.9	Yield and Ultimate Deformation of Abutments	106
5.1	Modal Properties of the Typical Bridges	109
6.1	Parameters and Variation	157
6.2	Sensitivity of Parameters on the MSSS Steel Bridge	172
6.3	Sensitivity of Parameters on the MSC Steel Bridge	172
7.1	Matrix of Dynamic Tests	205

7.2	Summary of Calculations for Dynamic Tests of Elastomeric Bearings	213
7.3	Test Matrix Describing the Differences Between the Cable Restrainer Tests	218
7.4	Summary of Effective Stiffness, Ultimate Strength, and Ultimate Deformation for Cable Restrainer Tests	250
7.5	Stiffness and Deformation Characteristics of Single Restrainer Used In Analysis	258
7.6	Characteristics of Synthetic Ground Motions Used in Analysis	259
7.7	Maximum Hinge Opening Results for MSSS Bridge	262
7.8	Maximum Hinge Opening Results for Continuous Bridge	263
8.1	Comparison of NZMWD and the Suggested Method for Designing of Lead-Rubber Bearings	275
8.2	Maximum Values of Critical Responses for Retrofitted MSSS Bridges	287
8.3	Maximum Values of Critical Responses for Retrofitted MSC Bridges	291
8.4	Maximum Values of Critical Responses for Retrofitted SS Bridges	294
B.1	Mean and COV of Responses of MSSS Steel Bridge	311
B.2	Mean and COV of Responses of MSSS Concrete Bridge	312
B.3	Mean and COV of Responses of MSC Steel Bridge	315
B.4	Mean and COV of Responses of MSC Concrete Bridge	317
B.5	Mean and COV of Responses of SS Steel Bridge	319
B.6	Mean and COV of Responses of SS Concrete Bridge	320
C.1	Natural Periods of MSSS Steel Bridge from DRAIN-2DX and MATLAB	325
C.2	Natural Periods of MSC Steel Bridge from DRAIN-2DX and MATLAB	326
C.3	Natural Periods of SS Steel Bridge from DRAIN-2DX and MATLAB	328

D.1a PSDM of Components in MSSS Steel Bridge 332

D.1b PSDM of Components in MSSS Steel Bridge Retrofitted with Elastomeric Bearings 332

D.1c PSDM of Components in MSSS Steel Bridge Retrofitted with Lead Rubber Bearings 333

D.1d PSDM of Components in MSSS Steel Bridge Retrofitted with Restrainer Cables 333

D.1e PSDM of Components in MSSS Steel Bridge Retrofitted with Restrainer Cables and Elastomeric Bearings 334

D.2a PSDM of Components in MSSS Concrete Bridge 336

D.2b PSDM of Components in MSSS Concrete Bridge Retrofitted with Elastomeric Bearings 336

D.2c PSDM of Components in MSSS Concrete Bridge Retrofitted with Lead Rubber Bearings 337

D.2d PSDM of Components in MSSS Concrete Bridge Retrofitted with Restrainer Cables 337

D.2e PSDM of Components in MSSS Concrete Bridge Retrofitted with Restrainer Cables and Elastomeric Bearings 338

D.3a PSDM of Components in MSC Steel Bridge 340

D.3b PSDM of Components in MSC Steel Bridge Retrofitted with Elastomeric Bearings 340

D.3c PSDM of Components in MSC Steel Bridge Retrofitted with Lead Rubber Bearings 341

D.3d PSDM of Components in MSC Steel Bridge Retrofitted with Restrainer Cables 341

D.3e PSDM of Components in MSC Steel Bridge Retrofitted with Restrainer Cables and Elastomeric Bearings 342

D.4a PSDM of Components in MSC Concrete Bridge 344

D.4b PSDM of Components in MSC Concrete Bridge Retrofitted with Elastomeric Bearings 344

D.4c PSDM of Components in MSC Concrete Bridge Retrofitted with Lead Rubber Bearings 345

D.4d PSDM of Components in MSC Concrete Bridge Retrofitted with Restrainer Cables 345

D.4e PSDM of Components in MSC Concrete Bridge Retrofitted with Restrainer Cables and Elastomeric Bearings 346

D.5a PSDM of Components in SS Steel Bridge 347

D.5b PSDM of Components in SS Steel Bridge Retrofitted with Elastomeric Bearings 348

D.5c PSDM of Components in SS Steel Bridge Retrofitted with Lead Rubber Bearings 348

D.5d PSDM of Components in SS Steel Bridge Retrofitted with Restrainer Cables 348

D.5e PSDM of Components in SS Steel Bridge Retrofitted with Restrainer Cables and Elastomeric Bearings 349

D.6a PSDM of Components in SS Steel Bridge 350

D.6b PSDM of Components in SS Steel Bridge Retrofitted with Elastomeric Bearings 350

D.6c PSDM of Components in SS Steel Bridge Retrofitted with Lead Rubber Bearings 350

D.6d PSDM of Components in SS Steel Bridge Retrofitted with Restrainer Cables 351

D.6e PSDM of Components in SS Steel Bridge Retrofitted with Restrainer Cables and Elastomeric Bearings 351

LIST OF FIGURES

Figures		Page
3.1	Eleven States Considered in Seismic Hazard Analysis of Mid-America	13
3.2	Seismicity of the Central and Southeastern United States (CERI, 2001)	16
3.3	Location of New Madrid Seismic Zone	16
3.4	Hazard Curves for West Coast and Mid-America (Leyendecker and Hunt, 2000)	19
3.5	Comparing Seismic Effect in Mid-America and West Coast	20
3.6a	Probabilistic Ground Motion Map for Mid-America Showing Peak Acceleration with 10% Probability of Exceedance in 50 Years(USGS, 1996)	22
3.6b	Probabilistic Ground Motion Map for Mid-America Showing Peak Acceleration with 2% Probability of Exceedance in 50 Years(USGS, 1996)	22
3.7	Representative Time Histories of Ground Motions for 10% and 2% Probability of Exceedance in 50 Years in Memphis, Carbondale and St. Louis	23
3.8a	Comparing Mean Response Spectra of G1 and Caltrans Designs Spectra	26
3.8b	Comparing Mean Response Spectra of G2 and Caltrans Designs Spectra	26
3.9a	Mean Response Spectra of Memphis Ground Motions	27
3.9b	Mean Response Spectra of Carbondale Ground Motions	27
3.9c	Mean Response Spectra of St. Louis Ground Motions	28
4.1	Typical Multi-Span Simply Supported Bridge with Steel Girders	36
4.2	Typical Multi-Span Simply Supported Bridge with Concrete Girders	37
4.3	Bearing System of Typical MSSS Bridge with Concrete Girders	38

4.4	Typical Continuous Bridge with Steel Girders	40
4.5	Typical MSSS Concrete Bridge Made Continuous by Casting Parapet Between Girders	41
4.6	Typical Single Span Bridge with Steel Girders	42
4.7	Steel Bearings in Typical Multi-Span Continuous Steel Bridge (Unit: mm)	44
4.8	Steel Bearings in Typical Single Span Bridge (Unit: mm)	45
4.9	Modeling of MSSS Bridge with Steel Bearings	47
4.10	Shape of Steel Bearings Typically Found on Mid-America Bridges	49
4.11	Details of Rocker Bearings Typically Found on Mid-America Bridges	52
4.12	Details of Sliding Bearings Typically Found on Mid-America Bridges	52
4.13	Response of High Type Fixed Steel Bearing Mounted on Steel Base and Concrete Pedestal (Mander et al., 1996)	53
4.14	Dimension of High Type Fixed Bearing (Unit: mm)	56
4.15	Hysteresis Loop for High Fixed Bearing in Longitudinal Direction from Previous Study (Mander et al. , 1996)	57
4.16	Dimension of High Type Rocker Bearing (Unit: mm)	58
4.17	Hysteresis Loop for High Type Rocker Bearing in Longitudinal Direction from Previous Study (Mander et al., 1996)	59
4.18	Dimension of Low Type Fixed Bearing (Unit: mm)	60
4.19	Hysteresis Loop for Low Type Fixed Bearing in Longitudinal Direction from Previous Study (Mander et al., 1996)	61
4.20	Dimension of Low Type Sliding Bearing (Unit: mm)	62
4.21	Hysteresis Loop for Low Type Sliding Bearing in Longitudinal Direction from Previous Study (Mander et al., 1996)	63
4.22	Typical Hysteresis Loops for Cyclic Dowel Action	66

4.23	Typical Configuration of Elastomeric Pads in Concrete Bridges	66
4.24	Model and Analytical Result of Dowel in ABAQUS	67
4.25	Hysteresis Loop of Dowel Bar	68
4.26	Analytical Model To Represent the Behavior of Two Dowels and An Elastomeric Pad	69
4.27	Various Types of Abutments	71
4.28	Analytical Model of Abutment is Passive and Active Action	75
4.29a	Location of Pounding Element on Bridge Decks	77
4.29b	Analytical Model for Pounding in DRAIN-2DX	78
4.30	Layout of Multi-Column Bent	79
4.31a	Comparison of Unconfined Concrete Models of UCFyber and DRAIN	81
4.31b	Comparison of Confined Concrete Models of UCFyber and DRAIN	81
4.32	Comparison of Steel Reinforcement Models of UCFyber and DRAIN	82
4.33	Fibers in Cross Section of Columns	83
4.34	Moment-Curvature Relationship for Columns	84
4.35	Fiber Element for A Column in Typical MSSS and Continuous Bridge	84
4.36	Layout and Model of Pile Foundation	85
4.37	Vertical Pile Stiffness Solution Graphs of Load-Displacement Curves	92
4.38	Dimension of Footings	93
4.39	Damage State Levels of High Type Fixed Bearings	94
4.40	Static Pushover Analysis of the Column of the MSSS Steel Bridge	101
4.41	Static Pushover Analysis of the Column of the Continuous Steel Bridge	102

4.42 Pile Foundation Configuration of MSSS Bridge for Moment Rotation Study 104

4.43 Damage State Levels of Abutments 106

5.1 First Mode Shape of Typical Bridges in Mid-America 110

5.2 Location of the Fundamental Period of the Typical Bridges in the Longitudinal Direction with MARS of G1 112

5.3 Location of the Fundamental Period of the 6 Bridges in the Longitudinal Direction with MARS of G2 112

5.4 Critical Responses of Interest for the MSSS Steel Bridge 114

5.5a Time Histories of Hinge Opening of MSSS Steel Bridge 116

5.5b Time Histories of Column Drift of MSSS Steel Bridge 116

5.5c Hysteresis Loops of Fixed & Expansion Bearings in MSSS Steel Bridge 117

5.5d Hysteresis Loops of Impact Elements in MSSS Steel Bridge 118

5.5e Hysteresis Loops of Abutments in MSSS Steel Bridge 118

5.5f Hysteresis Loops of Columns in MSSS Steel Bridge 118

5.6 Response of MSSS Concrete Bridge 119

5.7a Time Histories of Hinge Opening of MSSS Concrete Bridge 120

5.7b Time Histories of Column Drift of MSSS Concrete Bridge 120

5.7c Hysteresis Loops of Fixed & Expansion Dowels in MSSS Concrete Bridge 121

5.7d Hysteresis Loops of Impact Elements in MSSS Concrete Bridge 122

5.7e Hysteresis Loops of Abutments in MSSS Concrete Bridge 122

5.7f Hysteresis Loops of Columns in MSSS Concrete Bridge 122

5.8 Response of MS Continuous Steel Bridge 123

5.9a Time Histories of Hinge Opening in MSC Steel Bridge 124

5.9b Time Histories of Column Drift in MSC Steel Bridge 124

5.9c Hysteresis Loops of Fixed & Expansion Bearings in MSC Steel Bridge 125

5.9d Hysteresis Loops of Impact Elements in MSC Steel Bridge 125

5.9e Hysteresis Loops of Abutments in MSC Steel Bridge 126

5.9f Hysteresis Loops of Columns in MSC Steel Bridge 126

5.10a Time Histories of Hinge Openings in MSC Concrete Bridge 128

5.10b Time Histories of Column Drifts in MSC Concrete Bridge 128

5.10c Hysteresis Loops of Fixed & Expansion Dowels in MSC Concrete Bridge 129

5.10d Hysteresis Loops of Abutments in MSC Concrete Bridge 130

5.10e Hysteresis Loops of Columns in MSC Concrete Bridge 130

5.11a Time Histories of Hinge Opening in SS Steel Bridge 131

5.11b Hysteresis Loops of Fixed & Expansion Bearings in SS Steel Bridge 131

5.11c Hysteresis Loops of Abutments in SS Steel Bridge 132

5.12a Time Histories of Hinge Opening in SS Concrete Bridge 133

5.12b Hysteresis Loops of Fixed & Expansion Dowels in SS Concrete Bridge 133

5.12c Hysteresis Loops of Abutments in SS Concrete Bridge 134

5.13a Response of Columns Ductility in MSSS Steel Bridge 137

5.13b Response of Expansion Bearings Deformation in MSSS Steel Bridge 138

5.13c Response of Fixed Bearings Deformation in MSSS Steel Bridge 138

5.13d Response of Abutment1 Deformation in MSSS Steel Bridge 139

5.14a Response of Columns Ductility in MSSS Concrete Bridge 141

5.14b Response of Expansion Dowels Deformation in MSSS Concrete Bridge 141

5.14c Response of Fixed Dowels Deformation in MSSS Concrete Bridge 142

5.14d Response of Abutment1 Deformation in MSSS Concrete Bridge 142

5.15a Response of Columns Ductility in MSC Steel Bridge 144

5.15b Response of Fixed Bearings Deformation in MSC Steel Bridge 144

5.15c Response of Expansion Bearings Deformation in MSC Steel Bridge 145

5.15d Response of Abutment1 Deformation in MSC Steel Bridge 145

5.16a Response of Columns Ductility in MSC Concrete Bridge 148

5.16b Response of Fixed Dowels Deformation in MSC Concrete Bridge 148

5.16c Response of Expansion Dowels Deformation in MSC Concrete Bridge 149

5.16d Response of Abutment1 Deformation in MSC Concrete Bridge 149

5.17a Response of Fixed Bearings Deformation in SS Steel Bridge 150

5.17b Response of Expansion Bearings Deformation in SS Steel Bridge 151

5.17c Response of Abutment1 Deformation in SS Steel Bridge 151

5.18a Response of Fixed Dowels Deformation in SS Concrete Bridge 152

5.18b Response of Expansion Dowels Deformation in SS Concrete Bridge 153

5.18c Response of Abutment1 Deformation in SS Concrete Bridge 153

6.1a Effect of Frictional Coefficient in MSSS Steel Bridge 162

6.1b Effect of Deck Mass in MSSS Steel Bridge 163

6.1c Effect of Gap Size bet. Deck and Abutment in MSSS Steel Bridge 163

6.1d Effect of Gap Size bet. Decks in MSSS Steel Bridge 164

6.1e Effect of Rotational Stiffness of Pile Foundation in MSSS Steel Bridge 164

6.2a Effect of Frictional Coefficient in MSC Steel Bridge 168

6.2b Effect of Deck Mass in MSC Steel Bridge 168

6.2c Effect of Gap Size on Abutment in MSC Steel Bridge 169

6.2d Effect of Rotational Stiffness of Pile Foundation in MSC Steel Bridge 169

6.3 Sensitivity of Deck Mass on Ductility of Columns in MSSS Steel Bridge 171

7.1 Elevation and Cross-section of Test Setup 176

7.2 Partial Illustration of the Testing Facility at the Georgia Institute of Tech 179

7.3 Reinforcement Cage and Form for the Construction of the Piers 180

7.4 Pier Reinforcement Details (Elevation) 181

7.5 Concrete Pedestal Reinforcement Details 182

7.6 Details of Steel Laminated Elastomeric Bearings 184

7.7 Elastomeric Bearing Assembly 185

7.8 Two Concrete Blocks Representing the Dead Weight of the Bridge 186

7.9 Reinforcement of the Concrete Dead Weight Block Between Girders 187

7.10 Details of Structural Tube Section (14”x14”x1/2”) 189

7.11 Columns Used to Restrict Out-plane-movement 192

7.12 Actuator Extender Tube and Connection Elements to the Reaction Wall 193

7.13 Wire Rope End Termination Used a Thimble and 4 Wire Rope Clips 194

7.14 Cable Restrainers were Attached Between Girder Flange and Pier 195

7.15 Original Tennesse DOT Cable Restrainer Assemble Tested on Bridge Model 196

7.16 Installation Procedure for Undercut Anchors 197

7.17 Instrumentation of Test Setup 200

7.18 Seismic Accelerometers Mounted at top and Bottom of Dead Weight Block 203

7.19 Loading Displacement Time History Plot for Test H 206

7.20 Loading Displacement Time History Plot for Test R 206

7.21 Bearing Shear Stress vs. Bearing Shear Strain for +/- 0.5" Sine Wave at 0.5Hz 208

7.22 Bearing Shear Stress vs. Bearing Shear Strain for +/- 0.5" Sine Wave at 2.0Hz 208

7.23 Bearing Shear Stress vs. Bearing Shear Strain for +/- 2" Sine Wave at 0.125Hz 209

7.24 Bearing Shear Stress vs. Bearing Shear Strain for +/- 2" Sine Wave at 0.75Hz 209

7.25 Bearing Displaced to 100% Shear Strain 211

7.26 Cracks Formed in Pedestal After Bearing was Subjected to 100% Shear Strain 211

7.27 Bearing Effective Stiffness vs Bearing Shear Strain 214

7.28 Dearing Energy Per Cycle vs. Bearing Shear Strain 214

7.29 Plot Showing Energy Dissipated and Maximum Strain Energy of Experimental Component 215

7.30 Bearing Equivalent Viscous Damping Ratio vs. Bearing Test Displacement 216

7.31 Specifications of Current TDOT Cable Restrainer Assembly as Tested on Model Bridge 220

7.32 Bent Plate Pier Connection Tested on Model Bridge 221

7.33 Bent Plate Girder Connection Tested on Model Bridge 221

7.34 Load-Displacement Behavior of Current DOT Practice Cable Restrainer Assembly 222

7.35 Bent Plate Connection During Test - Notice Crack at Bend in Plate 223

7.36 Specifications of Retrofit Modification 1 Cable Restrainer Assembly as Tested on Model Bridge 224

7.37 L8x4x1/2” Steel Angle Used at the Girder Connection as Part of Retrofit Modification 1 225

7.38 Load-Displacement Behavior of Retrofit Modification 1 Cable Restrainer Assembly 226

7.39 Bent Plate Pier Connection Failure After Test Retrofit Modification 1 226

7.40 Angle Girder Connection Used in Retrofit Modification 1 With Ductile Deformation 227

7.41 Specifications of Retrofit Modification 2 Cable Restrainer Assembly as Tested on Model Bridge 228

7.42 Two L6x6x1/2” Steel Angles Back-to-back Used in Retrofit Modification 2 229

7.43 L6x6x1/2” Steel Angle Used at Girder Connection in Retrofit Modification 2 229

7.44 Load-displacement Behavior of Retrofit Modification 2 Cable Restrainer Assembly 230

7.45 Angle Connection at Girder Used in Retrofit Modification 2 231

7.46 Specifications of Retrofit Modification 3 Cable Restrainer Assembly as Tested on Model Bridge 232

7.47 L8x8x1” Steel Angle Used in Retrofit Modification 3 on Model Bridge 233

7.48 Load-displacement Behavior of Retrofit Modification 3 Cable Restrainer Assembly 234

7.49 L8x8x1” Steel Angle Connection Used Tested in Retrofit Modification 3 234

7.50 Girder Connection During Testing With Cracks Forming in K-zone 235

7.51 Specification of Retrofit Modification 4 Cable Restrainer Assembly as Tested on Model Bridge 236

7.52 Stiffened L6x6x1/2” Angle Used in Retrofit Modification 4 on Model Bridge 237

7.53	Load-displacement Behavior of Retrofit Modification 4 Cable Restrainer Assembly	238
7.54	Stiffened Steel Angle Girder Connection Tested in Retrofit Modification 4	238
7.55	Damage Due to Prying Action of Pier Connection	239
7.56	Failure of Undercut Anchor at Pier Connection in Retrofit Modification 4	239
7.57	Specifications of Retrofit Modification 5 Cable Restrainer Assembly as Tested on Model Bridge	241
7.58	Pier Connection Used for Retrofit Modification 5 on Bridge Model	242
7.59	Load-displacement Behavior of Retrofit Modification 5 Cable Restrainer Assembly	243
7.60	Brittle Failure of L8x8x1” Steel Angle Tested in Retrofit Modification 5	243
7.61	Specifications of Retrofit Modification 6 Cable Restrainer Assembly as Tested on Model Bridge	245
7.62	Side View of Girder Connection Used in Retrofit Modification 6	246
7.63	View of Girder Connection Showing Bolts and Shackle	246
7.64	Load-displacement Behavior of Retrofit Modification 6 Cable Restrainer Assembly	247
7.65	Failure of Wire Rope Clip Near Thimble on Pier Connection of Retrofit Modification 6	248
7.66	Load-displacement Behavior of Bridge with Each Cable Restrainer Assembly	249
7.67	Layout of Typical Multi-span Simply Supported Bridge with Steel Girders, Elastomeric Bearings, and Restrainers	253
7.68	Layout of Typical Continuous Bridge with Steel Girders, Elastomeric Bearings, and Restrainers	254
7.69	Model of MSSS Bridge Used in DRAIN-2DX	255

7.70 Experimental Force-Displacement Behavior of Cable Restrainers Used in Analysis 257

7.71 Multi-linear Tension Only Element Used to Model Restrainers 257

7.72 Synthetic Ground Motion Time History for Carbondale, IL (2% Exceedance in 50 Years) 259

7.73 Synthetic Ground Motion Time History for Memphis, TN (2% Exceedance in 50 Years) 260

8.1 Typical Unreinforced and Reinforced Elastomeric Bearings 267

8.2 Strain and Deformation of Elastomeric Bearings 267

8.3 Bilinear Modeling of Elastomeric Bearings 272

8.4 Experimental Result of An Elastomeric Bearing of Shear Force vs. Displacement Relationship (Roeder et al., 1987) 272

8.5 Typical Square Lead-Rubber Bearing 276

8.6 Hysteresis Loops of a Lead-Rubber and an Elastomeric Bearing 276

8.7 Behavior of Lead-Rubber Bearings 277

8.8 Damping Ratio of the Lead-Rubber Bearing 277

8.9 Typical Cable Restrainer and Swaged Fitting 278

8.10 Load Deformation Relationship for Restrainers 279

8.11 Typical Connection of Restrainer Cables for Steel Bridges (Piefer, 2001) 279

8.12 Typical Connection of Restrainer Cables for Concrete Bridges 280

8.13 Restrainer Connection between Decks for Steel Bridges (Xanthakos,1996) 282

8.14 Longitudinal Motion Restrainer at Abutment (Xanthakos, 1996) 282

8.15 Analytical Models for Two Types of Restrainer Cables 283

8.16 Installation of Retrofit Measures 284

8.17a Comparison of Responses for As-Built and Retrofitted MSSS Steel Bridges 288

8.17b Comparison of Responses for As-Built and Retrofitted MSSS Concrete Bridges 289

8.18a Comparison of Responses for As-Built and Retrofitted MSC Steel Bridges 292

8.18b Comparison of Responses for As-Built and Retrofitted MSC Concrete Bridges 293

8.19a Comparison of Responses for As-Built and Retrofitted SS Steel Bridges 295

8.19b Comparison of Responses for As-Built and Retrofitted SS Concrete Bridges 296

A.1 Stability of Expansion Steel Bearing (h>r) 308

A.2 Stability of Expansion Steel Bearing (h>r) 309

C.1 5 DOFs System of MSSS Steel Bridge in MATLAB 323

C.2 Simplified Bilinear Model of Fixed Steel Bearing 323

C.3 Linear Model of the Unit of Columns and Pile Foundations of MSSS Bridge 324

C.4 Linear Model of the Unit of Columns and Pile Foundations of Continuous Steel Bridge 325

C.5 3 DOFs Model of Continuous Steel Bridge in MATLAB 326

C.6 Single DOF Model of Single Span Steel Bridge in MATLAB 327

C.7 Linear Model of Low Type Fixed Bearing of Single Span Steel Bridge 327

D.1 Regression Analyses of PSDM as A Function of PGA for the MSSS Steel Bridge 331

D.2 Regression Analyses of PSDM as A Function of PGA for the MSSS Concrete Bridge 335

D.3 Regression Analyses of PSDM as A Function of PGA for the MSC Steel Bridge 339

D.4 Regression Analyses of PSDM as A Function of PGA for the MSC

Concrete Bridge 343

D.5 Regression Analyses of PSDM as A Function of PGA for the SS Steel Bridge 347

D.6 Regression Analyses of PSDM as A Function of PGA for the SS Concrete Bridge 349

E.1 Schaevitz Linear Variable Differential Transformer 353

E.2 RDP Linear Variable Differential Transformer 354

E.3 MTS 243.45T Actuator 355

E.4 Wilcoxon Ultra Low Frequency Seismic Accelerometer 356

E.5 Optim MEGADAC 3415AC 357

F.1 Plots From Test A 359

F.2 Plots From Test B 360

F.3 Plots From Test C 361

F.4 Plots From Test D 362

F.5 Plots From Test E 363

F.6 Plots From Test F 364

F.7 Plots From Test G 365

F.8 Plots From Test H 366

F.9 Plots From Test I 367

F.10 Plots From Test J 368

F.11 Plots From Test K 369

F.12 Plots From Test L 370

F.13 Plots From Test M 371

F.14 Plots From Test N 372

F.15 Plots From Test O 373

F.16 Plots From Test P 374

F.17 Plots From Test Q 375

F.18 Plots From Test R 376

CHAPTER 1

INTRODUCTION

1.1 Problem Description

Bridges are key nodes in any transportation network, and past earthquakes have shown that they are susceptible to damage and/or collapse during moderate to strong ground motions. However, most bridges in the central and southeastern United States (Mid-America) were constructed in the 1960's and 1970's and were designed without adequate consideration of seismic forces. This posses a significant risk since the transportation system in the Mid-America region provides a critical link for transportation of goods and passengers from the West Coast to the East Coast of the United States. It is estimated that over $2.01 trillion in goods originates, goes through, or ends in the Mid-America seismic zone (US department of commerce, 1993). Previous studies have shown that a major earthquake in Mid-America can lead to an economic loss of well over $26.4 billion (ATC-25, 1991). This economic loss is similar to that from the 1994 Northridge earthquake ($20-40 billions; Wald, 2000), and is considerably more than that from the 1989 Loma Prieta ($6-10 billions; Donlin, 1999) earthquake.

To mitigate the potential economic loss due to earthquakes, bridges need to be retrofitted to increase their seismic resistance to earthquakes. Such mitigation strategies have been very successful in highly seismic areas, such as California. Following the 1971 San Fernando earthquake, the California Department of Transportation (Caltrans)

initiated an aggressive retrofit program. From 1971 to 1994, over $2.4 billion was invested to strengthen the transportation system in California. It is generally agreed that these measures were instrumental in limiting the damage to bridges following the 1989 Loma Prieta and 1994 Northridge earthquakes.

Since there has not been a major earthquake in Mid-America since the 1811-1812 New Madrid and the 1886 Charleston earthquakes, there has been little focus on seismic resistant design and retrofit of bridges in this region. Recent changes in the seismic maps have called for higher design acceleration in many parts of Mid-America (AASHTO, 1992). These changes have led to the reevaluation of the seismic design criteria for bridges, and initiation of retrofit programs for deficient bridges. This study provides a comprehensive look at the seismic behavior of typical bridges in Mid-America with the goal of evaluating the effectiveness of various retrofit strategies.

1.2 Objectives of Research

The goal of this study is to evaluate the seismic vulnerability of typical bridges in Mid-America and explore economical methods for modifying their seismic response. The emphasis in this thesis is on superstructure retrofits. Field reconnaissance reports from past earthquakes indicate that many bridge failures could have been prevented with simple mitigation measures such as elastomeric bearings, isolation bearings or restrainer cables (Saiidi et al., 1995; Mayes, 1993). These mitigation strategies are commonly used on the West Coast. However, their effectiveness in Mid-America in not well understood.

To achieve the objectives, the bridge inventory in Mid-America must first be

characterized. Next, nonlinear analytical models are developed to determine the response of bridges due to ground motions that is likely to be observed. The effect of several retrofit strategies will then be investigated analytically and experimentally. Probabilistic studies are performed and fragility curves for typical bridges are developed. Finally, recommendations/guidelines for analysis and retrofit of bridges in Mid-America will be developed.

The specific objectives of the research are:

- Develop an inventory profile of typical bridges in Mid-America.
- Develop 2D nonlinear analytical models of typical bridges.
- Evaluate the seismic response of typical bridges in Mid-America subjected to likely ground motions.
- Evaluate the parameters that affect the response of typical bridges through extensive parameter studies.
- Evaluate the effect of various retrofit strategies using deterministic studies.
- Perform experimental tests on typical existing retrofit components, such as elastomeric bearings and restrainer cables.

1.3 Outline of Report

This report is organized into 10 chapters with the following contents:

Chapter 2 summarizes previous research in this area.

Chapter 3 discusses typical bridge types, seismic hazards, and ground motions in Mid-America.

Chapter 4 provides an overview of bridge components and presents the development of analytical models of bridges. In addition, the chapter evaluates the capacity of bridge components.

Chapter 5 presents the analytical results of the typical bridges subjected to synthetic ground motions.

In chapter 6, a parameter study examines the effects of several key parameters in the response of the typical bridges.

Chapter 7 presents the experimental setup and results.

Chapter 8 analytically evaluates the bridge response after several retrofit strategies have been incorporated.

Chapter 9 presents the conclusions of the study and discusses possible extensions of the research.

CHAPTER 2

SUMMARY OF PREVIOUS STUDIES ON BRIDGES IN MID-AMERICA REGION

2.1 Seismic Performance of Bridges

In recent decades, the seismic susceptibility of highway bridges sparked researcher's interests. From the examination of the damaged bridges during the 1971 San Fernando earthquake, it was found that deficiencies at hinged and rocker bearings played a major role in the collapse of many bridges (Iwasaki et al., 1971). Collapse of simply supported bridges was initiated by the bridge spans falling off their supports at abutments and piers due to large displacement of the spans relative to their supports.

In general, hinge opening at expansion joints is a very critical problem in multi-span simply supported (MSSS) bridges. Studies by Tseng and Penzien (1973), Zimmerman and Brittain (1979), and Imbsen and Penzien (1986), indicated that the hinge opening in multi-span simply supported bridges during previous earthquakes approached the maximum allowable displacement. Zimmerman explained that the relative motion between the ends of decks and pier caps can be severe, particularly when there are only roller connections. The minimum required seat width at the expansion joint was obtained by considering the most critical of: (i) the maximum possible expansion joint opening; and (ii) the maximum displacement of the columns prior to failure due to longitudinal and

transverse direction seismic excitation (Dicleli and Bruneau, 1995a). A mathematical expression for the minimum required seat width in the longitudinal and transverse direction, which is a function of span length, column height, and temperature, was derived to check the adequacy of seat widths in existing multi-span simply supported steel highway bridges (Dicleli, 1993). Parametric studies were conducted to identify the factors important in predicting span unseating, and new design procedures of cable restrainers to restrict the hinge opening were proposed (Yang et al., 1994; Trochalakis et al., 1996; DesRoches and Fenves, 1997; Randall et al., 1999;).

The other serious problem on multi-span simply supported bridges is the impact between decks or deck and abutment. Dicleli and Bruneau (1995a) conducted linear elastic analyses in longitudinal direction to investigate factors affecting the seismic capacity of multi-span simply supported steel bridges. The study indicated that since the maximum column displacement before failure was larger than the expansion joint gap, the impact of the decks is an important problem for longitudinal excitation. The minimum peak ground acceleration for first impacting to occur was calculated as a function of gravitational acceleration, expansion joint widths, and properties of bridges. It was found that the peak ground accelerations required to generate impact increase with span length, but the maximum is less than 0.1g. Therefore, pounding of the decks in the longitudinal direction was generally unavoidable. However, Rashidi and Saadeghvaziri (1997) indicated that generally impact does not lead to an increase in column shear or displacement. Moreover, they found that bearing failure due to impact generally reduces the demand on columns.

A parametric study (Saadeghvaziri and Rashidi, 1997a) was conducted on a multi-span simply supported bridge by varying the stiffness of bearings in longitudinal and transverse direction. Results of the study indicated that the effect of fixed steel bearing stiffness in longitudinal direction was negligible. In the transverse direction, the response was rather sensitive to the bearing stiffness. Based on the results of the study, it was recommended that although it is ideal to replace every fixed bearing with elastomeric bearings, increasing the seat length and installing cable restrainers is an adequate alternative for the retrofitting the bridge superstructure. Increasing the bearing stiffness was an undesirable option since it may lead to collapse by increasing the demand on the columns/piers that often do not posses adequate ductility.

Dicleli (1993) and Saadeghvaziri and Rashidi (1997a) conducted seismic analyses of multi-span simply supported bridges in the transverse direction. This resulted in the response in transverse direction being rather sensitive to the bearing stiffness. The total stiffness of the structure was largely affected by the transverse stiffness of the columns, which was partly a function of the stiffness of the bearings located on the columns. When seismic excitation was applied in transverse direction, the columns displaced in both directions, longitudinal and transverse. The contribution of the deck stiffness to the overall transverse stiffness of two-span simply supported bridge was more effective when bearings having larger stiffness were used at the abutments, resulting in less lateral displacements of the columns.

Three-dimensional bridge models of MSSS bridges were used to capture interaction of the responses in longitudinal and transverse direction (Dicleli and Bruneau, 1995a;

Saiidi et al., 1995; Randall et al., 1999). Dicleli and Bruneau indicated that the bending of the decks in transverse direction resulted in the bearing forces in longitudinal and transverse direction. Saiidi et al. (1995) and Randall et al. (1999) used 3D bridge models to evaluate the effect of restrainer cables. Especially, Saiidi et al. (1995) included impact, friction, and rotational stiffness of the decks at the expansion joints in their model. They found several characteristics of the seismic behavior of bridges in their study; (i) the peak longitudinal displacement of decks are larger than those of the transverse direction, (ii) the ductilities of columns in the transverse direction are much less than 1 because the columns are relatively strong in the direction, and the ductilities without restrainer cables are greater than those with cables, and (iii) in general, the intermediate hinge maximum relative displacements in the longitudinal direction are higher for the cases without restrainer cables than the cases with cables.

The review of the damage to the multi-span simply supported bridges revealed that the longitudinal response appeared to cause more damage to bridge components such as bearings, columns, and abutments, than the transverse response (Zimmerman and Brittain, 1979).

Multi-span continuous bridges are also very common in Mid-America. However, limited research on the seismic behavior of these bridges has been conducted. In general, since multi-span continuous bridges do not have internal expansion joints, they are believed to be less vulnerable to seismic damage than MSSS bridges. The seismic performance of existing multi-span continuous slab-on-girder steel highway bridges was studied by Dicleli and Bruneau (1995b). In their study, both linear elastic and nonlinear

inelastic dynamic analyses were performed to determine the seismically induced bearing forces and column moments. The study showed that the bridges with more spans had more resistant capacity to earthquake excitation before the bearings fail. However, after bearings' fail, bridges with more spans had less seismic resistance.

2.2 Seismic Retrofit of Bridges

The most commonly used retrofitting devices to modify the seismic response of bridges are elastomeric bearings, lead-rubber bearings, and restrainers. In general, elastomeric and lead-rubber bearings as an isolation device are used in both buildings and bridges (Kelly, 1981; Hoerner et al., 1986; Maragakis et al., 1992; Clark et al., 1993). Lead-rubber bearings have been utilized for the seismic isolation of bridges in New Zealand since 1978. In the United States, isolation bearings were not used until 1985 when the Sierra Point Overhead in California was seismically retrofitted.

Seismic isolation has been considered to be an effective measure to reduce earthquake forces and ductility demands on bridge structures (Blakely, 1982; Buckle and Mayes, 1989; Maragakis et al., 1992). Bridges are particularly suitable for isolation and literature surveys indicate that more than 90% of the world's isolated structures are, in fact, bridge structures (Buckle and Mayes, 1989). Applications of seismic isolation include both the design of new bridges and the retrofitting of existing bridges. Implementation within the United States has only occurred within the last few decades and then predominantly as a retrofit measure rather than in new constructions.

Hoerner et al. (1986) conducted dynamic analyses of a retrofitted bridge with lead-rubber or elastomeric bearings. Hoerner and his colleague found that the retrofitted bridge performance was far superior to the as-built bridge. Saiidi and Maragakis (1999) have shown that seismic isolators reduced the force and displacements on the superstructures of a six-span bridge effectively. In addition, it was also shown that the use of isolators does not necessarily increase the displacement of the superstructure. Finally, their study indicated that a reasonable estimate of the isolator response can be obtained even when the coupling effect in modeling of the isolators is ignored.

Maragakis et al. (1992) performed parametric studies on a retrofitted bridge with lead-rubber bearings. In the study, the parameters varied are the flexibility of the deck and the location of the isolator. The deck was modeled as a rigid or an elastic beam, and the isolator is located at the connections between the deck and the bents or at the bottom of the pier. Their study indicated that; (i) the flexibility of the deck can be ignored for the evaluation of the effects of base isolation; and (ii) the deck displacements were not sensitive to the location of the isolator.

Although elastomeric and lead-rubber bearings as isolators have shown significant benefits on modifying seismic response of bridges, some researches have raised questions about using elastomeric and lead-rubber bearings due to potential problems with stability (Kelly et al., 1987; Stanton et al., 1990; Roeder et al., 1987; Nagarajaiah and Ferrell, 1999;) and pounding due to large displacement of the superstructure (Jankowski et al., 1998). Kelly et al. (1987) indicated that when elastomeric bearings are used for seismic isolation, their height requirements might not be satisfied due to bearing instability and/or

geometric constraints. Stanton et al. (1990) and Roeder et al. (1987) studied the stability of laminated elastomeric bearings experimentally and theoretically with due consideration given to axial shortening. Koh and Kelly (1989) developed a viscoelastic stability model and a mechanical model based on bearing test results. Nagarajaiah and Ferrell (1999) developed a nonlinear model of elastomeric bearings to predict postcritical behavior that is unstable.

Bridge restrainers are intended to limit the relative movements at expansion joints and prevent the loss of support. Restrainers can be in the form of plates, rods, or cables. The most common type of restrainers in the United States is the steel restrainer cable. Restrainer cables were first employed in the United States by California Department of Transportation (Caltrans) following the 1971 San Fernando Earthquake (Jennings, 1983). The 1971 San Fernando earthquake in California resulted in many highway bridges collapses because of excessive longitudinal movements at expansion joints and supports. Since then, Caltrans initiated a retrofit program consisting of using restrainer cables at internal hinges of bridges with short seat widths. Approximately 1400 bridges were retrofitted under the Caltrans Phase I retrofit program (Randall et al., 1999). The performance of restrainer cables was tested in the past earthquakes such as the 1989 Loma Prieta Earthquake and the 1994 Northridge Earthquake in California. They mostly performed well, but some bridges were damaged or collapsed (Saiidi et al., 1995; DesRoches and Fenves, 1997; Randall et al., 1999). Several states in Mid-America including Tennessee, Illinois, and Missouri have recently begun using restrainer cables. Indiana and South Carolina plan to incorporate restrainers in the design of bridges in the

near future (Lam, 2000).

Most of the studies on restrainer cables were related to the optimum design (Saiidi et al., 1996; DesRoches and Fenves, 1997; Randall et al., 1999). Yang et al. (1994) performed an analytical parametric study to consider some parameters affecting the seismic response of bridge frames connected by restrainers, and Saiidi et al. (1992) determined important parameters in bridge restrainer design for seismic retrofit. Experimental tests were conducted to determine the characteristics of the behavior of restrainer cables (Selna et al., 1989). The test was performed on restrainer cables used in box-girder-type construction typically found in bridges on the West Coast. Tests being performed at Georgia Tech (Pfeifer, 2001) will be the first results of tests of restrainer cable setups found in MSSS and MS continuous bridges.

CHAPTER 3

SEISMIC HAZARDS AND GROUND MOTIONS IN MID-AMERICA

3.1 Historical Earthquakes and Seismic Hazards in Mid-America

The term Mid-America in this study is taken as that region of the central and southeastern portions of U.S. which includes Illinois, Indiana, Kentucky, Tennessee, Mississippi, Arkansas, Missouri, Georgia, South Carolina, North Carolina, and Virginia as shown in Figure 3.1. Many parts of these 11 states have anticipated ground motions greater than 0.1g for the 10% probability of exceeding 0.1g in a 50-year period (FEMA, 1995).

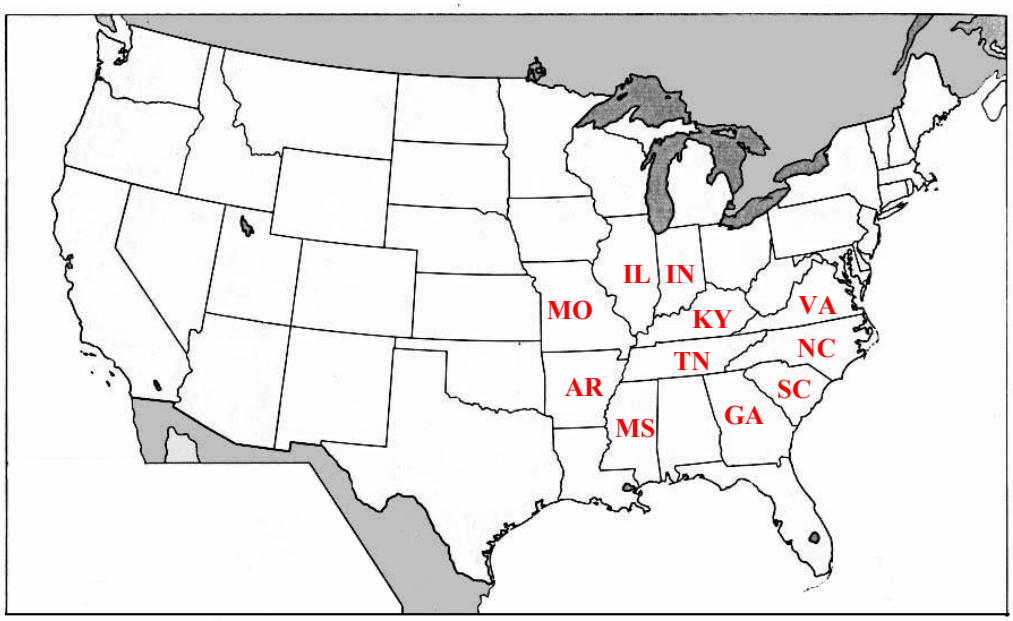

Figure 3.1 Eleven States Considered in Seismic Hazard Analysis of Mid-America

Three large earthquakes of approximately equal strength centered near New Madrid, Missouri occurred on December 16, 1811, January 23, 1812, and February 7, 1812 (U.S. Geological Survey, 1912). This sequence is believed to have had events with moment magnitudes greater than 7.0, including two events of magnitude greater than 8.0. Numerous aftershocks were also reported for a year after the initial shock. As shown in Table 3.1, the Feb. 7, 1812 earthquake in New Madrid is one of the ten largest earthquakes in United States history and is the largest in the continental U.S.

Table 3.1 Ten Largest Earthquakes in United States

No.	Location	Magnitude (M_w)	Date
1	Prince William Sound, AK	9.2	Mar. 28, 1964
2	Andreanof Islands, AK	8.8	Mar. 9, 1957
3	Rat Islands, AK	8.7	Feb. 4, 1965
4	East of Shumagin Islands, AK	8.3	Nov. 10, 1938
5	Lituya Bay, AK	8.3	Jul. 10, 1958
6	Yakutat Bay, AK	8.2	Sep. 10, 1899
7	near Cape Yakataga, AK	8.2	Sep. 4, 1899
8	Andreanof Islands, AK	8.0	May 7, 1986
9	**New Madrid, MO**	**8.0**	**Feb. 7, 1812**
10	Fort Tejon, CA	7.9	Jan. 9, 1857

The seismic hazard in Mid-America is not only from the New Madrid Seismic Zone (NMSZ). Charleston, South Carolina, had a very large earthquake on August 31, 1886,

which had a Modified Mercalli Intensity (MMI) of X (Wiegel, 1970). Twenty seven lives were lost and $5-6 million of damage was reported. Further, more than 18 earthquakes, having shaking intensities between VII and VIII on the MMI scale have occurred in the central and southeastern US between 1774 and 1980.

Figure 3.2 shows the recorded earthquakes in the Central and Southeastern United States from 1970-1999. None of these earthquakes have had moment magnitudes greater than 6. However, trends of low level seismicity may be useful in determining the seismicity in the region. In the New Madrid Seismic Zone, the low-level seismic activity has delineated what are believed to be fault zones associated with the major earthquakes of 1811-12. The low magnitude seismic activity in eastern Tennessee shown in Figure 3.2 may delineate a zone of important future activity, but no large shocks are known to have occurred in this area in recent history. Although the Mid-America may have ground shaking from a variety of sources, this study will focus on the effects of the New Madrid seismic hazard.

3.2 New Madrid Seismic Zone

The New Madrid Seismic Zone (NMSZ), shown in Figure 3.3, lies within the central Mississippi Valley, covering the region of northeast Arkansas, southeast Missouri, western Tennessee, western Kentucky and southern Illinois. Most quakes in eastern United Sates occur in the New Madrid Seismic Zone shown in red in Figure 3.3(a). Crosses in Figure 3.3(b) show the locations of the earthquakes which have been recorded in the New Madrid Seismic Zone since 1974.

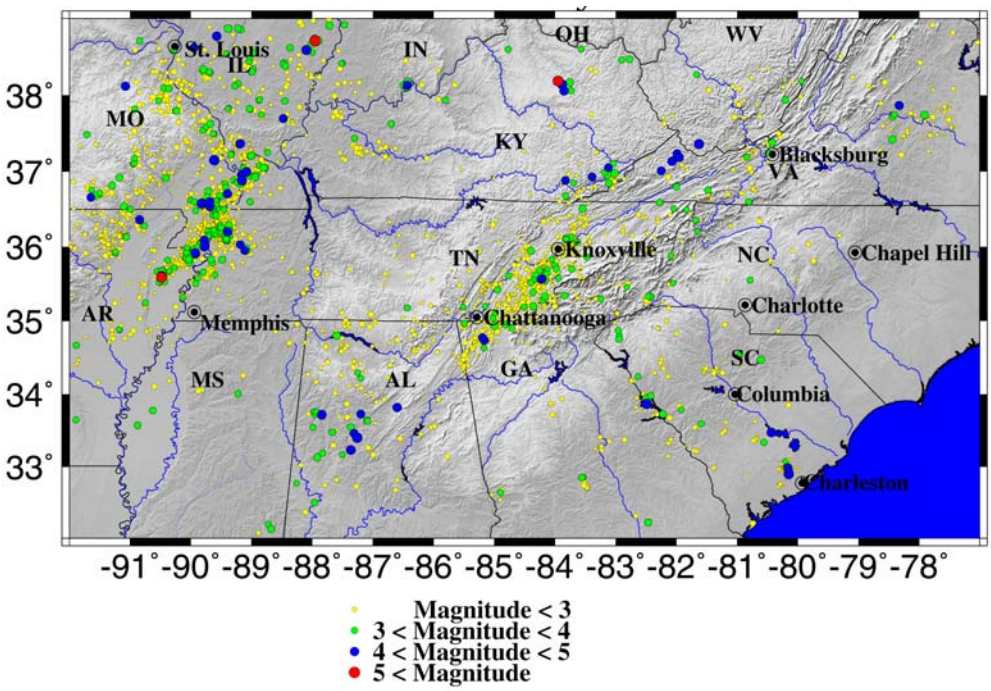

Figure 3.2 Seismicity of the Central and Southeastern United States (CERI, 2001)

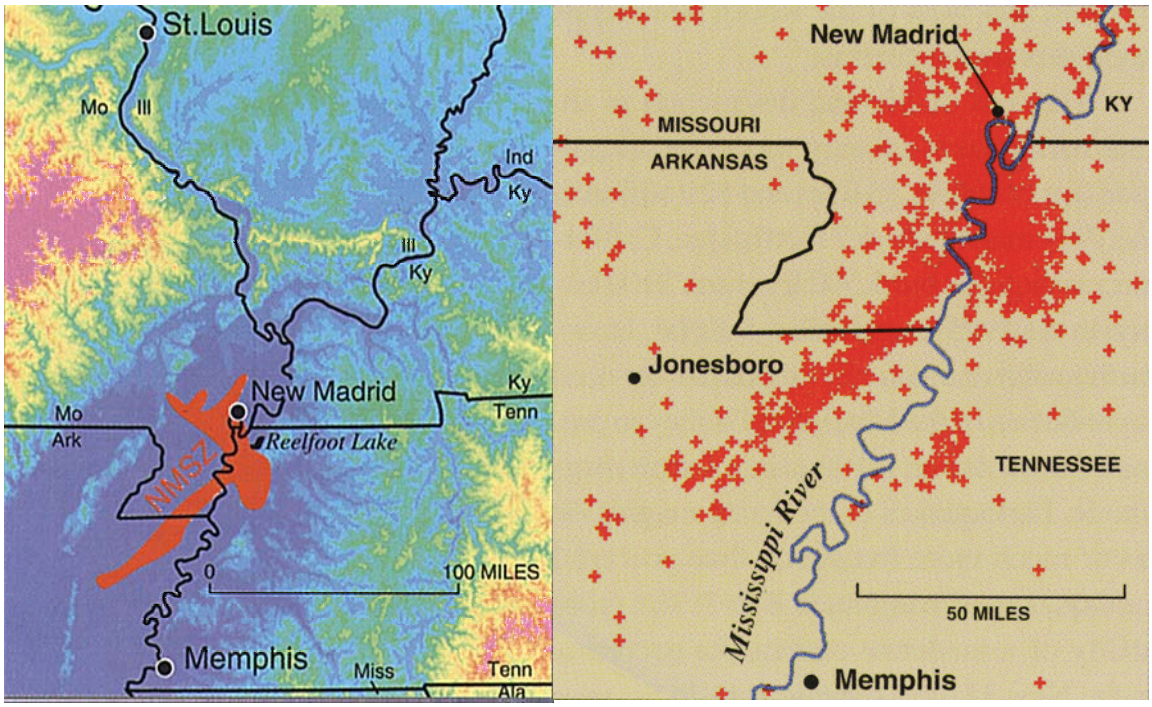

(a) (b)

Figure 3.3 Location of New Madrid Seismic Zone

As previously mentioned, this area has been the site of some of the largest earthquakes in North America. Between 1811 and 1812, 3 catastrophic earthquakes, with magnitude estimated greater than 7.0, occurred during a 3-month period. Hundreds of aftershocks followed over a period of several years. The largest earthquakes to have occurred since then were on January 4, 1843 and October 31, 1895 with magnitude estimates of 6.0 and 6.2, respectively. In addition to these events, seven events of magnitude greater than or equal to 5.0 have occurred in the area. Instruments were installed in and around this area in 1974 to closely monitor the seismic activity. Since then, more than 4000 earthquakes have been located, most of which are too small to be felt.

The likelihood of a repeat of a great earthquake in the New Madrid seismic zone is small. It is believed that catastrophic events like those of the 1811-12 occur in the NMSZ every 550-1200 years (CERI, 2001), which means an event greater than magnitude 8.0 has roughly the probability of 0.3-1.0% within the next 15 years and 2.7-4.0% within 50 years. For a magnitude 7.0 earthquake, there is a 5-9% probability within the next 15 years and a 19 to 29% probability within the next 50 years. For a magnitude 6.0, the probability of occurrence is 40-63% probability within the next 15 years and 86-97% probability within the next 50 years. It is believed that magnitude 6.0 earthquake would cause damage to older structures, especially those of unreinforced masonry construction.

Paleoliquefaction investigations have provided constraints on recurrence in the New Madrid Seismic Zone. Following the above statement, the probability of a larger earthquake is less than that of the smaller. However, the paleoliquefaction interpretations

suggest that large earthquakes like those of 1811-1812 may be "characteristic earthquakes". In other words, the recurrence rates of small events, whose magnitude is less than 5.0, and the largest earthquakes cannot be simply related. Paleoliquefaction features that might be associated with moderate earthquakes are absent from the geologic record, and an earthquake, whose magnitude is larger than 6.0, has not occurred since 1895. In short, the largest earthquakes might occur much more frequently than the rate of smaller earthquakes would imply.

Among the recorded earthquakes in the Southeastern United States from 1970-1999 shown in Figure 3.2, none of these earthquakes have had moment magnitudes greater than 6. Therefore, because the New Madrid events occurred prior to the development of modern seismological instruments, recordings of strong ground motions in the central US do not exist.

3.3 Comparing Seismic Hazards for Mid-America and the West Coast

In California, many earthquakes are associated with surface faulting, so that the relationship between geological structure and earthquake occurrence is reasonable well known. The seismicity in the past has been investigated through this relationship, which has provided the information of magnitude of earthquake likely to occur on individual faults, the recurrence rates of large earthquakes, and related data. With few exceptions, meaningful relationships between the surface trace of faults and earthquake occurrence in Mid-America have not been established.

In addition, the probabilistic seismic hazard for the Mid-America region is different

from that of the West Coast. As shown in Figure 3.4, the slopes of the hazard curves for Charleston and Memphis in the Mid-America are relatively steep compared to the slopes for San Francisco and Los Angeles in the West Coast. The 0.2 second spectral acceleration of the 10% probability of exceedance in 50 years for Los Angeles is about 1.0g, and the corresponding value for Memphis is about 0.3g. For the 2% probability of exceedance in 50 years, the values of 0.2 second spectral acceleration for Los Angeles and Memphis are approximately equal.

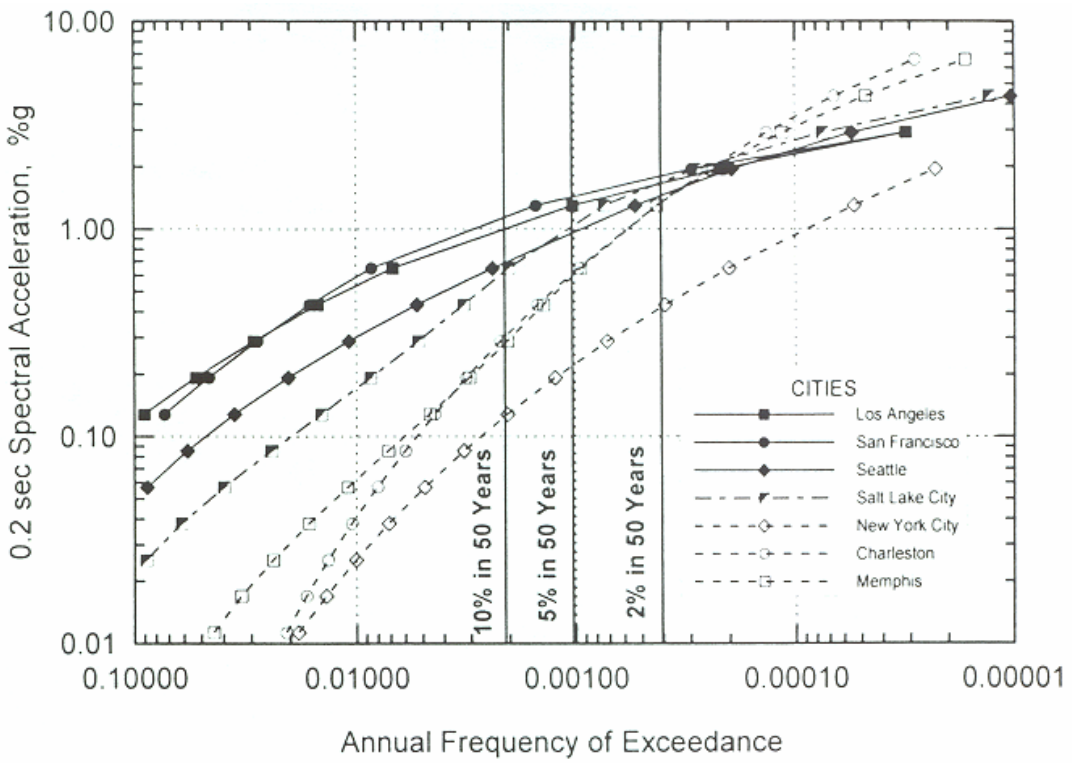

Figure 3.4 Hazard Curves for West Coast and Mid-America (Leyendecker and Hunt, 2000)

Figure 3.5 shows the seismic effects of the two earthquakes in the West Coast, 1906 San Francisco and 1971 San Fernando, and the two in Mid-America, 1811 New Madrid and 1886 Charleston. The estimated moment magnitudes of the 1906 San Francisco and the 1971 San Fernando earthquake are 8.3 and 6.3, respectively. The magnitudes for the two earthquakes in Mid-America are 8.6 (1811 New Madrid) and 7.8 (1886 Charleston), respectively. From the figure, the seismic effect of an earthquake in Mid-America is much wider than that of West Coast. This is due to the fact that the Mid-America region has less rapid attenuation of ground motions with distance compared with the West Coast. As shown below, a repeat of the 1811-1812 New Madrid earthquake may be strongly felt over 14 states.

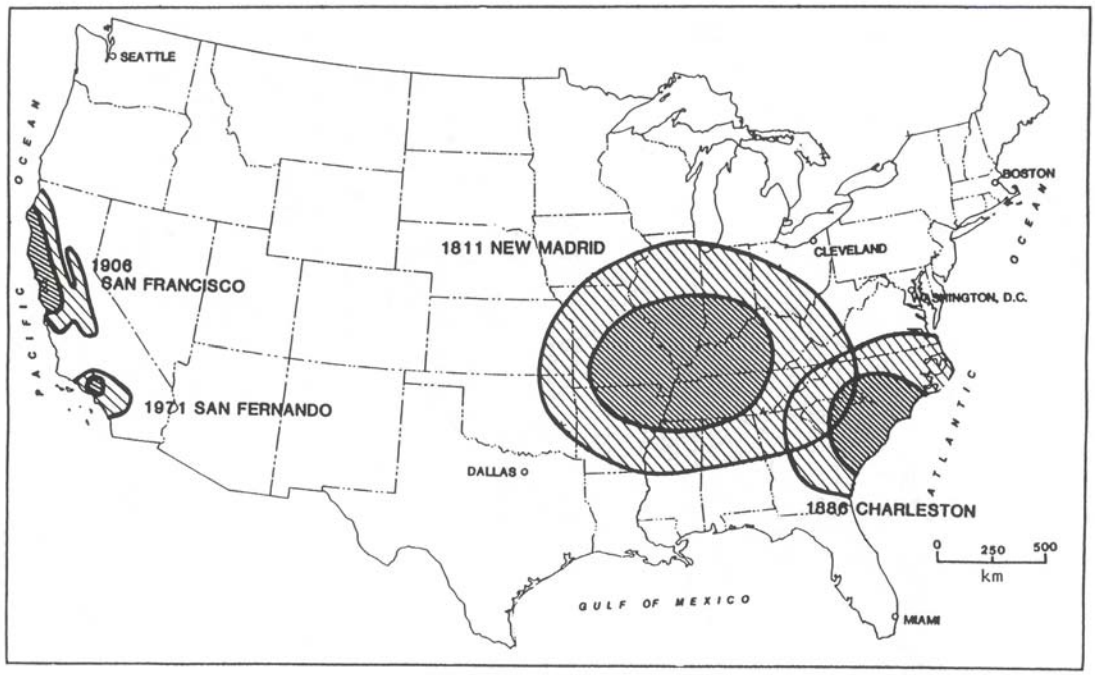

The dark areas are intensity VIII and greater; the light areas are intensity VI-VII.

Figure 3.5 Comparing of Seismic Effect in Mid-America and West Coast

3.4 Ground Motions in Mid-America

In order to assess the seismic hazard of bridges in Mid-America, ground motions that are likely to occur in the Mid-America must be determined. Since few recorded strong ground motions exist in the region, synthetic ground motion records must be generated. Using the latest regional information and stochastic ground motion models, Wen and Wu (2001) developed a suit of synthetic uniform hazard ground motions for Memphis, TN, Carbondale, IL, and St. Louis, MO. These cities are selected as earthquake sites because they present a cross-section of the Mid-America cities at risk. The ground motion simulation method basically follows the procedure proposed by Herrmann and Akinci (1999) that is largely based on Boore's point-source simulation method SMSIM (1996). However, the finite fault model by Beresnev and Atkinson (1997, 1998) is also used for magnitude-8 events to catch some of the important near-source effects due to large events. The soil amplification is modeled by the quarter-wavelength method by Boore and Joyner (1991, 1997). The tectonic and seismological data are mainly taken from USGS Open-File Report 96-532 (Frankel et al. 1996).

For each of the three cities, two uniform hazard level ground motion records are generated: 10% probability of exceedance in 50 years (G1) and 2% probability of exceedance in 50 years (G2). Each suite has 10 ground motions, resulting in the development of a total of 60 ground motion records. The probabilistic ground motion maps of the suites are shown in Figure 3.6. Figure 3.7 shows the representative sample of each suite of ground motion records.

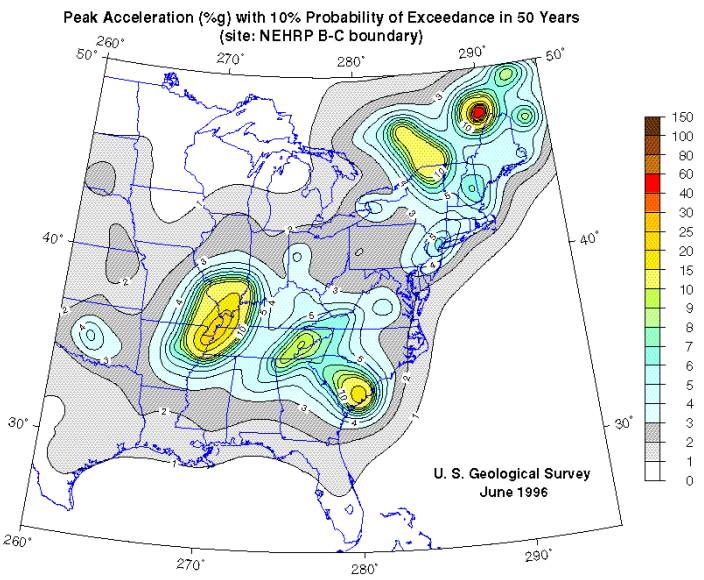

Figure 3.6a Probabilistic Ground Motion Map for Mid-America Showing Peak Acceleration with 10% Probability of Exceedance in 50 Years (USGS, 1996)

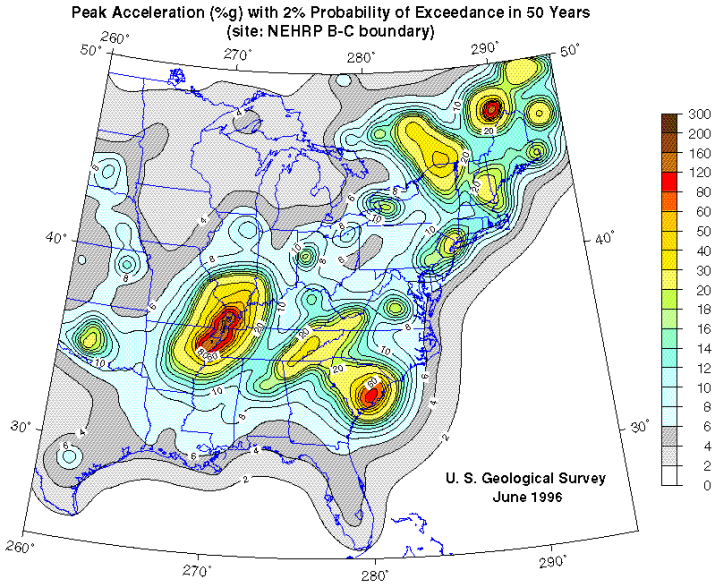

Figure 3.6b Probabilistic Ground Motion Map for Mid-America Showing Peak Acceleration with 2% Probability of Exceedance in 50 Years (USGS, 1996)

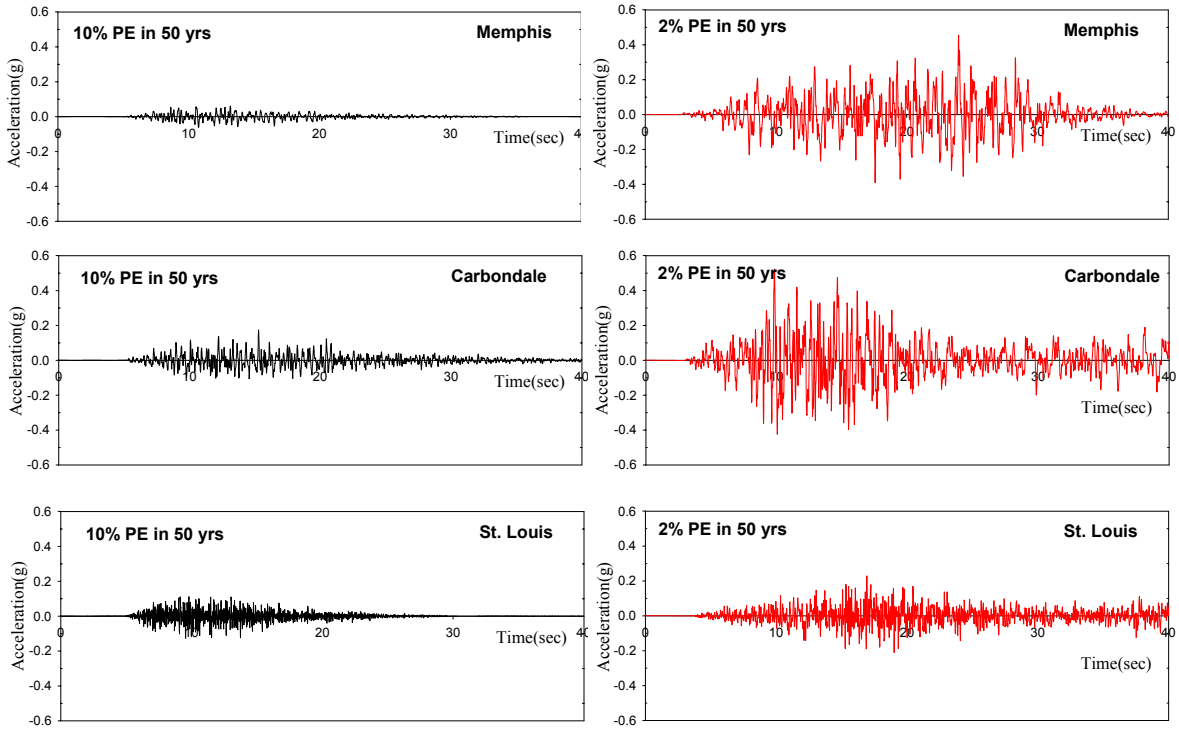

Figure 3.7 Representative Time Histories of Ground Motions for 10% and 2% Probability of Exceedance in 50 Years in Memphis, Carbondale, and St. Louis

3.4.1 Characteristics of Ground Motions

Amplitude, frequency content, and duration are the three main parameters that characterize strong ground motions (Jennings, 1983). Peak ground acceleration can represent earthquake amplitude. One method of ascertaining frequency content is from response spectra of ground motions. Duration is typically defined as the time length between the first and the last exceedances of 0.05g. Table 3.2 shows the mean values of moment magnitude (M_w), epicentral distance, duration, peak ground acceleration, and characteristic period (T_g). Table 3.3 shows the parameters for each ground motion record.

Table 3.2 Mean Values of Ground Motion Parameter for Suite of Synthetic Ground Motion Records for Mid-America

Ground Motions for 10% Probability of Exceedance in 50 years					
	Moment Magnitude(M_w)	Epicentral Distance (km)	Duration (sec)	PGA (g)	T_g (sec)
Memphis	6.4	88	4.4	0.08	0.45
Carbondale	6.4	122	14.2	0.17	0.16
St. Louis	6.4	193	12.1	0.11	0.17
Ground Motions for 2% Probability of Exceedance in 50 years					
	Moment Magnitude(M_w)	Epicentral Distance(km)	Duration (sec)	PGA (g)	T_g (sec)
Memphis	8.0	151	31.2	0.38	0.99
Carbondale	8.0	158	59.5	0.51	0.88
St. Louis	7.2	195	31.9	0.33	0.16

The peak ground acceleration as a factor of amplitude is usually proportional to moment magnitude and inversely proportional to epicentral distance. Therefore, generally speaking, the peak ground acceleration of the artificial ground motions is proportional to moment magnitude and inversely proportional to epicentral distance.

To investigate the frequency contents of ground motion suites, Mean Response Spectra (MRS) for 5% damping are calculated as shown in Figure 3.8. The MRS are compared with the two response spectra, Caltrans design spectra and spectra from NEHRP (National Earthquake Hazards Reduction Program). The PGA of Caltrans design spectra is scaled down to 0.1g and 0.4g to allow comparison with the MRS of the synthetic ground motions, G1 and G2, respectively.

As shown in Figure 3.8a, the MRS of Carbondale ground motions is the largest in the

short period range. The MRS of St. Louis is larger than that of Memphis for periods less than 0.25 second.

In the G2 suite shown in Figure 3.8b, the MRS of Memphis and Carbondale ground motions are much higher than that of St. Louis. This is a result of the fact that Memphis and Carbondale soil profiles contain softer soils compared with St. Louis.

From NEHRP, the MRS of 2 and 10% probability of exceedance in 50 years for the three sites, Memphis, Carbondale, and St. Louis, are shown in the Figure 3.9. Ten sites for Memphis and St. Louis, respectively and one site for Carbondale are selected to obtain the MRS from NEHRP. In the figure, the MRS from MAEC (Mid-America Earthquake Center) are plotted with mean±standard deviation.

The MRS from MAEC is close to the MRS of NEHRP in the ground motions of 10% probability of exceedance in 50 years. However, in the 2% case, the MRS of MAEC is not in accord with that of NEHRP. The spectra from NEHRP are higher than that of MAEC in Memphis, but it becomes smaller at the period of 1.0 sec. This trend is reversed for the St. Louis spectra. In the case of Carbondale, the trend of NEHRP is similar to that of MAEC. The magnitude of NEHRP is lower than that of MAEC in the long period.

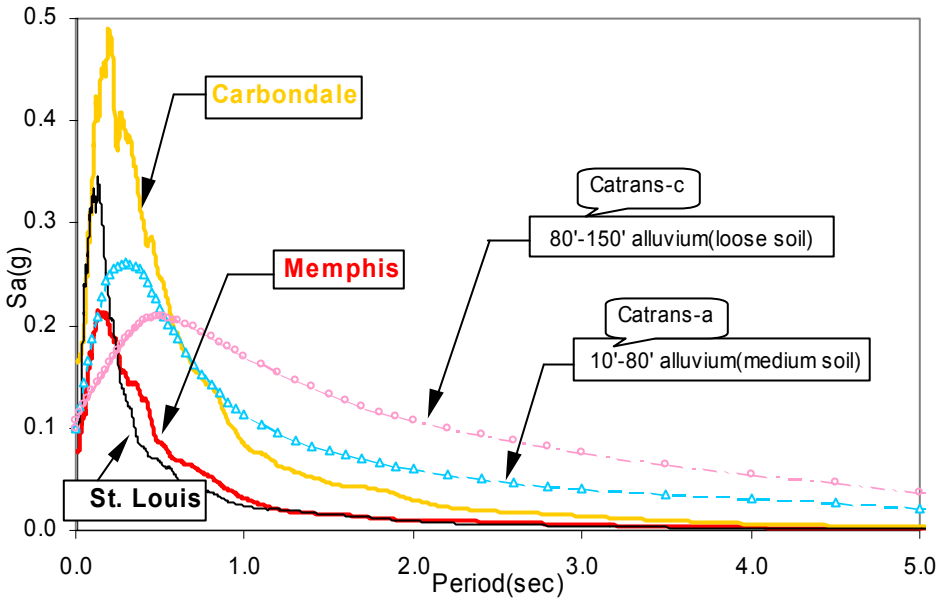

Figure 3.8a Comparing Mean Response Spectra of G1 and Caltrans Design Spectra

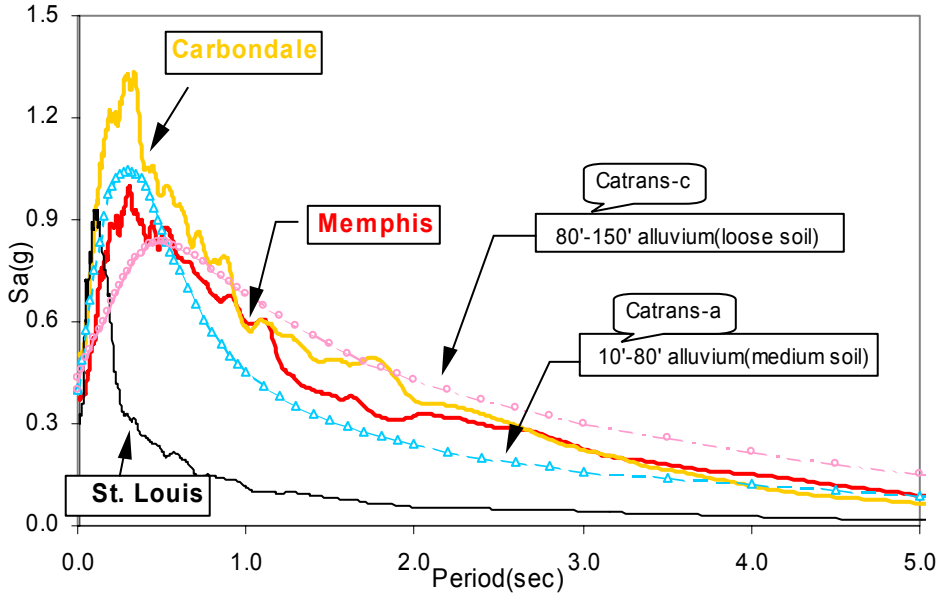

Figure 3.8b Comparing Mean Response Spectra of G2 and Caltrans Design Spectra

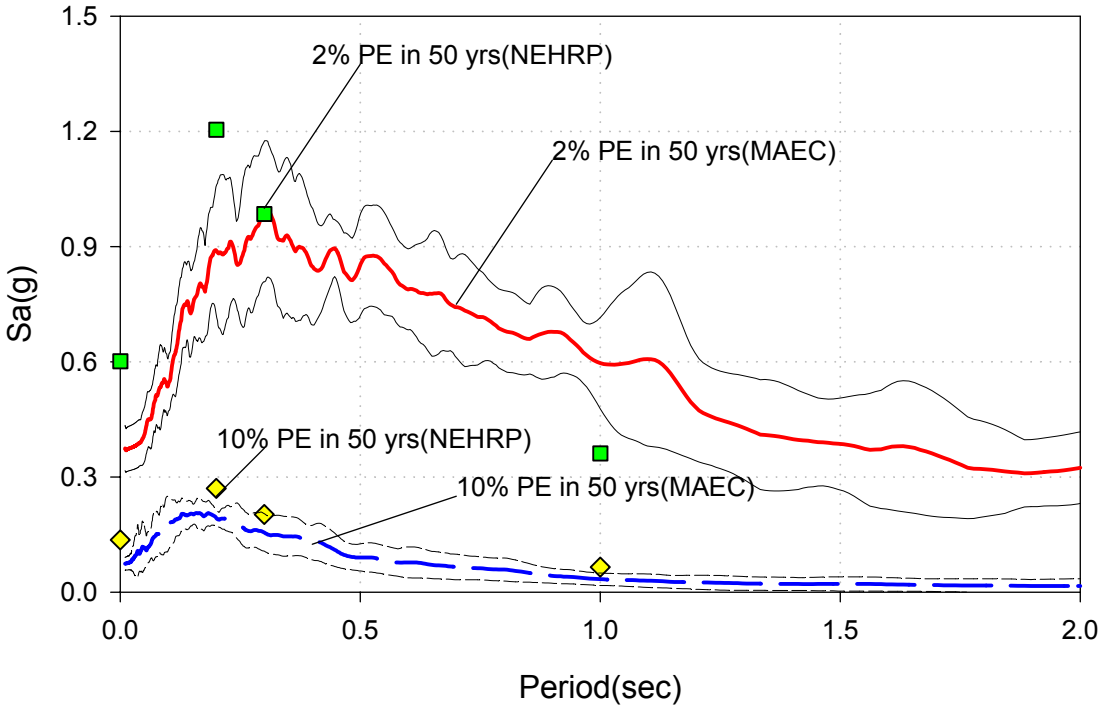

Figure 3.9a Mean Response Spectra of Memphis Ground Motions

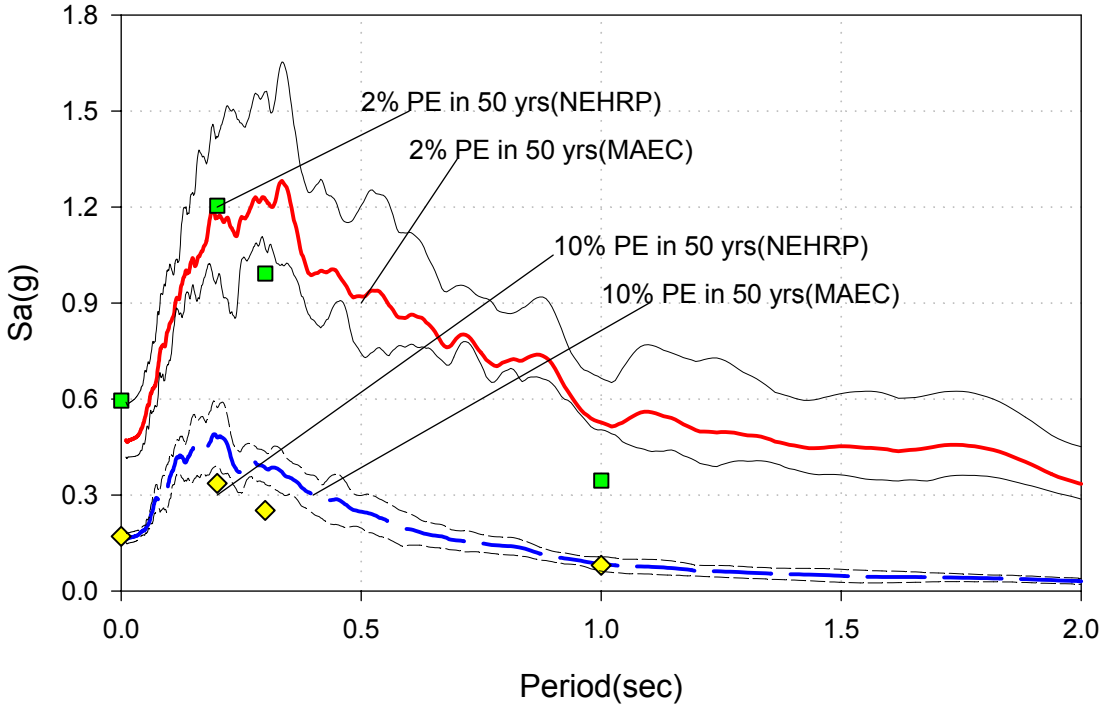

Figure 3.9b Mean Response Spectra of Carbondale Ground Motions

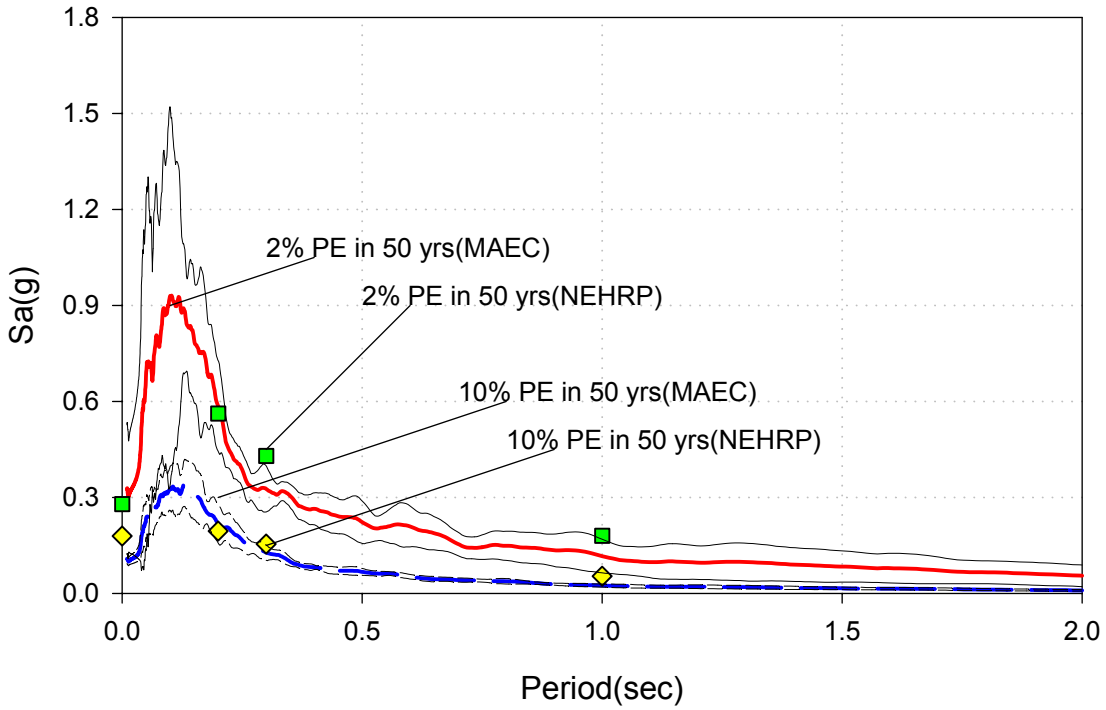

Figure 3.9c Mean Response Spectra of St. Louis Ground Motions

Another parameter of the ground motions is the characteristic period, T_g, of the ground motions which is defined as the period at which the input energy of a 5% damped linear elastic system is maximum. Since the maximum pseudo-velocity is related to the maximum kinetic energy, the characteristic period of the ground motions is estimated by the peak of the pseudo-velocity response spectrum maximum (Uang and Bertero, 1990). The estimated characteristic periods are shown in Table 3.3.

The duration is related to the time required for release of accumulated strain energy by rupture along the fault. As the length of fault rupture increases, the time for releasing earthquake energy increases. Therefore, the duration of strong ground motions increases with increasing earthquake magnitude. Thus, earthquake duration can be important in

nonlinear structural analysis because longer duration of strong shakings can lead to the accumulation of plastic deformation.

Table 3.3 Characteristics of Synthetic Ground Motion Records

	M_w	Ed (km)	Du (sec)	PGA (g)	T_g (sec)	M_w	Ed (km)	Du (sec)	PGA (g)	T_g (sec)	M_w	Ed (km)	Du (sec)	PGA (g)	T_g (sec)
Ground Motions for 10% Probability of Exceedance in 50 years															
No.	Memphis					Carbondale					St. Louis				
1	6.7	138	7.92	0.06	0.38	7.1	150	20.5	0.17	0.52	6.0	76	12.6	0.13	0.16
2	6.3	121	3.56	0.08	0.60	6.4	121	13.9	0.17	0.31	6.8	201	14.0	0.10	0.15
3	5.9	123	3.74	0.07	0.65	6.1	69	14.2	0.15	0.33	7.2	237	9.23	0.09	0.22
4	6.8	92	7.26	0.07	0.69	6.4	103	14.9	0.17	0.45	6.3	252	8.44	0.11	0.16
5	6.2	41	3.40	0.11	0.35	5.8	62	11.8	0.18	0.21	5.5	123	9.98	0.13	0.20
6	8.0	171	1.35	0.05	0.63	6.2	120	10.6	0.18	0.35	6.2	208	12.0	0.11	0.14
7	6.5	59	4.86	0.07	0.43	5.8	125	9.32	0.13	0.37	6.9	194	14.2	0.10	0.13
8	6.0	30	4.33	0.09	0.19	6.3	96	12.6	0.17	0.29	6.2	175	13.3	0.19	0.23
9	5.3	32	4.42	0.09	0.18	6.8	186	19.7	0.18	0.54	6.2	221	12.3	0.11	0.14
10	5.8	76	3.12	0.06	0.42	6.7	186	14.7	0.18	0.20	6.9	237	14.6	0.08	0.16
Ground Motions for 2% Probability of Exceedance in 50 years															
No.	Memphis					Carbondale					St. Louis				
1	8.0	148	30.7	0.44	1.04	8.0	166	57.1	0.52	0.54	8.0	267	46.8	0.23	0.13
2	8.0	186	21.5	0.33	0.93	8.0	193	21.2	0.42	0.78	8.0	229	46.9	0.25	0.15
3	8.0	163	20.2	0.36	1.04	8.0	166	43.4	0.55	0.72	5.4	29	7.35	0.83	0.10
4	8.0	100	55.3	0.32	0.95	8.0	166	45.9	0.45	0.90	7.1	253	32.1	0.25	0.17
5	8.0	98	57.8	0.48	1.14	8.0	122	91.0	0.60	0.89	8.0	254	37.8	0.19	0.22
6	8.0	118	43.5	0.42	1.14	8.0	137	92.1	0.50	1.13	6.8	224	23.8	0.24	0.15
7	8.0	146	23.0	0.37	0.96	8.0	176	81.7	0.42	0.71	8.0	196	59.5	0.24	0.20
8	8.0	197	18.0	0.29	1.09	8.0	98	76.6	0.41	0.95	8.0	260	24.7	0.24	0.17
9	8.0	170	22.2	0.34	0.66	8.0	169	27.9	0.67	0.87	6.8	185	26.4	0.26	0.19
10	8.0	188	19.7	0.41	0.91	8.0	183	58.4	0.50	1.27	5.9	48	13.9	0.54	0.12

M_w : Moment Magnitude Ed : Epicentral Distance Du : Duration T_g : Predominate Period

CHAPTER 4

TYPICAL BRIDGES AND ANALYTICAL MODELS IN MID-AMERICA

4.1 Inventory of Bridges and Typical Bridges in Mid-America

To better understand the seismic risks to the transportation systems in Mid-America, we must first evaluate the characteristics of typical bridges in the region. This is accomplished by developing an inventory profile of the bridges and their characteristics. Using data from the National Bridge Inventory Program (NBIP), the distribution of bridges is developed, as shown in Table 4.1. The multi-span simply supported bridge makes up 41.8% of the bridge inventory, the multi-span continuous bridge constitutes 28.2% of the bridges, and the single span simply supported bridge makes up 25.1% of the bridges. Since these three types of bridges account for more than 95% of the total bridges in Mid-America, the studies in this thesis will focus on these bridges. Table 4.2 shows the distribution of superstructure material for the bridges in Mid-America. It is observed that 32% and 20% of the bridges have steel girder or PSC girder superstructure, respectively. RC superstructure accounts for over 43% of the bridges. The distribution for the RC superstructure includes T-beam, slab, and culvert. Since bridges with a slab or culvert superstructure are generally not considered seismic hazard, they are not evaluated as part of the study. Therefore, the two superstructure types considered in this study are PS concrete girder and steel girder beams.

Based on the above information, the six types of bridges considered as the typical bridges in the Mid-America region are; (1) Multi-span simply supported (MSSS) steel girder bridge, (2) Multi-span simply supported (MSSS) PS concrete girder bridge, (3) Multi-span continuous (MSC) steel girder bridge, (4) Multi-span continuous (MSC) PS concrete girder bridge, (5) single span (SS) steel girder bridge, (6) single span (SS) PS concrete girder bridge.

In this study, curved and/or skew bridges will not be considered. Most highway bridges are not curved except connectors at highway junctions. The seismic behavior of the bridges will be estimated only in the longitudinal direction since the previous studies showed that the unseating and the impact in the longitudinal direction are the serious problems in the seismic behavior of bridges (Imbsen and Penzien, 1986; Dicleli and Bruneau, 1995a).

Table 4.1 Inventory of Bridges in Mid-America According to Structure Type

State	Total	MSSS[1] (%)	Single Span (%)	MSC[2] (%)	Other (%)
Georgia	**14809 (100.0)**	12089 (81.6)	1100 (7.4)	1620 (10.9)	0 (0.0)
Tennessee	**19402 (100.0)**	5413 (27.9)	3306 (17.0)	10683 (55.1)	0 (0.0)
S-Carolina	**7994 (100.0)**	2481 (31.0)	4766 (59.6)	639 (8.0)	108 (1.4)
Mississippi	**5332 (100.0)**	124 (2.3)	2863 (53.7)	1067 (20.0)	1278 (24.0)
Arkansas	**6956 (100.0)**	5769 (82.9)	372 (5.3)	815 (11.7)	0 (0.0)
Missouri	**9902 (100.0)**	3080 (31.1)	21 (0.2)	6797 (68.6)	4 (0.0)
Illinois	**27574 (100.0)**	10418 (37.8)	11022 (40.0)	6087 (22.1)	47 (0.2)
N-Carolina	**17193 (100.0)**	6265 (36.4)	3934 (22.9)	3090 (18.0)	3904 (22.7)
Total	**109162 (100.0)**	**45639 (41.8)**	**27384 (25.1)**	**30798 (28.2)**	**5341 (4.9)**

MSSS[1] : Multi-Span Simply Supported

MSC[2] : Multi-Span Continuous

Table 4.2 Inventory of Bridges in Mid-America According to Material Type of Superstructure

State	**Total**	Steel (%)	PSC[1] (%)	RC[2] (%)	Wood (%)	Other (%)
Georgia	**14809 (100.0)**					
Tennessee	**19402 (100.0)**	3143 (16.2)	3817 (19.7)	11835 (61.0)	596 (3.1)	11 (0.0)
S-Carolina	**7994 (100.0)**	1475 (18.5)	1527 (19.1)	4825 (60.4)	165 (2.1)	0 (0.0)
Mississippi	**5332 (100.0)**	991 (18.6)	2149 (40.3)	2191 (41.1)	1 (0.0)	0 (0.0)
Arkansas	**6956 (100.0)**	2417 (34.7)	57 (0.8)	4281 (61.5)	181 (2.6)	20 (0.0)
Missouri	**9902 (100.0)**	4002 (40.4)	924 (9.3)	4951 (50.0)	21 (0.2)	2 (0.0)
Illinois	**27574 (100.0)**	8893 (32.3)	8532 (30.9)	9839 (35.7)	173 (0.6)	137 (0.0)
N-Carolina	**17193 (100.0)**	9300 (54.1)	2149 (12.5)	3158 (18.4)	1906 (11.1)	58 (0.0)
Total	**109162 (100.0)**	**30221 (32.1)**	**19155 (20.3)**	**41080 (43.6)**	**3043 (4.0)**	**228 (0.0)**

PSC[1] : Pre-Stressed Concrete

RC[2] : Reinforced Concrete

Table 4.3 Inventory of Bridges in Mid-America According to Superstructure Type

State	**Total**	Slab (%)	Multi-Beam (%)	T-Beam (%)	Culvert (%)	Box Girder (%)	Girder (%)	Truss (%)	Arch (%)	C Stay (%)	Other (%)
Georgia	**14809 (100.0)**	1226 (8.3)	5555 (37.5)	2145 (14.5)	5249 (35.4)	394 (2.7)	80 (0.5)	61 (0.4)	59 (0.4)	1 (0.0)	39 (0.3)
Tennessee	**19402 (100.0)**	299 (1.5)	7779 (40.1)	26 (0.1)	7928 (40.9)	2051 (10.6)	2 (0.0)	118 (0.6)	185 (1.0)	0 (0.0)	1014 (5.2)
S-Carolina	**7994 (100.0)**	3739 (46.8)	2485 (31.1)	983 (12.3)	0 (0.0)	1241 (15.5)	330 (4.1)	3 (0.0)	42 (0.5)	0 (0.0)	0 (0.0)
Mississippi	**5332 (100.0)**	224 (4.2)	124 (2.3)	169 (3.2)	1316 (24.7)	293 (5.5)	1706 (32.0)	21 (0.4)	6 (0.1)	0 (0.0)	0 (0.0)
Arkansas	**6956 (100.0)**	1365 (19.6)	3131 (45.0)	529 (7.6)	1755 (25.2)	21 (0.3)	33 (0.5)	70 (1.0)	41 (0.6)	0 (0.0)	11 (0.2)
Missouri	**9902 (100.0)**	1082 (10.9)	2461 (24.9)	775 (7.8)	2931 (29.6)	219 (2.2)	26 (0.3)	280 (2.8)	42 (0.4)	0 (0.0)	2084 (21.0)
Illinois	**27574 (100.0**	3018 (10.9)	8299 (30.1)	841 (3.0)	4298 (15.6)	7330 (26.6)	959 (3.5)	596 (2.2)	155 (0.6)	4 (0.0)	2074 (7.5)
N-Carolina	**17193 (100.0)**	215 (1.3)	1170 (6.8)	757 (22.7)	3904 (22.7)	4 (0.0)	10589 (61.6)	80 (0.5)	30 (0.2)	0 (0.0)	4444 (25.8)
Total	**109162 (100.0)**	**11168 (10.2)**	**31004 (28.4)**	**6225 (5.7)**	**27381 (25.1)**	**11553 (10.6)**	**13725 (12.6)**	**1229 (1.1)**	**560 (0.5)**	**5 (0.0)**	**9666 (8.9)**

4.1.1 Multi-Span Simply Supported (MSSS) Bridge

The most common configuration of bridges found in Mid-America is the MSSS bridge. Typical MSSS bridges generally consist of 2-5 spans with each span ranging from 9 m to 50 m (30-160 ft) and width ranging from 12 m to 30 m (40-100 ft). For long span bridges in general, a greater economy can be realized by using plate girders in lieu of the predefined rolled beam shapes. Each girder is typically supported by fixed type steel bearing (high/low type fixed bearing) at one end and expansion steel bearing (rocker bearing/sliding bearing) at the other.

- **Steel Girder**

The typical MSSS Bridge with steel girders considered in this study is shown in Figure 4.1. The bridge has 3 spans and 2 multi-column bents. Each bent has 4 columns and each span has 11 girders. The span lengths are 12.2, 24.4, and 12.2 m (40, 80, and 40 ft), respectively, and the width is 20.5 m (67.0 ft). The column height of the piers is 4.6 m (15 ft). A 20.5 m × 2.4 m (67 ft × 8 ft, W×H) pile bent abutment with 13 piles is used. The nominal gap between deck and abutment is 38.1 mm (1.5 in.) and the nominal gap between decks is 25.4 mm (1.0 in.). The concrete slabs of the MSSS bridges are supported by steel girders resting on steel bearings. The steel bearings are mounted on abutments and cap beams. Two adjacent decks are separated by expansion joints above the bents.

The MSSS bridge with steel girders has several known deficiencies in regards to seismic loading; i) pounding between decks, ii) failure of steel fixed and rocker bearings,

and iii) unseating from the support. The pounding can produce local damage on decks and large deformation to steel fixed bearings and abutments. In addition, rocker bearings can be unstable due to the large deck displacement. Finally, if the allowable seat width is not adequate, unseating may occur.

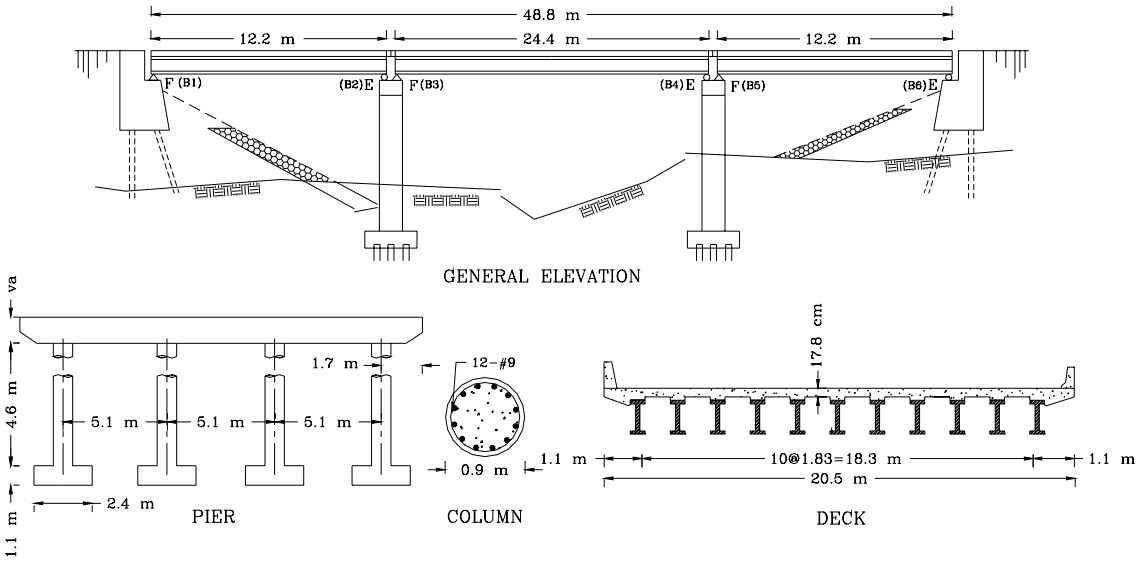

Figure 4.1 Typical Multi-Span Simply Supported Bridge with Steel Girders

- **PS Concrete Girder**

A typical MSSS concrete bridge is shown in Figure 4.2. The bridge has 3 prestressed concrete beam spans and 2 multi-column bents. There are 4 columns in a bent and 11 girders in a deck. The general properties of the concrete bridge are the same as those of the steel bridge in the above section. However, the weight of the prestressed concrete girders is heavier than that of the steel girders.

In the MSSS bridge with prestressed concrete girders, dowels, whose diameter is 25.4 mm (1.0 in.), and Neoprene pads restrict the movement of decks at the end of each girder as shown in Figure 4.3. At the end of girder, there are slots in the longitudinal direction to allow for any movement such as thermal expansion; one is 31.8 mm (1.25 in.) for the fixed type and the other is 76.2 mm (3.0 in.) for the expansion type.

There are two typical dowels at the end of a girder. However, the dowels in general are not strong enough to restrain the movement of decks against moderate or strong ground motions. When the dowels are fractured, sliding is restricted only by friction between the concrete surface and the rubber pads which may lead to unseating of the deck. The weight of the PS concrete decks is much heavier than the steel girder resulting in higher seismic loads.

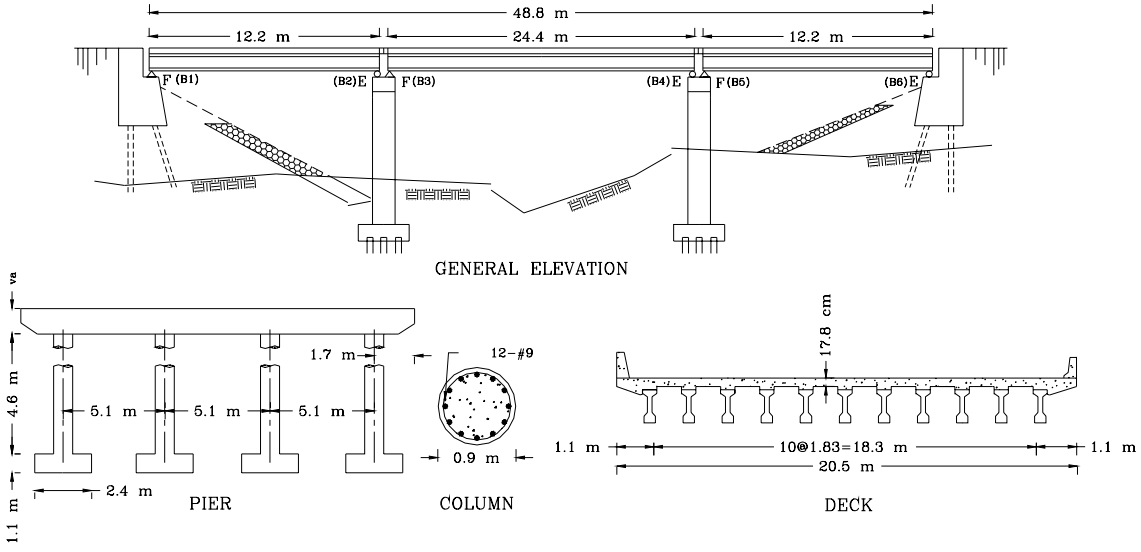

Figure 4.2 Typical Multi-Span Simply Supported Bridge with Concrete Girders

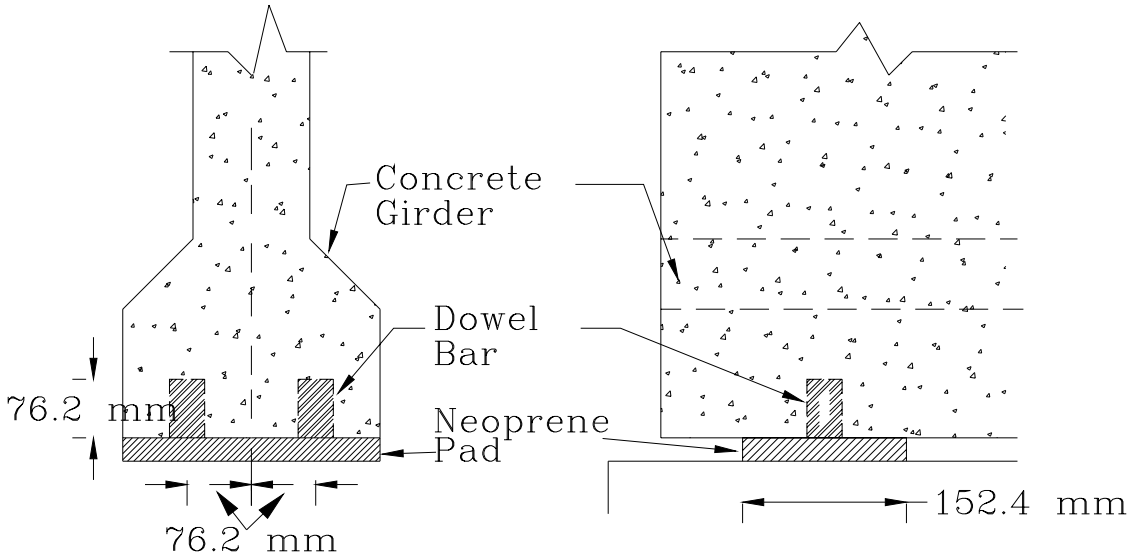

(a) End View (b) Side View

Figure 4.3 Bearing System of Typical MSSS Bridge with Concrete Girders

4.1.2 Multi-Span Continuous (MSC) Bridge

The second most common bridge configuration is the multi-span continuous (MSC) bridge. When the term "continuous bridge" is used in this study, it implies a longitudinally continuous span with primary members extending across a pier uninterrupted. There are many benefits to be realized by the use of continuous beams in highway bridge construction. Compared with a simply supported bridge, continuous bridges offer the advantages of; i) reducing the number of deck joints, ii) reducing the number of bearings, iii) increasing span lengths, and iv) reducing the size of girders.

The most significant item listed above is the first: elimination of deck joints. There could be problems associated with leakage at deck joints. From a long term cost standpoint, the detrimental effects of joint leakage can have a severe impact on the

overall cost of a bridge. Damage from this type of deterioration can affect the superstructure as well as the substructure. From the point of view of seismic effects, since the elimination of deck joints reduces the moving tolerance of deck, it may help to improve the seismic response of the bridge.

For continuous bridges, the number of bearings is half of that of simple spans at any given pier. This is beneficial not only from the initial cost savings but also with regard to having to maintain fewer bearings over the life of the bridge.

Continuous bridges, however, incur greater fabrication costs than their simply supported counterparts. Continuous span bridges are also more susceptible to settlement problems than simply supported bridges. All things being equal, simple spans are generally best suited for short crossings and where speed of construction is an issue. Continuous bridges are typically favored when a sound foundation is available and span lengths are greater.

- **Steel Girder**

Figure 4.4 shows a three-span continuous bridge with steel girders located in Shelby County, Tennessee. The span lengths of the bridge are 30.3 m (99.5 ft), 37.9 m (124.5 ft), and 32.8 m (107.5ft), respectively. A 17.7 m (58 ft) wide bent cap is supported on four columns of approximate height 4.9 m (16 ft). Decks are composite steel girders with a concrete slab. Fixed bearings are located on cap beams, and rocker bearings are on abutments.

The abutment is similar to that of the MSSS bridge. The size of the left abutment is

17.7m × 2.4m (58ft × 8ft, W×H), and the number of piles in the abutment is 17. The height of the right abutment is 7.6 m (25 ft) with 17.7 m (58 ft) width and the number of piles is 84. The gap size of the expansion joints at the abutments is 76.2 mm (3.0 in.).

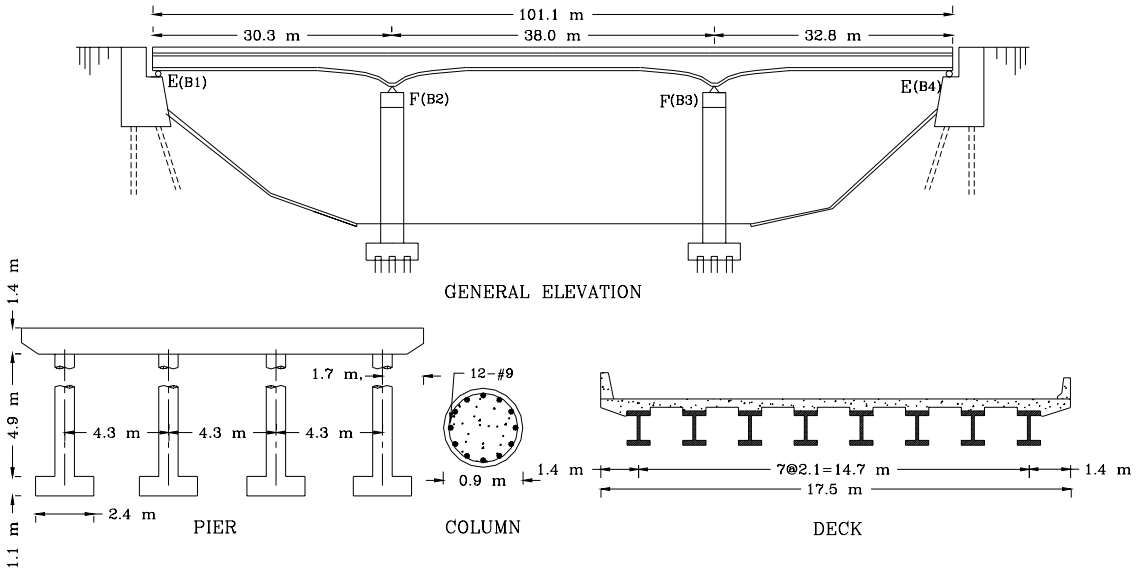

Figure 4.4 Typical Continuous Bridge with Steel Girders

Generally, the weight of the continuous bridge deck is larger than the MSSS bridge, resulting in the large pounding forces at the abutments. The rocker bearings on abutments can be unstable due to large deck displacement, resulting in the potential for unseating.

- **PS Concrete Girder**

Most PS concrete girder bridges are not constructed continuous. However, as shown

in Figure 4.5, MSSS PSC girder bridges are typically made continuous by casting a parapet between decks. This is done to reduce maintenance and the dead load moment. The gap between deck and abutment, however, is not filled with concrete to allow the thermal expansion. The dowel bars are anchored on the concrete girders to build the concrete connections.

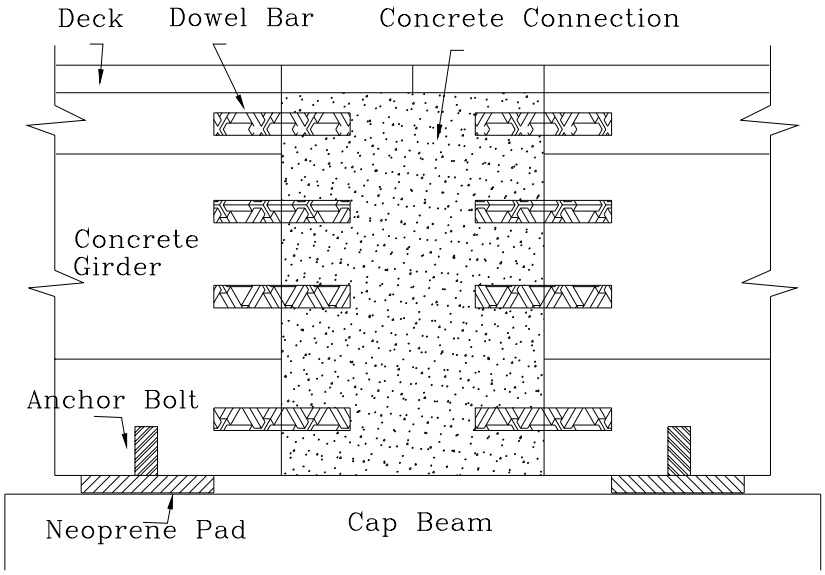

Figure 4.5 Typical MSSS Concrete Bridge Made Continuous by Casting Parapet between Girders

4.1.3 Single Span (SS) Bridge

Single span (SS) bridges are usually used in locations that have short spans and/or may not accommodate any intermediate column. For a single span (SS) bridge, the inertial loads are transferred directly from the deck to the bearings and into the abutments.

- **Steel Girder**

The typical single span bridge with steel girders is shown in Figure 4.6. It has a span of 34.4 m (113 ft) and width of 8.7 m (28.5 ft). The deck consists of a slab and 5 steel girders. There are low type fixed steel bearings on one abutment and high type rocker steel bearings on the other. The dimension of the left abutment, whose type is pile bent abutment, is 11.0m × 7.3m (36ft × 24ft, W×H) and the number of piles under the abutment is 74. The right abutment height is 6.7 m (22 ft) with the same width, and it has 31 piles. The gap size at the abutments is 101.6 mm (4.0 in.).

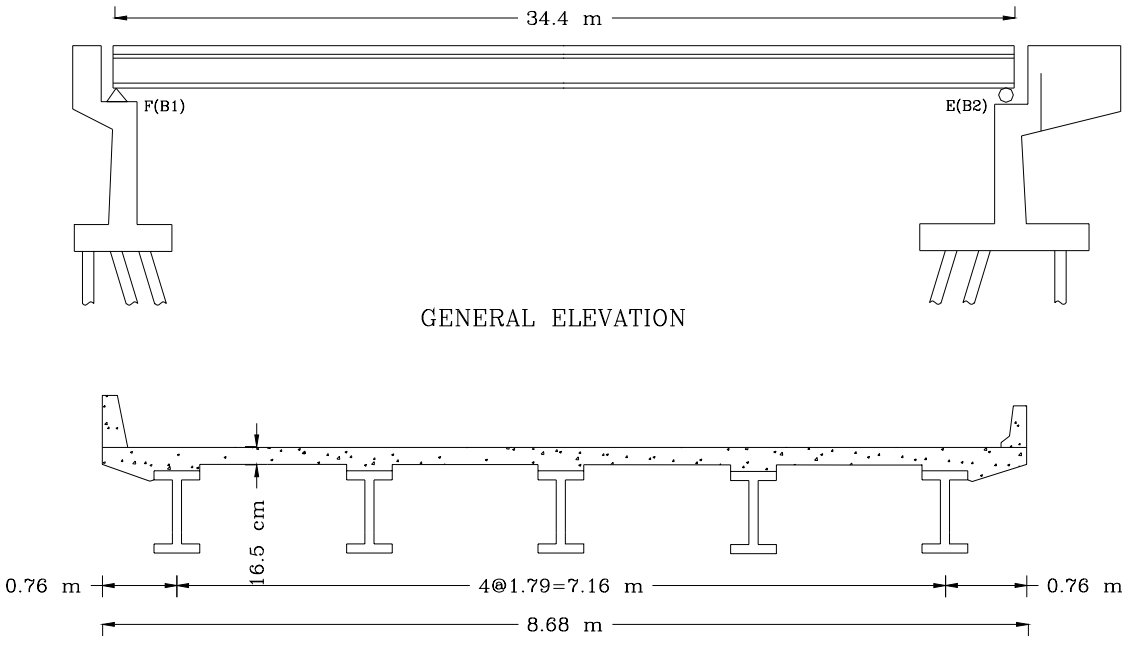

Figure 4.6 Typical Single Span Bridge with Steel Girders

In this bridge, the deck movement primarily depends on the fixed bearing deformation. In the fixed bearing, pintles resist the movement of the deck. Therefore,

the movement of rocker bearings and the relative displacement on the right abutment is typically small.

- **PS Concrete Girder**

The single span bridge with concrete girders is similar to the steel bridge except that the deck is supported by prestressed concrete girders which are supported by Neoprene pads. The property of Neoprene pads is the same as those of the typical MSSS concrete bridge.

4.2 Bearings Found in Typical Bridges

In this section, the steel bearings used in the typical steel bridges are discussed. The deck of the MSC steel bridge is supported by the fixed bearings and the rocker bearings shown in Figure 4.7, and the steel bearings shown in Figure 4.8 are typically used in the SS steel bridges. The MSSS steel bridge is assumed to be supported by the similar steel bearings shown in Figure 4.7 such as high type fixed and expansion rocker bearings.

The high type fixed bearing has a bearing plate between the sole plate and masonry plate. The low type fixed bearing, however, does not have the bearing plate. Both types of fixed bearings resist the translational movement by pintles on bearing plate in high type or masonry plate in low type. The pintles' connection, however, permits rotational movement.

The rocker bearings allow the translational movement with the rolling of the rocker plate on the masonry plate. In the low type fixed bearing, the sole plate is resisted by the pintle on the masonry plate. The round surface of the sole plate and the pintle permit the

rotational movement of the bearing.

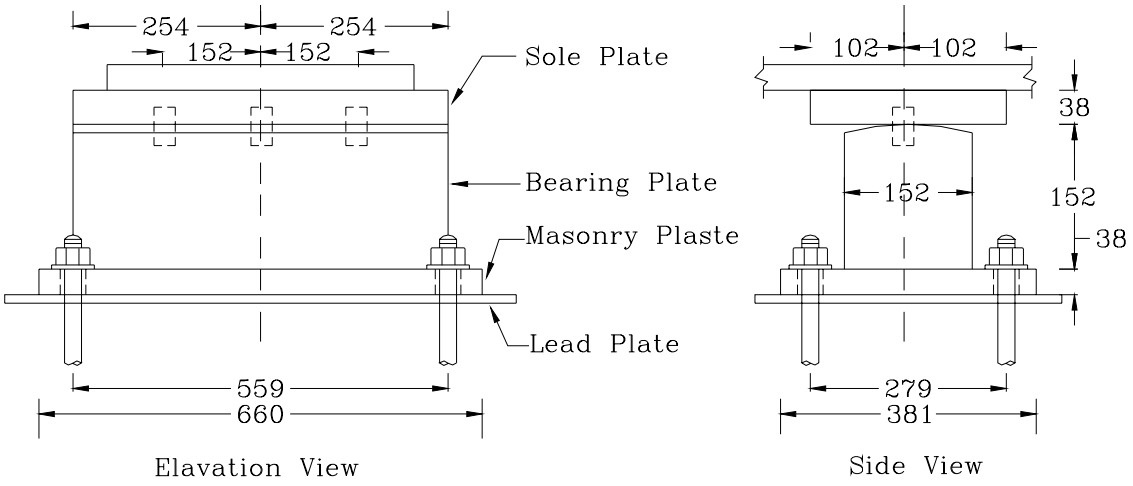

(a) Details of High Type Fixed Steel Bearing

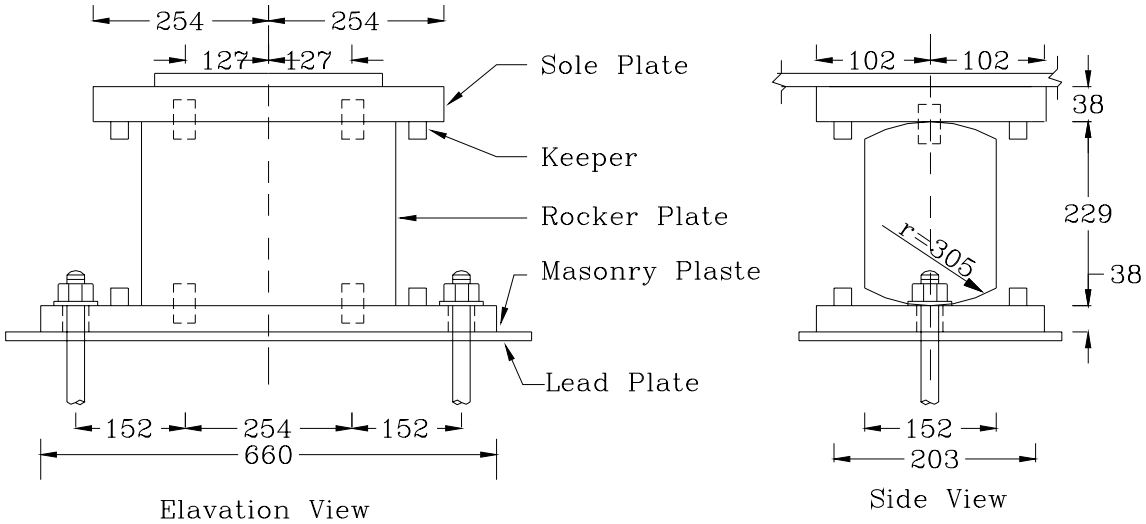

(b) Details of High Type Rocker Steel Bearing

Figure 4.7 Steel Bearings in Typical Multi-Span Continuous Steel Bridge (Unit : mm)

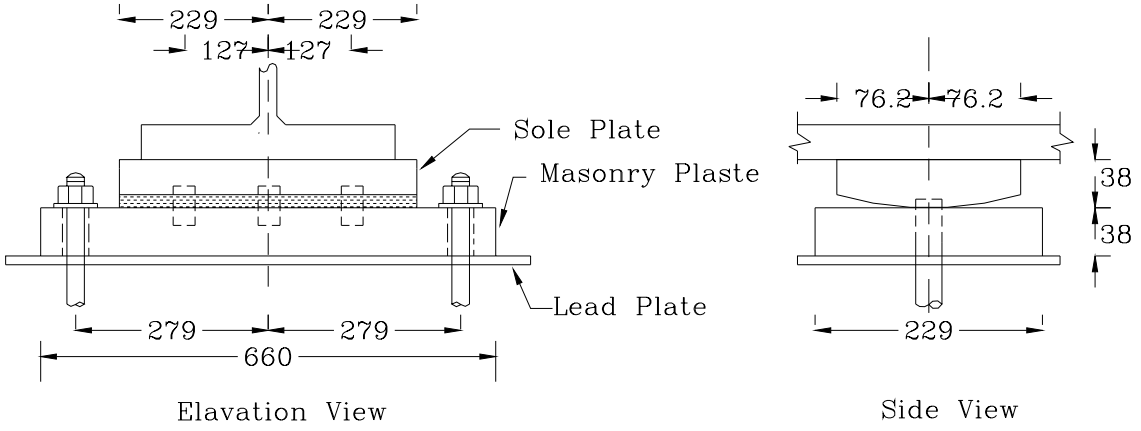

(a) Details of Low Type Fixed Steel Bearing

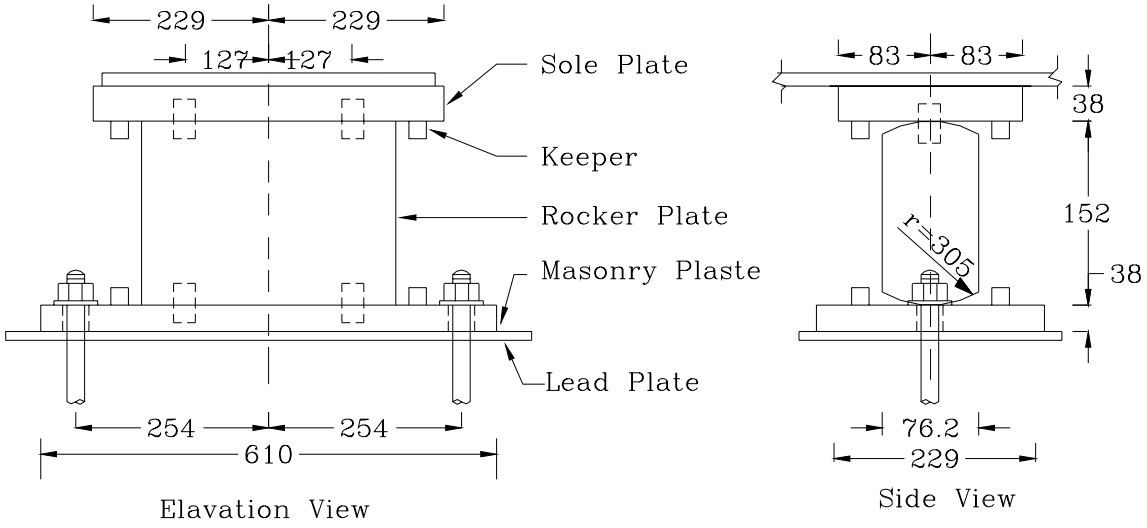

(b) Details of High Type Rocker Steel Bearing

Figure 4.8 Steel Bearings in Typical Single Span Bridge (Unit : mm)

4.3 Analytical Models of Typical Bridges

The six types of typical bridges in Mid-America are modeled using DRAIN-2DX (Prakash et al., 1992). DRAIN-2DX is a nonlinear finite element structural analysis program used to perform many types of analyses with various types of loading such as modal analysis, response spectral analysis, and time history analysis. Time history analysis is used in this study.

The seismic demand on a bridge is estimated by developing and analyzing a mathematical model of the superstructure and substructure of the bridge subjected to representative ground motions. The models shown represent the geometry, boundary conditions, mass distribution, energy dissipation as well as the interaction between elements. Since the bridge consists of many components that exhibit nonlinear behavior, a fully 2D nonlinear model is developed.

The superstructure is modeled using linear elements, since the superstructure is expected to remain elastic under the seismic loads applied. Dependent on the bridge types, the superstructure is either prestressed concrete beams or steel girders with concrete slab. It should be noted that the stiffness of superstructure does not have a significant effect on the seismic response of the bridge since the longitudinal response is typical governed by the bearings, columns, abutments, and foundation.

In the model of a typical MSSS bridge as shown in Figure 4.9, the following types of elements are used; beam-column elements for the decks (Type #4); fiber element for the columns (Type #15); truss elements for expansion and fixed steel bearings (Type #1); link elements for fixed steel bearing, abutments, dowels, and impact elements (Type #9);

and connection elements for elastomeric pads and foundation springs (Type #6).

Since damping is based on initial stiffness, very stiff elements will produce unrealistically high forces resulting in inaccurate results. Therefore, stiffness proportional damping is only applied to the fiber elements of the columns. It is expected that the damping provided by hysteretic elements will exceed that from viscous damping.

The damping ratio of the first mode in the bridge models is controlled to be 5% of critical.

The damping ratio of the abutments is usually larger than 5% (Goel and Chopra, 1997). However, abutments of the bridge in this study do not have any proportional damping.

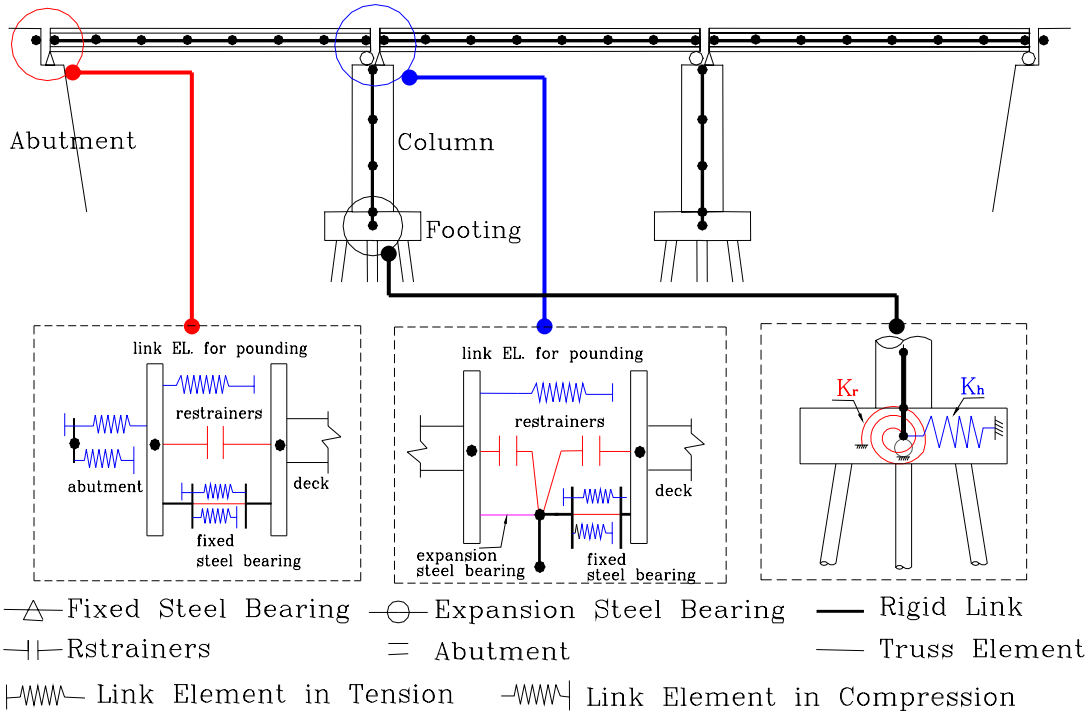

Figure 4.9 Modeling of MSSS Bridge with Steel Bearings

In the MSSS steel and concrete bridges, there are 10 beam-column elements on the first and the third deck, and 20 elements on the middle deck. The length of each element on the deck is 1.22 m (4 ft). The cap beams and the footings in piers are modeled as rigid elements with discrete mass. To obtain more accurate representation of the yielding in the columns, the bottom portion of columns is modeled with a finer element mesh.

The model of the continuous steel bridge contains 99 beam-column elements in the deck. The length of elements of the deck varies from 0.61 m (2 ft) to 1.52 m (5 ft). The remainder of the bridge is modeled in a similar fashion to the MSSS bridges.

The model of the typical single span bridge has 23 beam-column elements, 1.52 m (5 ft) in length, in the deck.

Table 4.4 shows the sectional properties of superstructure. Young's modulus for steel and concrete bridges are 2.0e5 MPa (29000 ksi) and 2.78e4 MPa (4030 ksi), respectively. The second moment and area for the continuous steel bridge represents the properties near the column supports. The following sections provide details on the modeling assumptions for each component.

Table 4.4 Superstructure Section Properties for Typical Bridges

	Steel Bridge			Concrete Bridge		
	MSSS	MSC	SS	MSSS	MSC	SS
Second Moment (m^4)	8.65e-2 2.44e-1 8.65e-2	2.00e-1 2.89e-1	8.51e-2	9.86e-1 1.53 9.86e-1	9.86e-1 1.53 9.86e-1	9.36e-1
Area (m^2)	7.01e-1 7.95e-1 7.01e-1	5.23e-1 6.42e-1	4.56e-1	5.10 6.88 5.10	5.10 6.88 5.10	3.19
Weight (kN)	1320 2810 1320	3320 4090 3550	2000	1770 4360 1770	1770 4360 1770	2680

4.4 Analytical Models of Bridge Components

4.4.1 Steel Bearings

4.4.1.1 Overview of Steel Bearings

Steel bridge bearings can be categorized generally in two types; fixed bearings and expansion bearings. While steel bridge bearings come in a variety of shapes and sizes in the Mid-America region, they all have the same function. In general, the movement accommodated by fixed bearings is rotation only, but expansion bearings allow for rotation and translation. Figure 4.10 illustrates typical expansion bearings and fixed bearings used in Mid-America.

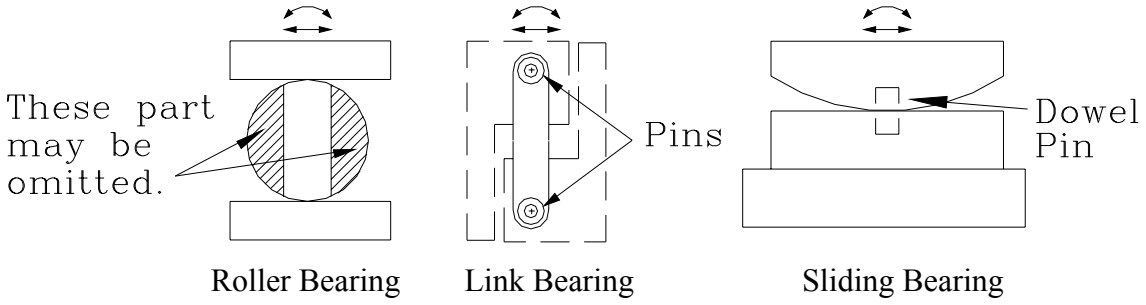

(a) Steel Bearings of Expansion Type

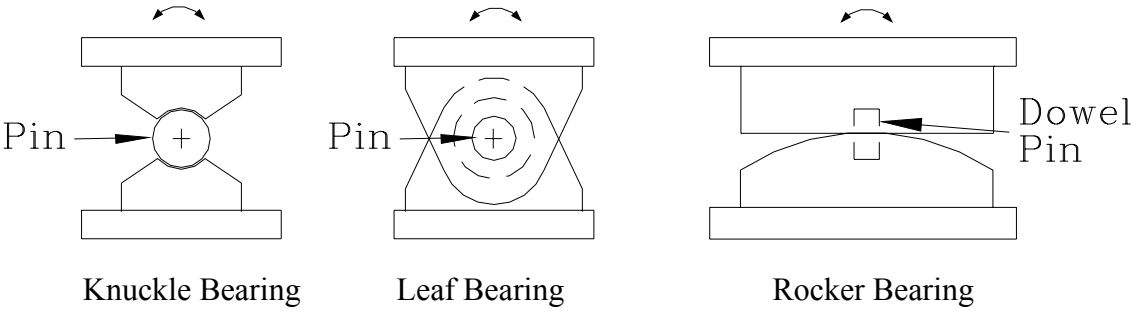

(b) Steel Bearings of Fixed Type

Figure 4.10 Shape of Steel Bearings Typically Found on Mid-America Bridges

Among these six types of bearings, rocker bearings, roller bearings, and sliding bearings are most commonly used in highway bridges in Mid-America. A rocker bearing is a type of pinned bearing that is used to accommodate large live load deflections. To prevent the rocker in a bearing from walking, pintles are used which resist transverse force. A pintle is a trapezoidal extrusion which extends upward from the masonry plate. Rotation in both fixed and expansion bearings are facilitated through the use of a solid circular pin. This pin acts as a hinge which allows for translation and rotation in expansion bearings and rotation in fixed bearings. The rocker bearing resists forces from a combination of rolling resistance at the base of the rocker and Coulomb friction at the hinge of the sole plate-rocker interface.

A roller bearing is a form of pinned bearing, and therefore its function is similar to a rocker bearing in many ways. In this type of bearing, translation is facilitated by the use of a roller or nest of rollers. Rotation can be accommodated by a pin or by the rolling action of the rollers themselves. Roller bearings, however, are intended only for spans of moderate length.

A sliding bearing utilizes one plate sliding against another to accommodate translational movement. Whether or not rotation is accommodated by this type of bearing is dependent on the magnitude of anticipated rotation. Copper has traditionally been used for the material for sliding surface. However, in recent years, Teflon has been used.

Link bearings have been commonly used to support suspended spans in multi-span bridge units. Link bearings consist of plate, rod, and I or tubular section members

connected at their ends by pins to opposite sides of a joint to transmit vertical shear or a bearing reaction. They permit rotation and longitudinal movement by sway about a vertical axis. They are unsuitable for carrying transverse loads and are normally used in conjunction with a lateral restraint bearing free to slide vertically, and longitudinal and positioned at the deck center. In new design and construction, elastomeric bearings and shear keys are used instead of these types of bearings.

Knuckle bearings consist of a steel pin housed between an upper and lower support member each having a curved surface which mates with the pin. Lateral loads are transmitted by flanges on the ends of the pin. These bearings permit rotation by sliding of one part on another. This type of bearing usually is intended for long span bridges.

Leaf bearings consist essentially of a pin passing through a number of interleaved plates fixed alternatively to the upper and lower bearing plates. Leaf bearings can be designed to resist uplift and for long span bridges. Figures 4.11 and 4.12 show the details of steel bearings used for analytical models in this study. These types of steel bearings are most common in Mid-America bridges.

A steel bridge bearing is a system with many moving parts. Therefore corrosion and aging can limit the free movement of the bearing. The accumulated debris in moving parts can increase the friction between bearing surfaces and subsequently develop larger forces than expected which are transferred to substructures (Mander et al., 1996).

Fixed steel bearings have very small elastic range and low ductility capacity. Rocker expansion bearings with large displacement may produce a stability problem. In the transverse direction, the movement of steel bearings is restricted by keeper plates.

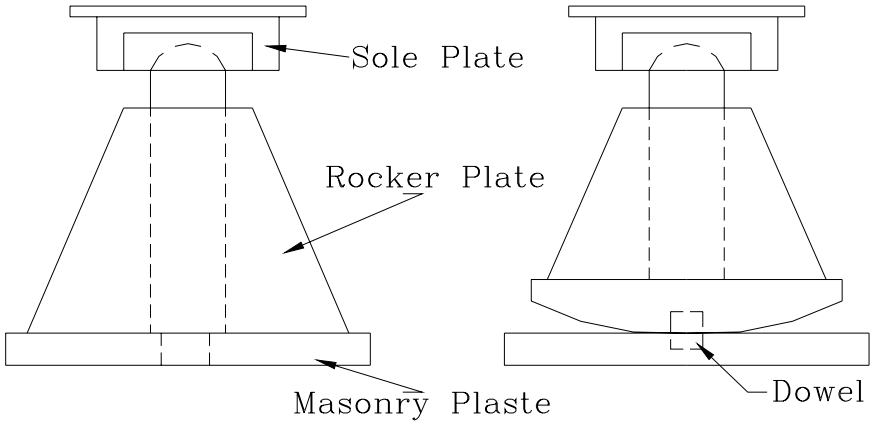

(a) Fixed Type (b) Expansion Type

Figure 4.11 Details of Rocker Bearings Typically Found on Mid-America Bridges

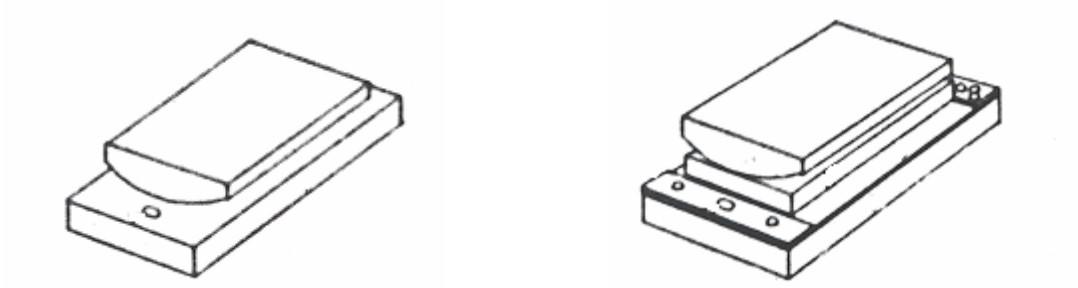

(a) Fixed Type (b) Expansion Type

Figure 4.12 Details of A Sliding Bearings Typically Found on Mid-America Bridges

The keeper plate, however, can be easily fractured. Because of these issues, steel bearings are generally believed to behavior poorly during an earthquake (Saadeghvaziri and Rashidi, 1997b). Many have proposed rehabilitation techniques for steel bearing (Mander et al., 1996). These techniques may increase the ductility and the strength of steel bearings. However, this typically occurs at the expanse of increased demands on piers, which is undesirable.

4.4.1.2 Analytical Models of Steel Bearings

There are several studies on the seismic behavior of steel bearings. Mander et al. (1996) conducted the experimental tests with the retrieved steel bearings from existing bridges. The experiments have been conducted to obtain the force-deformation behavior of steel bearings with reversed cyclic loading. From these results, theoretical stiffness and strength analyses have been performed and nonlinear models for steel bearings' behavior were proposed. Mander conducted most of his experiments on a steel base. However, the steel bearings usually are on a concrete base. Therefore, Mander subsequently tested steel bearings on the concrete pedestal and compared the results with those on the steel base. As expected, the stiffness and strength of steel bearings on concrete pedestal is less than those on the steel base, and the deformation capacity on a concrete base is larger than that on steel base, as shown in Figure 4.13.

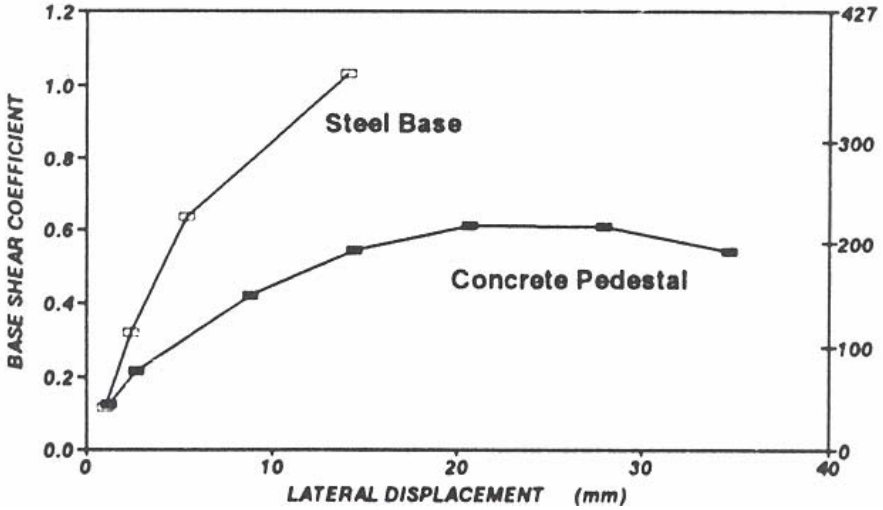

Figure 4.13 Response of High Type Fixed Steel Bearing Mounted on Steel Base and Concrete Pedestal (Mander et al., 1996)

In Mander's test, the concrete cover is 50 mm (2 in.) and was spalled due to the rocking the bearing on the pedestal. However, a test of anchor connections in concrete showed that the anchors had experienced yielding and had fractured (Cook and Klingner, 1992). In Cook's experiment, the concrete base is much larger than the base plate that is the same as the masonry plate of steel bearings (Cook and Klingner, 1992). The concrete cover of steel bearings in bridges is usually greater than 50 mm (2 in.). Therefore, the actual stiffness and strength of the high type fixed steel bearing might be somewhere between the two curves in Figure 4.13.

Rashidi and Saadeghvaziri (1997) conducted numerical analysis of steel bearing and steel bearing base using ADINA. They found that in the longitudinal direction, there are three stiffnesses for steel bearings that must be considered, namely: the stiffness of the girder-sole plate connection; the stiffness of the bearing (casing and pin); and the stiffness of the seat (base plate, anchorbolts, and concrete). The stiffness of the girder-sole plate connection was found to be much larger than the other two stiffnesses and may be ignored. They evaluated the stiffness of steel bearings and the base plate analytically. It is found from their analyses that the stiffness of the base is less than that of steel bearing itself for steel bearings larger than 380 mm (15 in.) wide. From the studies by Rashidi and Saadeghvaziri (1997) and Mander et al. (1996), it is found that the critical stiffness of steel bearings is the stiffness of the anchor bolts connected to the concrete base.

Dicleli and Bruneau (1995a) considered the deformation of steel bearings due to the bending of bearing bar and the elongation of anchor bolts to calculate a bearing stiffness.

Since the bearing bar and the anchor bolts are acting as springs connected in series, the stiffness of the bearings was calculated from the serial combination of the two components.

Dicleli (1993) calculated the stiffness of the bearing considering only the flexural stiffness of the bearing bar when the bottom plate of the bearing was welded to the top of the column or connected by short bolts to another plate welded to the column.

From the review of the previous research, it is considered that Mander's steel bearing models (Mander et al., 1996) are most appropriate for this study. The concrete pedestal is fairly representative of the type of construction for most bridges in Mid-America. Therefore, the models from the experiments on concrete base are adapted for the high type fixed bearing. However, the models of a high type rocker bearing and a low type fixed bearing are based on the test on the steel base, since these bearings were not tested on a concrete pedestal.

- **High Type Fixed Bearing**

For the analytical model of the high type fixed bearings, one bilinear truss and two link elements in DRAIN-2DX were used in parallel. The bilinear truss element (#1) was used to model part of the prying of the masonry plate with values: k_e = 86 kN/mm (491 kips/in.), k_p = 6% of k_e, and F_y = 75 kN (17 kips) as shown in Figure 4.15a.

With continued loading, the partial bond failure led to anchor bolts pulling out slightly and progressive decrease in stiffness. Since the bearing was rocked on the pedestal with the displacement of 20 mm (0.79 in.), cover concrete started to crack and spall beneath

the masonry plate. Link elements (#9) were selected to simulate stiffness deterioration and rocking as illustrated in Figure 4.15a. The initial stiffness, $k_{1,}$ is equal to 93 kN/mm (531 kips/in.) up to a displacement limit u_1 = 0.4 mm (0.016 in.). The total initial elastic stiffness is 179 kN/mm (1022 kips/in.). The plastic stiffness, k_2, is 7% of k_1, up to displacement limit u_2 =20.0 mm (0.79 in.), deteriorated stiffness, k_3, is 5% of k_1, and unloading stiffness, k_4, is 100% of k_1. The tested fixed steel bearing is shown in Figure 4.14, and Figure 4.15 shows the experimental and the analytical results of the fixed bearing, in which the solid line represents the experimental result and the dotted line represents the analytical model used in this study.

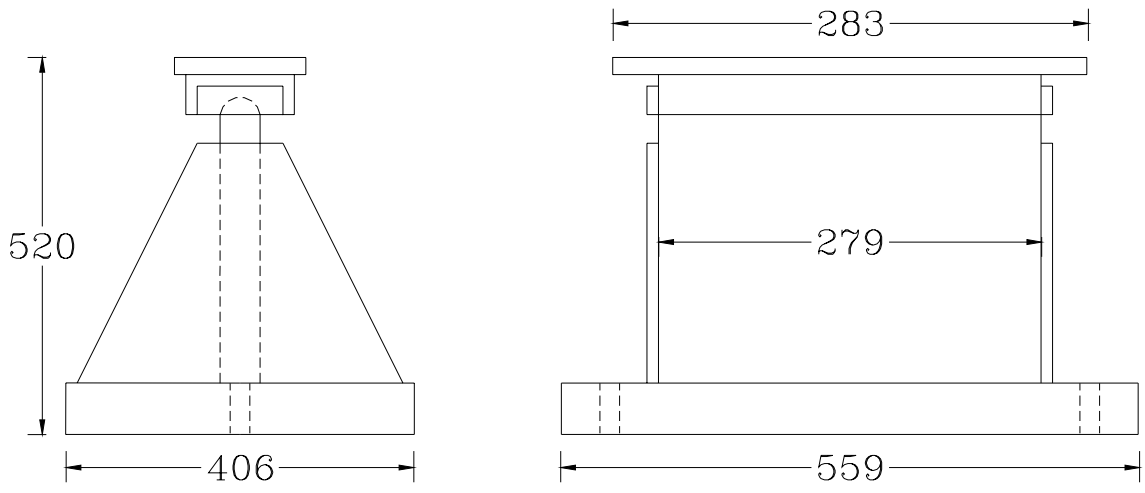

(a) Side View (b) Elevation View

Figure 4.14 Dimension of High Type Fixed Bearing (Unit : mm)

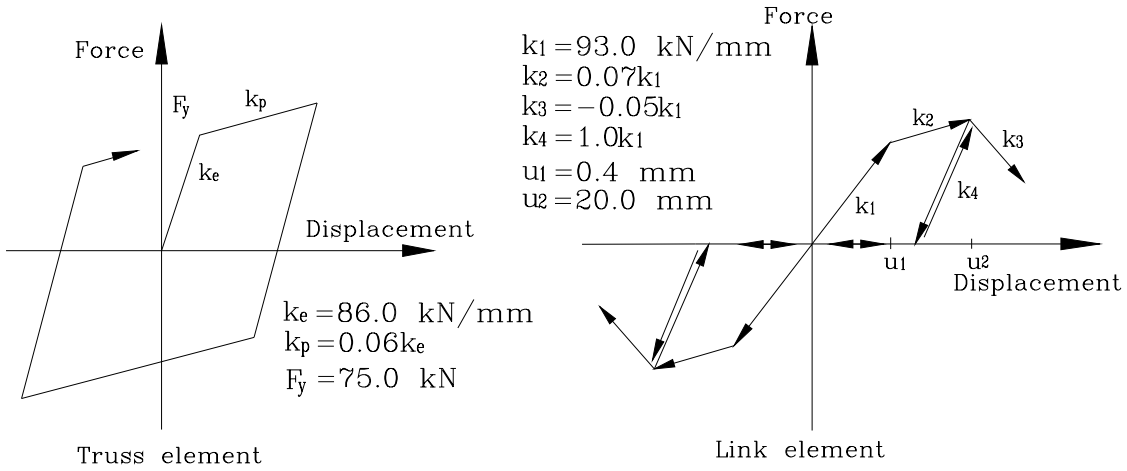

(a) Combination of DRAIN-2DX Elements for Fixed Bearing

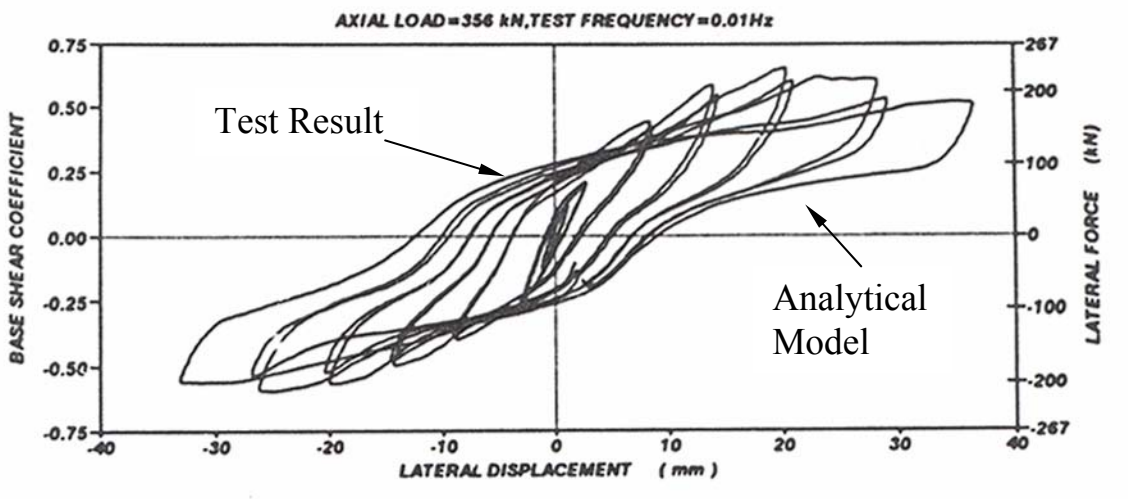

(b) Experimental and Analytical results of Force-Displacement Relationship

Figure 4.15 Hysteresis Loop for High Type Fixed Bearing in Longitudinal Direction from Previous Study (Mander et al., 1996)

- **High Type Rocker Bearing**

In the high type rocker bearings as shown in Figure 4.16, friction caused by a combination of rolling resistance at the base of the rocker and Coulomb friction at the hinge of the sole plate-rocker interface generated the hysteresis behavior shown in Figure 4.17. However, due to the presence of accumulated debris as well as corrosion on the steel, the hysteresis loops for the bearings tended to be irregular. For the analytical model of the bearing, one bilinear truss element was utilized with the values of k_e = 14 kN/mm (80.0 kips/in), k_p = 0.018% of k_e, and the friction coefficient, μ = 0.04 as shown in Figure 4.17. The normal force, N, is the weight of the bridge deck.

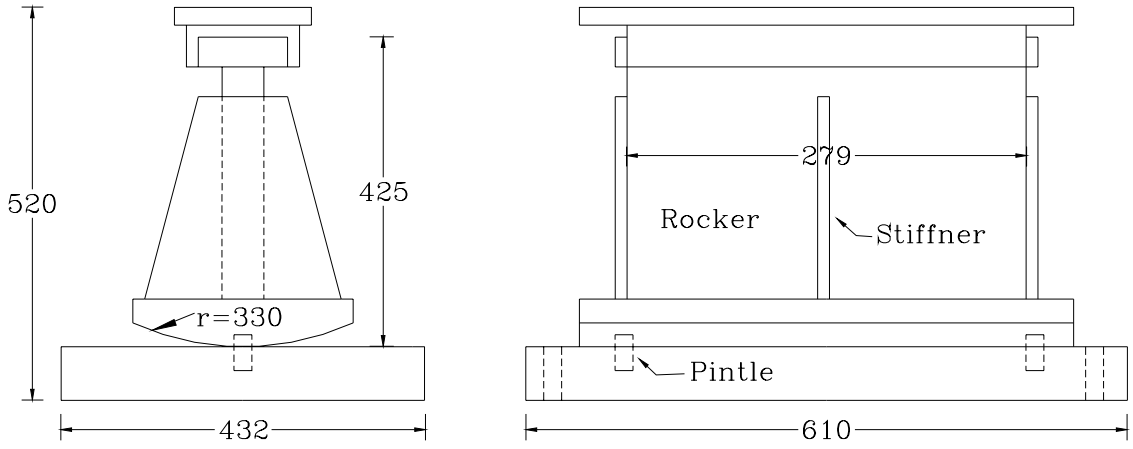

(a) Side View (b) Elevation View

Figure 4.16 Dimension of High Type Rocker Bearing (Unit : mm)

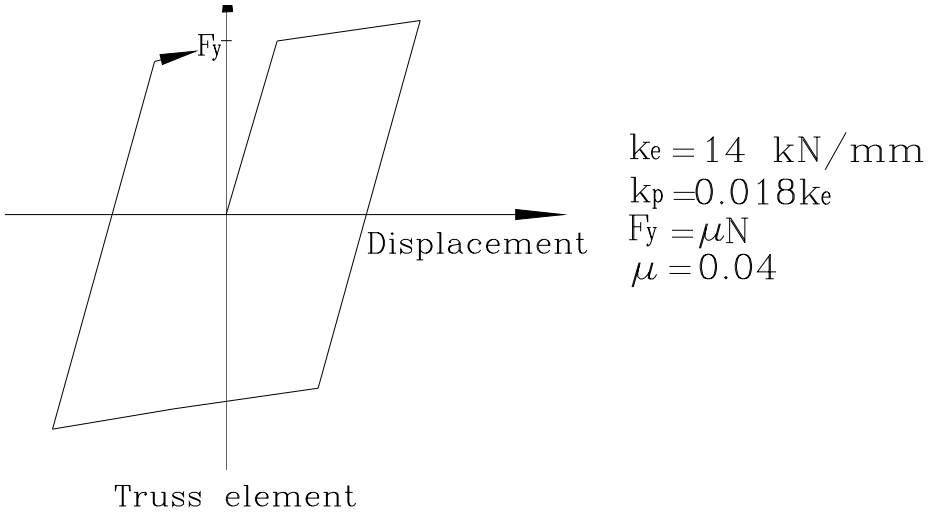

(a) DRAIN-2DX Element for Expansion Bearing

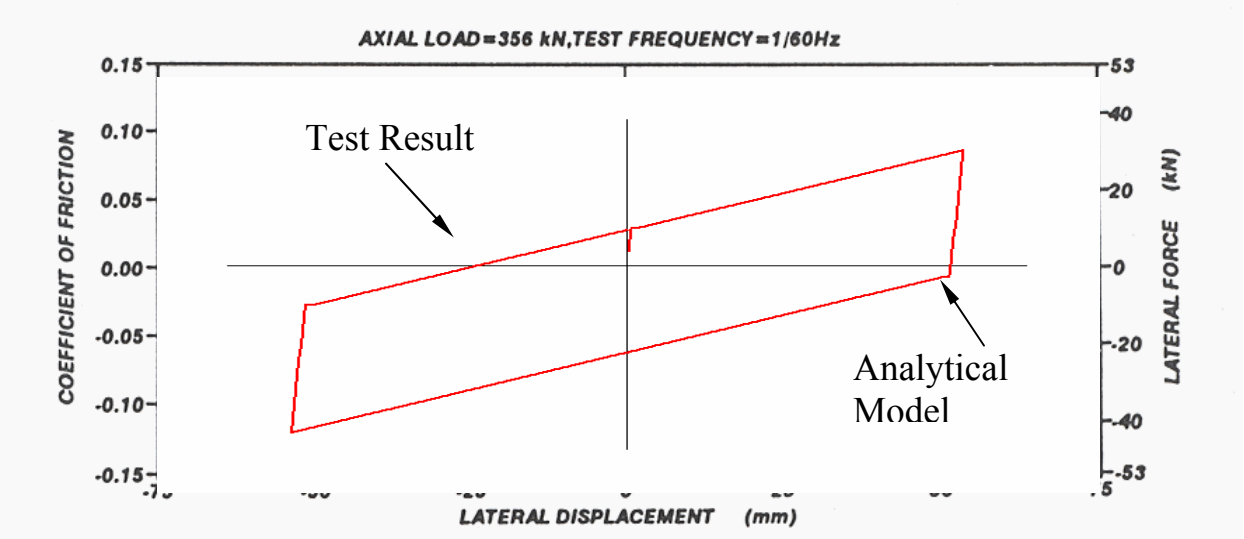

(b) Experimental and Analytical Results of Force-Displacement Relationship

Figure 4.17 Hysteresis Loop for High Type Rocker Bearing in Longitudinal Direction from Previous Study (Mander et al., 1996)

- **Low Type Fixed Bearing**

Figure 4.18 shows the low type fixed steel bearing tested by Mander, and Figure 4.19 presents the experimental result and the analytical model of the bearing. The combination of a truss and two link elements in parallel is chosen for the analytical model of the bearing behavior. The sliding between assembly clearance can be modeled with an elasto-perfectly plastic element with k_e=356 kN/mm (2033 kips/in.), represents a frictional coefficient, μ=0.37.

The behavior of the bearing after the sole plate striking the pintles can be modeled using two link elements for each direction with the following values: 2.0 mm (0.079 in.) gap, elastic striking stiffness k_1=210 kN/mm (1199 kips/in.) up to displacement limit u_1=0.5 mm (0.02 in.), plastic striking stiffness $k_2=k_3=0.25k_1$, and unloading stiffness $k_4=k_1$.

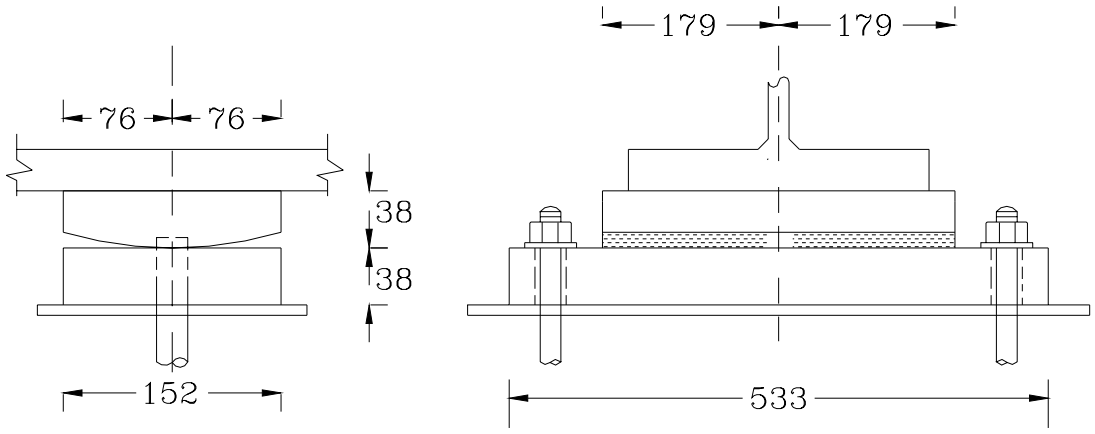

(a) Side View (b) Elevation View

Figure 4.18 Dimension of Low Type Fixed Bearing (Unit : mm)

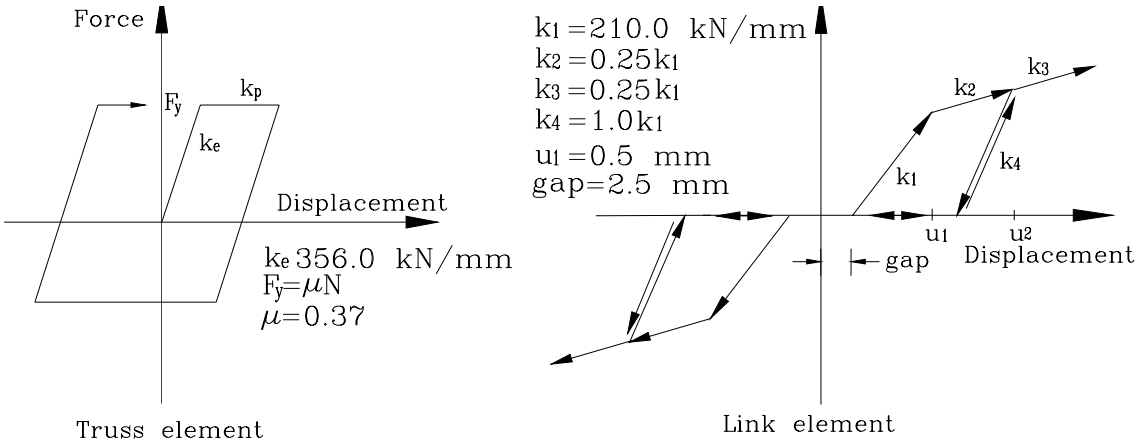

(a) Combination of DRAIN-2DX Elements for Fixed Bearings

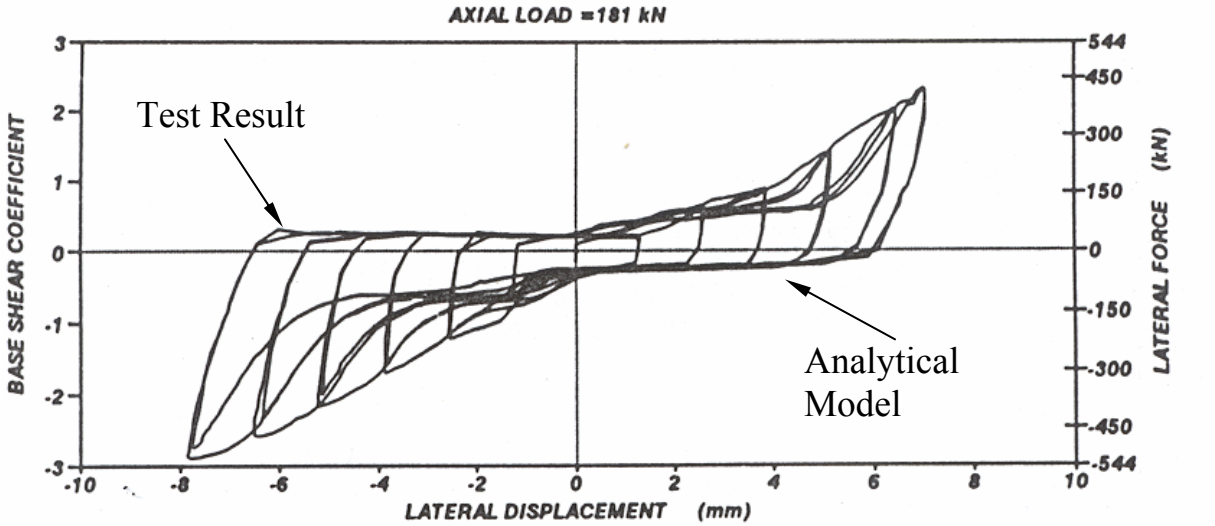

(b) Experimental and Analytical Results of Force-Displacement Relationship

Figure 4.19 Hysteresis Loop for Low Type Fixed Bearing in Longitudinal Direction from Previous Study (Mander et al., 1996)

- **Low Type Sliding Bearing**

Figure 4.20 shows the low type expansion steel bearing tested by Mander. Figure 4.21 presents the experimental result and the analytical model. For analytical modeling of the low type sliding bearing, an elasto-perfectly plastic truss element was used to represent Coulomb friction between the masonry and sole plate. The elastic stiffness, k_e=123 kN/mm (702 kips/in.), and frictional coefficient, μ=0.2, was observed experimentally.

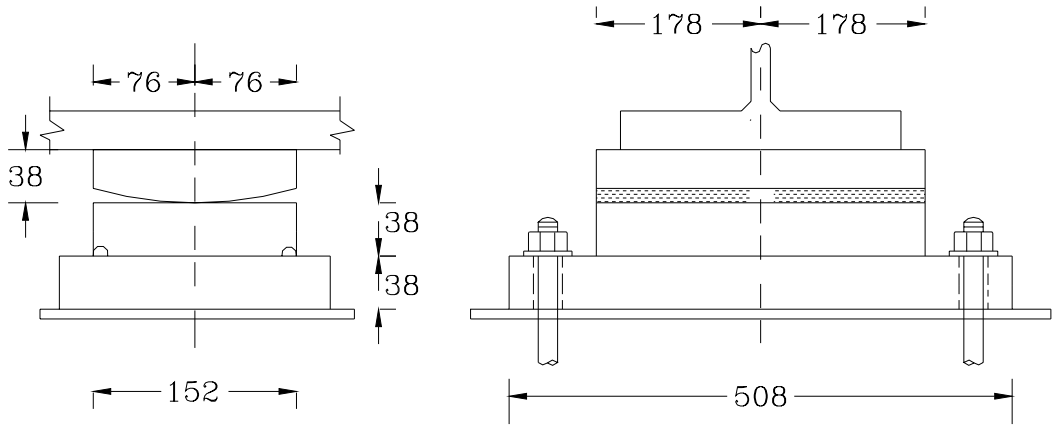

Figure 4.20 Dimension of Low Type Sliding Bearing (Unit : mm)

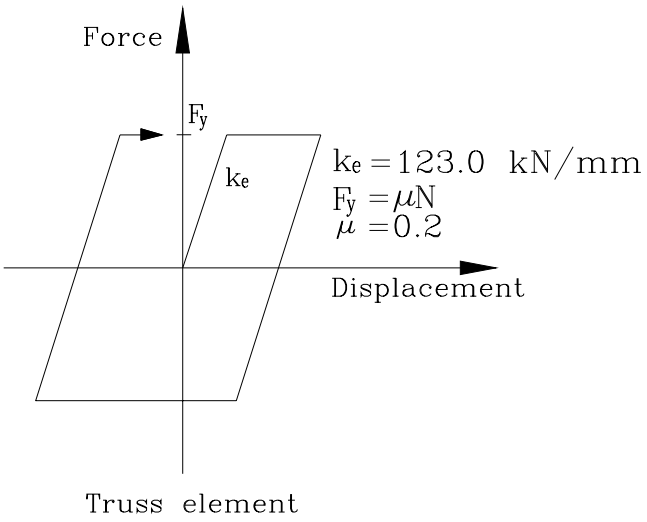

(a) Truss Element of DRAIN-2DX

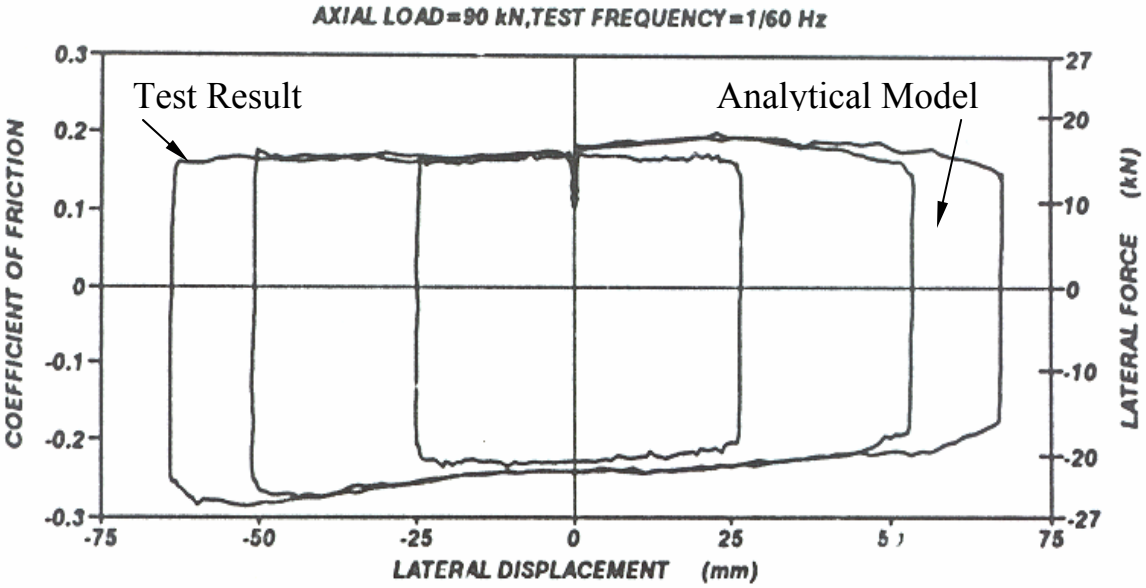

Figure 4.21 Hysteresis Loop for Low Type Sliding Bearing in Longitudinal Direction from Previous Study (Mander et al., 1996)

4.4.2 Elastomeric Pads and Dowels

4.4.2.1 Overview of Elastomeric Pads and Dowels

The forces in the PS concrete girder are transferred to the substructure by dowel bars and elastomeric bearing pads. In concrete bridges, typically one side of the dowel bar is projected into the holes in concrete girders, while the other side is embedded in concrete bent caps as shown in Figure 4.5. Therefore, the loading mechanism of the dowels in concrete bridges is beam action rather than dowel action (Taylor, 1969). Since elastomeric pads are located between concrete interfaces, the frictional force is developed between the surfaces. To describe the behavior of dowel bars and elastomeric pads in this study, an analytical model is developed for each component and added in parallel.

4.4.2.2 Analytical Models of Elastomeric Pads and Dowels

For moderate seismic loading, the behavior of dowel bars is usually in the inelastic range. However, the modeling a dowel as a beam resting on elastic and cohesionless foundation (BEF model) is still the most expedient way to describe the mechanism. The behavior of the BEF model is linear because the dowel bar and the surrounding concrete are merged into a uniaxial linear element.

Linear models can represent the dowel action with a single parameter. However, they are valid only under working loads. Therefore, nonlinear models are required to represent dowels' behavior up to failure (ultimate loads). An experiment (Poli et al., 1993) showed that the behavior of a dowel embedded in an unlimited concrete mass is linear-plastic. Another study (Vintzeleou and Tassios, 1987) found that there was a very

pronounced pinching effect in the hysteresis behavior of cyclic dowel action as shown in Figure 4.22.

Hence, a link element in DRAIN-2DX can be used to model the behavior of the dowel as shown in Figure 4.22. The element is activated on tension only or compression only action. In addition, it can describe the abrupt fracture behavior of dowels.

The dowel bar having the height and the diameter of 76.2 mm (3.0 in.) and 25.4 mm (1.0 in.), respectively, and elastomeric pads are installed in the PS concrete girder bridges to restrict the movement of decks. There are two bars at the end of each girder. The expansion type of dowel has a 76.2 mm (3.0 in.) slot as shown in Figure 4.23. The dimension of the pad, which is installed at both end and middle spans of the MSSS concrete bridge, is 406 mm × 152 mm (16 in. × 6 in., Length×Width) and 559 mm × 203 mm (22 in. × 8 in.), respectively.

To obtain the analytical model of dowels' behavior, at first, a dowel bar is modeled with 3D solid elements in ABAQUS, as shown in Figure 4.24. Since the thickness of elastomeric pad is 25.4 mm (1.0 in.), a static force is applied at the 25.4 mm (1.0 in.) height point from the bottom to obtain yielding condition in every bottom element due to the Von Mises criterion. The bottom of the model is fixed. Therefore, the stiffness of concrete is not considered in this model. In Figure 4.24, the force-deformation relationship of a dowel bar is presented. The deformation is measured at the loading point. This result corresponds closely to the previous study (Poli et al., 1993).

The elastic stiffness of the bilinear model is 45.6 kN/mm (260.4 kips/in.) and hardening ratio is 0.012. The yield deformation is 1.23 mm (0.048 in.) with the yield

strength of 56.0 kN (12.6 kips) and the deformation at failure is 5.33 mm (0.21 in.) with the ultimate strength of 57.8 kN (13.0 kips). After the dowel is fractured, it can be assumed that the dowel bars do not have any resistance. This behavior with the abrupt fracture can be described with the combination of two link elements in DRAIN-2DX as shown in Figure 4.25.

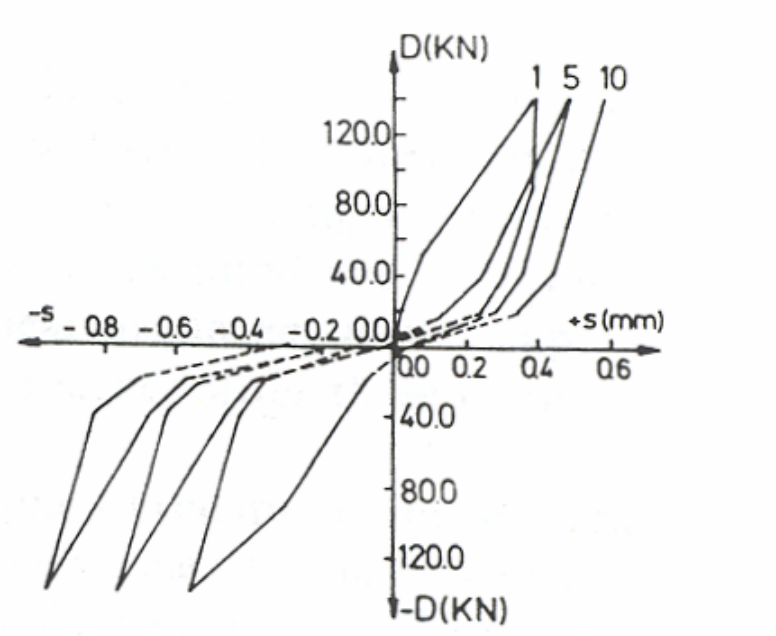

Figure 4.22 Typical Hysteresis Loops for Cyclic Dowel Action

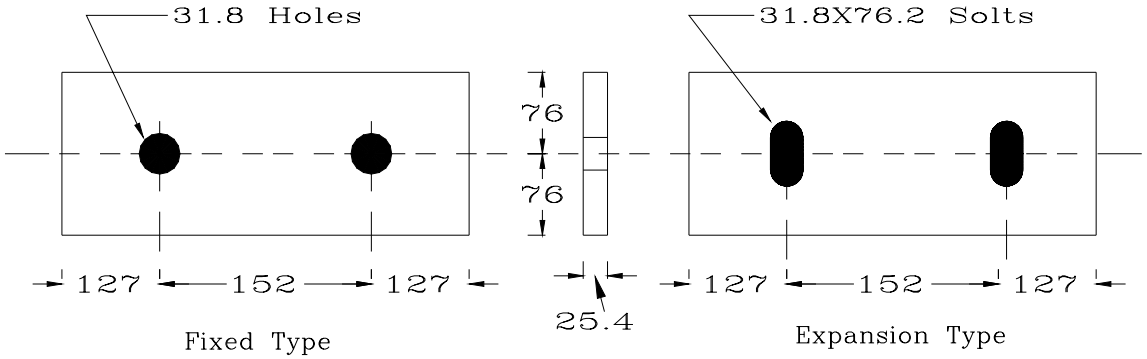

Figure 4.23 Typical Configuration of Elastomeric Pads in Concrete Bridges

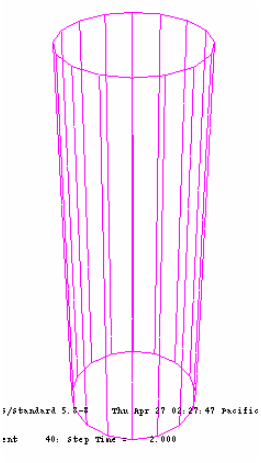

(a) Model of A Dowel

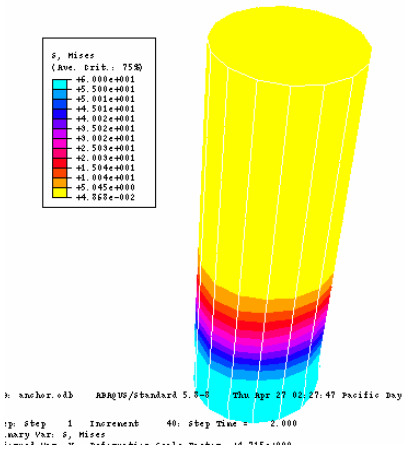

(b) Deformed Shape of A Dowel

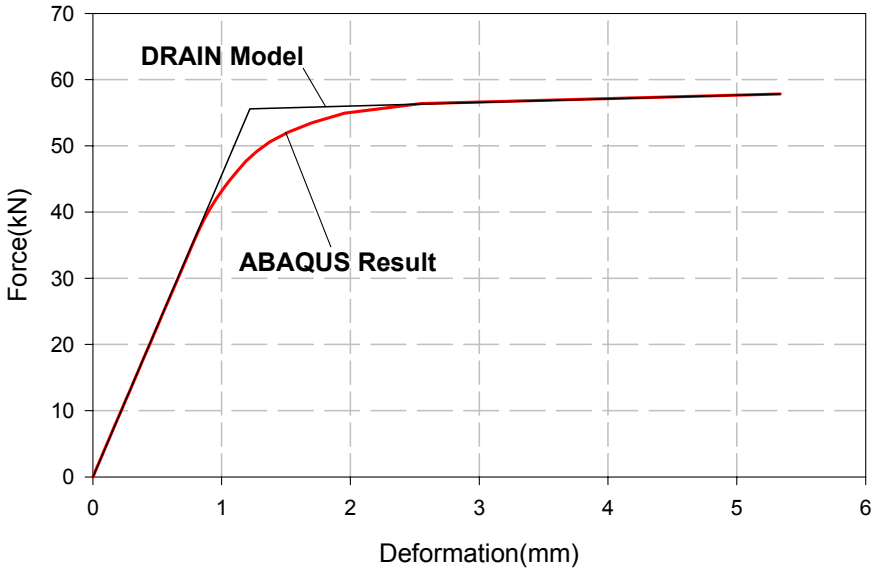

(c) Analytical Result and Model of A Dowel

Figure 4.24 Model and Analytical Result of Dowel in ABAQUS

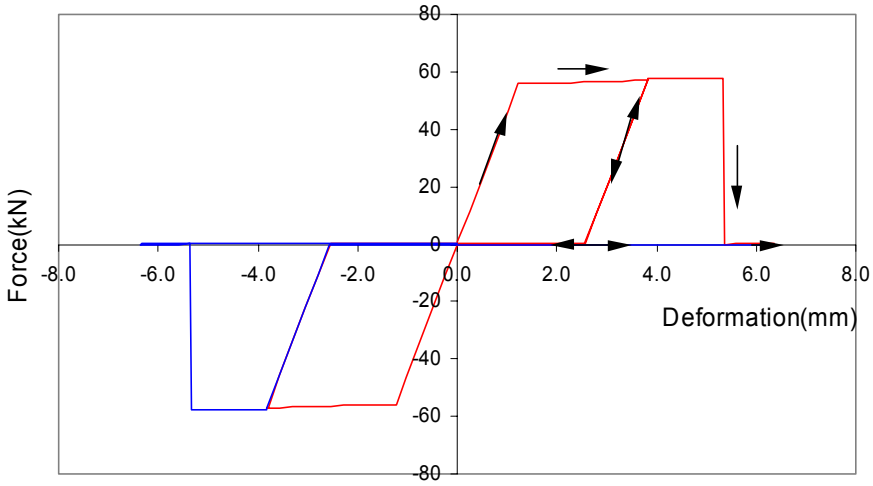

Figure 4.25 Hysteresis Behavior of Dowel Bar

The estimated yield strength of the dowel (56.0 kN, 12.6 kips) in this study is the half of the estimated value (111.7 kN, 25.1 kips) by Hwang et al. (2000b) based on the experimental results obtained by Mander et al. (1996). The reason is that in the Mander's test the two cross sections of the dowel were involved simultaneously.

The behavior of elastomeric pads can be characterized by sliding. Thus, the behavior of the analytical model of the pad can be elasto-perfectly plastic. The frictional coefficient of the elastomeric pads on concrete surface is the function of normal stress acting on the pads, and has been described as follows (Schrage, 1981);

$$\mu = 0.05 + 0.4/\sigma_m \qquad (4.1)$$

where:

μ = Frictional coefficient of elastomeric pads on concrete surface

σ_m = Normal stress action on elastomeric pads in MPa

The frictional coefficient for the small pad is 0.36 (σ_m = 1.29 MPa), and that for the large is 0.27 (σ_m = 1.83 MPa). The initial stiffness of the model is assumed to be 7.36 kN/mm (42.0 kips/in.) based on Schrage's tests (Schrage, 1981). The ultimate forces of the small and large pad are 28.8 (6.5) and 55.8 kN (12.5 kips) in the MSSS and continuous bridge, respectively. In Figure 4.26, the combined behavior of the two dowels and an elastomeric pad is shown.

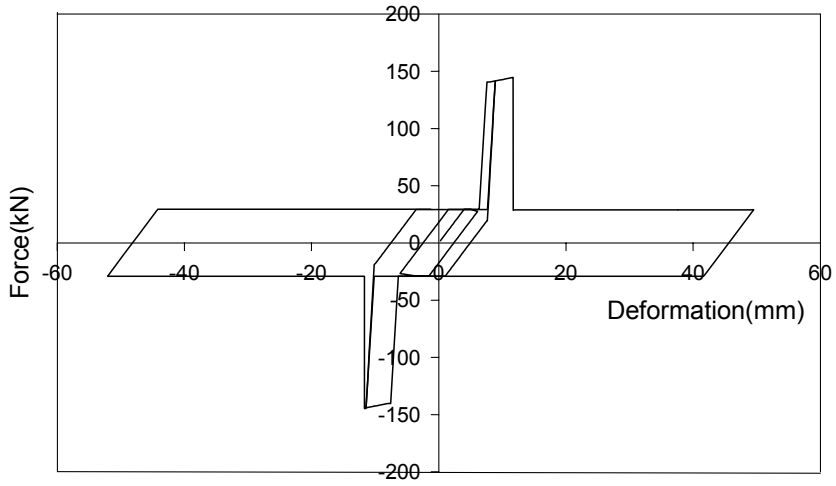

Figure 4.26 Analytical Model to Represent the Behavior of Two Dowels and An Elastomeric Pad

4.4.3. Abutments

4.4.3.1 Overview of Abutments

Abutments in bridges act as a retaining wall for backfill soil and serve an additional function of providing resistance to deformation along the longitudinal and transverse bridge axis to earthquake induced inertial loads from the bridge deck.

Under longitudinal response earth pressures on the abutment increase due to seismic acceleration. Impact of the bridge deck with the abutment may generate high passive pressures, which will induce a further increase in lateral pressures at levels below the point of the deck or superstructure impact.

There are several types of abutments used in bridges. The most common types are gravity abutment, U abutment, spill-through abutment, and pile bent abutment as shown in Figure 4.27. Since the pile bent abutment is generally used in Mid-America, it is used in all the models in this study. The abutment consists of a single cap beam, acting as a bridge seat, supported by one or two rows of piles. Batter piles are usually used to resist the overturning movement.

4.4.3.2 Analytical Models of Abutments

Past experience has demonstrated that abutments play an important role in the overall behavior of bridge structures under seismic loading. For many highway bridges, abutments attract a large portion of the seismic force in the longitudinal direction and it is now recognized that proper modeling of abutments is a significant factor in the overall evaluation of bridge performance. Therefore, quantifying the abutment stiffness and ultimate passive pressure capacity for modeling purposes is critical. Most specification and guidelines for earthquake design of highway bridges require that abutment-soil systems be included in the analytical model as discrete equivalent linear springs (Caltrans, 1988 and 1989; ATC-6, 1981; AASHTO-83, 1988). In the Caltrans modeling procedure, the passive abutment-soil stiffness used is 115 kN/mm/m (200 kips/inch/linear

foot) for standard 2.4 m (8 ft) height of wall, and the stiffness of a pile is 7.0 kN/mm/pile (40 kips/inch/pile) for standard 45 and 70 ton, and 406.4 mm (16 in.) Cast-In-Drilled-Hole (CIDH) piles.

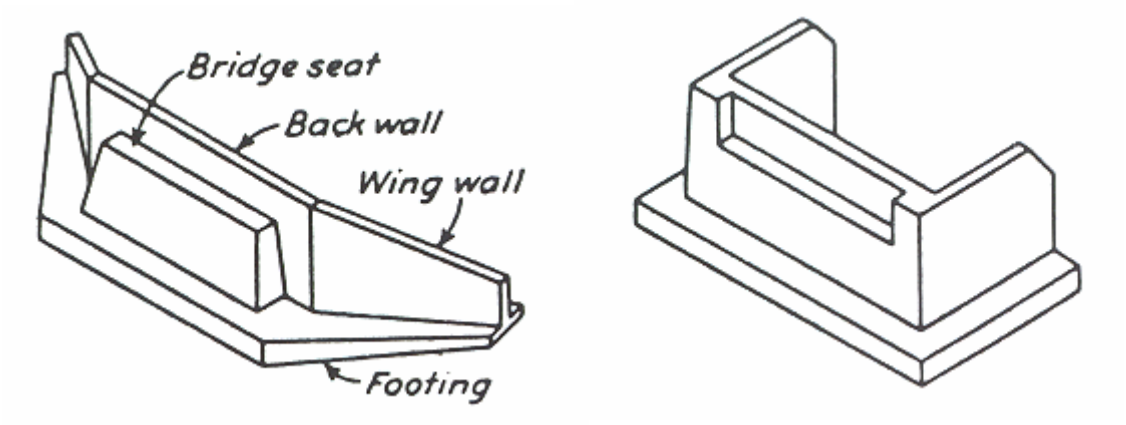

(a) Gravity Abutment (b) U Abutment

(c) Spill-through Abutment (d) Pile Bent Abutment

Figure 4.27 Various Types of Abutments

In the transverse direction of a bridge, two-thirds of the length of the wingwalls is assumed to be effective. As an abutment displaces in a transverse direction, the wingwall moving into the soil is assumed to be capable of developing the full passive resistance of the soil. Thus, the design passive resistance of the soil outside the wingwalls is estimated as a third the full passive resistance. Ultimate strength capacities of an abutment are normally assumed to be limited by a maximum soil stress under a dynamic load of 0.37 MPa (7.7 ksf) based on a judgement that estimates the static shear strength of typical embankment material to be 0.24 MPa (5.0 ksf). This value is then increased by 1/0.65 to account for an increase in strength due to the higher strain rate at which the earthquake load is applied.

Two end-diaphragm abutments, approximately one-half scale, are constructed to verify the stiffness and strength of abutments suggested by some provisions (Maroney et al. 1994). Static tests of half scale abutments not only in longitudinal and transverse direction, but also in passive (compression/or pushing) and active (tension/or pulling) direction were conducted. It is found that the passive stiffness is significantly overestimated, while the ultimate strength compared well and demonstrated some level of conservatism. The stiffness of abutments in active action is about a fifth of the passive stiffness.

Martin and Yan (1995) conducted parametric studies on sands and clays to investigate the earth pressure in the backfill soil of the abutments. They used finite difference grids in their numerical analyses. From the curve of passive pressure versus lateral displacement it is found that the ultimate passive earth pressure is mobilized at a

displacement of abutment of approximate 6% of the wall height for most of the cases. With regard to the Caltrans assumptions, it is hard to achieve a static passive soil resistance of 0.24 MPa (5.0 ksf) for a 2.4 m (8 ft) high abutment wall in a cohesionless soil. If the soil is cohesive, it is possible to achieve the same static passive soil resistance in practice.

Goel and Chopra (1997) evaluated the stiffness of abutments during earthquakes. In their numerical bridge model the abutment consists of a linear spring and a damper. The estimated stiffness is compared with the stiffness from the current design procedures. Evaluation of the current design procedures indicates that the Caltrans procedure leads to a good estimate of the transverse abutment stiffness, provided the deformation assumed in computing the stiffness is close to the actual deformation during the earthquake. The Caltrans procedure also leads to a good estimate of the abutment capacity in this direction. However, this procedure may overestimate the normal abutment capacity and stiffness by a factor of two or more, indicating that the assumed value of 0.37 MPa (7.7ksf) for the ultimate passive resistance of the soil used in the Caltrans procedure may be too high.

Geol (1997) used system identification to estimate the periods, damping ratios, and mode shapes of a bridge from recorded responses of the bridge. It is indicated from the results that the abutments provided significant restraint to the bridge movement during low-level shaking. However, during more intense shaking, the amount of restraint provided by abutments reduced by a factor of four.

The abutments are modeled by nonlinear springs to represent the seismic condition

and soil backfill. An abutment has two types of stiffness; one is the passive stiffness and the other one is the active stiffness. The passive stiffness acts in compression only, and the active stiffness acts in tension only. The passive stiffness is composed of soil resistance and piles' resistance. However, the active stiffness consists of the piles' resistance only.

- **Stiffness and Strength in Longitudinal Direction**

The abutment passive stiffness recommended by Caltrans is 115.0 kN/mm/m (200kips/in/foot). However, it is generally believed that this value is overestimated (Maroney et al., 1994; Geol and Chopra, 1997). Therefore, based on Maroney's experimental results, Caltrans specification of 115.0 kN/mm/m (200 kips/in/foot) should be reduced to 34.5 kN/mm/m (60 kips/in/foot), and the ultimate strength of 0.37 MPa (7.7 kips/ft^2) should remain the same (Maroney et al., 1994).

If the height of an abutment is less than 2.4 m (8 ft), the ultimate strength (0.37 MPa, 7.7 ksf) should be multiplied by the square root of the ratio of the actual activated soil height divided by 2.4 m (8 ft) (Caltrans, 1990). The ultimate passive earth pressure is mobilized at the displacement of the abutment of 6% of the wall height for most cases (Martin and Yan, 1995). In this study, the multi-linear behavior of abutments in passive action is suggested from the above considerations. Table 4.5 shows the values used for the abutment model in active and passive action. In the table, Δ represents the abutment displacement at the top, and h stands for the height of abutment. The behavior of abutment in passive action is perfectly plastic beyond the displacement $\Delta/h=0.06$. The

unloading stiffness is the same as the initial stiffness.

The abutment stiffness in active action is dependent on the resistance of piles. Caltrans recommendation (Caltrans, 1990), 119 kN/pile (40 kips/pile), is accepted in this study. However, the behavior of abutments in active action is not linear to the ultimate strength. The initial stiffness in active action degrades with surface soil yielding. Therefore, in this study, a trilinear model is selected for the active stiffness as shown in Figure 4.28.

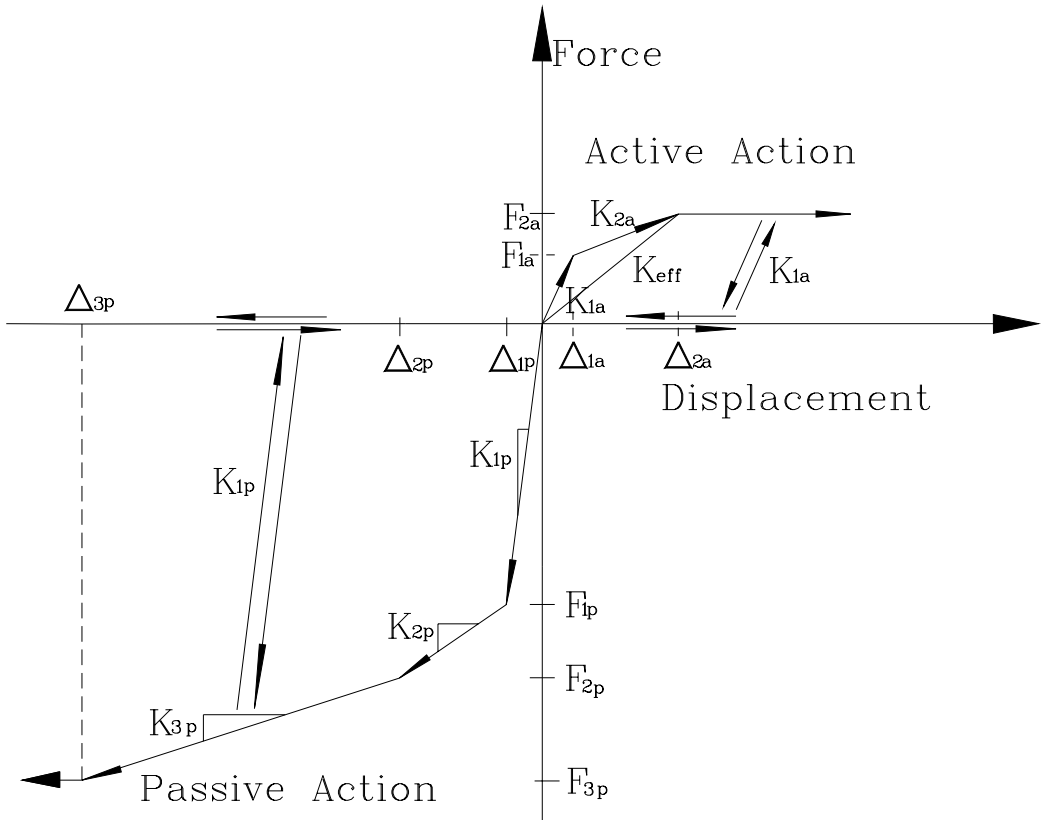

Figure 4.28 Analytical Model of Abutment in Passive and Active Action

The Caltrans recommendation is accepted to calculate the effective stiffness and the ultimate strength in active action, which is 119 kN/pile (40 kips/pile). The behavior of the abutment in active action is perfectly plastic after reaching the ultimate deformation (25.4 mm, 1.0 in). It is assumed that first yielding occurs at 30% of the ultimate deformation and the yielding force is 70% of the ultimate force. The corresponding forces for each step can be calculated from the stiffness and the deformation.

Table 4.5 Properties of Abutment in Passive and Active Action

Properties	Notations	Values
Passive Action		
Initial Stiffness	$K_{1(p)}$	34.5 kN/mm/m × width (60 kips/in/foot × width)
Displacement 1 at the top	$\Delta_{1(p)}/h$	0.6%
Second Stiffness	$K_{2(p)}$	0.167 $K_{1(p)}$
Displacement 2 at the top	$\Delta_{2(p)}/h$	1.5%
Third Stiffness	$K_{3(p)}$	0.071 $K_{1(p)}$
Displacement 3 at the top	$\Delta_{3(p)}/h$	6.0%
Active Action		
Effective Stiffness	K_{eff}	7.0 kN/mm/pile × number of piles (40 kips/in/pile × number of piles)
Initial Stiffness	$K_{1(a)}$	2.333 × K_{eff}
Displacement 1 at the top	$\Delta_{1(a)}$	7.62 mm (0.3 in.)
Second Stiffness	$K_{2(a)}$	0.428 × K_{eff}
Displacement 2 at the top	$\Delta_{2(a)}$	25.4 mm (1.0 in.)

4.4.4 Analytical Model of Impact Element

In this study, the contact-element approach is utilized to model pounding between two adjacent structures (Maison and Kasai, 1992). Previous studies have shown that when a linear element with very high stiffness is used for impact, it can produce unrealistically high impact forces and acceleration (DesRoches and Fenven, 1997). Therefore, a trilinear and elastic loading/unloading element, as shown in Figure 4.29, is selected for pounding. The compression only impact elements are located at expansion joints and abutments. The size of the gap of this element is the same as that of the gap at expansion joints. The stiffness of impact element, K_3 = 8.76e3 kN/mm (5.0e4 kis/in.), K_2= 1/2 K_3, and K_1 = 1/3 K_3, is controlled to ensure that the penetration of pounding is less than 2.54 mm (0.1 in.) when peak ground acceleration of ground motion applied is 0.4g. One link element in DRAIN-2DX is used for an impact element.

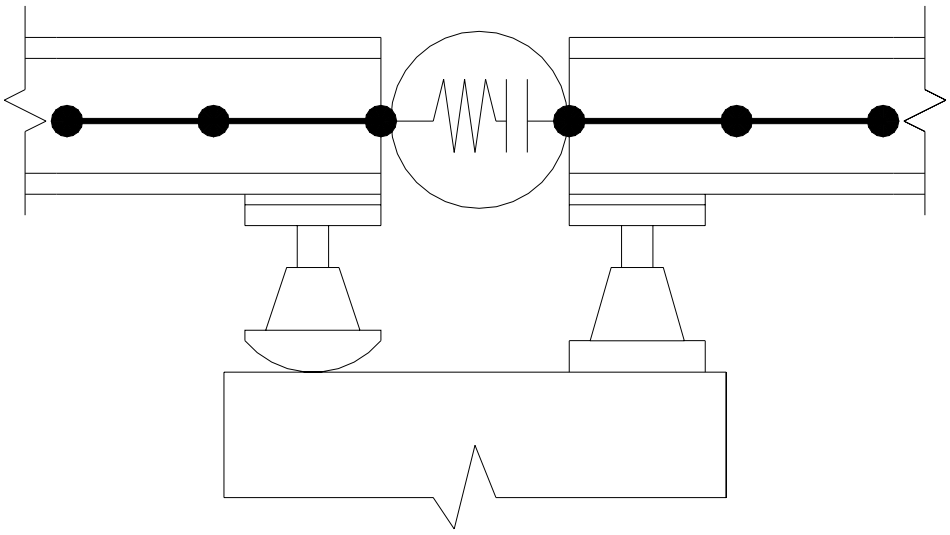

Figure 4.29a Location of Pounding Element on Bridge Decks

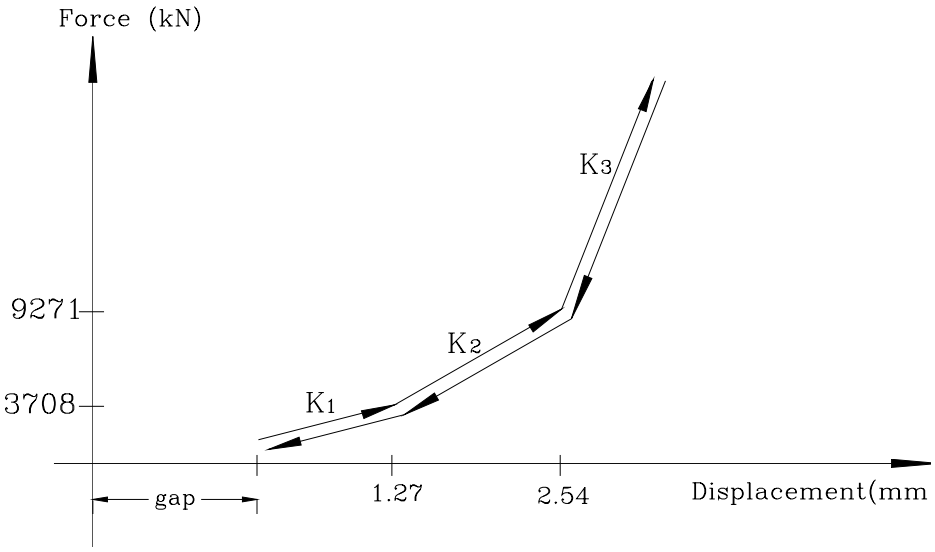

Figure 4.29b Analytical Model for Pounding in DRAIN-2DX

4.4.5 Multi-Column Bents

4.4.5.1 Overview of Multi-Column Bents

Among the various types of piers found in Mid-America, the multi-column piers bent in Figure 4.30 represents one of the most popular forms for highway bridges. The column bent is supported on either spread footing or pile foundation and is made of conventionally reinforced concrete. The supporting columns can be either circular or rectangular in cross section, although the circular cross section is more prevalent in Mid-America.

4.4.5.2 Material Models of Columns

The reinforced concrete section analysis program, UCFyber (Chadwell., 1999), was used to validate the DRAIN-2DX fiber model. UCFyber uses the Mander model (Mander

et al., 1988) to represent the uniaxial stress-strain behavior of concrete and performs moment-curvature analysis under monotonic loading.

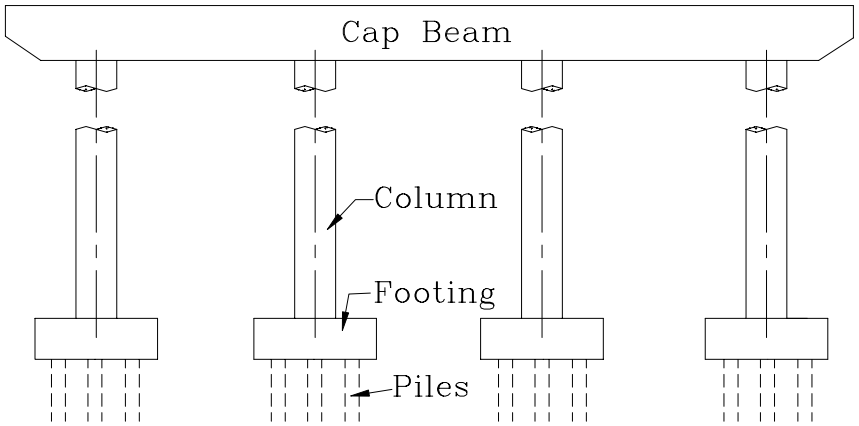

Figure 4.30 Layout of Multi-Column Bent

The peak strain of the unconfined concrete is assumed to be ε_o=0.002, and the unconfined peak compressive stress is assumed to be 27.6 MPa (4.0 ksi). The maximum stress of the confined concrete is 28.5 kPa (4.13 ksi), which is multiplied by the factor, K (Park et al., 1982) below, to the unconfined peak compressive stress at a strain of ε = 2.064e-3 ($K\varepsilon_o$).

$$K = 1 + \frac{\rho_s f_{y_h}}{f'_c} \tag{4.2}$$

where :

ρ_s = ratio of volume of steel hoops to volume of concrete core measured to outside of the peripheral hoop

f_{yh} = yield strength of steel hoops

f'_c = concrete compressive cylinder strength.

The spacing of hoop reinforcement, bar #4, in the columns is assumed to be 305 mm (12.0 in.), based on bridge plan from typical Mid-America bridges. Using grade 60 reinforcement, ρ_s and K are calculated to be 2.2e-3 and 1.0, respectively.

UCFyber uses the Mander model explicitly for the confined concrete model, whereas the DRAIN-2DX model requires a piecewise linear approximation for the model. The steeply descending stress-strain branch that is present in the UCFyber confined concrete model causes problems with converging to an equilibrium solution. For this reason, the confined concrete material model shown in Figure 4.31(b) is used for the nonlinear analysis of DRAIN-2DX. However, since the unconfined concrete model is only used for the cover, the sharp decreasing behavior of the concrete dose not produces equilibrium problems. Figure 4.32 shows the properties of reinforcement used in DRAIN-2DX and UCFyber.

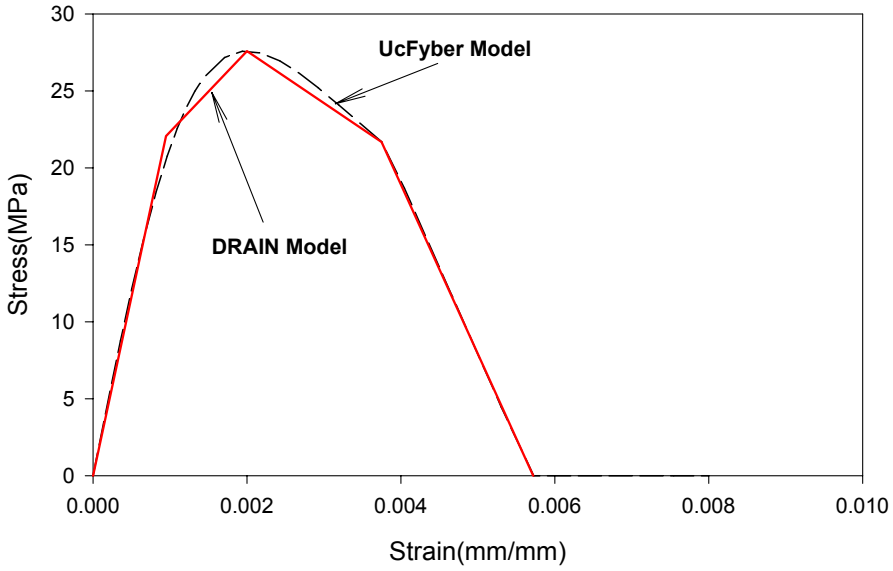

Figure 4.31a Comparison of Unconfined Concrete Models of UCFyber and DRAIN

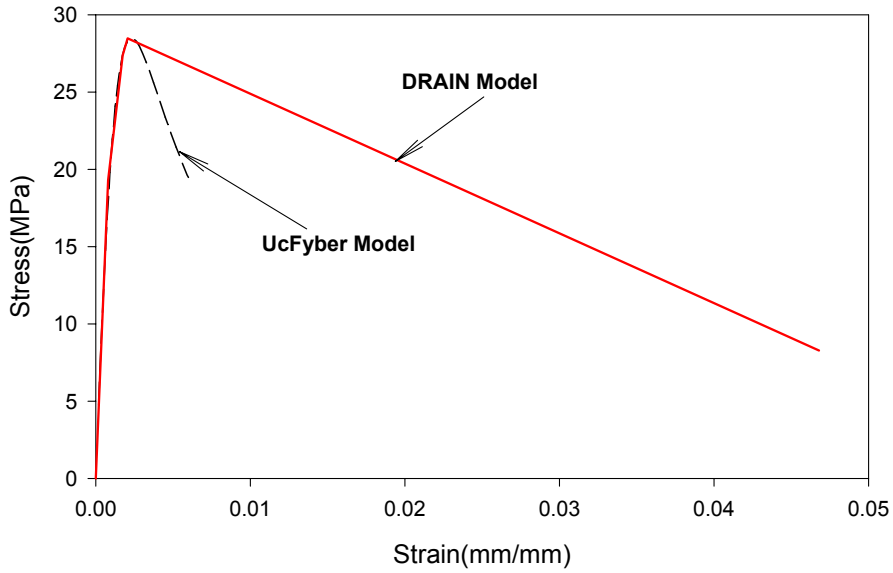

Figure 4.31b Comparison of Confined Concrete Models of UCFyber and DRAIN

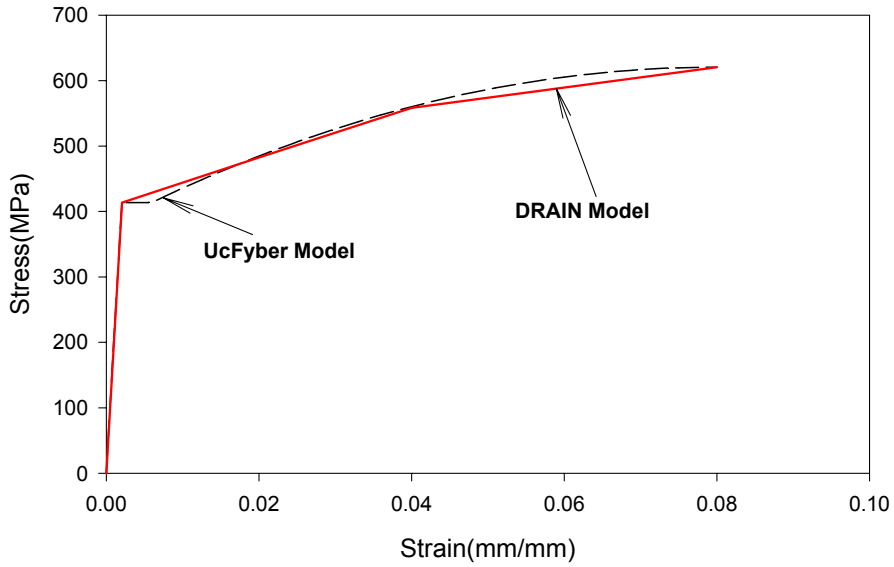

Figure 4.32 Comparison of Steel Reinforcement Models of UCFyber and DRAIN

4.4.5.3 Cross Section Behavior of Columns

The cross-sectional discretizations of the columns for UCFyber and DRAIN-2DX model are shown in Figure 4.33. About 2000 fibers are used to analyze the cross section in UCFyber. However, the cross section is represented by 24 concrete and 12 steel fibers in DRAIN-2DX. The concrete fibers are placed at the geometric centroids of the concrete areas shown in the cross-sectional discretization and the steel fibers are placed at the points shown in the figure. When fibers have the same value of centroid, they are merged into a fiber.

The moment-curvature relationship for the column cross section from DRAIN-2DX and UCFyber reference model are compared in Figure 4.34 for y-axis bending without axial load. The moment-curvature relationship is obtained by push-over analysis of only

a column model in DRAIN-2DX, which is shown in Figure 4.35. The yield curvature of the cross-section is 3.436e-3 rad/m (8.728e-5 rad/in.).

The moment-curvature relationship under monotonic loading is similar in both DRAIN-2DX and UCFyber, despite the more highly descretized UCFyber model. Therefore the DRAIN-2DX fiber element is thought to adequately represent the response.

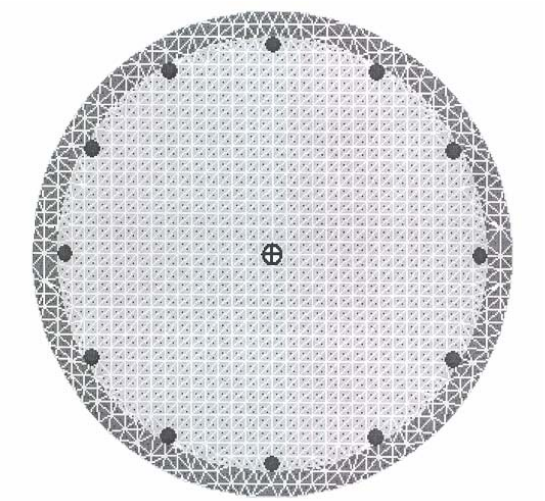

(a) Discretization of Column Cross Section in UCFyber

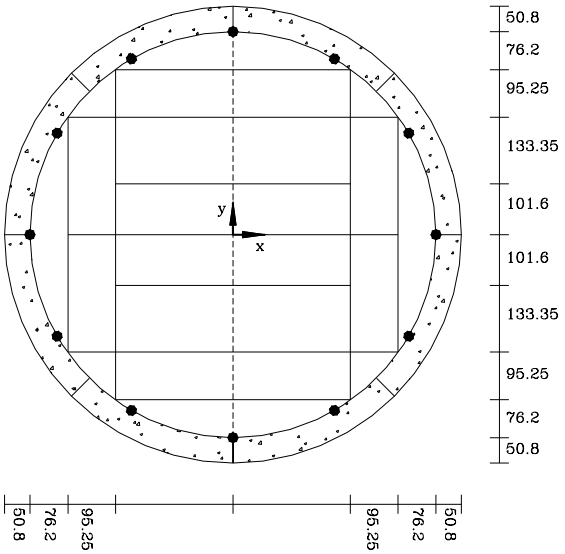

(b) Discretization of Column Cross Section in DRAIN-2DX

Figure 4.33 Fibers in Cross Section of Columns

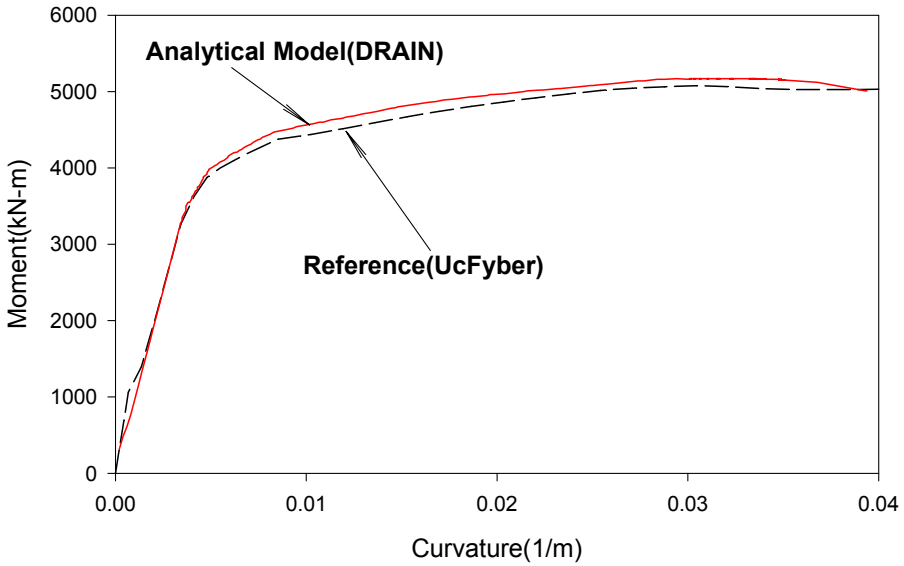

Figure 4.34 Moment-Curvature Relationship for Columns

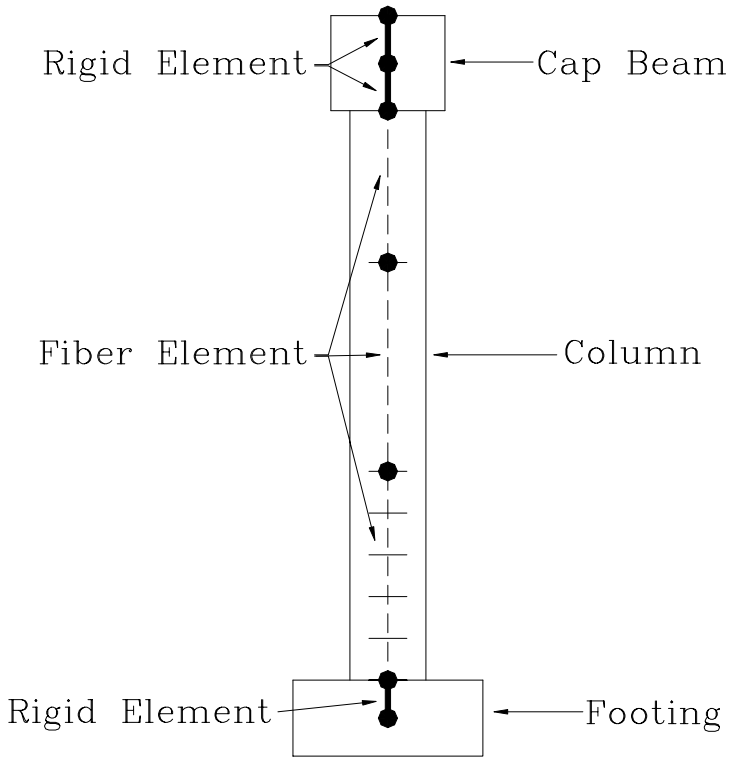

Figure 4.35 Fiber Elements for A Column in Typical MSSS and Continuous Bridge

4.4.6 Pile Foundations

4.4.6 1 Overview of Pile Foundations

Most bridges, especially long span bridges, are supported on pile foundations. A typical foundation shown in Figure 4.36 consists of vertical and battered piles supporting a footing. The piles may penetrate several layers of soil with varying strength and stiffness.

In the last two decades, several numerical and analytical methods have been developed to compute the dynamic stiffness and the seismic response of pile foundations accounting for soil-structure interaction. Soil-structure interaction refers to the effects that the foundation soil has on the dynamic response of a structure and, conversely, the effects of the structure on the soil motion.

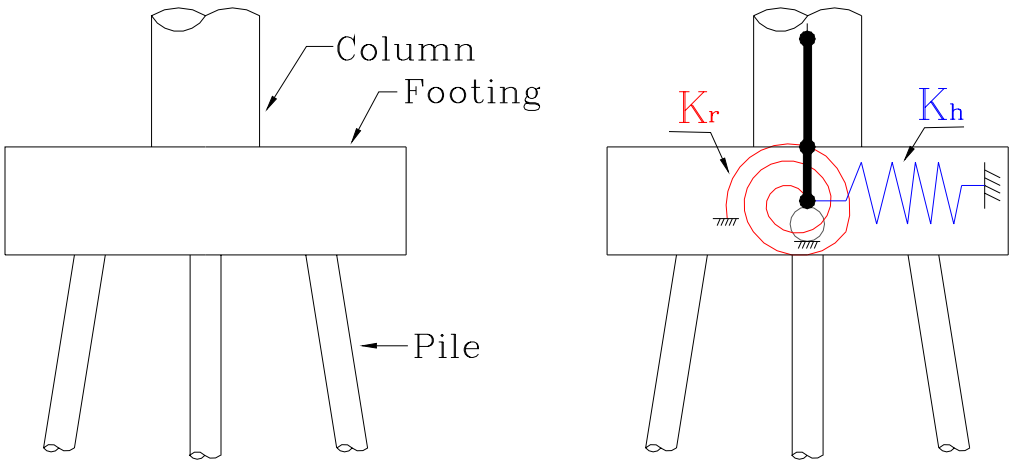

Figure 4.36 Layout and Model of Pile Foundation

The influence on the structural response often includes an amplification of the translational motion, an increase in the flexibility of the system, the addition of damping from hysteretic action of the soil (hysteretic damping), and radiation of energy away from the structure in the form of outward-propagating soil waves (radiation damping). The seismic response of a pile foundation is the result of complex interaction between the pile cap, the piles and the soil.

Two general approaches are available for incorporating soil-structure interaction effects into structural analysis (Wolf, 1985). In the direct method, the structure and a portion of the foundation soil are both incorporated into a finite element mesh. This is the simplest approach conceptually, but a number of drawbacks, including the need for a large model, energy absorbing boundaries, and detailed soil properties, make its use prohibitive for all but the most extreme analysis demands.

An analytical model intended to capture every aspect of the seismic response would use solid elements to represent the components of the foundation and appropriate structural and geotechnical constitutive relationships. This type of model is beyond the state of the practice in the structural engineering community, however.

A simpler, more efficient approach is the substructure method. With this method, the structure and the soil are analyzed separately. A simplified model is constructed that can approximate the behavior of the soil as the foundation. This simplified model is then coupled with the structure at the supports, and the structure is analyzed. The foundation model is composed of sets of structural elements, ranging in complexity from elastic springs to complicated nonlinear spring/damper combinations arranged in series and/or

parallel for each degree of freedom. They are chosen on the basis of the assumed foundation behavior, which is obtained either experimentally or analytically.

Practical models are built using beam elements to represent the piles and uncoupled, distributed springs to represent the soil. This type of model neglects any inertial effects in the soil, the interaction between piles, and coupling of the soil stiffness between different elements.

The performance of such structure-foundation systems in the recent Northridge (1994) and Kobe (1995) earthquakes have come under scrutiny. Buckle (1994) gives a comprehensive account of the performance of highway bridges in the 1994 Northridge, California, earthquake. These recent cases have generated sufficient reason to believe that the subject of soil-pile-structure interaction should be investigated with greater rigor and precision.

Closed-form expressions for the static stiffness of single pile have been derived by fitting finite element results of the static problem (Gazetas, 1984). The accuracy of these expressions has been verified by comparing their results with the solution of Blaney et al. (1976) for lateral and vertical pile motion in homogeneous soil, and the solution of Randolph (1981) for lateral pile motion in nonhomogeneous soil with modulus proportional to depth. The horizontal and vertical static stiffness of a single pile are also computed with the procedure developed by Trochanis et al. (1991). The procedure is based on one-dimensional analysis, which utilizes a realistic hysteretic model that has been calibrated using a three-dimensional finite element analysis of the soil-pile system. The results at small deflection are close to those from the Gazetas formulations.

Today, numerous rigorous and approximate procedures are available to compute the response of piles and pile groups under dynamic loads. A recent comprehensive review on the subject has been presented by Novak (1991). On the other hand, during the same period, the software for structural analysis has been considerably developed and expanded so that complex structures with sophisticated behavior can be rigorously analyzed.

4.4.6 2 Analytical Model of Pile Foundations

To describe the behavior of pile foundations, a linear spring model is selected in horizontal and rotational directions shown in Figure 4.36. The vertical movement is restricted since vertical ground motion will not applied in this study.

The response of piles laterally loaded (by horizontal forces and moment) is independent of their length, in most practical situations. Only the uppermost part of the pile, length, l_c, experiences appreciable displacement. It is along this active length, l_c, that the imposed load is transmitted to the supporting soil. The length, l_c, is typically on the order of 5 to 10 pile diameters; for a given soil profile, and is a function of the pile with respect to the soil. Fang (1999) presents simple algebraic expressions for estimating l_c of a circular solid pile with diameter d and Young's modulus, E_p, for parabolic increases of soil modulus.

$$l_c = 2d\,(E_p / \hat{E}_s)^{0.22} \tag{4.3}$$

Where $\hat{E}_s$ is the reference Young's modulus of the soil at a depth, z=d and d is the

diameter of a pile.

Fang (1999) also presents formulas to calculate the horizontal, and rotational stiffness of a pile foundation, which, however, are valid only for piles with length; $L > l_c$

$$K_h = 0.8\ d\ \hat{E}_s\ (E_p / \hat{E}_s)^{0.28} \tag{4.4}$$

$$K_r = 0.15\ d^3\ \hat{E}_s\ (E_p / \hat{E}_s)^{0.77} \tag{4.5}$$

where:

K_h = Horizontal stiffness of a pile

K_r = Rotational stiffness of a pile

d = Diameter of a pile

then calculated using following the equation (4.6) and (4.7) (Martin and Lam, 1995).

$$K_{h,\ total} = N \cdot K_h \tag{4.6}$$

$$K_{r,total} = N \cdot K_r + \sum K_v \cdot S_n^{\ 2} \tag{4.7}$$

where:

N = Number of piles in a footing

K_h = Horizontal stiffness of a pile

S_n = Distance from the center of pile group

K_v = Vertical stiffness of a pile

$K_{h,\ total}$ = Total horizontal stiffness of a pile footing

$K_{r,\ total}$ = Total rotational stiffness of a pile footing

The reference modulus of sand varies from 34.5 MPa (5 ksi) to 68.9 MPa (10 ksi). In

this study, the minimum reference modulus of sand, 34.5 MPa (5ksi), is used for the conservatism. The piles are assumed to be made of concrete (E_p = 21994 MPa, 3190 ksi), and the diameter and length of piles is assumed to be 305 mm (12 in) and 15.3 m (50 ft), respectively. With the above information, the maximum active length for sand is about 2.4 m (8 ft). The horizontal, and rotational stiffness of the pile are 51.3 kN/mm (293 kips/in.), and 2.11e4 kN-m/rad (1.87e5 kips-in/rad).

However, the horizontal stiffness of the piles is about 3 times that of the initial stiffness of piles used in the abutments in active action. Therefore, in this study, a third of the horizontal stiffness of a pile is used to calculate the total horizontal and rotational stiffness of a pile footing.

To calculate the total rotational stiffness of a pile footing, the vertical stiffness of the pile is required. The value of K_v is calculated following the method in Martin's study (Martin and Lam, 1995). The pile has the ultimate capacity of 801 kN (180 kips) for compression (Lam, 1994). Assuming frictional capacity of 534 kN (120 kips) and bearing capacity of 267 kN (60 kips), the procedure to calculate the vertical stiffness of the pile is like below:

1. Calculate coordinate of friction resistance-displacement curve using the below formulation:

$$F = F_{\max}\left[2\sqrt{\frac{Z}{Z_c}} - \frac{Z}{Z_c}\right] \tag{4.8}$$

where:

F_{max} = Frictional capacity of the pile

Z = Displacement in vertical direction

Z_c = Ultimate displacement (5.08 mm, 0.2 in.)

2. Calculate the coordinate of the tip resistance-displacement curve using the below equation:

$$Q = Q_{max} \sqrt[3]{\frac{Z}{Z_c}} \tag{4.9}$$

where:

Q_{max} = Frictional capacity of the pile

Z = Displacement in vertical direction

Z_c = Ultimate displacement (=0.05*Diameter)

3. Calculate the rigid-pile solution with summation of friction and tip resistance values along the curve.

4. Calculate the flexible-pile solution with adding displacement component at each load level to reflect the pile compliance to the rigid-pile solution. The compliance is calculated using the following equation:

$$\delta = QL/AE \qquad (4.10)$$

where L is the length, A is the area, and E is the Young's modulus of the pile.

5. Develop approximate solution by averaging the rigid and flexible pile solution.

6. Estimate the vertical stiffness from the curve.

Figure 4.37 shows the vertical pile stiffness solution graphs of load-displacement curves. The estimated vertical stiffness of the pile is approximately 175 kN/mm (1000 kips/in.).

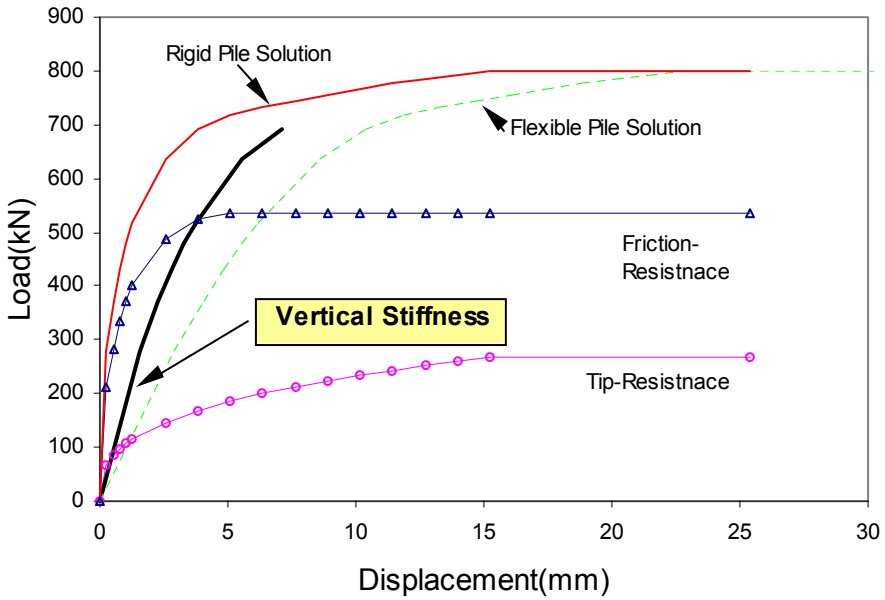

Figure 4.37 Vertical Pile Stiffness Solution Graphs of Load-Displacement Curves

The reduction of the horizontal stiffness was accepted because the soil strain would be larger in an earthquake and pile group effects would reduce the effective stiffness. It

is recognized, however, that the foundation modeling is approximate.

In Table 4.6, the stiffness of pile foundations in horizontal and rotational direction for each bridge type is shown. There are four footings in each bridge, and the dimensions of the footings are shown in Figure 4.38.

Table 4. 6 Stiffness of Pile Foundations

Bridge Type	Horizontal kN/mm (kips/in)	Rotational kN-m/rad (kips-in/rad)
	Total stiffness of 4 footings	Total stiffness of 4 footings
MSSS-Steel MSSS-Concrete Continuous-Concrete	547 (3123)	5.60×e6 (4.92×e7)
Continuous-Steel	820 (4684)	1.04×e7(9.18×e7)

(a) MSSS Bridge (b) MS Continuous Bridge

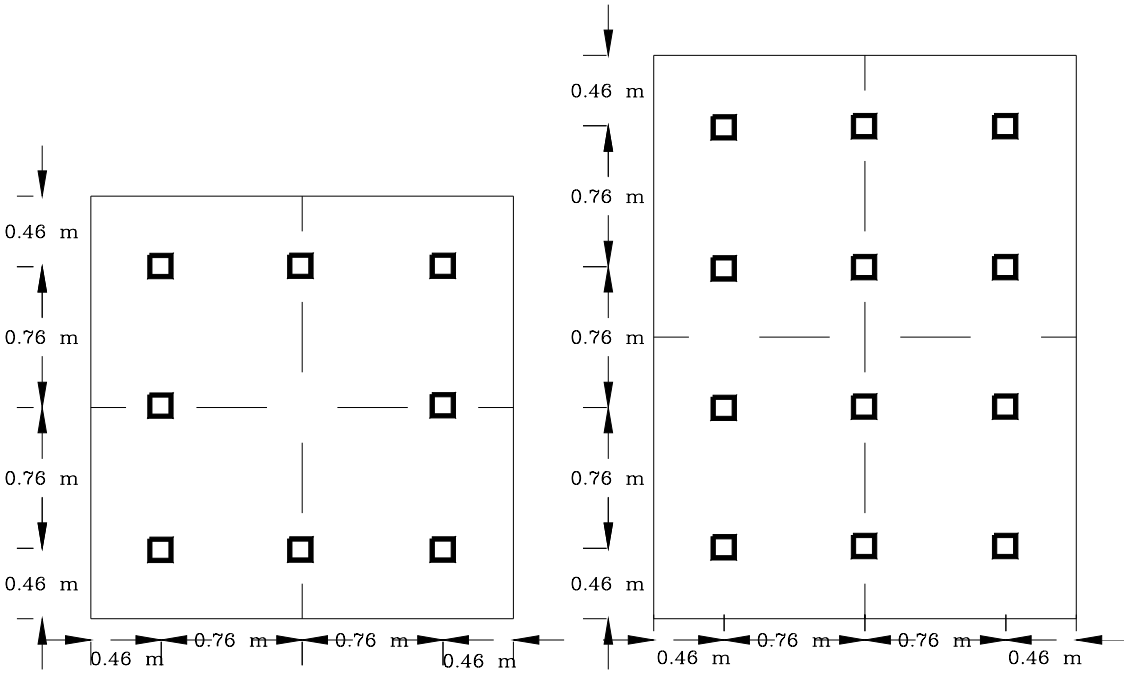

Figure 4.38 Dimension of Footings

4.5 Capacity Estimation of Bridge Components

Analytical bridge components developed in the above sections are simply linear elastic or the combination of fully nonlinear elements. To assess the damage state of each component, it is required to estimate the capacity of components such as yield and ultimate state, or failure point.

4.5.1 Fixed Steel Bearing Capacity

Two types of fixed steel bearings are used in this study, high type and low type as shown previously in Figures 4.11 and 4.12. The experimental test of the bearing is shown in Figure 4.39 to illustrate the various damage states.

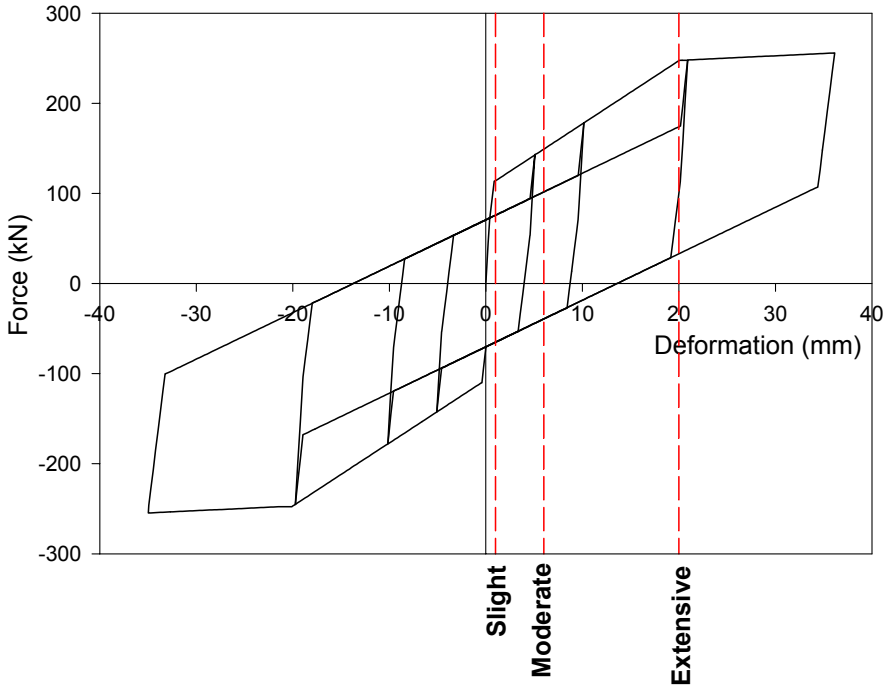

Figure 4.39 Damage State Levels of High Type Fixed Bearing

In the low type fixed steel bearing, the pintle yields at the displacement of 3.30 mm (0.13 in.) as shown in Figure 4.19. The experimental result was based on the steel base. When assuming that the bearings are on concrete pedestal, the damage states of the bearings can follow the definition of damage states for the high type fixed bearings. Since the low type fixed bearings have gap of 2.5 mm, this gap size should be included.

4.5.2 Expansion Steel Bearing Capacity

The procedure for determining the expansion bearings' capacity is illustrated in Appendix A. Following the formulations, the maximum allowable displacement of the three expansion bearings can be calculated and listed in Table 4.7. EXB-I is the Mander's test bearing in Figure 4.17, EXB-II is the expansion bearing on the continuous bridge in Figure 3.5, and EXB-III is the bearing of the single span bridge in Figure 3.8. These three expansion bearings are stable until the contact point beyond the edge. In the case, the maximum allowable displacement of the expansion bearings is independent of the frictional coefficient (μ) but depends on the configuration of the bearings. As expected, the expansion bearing, EXB-III, can be unstable easily as shown in Table 4.7.

Table 4.7 Maximum Allowable Displacement of Expansion Steel Bearings

Bearing Type	Height of Bearing (h) (mm)	Radius of Rocker (r) (mm)	Angle of Rocker (ψ) (radian)	Maximum Allowable Displacement (mm)
EXB-I	381.0	330.2	0.446	179.8
EXB-II	228.6	304.8	0.247	58.2
EXB-III	152.4	304.8	0.125	19.3

4.5.3 Capacity of Columns

There is still a wide divergence of the evaluation of shear capacity of bridge columns. Some factors; such as the contribution of the concrete, the transverse and longitudinal reinforcement, and the axial force resisted by a column, affect the shear capacity of the column. Based on experimental testing of reinforced concrete columns, various theories have been proposed for shear strength capacity (Aschheim and Moehle, 1996).

ASCE-ACI Committee 426 estimates the shear strength of bridge columns. The column shear strength is given as:

$$V_n = V_c + V_s \tag{4.11}$$

where V_c is the concrete component of shear strength, and V_s is the steel component. The concrete component, V_c in psi, of the column shear strength is given as:

$$V_c = (1 + \frac{3P}{f_c' A_g})(0.8 + 120\rho_t)\sqrt{f_c'} A_e \tag{4.12}$$

where:

f_c' = Compressive strength of concrete in ksi.

A_e = Effective shear area, taken as $0.8A_{gross}$ in in^2

ρ_t = Tension steel ratio, taken as 0.5ρ.

P = Axial load, taken negative for tension in kips.

V_c= Concrete component of shear strength in kips.

The contribution of the transverse reinforcement, V_s in psi, is given as:

$$V_s = \frac{A_v f_{yh} D}{s} \tag{4.13}$$

where:

A_v = Total area of transverse reinforcement in a layer in the direction of the shear force,

s = Spacing of transverse reinforcement layers along member axis

f_{yh}= Yield strength of transverse reinforcement

D = Effective depth, taken as 0.8D for columns

V_s= Steel component of shear strength

The MSSS and continuous bridges have the same cross-section of columns shown in Figures 3.1, 3.2, and 3.4. The estimated shear strength of each column following the above equations is 1357 kN (305 kips), and the total shear strength of a pier is 4 times of that, 5427 kN (1220 kips).

However, this estimation shows the shear strength of a column with elastic or a small amount of inelastic deformation called the brittle capacity. The shear strength under large inelastic deformation is called the ductile capacity. Priestley and his colleagues (Priestely et al., 1994; Priestely et al., 1996) suggested the formulation to estimate the ductile shear capacity. The formulation of column shear strength is given as:

$$V_n = V_c + V_s + V_p \tag{4.14}$$

where V_c is the concrete component of shear strength, V_s is the steel component, and V_p is the contribution of the axial force. The concrete component, V_c in MN, is equal to:

$$V_c = k\sqrt{f_c'}A_e \tag{4.15}$$

where:

k = Factor to account for member ductility. This factor is related to curvature ductility, as suggested by Priestley et al. (1996).

$$= \left\{ \begin{array}{ccc} 0.29 & for & \mu \le 3 \\ 0.43 - 0.048\mu & for & 3 < \mu \le 7 \\ 0.15 - 7.3\times10^{-3}\,\mu & for & 7 < \mu \le 13 \\ 0.042 & for & \mu > 13 \end{array} \right\} \text{ for uniaxial ductility}$$

μ = Curvature ductility

f_c' = Compressive strength of concrete in MN.

A_e = Effective shear area, taken as $0.8A_{gross}$ in m^2

V_c= Concrete component of shear strength in MN.

The contribution of the transverse reinforcement, V_s, is given as:

$$V_s = \frac{A_v f_{yh} D}{s} \tag{4.16}$$

where:

A_v = Total area of transverse reinforcement in a layer in the direction of the shear force

s = Spacing of transverse reinforcement layers along member axis

f_{yh}= Yield stress of transverse reinforcement

D = Effective depth, taken as 0.8D for columns

V_s= Steel component of shear strength

V_p is given as:

$$V_p = \frac{D-c}{2a} P \tag{4.17}$$

where:

D = Overall section depth or diameter

c = Depth of the flexural compression zone

a = L for single bending, L/2 for double bending

P = Axial load in member (positive for compression)

V_p= Axial component of shear strength

As shown in the equation (4.12), the shear capacity of concrete depends on the curvature ductility of a column. The brittle shear capacity of the columns is determined using k=0.29. The ductile capacity is calculated using k=0.10, which corresponds to a curvature ductility of μ=7.2. Figures 4.40 and 4.41 show the variation of the curvature ductility and the shear capacity of columns of the MSSS steel bridge and the continuous steel bridge with respect to the lateral displacement at the top of the columns.

In the Table 4.8, there is the estimation of the shear capacity for columns of each type of bridges.

Table 4.8 Shear Capacity of Columns

Bridge Type	Brittle Capacity (V_{nb}, kN)		Ductile Capacity (V_{nd}, kN)
	ACI	Priestely	Priestely
MSSS Steel Bridge	1334	1603	1074
MSSS Concrete Bridge	1337	1605	1081
MSC Steel Bridge	1344	1607	1082
MSC Concrete Bridge	1337	1605	1081

The ACI approach gives brittle shear capacities that are about 83% of the capacities according to Priestely et al. (1994). The ductile shear capacity of columns is about 67% of the brittle shear capacity. The ACI estimation is used in this study to check shear failure because of the two reasons; (1) the ductility of columns of typical bridges is usually found less than 3.0; and (2) the ACI estimation has more conservatism than the Priestely approach.

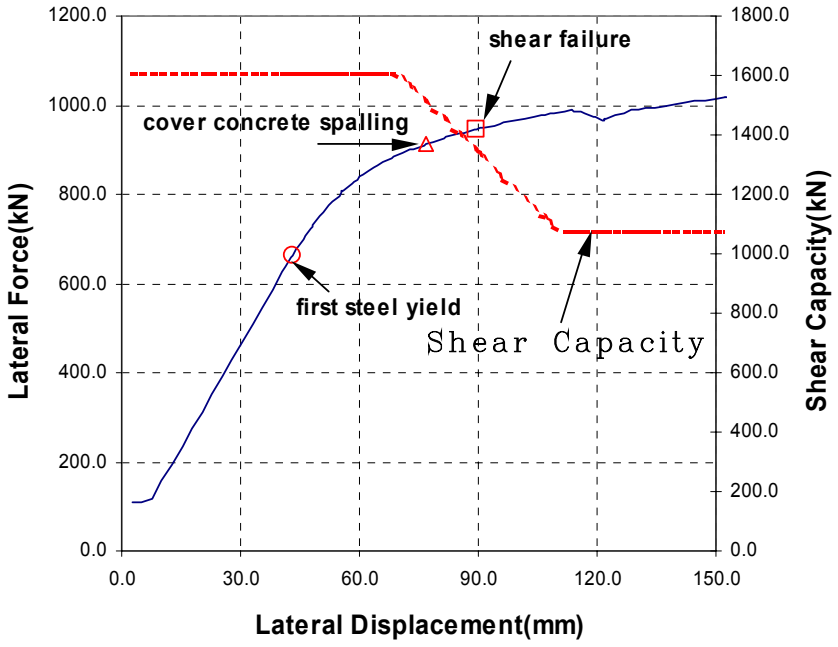

(a) Shear Capacity and Lateral Force

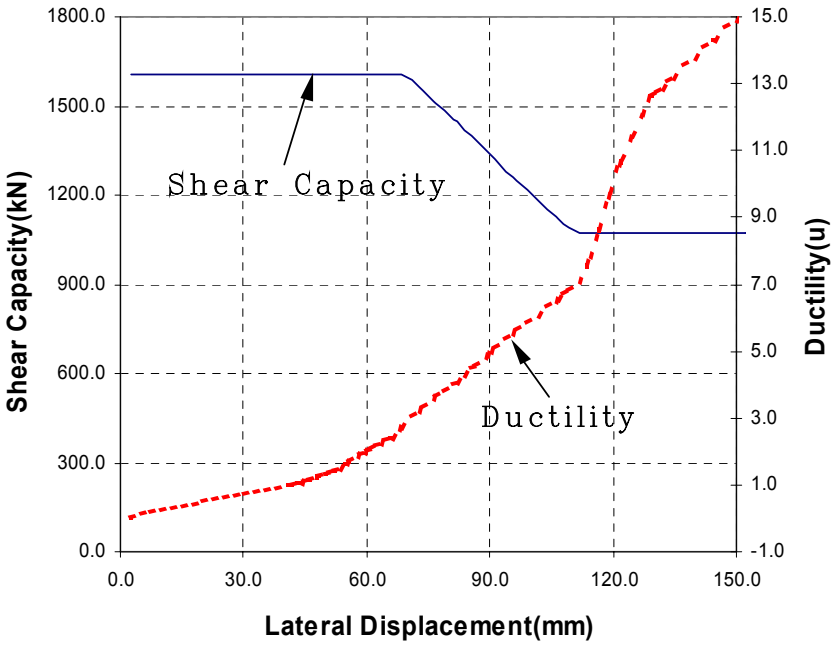

(b) Curvature Ductility and Shear Capacity

Figure 4.40 Static Pushover Analysis of the Column of the MSSS Steel Bridge

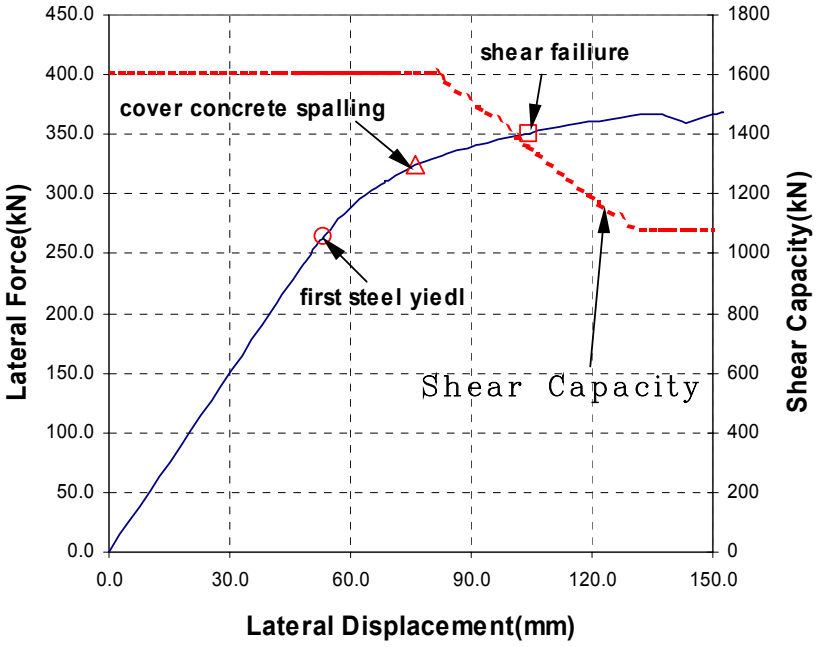

(a) Shear Capacity and Lateral Force

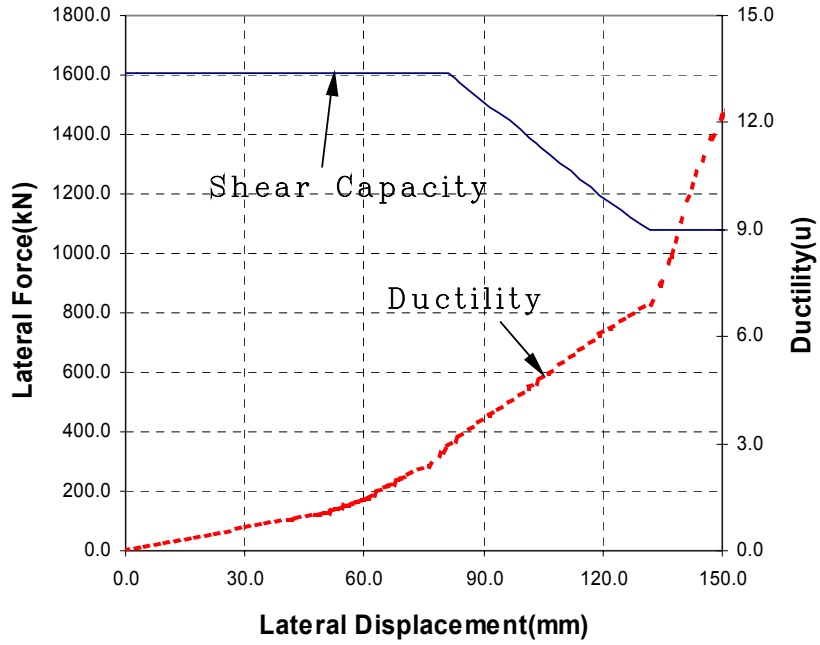

(b) Curvature Ductility and Shear Capacity

Figure 4.41 Static Pushover Analysis of the Column of the Continuous Steel Bridge

4.5.4 Foundation Capacity

In seismic analysis, the horizontal displacement of pile groups is often considered important on the overall response of bridges. However, it is found that moment-rotational characteristics of a pile group can have a more dominating effect on the response of the structure as compared to the horizontal stiffness. Therefore, the investigation of the both responses in the horizontal and rotational direction is required.

To determine the failure of a foundation in the horizontal direction, a criterion is necessary. In the above section of the abutments, the ultimate capacity of a pile in the horizontal direction is 178 kN (40 kips). This value can be used as the criterion of failure of a pile in a foundation. The failure strength of the pile footing on the MSSS bridge in horizontal direction is 5694 kN (1280 kips). The failure strength of the pile footing of the continuous steel bridge is 8541 kN (1920 kips).

To establish the criterion for the moment capacity of a pile foundation, at first, it is necessary to determine the vertical load capacity because the moment capacity depends on the capacity of each pile for both compression and uplift loading. The moment capacity also depends on the configuration of the pile foundation. In this study, the pile in a foundation has been assumed to be a 15.2 m (50 ft) long and 304.8 mm (12 in.) concrete pile. Lam (1994) showed that the ultimate capacities of the pile for compression and tension are 801 kN (180 kips) and 400 kN (90 kips), respectively.

Figure 4.42 presents various capacity criteria for the pile footing of the MSSS bridge. Under conventional practice, the moment capacity at the center of the pile footing would be 1831 kN-m (16200 kips-in.). This capacity rises from assuming a linear distribution in

pile reaction across the pile footing.

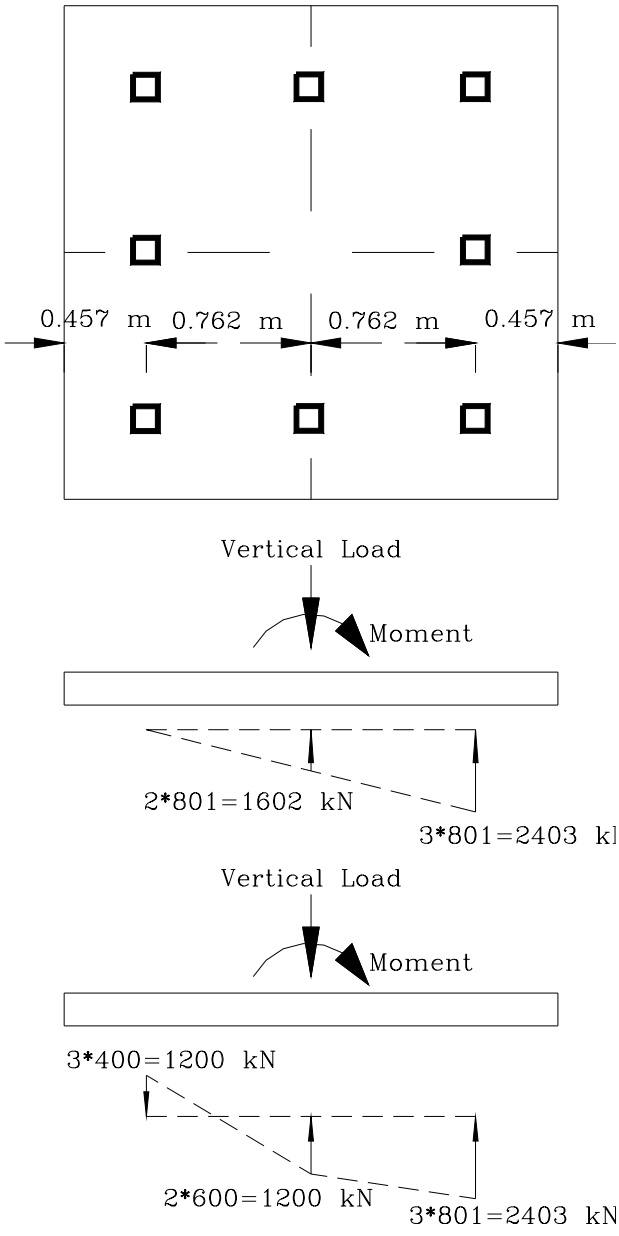

(a) Conventional Design Criterion

Moment Capacity

= 1831.1 kN-m

(b) Ultimate moment Capacity

Moment Capacity

= 2745.5 kN-m

Figure 4.42 Pile Foundation Configuration of MSSS Bridge for Moment Rotation Study

Figure 4.42 shows the moment capacity that can be achieved from a nonlinear moment-rotation analysis of the pile footing. As the moment load increases above the conventional capacity, nonlinear load-displacement characteristics of the pile are simulated to allow additional load to be distributed to the other less loaded piles in the pile group. As shown in Figure 4.42, the ultimate capacity of 2746 kN-m (24300 kips-in.), which is 1.5 times the conventional capacity, can be achieved by nonlinear analysis.

From Lam's study (1994), it is found that the conventional moment capacity of a pile footing corresponds to the yield point of the pile footing, and the ultimate moment capacity corresponding to the failure point of the pile footing. Therefore, the conventional moment capacity can be the criterion of the yield point, and the ultimate moment capacity can be the criterion of the failure point.

Following the same method, the yield and ultimate moment capacity of the pile foundation for the continuous steel bridge are 2441 kN-m (21600 kips-in.) and 3660.7 kN-m (32400 kips-in.), respectively.

Therefore, the total moment capacities of the MSSS bridge pile foundation are 7320 kN-m. (= 4 × 1830, 64800 kips-in.) and 10982 kN-m. (= 4 × 2745.5, 97200 kips-in.) for the yield and ultimate state, respectively. The values of the continuous steel bridge are 9762 kN-m (86400 kips-in.) and 14642.8 kN-m (129600 kips-in.) for the yield and ultimate state, respectively.

4.5.5 Abutment Capacity

The analytical model of abutments is a fully nonlinear behavior. In the model, the

ultimate strength can be easily determined. However, the yield point is not clearly identified. Thus, it is needed to define the yield point in the analytical model of abutments. The yield deformation of abutments can be defined as the first yield point in the analytical model. Following the definition, the yield and ultimate deformation of the abutments for 6 bridges are listed in Table 4.9. Figure 4.43 shows the damage state of the abutment of the MSSS steel bridge.

Table 4.9 Yield and Ultimate Deformation of Abutments

Bridge Type	First Yield Deformation (mm)				Ultimate Deformation (mm)			
	Left		Right		Left		Right	
	Act.	Pas.	Act.	Pas.	Act.	Pas.	Act.	Pas.
MSSS-SG, MSSS-CG, CON-CG	7.6	14.6	7.6	14.6	25.4	146.0	25.4	146.0
CON-SG	7.6	14.6	7.6	45.7	25.4	146.0	25.4	457.0
SS-SG, SS-CG	7.6	43.9	7.6	39.4	25.4	439.0	25.4	394.0

Ref. Act. : Active Action Pas. : Passive action

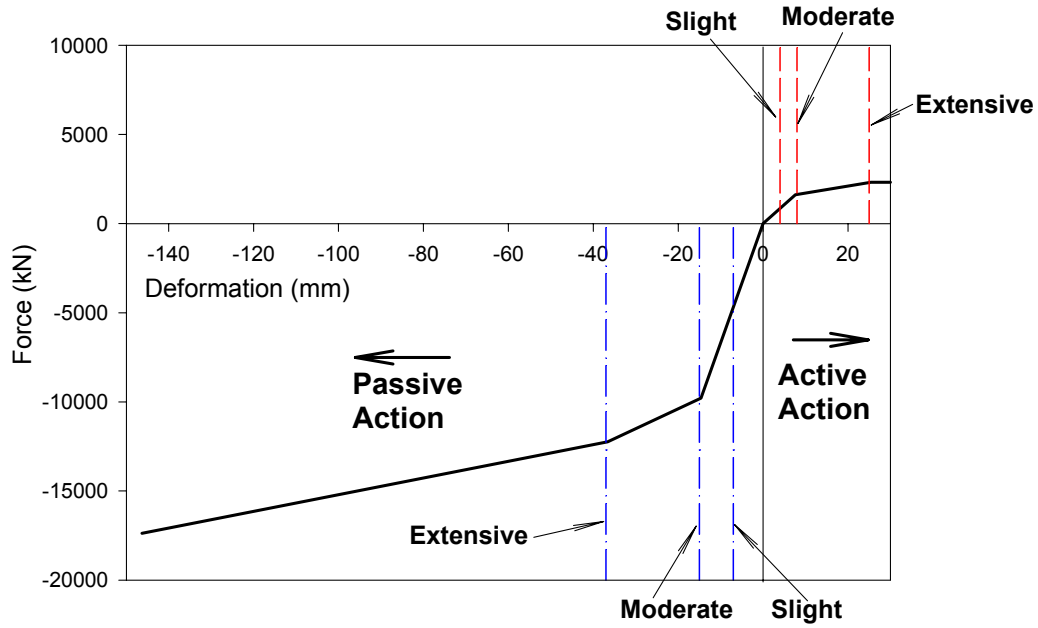

Figure 4.43 Damage State Levels of Abutment

CHAPTER 5

DETERMINISTIC SEISMIC RESPONSE ANALYSIS OF TYPICAL BRIDGES

In this chapter, the seismic responses of the six types of typical bridges are evaluated. The analytical responses are based on a suite of ground motions developed for Mid-America. The goal of the analysis is to determine the seismic demands on the critical components of the bridges and to determine the likely failure modes.

First, the vibration properties from the typical bridges are summarized. Next, the seismic response of each bridge to a representative ground motion record is reviewed. Mean global displacement as well as element force-deformation relationships for critical components are presented. Finally, using the suite of special ground motions developed for Memphis, Carbondale, and St. Louis, the mean responses of critical bridge components are reported for each bridge type.

5.1 Modal Analysis

Prior to conducting the response history analysis of the bridge, a modal analysis of the 6 typical bridges is first conducted. The dynamic properties are based on the initial state of elements in the bridge. Table 5.1 lists the vibration characteristics such as periods and participating mass in the x and y-direction of the first 5 modes for each

bridge. Five- percent viscous damping is assumed for the first significant longitudinal mode. Mass proportional damping is applied to every mass. However, the stiffness proportional coefficient is applied only to the columns (fiber elements). Since the initial stiffness of the bearing elements is orders of magnitude larger than the columns' stiffness, they provide unrealistic viscous forces. This results in only being able to provide 5% damping in one mode. However, since this mode typically consist of over 80% of the effective mass in all bridges, this approximation is adequate. The corresponding mode shapes for the primary mode for each bridge type are shown in Figure 5.1.

The results of the modal analyses of the MSSS bridges and single span bridges show that the fundamental periods in the longitudinal direction with concrete girders are longer than the periods with steel girders. This is due to the larger weight of concrete bridge girders compared with steel girders. However, the first period of the MS continuous steel bridge is longer than that of the MS continuous concrete bridge since the steel bridge deck chosen in this study is longer and heavier than the concrete bridge.

Figures 5.2 and 5.3 graphically show the location of the fundamental period of the six typical bridges in the longitudinal direction plotted along with the mean acceleration response spectra (MARS) for the suite of synthetic ground motion records used in this study.

In Figure 5.2 for G1 ground motion records, the MARS at the funamental period of the MSSS bridge with steel girders is higher than that of the MSSS concrete bridge. Since the periods of the two continuous bridges is close to each other, the MARS at the periods of the bridges are not significanlty different. The period of the single span steel

bridge is located on almost the peak of the MARS in the case of Memphis and St. Louis. Therefore, the MARS at the period of the single span steel bridge is higher that that of the single span concrete bridge.

Table 5.1 Modal Properties of the Typical Bridges

	MSSS Bridge					
	Steel Girders			**Concrete Girders**		
No. of Mode	Period (sec)	Effective Modal Mass		Period (sec)	Effective Modal Mass	
		Longitudinal (%)	Vertical (%)		Longitudinal (%)	Vertical (%)
1st	**0.271**	**81.3**	0.0	**0.516**	**80.6**	0.0
2nd	0.181	0.0	30.9	0.252	0.0	0.0
3rd	0.147	1.0	0.0	0.241	0.0	36.0
4th	0.080	10.9	0.0	0.237	13.9	0.0
5th	0.076	0.0	0.0	0.117	0.0	0.0
	MS Continuous Bridge					
	Steel Girders			**Concrete Girders**		
No. of Mode	Period (sec)	Effective Modal Mass		Period (sec)	Effective Modal Mass	
		Longitudinal (%)	Vertical (%)		Longitudinal (%)	Vertical (%)
1st	**0.414**	**94.5**	0.0	**0.322**	**91.3**	0.0
2nd	0.380	0.0	0.4	0.165	0.0	21.5
3rd	0.255	0.0	4.0	0.095	4.5	0.0
4th	0.191	0.0	57.0	0.094	0.0	2.3
5th	0.096	0.0	0.2	0.061	1.0	0.0
	Single Span Bridge					
	Steel Girders			**Concrete Girders**		
No. of Mode	Period (sec)	Effective Modal Mass		Period (sec)	Effective Modal Mass	
		Longitudinal (%)	Vertical (%)		Longitudinal (%)	Vertical (%)
1st	0.451	0.0	84.1	0.522	0.0	84.1
2nd	0.113	0.0	0.0	**0.389**	**100.0**	0.0
3rd	**0.099**	**100.0**	0.0	0.131	0.0	0.0
4th	0.050	0.0	9.1	0.058	0.0	9.1
5th	0.028	0.0	0.0	0.033	0.0	0.0

(a) 1st Mode Shape (T=0.271 sec.) of MSSS Steel Bridge

(b) 1st Mode Shape (T=0.516 sec.) of MSSS Concrete Bridge

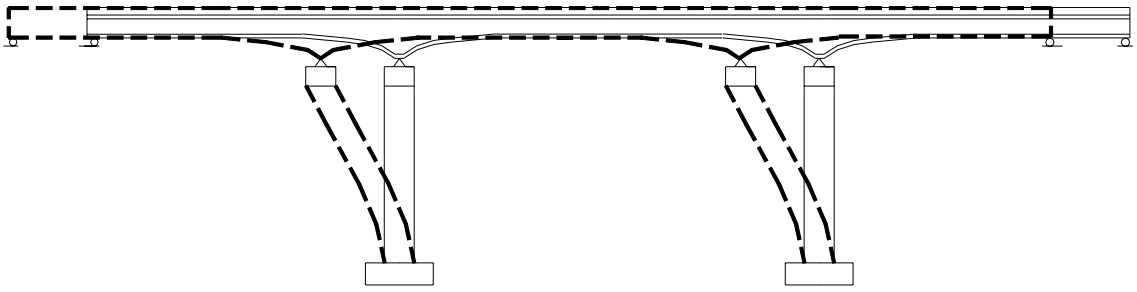

(c) 1st Mode Shape (T=0.414 sec.) of MS Continuous Steel Bridge

(d) 1st Mode Shape (T=0.322 sec.) of MS Continuous Concrete Bridge

Figure 5.1 First Mode Shape of Typical Bridges in Mid-America

(e) 1st Mode Shape (T=0.451 sec.) of Single Span Steel Bridge

(f) 1st Mode Shape (T=0.522 sec.) of Single Span Concrete Bridge

Figure 5.1 First Mode Shape of Typical Bridges in Mid-America

In Figure 5.3 for G2 ground motion records, since the period of the MSSS steel bridge is located on almost the peak of the MARS of Memphis and Carbondale, and the period of the MSSS concrete bridge is deviated from the peak of the two ground motions, the MARS of the MSSS steel bridge is larger than that of the MSSS concrete bridge. The MARS of the two continuous bridges is also similar in this case. The period of the single span steel bridge is placed on exactly the peak of the MARS for St. Louis. Hence, the MARS of the single span steel bride for St. Louis is about two times that of the single span concrete bridge. However, for the Memphis and Carbondale ground motions, the MARS of the single span concrete bridge is larger than that of the steel bridge.

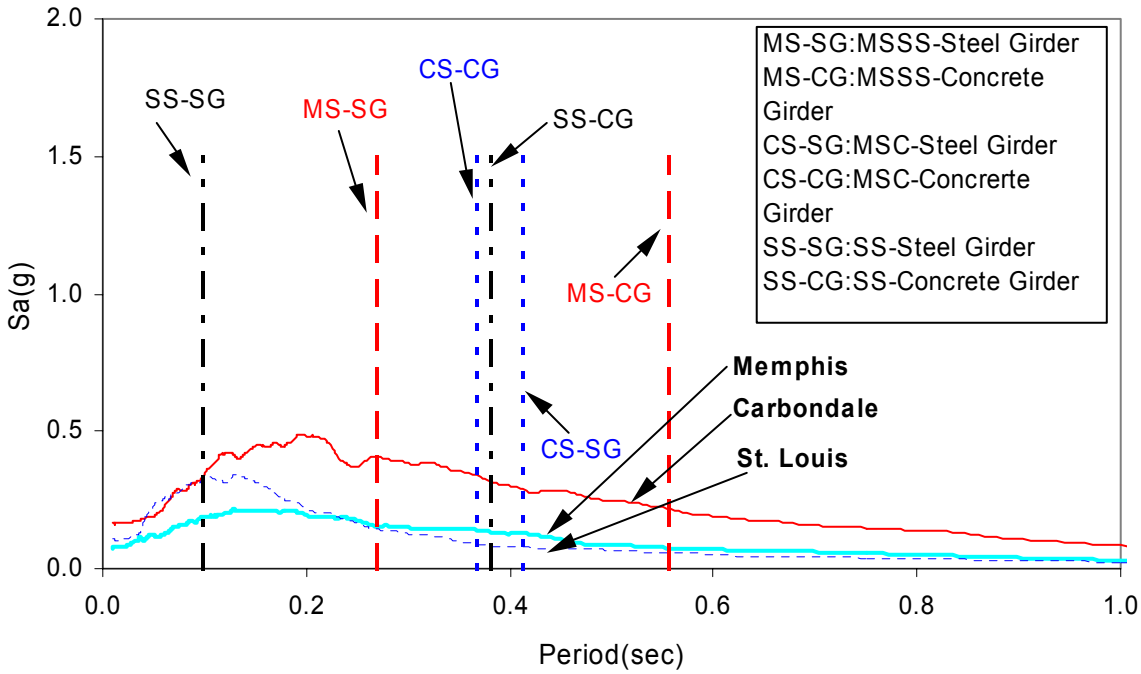

Figure 5.2 Location of the Fundamental Period of the Typical Bridges in the Longitudinal Direction with MARS of G1

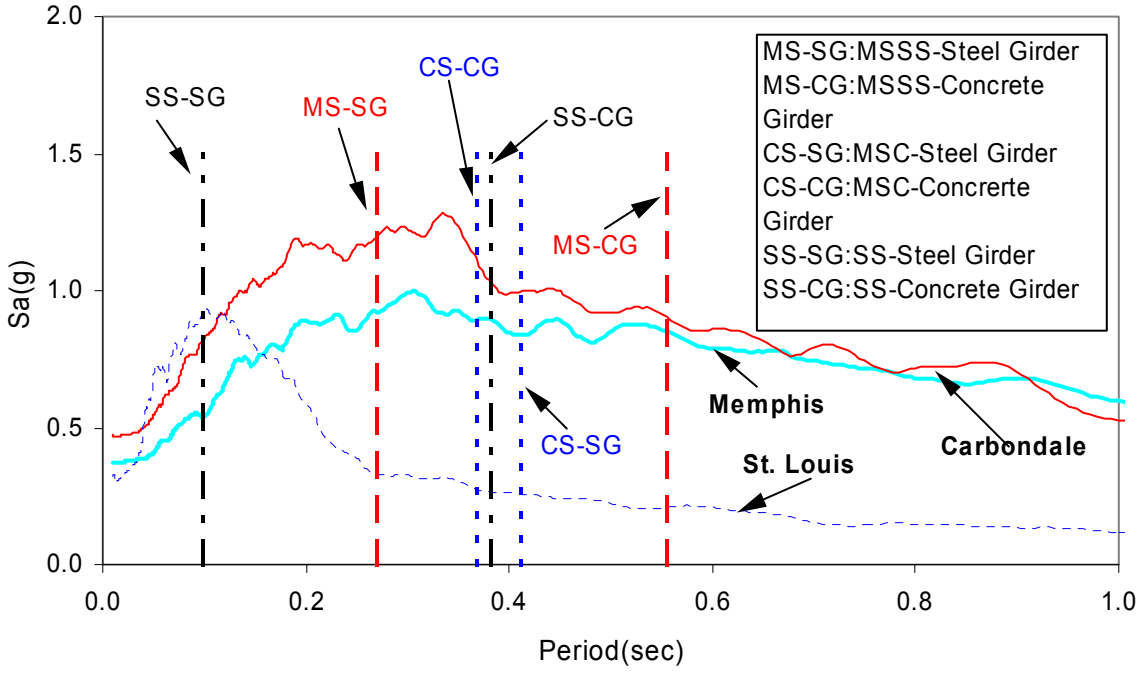

Figure 5.3 Location of the Fundamental Period of the 6 Bridges in the Longitudinal Direction with MARS of G2

5.2 Seismic Response Analysis of Typical Bridges

The seismic response of each type of bridge will be discussed in this section. Response histories as well as force-displacement plots are presented to illustrate the seismic behavior of the bridges. The #5 record from the G2 Carbondale suite having the PGA of 0.6g is used in the analysis.

- **MSSS Steel Bridge**

Figure 5.4 shows the responses of interest for the analyses. As shown below, the critical deformation responses are the column drift and ductility, hinge opening at the abutments and intermediate hinges, and bearing deformation. Other responses evaluated include the abutment forces ad impact forces between the decks.

Figure 5.5 shows the displacement histories and force-displacement curves for critical responses for the MSSS steel bridge. The hinge openings, Δ_1 and Δ_3, have maximum displacements of 65.4 mm (2.6 in.) and 47.7 mm (1.9 in.), respectively. The opening at Hinge 2 is relatively small because Deck 2 and 3 move in-phase. Since the typical seat width on bridges range from 102 mm (4.0 in.) to 250 mm (10 in.), this bridge is not in the jeopardy of collapse due to unseating. Figure 5.5b shows the column drift and corresponding displacement. The drift is the top displacement of a column divided by the length of the column. The drift of Column 1 is larger than that of Column 2, since Column 1 responds with Deck 2 which is heavier than Deck 3. The second reason for the larger displacement in Column 1 is the moving tolerance. Deck 2 on Column 1 has more

moving tolerance than Deck 3 on Column 2. The drift ratio of Column 1 approaches 1% which has been shown to be the critical value where lap splices may occur in nonseismically designed bridges in Mid-America (Lin et al., 1998).

FXB: Fixed Steel Bearing, EXB: Expansion Steel Bearing

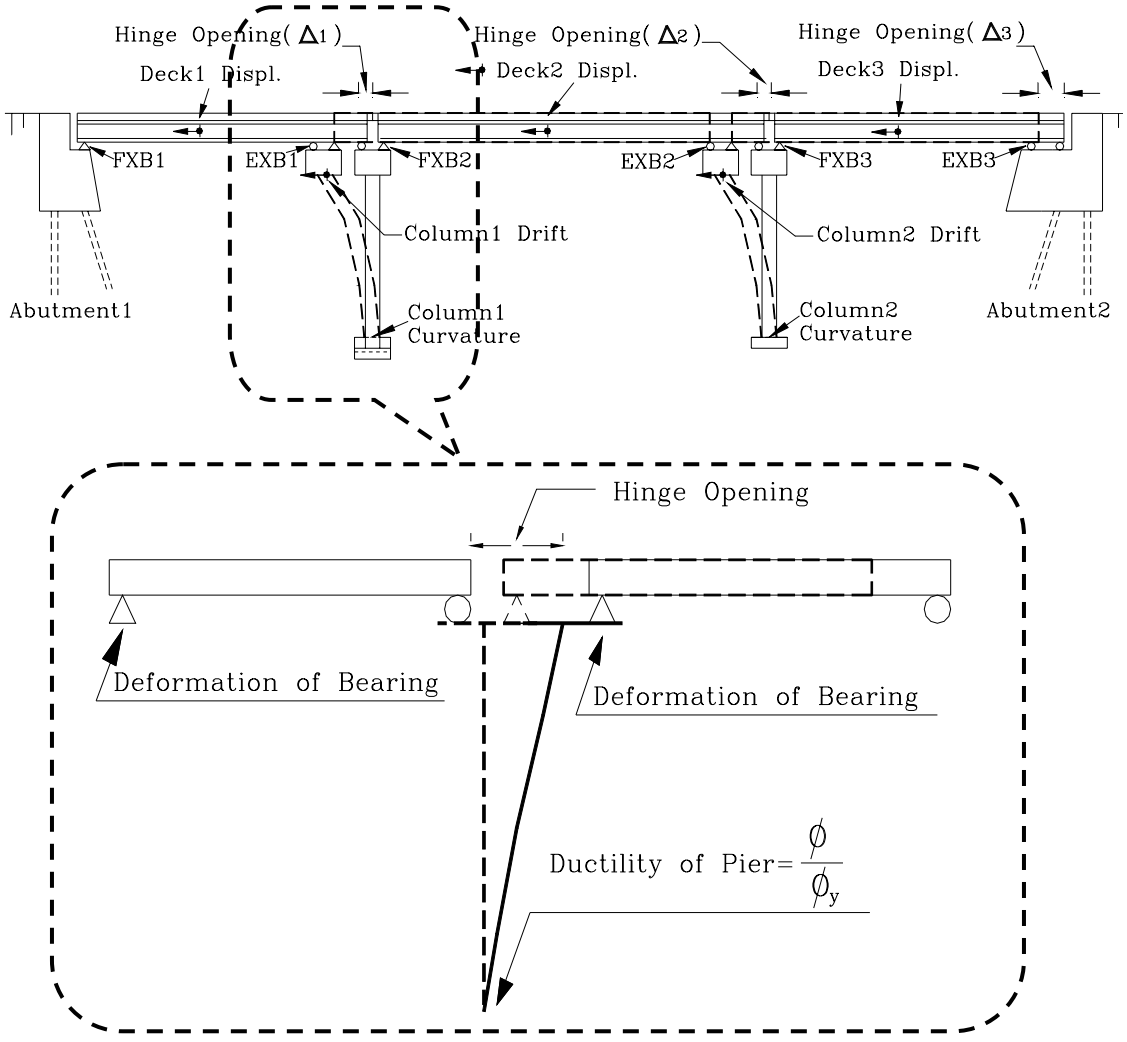

Figure 5.4Critical Responses of Interest for MSSS Steel Bridge

Figure 5.5c shows the force-displacement responses for the fixed bearings on the bridge. The results show considerable inelastic response in Fixed Bearing 1. The 18 mm (0.7 in.) deformation is beyond the point where yielding would occur, resulting in failure of the bearing. This large deformation is primarily due to the impact force generated on Deck 2. Deck 2 impacts into Deck 1, transferring large forces to the fixed bearing at the abutment.

The deformation of the expansion bearings, which also corresponds to the hinge openings, is shown in Figure 5.5c. The maximum deformation of Bearing 1, 65.4 mm (2.57 in.), exceeds the criterion of the stable limit, 58.2 mm (2.30 in.), as was calculated in the chapter 4.

Figure 5.5d shows the behavior of the impact elements between decks. These large impact forces are developed when the gap, 25.4 mm (1.0 in.), closes and the decks come into contact. These forces are transferred through the deck and into the bearings and/or columns.

Figure 5.5e shows the response of the abutments. The force from the bearing on the abutments dominates the behavior of the abutments in pulling action. However, in pushing action, the pounding force governs the behavior. Therefore, Abutment 1, which has fixed bearings, has large forces and deformations in the both actions. However, Abutment 2, which has the expansion bearings, has small force in pulling action, but it has large forces from pounding.

Figure 5.5f shows the moment-curvature response for the two columns. As shown in the figure, both columns have yielded and experience the pinching effect.

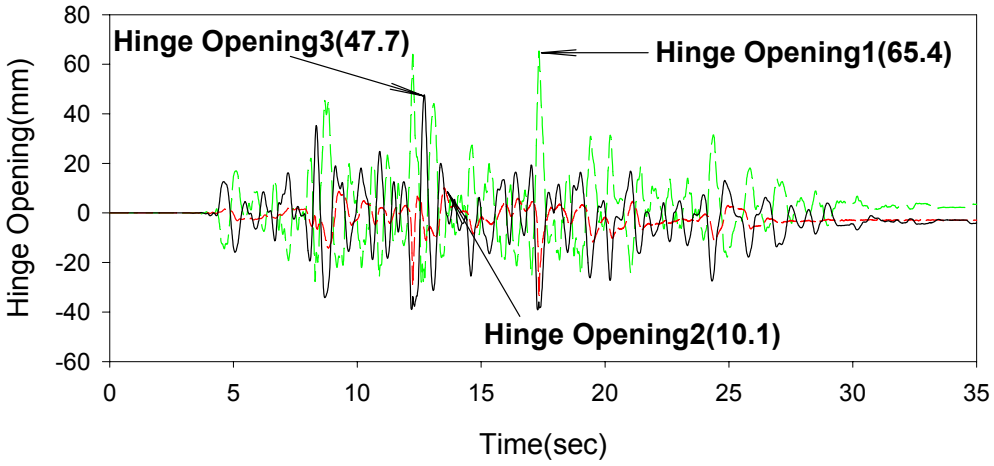

Figure 5.5a Time Histories of Hinge Opening of MSSS Steel Bridge

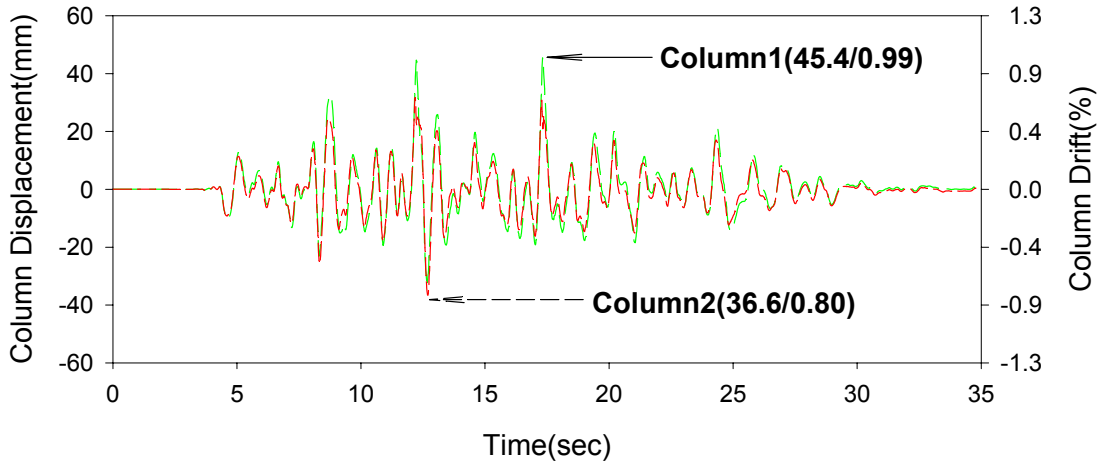

Figure 5.5b Time Histories of Column Drift of MSSS Steel Bridge

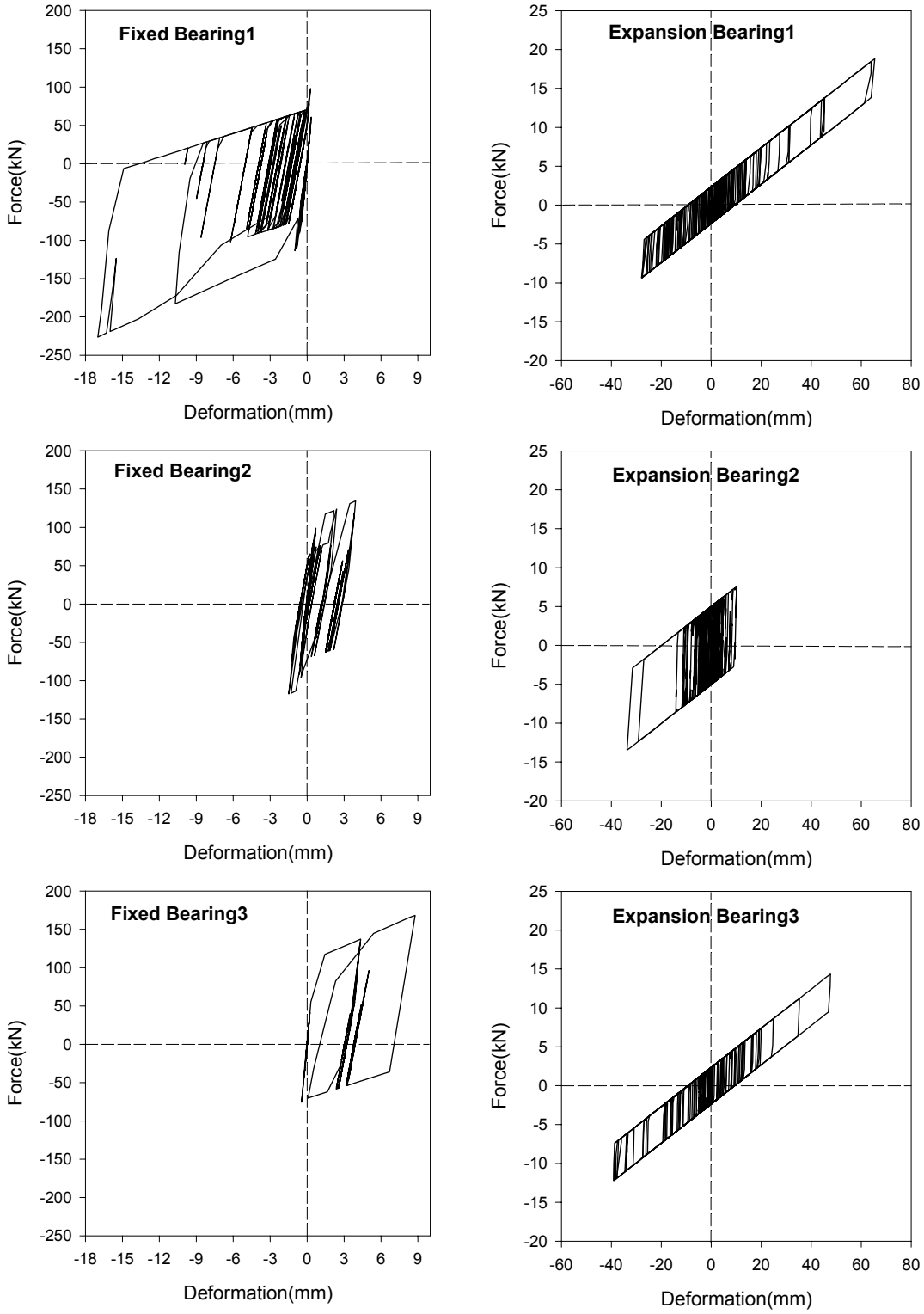

Figure 5.5c Hysteresis Loops of Fixed & Expansion Bearings in MSSS Steel Bridge

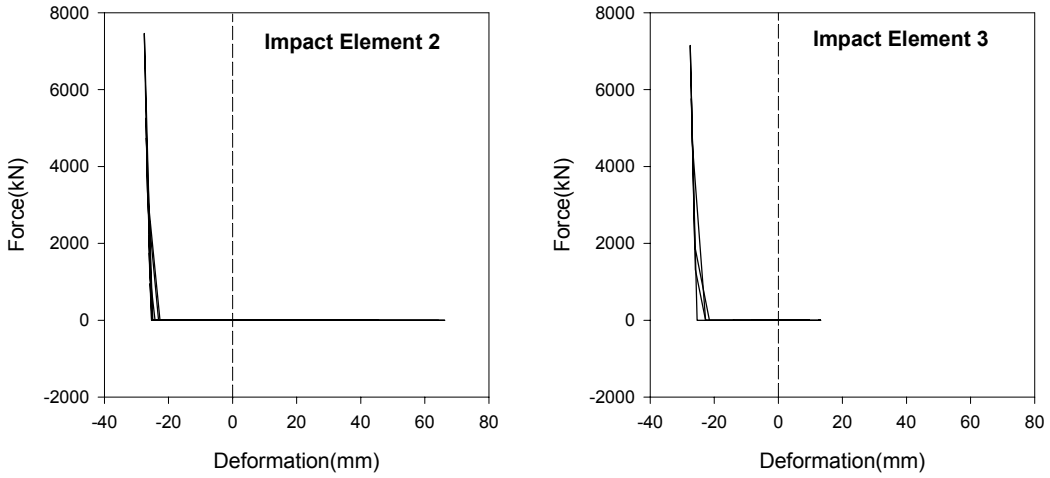

Figure 5.5d Hysteresis Loops of Impact Elements in MSSS Steel Bridge

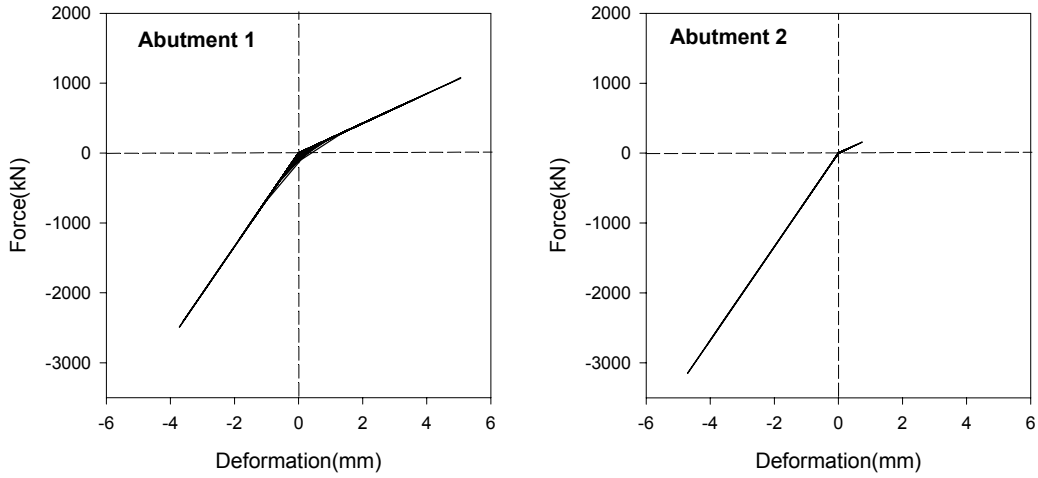

Figure 5.5e Hysteresis Loops of Abutments in MSSS Steel Bridge

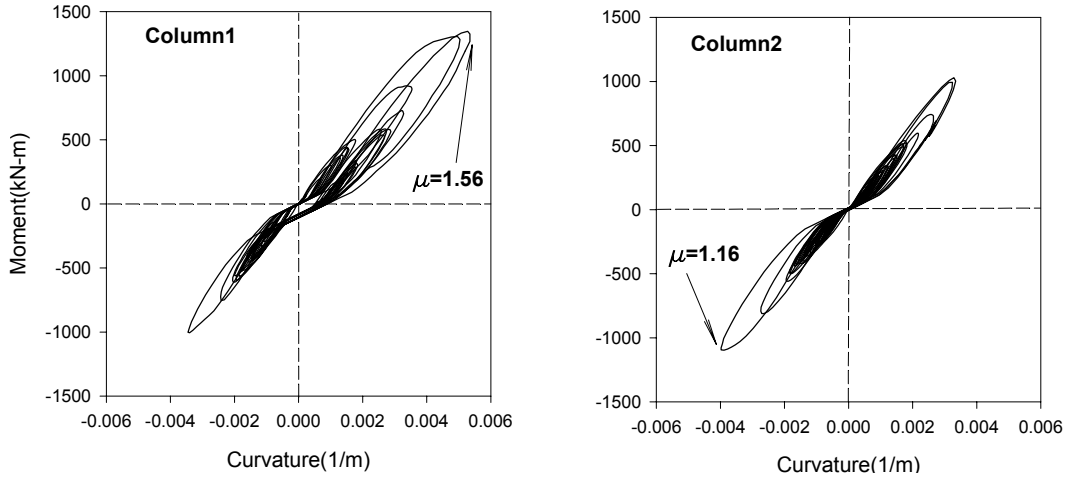

Figure 5.5f Hysteresis Loops of Columns in MSSS Steel Bridge

• **MSSS Concrete Bridge**

In the MSSS concrete bridge, response quantities to be determined are similar to those in the MSSS steel bridge, as illustrated in Figure 5.6. Figure 5.7a shows the relative hinge opening at the abutment for the MSSS concrete bridge. The large hinge opening in the MSSS concrete bridge compared with the MSSS steel bridge is due to both its longer natural period and the nonlinear behavior of the dowel bars.

Dowels usually are not strong enough to resist deck movement against moderate or strong seismic loading. As shown in Figure 5.7d and 5.7e, the dowels are fractured at every hinge, as indicated by the decrease in strength and stiffness in the dowel element. Subsequent, the displacement of decks in the MSSS concrete bridge becomes large since the only resistance is provided by friction in the elastomeric pads. The column drifts are similar to that in the MSSS steel bridge but approach the point where lap splice failure may occur.

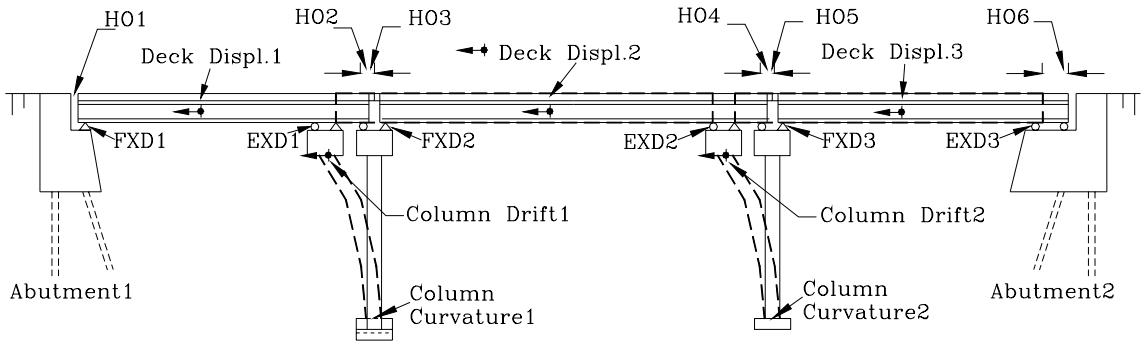

HO: Hinge Opening, FXD: Fixed Type Dowel, EXD: Expansion Type Dowel

Figure 5.6 Response of MSSS Concrete Bridge

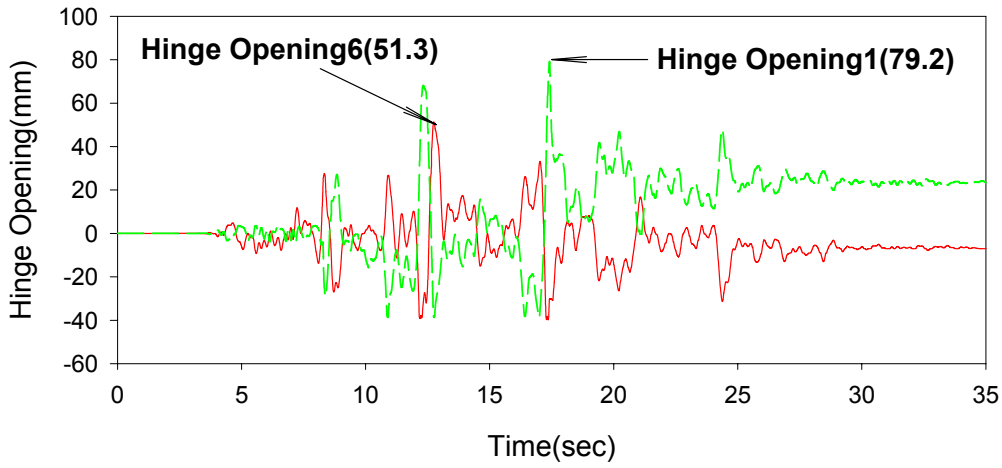

Figure 5.7a Time Histories of Hinge Opening of MSSS Concrete Bridge

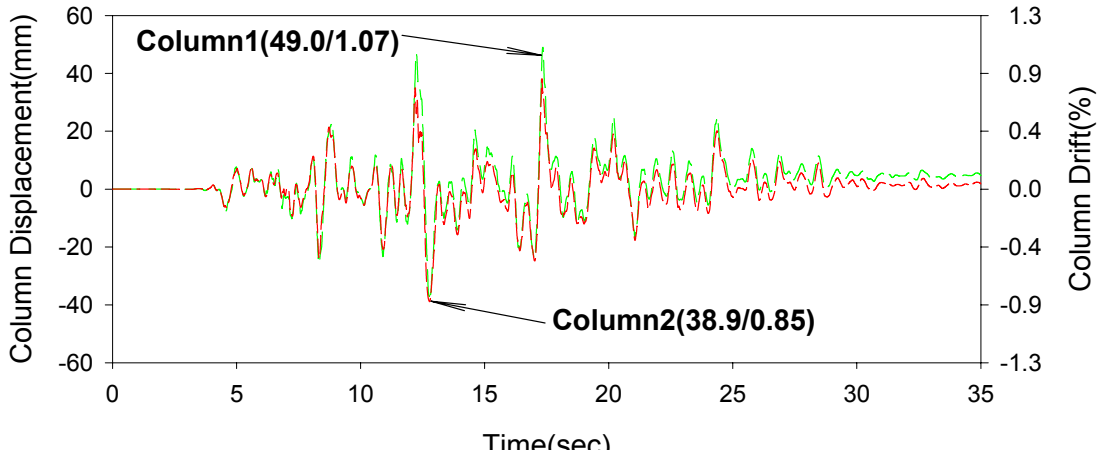

Figure 5.7b Time Histories of Column Drift of MSSS Concrete Bridge

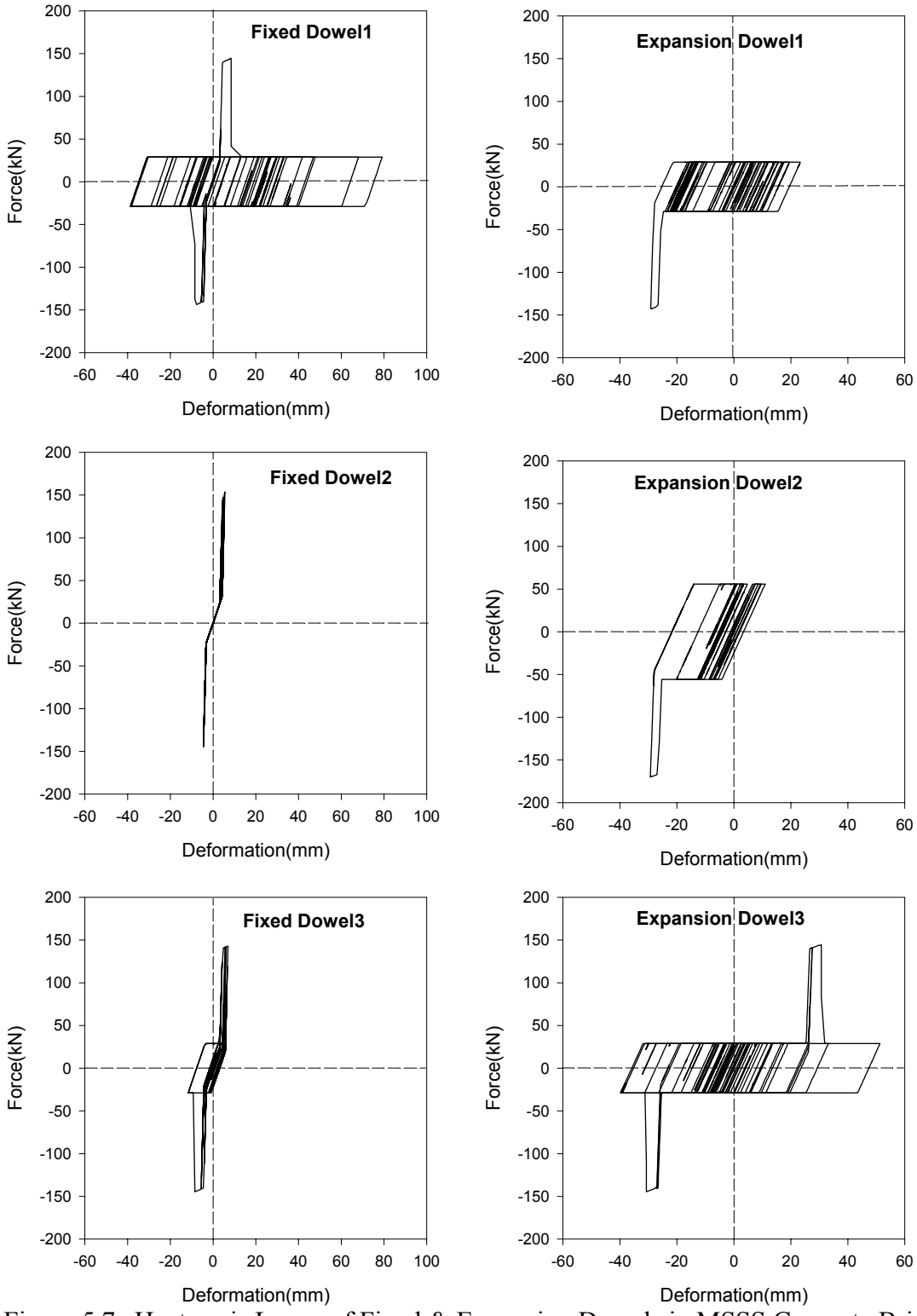

Figure 5.7c Hysteresis Loops of Fixed & Expansion Dowels in MSSS Concrete Bridge

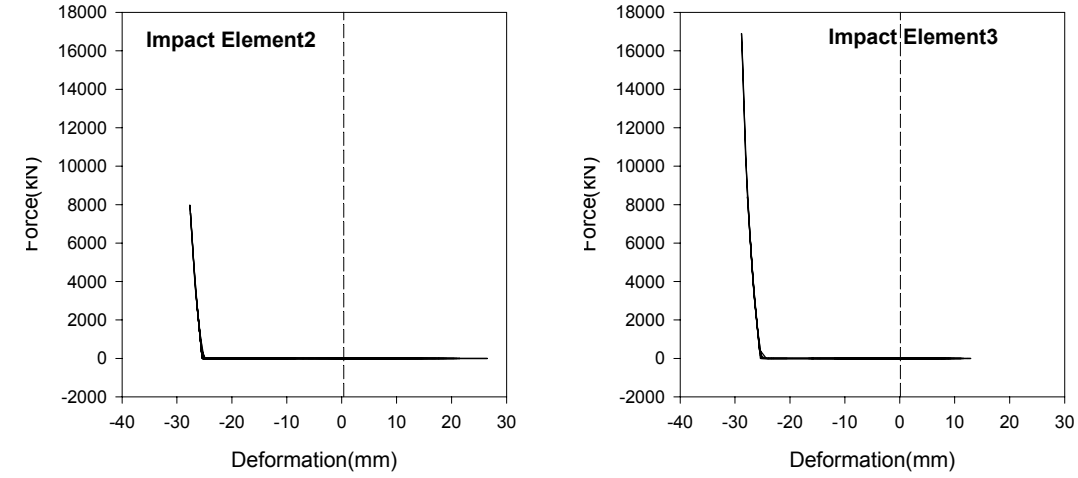

Figure 5.7d Hysteresis Loops of Impact Elements in MSSS Concrete Bridge

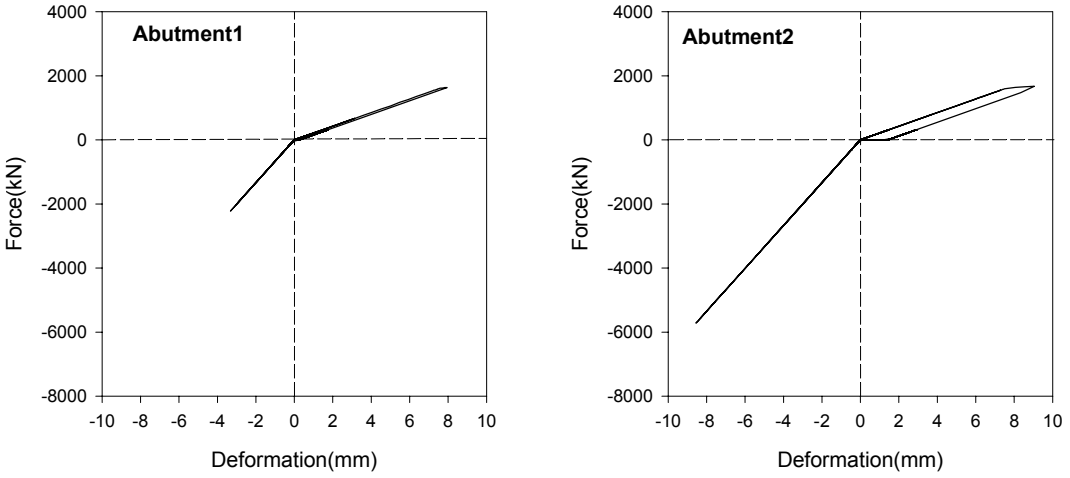

Figure 5.7e Hysteresis Loops of Abutments in MSSS Concrete Bridge

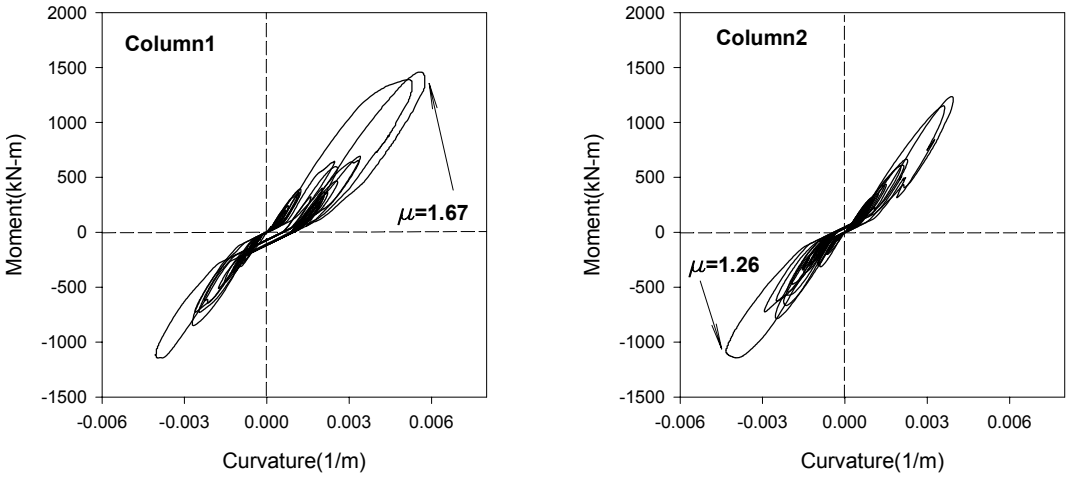

Figure 5.7f Hysteresis Loops of Columns in MSSS Concrete Bridge

- **MSC Steel Bridge**

Figure 5.8 shows the responses of the interest in the multi-span continuous steel bridge. In this bridge, fixed bearings are located on piers, and expansion bearings at the abutments. Figure 5.9 shows the time histories and hysteresis plots of the response of the bridge.

FXB: Fixed Steel Bearing, EXB: Expansion Steel Bearing

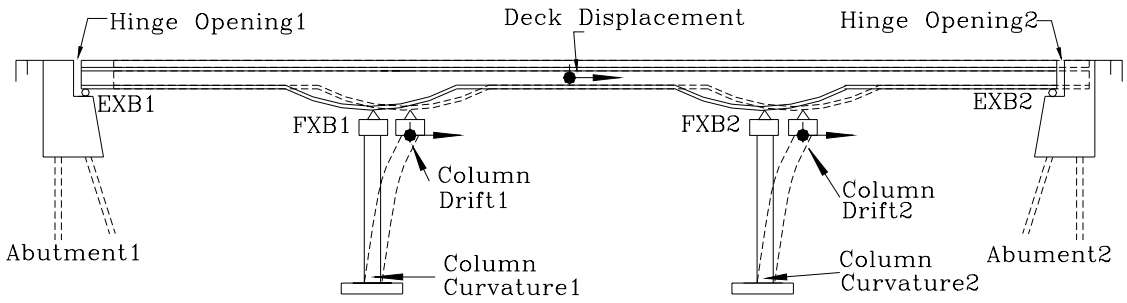

Figure 5.8 Response of MS Continuous Steel Bridge

The MS continuous steel bridge has large deck displacement and hinge openings compared to the MSSS steel and concrete bridge as a result of the large gap size at the abutments (76.2 mm, 3.0 in.). However, the maximum hinge opening does not exceed the collapse point of 254 mm (10 in.). The drift and ductility exceed 1% and are larger than that of the MSSS bridges.

The deformation of fixed bearings is small since the bearings are located on the flexible columns as shown in Figure 5.9c. However, the deformation of the expansion

bearings exceeds the failure criterion of the bearing, 58.2 mm (2.3 in.). In abutments, the deformation in active (pulling) action is small, but, in passive (pushing) action, the deformation is large due to the pounding between the deck and the abutments. Abutment 1 is weaker in passive action than Abutment 2 as shown in Table 4.10; the first yield deformation of Abutment 1 is 14.6 mm (0.58 in.), and the yield deformation of Abutment 2 is 45.7 mm (1.80 in.). Thus, only Abutment 1 has yielded in passive action as shown in Figure 5.9g.

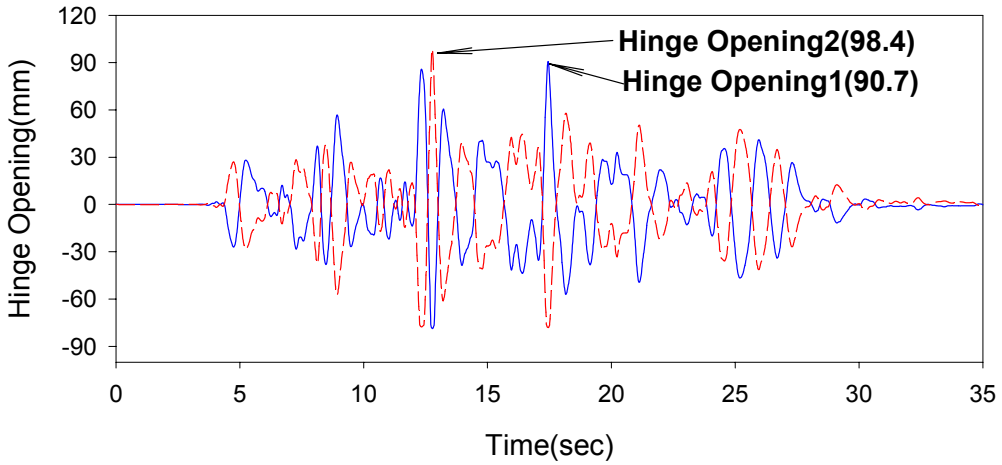

Figure 5.9a Time Histories of Hinge Opening in MSC Steel Bridge

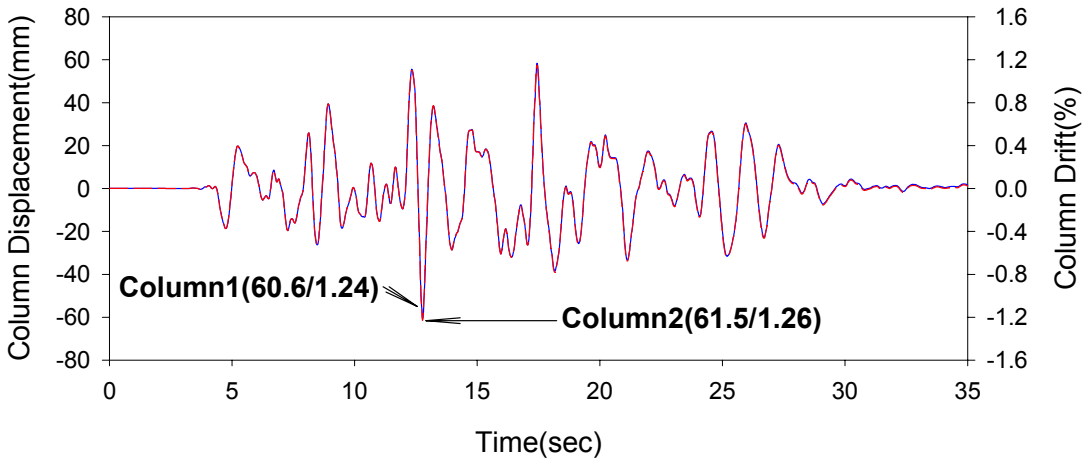

Figure 5.9b Time Histories of Column Drift in MSC Steel Bridge

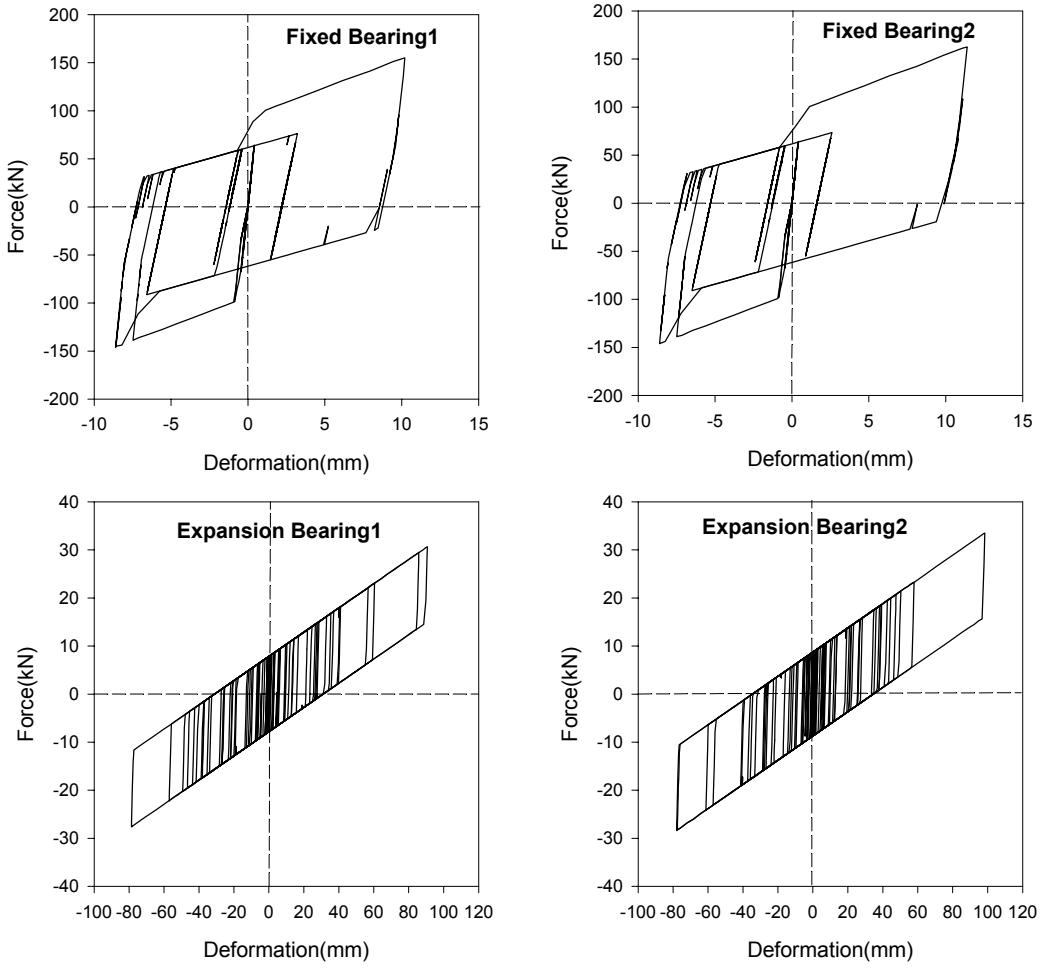

Figure 5.9c Hysteresis Loops of Fixed & Expansion Bearings in MSC Steel Bridge

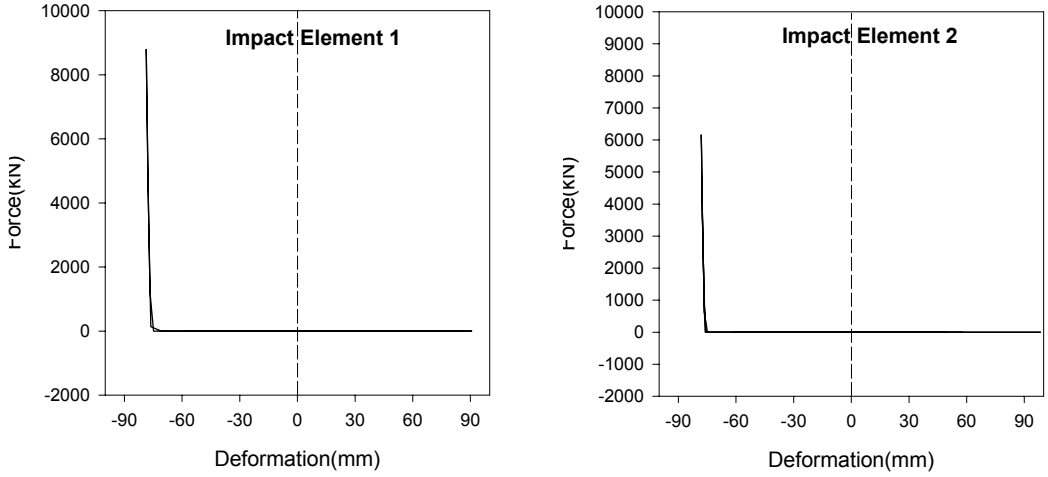

Figure 5.9d Hysteresis Loops of Impact Elements in MSC Steel Bridge

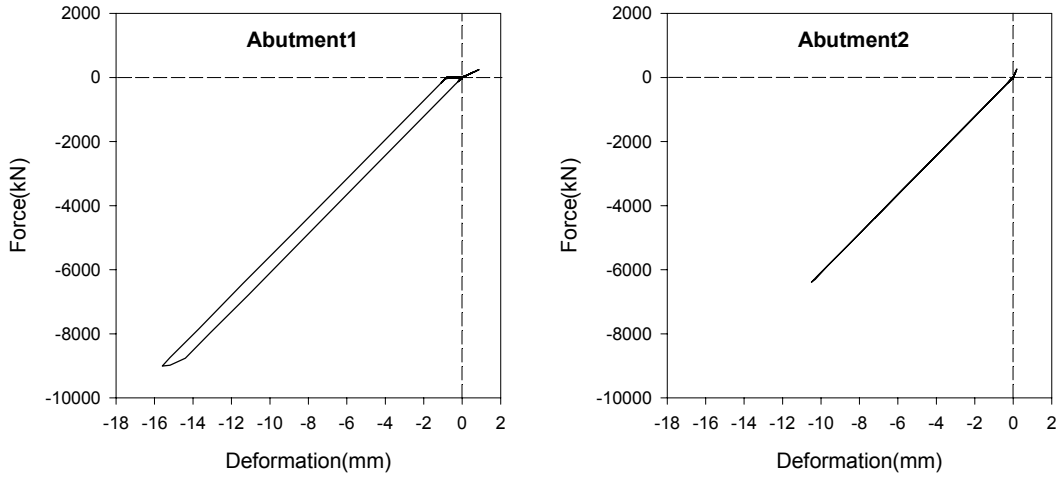

Figure 5.9e Hysteresis Loops of Abutments in MSC Steel Bridge

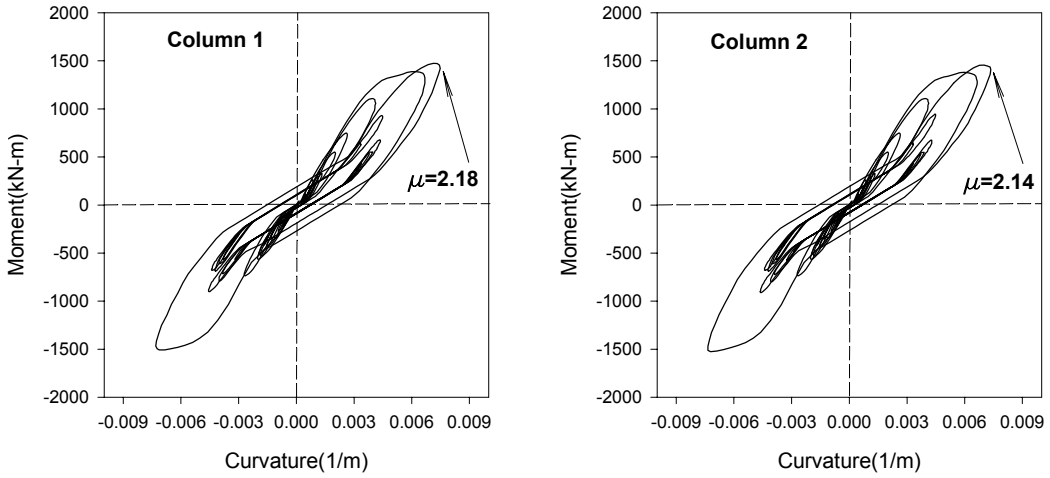

Figure 5.9f Hysteresis Loops of Columns in MSC Steel Bridge

- **MSC Concrete Bridge**

As mentioned in chapter 4, the MS continuous concrete bridge is made from the MSSS concrete bridge by casting a parapet between decks. This is commonly done to make the bridge continuous and reduce dead and live load moments. As shown in Figure 5.10, the continuity of the bridge modifies the response of the MSC concrete bridge

greatly compared to that of the MSSS concrete bridge. The continuity removes the gaps between decks, thereby reducing the moving tolerance of the deck in the bridge. This can improve the response of the bridge. Deck displacement, hinge opening, and column drift decrease sharply. The ductility of the columns in Figure 5.10h is less than 1.0. The columns of the MS continuous concrete bridge do not yield, while the other types of bridges have the yielded columns.

The dowels in the fixed bearing are fractured, but dowels in expansion type are not activated. Since the maximum displacement of the deck is smaller than the gap between the deck and abutments, there is not any pounding between them. Thus, impact elements are not activated. The deformation of the abutments in passive action is small because of the absence of impact on abutments. In active action, Abutment 1 yields, but Abutment 2 remains elastic. The fixed dowels with 3.2 mm (0.125 in.) slack are activated with small deck displacement. These activated dowels pull Abutment 1, resulting in yielding. However, since Expansion dowel 3, which has 25.4 mm (1.0 in.) slack, is not activated, only the small frictional force of rubber pads on Abutment 2 is acting on the abutment.

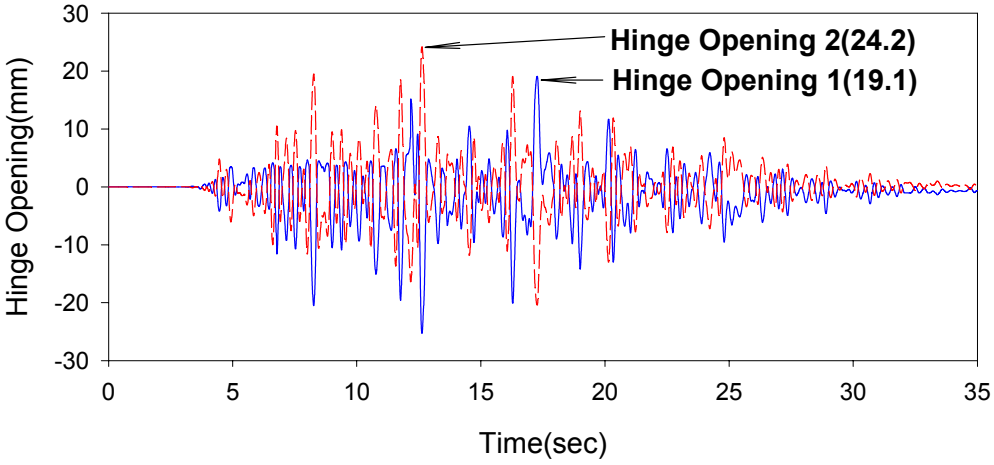

Figure 5.10a Time Histories of Hinge Openings in MSC Concrete Bridge

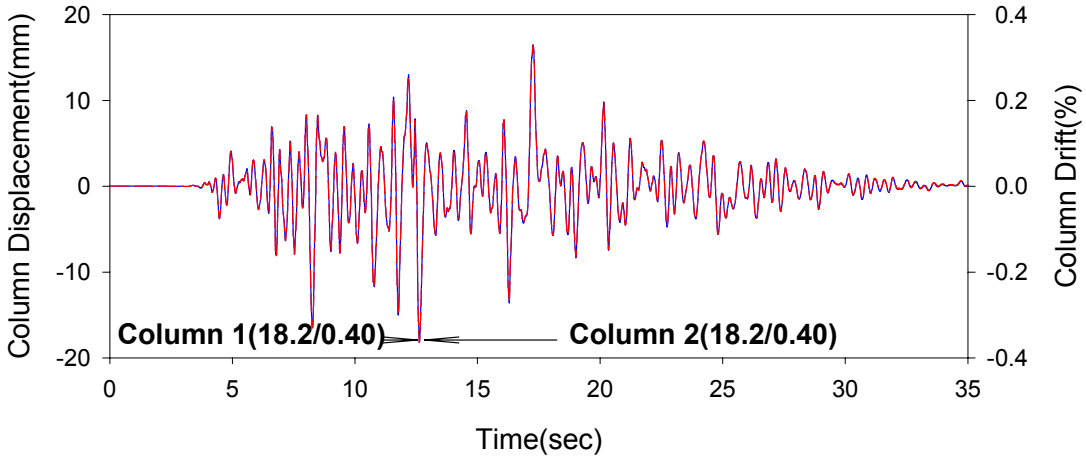

Figure 5.10b Time Histories of Column Drifts in MSC Concrete Bridge

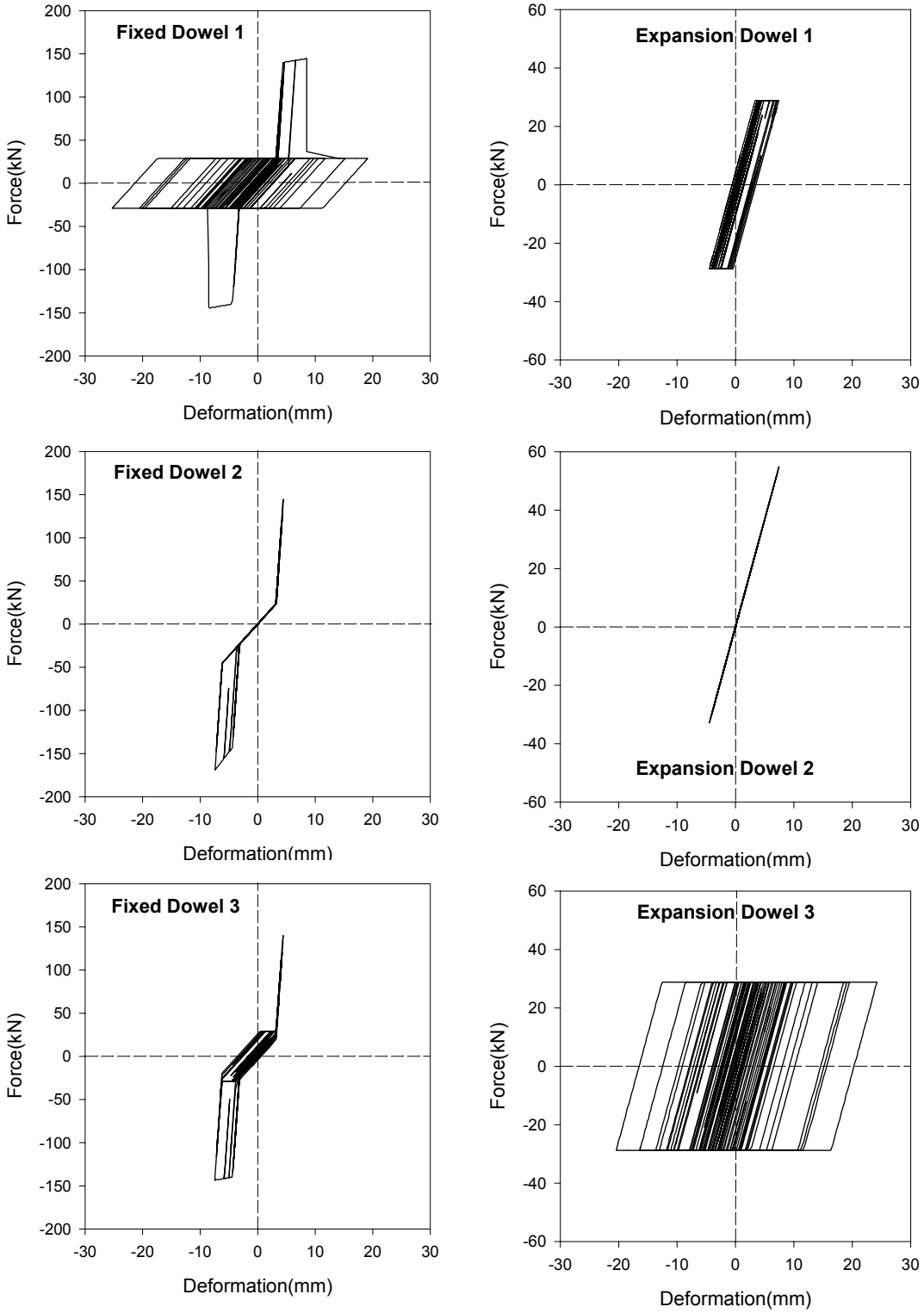

Figure 5.10c Hysteresis Loops of Fixed & Expansion Dowels in MSC Concrete Bridge

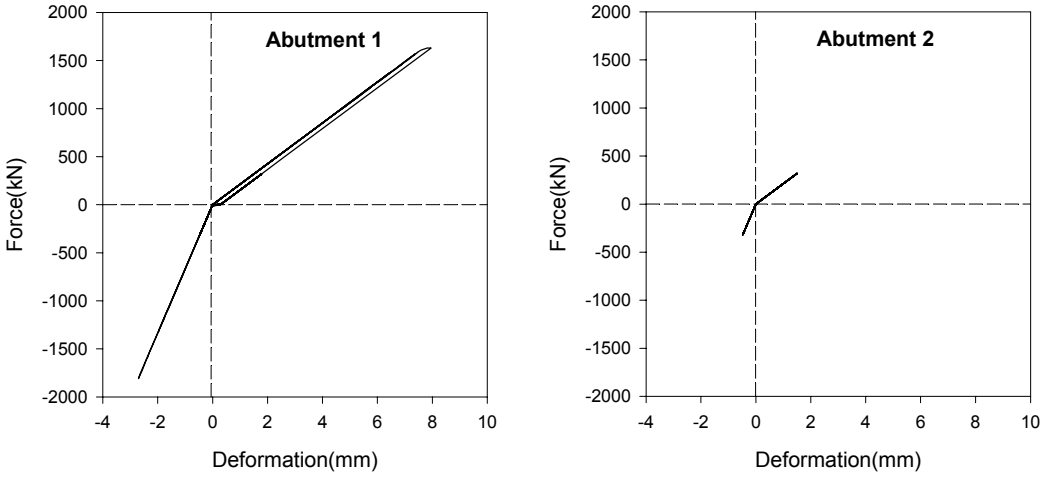

Figure 5.10d Hysteresis Loops of Abutments in MSC Concrete Bridge

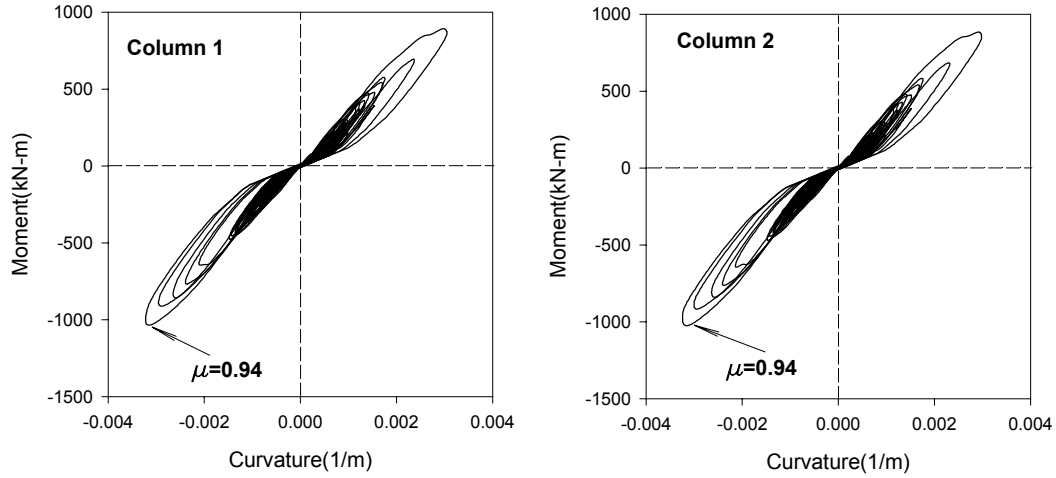

Figure 5.10e Hysteresis Loops of Columns in MSC Concrete Bridge

- **Single Span Steel Bridge**

In the single span bridge, the inertia force in the deck is transferred to the abutments through the fixed and expansion bearings. Therefore, the bearings are a critical element in the response of the SS steel bridge. Figure 5.11 shows the deformation response of the

fixed and expansion bearings. The maximum deformation of the fixed bearing exceeds the yield point, but is less than the ultimate deformation. The abutment response remains in the elastic range.

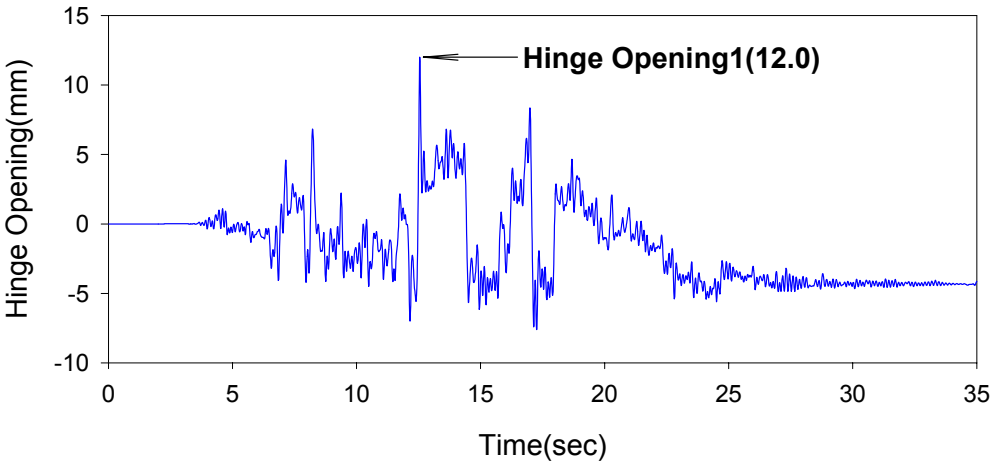

Figure 5.11a Time Histories of Hinge Opening in SS Steel Bridge

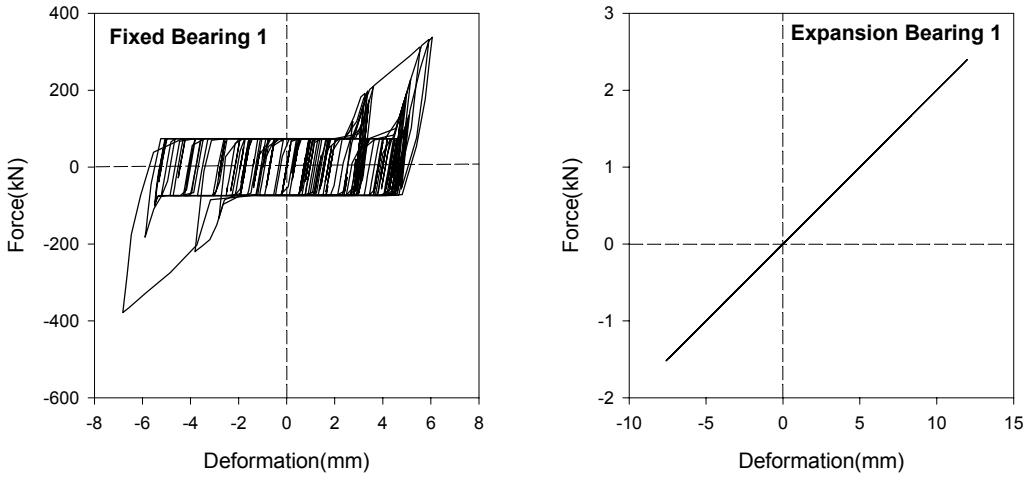

Figure 5.11b Hysteresis Loops of Fixed & Expansion Bearings in SS Steel Bridge

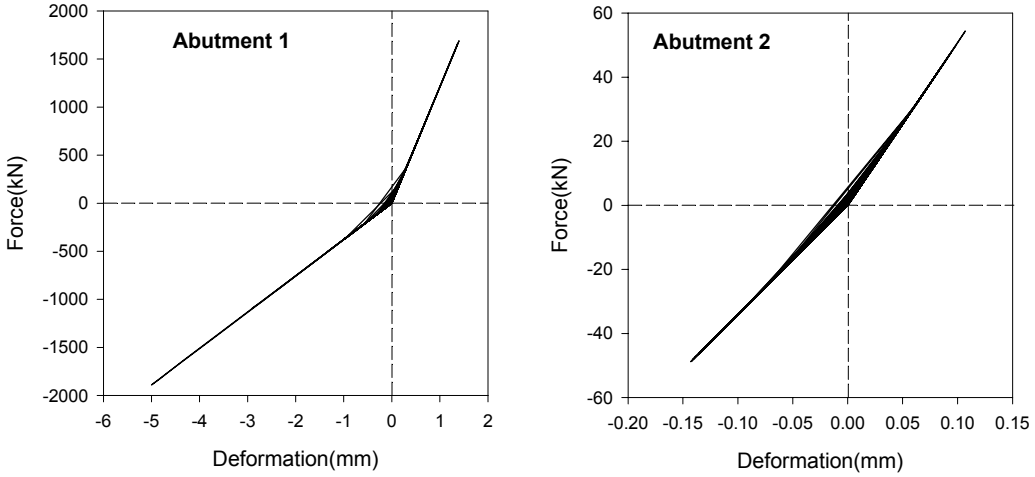

Figure 5.11c Hysteresis Loops of Abutments in SS Steel Bridge

- **Single Span Concrete Bridge**

As previously mentioned, dowels are not strong enough to restrain the deck movement in the single span concrete bridge. The two dowels, fixed and expansion type, fracture, resulting in large deck movements. Therefore, the deck displacement and the hinge opening are very large. However, the maximum deck displacement is less than the gap size on the abutments, 101.6 mm (4.0 in.), thus impact elements are not activated.

Without pounding, both abutments are in the elastic range in passive action. Even though the dowels are fractured, the abutments do not yield in active action. The MSSS and the MS continuous concrete bridge have 11 girders and 22 dowels on each abutment. The single span concrete bridge, however, has 5 girders and 11 dowels on each abutment.

Therefore, the total force delivered from dowels to abutments in the single span concrete bridge is smaller than that in the MSSS or MS continuous concrete bridge.

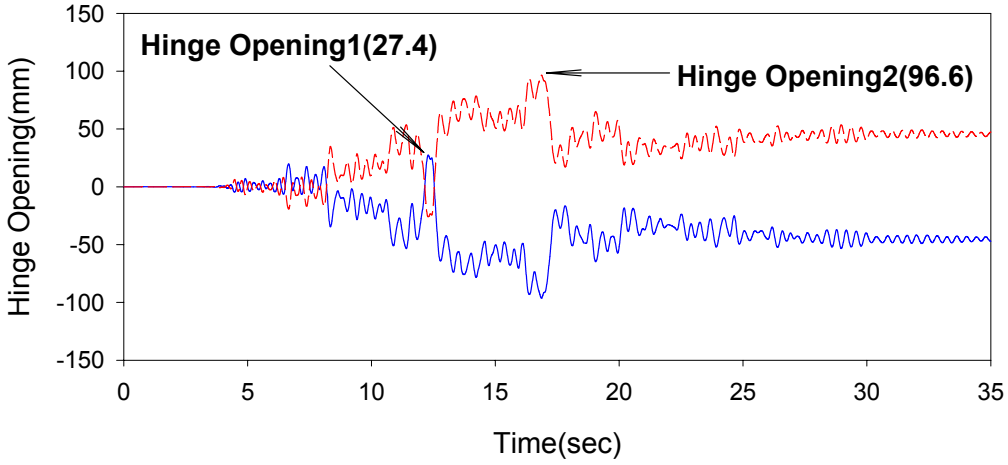

Figure 5.12a Time Histories of Hinge Opening in SS Concrete Bridge

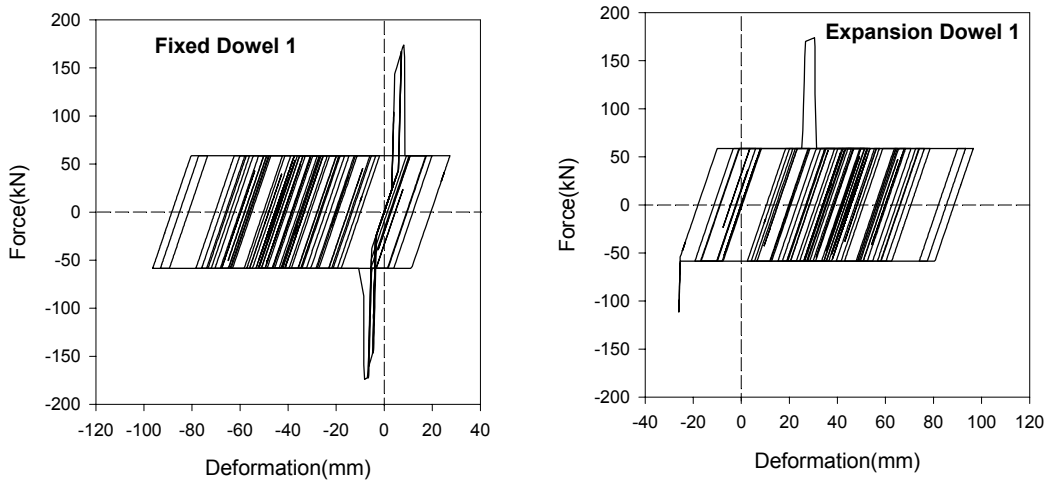

Figure 5.12b Hysteresis Loops of Fixed & Expansion Dowels in SS Concrete Bridge

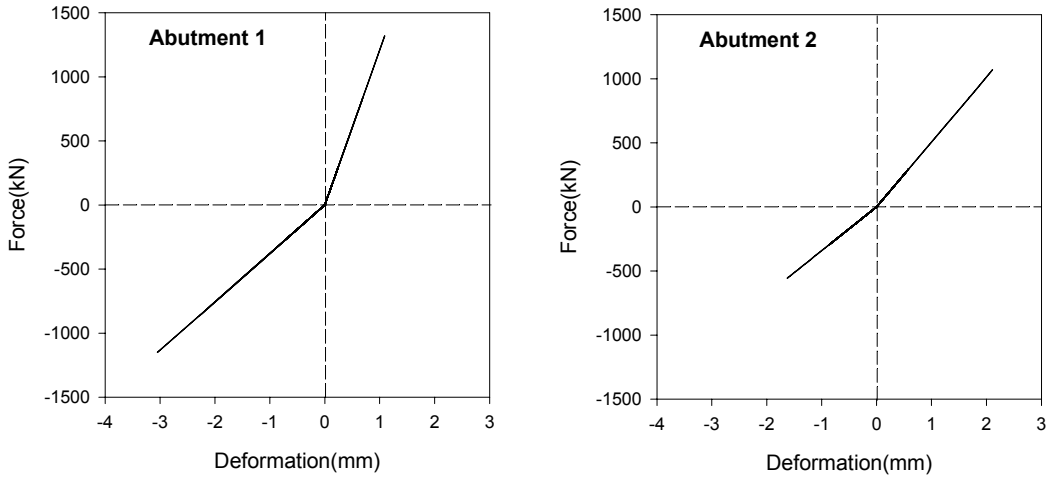

Figure 5.12c Hysteresis Loops of Abutments in SS Concrete Bridge

5.3 Statistical Analysis of Typical Bridges Subjected to Ground Motions

The previous section presented the response of typical bridges to one ground motion record. The results highlighted the overall behavior of the bridges as well as the critical components. However, a more appropriate understanding of the seismic behavior of these typical bridges can be obtained by looking at the mean responses from a suite of ground motions. In this study, the mean and the standard deviation of the response for the suite of synthetic ground motions discussed in chapter 3 will be presented. Each bridge is subjected to the suite of ground motions listed in Tables 3.3, 3.4, and 3.5, which represents two hazard levels: 2% probability of exceedance in 50 years and 10% probability of exceedance in 50 years. For each bridge, the mean and the standard deviation of the responses are provided in Appendix B. In this section, the mean and the standard deviation are compared to the capacity of each component to estimate the damage-state of the component.

Each ground motion is applied in both longitudinal directions. The mean responses in the both directions are calculated, and the maximum of the two values is shown in the graphs and tables in Appendix B.

5.3.1 Performance of MSSS Steel Bridge

Figure 5.13 shows the mean and the standard deviation of the critical seismic responses for the MSSS steel bridge, for the 3 suites of ground motions and 2 hazard levels. For the G1 (10% PE in 50 years) ground motions, the responses of all the bridge components are very low and remain in the elastic range.

Using G2 (2% PE in 50 years) ground motions, the mean column drift varies from 0.16% in St. Louis to 0.86% for Carbondale. For all 3 ground motion suites, the response is less than that which would initiate lap splice failure, as discussed in section 5.2. In addition, the shears of the columns are well below the shear capacities. The maximum mean of the fixed bearings occurs at the first bearing. This occurs due to pounding between Deck 1 and Deck 2 as discussed in section 5.2. The mean values in the Memphis and Carbondale ground motions, 12.2 mm (0.48 in.) and 16.1 mm (0.63 in.), respectively, exceed the yield value for the fixed bearings, as defined above.

The expansion rocker bearings have mean values as large as 59.5 mm (2.34 in.) for the Carbondale suite of ground motions. As previously mentioned, this is slightly larger than the value corresponding to instability of the bearing, EXB-II. The maximum largest opening of 59.5 mm (2.34 in.), is much less than the typical allowable hinge seat of 102 mm (4 in.).

Table B1b shows that large forces are observed in the abutment in passive (pushing) action. These forces are primarily due to impact between the deck and abutments. In active (pulling) action, the large abutment force is transferred to Abutment 1 through Fixed Bearing 1. However, both abutments remain in the linear elastic range. The maximum force of the pile foundations is less than 20% of the ultimate value. However, the maximum moment reaches 86.8% of the yield point for the Carbondale suites of ground motions.

The coefficient of variation (COV) of the responses in Table B1 in Appendix B is generally less than 30%. However, in some responses, such as the deformation of

Abutment 2 in passive action and Fixed Bearing 3, the COV is very high. This is due to the highly nonlinear pounding behavior. For the G1 suites of ground motion and G2 of St. Louis, the COV is small because pounding of spans does not occur.

Moderate ground motions, G2 (2% PE in 50 years), usually lead to moderate damage on columns, expansion bearings, and fixed bearings. However, abutments are damaged slightly in active action and no damage in passive action. The moderate ground motions for St. Louis produce small responses compared with those from the ground motions for the other sites. It is noticeable, however, that G2 ground motions for St. Louis result in relatively large deformation at Abutment 1.

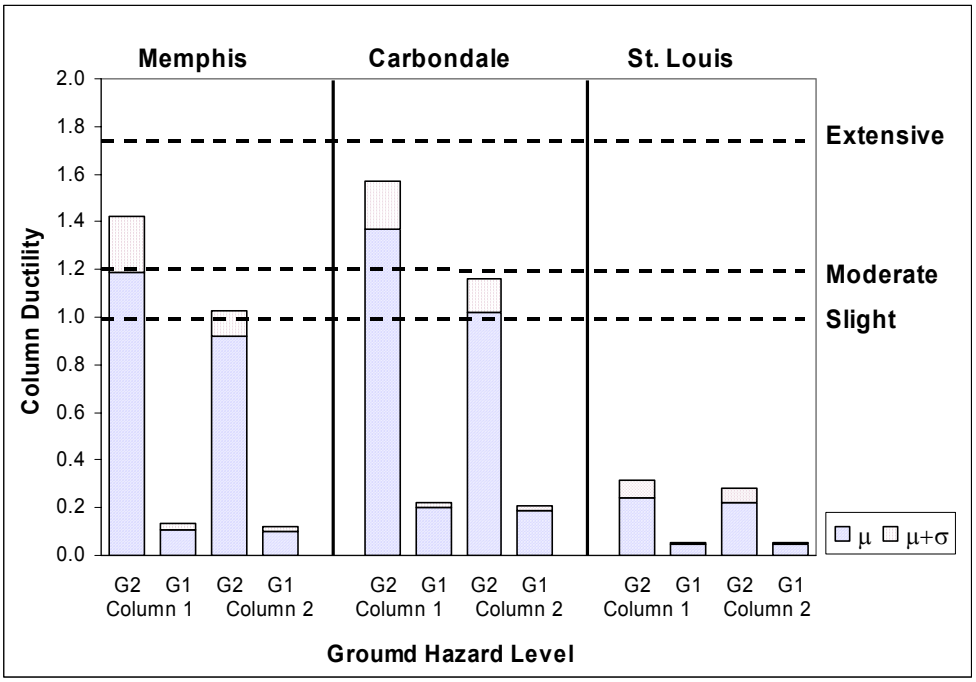

Figure 5.13a Response of Columns Ductility in MSSS Steel Bridge

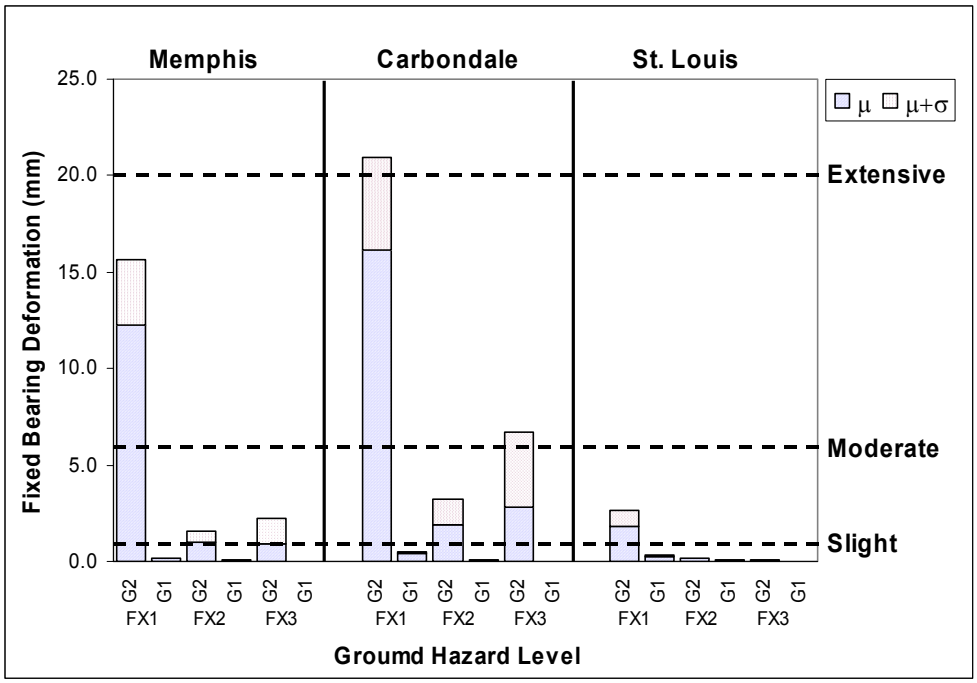

Figure 5.13b Response of Fixed Bearings Deformation in MSSS Steel Bridge

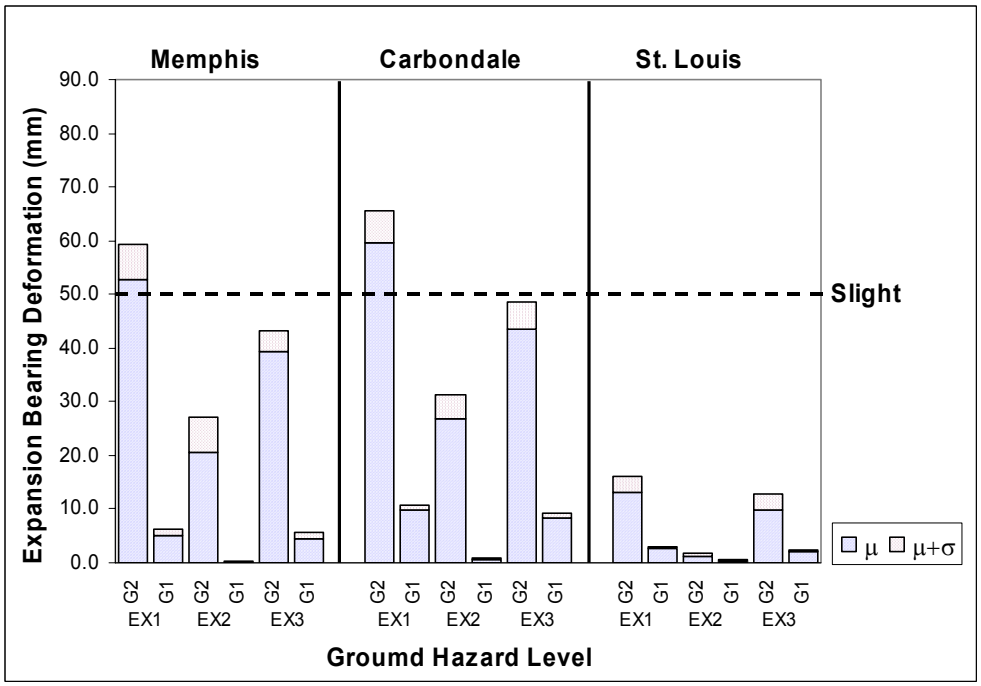

Figure 5.13c Response of Expansion Bearings Deformation in MSSS Steel Bridge

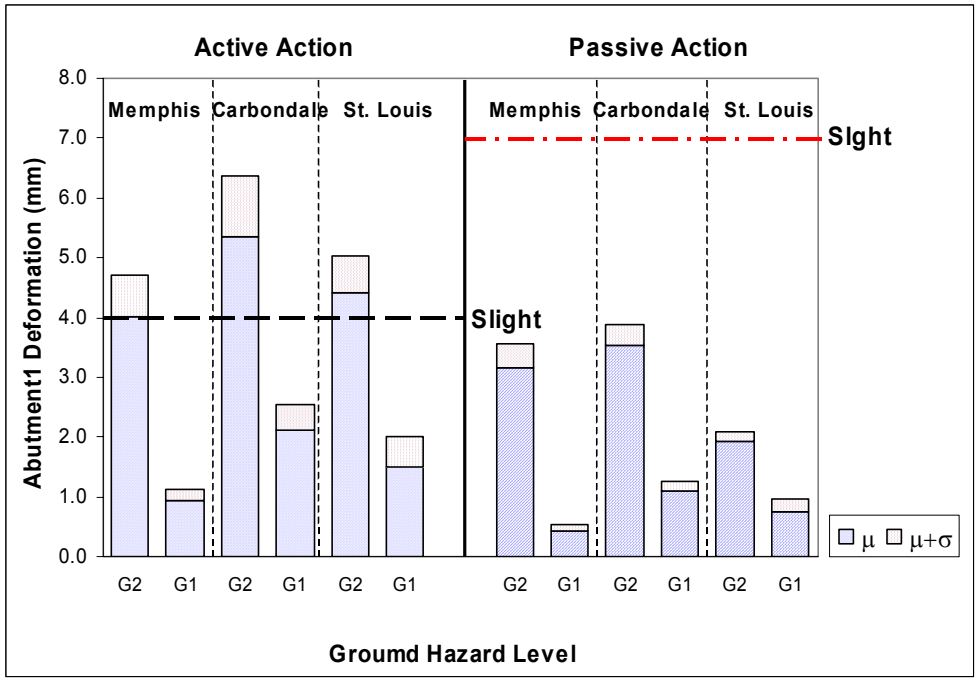

Figure 5.13d Response of Abutment1 Deformation in MSSS Steel Bridge

5.3.2 Performance of MSSS Concrete Bridge

The mean and the standard deviation of the critical responses for the MSSS concrete bridge are shown in Figure 5.14 for the three ground motion suites. The values are also listed in Table B2 in Appendix B.

The seismic responses of the columns are similar to those of the MSSS steel bridge because both bridges have the same moving tolerance. The maximum drift and ductility of the columns is 0.86% and 1.37%, respectively, for the G2 suites for Carbondale. The shear forces in the columns are also much lower than the shear capacity.

The fixed dowels in the bridge are fractured or yielded for the G2 ground motion suite from Memphis and Carbondale. However, the mean response of the expansion type dowels do not exceed the fractured/yield point even for G2 ground motions except for the

Expansion-dowel 3 for the G2 suite of Carbondale. The dowels can resist the seismic loads for all G1 ground motions and G2 ground motions for St. Louis.

For hinge openings, only Δop_1 and Δop_6, which are illustrated in Figure 5.12, are listed because these are generally the locations of maximum displacement. The maximum hinge opening is 49.7 mm (1.96 in.) with G2 of Carbondale; this value is much less than the unseating limit.

As previously mentioned in section 5.1, large forces develop in abutments in active action due to the dowels' behavior on abutments. The active deformation of 7.67 mm (0.30 in.) and 8.41 mm (0.33 in.) at Abutment1, and the active deformation of 8.19 mm (0.32 in.) at Abutment 2 for G2 suite from Memphis and Carbondale, respectively, exceed the yield point of the abutment. The maximum deformation of the abutments in passive action is 5.83 mm (0.23 in.) which is about 40% of the yield deformation (14.6 mm, 0.57 in.).

For pile foundations, the maximum force is approximately 20% of the ultimate value, and the maximum moment is 85% of the yielding point.

The COV of the responses in Table B2 are higher than those of the MSSS steel bridge. Since the difference of response before and after the fracture of dowels is large, it produces high COV, especially in Hinge-opening 1 with G2 of Memphis. The COV of the response of Abutment 2 for G1 of Memphis and G2 of St. Louis are zero. In these cases, the dowel bars are not activated and there are no poundings.

The maximum damage level on the columns is moderate, and dowels are usually damaged with G2 ground motions for Memphis and Carbondale. The active deformation

of the abutment is much higher than the moderate damage level with G2 for Carbondale, however, the passive deformation is below than the slight damage level.

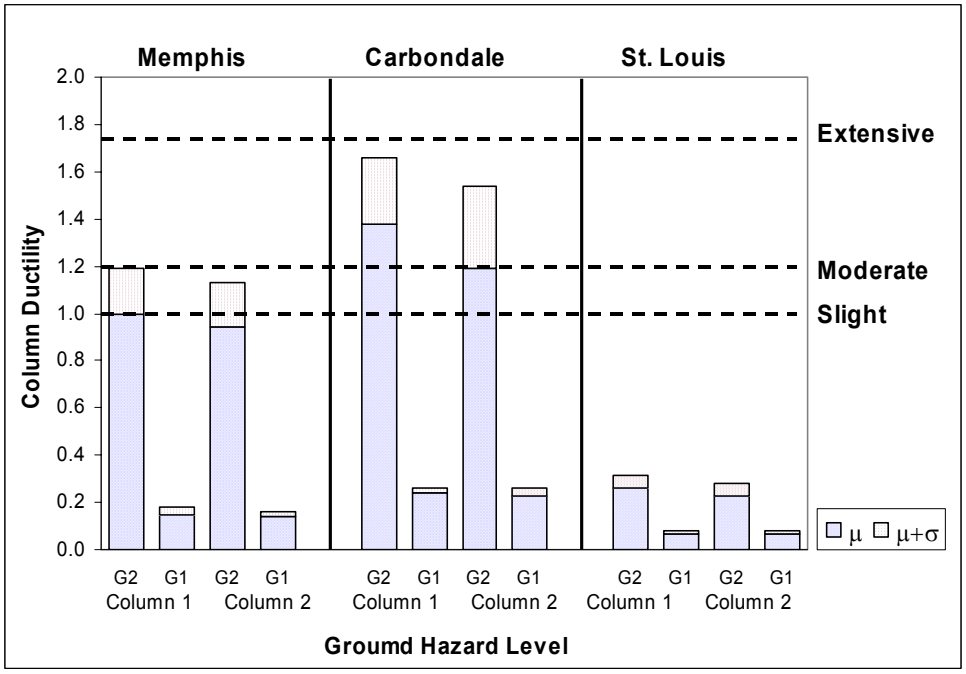

Figure 5.14a Response of Columns Ductility in MSSS Concrete Bridge

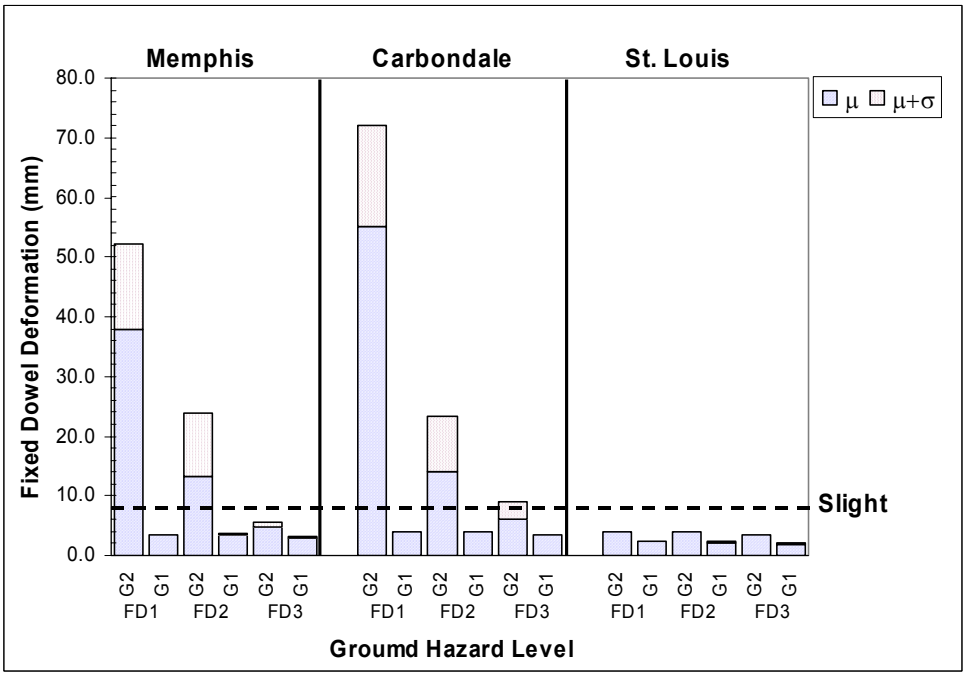

Figure 5.14b Response of Fixed Dowels Deformation in MSSS Concrete Bridge

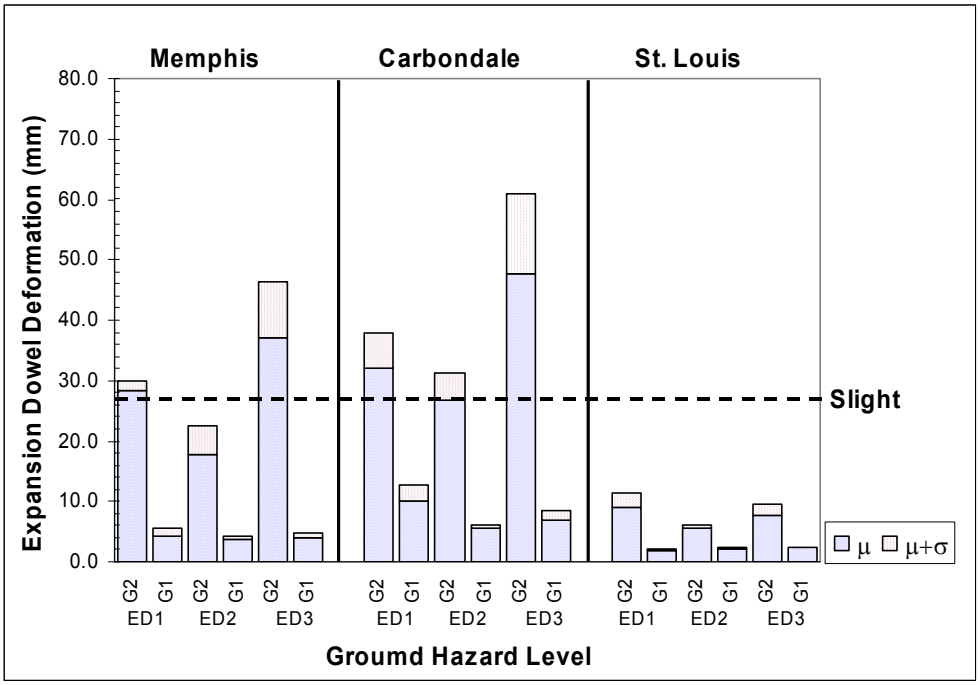

Figure 5.14c Response of Expansion Dowels Deformation in MSSS Concrete Bridge

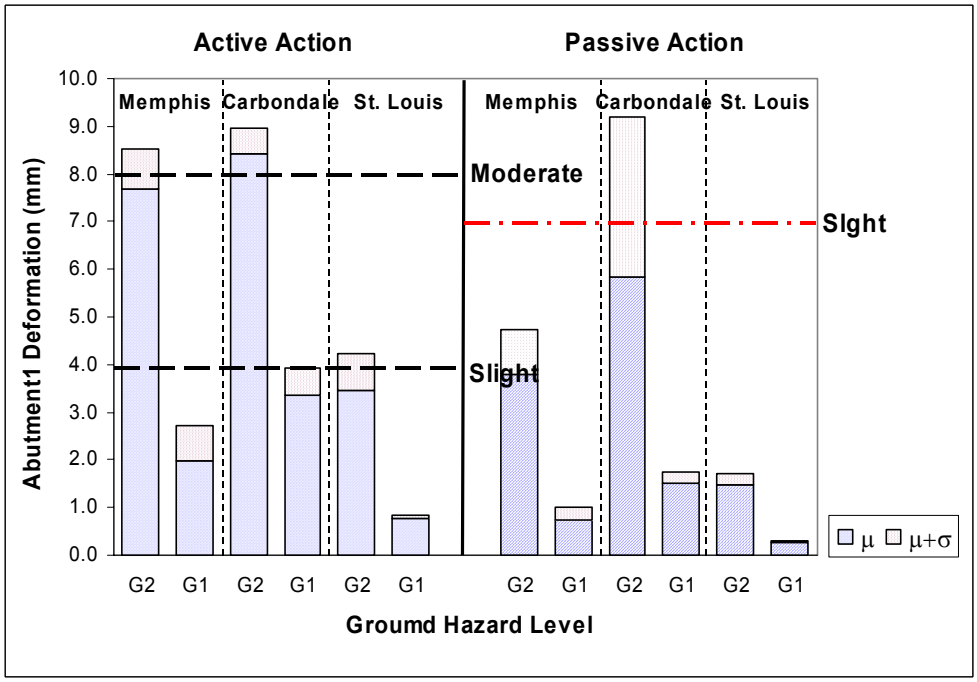

Figure 5.14d Response of Abutment1 Deformation in MSSS Concrete Bridge

5.3.3 Performance of MSC Steel Bridge

The MSC steel bridge has larger gaps on the abutments and longer columns than the MSSS bridges. However, the bridge is essentially linear for the 3 suites of G1 ground motions and G2 ground motions for St. Louis. Thus, the responses of G2 ground motions of Memphis and Carbondale will be discussed below.

The drifts in the columns are larger than that of the MSSS bridges. The drifts of columns are 1.12% and 1.24% for G2 of Memphis and Carbondale, respectively, which exceed the limit of lap splice failure. In addition, the ductilities of columns, μ=2.02 and μ=2.32 for G2 of Memphis and Carbondale, respectively, are larger than over the extensive damage-state (μ=1.76). However, the maximum shear is about 20% of the capacity.

For the bearings, the deformation of the fixed bearings on the columns is slightly larger than the moderate damage-state (6.0 mm, 0.24 in.). Moreover, the deformation of expansion rocker bearings on the abutments exceeds the limit for instabilities due to large deck movements. The maximum damage level of the expansion bearings is also extensive damage-state. The maximum opening (94.4 mm, 3.72 in.) is much larger than those of the MSSS bridges, and thus if the width is small, the unseating may occur.

The passive deformation of Abutment 1 is 13.5 mm (0.53 in.), which is close to the yield deformation of the abutment (14.6 mm, 0.57 in.). However, the passive deformation of Abutment 2, 12.8 mm (0.50 in.), is much less than the yield point of the abutment (45.7 mm, 1.80 in.). The active deformations/forces of the abutments are small because there are rocker bearings on the abutments. The damage level of the abutments

in passive action exceeds the slight damage-state, however the active deformation is much less than the slight damage level.

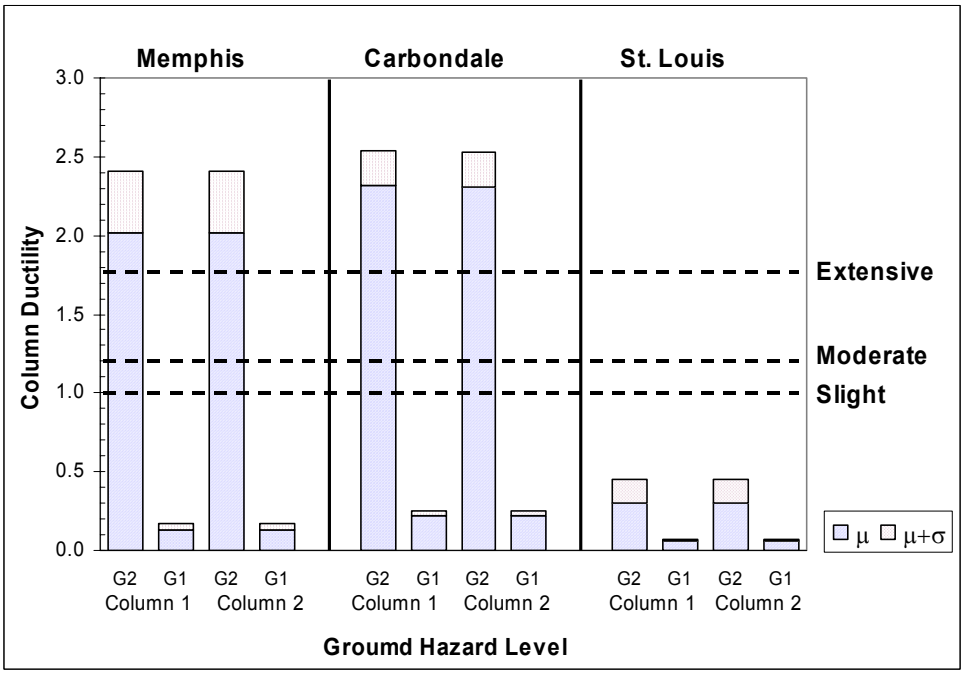

Figure 5.15a Response of Columns Ductility in MSC Steel Bridge

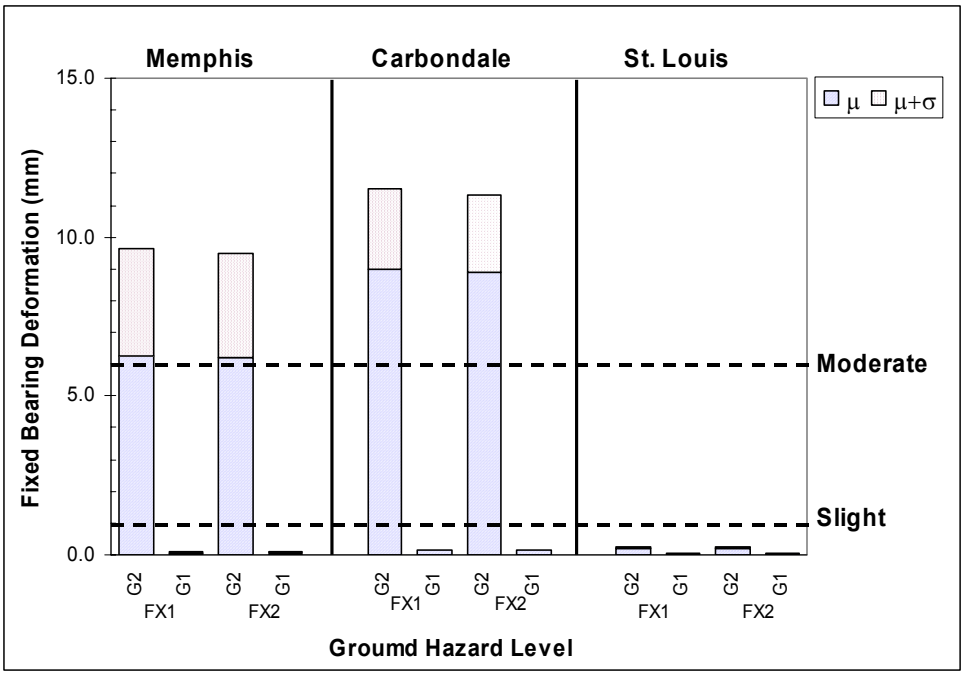

Figure 5.15b Response of Fixed Bearings Deformation in MSC Steel Bridge

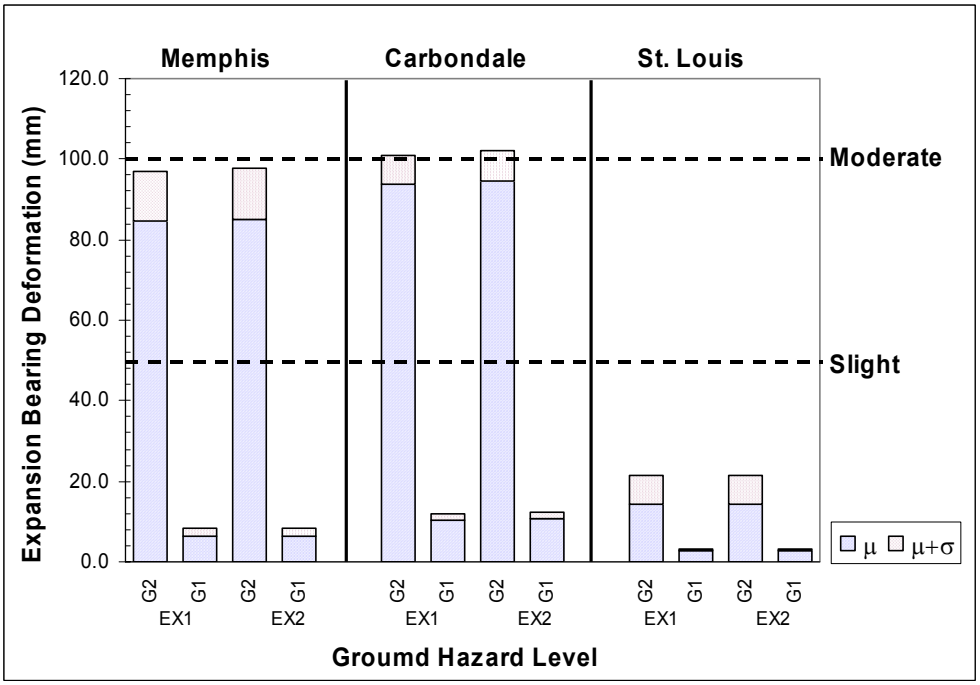

Figure 5.15c Response of Expansion Bearings Deformation in MSC Steel Bridge

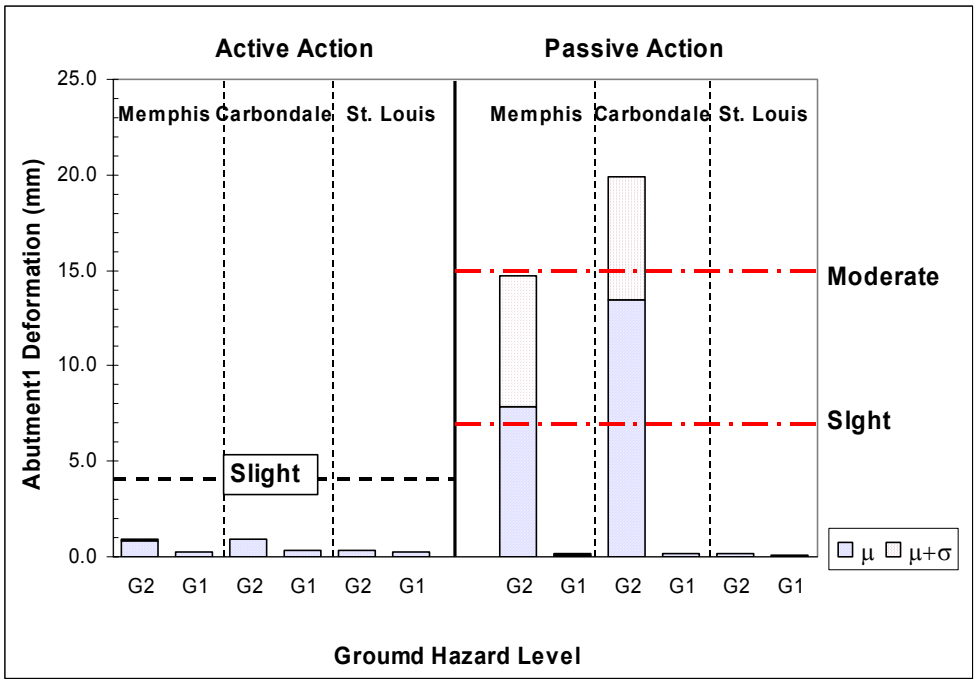

Figure 5.15d Response of Abutment1 Deformation in MSC Steel Bridge

The responses of the pile foundations in the bridge become improved from those of the MSSS bridges. The maximum force and moment are 15.5% and 83.9% of the ultimate, respectively, for G2 ground motions of Carbondale.

5.3.4 Performance of MSC Concrete Bridge

As previously mentioned in chapter 3, the MSC concrete bridge is retrofitted from the MSSS concrete bridge by casting a parapet between two decks. Thus, it is very meaningful to compare the response of the two bridges.

The maximum ductility and drift of the columns in the bridge are 0.94% and 0.34%, respectively. The ductility, μ=0.94, is 68% of the maximum value of the MSSS concrete bridge, and the drift, 0.34%, is 39% of the value for the MSSS concrete bridge. For shears, however, the maximum is 44.3% of the capacity, which is 2.2 times of the maximum shear in the MSSS concrete bridge. Since the deck is continuous in the bridge, more inertia forces are transferred to columns. In the MSC concrete bridge, the columns are not damaged even with the moderate ground motions (2% PE in 50 years).

The maximum deformation of the fixed-dowel is 30.4 mm (1.2 in.), which is 55% of the maximum value in the MSSS concrete bridge. However, the maximum values of the other two dowels in the MSC concrete bridge are larger than those in the MSSS concrete bridge. In the MSSS concrete bridge, the seismic demand is concentrated on Fixed dowel 1. In the MSC concrete bridge, however, the demand is distributed on the three fixed dowels.

The maximum opening is 30.8 mm (1.21 in.) with G2 of Carbondale, which is 62% of

the maximum value for the MSSS concrete bridge. Based on this fact, it is known that the deck displacement of the MSC concrete bridge is less than that of the MSSS concrete bridge.

The active deformation of Abutment 1 in the bridge is similar to that of the MSSS concrete bridge and the abutment yields with G2 for Memphis and Carbondale. The maximum damage level of the abutment in active action is also moderate. However, the pounding force on Abutment 2 in the bridge, whose value is 421 kN (94.6 kips) with G2 for Memphis, is approximately 19% of the pounding force found in the MSSS concrete bridge (2242 kN, 504 kips). Therefore, it is found that the continuity can reduce the pounding forces in the MSC continuous bridge.

For the pile foundations, the maximum force in the bridge is 41% of the ultimate capacity, which is 2 times that of the MSSS concrete bridge. The maximum moment is 93% of the yield capacity.

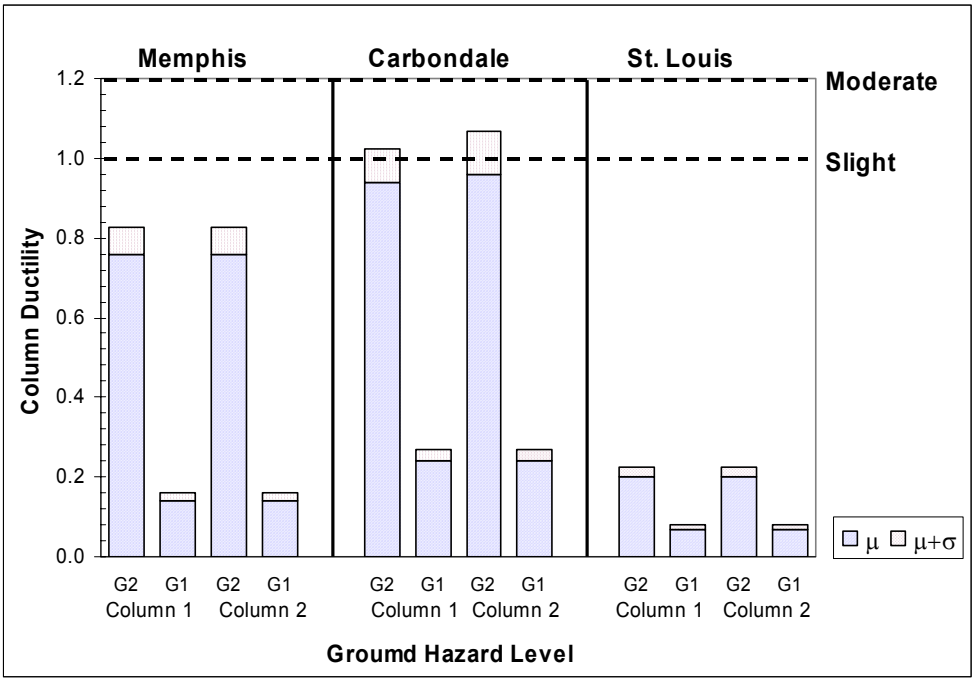

Figure 5.16a Response of Columns Ductility in MSC Concrete Bridge

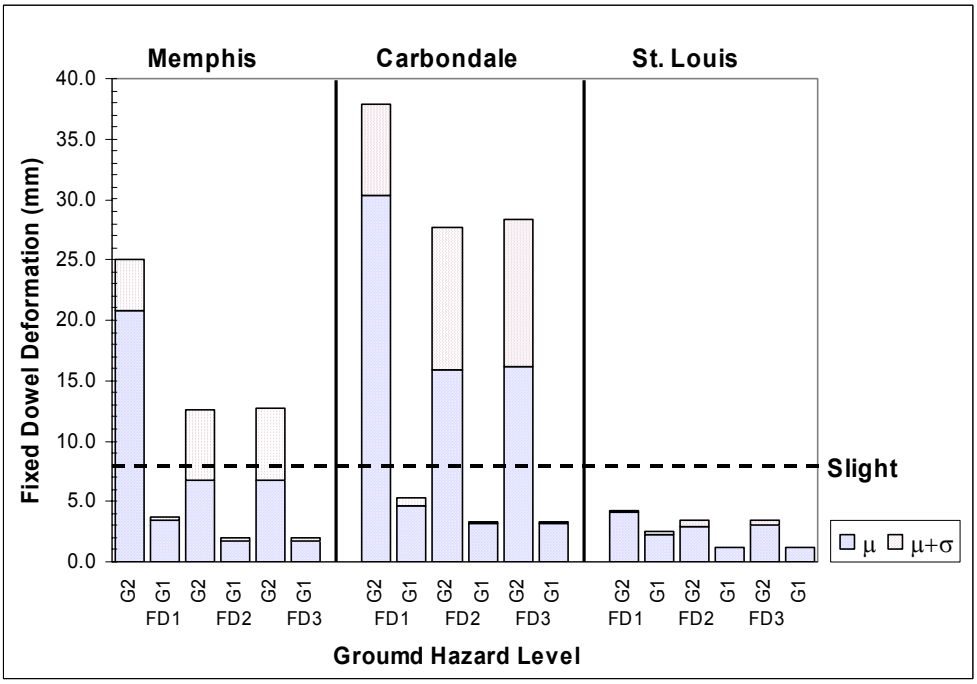

Figure 5.16b Response of Fixed Dowels Deformation in MSC Concrete Bridge

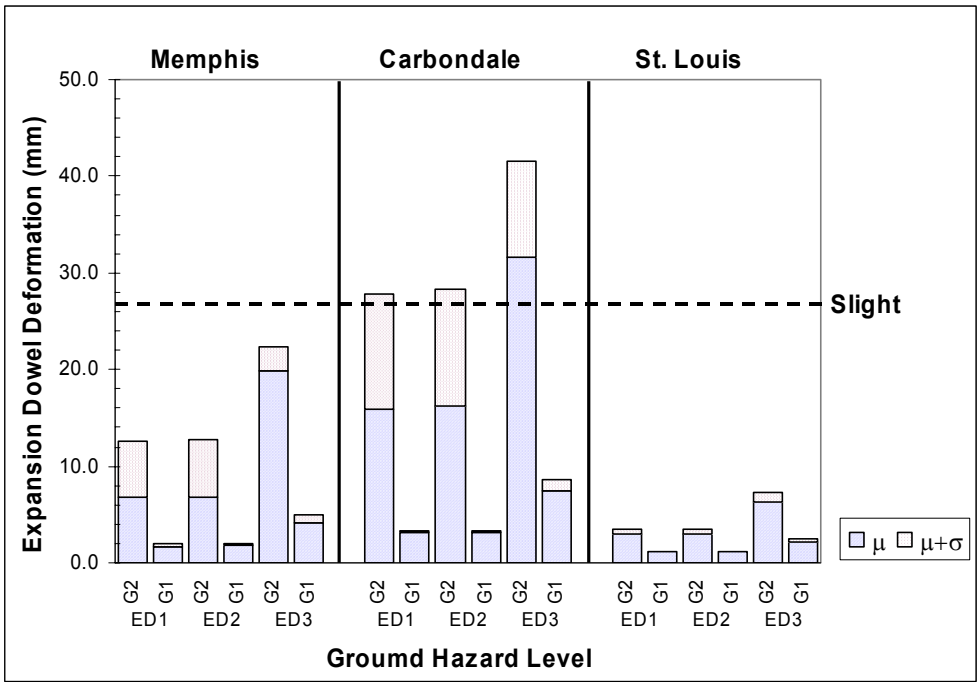

Figure 5.16c Response of Expansion Dowels Deformation in MSC Concrete Bridge

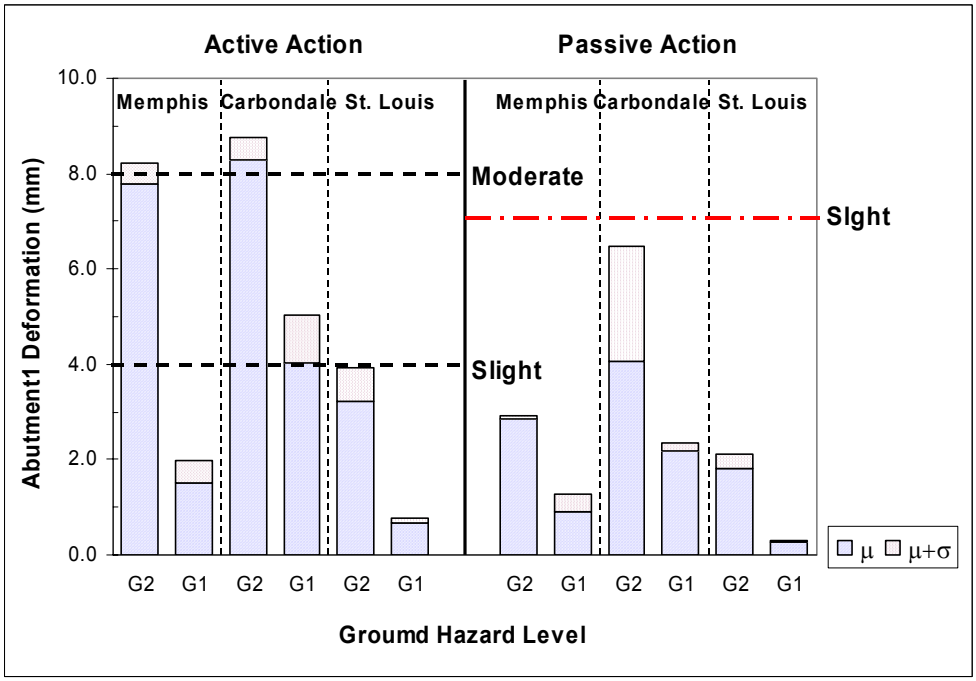

Figure 5.16d Response of Abutment 1 Deformation in MSC Concrete Bridge

5.3.5 Performance of SS Steel Bridge

The results of the single span steel bridges are listed in Figure 5.17. The behavior of the single span bridge is relatively simple. The critical factor is the deck's mass, and the fixed bearings govern the seismic behavior of the bridge. The maximum deformation of the fixed bearing is 6.6 mm (0.26 in.) for the G2 suite of Carbondale, which is just over the slight-damage state.

Since the deformation of the expansion bearing and the opening depend on the deformation of the fixed bearing and abutments, they are very small. The abutments remain in elastic range for all kinds of ground motions. In this bridge, only the fixed bearing is damaged slightly and the other components do not have any damage.

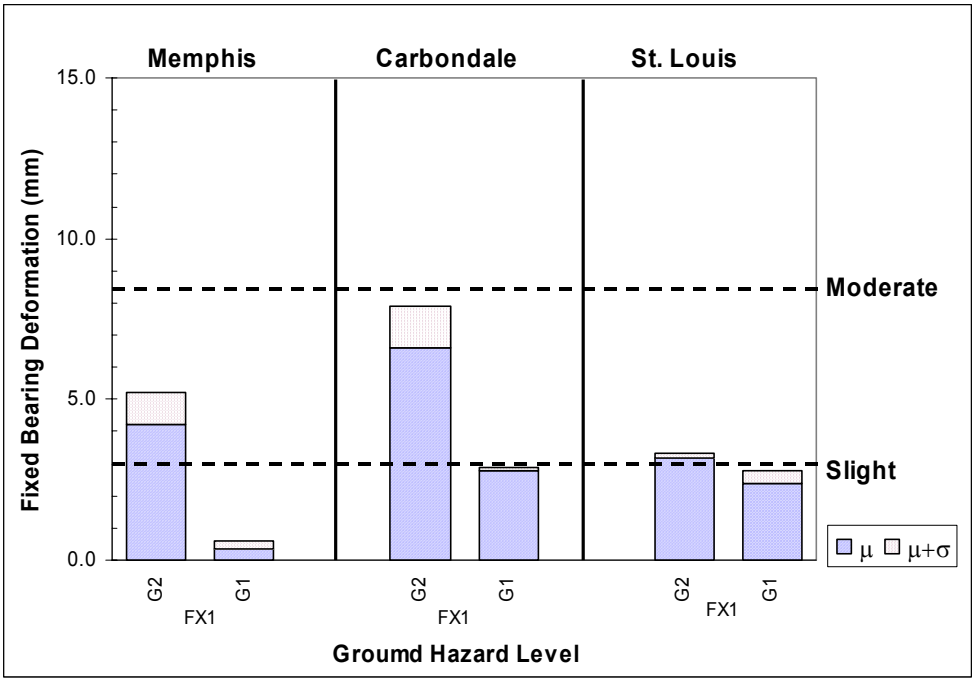

Figure 5.17a Response of Fixed Bearing Deformation in SS Steel Bridge

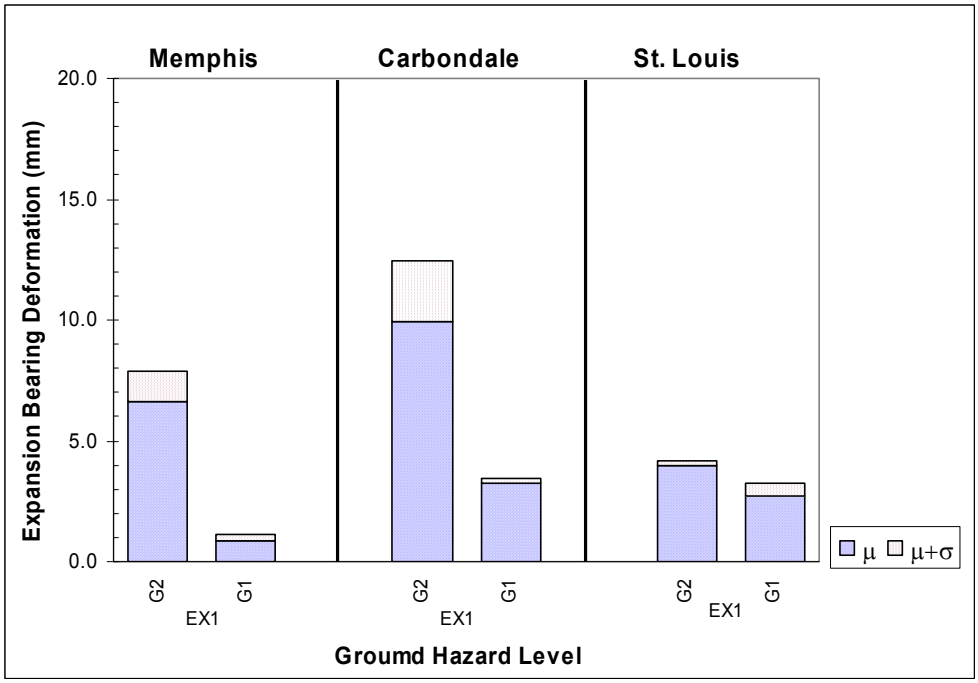

Figure 5.17b Response of Expansion Bearing Deformation in SS Steel Bridge

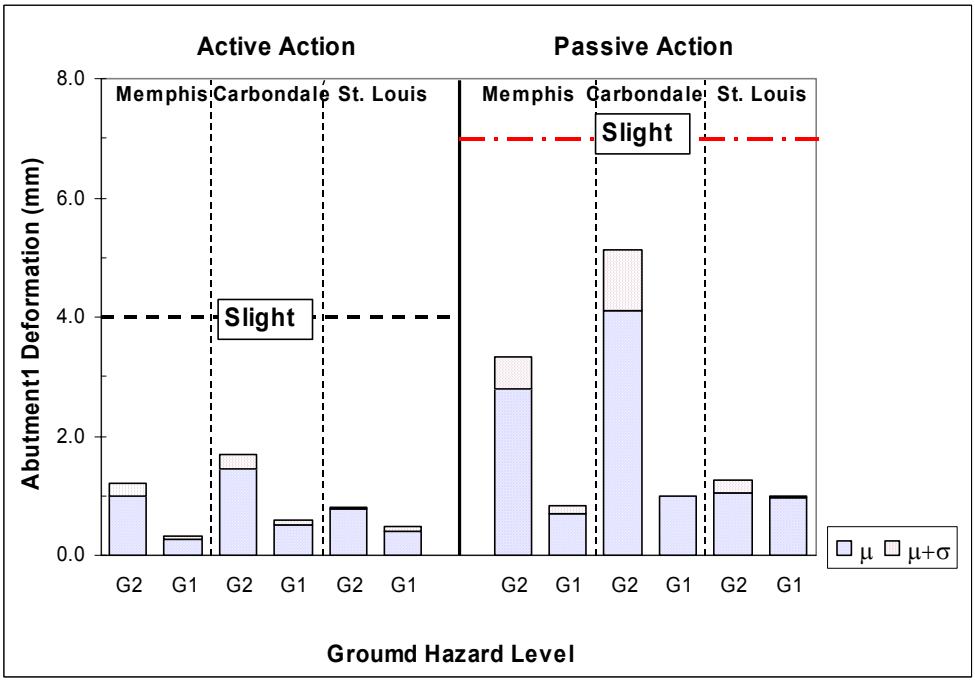

Figure 5.17c Response of Abutment1 Deformation in SS Steel Bridge

5.3.6 Performance of SS Concrete Bridge

As shown in Figure 5.18, the fixed dowel is broken even with G1 suites for Carbondale. In addition, the expansion dowel is fractured for G2 ground motions of Memphis and Carbondale. Due to the easy fracture of dowels, the maximum opening reaches 63.3 mm (2.5 in.). From the above fact, the SS concrete bridge can sustain damage with the G1 suite of ground motions and very vulnerable to seismic loading.

Although the dowels are fractured easily, there is not any pounding to abutments because of the large gap between the deck and the abutments, 101.6 mm (4.0 in.). Thus, the abutments remain in elastic range and no damage in both actions.

The COV of the response of the fixed dowel is low compared to that of the fixed bearing in the SS steel bridge.

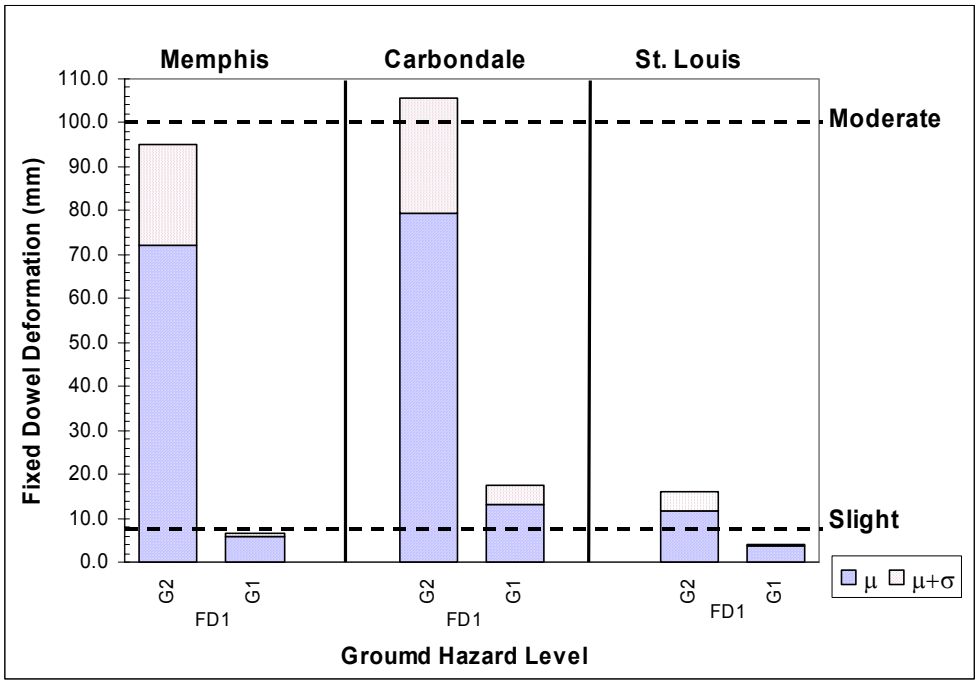

Figure 5.18a Response of Fixed Dowel Deformation in SS Concrete Bridge

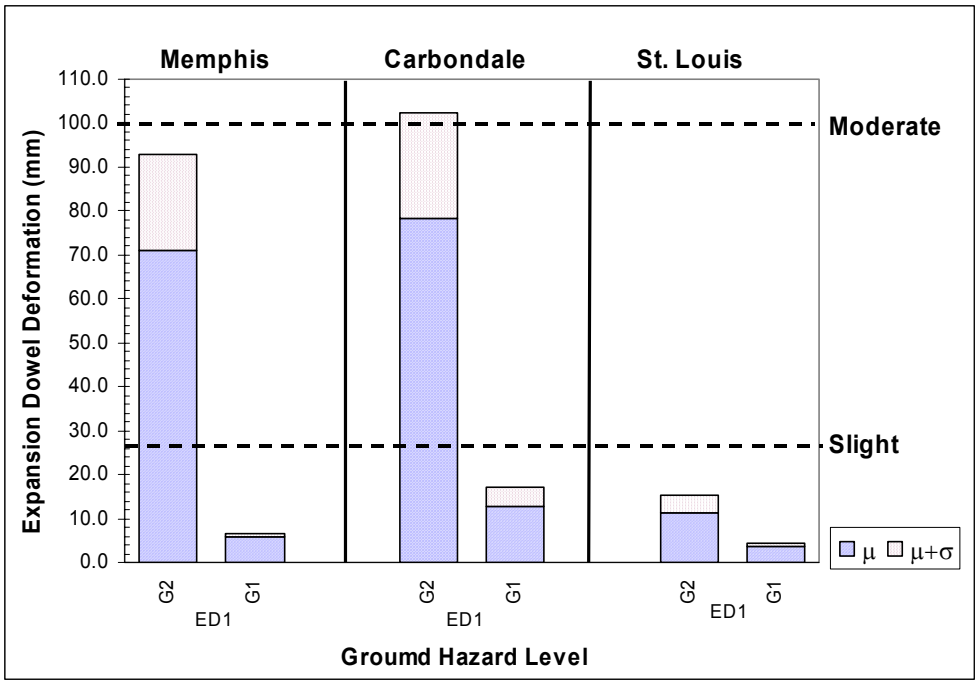

Figure 5.18b Response of Expansion Dowel Deformation in SS Concrete Bridge

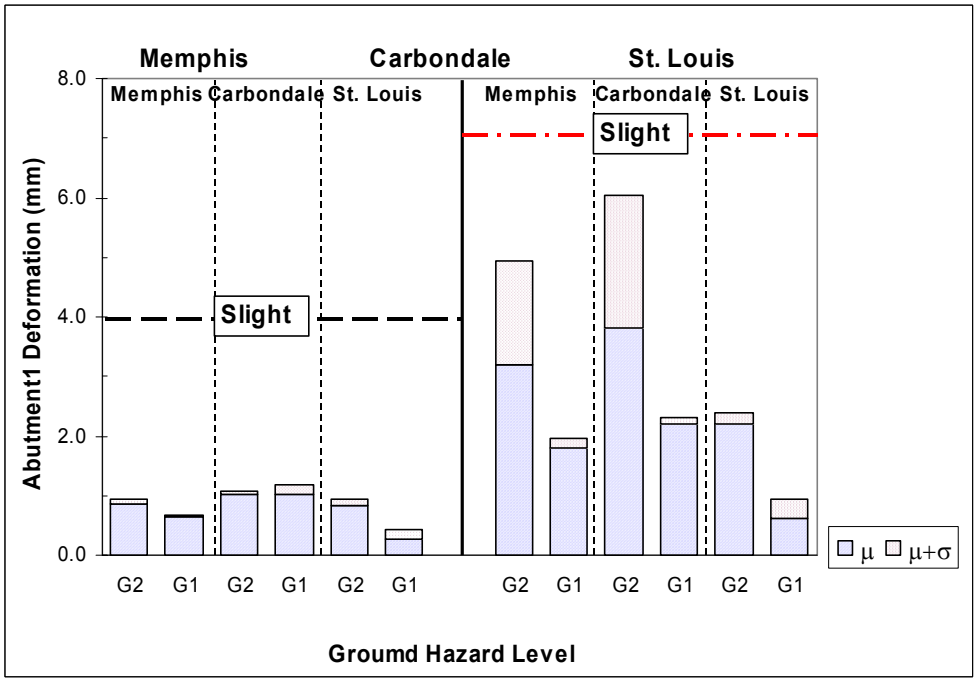

Figure 5.18c Response of Abutment1 Deformation in SS Concrete Bridge

5.4. Summary

The three suites of ground motions for two hazard levels were applied to evaluate the seismic response of the typical bridges in Mid-America. Responses, in general, are linear for all ground motions with 10% probability of exceedance in 50 years except the single span concrete bridge. Therefore, the bridge is estimated as highly vulnerable bridge to seismic loading.

The critical elements in the responses of the MSSS bridges are the columns. Additionally, the expansion rocker bearings in the steel bridges and dowels in the concrete bridges can be damaged easily for the ground motion records of 2% probability of exceedance in 50 years. The MSSS concrete bridge is estimated as the bridge with the highest seismic risk.

For the multi-span continuous concrete bridge rehabilitated from the multi-span simple supported concrete bridge, the maximum ductility of columns is reduced to 0.94 from the value of 1.38 by the continuity, and the maximum hinge opening is reduced by 38%. Therefore, it is found that the continuity in the MSC concrete bridge can improve the seismic response.

Finally, although AASHTO (1996) specify that single span bridges do not require seismic analysis, dowels are damaged and unseating may be expected in the single span concrete bridge. Therefore, the dynamic seismic analysis is necessary to inspect the seismic vulnerability for single span concrete bridges.

CHAPTER 6

PARAMETRIC AND SENSITIVITY STUDY OF TYPICAL BRIDGES

The previous chapter evaluated the statistical response of typical bridges to a suite of ground motions. Conclusions and observations were made based on a fixed set of properties for the six types of bridges in Mid-America. However, for each type of bridge, the response will vary as a function of the actual properties. Therefore, in this chapter, various bridge properties, such as deck mass, bearing stiffness and strength, gap size, and pile foundation stiffness are varied to determine the effect on the response of the typical bridges.

In this study, a parameter is varied, while the other parameters remain constant. For the parametric study, the G2 ground motions (2% PE in 50 years) for Carbondale are applied for each type of bridge. The concrete bridges are not included in this study because the trend of the response would be similar to that of the steel bridges.

6.1 Description of Parameters

In this study, there are five parameters; frictional coefficient of expansion rocker bearings, deck mass, gap size between decks, gap size between deck and abutment, and the rotational stiffness of pile foundations. Each of the parameters is discussed below.

Frictional Coefficient of Expansion Steel Bearings

The strength and stiffness of the expansion rocker bearings depends on the surface condition of the bearings and the moving mechanism of expansion such as sliding and rolling. With aging, the corrosion and accumulated debris can increase the frictional coefficient of the surface and strength of the bearing (Mander et al., 1996). The frictional coefficient, μ, can vary from 0.04 to 0.20 for typical bearings in Mid-America. The frictional coefficient of expansion bearings used in the analyses in chapter 5 is 0.04. The variation of the coefficient in the parametric study is varied from 0.01 to 0.2.

Mass of Decks

The mass of the bridge deck can have a significant effect on the response of typical bridges. Larger masses can lead to an increased period for the bridge and can effect the nonlinear behavior of impact at the expansion joints. To evaluate the effect of deck mass on the seismic response of bridges, the mass of the deck is varied for 50% of the base case to 200% of the base case.

Gap Size

The gap in the bridges is usually located at expansion joints to accommodate the deck length changes due to thermal, creep, and shrinkage effects. Based on typical variation in temperature of approximately 90°F between winter and summer and the coefficient of thermal expansion for concrete, the gap can vary by up to 25 mm (1.0 in.).

The gap in bridges is a significant factor in responses of bridges because of pounding.

Previous studies have shown the pounding can increase or decrease the response of bridges, depending on the gap (Dicleli and Bruneau, 1995a). In this study, the gap between deck and abutment and the gap between decks are discussed separately. The gap size between deck and abutment is varied from 0.0 to 152.4 mm (0-6 in.). The gap size between decks is varied from 0.0 to 50.8 mm (0-2 in.).

Rotational Stiffness of Pile Foundations

The rotational stiffness of the pile foundation varies depending on the reinforcement and type of foundation. To consider this effect, the rotational stiffness of pile foundations is varied from 25% to 300% of the base case. Table 6.1 shows the parameters discussed in this parametric study and their variation.

Table 6.1 Parameters and Variation

Parameters	MSSS Bridge	MSC Bridge	Variation
Frictional Coefficient	0.04	0.04	50 - 500%
Deck Mass (kN sec^2/m)	134.0 287.0 134.0	325.0 417.0 362.0	50 - 150%
Gap bet. Deck & Abutment (mm)	38.1	N/A	0 – 400%
Gap bet. Decks (mm)	25.4	76.2	0 – 200%
Rotational Stiffness of Pile Foundations (kN-m/rad)	5.56 × e6	1.04 × e7	25 - 300%

N/A: Not Available

6.2 Results of MSSS Steel Bridge

The parameters described in the above section are evaluated in the MSSS steel bridge. The responses that will be evaluated are column ductility, relative hinge opening, fixed bearing deformation, and abutment deformation. These quantities were estimated as the most important in chapter 5. The other responses will not be discussed in this parametric study.

6.2.1 Frictional Coefficient of Expansion Bearings

As previously mentioned, the frictional coefficient can vary as a function of the type of rocker and condition of the bearing. Figure 6.1a shows that increasing the coefficient of expansion steel bearings slightly reduces the response of Column 1. A 100% increase in the frictional force in the expansion bearing results in a 7% reduction in ductility of the column. This can be explained by looking at the configuration of the MSSS steel bridge in Figure 4.1. The displacement of the pier is restricted by the friction in Expansion bearing 2. The displacement of Column 2, however, is a function of many other parameters and is therefore not sensitive to the coefficient of friction.

Opening 2 is very sensitive to the coefficient of friction. When the friction increases 100%, the opening is reduced by approximately 56%. A stronger rocker bearing can connect the second frame and the third tightly. Opening 1 and 3 are not sensitive to the coefficient. Opening 1 is reduced slightly with increasing the friction, but Opening 3 increases slightly with increasing frictional coefficient.

The deformation of fixed bearings is sensitive to the frictional force. A 100%

increase in the force results in approximately 12-19% reduction in the deformation. Stronger expansion rocker bearings have more energy dissipation, thus they can reduce the pounding force and the deformation of the fixed bearings.

For abutments, the active deformation of Abutment 1 is not sensitive to the frictional force because the deformation depends largely on the inertia force of Deck 1. However, Abutment 2 deformation in active action increases by approximately 19% with a 100% increase in the frictional force. The deformation of abutments is not sensitive to the frictional force.

6.2.2.Mass of Decks

The deck mass can affect the dynamic properties of the bridge as well as the inertia forces transferred to spans, abutments, and bearings. Figure 6.1b shows that an increase in the deck mass results in an increase in column ductility. This is primarily due to the increasing response at the longer structural period and the increasing inertia force of the decks.

The increasing deck mass also leads to larger hinge openings and fixed bearing deformations. The increasing inertia force increases the deformation of abutments. However, the active deformation of Abutment 2 depends on the strength of expansion bearings, thus it is not sensitive to the variation of deck masses.

6.2.3 Gap between Deck and Abutment

Increasing the gap between the deck and abutment affects the movement of the deck

and pounding significantly. Generally, the larger gap decreases the pounding force at the abutments. However, the deck displacements increase.

The ductility of the columns increases with larger gap at first, however, as the gap size approaches 50.8 mm (2.0 in.), the ductility remains constant as shown in Figure 6.1. Column 1 displacement is more sensitive to the gap size than Column 2.

The larger gap size also increases the relative displacement and the displacement of expansion bearings. However, Opening 2 is not sensitive to the gap size since the hinge opening is primarily a function of the relative movement between the second and the third deck. Since Opening 3 is measured as the maximum relative displacement between Deck 3 and Abutment 2, the gap variation does not affect the opening. However, for small gaps, the pounding between Deck 3 and Abutment 2 can affect Opening 3.

The deformation of the first fixed bearing increases with larger gaps. When the gap on the abutments is small, the pounding force is transferred to abutments directly. The larger gaps, however, permit the larger deformation of the fixed bearing. The deformation of other fixed bearings decreases with the larger gaps.

The passive deformation of abutments is reduced sharply at first and decrease less rapidly with larger gap because there is not pounding between decks and abutments. The active deformation of abutments is not related to the gap size. However, it is considered that the pounding between decks and abutments with small gap affects the active deformation of Abutment 1.

6.2.4 Gap between Decks

Increased gap between decks reduces column ductilities, as expected. The gap at the deck has little effect on the ductility of Column 2, since this is controlled by the abutment gap. The relative hinge opening, however, is not strongly affected by the gap. The deformation of Fixed bearing 1 decreases sharply with increasing gap. The active deformation of abutments is not sensitive to the gap size, but the passive deformation is highly affected by the gap.

6.2.5 Rotational Stiffness of Pile Foundations

The increased rotational stiffness of the foundations decreases the rotation at the bottom of the columns. This reduces the columns' drift but increases the ductility as shown in Figure 6.1e. Other responses are not affected significantly by the variation of the rotational stiffness of foundations.

Since the stiffer foundations reduce the deck movement and the pounding force, the fixed bearings' deformation and the passive deformation of abutments are decreased with the stiffer foundations

6.2.6 Summary

The parametric study on the response of the MSSS bridge highlighted some of the factors that affect the response. The study shows that the column ductility decreases with increasing friction at the expansion rocker bearings and increases with increasing deck mass. The gap size has a significant effect on column ductilities. Decreasing the gap

restricts the movement of the spans, resulting in decreases in column ductility.

The relative hinge opening is most affected by the size of the gap between decks. Larger gap sizes result in larger relative hinge displacement.

The deformation of the fixed bearings is strongly affected by the mass of the deck. Larger masses result in larger inertia forces transferred to the fixed bearings during impact. In addition, the gap between deck and abutment has a significant effect on the deformation of fixed bearings.

Finally, the abutment deformations are most affected by the deck mass and the gap at the abutment.

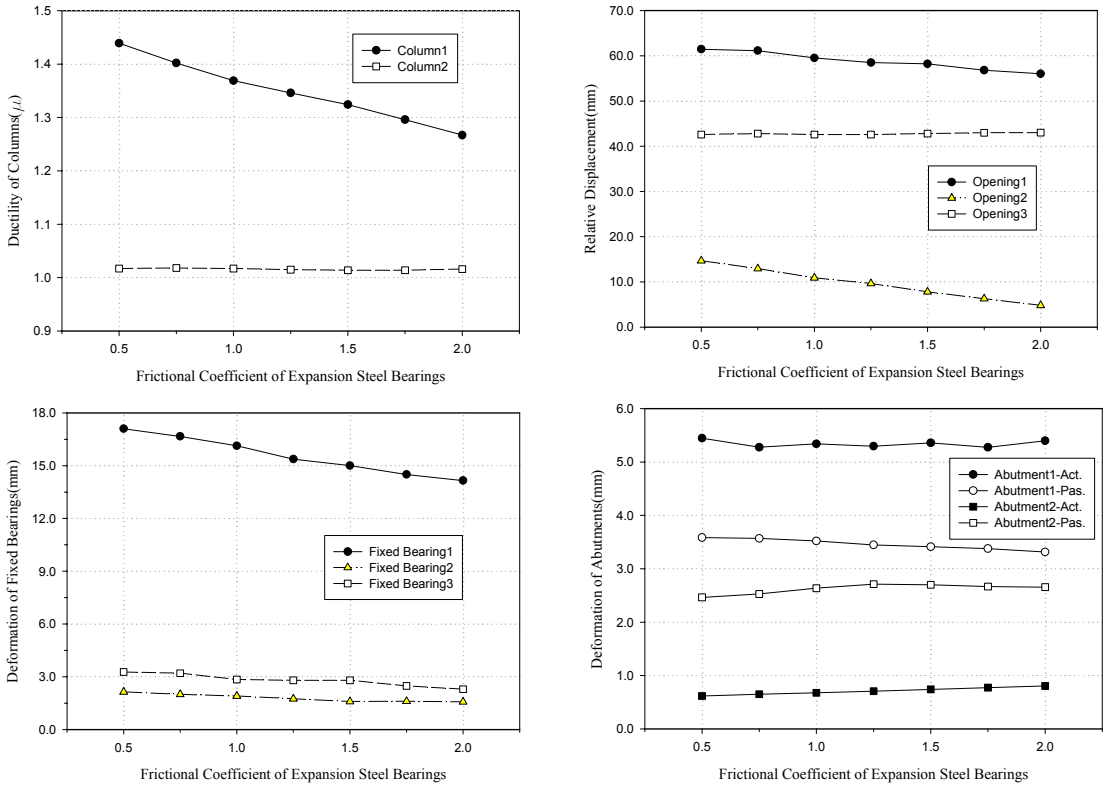

Figure 6.1a Effect of Frictional Coefficient in MSSS Steel Bridge

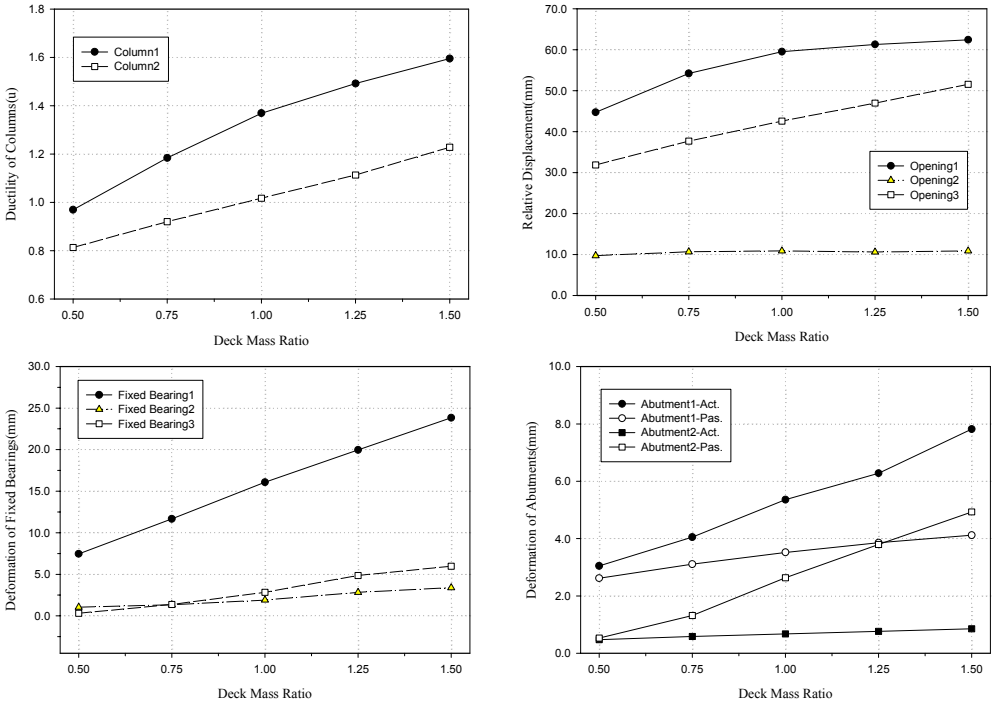

6.1b Effect of Deck Mass in MSSS Steel Bridge

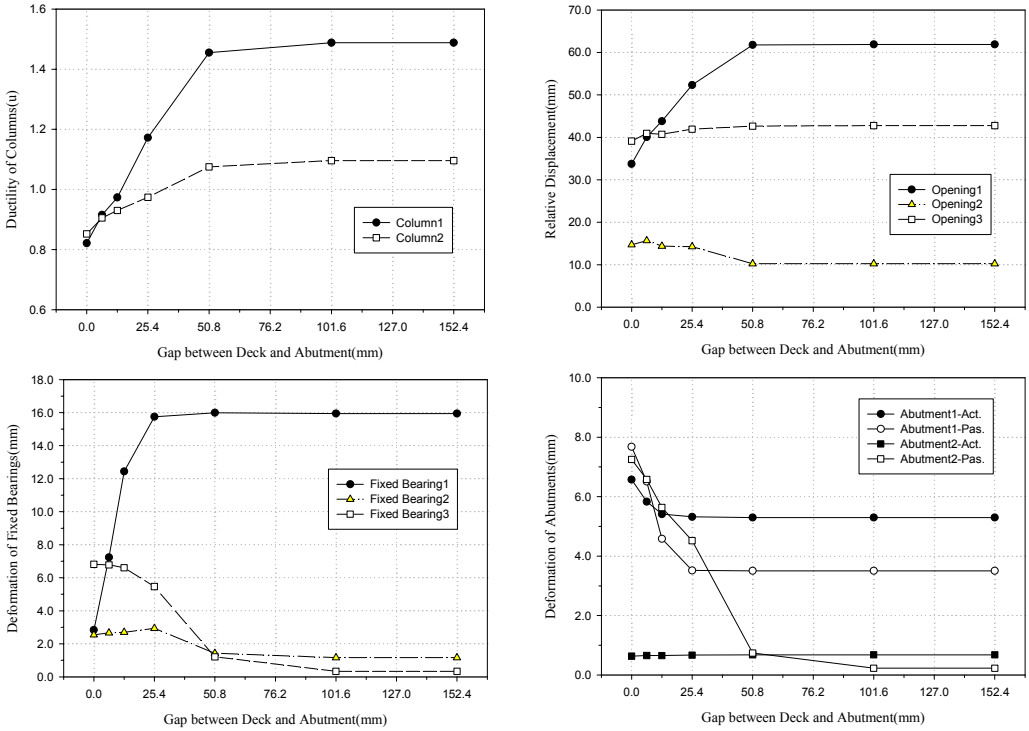

Figure 6.1c Effect of Gap Size bet. Deck and Abutment in MSSS Steel Bridge

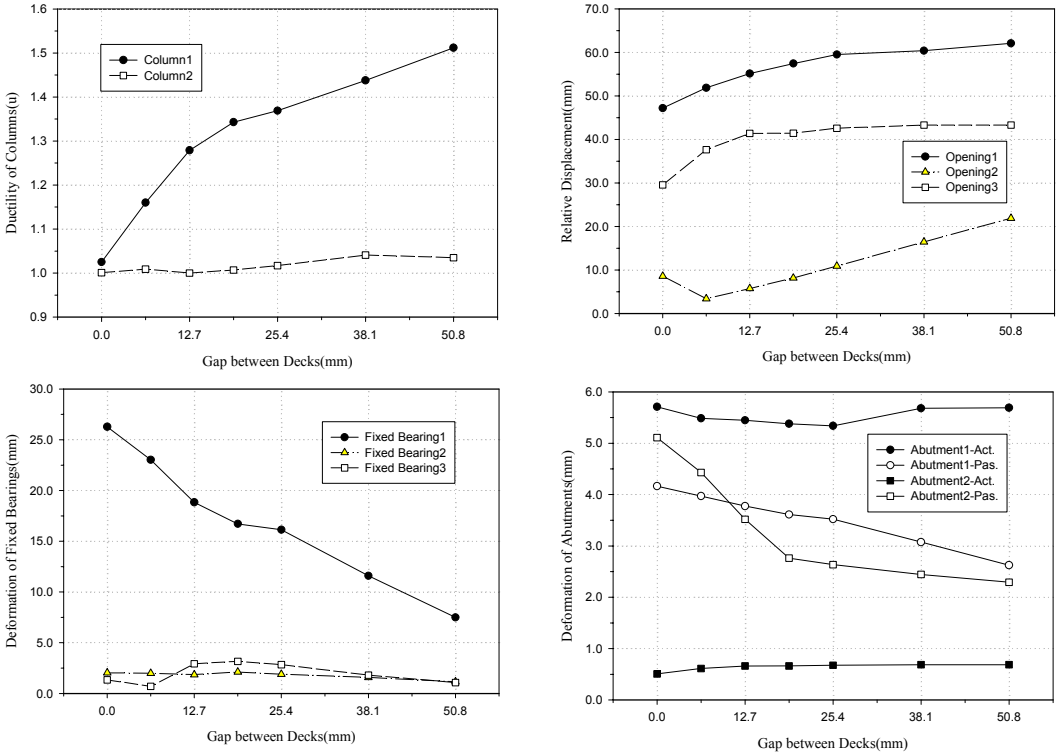

Figure 6.1d Effect of Gap Size bet. Decks in MSSS Steel Bridge

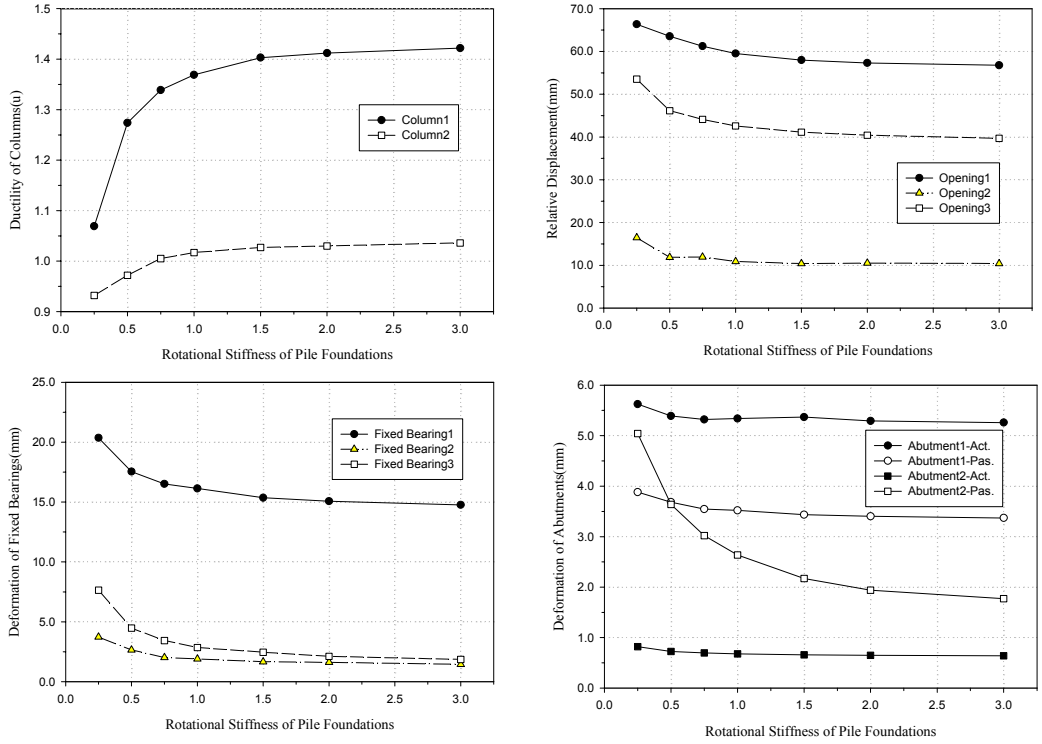

Figure 6.1e Effect of Rotational Stiffness of Pile Foundations in MSSS Steel Bridge

6.3 Results of MSC Steel Bridge

In the continuous steel bridge, the gap between decks does not exist. Thus, this parameter is excluded in this section. The results are displayed in Figure 6.2.

6.3.1 Frictional Coefficient of Expansion Bearings

The behavior of the MSC steel bridge is relatively simple compared to that of the MSSS steel bridge since there is not a gap between the decks.

The increased frictional coefficient of the expansion bearings in the bridge restricts the deck movement more, thus most responses are slightly improved. A 100% increase in the frictional force of the bearings reduces by less than 5% of the ductility of the columns and the relative hinge openings. The deformations of fixed bearings are reduced about 13% and the passive deformations of abutments are decreased about 20% with a 100% increase in the frictional force.

However, the active deformations of the abutments increased with increasing coefficient of friction.

6.3.2 Mass of Decks

As previously mentioned, the major reasons for the increasing responses with increasing deck mass are the increased inertia force and the effect of the longer period. The ductilities of the columns and the hinge openings are increased by approximately 18% and 11% with a 50% increase in the deck mass. However, the passive deformations increase by 90% with a 50% increase.

6.3.3 Gap between Deck and Abutment

The effect of gap size on the response of bridges can be understood more easily in the continuous bridge because there is not a gap between decks. In the MSC steel bridge, it is expected that the demand of the columns increases at first with larger gap and reaches to the maximum beyond a point. In general, when the demand of columns increases, the demand on the foundations also increases.

The larger gap permits more movement of the deck and generates increased responses on the columns and hinge openings. The larger gap, however, decreases the pounding force, thus the passive deformations of abutments decrease. When the deck comes in contact with the abutments, the deck transfers larger force directly to the abutments. Therefore, in this case, the passive deformations of abutments are larger than the other cases. However, if there is any gap between them, when the deck reaches the maximum velocity, the pounding force is maximized. With the gap size of 19.05 mm (0.75 in.), the deck has the maximum velocity.

Although the pounding force decreases with larger gap, the fixed bearings' deformation increases because the deck can move more with the larger gap.

6.3.4 Rotational Stiffness of Pile Foundations

The stiffer foundations reduce the displacement of the deck in the continuous bridge. This reduces the columns' drift and the relative hinge displacement. However, the stiffer foundations increase the ductility of columns and the deformation of fixed bearings. The result of the fixed bearings is contrary to the fixed bearings' deformation in the MSSS

steel bridge. As mentioned above, in the MSSS steel bridge, impact is a major effect on the deformation of the bearings. In the continuous bridge, however, pounding is not a critical factor. With stiffer foundations, the pounding force is reduced since the deck movement is smaller. Therefore, the substructure stiffness and the inertia force of the deck are the two major effects on the fixed bearing deformation in the continuous bridge.

6.3.5 Summary

The parametric study on the MSC steel bridge shows that the effect of the parameters on the responses can be different from that on the MSSS steel bridge.

The columns' demand is reduced by increasing the friction of the expansion bearings, but the effect is much less than that on the MSSS steel bridge. The ductilities of columns are significantly affected by the increasing of the deck mass, the gap size, and the rotational stiffness of foundations.

The hinge openings increase with increasing deck mass and the gap but decrease with increasing frictional force of the expansion bearings and the stiffness of foundations.

The deformation of fixed bearings and the passive deformation of abutments are influenced significantly by increasing the deck mass and the gap size.

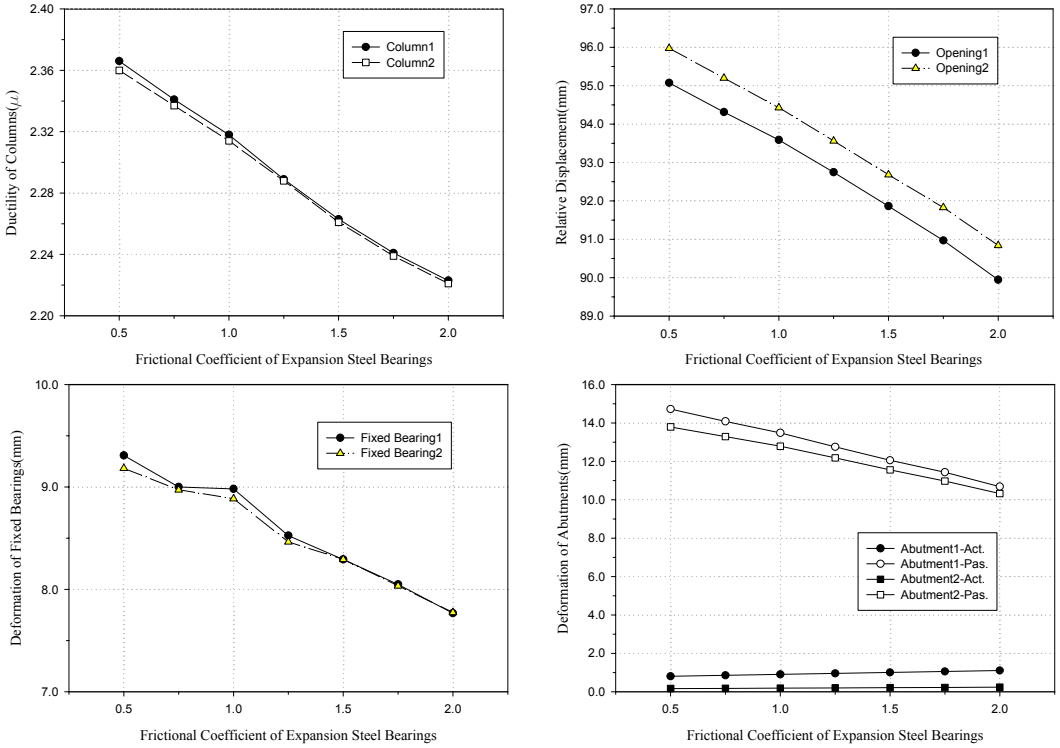

Figure 6.2a Effect of Frictional Coefficient in MSC Steel Bridge

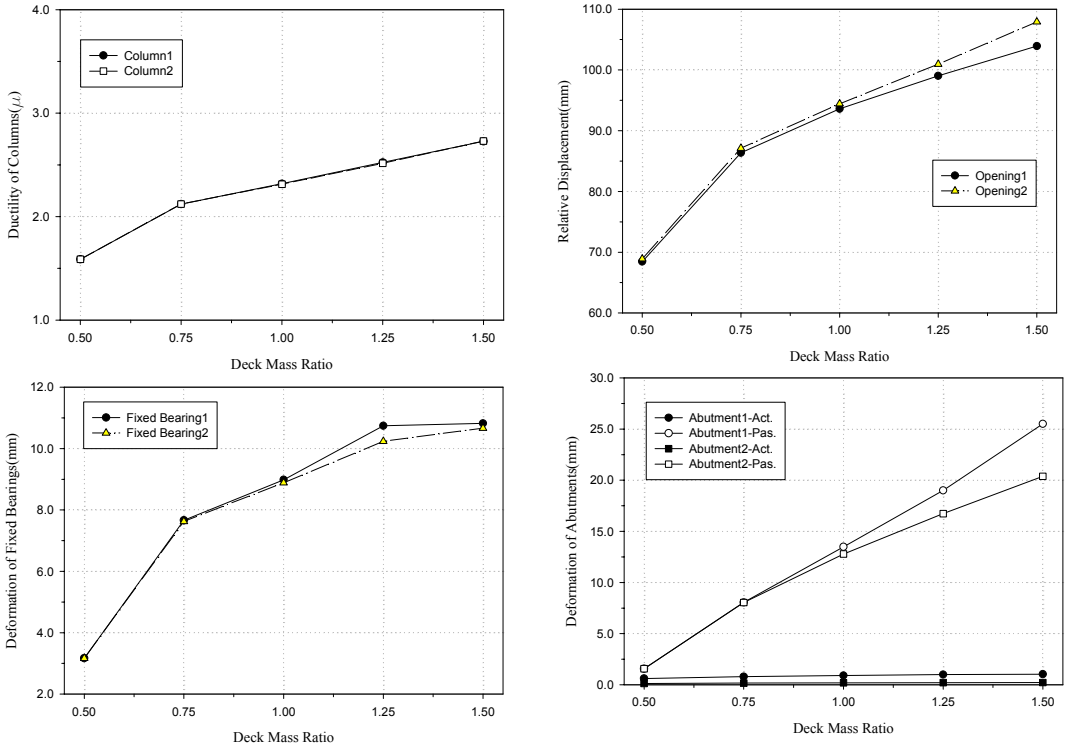

Figure 6.2b Effect of Deck Mass in MSC Steel Bridge

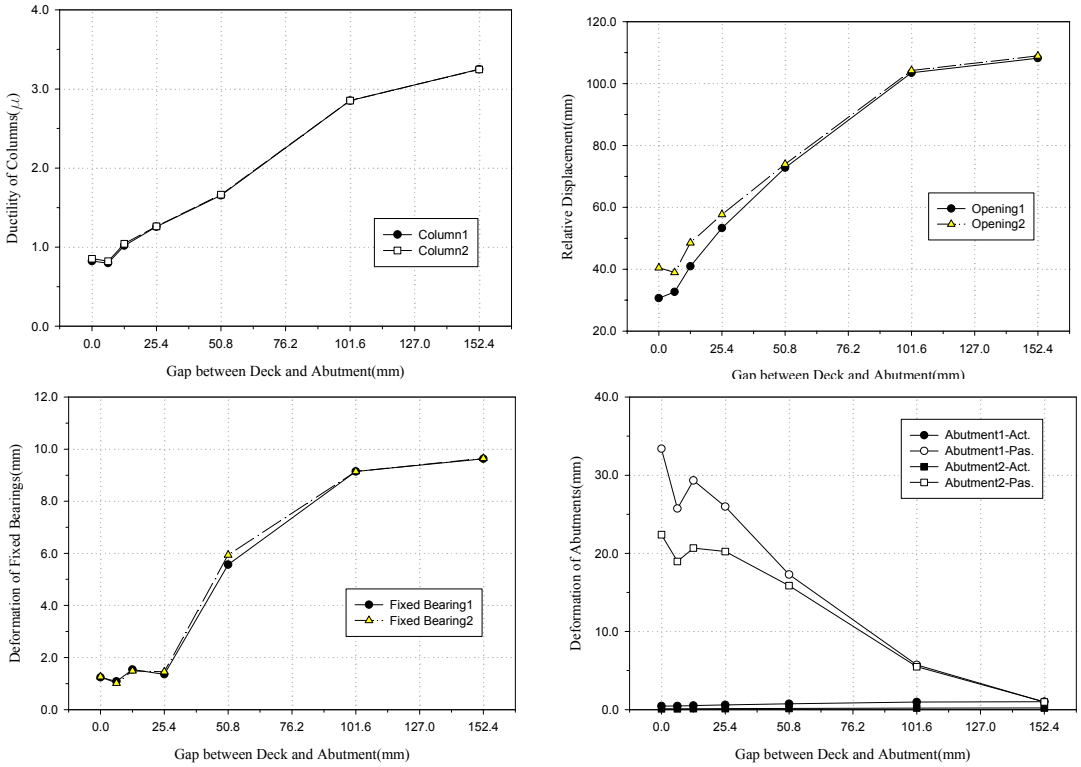

Figure 6.2c Effect of Gap Size on Abutments in MSC Steel Bridge

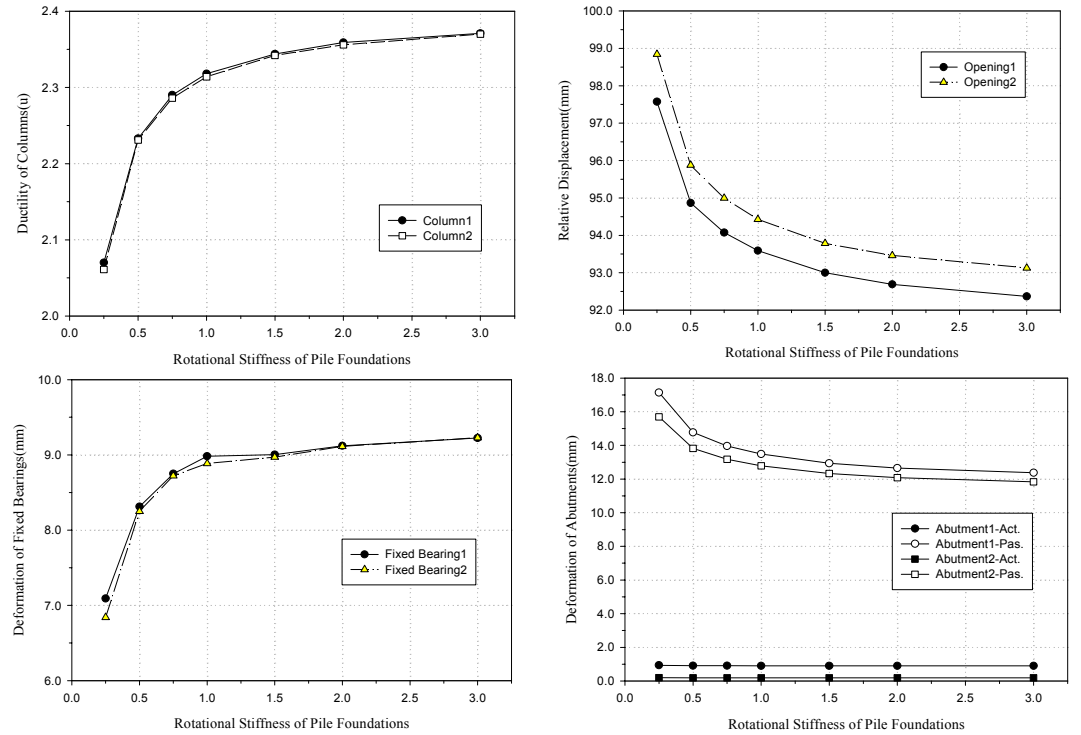

Figure 6.2d Effect of Rotational Stiffness of Pile Foundation in MSC Steel Bridge

6.4 Sensitivity of Parameters

It is necessary to investigate the sensitivity of each parameter to understand how much effect on the response of a bridge a parameter has. In general, the trend of the ductility demand of columns is similar to that of the deformation of expansion bearings, hinge openings, and the demand of foundations. The deformation of fixed bearings and the passive deformation of abutments depend on the pounding force. Therefore, considering the three responses, a bridge is screened to obtain the sensitivity of each parameter. The response from G2 ground motions for Carbondale are utilized to calculate the sensitivity which is the slope of each response in the graphs drawn in the sections 6.2 and 6.3. Before calculating the slope for each parameter, the responses are normalized by the response of the as-built bridges, and parameters are also normalized by the parameter value of the as-built bridges. In general, the sensitivities of responses are nonlinear. Therefore, only the three points are used; one is the reference point and the other two are the points beside the reference, to calculate the sensitivity since the points in the far sides can distort the sensitivity.

In the MSSS steel bridge, the sensitivity for the ductility of both columns, the deformation of Fixed-bearing 1 which has the maximum deformation, and the passive deformation of Abutment 2 are considered. In the MSC steel bridge, the second column is excluded because the trend of the second column is almost the same as that of the first column.

Figure 6.3 shows an example how to obtain the sensitivity of the parameter of deck mass on the ductility of columns in the MSSS steel bridge. In the figure, the sensitivity

of Column 1 is 0.45. Table 6.1 and 6.2 shows the result of the sensitivity study on the both bridges, the MSSS and the MS continuous steel bridge, respectively.

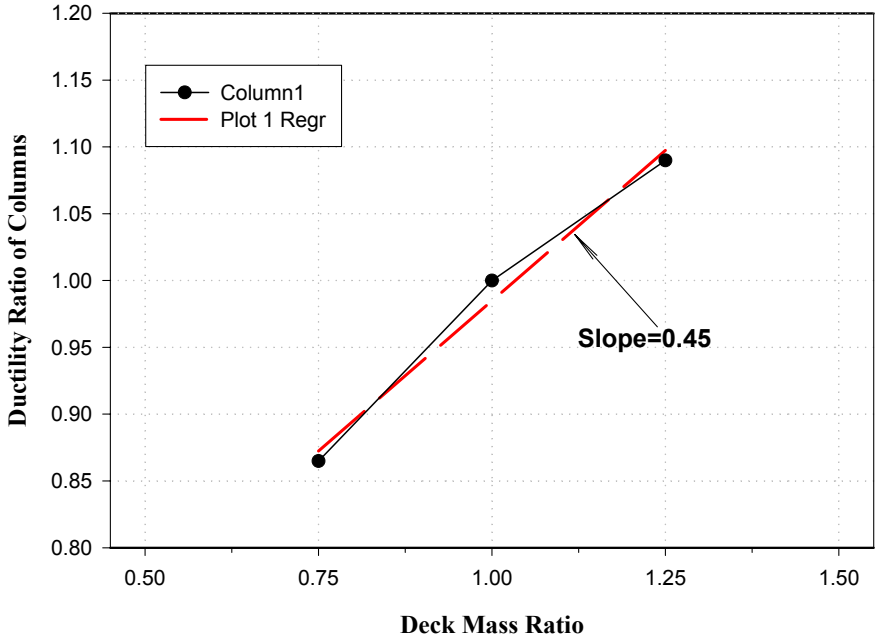

Figure 6.3 Sensitivity of Deck Mass on Ductility of Columns in MSSS Steel Bridge

From Table 6.2, the ductilities of Column 1 and 2 are most sensitive to the variation of the deck mass. The variation of the gap on abutments and the deformation of the fixed bearing have the most effect on the passive deformation of Abutment 2. The variation of deck masses is very sensitive to almost every response of the bridge. The gaps on abutments have large sensitivity on the deformation of fixed bearings and abutments. The friction of expansion bearings, gap between decks, and rotational stiffness of foundations have a small effect on the global responses of the bridge.

As shown in Table 6.3, in the MSC steel bridge, the gaps on abutments have the most effect on the ductility of columns and the deformation of fixed bearings. The deck mass has the largest sensitivity on the deformation of abutments.

Table 6.2 Sensitivity of parameters on the MSSS Steel Bridge

Parameter	Column 1 Ductility	Column 2 Ductility	Fixed Bearing 1 Deformation	Abutment 2 Deformation
Friction	8.18e-2	5.90e-3	1.60e-1	8.56e-1
Mass	**4.50e-1**	**3.80e-1**	4.26e-1	1.88
Gap-A	3.46e-1	1.44e-1	**9.92e-1**	**1.90**
Gap-D	9.37e-2	4.50e-2	4.43e-1	1.59e-1
R-Stiffness	6.05e-2	2.75e-2	9.57e-2	4.19e-1

Table 6.3 Sensitivity of Parameters on the MSC Steel Bridge

Parameter	Column 1 Ductility	Fixed Bearing 1 Deformation	Abutment 2 Deformation
Friction	4.49e-2	1.06e-1	1.73e-1
Mass	3.48e-1	6.86e-1	**1.36**
Gap-A	**7.00e-1**	**8.28e-1**	1.16
R-Stiffness	2.98e-2	1.49e-1	8.57e-2

Based on the above results, the mass of decks and the gaps between decks and abutments are estimated as the most effective parameters. The deck mass of a bridge is not varied without replacing the deck with lighter or heavier material. The gaps, however, is varied with temperature. Consequently, it is found from this parametric study that the gap size is the most sensitive parameter.

CHAPTER 7

EXPERIMENTAL TESTS

7.1 Experimental Setup

This chapter describes the experimental test setup and the components used in the testing of the full-scale bridge model. The chapter begins with an overview of the experimental setup and the tests that were conducted. Next, the Structural Engineering Mechanics and Materials Laboratory testing facility at the Georgia Institute of Technology is described and details are given on the various components used in the experimental tests. The bridge components used in the experimental model are described including the piers, the concrete pedestals, elastomeric bearings, and steel cable restrainers. Information on the assembly of the bridge model and the seismic cable restrainer retrofits conducted on the bridge are also included.

7.1.1 General Overview

The experimental portion of the Mid-America Earthquake Center's Project ST-12: Response Modification of Bridges consisted of testing two commonly used retrofit measures in Mid-America - elastomeric bearings and cable restrainers. A full-scale model of a typical steel girder bridge is used to test these retrofit strategies under quasi-static and dynamic loadings. Previous research on elastomeric bearings was mostly based on tests of individual bearings under static loadings. The individual bearings were subjected to a vertical compressive loading from one actuator to represent the dead

weight of the bridge and a lateral loading from another actuator. Dynamic testing of the individual bearings under large compressive loads was difficult to achieve due to instability of the actuator producing the dead weight load. Therefore, most of the experimental data obtained for the individual bearings only gave response characteristics for bearings under static lateral loading or dynamic lateral loading with small compressive loads. Experimental research on seismic cable restrainer assemblies is also very limited. Tests conducted on a full-scale model of the bridge would produce results which are more representative of the elastomeric bearings and cable restrainers on existing bridges.

The full-scale bridge model was based on an existing steel girder bridge in Tennessee, which has been considered for seismic cable restrainer retrofit, as shown in Figure 7.1. The two main girders were A36 W30x292 steel sections and span 40'-0" at a distance of approximately 7'-9 ½" from centerline of girder to centerline of girder. Three transverse stiffener beams (W30x124) were spaced between the main girders such that the loading of the bridge will remain in-plane and thus minimize torsional effects. The dead weight of the bridge deck was represented by casting a large concrete block between the main girders. The concrete block also provided a bearing surface to which loading from the actuator can be transmitted. The superstructure of the bridge, described above, rested on top of the elastomeric bearings. The bearings, in turn, sat atop concrete pedestals which were cast on the pier caps. The piers were post-tensioned to the structural floor to prevent any movement or sliding that could occur during the loading. The steel reinforcement in the concrete piers was designed similar to piers on actual

bridges in order to accurately predict the behavior of the cable restrainer connections at the pier caps.

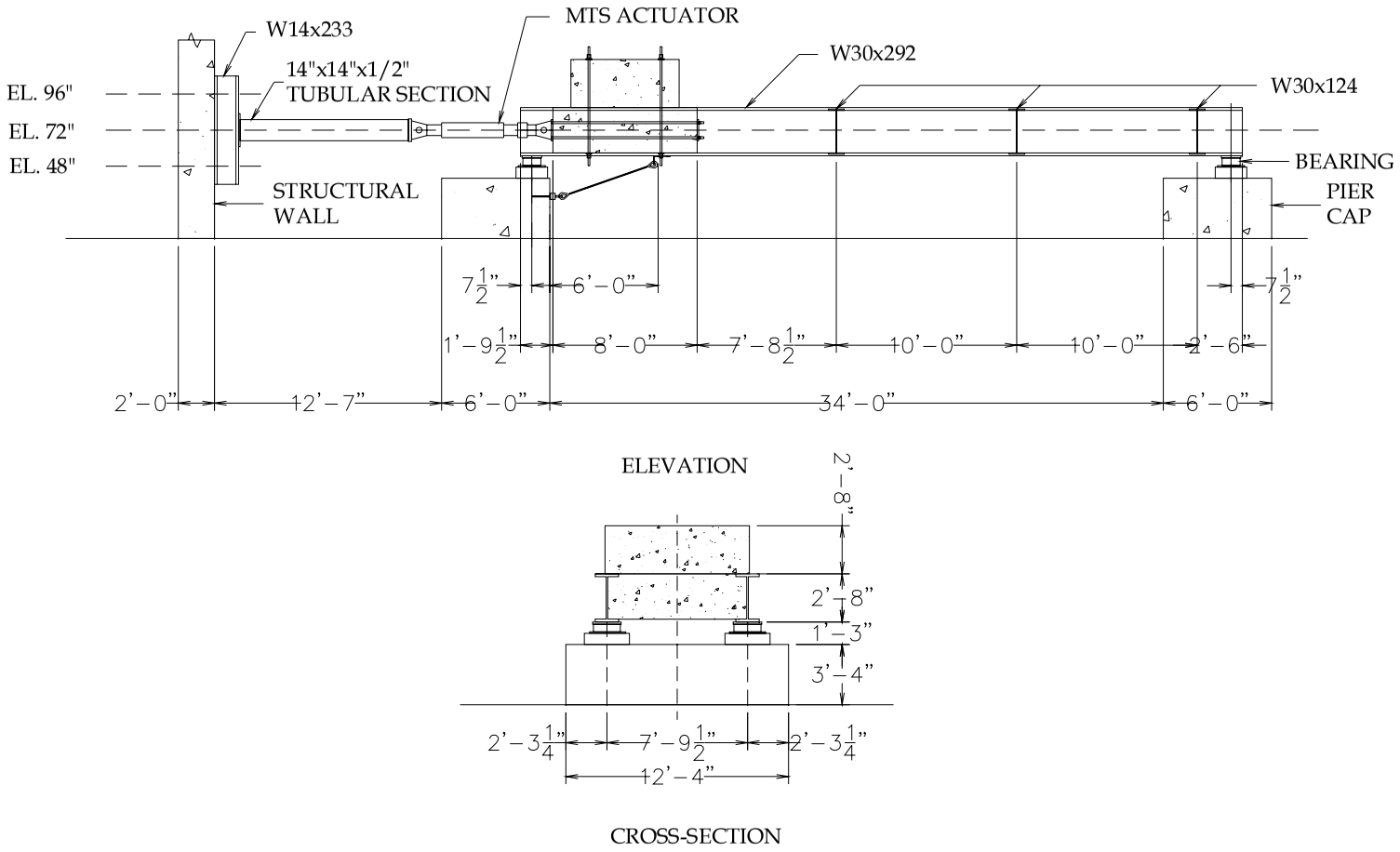

Figure 7.1 Elevation and cross-section of test setup.

The loading of the bridge model was achieved through the use of an MTS 243.45T actuator powered by a 150 gpm hydraulic power supply and dual 60gpm servovalves. This loading system was designed to achieve a maximum speed of 8 inches per second, with maximum forces of 100 kips in tension and 150 kips in compression. The actuator was attached to the reaction wall in the laboratory and the concrete block between the two steel girders.

The main objective of the study is to evaluate the force-deformation behavior of the elastomeric bearings and seismic cable restrainers. The components tested on the bridge were supplied by manufacturers that have been used to supply similar bridge components throughout the Mid-America region. The elastomeric bearings were tested statically and dynamically over various displacements and frequencies. Seven different cable restrainer configurations were tested statically on the model bridge.

7.1.2 Testing Facility

The structural engineering laboratory at the Georgia Institute of Technology consisted of a 6 ft. thick concrete strong floor and a large L-shaped reaction wall. The reaction wall has a 2ft. thick wall with buttresses that extend back 12 ft., allowing for rigid boundary conditions for the test setup. The reaction wall is 24 ft. high on one side and 36 ft. high on the other. The laboratory was built specifically so that large external loading frames were not needed for experimental tests. Figure 7.2 shows a partial view of the wall in the testing facility.

Contained within the walls and floor are a series of anchor points at 4ft. on-centers. This four-foot pattern extends the length and height of the wall and the length of the floor inside the designated testing areas. Anchor points on the wall are straight, horizontal tubes in an 8" square pattern that accommodate high strength threaded Dywidag bars which are threaded through and extend beyond either face of the wall. Each Dywidag bar has a service capacity of 50 kips with a total of four bars per anchorage point for a total service capacity of 200 kips. It is important to point out that the safety factor on these bars is over 2.5 to provide a comfortable margin for low cycle fatigue loading.

To provide an anchorage to the wall, a Dywidag bar is inserted in the tube, a nut is threaded onto one side of the wall to prevent pullout, and post-tensioning is applied from the other side of the wall. Anchorage to the strong floor is accomplished in a slightly different manner. Holes in the specimen are cast-in-place and Dywidag bars are inserted through the holes. The bars are threaded into anchorage blocks on the slab and post-tensioned vertically through the specimen. The anchorage blocks in the slab have a service capacity of 200 kips and are in an 8"x8" pattern as in the wall.

Figure 7.2 Partial illustration of the testing facility at the Georgia Institute of Technology.

7.1.3 Bridge Substructure

The bridge substructure consists of two large reinforced concrete piers, four reinforced concrete bearing pedestals, and four elastomeric bearings. The next three sections will discuss the bridge superstructure in more detail.

7.1.3.1 Piers

The reinforced concrete piers were 12’-4" wide x 6’-0" long x 3’-4" high. The width was selected to accommodate the spacing of the girders. The height allowed concrete cone failure of the connection of the cable restrainers at the face of the pier, if it were to occur.

Figure 7.3 Reinforcement cage and form for the construction of the piers.

Pier 1, which was closest to the structural wall, had a 28-day concrete compressive strength of 3,370 psi. Pier 2, at the far end, was cast on a different day and had a concrete strength of 4,055 psi. Figure 7.3 shows the steel reinforcement cage in the form prior to casting the piers. The reinforcement in both piers, illustrated in Figure 7.4, was modeled after the reinforcement in the pier cap of the model bridge in Tennessee. The reinforcement consisted of fourteen #10 top longitudinal rebars, nine #10 bottom longitudinal rebars, two #6 longitudinal rebars on each face of the pier, and ten #5 stirrups.

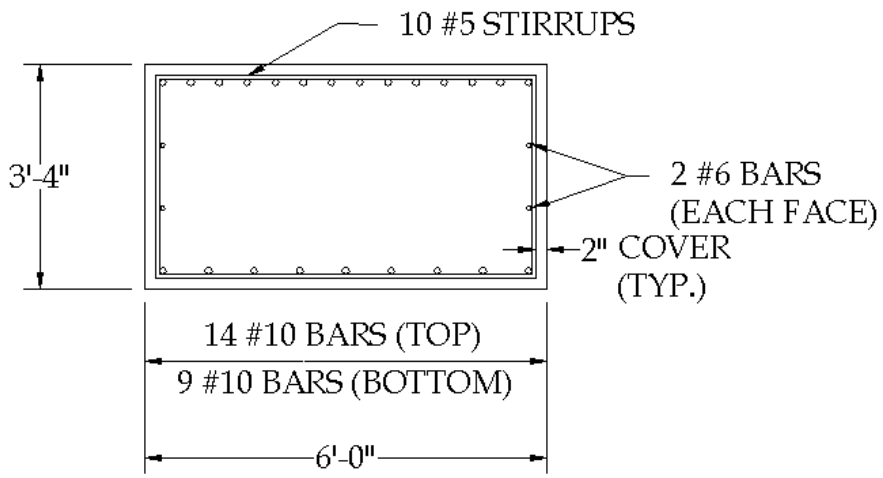

Figure 7.4 Pier reinforcement details (elevation).

To prevent sliding of the piers along the structural floor during testing, the piers were post-tensioned to the floor with eight Dywidag bars. The Dywidag bars were located along the centerline of the pier to prevent obstruction of the bearings. The bars were post-tensioned to 65 kips per bar.

7.1.3.2 Concrete Pedestals

One of the most common retrofit measures is to replace steel rocker bearings with elastomeric bearing assemblies. In most cases, the elastomeric bearings are much smaller in height than the steel rocker bearings. To accommodate the height difference, on of two methods is used. In the preferred method, a steel section is attached between the elastomeric pad and the bridge girder. However, when the height difference is usually more than four inches, the use of steel sections becomes expensive and is not very practical. The second option is to construct a concrete pedestal. The latter method was used in this experiment.

To better replicate field conditions during retrofits, the pier was cast first. After the dimensions of the elastomeric bearing assemblies were finalized, the dimensions and reinforcement of the pedestals were designed (Figure 7.5). Each pedestal was 21" wide x 30" long x 7-7/16" high. Holes corresponding to the vertical reinforcement and anchor bolts for the bearing were cored in the piers. Four #6 bent rebars were epoxied into the 9" cored holes located at the corners of the three #3 stirrups. PVC pipes were used to prevent concrete from filling in the 12" cored holes for the anchor bolts. Concrete, with an average compressive strength of 5535 psi, was cast. The concrete was allowed to cure for one week, after which time, the PVC pipes were removed and the anchor bolts for the bearings were epoxied into the piers.

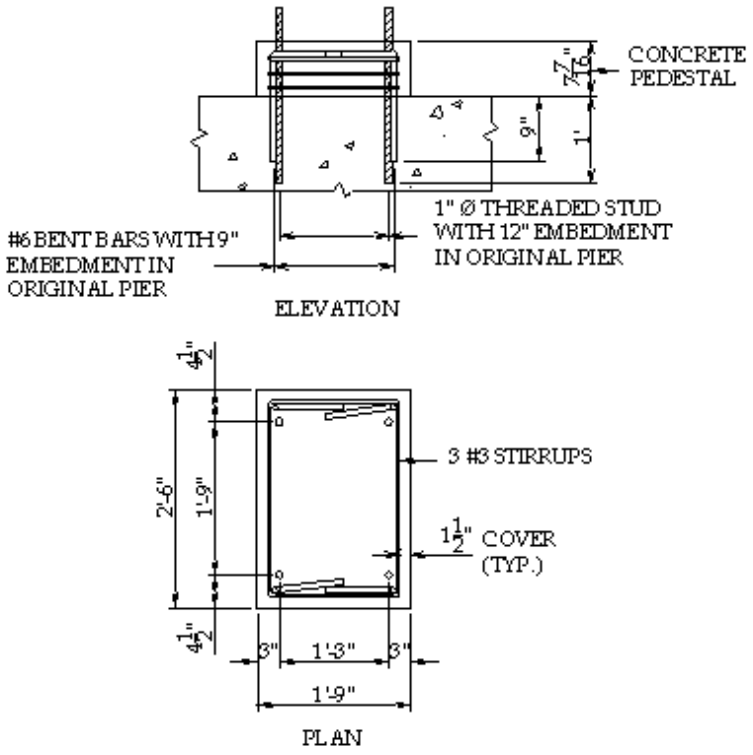

Figure 7.5 Concrete Pedestal reinforcement and details.

7.1.3.3 Elastomeric Bearing Assemblies

The elastomeric bearing assembly (Figure 7.6) consisted of an elastomeric pad vulcanized to two steel bearing plates. The pad was 12" wide x 18" long x 5-1/16" high with six (6) 3/16" steel laminates vulcanized to seven (7) 9/16" layers of rubber. The durometer reading (hardness) of the polyisoprene (natural rubber) used in these bearings was 56. The arbitrary scale for durometer ranges from 0 to 100 for soft to hard materials. The durometer for typical elastomeric bearings ranges between 50 to 70. The top bearing plate was 13" wide x 19" long x 1-1/2" thick. Four threaded holes accommodating 1" diameter threaded studs were made. The bottom bearing plate was 18" wide x 24" long x 1" thick. Four 1-1/2" diameter holes were drilled in the plate to accommodate 1" diameter threaded studs epoxied to the concrete pedestal. This design is currently being used in the Memphis, Tennessee area. Current designs have specified that top bearing plates should be bolted to the girders and bottom bearing plates should be bolted to the pier cap. This design prevents the bearing from "walking out" underneath the girders and causing collapse of the superstructure during a seismic event. Figure 7.7 shows the assembly of the bearings to the concrete pedestal and pier.

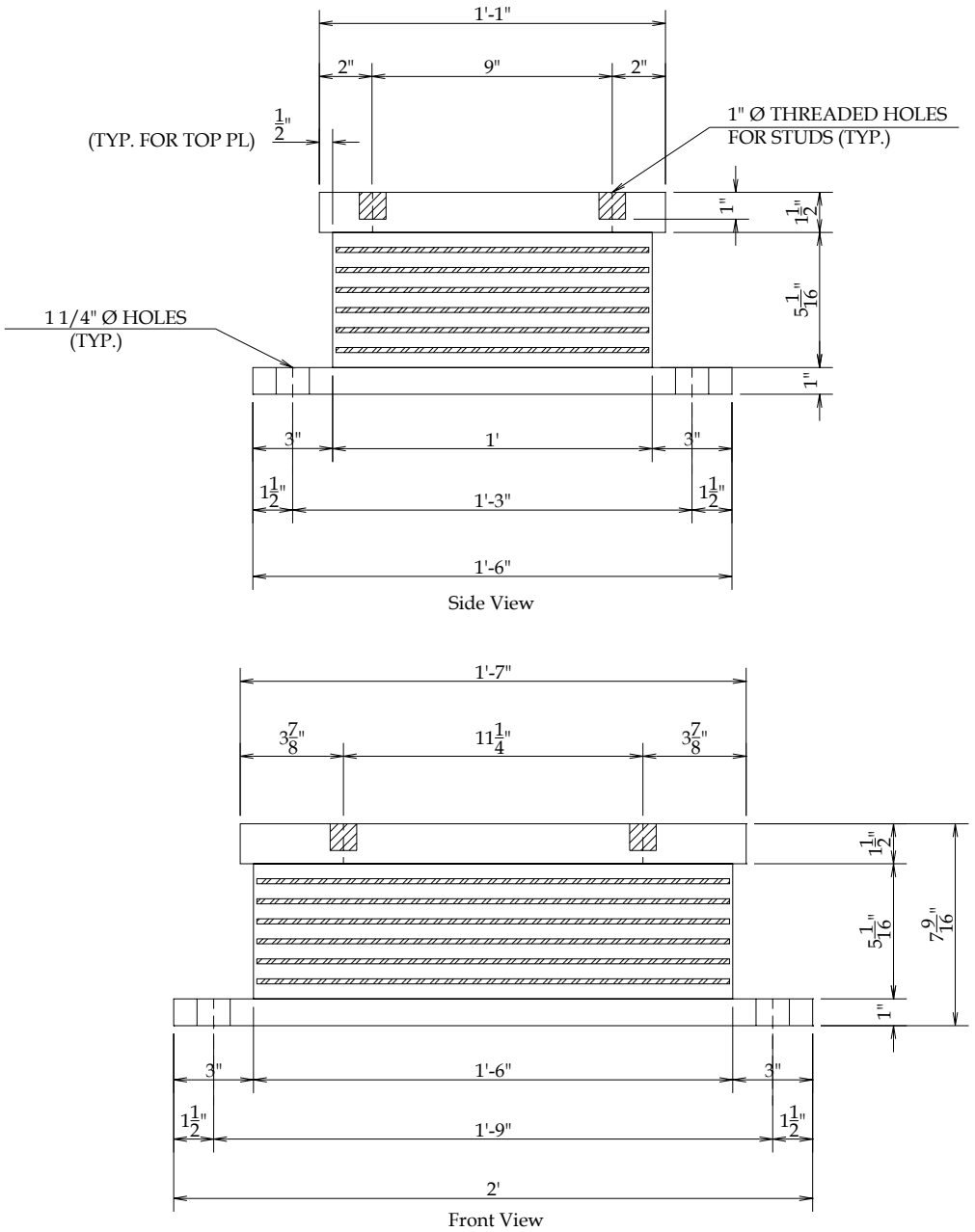

5 1/16" THICK ELASTOMERIC PAD INCLUDES:
SIX 3/16" STEEL LAMINATES
SEVEN 9/16" LAYERS OF RUBBER
RUBBER COVER: 1/8" MIN, 1/4" MAX

Figure 7.6 Details of steel laminated elastomeric bearings.

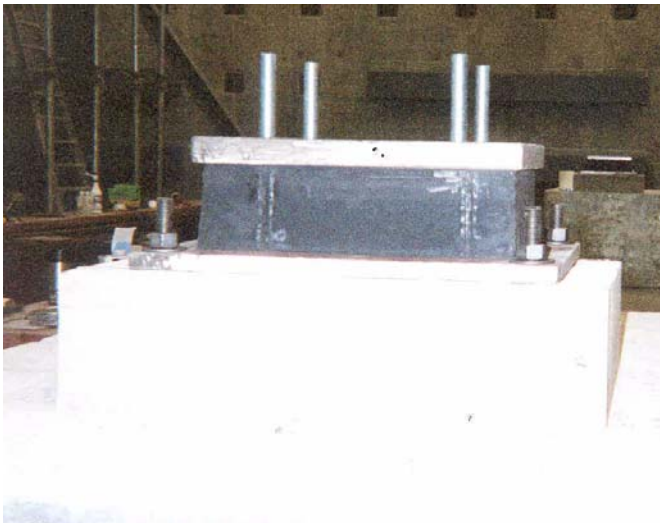

Figure 7.7 Elastomeric bearing assembly.

7.1.4 Bridge Superstructure

The bridge superstructure consists of two steel girders, three transverse beams, and two concrete blocks for dead weight. The main girders were composed of A36 W30x292 steel sections which were 40’-0" long. Three transverse stiffeners, which are A36 W30x124 steel sections, were attached to the main girders to ensure in-plane loading of the bridge.

The dead weight of the bridge consisted of the concrete bridge deck. The amount of dead weight used in the bridge model was based on plans from the aforementioned Tennessee bridge. In the bridge plans, the deck was 7" thick, the center lines of the girders were 8’-0" apart, and the span length was assumed to be 60’-0" long. Using these values, the tributary dead weight to represent a two-girder span was 42 kips.

The dead weight of the bridge was represented by casting two concrete blocks, which totaled 42 kips (Figure 7.8). Two blocks were cast because of the load limitation of the cranes. The first dead weight block, with a concrete strength of 4422 psi, was cast between the two main girders (Figure 7.9). It was 8'-0" long, 7'-8 1/2" wide, and 2'-6" high. Four horizontal tubes were cast with this block so that the actuator could be post-tensioned to the block with Dywidag bars. Four vertical tubes were also cast with the block to allow post-tensioning of the two blocks to prevent sliding between them. The block was reinforced with twelve #6 rebars. Holes drilled in the webs of the girders allowed for the placement of the rebars through both girders to prevent slipping of the block with the girders during loading. The second dead weight block, with a concrete strength of 3626 psi, was 6'-0" wide x 8'-0" long x 2'-8" high. It was cast with four vertical tubes. This block was not reinforced since it would not experience significant loads.

Figure 7.8 Two concrete blocks representing the dead weight of the bridge.

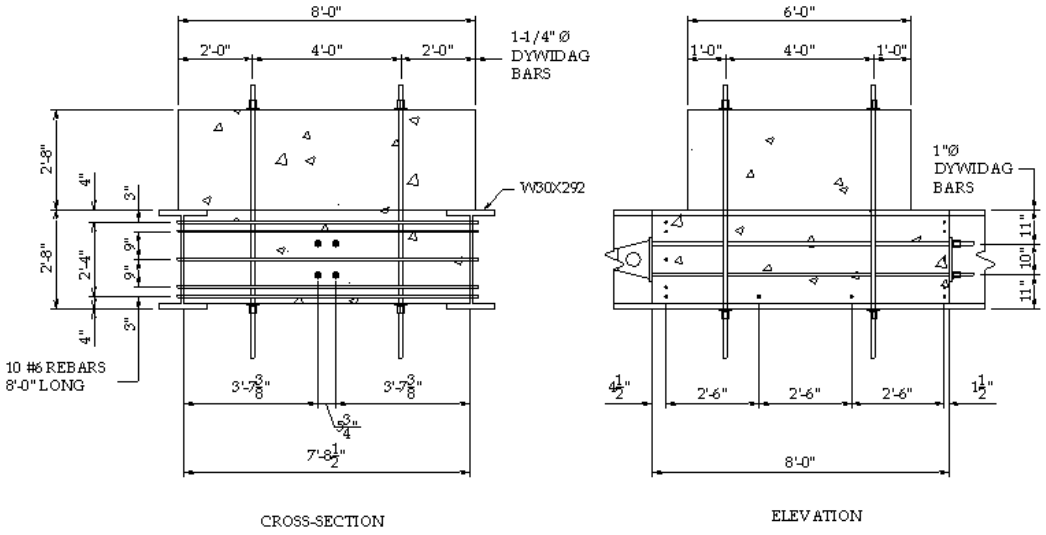

Figure 7.9 Reinforcement of the concrete dead weight block between the girders.

7.1.5 Bridge Assembly

In order to allow for concrete cone failure of the seismic cable restrainers on the face of the pier cap, sufficient height below the girders was needed to allow a realistic angle for the cable restrainers. Thus, the centerline of the actuator was located at an elevation of 6'-0" from the structural floor. Since the anchors on the structural wall were located at 4'-0" and 8'-0", a spreader beam was attached to the wall. The beam was a W14x233 steel section. Holes, which corresponded to the anchor holes in the wall, were drilled on the flange closest to the wall. That flange was then post-tensioned to the 2'-0" thick structural wall with eight 1-1/4" diameter Dywidag bars at a force of 50 kips per

bar. Holes, corresponding to the bolt holes in the connection of the actuator, were drilled in the flange farthest away from the structural wall.

Due to space limitations in the laboratory, the centerline of the bearings closest to the structural wall was located 17'-7" from the wall. Consequently, extender sections for the actuator were required. First, the W14x233 spreader beam was post-tensioned to the structural wall. Next, a 9'-7" long tubular section was attached (Figure 4.10). The section is a 14" x 14" x ½" square tube. The end plate near the spreader beam is 15" x 22" x 1" with four 1-½" diameter holes corresponding to the bolt holes in the actuator. The end plate near the actuator is 15" x 15" x 2" with four 1-½" diameter holes corresponding to the bolt holes in the actuator. A 2" thick plate was selected to prevent deflections due to actuator loading.

The first pier was located at a distance of 12'-7" from the structural wall to the closest face of the pier. Eight 1-1/4" Dywidag bars (at centerline locations of 13'-7" and 17'-7") were used to post-tension the pier to the structural floor. The second pier was located at a distance of 52'-7" from the structural wall to the closest face of the second pier. The second pier was also post-tensioned to the structural floor at locations 53'-7" and 57'-7".

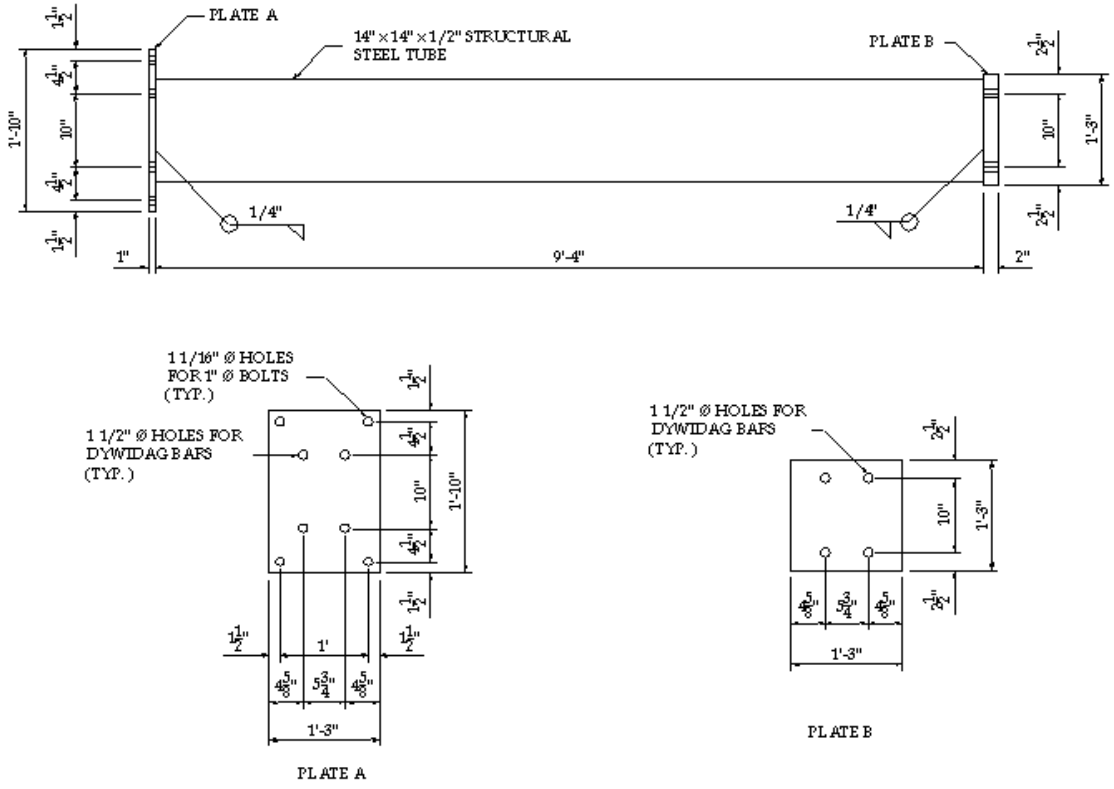

Figure 7.10 Details of structural tube section (14"x14"x1/2").

Next, the concrete pedestals were constructed. The center of the bearings was located at distances of 17'-7" and 56'-4" from the structural wall. The locations were determined according to minimum edge distances from Tennessee Department of Transportation specifications. The edge distance from the centerline of the bearing to the face of the pier is 12" and the distance from the centerline of the bearing to the edge of the girder is 7-1/2".

To construct the pedestals, holes were first core drilled into the original pier. Vertical rebars were epoxied into the holes; stirrups were tied to the vertical rebars; and

PVC pipes were inserted to prevent concrete fill-up in the anchor bolt holes. Concrete was cast into the forms and allowed to cure for one week before the threaded anchor bolts for the bearings were epoxied in the hole (after the PVC pipes were removed).

Next, the elastomeric bearings were placed on the concrete pedestals. Flat washers and hex-nuts were placed on the anchor bolts and tightened. Holes were drilled in the bottom flange of the bridge girders to correspond to the threaded studs embedded in the top bearing plate of the elastomeric bearing assemblies. The superstructure was then lowered into placed with the laboratory overhead cranes. Flat washers and hex-nuts were place on the threaded studs and tightened down.

The second dead weight concrete block was placed on top of the original block cast between the main girders. Four 1-1/4" diameter Dywidag bars were inserted through the holes of the two blocks. They were each post-tensioned to 40 kips to prevent the two blocks from sliding during loading.

Next, the actuator was placed between the tubular section and the concrete block. Four 1" diameter Dywidag bars were inserted from the spreader beam flange, through the tubular section, and through the bolt holes in the actuator. The Dywidag bars were post-tensioned to 50 kips per bar. Then, four 1" diameter Dywidag bars were inserted from the other end of the actuator, through a 1" bearing plate, through the concrete block, and through another 1" bearing plate. The Dywidag bars were post-tensioned to 50 kips per bar.

All post-tensioning forces provided a factor of safety of more than two against the expected forces. A value of two was deemed minimum to account for possible dynamic amplitude effects.

7.1.6 Bracing Frames

A lateral bracing frame was post-tensioned to the strong floor at a distance of 28'-7" from the structural wall, in the anchor points directly below the webs of the superstructure girders. The frame consisted of a 16'-0" spreader beam which was placed on the floor and post-tensioned so that it was perpendicular to the length of the bridge. Four columns were bolted to the spreader beams, one on each side of the superstructure girder, with a maximum distance of 1/2" from the superstructure girders. Additional resistance was provided by bolting channel sections to each set of columns above the superstructure girder. This frame provided bracing of the bridge model in case of out-of-plane loading (Figure 7.11).

During initial test runs of the bridge model and bearings, the cantilevered structural tube did not provide enough stiffness in the vertical and lateral directions. As a result, the tube caused severe vibration of the actuator and bridge model. To remedy this problem, several bracing members are constructed and installed. First, four 1/2" thick stiffener plates were welded on the W14x233 spreader beam on the wall to prevent rotation of the flange of the spreader beam.

Figure 7.11 Columns used to restrict out-plane-movent.

Next, a vertical column was attached to the strong floor beneath the structural tube at the end connected to the actuator. A small tube, placed between the vertical column and the structural tube, was welded to the top of the vertical column. Another small tube was placed on top of the structural tube. Dywidag bars were placed through the holes in the small tube to provide vertical restraint.

Finally, to increase the lateral stiffness, a lateral brace was constructed. A spreader beam was attached to the structural wall at a horizontal distance of 8’-0" from the W14x233 spreader beam. One T-stub was bolted and welded to the new spreader beam at an elevation of 6’-0". Another T-stub was welded to the structural tube at an elevation of 6’-0" near the end by the actuator. Double angles (two 7"x4"x3/4" angles) were then connected to the two T-stubs and welded to prevent slipping of the bolts.

Figure 7.12 shows the extender tube and the steel sections used to stiffen the tube in the vertical and horizontal directions.

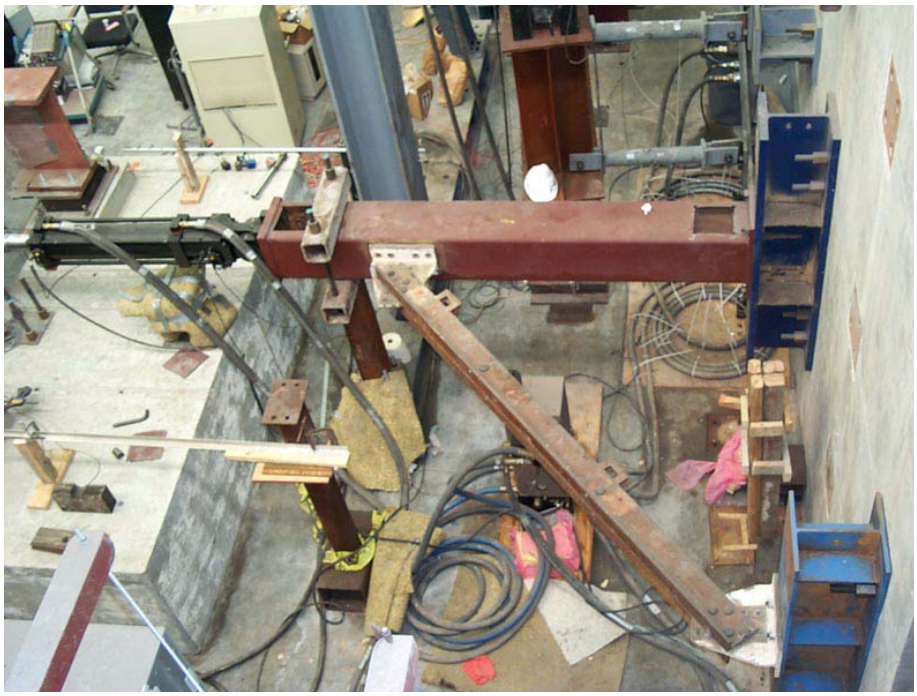

Figure 7.12 Actuator extender tube and connection elements to the reaction wall.

7.1.7 Cable Restrainer Retrofits

Cable restrainers were attached between each girder and the pier on the bridge model. The next three sections will describe the characteristics of the restrainer cable, pier connection, and the girder connection used in this experiment.

7.1.7.1 Restrainer Cable

Typical cable restrainers used in the Central and Southeastern US are 3/4-inch diameter and 0.22 square inch steel cables. They are made of 6x19 strands, galvanized

with a wire rope strand core, a right regular lay, and made of improved plow steel. The cables have a yield strength of 39.1 kips, which coincides with a yield stress of 176 ksi. The initial modulus of elasticity is 10,000 ksi. The post yield strength of the cables increases to an ultimate of about 53 kips per cable.

The cable restrainer system is composed of cables, thimbles, wire rope clips, and steel connections for the pier and girder. The ends of the cables were terminated using galvanized wire rope thimbles and four galvanized wire rope clips. According to the installation specifications, the wire rope clips were spaced 4" from each other and the bolts were torqued to 130 ft.-lbs. Figure 7.13 shows the wire rope end termination used on the cable restrainer assemblies tested in this experiment.

Figure 7.13 Wire rope end termination used a thimble and 4 wire rope clips.

Seismic cable restrainer retrofits were tested on the bridge model according to the specifications given by the Tennessee Department of Transportation. However, only one cable restrainer was used per girder instead of two specified due to loading limitations. The cable restrainers were attached to the pier and each girder on one side of the bridge model (Figure 7.14 and 7.15).

Figure 7.14 Cable restrainers were attached between girder flange and pier.

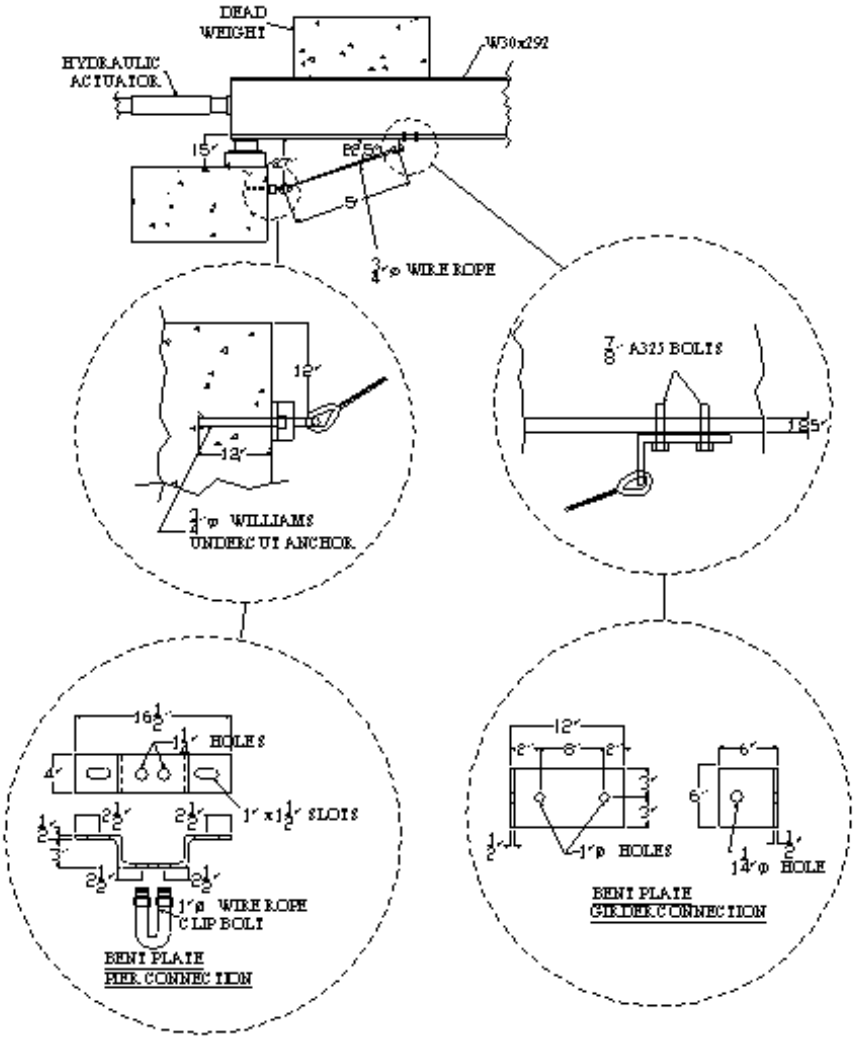

Figure 7.15 Original Tennessee DOT cable restrainer assemble tested on bridge model.

7.1.7.2 Restrainer Connections

The original pier connection specified by Tennessee DOT was a 1/2" bent plate connection. The steel pier connections were anchored to the concrete pier with two 3/4" diameter Williams S-9 undercut anchors with 12" embedment. These type of anchors were specified by Tennessee for use with their cable restrainer assemblies.

The undercut anchors were installed according to the manufacturer's specifications. First, a 1-1/8" diameter hole, 14" deep, was cored 12" inches below the top of the piers (Figure 7.16a). Next, the hole was undercut at 13-1/2" using the supplied undercut tool from the manufacturer (Figure 7.16b). After the hole was undercut, the anchor was installed in the hole and the hex nut was tightened approximately 12 revolutions to expand the anchor (Figure 7.16e). Finally, the hex nut was removed and the steel connection was attached and the nut was retightened (Figure 7.16f).

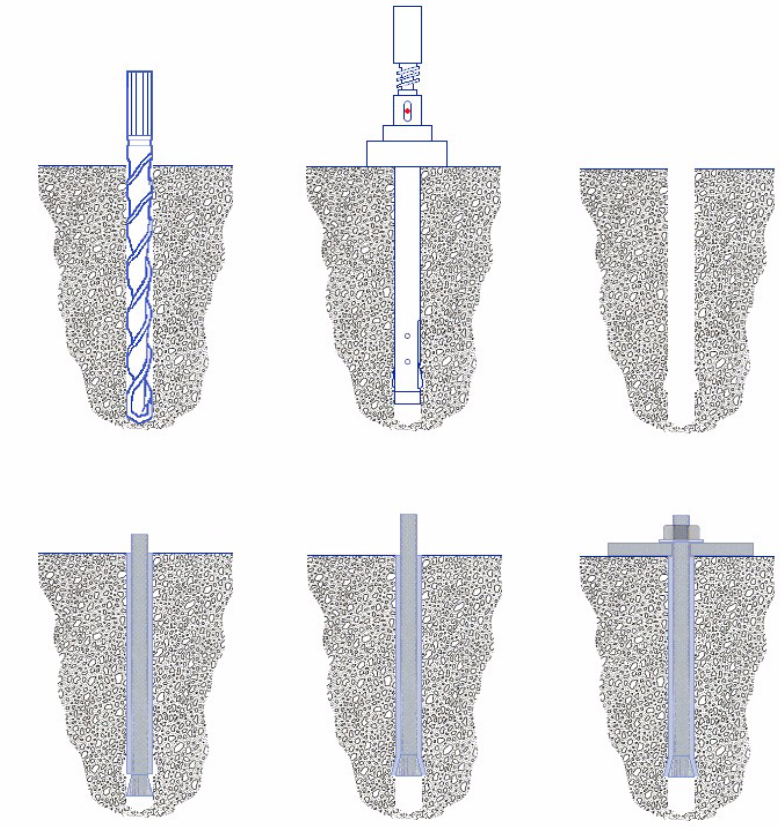

Figure 7.16 Installation procedure for undercut anchors.

The original girder connection specified by Tennessee DOT was a 1/2" bent plate connection. This connection was attached to the bottom of the girder flange using two 7/8" diameter A325 structural bolts.

7.2 Description of Tests and Results

This chapter describes the experimental test results on the full-scale model bridge. The first section gives information about the instrumentation used on the elastomeric bearing and cable restrainer tests. Specifications for the instrumentation used in this study can be found in Appendix A. The second section describes the loading system used for the elastomeric bearing and cable restrainer tests. The third section presents the test description and the results of the elastomeric bearing tests. Finally, the results and the description of the cable restrainers tests are presented.

7.2.1 Instrumentation

In order to monitor the data obtained from this experiment, an OPTIM Electronics MEGADC model 3415AC was used to take data readings from the sensors at a specified scan rate. This data acquisition system can sample data up to 25,000 times per second and has a maximum capacity of 300 channels of input. It can also provide constant current and constant voltage excitation for sensors if required.

The MEGADAC 3415AC is hooked up to an external computer and controlled remotely using OPTIM's Test Control Software (TCS). The system is capable of storing up to 64 megabytes of data internally. However, data is easily exported to an external computer hard drive using the TCS software. After each test was completed in this study, the data files were exported to the host computer as ASCII files to ensure proper storage of information.

Four different types of sensors were used to monitor data on the experimental tests. Instrumentation of the test setup with elastomeric bearing assemblies consisted of six linear variable differential transformers (LVDTs), twelve strain gauges, four accelerometers, and the load cell and LVDT located on the MTS actuator (Figure 7.17). The first type of sensor used to measure longitudinal displacement of the bridge was a linear variable differential transformer. The LVDTs used for the tests were manufactured by Lucas Schaevitz (Models 2000HCD and 3000HCD) and RDP (Model DCT2000). An LVDT is an electromechanical transducer, which consists of a coil assembly and a free-moving, rod-shaped ferrous core. When the primary coil is energized by and external AC source, voltages of opposite polarities are induced in the secondary coils. When the core is at the center, or the null position, in the coil assembly, the net output of the transducer is zero. When the core is moved from the null position, it causes the induced voltage of the closest secondary coil to increase, while the other voltage decreases. This results in an output that is a sinusoid with differential amplitudes and a 0 or 180 phase to the primary coil, which gives the displacement.

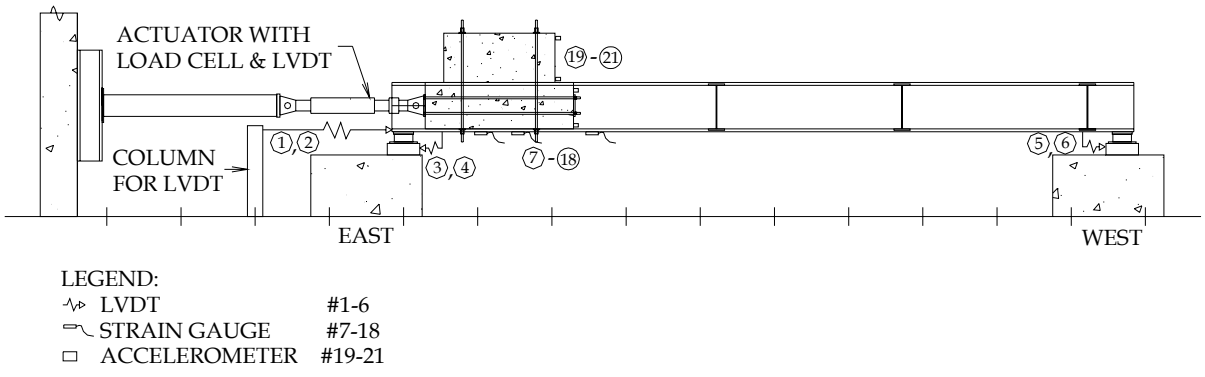

Figure 7.17 Instrumentation of test setup.

A total of six LVDTs were used to measure displacements during the elastomeric bearing tests. Figure 7.17 illustrates the locations and numbering schemes for the LVDTs. LVDTs #1 and #2 measured displacements of the bridge model. They were attached from a fixed location (the two columns) to each end of the bridge girders (on the outside of the flanges). LVDTs #3 and #4 measured the displacements of the east bearings, assuming that there was no slip between the bearings and the girders. They were attached from the underside of the girders, directly below the web, to the concrete pedestal. LVDTs #5 and #6 measured the displacements of the west bearings, assuming that there was no slip between the bearings and the girders. Their connections were similar to that of LVDTs #3 and #4. For the cable restrainer tests, only LVDTs #1 and #2 were used to measure displacements in the bridge model.

Strain gauges were used to measure the strain in the bottom flanges of the steel girders. The strain gauges used were Texas Measurements TML Model WFLA-6-11-1L. The gauge consists of a fine electric resistance wire, which is bonded to an electrical insulation base. This particular gauge is waterproof. It has a vinyl lead wire and the entire gauge and lead wire junction have been fully overcoated with a transparent, flexible epoxy resin, which is approximately 1 mm thick. The gauges were bonded to the underside of the bottom flanges of the two girders at locations of 4’-7-1/2", 6’-7-1/2", and 10’-7-1/2" from the end of the girder closest to the structural wall. These locations correspond to various distances from the cable restrainer connections on the girder. The strain gauges were placed on the bridge to measure strains in the girders from the cable

restrainer connections. However, the girder flanges were very thick and the strains measured were negligible.

Four Wilcoxon 731A Ultra-Quiet, Ultra Low Frequency seismic accelerometers were used to measure the acceleration of the bridge model. The accelerometers were mounted at the top and bottom of the dead weight blocks, as shown in Figure 7.18. The accelerometers are connected to a signal conditioner that sends voltages to the OPTIM MEGADAC. The 16 channel signal conditioner is an external PCB Piezotronics module that provides selectable gains of 1, 10, and 100 to 16 channels in four embedded 4-channel PCB 442A104 signal conditioners. Since the bridge model consists of significant mass, the inertia force was measured and subtracted from the load cell data. The accelerometers were only used on the dynamic tests of the bridge with elastomeric bearings.

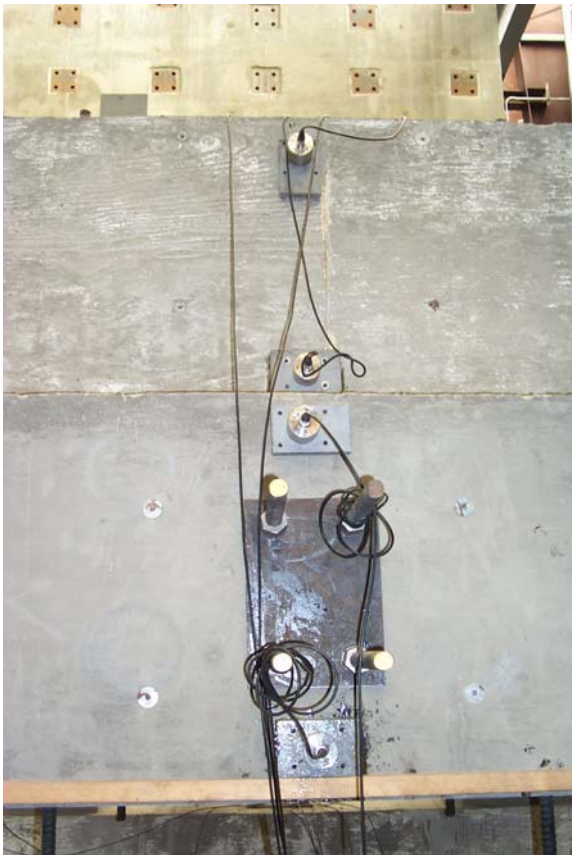

Figure 7.18 Seismic accelerometers mounted at top and bottom of dead weight blocks.

7.2.2 Loading Equipment

An MTS actuator (Model 243.45) with dual servovalves was used to displace the full-scale bridge during testing. Dual servovalves were required for dynamic testing and they allowed the actuator to theoretically displace up to a maximum speed of 12 inches per second. The actuator has a tensile capacity of 100 kips and a compressive capacity of 146 kips.

An MTS 407 Controller was used to control the actuator. This controller enables the user to use a function generator to transmit sine, square, and triangular waveforms for

testing. Prior to attaching the actuator to the bridge model, the PDIF gains on the controller were adjusted to fine tune the response of the actuator under a sine command. By plotting the curves for the command and feedback versus time and adjusting the PDIF gains, phase shifts between command and feedback were decreased and the difference in amplitudes between command and feedback were minimized. When the actuator was attached to the bridge model, the resistance of the bridge caused the actuator to become unstable at the gains previously set. Therefore, the PDIF gains were readjusted to produce a stable and smooth loading.

7.2.3 Elastomeric Bearing Tests

The first phase of this study was to test full-scale elastomeric bearings on the bridge model. The next section gives a description of the elastomeric bearing tests, followed by a presentation and discussion of the results.

7.2.3.1 Description of Elastomeric Bearing Tests

The full-scale bridge model with elastomeric bearings was tested statically and dynamically in the longitudinal direction. The two bearings closest to the actuator had a vertical axial compressive load of 114 psi and the other two bearings had an axial load of 46 psi. A total of eighteen dynamic tests were performed on the bridge with elastomeric bearings. The specimen was loaded under displacement control with the hydraulic actuator. The full-scale bridge was tested under fully reversed longitudinal loading cycles at varying displacements and frequencies. The displacements ranged from +/-

0.50 in. to +/- 2.0 in. and the frequencies ranged from 0.125 Hz to 2.0 Hz. Table 7.1 shows a matrix of the dynamic tests performed. Each test run consisted of five full span cycles and two to four ramp up and ramp down cycles. The ramp up/down cycles were necessary because the actuator takes time to get up to full speed. Figure 7.19 and Figure 7.20 show the time history of the loading displacement for Test H and Test R respectively.

Table 7.1 Matrix of dynamic tests.

Test	Displacement (in.)	Frequency (Hz)	Speed (in/sec)
A	0.5	0.5	1
B	0.5	1	2
C	0.5	1.5	3
D	0.5	2	4
E	1	0.25	1
F	1	0.5	2
G	1	0.75	3
H	1	1	4
I	1.5	0.167	1
J	1.5	0.333	2
K	1.5	0.5	3
L	1.5	0.667	4
M	2	0.125	1
N	2	0.25	2
O	2	0.375	3
P	2	0.5	4
Q	2	0.625	5
R	2	0.75	6

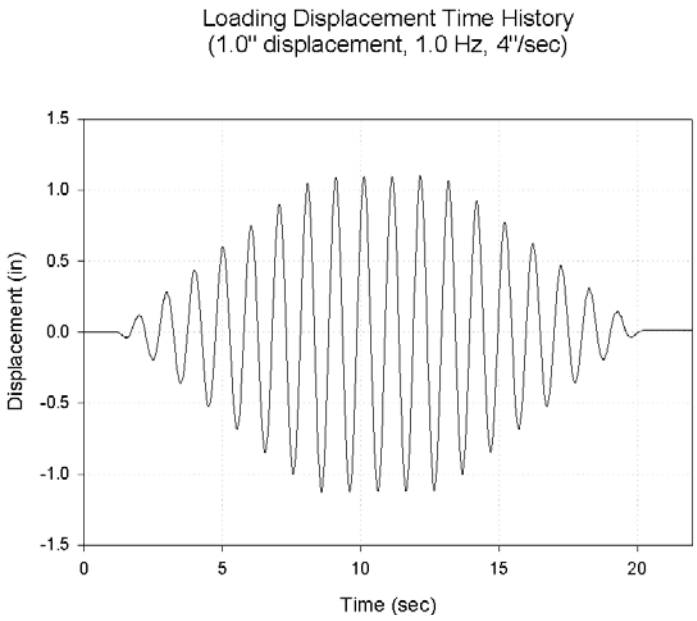

Figure 7.19 Loading displacement time history plot for Test H.

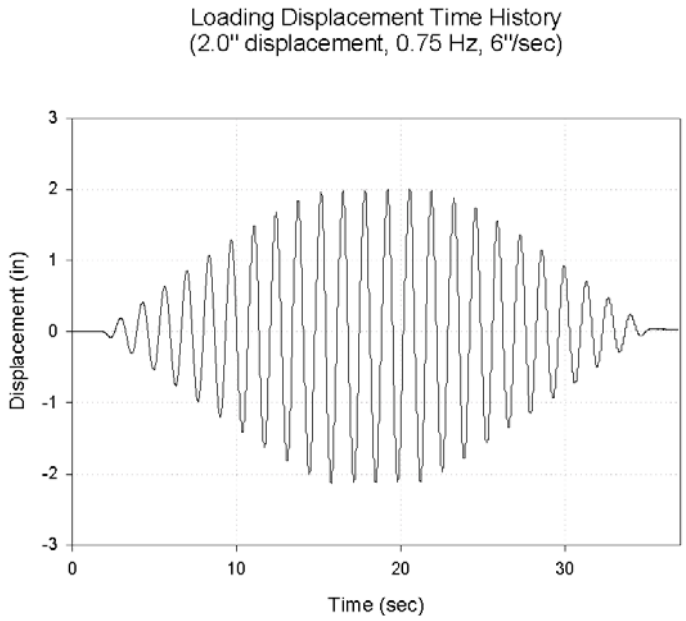

Figure 7.20 Loading displacement time history plot for Test R.

7.2.3.2 Elastomeric Bearing Tests Results

Data from the eighteen tests consisted mainly of the load and displacement obtained from the load cell and LVDT on the actuator. LVDTs #1 and #2 were used to verify the displacements from the actuator and eliminate any compliance in the loading elements. LVDTs #3 to #6 were used to monitor any lateral translations and slippage between the bearings and the bridge superstructure.

For each test run, the bearing shear stress-shear strain curves were plotted. The shear stress is calculated as the ratio between the load per bearing and the cross-sectional area of the bearing. The shear strain is calculated as the ratio between the bearing displacement and the total rubber height of the bearing. Figure 7.21 and Figure 7.22 show the bearing shear stress-shear strain curve for 0.5" displacement at 0.5Hz and 2.0Hz respectively. The shear stress-shear strain curves for the bearing displaced 2.0" at 0.125Hz and 0.75Hz are shown in Figure 7.23 and Figure 7.24. Appendix F contains load-deflection plots of the bridge model and shear stress-shear strain plots for the bearing.

At higher frequencies, the graphs do not follow a straight path during the loading phase of the bearing. This results from the inability of the accelerometers to produce accurate readings at these frequencies. The load cell on the actuator measures the total force in the system including the inertia force. The acceleration measured by the accelerometers is multiplied by the mass of the system to determine the inertia force at a given time. This force is then added to the load cell measurement to determine the force in the bearings.

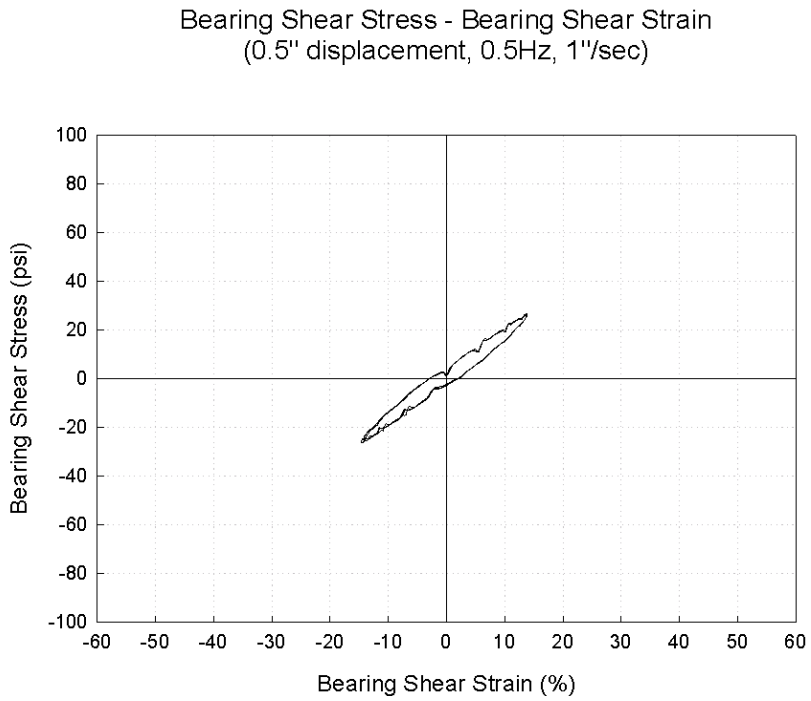

Figure 7.21 Bearing shear stress vs. bearing shear strain for +/- 0.5" sine wave at 0.5Hz.

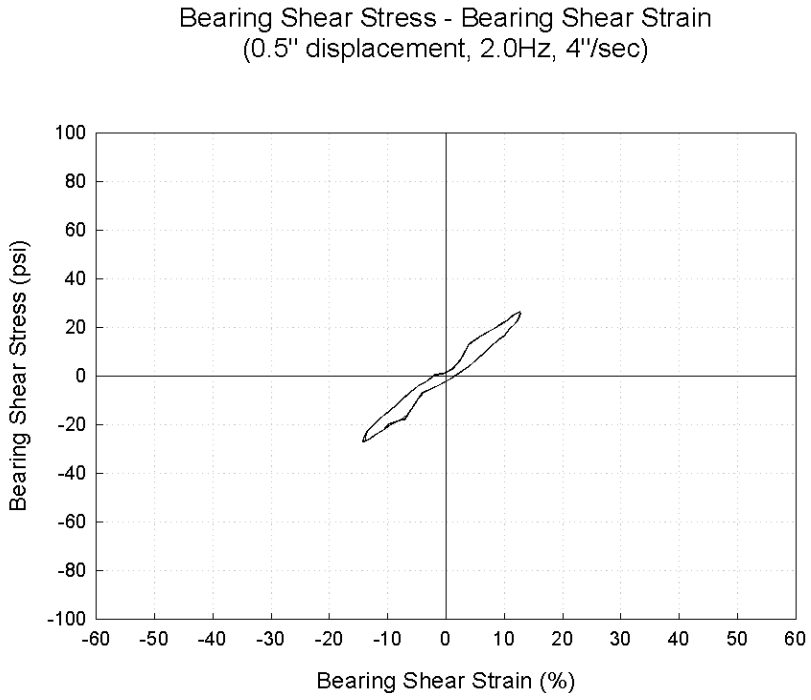

Figure 7.22 Bearing shear stress vs. bearing shear strain for +/- 0.5" sine wave at 2.0Hz.

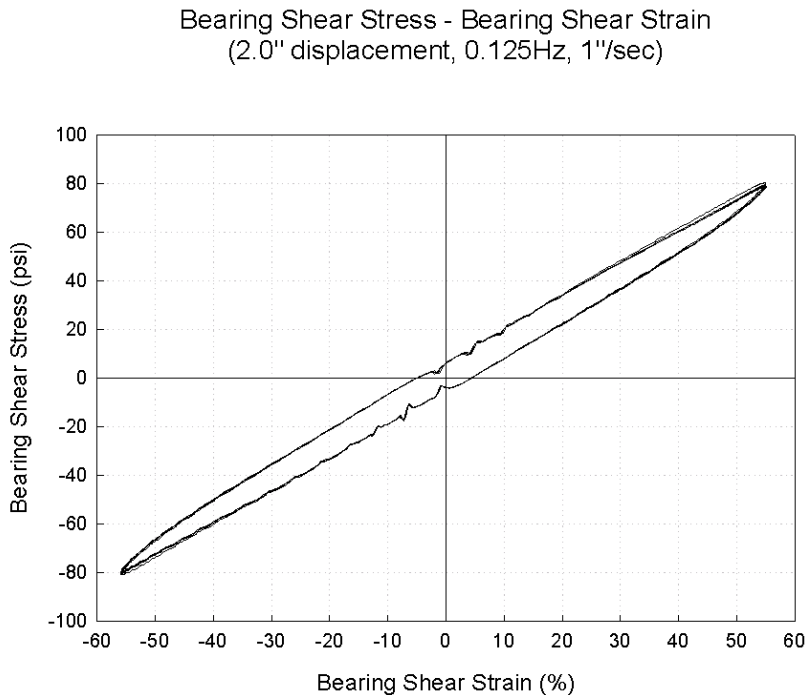

Figure 7.23 Bearing shear stress vs. bearing shear Strain for +/- 2.0" sine wave at 0.125Hz.

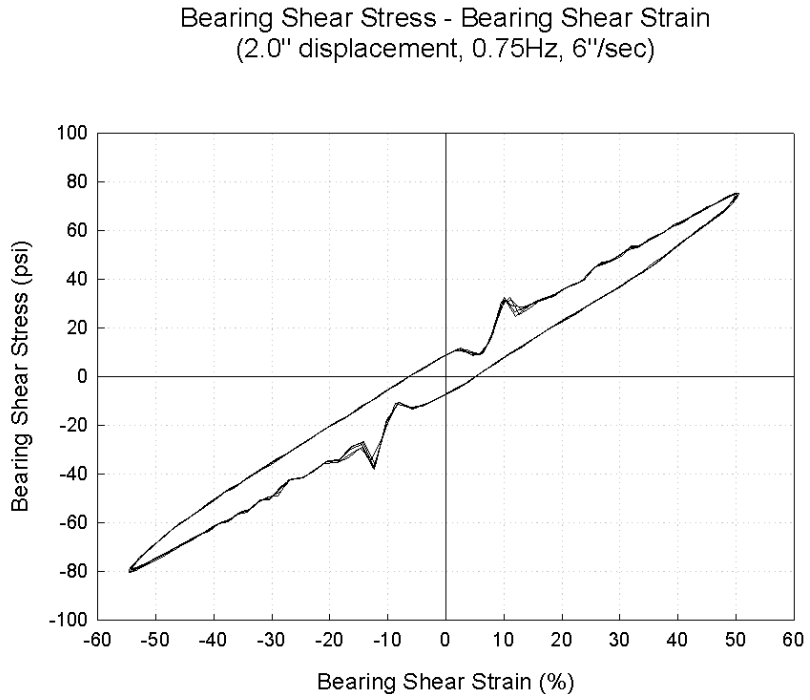

Figure 7.24 Bearing shear stress vs. bearing shear strain for +/- 2.0" sine wave at 0.75Hz.

The model bridge with elastomeric bearings was tested statically to confirm some of the inertia problems that occurred during the dynamic tests. Figure 7.25 shows the elastomeric bearing displaced to 100% shear strain. Even under such large deformations, the bearings are stable.

After the test to 100% shear strain, cracks were noticed on the reinforced concrete bearing pedestals. The cracks formed at the anchor bolts and ran down the pedestal to the top of the pier, as shown in Figure 7.26. The 1" diameter anchor bolts used to secure the bottom of the bearing to the pedestal yielded during the test and the concrete cracked around the bolts. The pedestals were heavily reinforced and the anchor bolts were embedded 12" into the pier.

Since these bearing pedestals were designed and constructed according to specifications of existing pedestals used in the field, the tests show that a failure of the existing pedestals can occur at large deformations. If the bearing seat is relatively small, a pedestal failure could result in the collapse of a bridge span. The current design practice should be investigated and modifications should be made to strengthen the pedestals.

Figure 7.25 Bearing displaced to 100% shear strain.

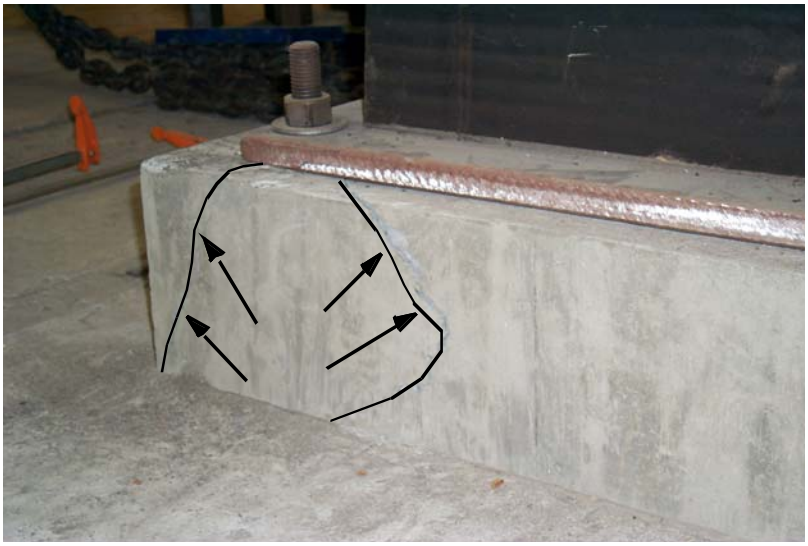

Figure 7.26 Cracks formed in concrete pedestal after bearing was subjected to 100% shear strain.

One of the goals of this study was to determine the characteristics of the bearing as a function of loading frequencies and shear strain. Therefore, the effective stiffness, energy per cycle, and equivalent viscous damping ratio were calculated for various loading frequencies and shear strains, as shown in Table 7.2. Figure 7.27 shows a plot of the bearing's effective stiffness versus the bearing shear strain. The effective stiffness of each test at the same shear strain for varying frequencies is very similar to each other. As the test shear strain increases, the effective stiffness of the bearing decreases. This has been shown in previous tests of elastomeric bearings (HITEC, 1999). Figure 7.28 shows a plot of the bearing's energy per cycle versus the bearing shear strain. At test shear strains of 12.5%, 25% and 37.5%, the energy per cycle for the same test shear strain at varying frequencies is very similar. However, the energy per cycle at the 50% test shear strain ranges from 8.46 k-in to 9.86 k-in.

Table 7.2 Summary of calculations for dynamic tests of elastomeric bearings

Test	Shear Strain (%)	Frequency (Hz)	Speed (in/sec)	Effective Stiffness (k/in)	Energy/cycle (k-in)	Equivalent Viscous Damping Ratio
A	12.5	0.50	1.0	11.49	1.0198	0.057
B	12.5	1.00	2.0	11.56	1.0041	0.055
C	12.5	1.50	3.0	11.58	1.0336	0.057
D	12.5	2.00	4.0	11.71	1.0286	0.056
E	25.0	0.25	1.0	9.97	3.1228	0.050
F	25.0	0.50	2.0	9.90	3.1862	0.051
G	25.0	0.75	3.0	9.94	3.1743	0.051
H	25.0	1.00	4.0	9.99	3.1853	0.051
I	37.5	0.167	1.0	8.93	5.5421	0.044
J	37.5	0.333	2.0	8.98	5.7334	0.045
K	37.5	0.50	3.0	9.01	5.6905	0.045
L	37.5	0.667	4.0	9.07	5.6709	0.044
M	50.0	0.125	1.0	8.64	8.4641	0.039
N	50.0	0.25	2.0	8.60	8.7229	0.040
O	50.0	0.375	3.0	8.78	9.8637	0.045
P	50.0	0.50	4.0	8.76	9.7814	0.044
Q	50.0	0.625	5.0	8.78	9.244	0.042
R	50.0	0.75	6.0	8.81	8.8349	0.040

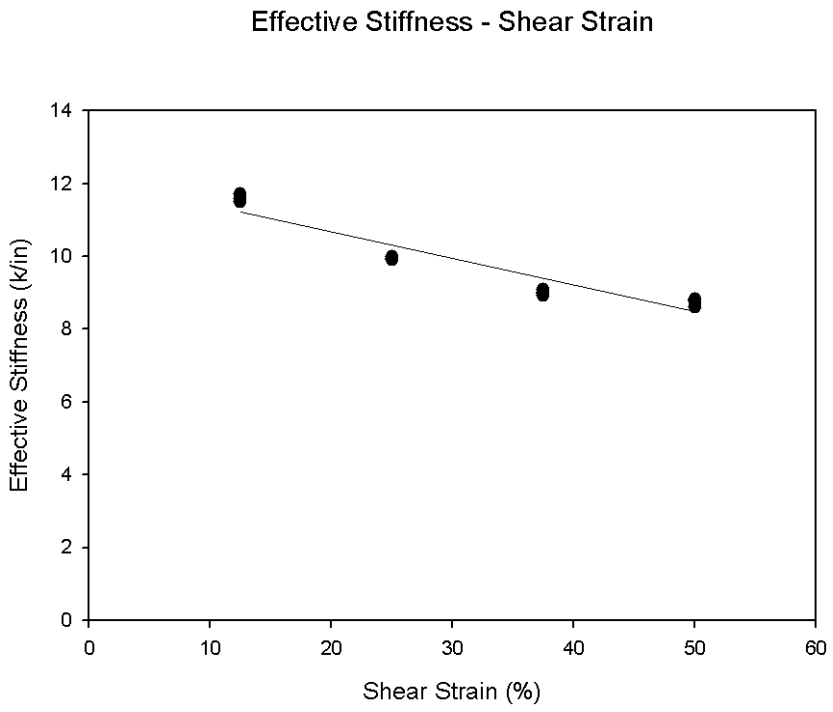

Figure 7.27 Bearing effective stiffness vs. bearing shear strain.

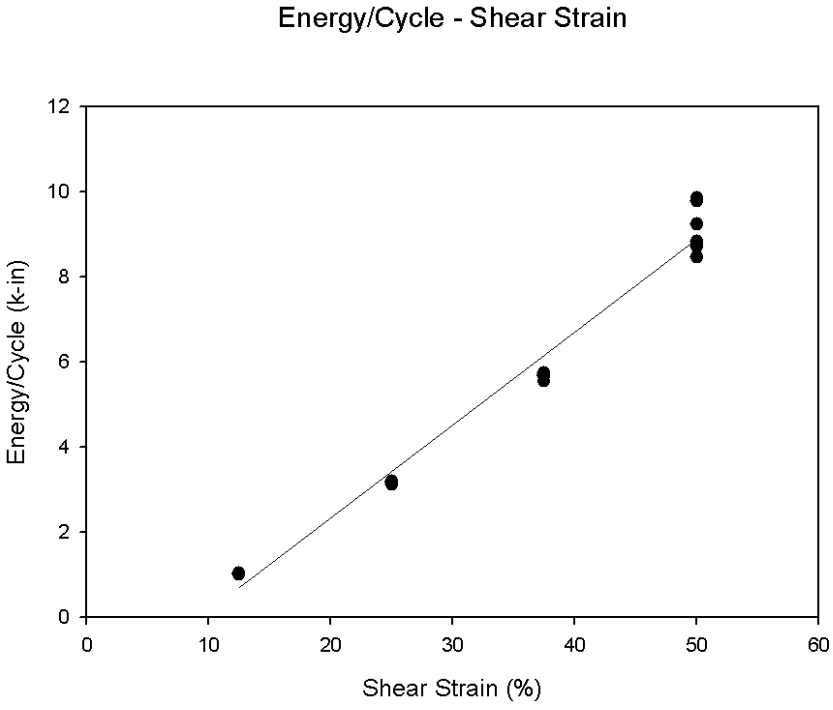

Figure 7.28 Bearing energy per cycle vs. bearing shear strain.

The equivalent viscous damping ratio for the bearing was calculated for each test. The simplest definition of equivalent viscous damping is based on the measured response of a system to harmonic force at exciting frequency equal to the natural frequency of the system. The equivalent viscous damping ratio (ζeq) was calculated by the following equation (Chopra, 1995):

$$\zeta_{eq} = \frac{1}{4\pi}\frac{E_D}{E_{So}}$$

ED is the energy dissipated by damping and ESo is the maximum strain energy of the component. Figure 7.29 illustrates ED and ESo on the component's force versus deformation plot.

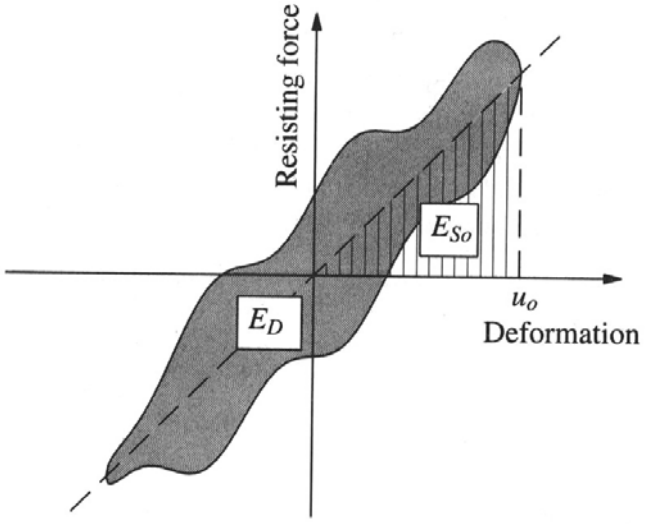

Figure 7.29 Plot showing energy dissipated and maximum strain energy of experimental component (Chopra, 1995).

In Figure 7.30, the equivalent viscous damping ratio of the bearing is plotted versus the bearing test displacement. The equivalent viscous damping ratio decreases as

the bearing test displacement increases. The damping ratio for these elastomeric bearings is relatively low (~ 5%); however, the bearings were made with natural rubber and do not use lead cores. Bearings made with high damping rubber have damping ratios of approximately 15% and lead-core elastomeric bearings have damping ratios of approximately 20% (Aiken et al., 1992).

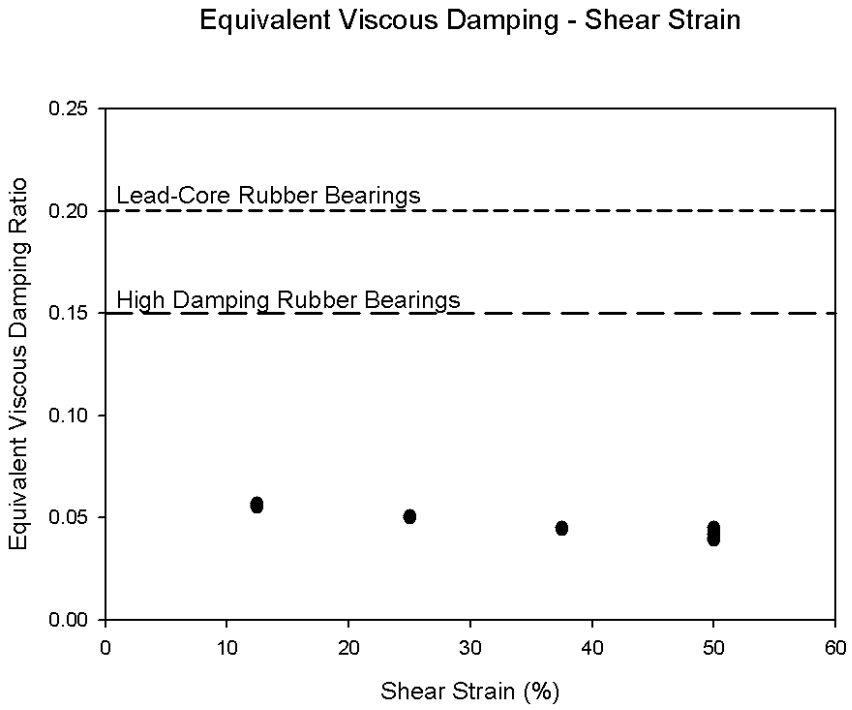

Figure 7.30 Bearing equivalent viscous damping ratio vs. bearing test displacement.

7.2.4 Cable Restrainer Tests

Many states in Mid-America are beginning to use cable restrainers as a seismic retrofit on existing bridges. Cable restrainers are used to prevent unseating of the girders, which may lead to collapse of the superstructure. The goal of this study is to test typical

cable restrainer assemblies in Mid-America and determine their failure modes and capacity. Seismic cable restrainers are connected to the bridge pier using steel bent plates, angles, and undercut anchors embedded in the concrete, as specified by typical bridge plans and discussed in the previous section. The full-scale bridge model was subjected to monotonic loading at a rate of 1"/min to test the capacity of the restrainer cable system and determine the modes of failure. The results of the experimental tests from the existing restrainer retrofits as well as the recommended modifications are presented. In the cable restrainer tests, the elastomeric bearing supports were replaced with steel rollers to decrease the demand on the actuator. The steel rollers also made it much easier to determine the exact load taken by the cable restrainers.

7.2.4.1 Description and Results of Cable Restrainer Tests

Seven restrainer cable assemblies were tested on the full-scale bridge model. The first test consisted of a restrainer cable retrofit currently used in the field as specified by the Tennessee Department of Transportation (TDOT). The remaining six tests were modifications of the current TDOT practice and represent hybrids of seismic cable restrainer retrofits used in other parts of the Central and Southeastern US, and New York. All of the modifications to the restrainer cable assemblies were changes in the connection elements at the girders and piers with the actual cable remaining the same. Previous studies have shown that the connection elements are often the weak link in cable restrainer assemblies and design codes usually specify a strength of connection elements 25% higher than the cable (Selna et al., 1989). Table 7.3 describes the differences

between the connections used in the seven tests. The following subsections describe the tests configurations in more detail.

Table 7.3 Test matrix describing the differences between the cable restrainer tests.

Test	Pier Connection	Girder Connection
Current DOT Practice	½" bent plate with 1" ϕ U-bolt	½" bent plate connected with two 7/8" ϕ A325 bolts
Retrofit Modification 1	½" bent plate with 1" ϕ U-bolt	L8x4x½" steel angle connected with two 7/8" ϕ A325 bolts
Retrofit Modification 2	Two L6x6x½" steel angles back-to-back with 1½" ϕ threaded stud	L6x6x½" steel angle connected with one 1-3/8" ϕ A325 bolts
Retrofit Modification 3	Two L6x6x½" steel angles back-to-back with 1½" ϕ threaded stud	L8x8x1" steel angle connected with two 7/8" ϕ A325 bolts
Retrofit Modification 4	Two L6x6x½" steel angles back-to-back with 1½" ϕ threaded stud	L6x6x½" steel angle stiffened with ½" plates and connected with one 1-3/8" ϕ A325 bolts
Retrofit Modification 5	½" bent plate with 1" ϕ U-bolt topped with two L6x6x½" steel angles back-to-back with 1½" ϕ threaded stud	L8x8x1" steel angle connected with two 7/8" ϕ A325 bolts
Retrofit Modification 6	Two L6x6x½" steel angles back-to-back with 1½" ϕ threaded stud	L7x4x¾" steel angle oriented longitudinally and connected with four 7/8" ϕ A325 bolts

7.2.4.1.1 Current DOT Practice

The first cable restrainer assembly tested on the model bridge was a configuration currently used on existing bridges as specified by TDOT. Two cable restrainers were attached to the bridge, one at each girder, as shown in Figure 7.31. The length of the wire rope used in the assembly is 5 ft from connection to connection. The connections at the pier and girders were made from 1/2" thick bent plate. Figure 7.32 shows the pier connection attached with two 3/4" undercut anchors embedded 12". This connection also uses a 1" diameter U-bolt to attach the cable restrainer to the bent plate. At the girder, the cable restrainer is attached directly to the bent plate by threading the thimble through a hole in the plate, as shown in Figure 7.33. The girder connection is attached to the

bottom flange of the girder using two 7/8" diameter A325 bolts. In the field the cable restrainers are installed with a 3" drape to accommodate superstructure movement from temperature changes. However, the restrainers installed on the bridge model were not installed with any slack because of constraints on the displacement of the supports.

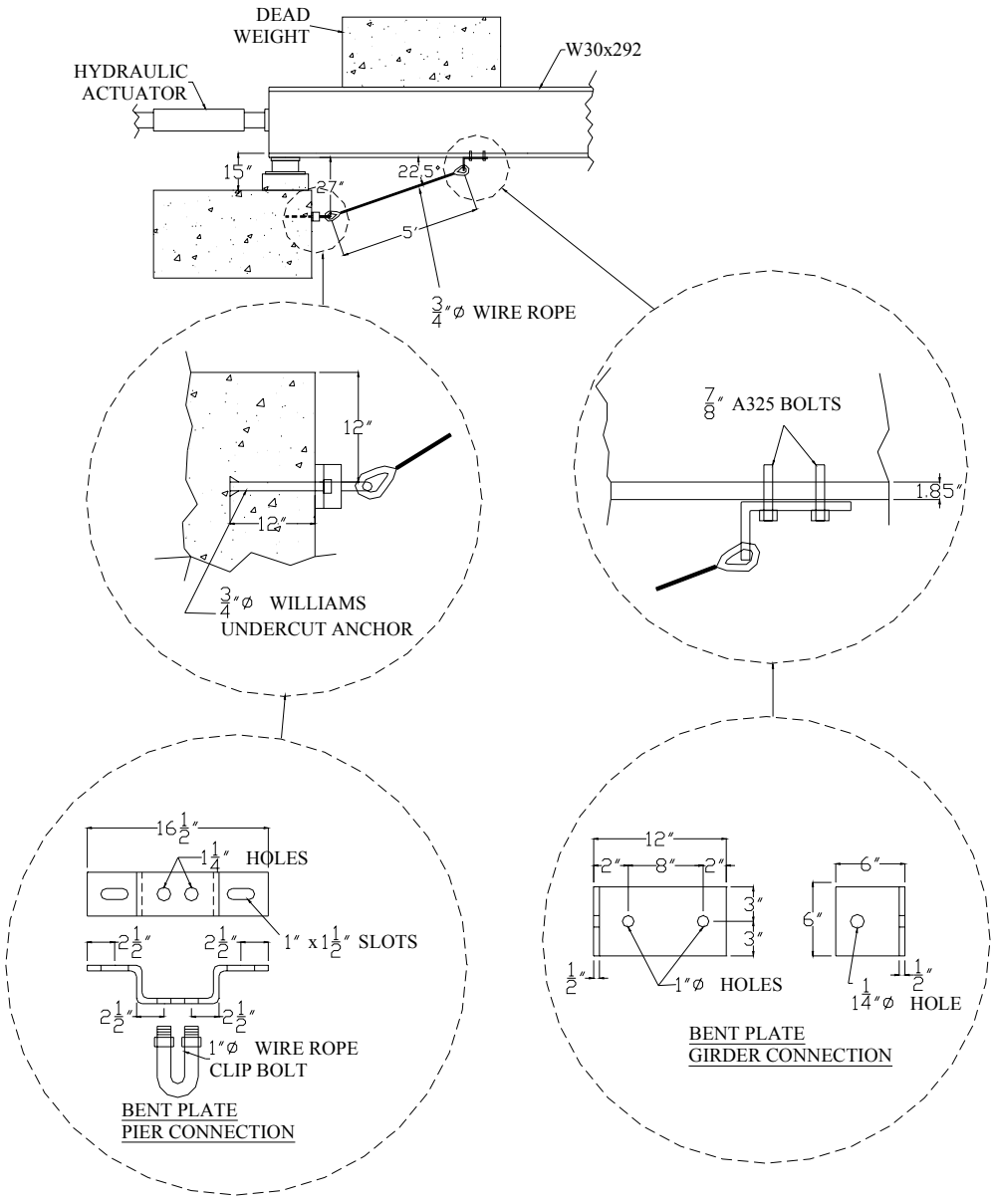

Figure 7.31 Specifications of current TDOT cable restrainer assembly as tested on model bridge.

Figure 7.32 Bent plate pier connection tested on model bridge.

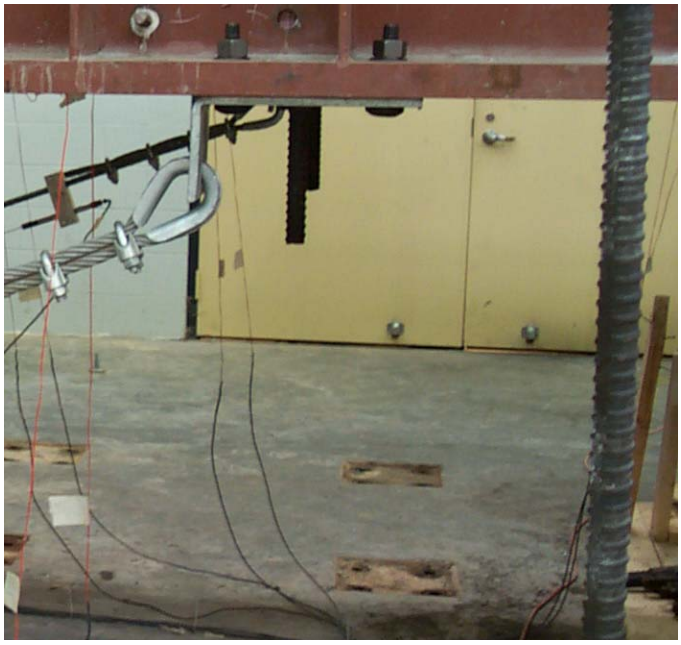

Figure 7.33 Bent plate girder connection tested on model bridge.

The bent plate connections at the girders failed in a brittle manner with a capacity of only 4 kips, as shown in Figure 7.34. The girder connections performed poorly and only resisted a 1" displacement of the bridge before failure occurred. The plates used in

these connections were cold bent to an angle of 90° which introduced large stress concentrations and possible cracks in the steel. The restrainer cable attaches to the bent plate at a large eccentricity from the bottom of the girder flange. This eccentricity introduces large moments which act on the weakest part of the bent plate. Figure 7.35 shows the crack in the connection plate near the bend after a small amount of displacement. The crack that formed in the bent plate was brittle and located within the section of the plate that was reduced by bending.

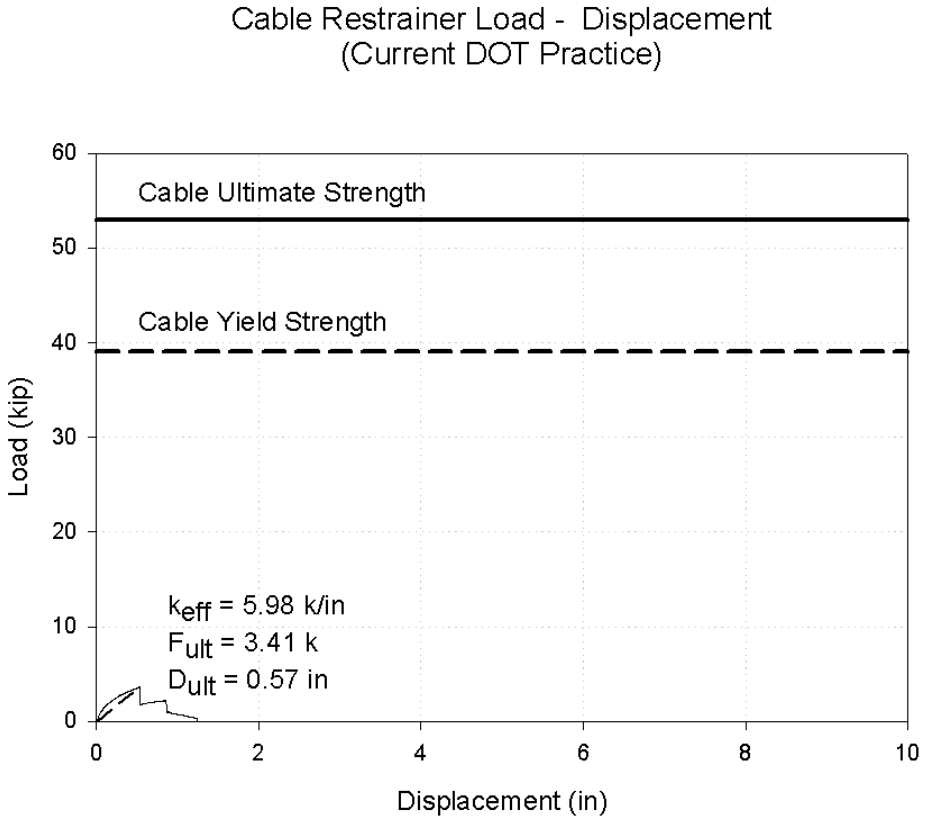

Figure 7.34 Load-displacement behavior of current DOT cable restrainer assembly.

Figure 7.35 Bent plate connection during test - notice crack at bend in plate.

7.2.4.1.2 Retrofit Modification 1

The second cable restrainer configuration tested used a modified connection at the girder, as illustrated in Figure 7.36. Instead of a 1/2" thick bent plate, an L8x4x1/2" steel angle (Figure 7.37) was chosen to improve the strength, stiffness, and ductility of the connection. A steel angle also allowed easy replacement of the original connection with only minor modifications to the girder flange. The original pier connection was not changed for retrofit modification 1.

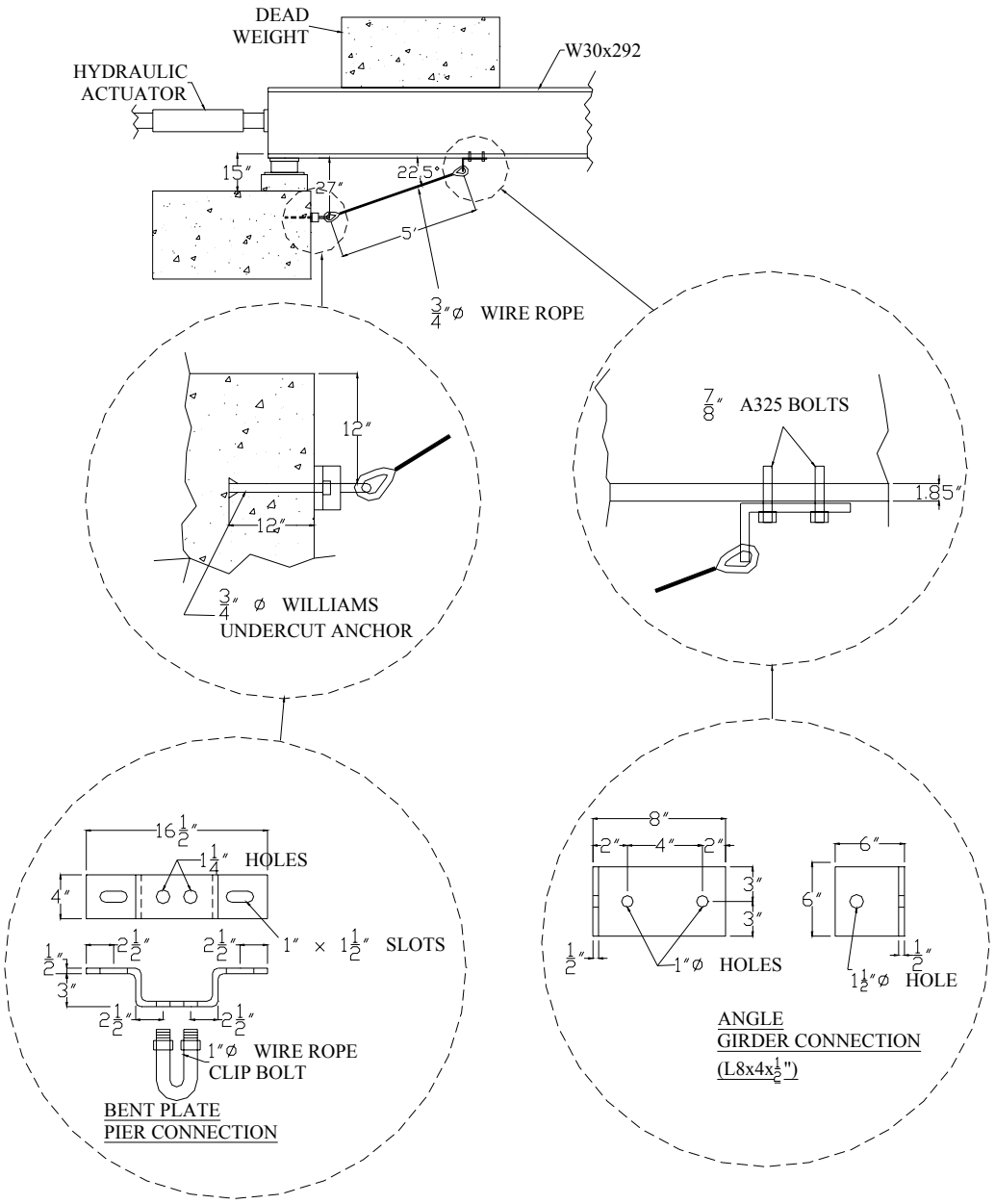

Figure 7.36 Specifications of retrofit modification 1 cable restrainer assembly as tested on model bridge.

Figure 7.37 L8x4x1/2" steel angle used at the girder connection as part of retrofit modification 1.

The L8x4x1/2" angle girder connection performed in a ductile manner compared to the original bent plate connection at the girder. However, bent plate connection at the pier failed at a capacity of 18 kips, as shown in Figure 7.38. The pier connection cracked in two different locations at the bends in the plate, as shown in Figure 7.39. This connection failed in a brittle manner and did not show any premature signs of weakness during the testing. Figure 7.40 shows the ductile deformation of the steel angle used in the girder connections.

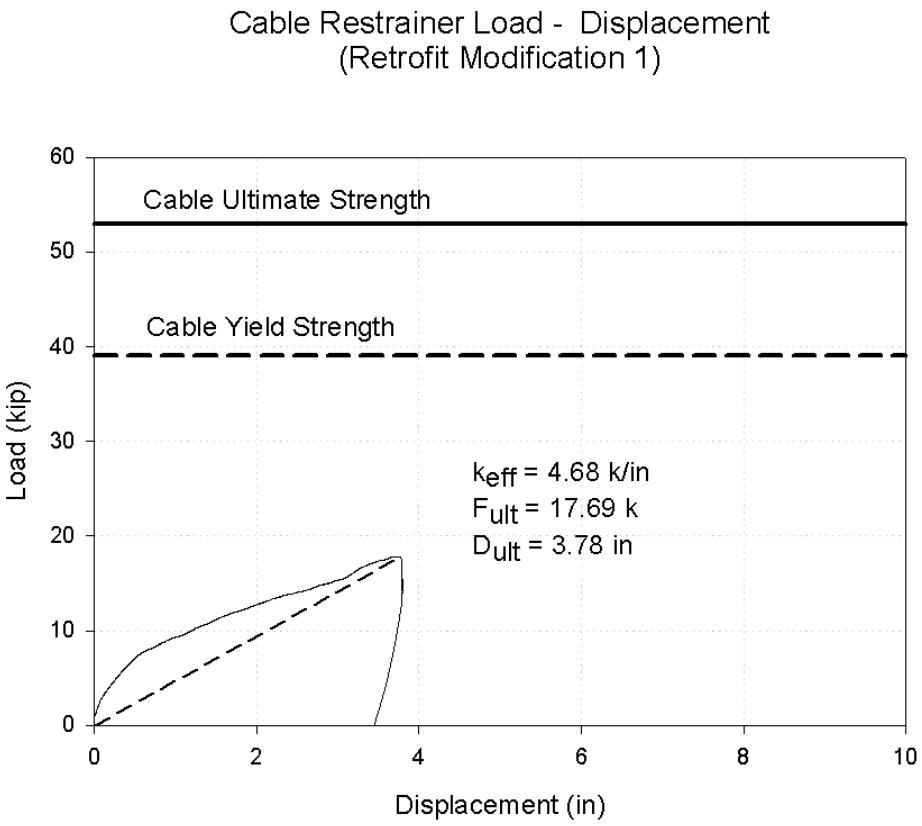

Figure 7.38 Load-displacement behavior of retrofit modification 1 cable restrainer assembly.

Figure 7.39 Bent plate pier connection failure after test retrofit modification 1.

Figure 7.40 Angle girder connection used in retrofit modification 1 with ductile deformation.

7.2.4.1.3 Retrofit Modification 2

The third cable restrainer configuration tested used a modified connection at the pier and girder, as shown in Figure 7.41. At the pier connection, two L6x6x1/2" steel angles were placed back-to-back and connected with a 1-1/2" diameter A193 B7 threaded stud, as shown in Figure 7.42. The cable restrainer thimble was connected directly to the threaded stud between the two angles. This modified connection used the existing undercut anchors embedded in the pier and did not require any major modifications for the installation. At the girder connection, an L6x6x1/2" steel angle was used for this test configuration. Figure 7.43 shows the girder connection as it was installed on the model bridge. For this connection, only one 1-3/8" Grade 5 bolt was used to connect the angle to the girder flange. A Grade 5 bolt was used because of the limited availability of a

structural bolt in the required diameter and the bolt strength was not calculated as a major failure mode. The only modification required to install this connection was to ream out a larger diameter hole in the girder flange to accommodate the larger bolt size.

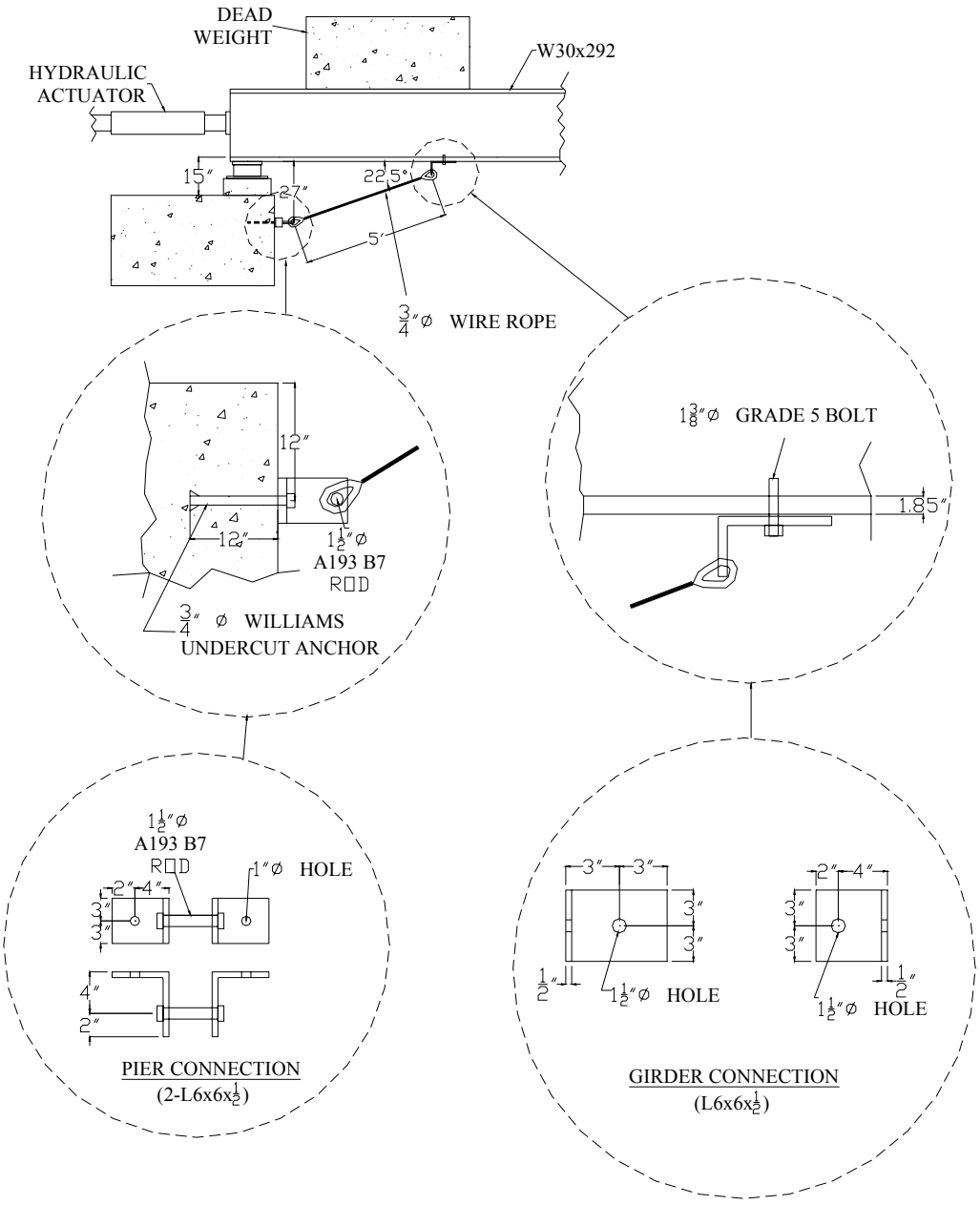

Figure 7.41 Specifications of retrofit modification 2 cable restrainer assembly as tested on model bridge.

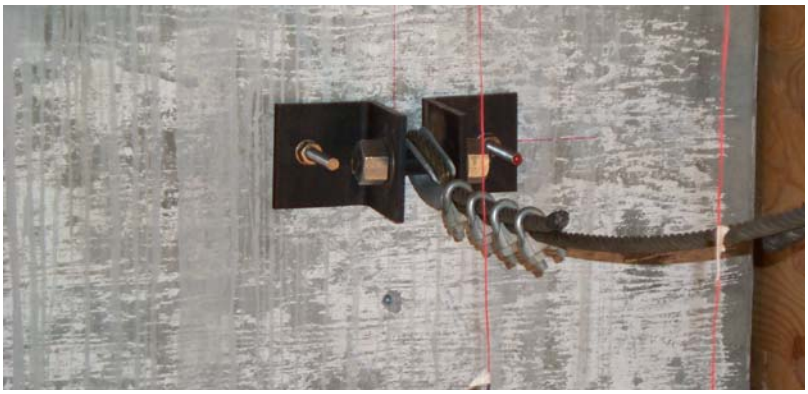

Figure 7.42 Two L6x6x1/2" steel angles back-to-back used in retrofit modification 2.

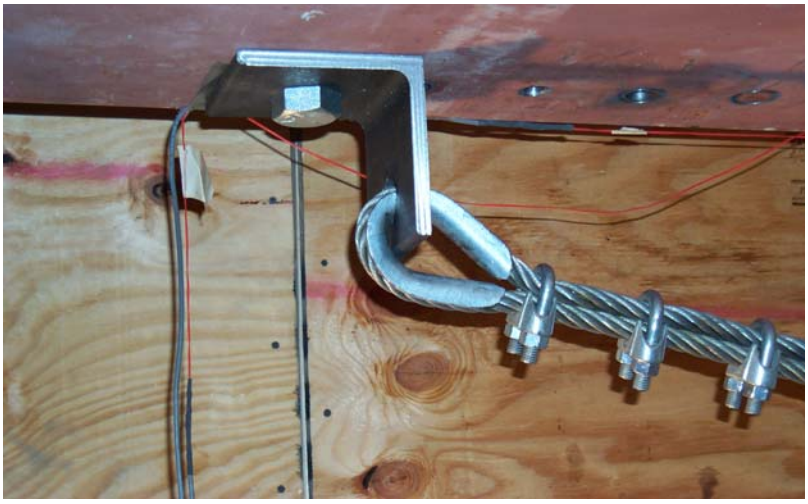

Figure 7.43 L6x6x1/2" steel angle used at girder connection in retrofit modification 2.

The L6x6x1/2" angle connection at the girders performed in a ductile manner, as shown in Figure 7.44, with a capacity of 33 kips before failure. To examine possible failure modes during the test, the actuator was held in displacement control at 5-1/2" of displacement for a few minutes. While the actuator was held in a constant displacement, the load taken by the cable restrainer assembly only dropped 4 kips. The bridge

displaced 6-1/2" before failure occurred in the angle connections at the girders. Figure 7.45 illustrates the ductile behavior of the steel angle connections. The modified connection at the pier performed well, with little deformation.

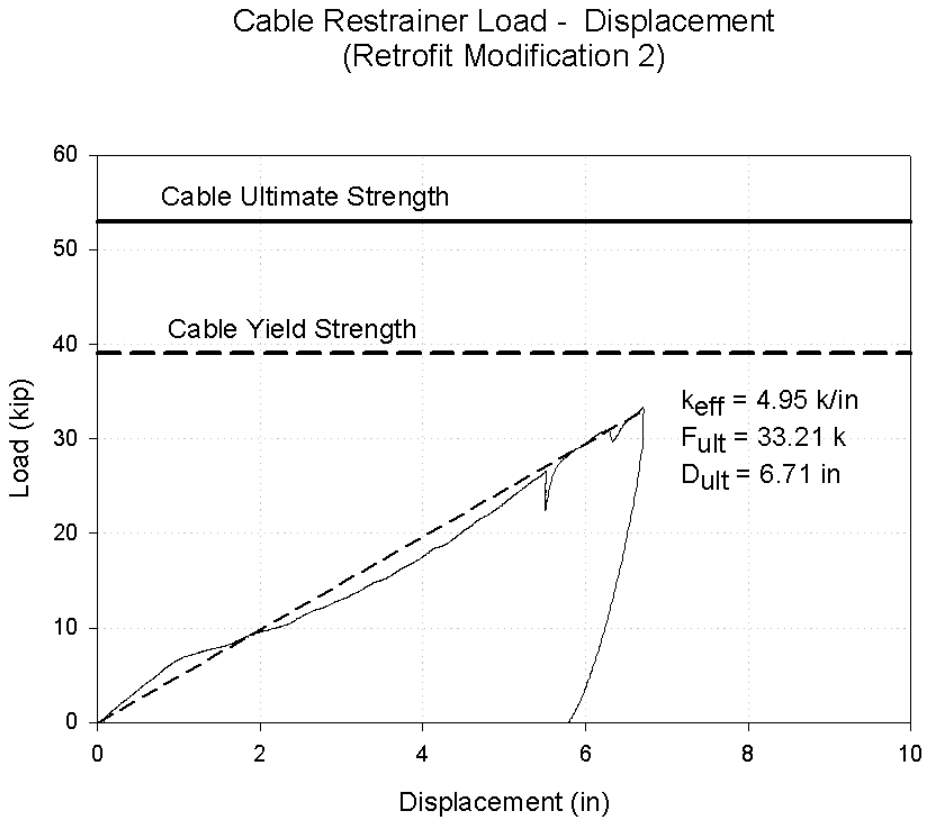

Figure 7.44 Load-displacement behavior of retrofit modification 2 cable restrainer assembly.

Figure 7.45 Angle connection at girder used in retrofit modification 2.

7.2.4.1.4 Retrofit Modification 3

The fourth cable restrainer configuration tested used the previous pier connection and an L8x8x1" steel angle connection at the girder, as illustrated in Figure 7.46. The L8x8x1" steel angle was chosen to increase the strength and stiffness of the connection. The larger angle also allowed the connection to use two bolts to connect to the girder flange. Figure 7.47 shows the steel angle attached to the bottom flange of the girder. This connection was easily installed with only modifications made to the bolt hole size and spacing on the girder flange.

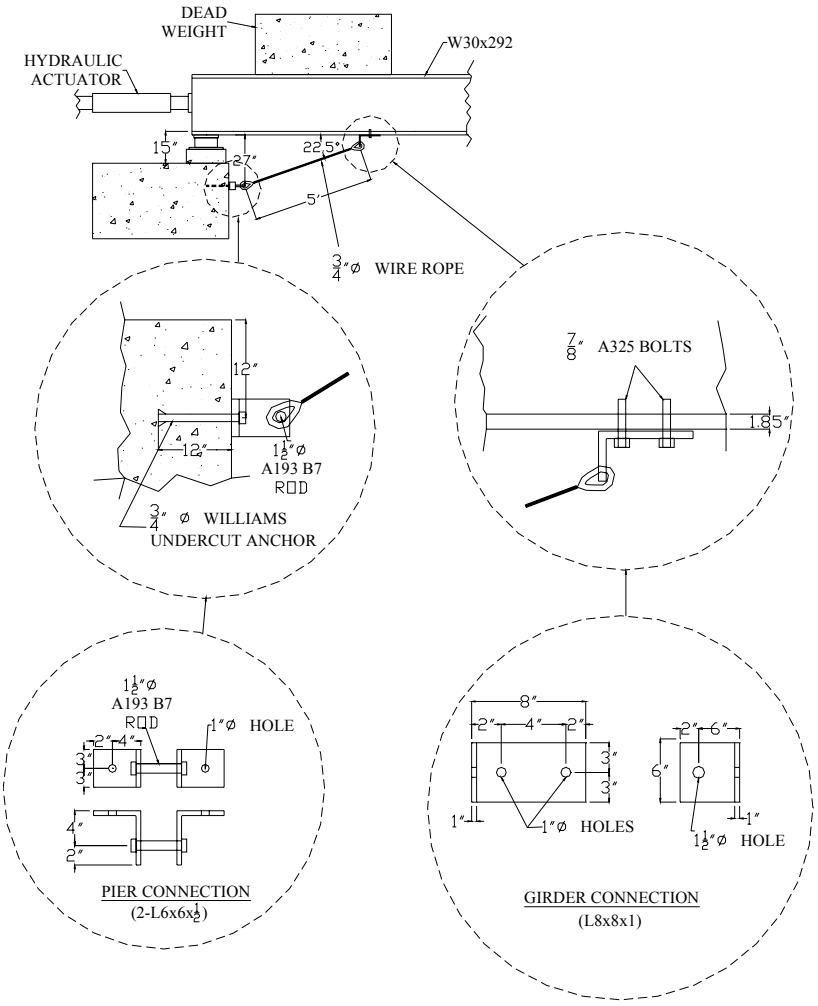

Figure 7.46 Specifications of retrofit modification 3 cable restrainer assembly as tested on model bridge.

Figure 7.47 L8x8x1" steel angle used in retrofit modification 3 on model bridge.

The L8x8x1" steel angle used in the girder connection failed at a capacity of 46 kips, as shown in Figure 7.48. The restrainer cables reached their yield strength with this assembly; however, the displacement before failure was close to 8". To examine possible failure modes during the test, the actuator was held in displacement control at 5-3/4" of displacement for a few minutes. While the actuator was held in a constant displacement, the load taken by the cable restrainer assembly only dropped 3 kips. Figure 7.49 shows a side view of the deformed angle connection during the test. Cracks in the k-zone of the angle formed during the test, as shown in Figure 7.50.

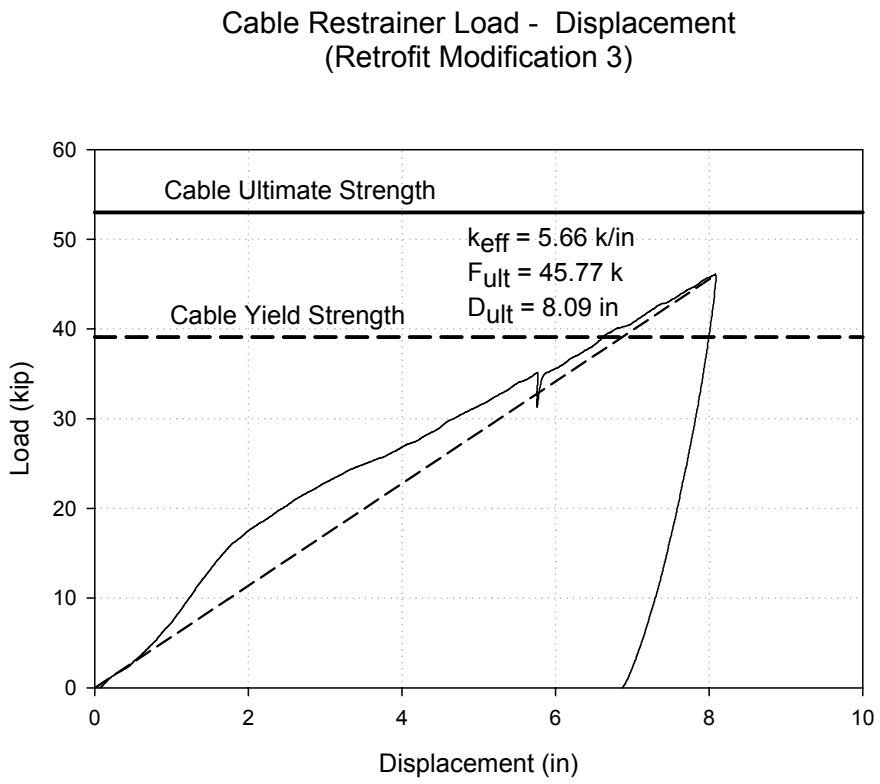

Figure 7.48 Load-displacement behavior of retrofit modification 3 cable restrainer assembly.

Figure 7.49 L8x8x1" steel angle connection used tested in retrofit modification 3.

Figure 7.50 Girder connection during testing with cracks forming in k-zone.

7.2.4.1.5 Retrofit Modification 4

The fifth cable restrainer configuration tested used the same pier connection as retrofit modification 3 and an stiffened L6x6x1/2" steel angle connection at the girder, as shown in Figure 7.51. The angle was stiffened with two 1/2" steel plates welded between the two legs of the angle, as shown in Figure 7.52. This cable restrainer assembly is similar to retrofit modification 2 with the exception of the plates used to stiffen the angle. The connection used at the girder for this configuration is very similar to the connections specified by Illinois DOT.

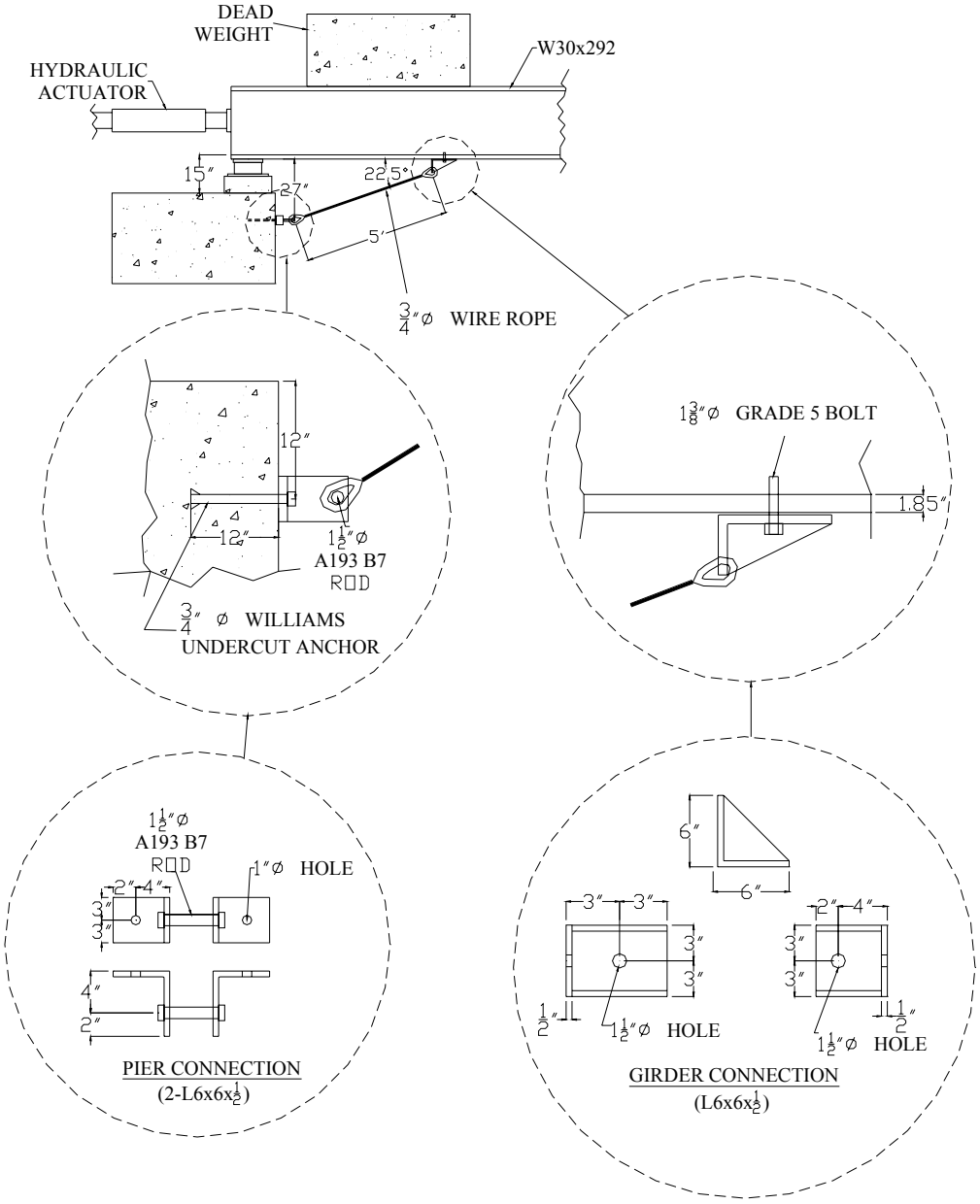

Figure 7.51 Specifications of retrofit modification 4 cable restrainer assembly as tested on model bridge.

Figure 7.52 Stiffened L6x6x1/2" angle used in retrofit modification 4 on model bridge.

The stiffened angle connections performed well with a capacity of 47 kips with less than 5” of displacement of the bridge deck, as shown in Figure 7.53. Figure 7.54 shows the stiffened angle girder connection after the test was completed. The restrainer assembly failed when an anchor broke due to repeated prying of the pier connection, as illustrated in Figure 7.55 and Figure 7.56. The undercut anchors used at the pier connection were not replaced after each test and these anchor had been used for the test of the original DOT connection and retrofit modifications 1-3. This cable restrainer assembly performed much better than the previous assemblies in terms of strength and stiffness. The total deformation at failure for the stiffened system was about half of the deformation for the unstiffened system used in retrofit modification 2.

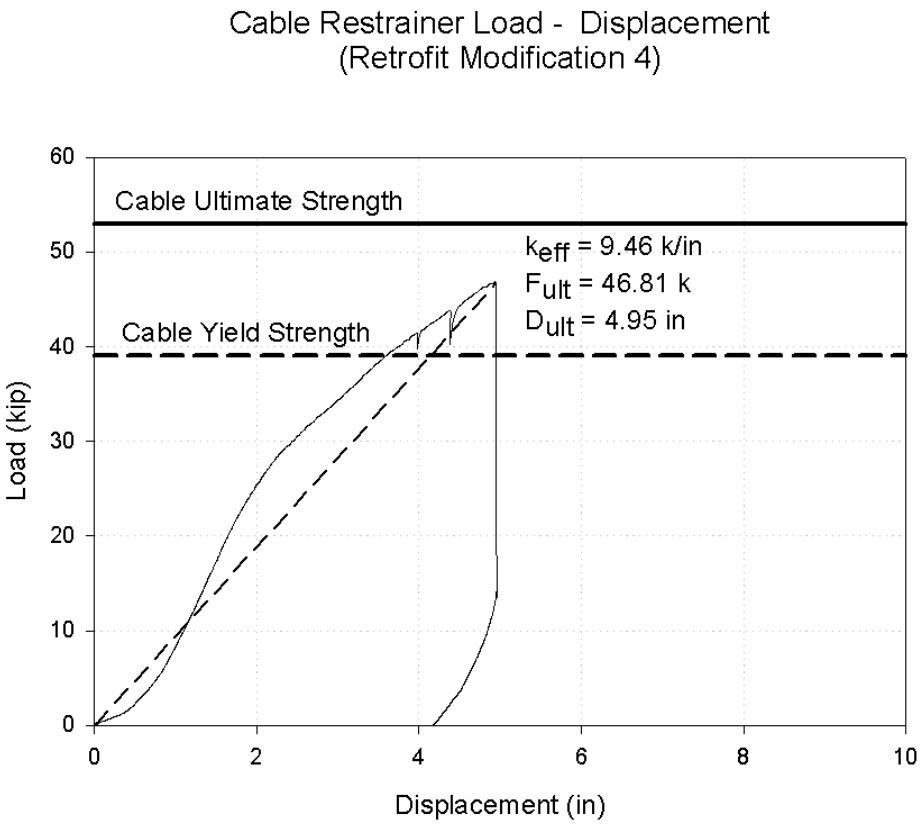

Figure 7.53 Load-displacement behavior of retrofit modification 4 cable restrainer assembly.

Figure 7.54 Stiffened steel angle girder connection tested in retrofit modification 4.

Figure 7.55 Damage due to prying action of pier connection.

Figure 7.56 Failure of undercut anchor at pier connection in retrofit modification 4.

7.2.4.1.6 Retrofit Modification 5

The sixth cable restrainer configuration tested used a modified pier connection and an L8x8x1" steel angle connection at the girder, as illustrated in Figure 7.57. The

pier connection used incorporated elements from the original TDOT bent plate connection and the modified connection used in previous retrofit modifications. The two L6x6x1/2" back-to-back angles connected with a 1-1/2" stud are placed on top of the original 1/2" thick bent plate connection, as shown in Figure 7.58. This configuration was proposed for testing by TDOT after the results of the original connection were presented. This connection allows easy retrofit to the existing connections in the field because the original connection will not have to be removed. The modified elements are designed to engage only when the original connection fails. The L6x6x1/2" angles required 1/2" plate extensions to be welded to one leg of the angle so they could accommodate the position of the cable thimble attached to the original connection.

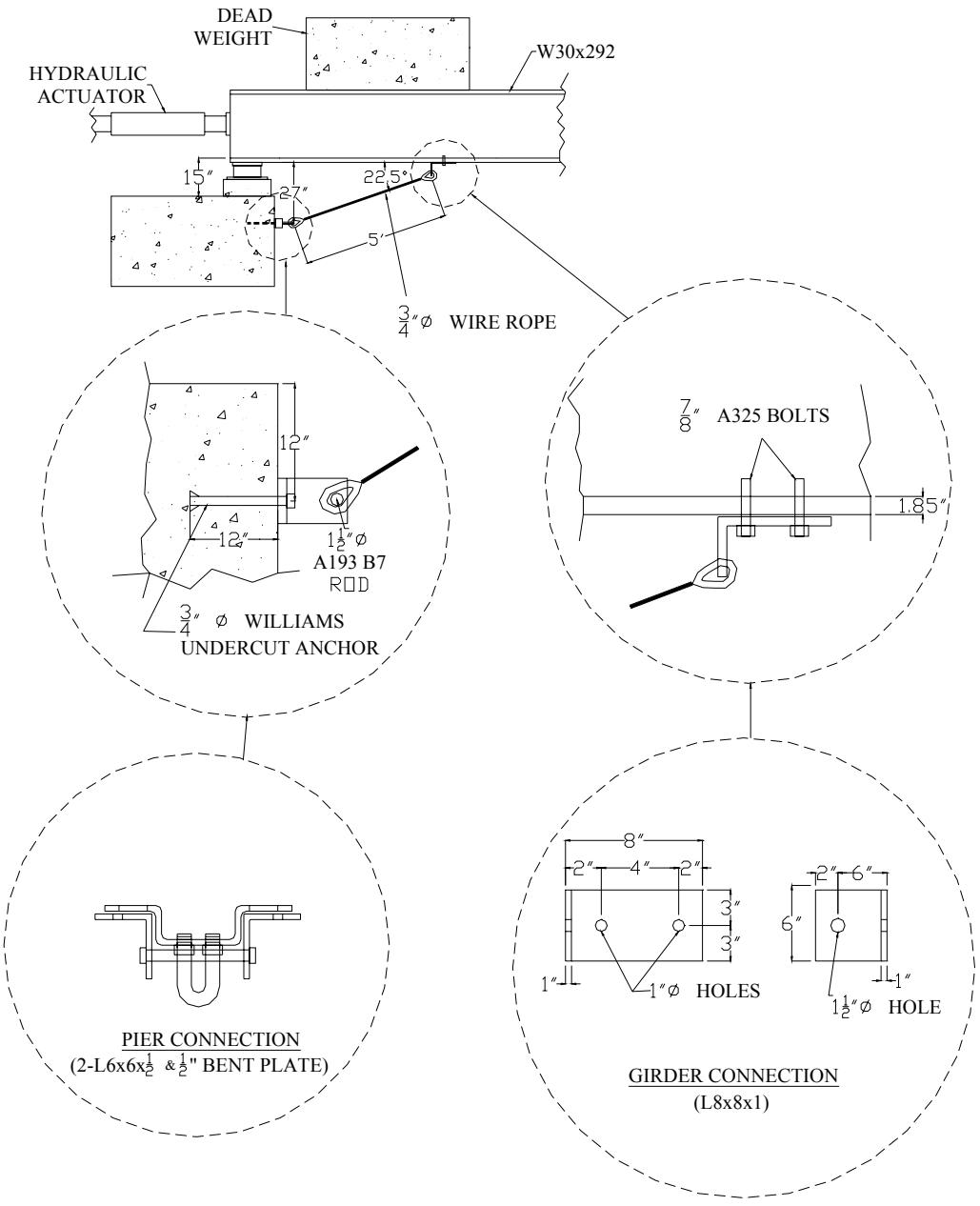

Figure 7.57 Specifications of retrofit modification 5 cable restrainer assembly as tested on model bridge.

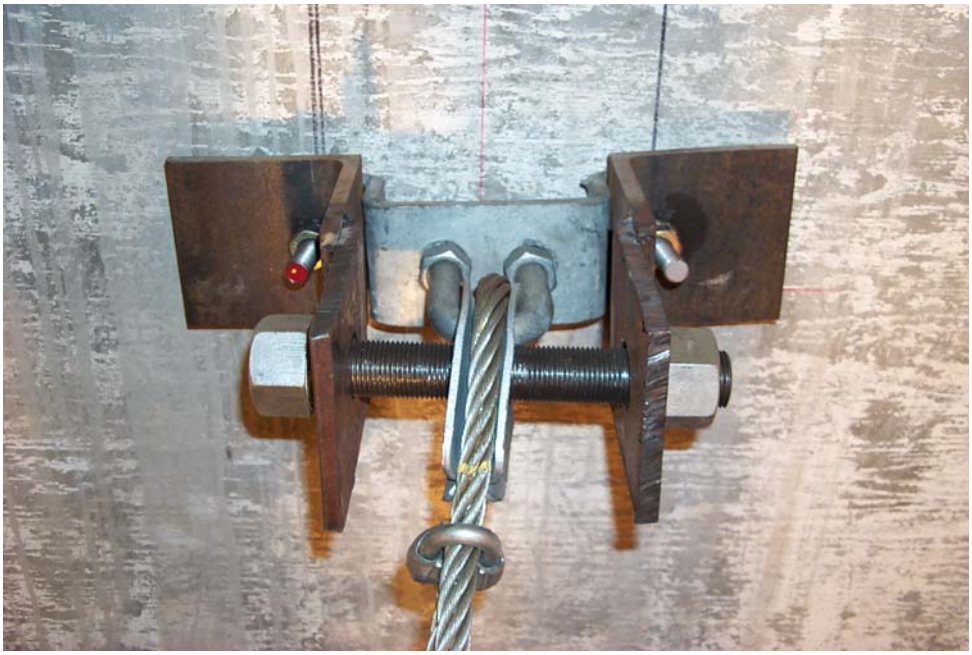

Figure 7.58 Pier connection used for retrofit modification 5 on bridge model.

The capacity of the restrainer assembly was 45 kips, but the bridge displaced over 9” before failure, as shown in Figure 7.59. The loss of load at 8-1/2" of displacement was caused by holding the actuator in displacement control for a short period of time. The pier connection performed well with little deformation before the angle connection at the girder formed a brittle crack, as seen in Figure 7.60. The failure of the steel angle was sudden and no major signs of weakness were seen before the failure occurred.

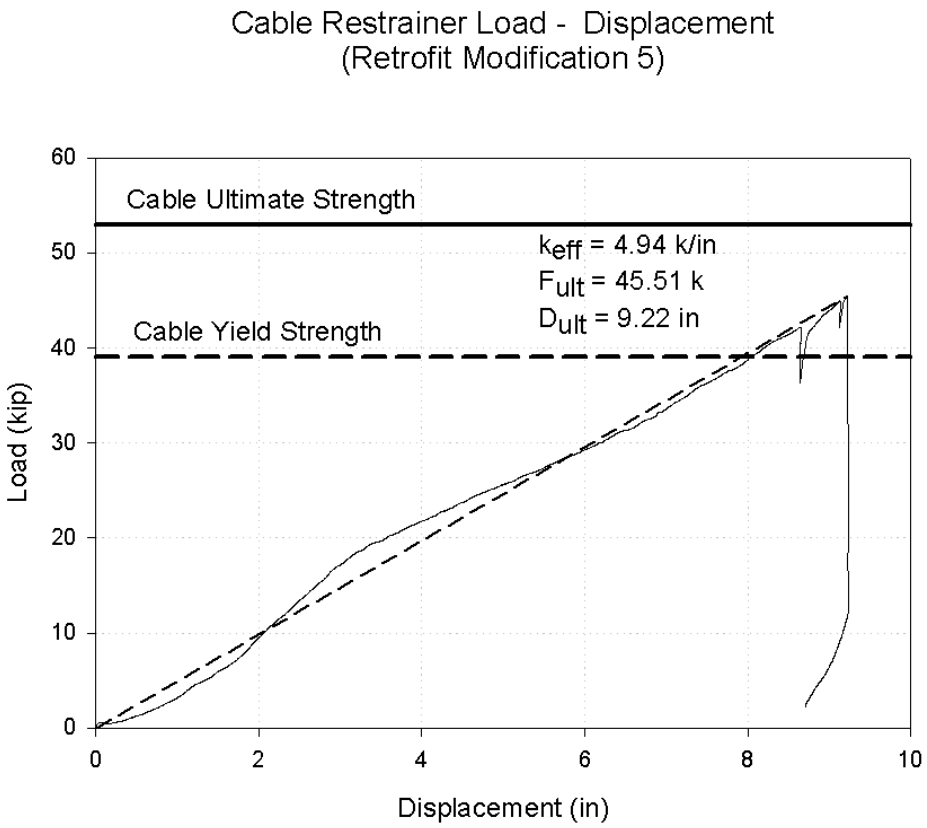

Figure 7.59 Load-displacement behavior of retrofit modification 5 cable restrainer assembly.

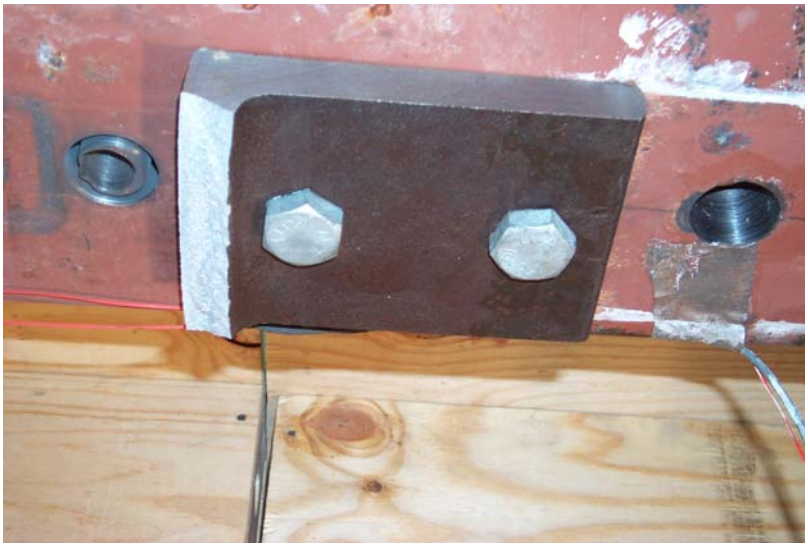

Figure 7.60 Brittle failure of L8x8x1" steel angle tested in retrofit modification 5.

7.2.4.1.7 Retrofit Modification 6

The seventh cable restrainer configuration tested used the same modified pier connection as retrofit modification 4 and an L7x4x3/4" steel angle connection at the girder, as shown in Figure 7.61. The girder connection is similar to connections currently used by the New York Department of Transportation (NYSDOT). The steel angle was oriented longitudinally to increase the strength and stiffness of the connection. With this orientation, the leg of the angle will not bend in the direction of the load like previous girder connections tested. This connection used a 1-1/4" diameter shackle to connect the cable restrainer to the steel angle. The steel angle was connected to the girder flange using four 7/8" diameter A325 bolts spaced 3" apart. Figure 7.62 and Figure 7.63 show different angles of the girder connection used in retrofit modification 6.

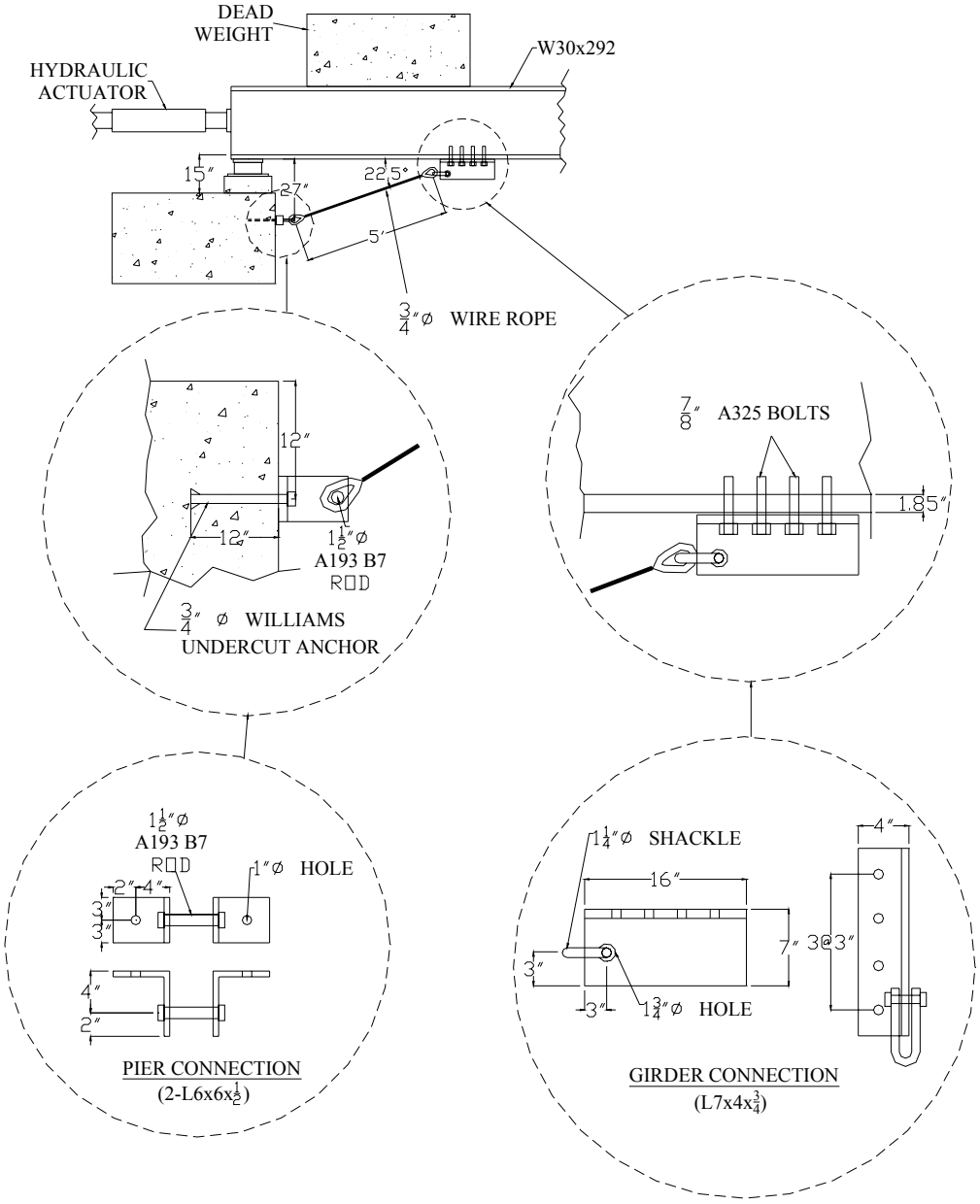

Figure 7.61 Specifications of retrofit modification 6 cable restrainer assembly as tested on model bridge.

Figure 7.62 Side view of girder connection used in retrofit modification 6.

Figure 7.63 View of girder connection showing bolts and shackle.

The restrainer assembly had a capacity of 42 kips with less than 5" of displacement before failure occurred, as shown in Figure 7.64. The angle connection at the girder performed well with little deformation before a clip on the restrainer cable failed at the pier connection, as seen in Figure 7.65. The girder connection used in this

retrofit modification displayed little or no deformation. The shackle used to connect the cable to the girder connection worked well and directed the load into the cable without binding on or yielding the leg of the angle.

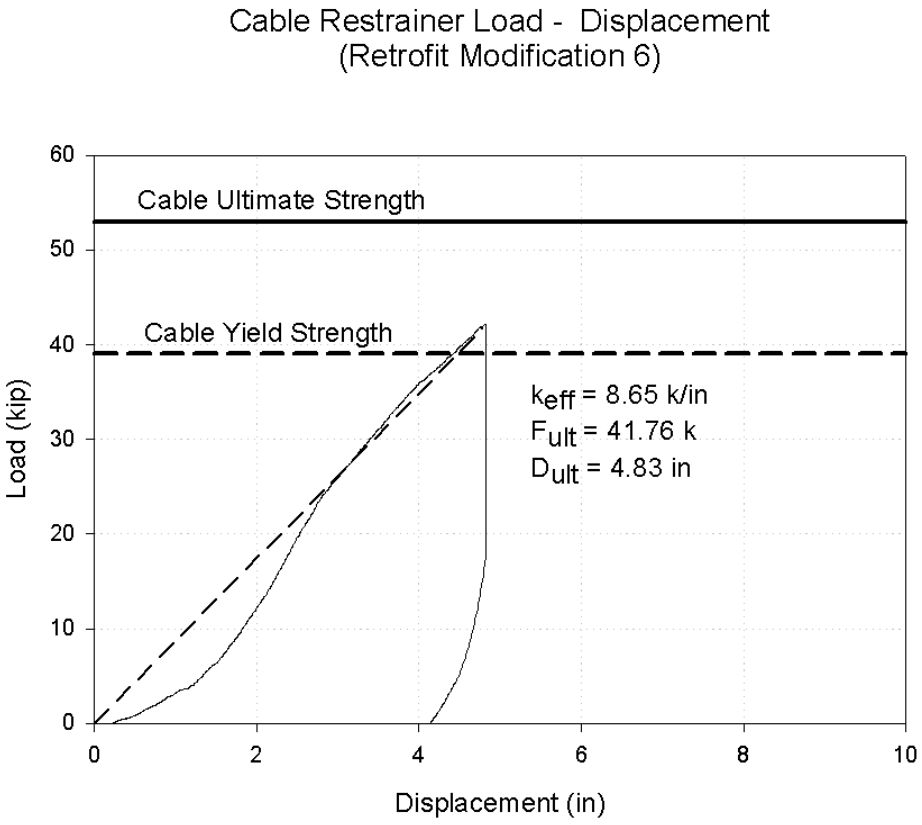

Figure 7.64 Load-displacement behavior of retrofit modification 6 cable restrainer assembly.

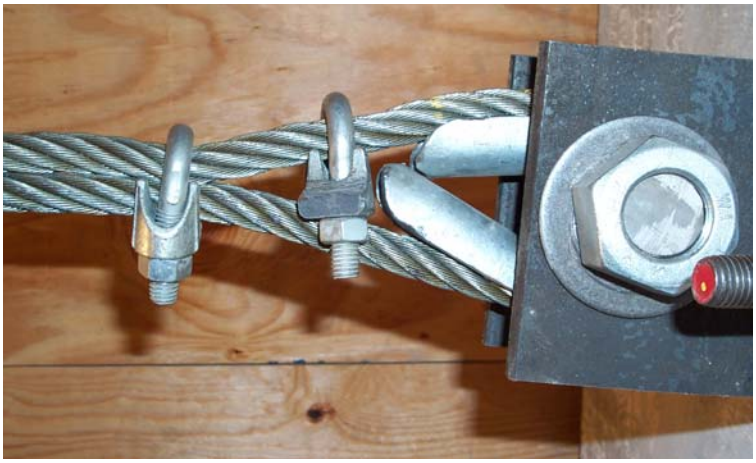

Figure 7.65 Failure of wire rope clip near thimble on pier connection of retrofit modification 6.

7.2.4.2 Summary of Cable Restrainer Tests Results

The load-displacement behavior of the bridge with each cable restrainer assembly is shown in Figure 7.66. The cable restrainer assembly currently used by TDOT failed at a load of 4 kips – less than 10% of the yield strength of the cable. Failure occurred in the bent plate connection at the girder because the plates were cold bent to 90°. The bent plate connections were replaced with steel angle connections that resulted in much higher capacity compared to the bent plates. Four of the six retrofit modifications failed at loads greater than the yield capacity (39 kips) of the restrainers. However, several of the retrofit modifications had large deformations before failure. To limit the large deformations in the bridge, a stiffened angle girder connection was used in retrofit modification 4. This cable restrainer assembly, similar to assemblies used by IDOT, had about half of the deformation than an unstiffened assembly. Retrofit modification 6 used a steel angle oriented longitudinally on the girder flange similar to cable restrainer

connections used by NYSDOT. This assembly also behaved much better than the currently used connections, in terms of stiffness and deformation. Table 7.4 shows a summary of the effective stiffness, ultimate strength, and ultimate displacement for the cable restrainer tests.

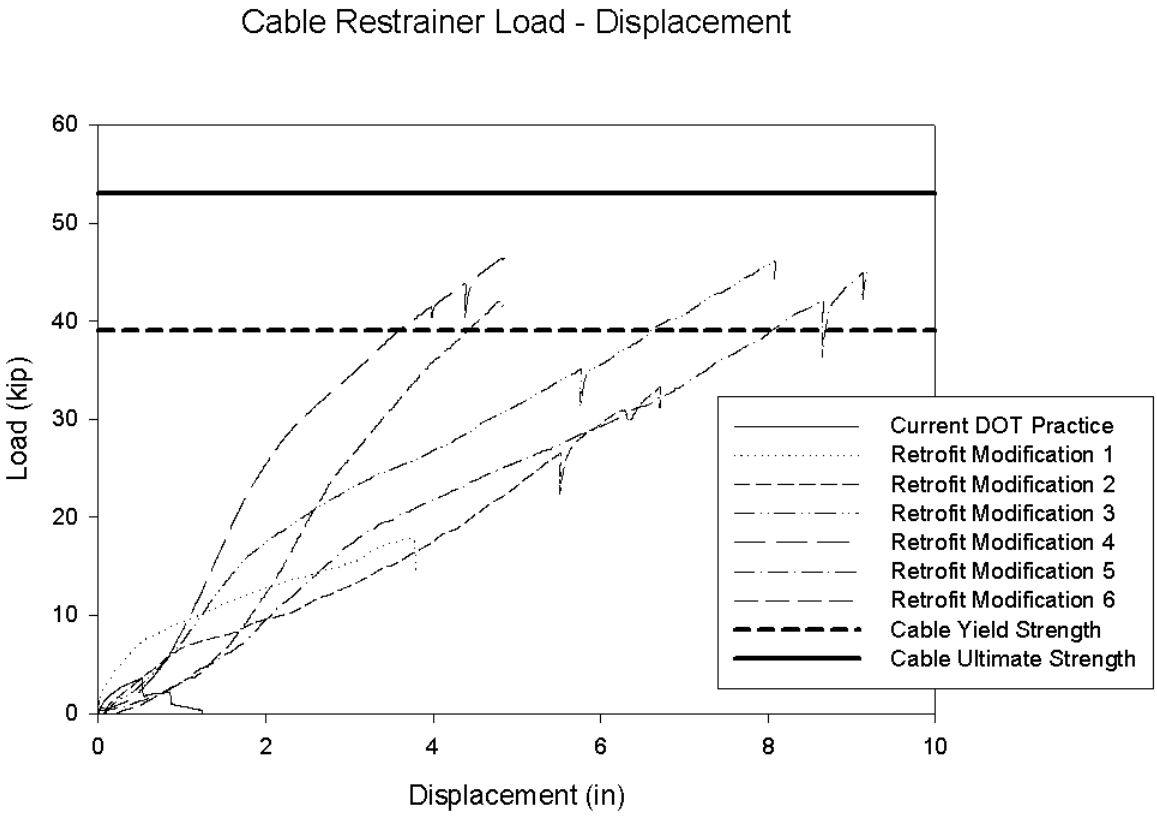

Figure 7.66 Load-displacement behavior of bridge with each cable restrainer assembly.

Table 7.4 Summary of effective stiffness, ultimate strength, and ultimate deformation for cable restrainer tests.

Tests	Effective Stiffness (k/in)	Ultimate Strength (kip)	Ultimate Displacement (in)
Current DOT	5.98	3.41	0.57
Retrofit Mod 1	4.68	17.69	3.78
Retrofit Mod 2	4.95	33.21	6.71
Retrofit Mod 3	5.66	45.77	8.09
Retrofit Mod 4	9.46	46.81	4.95
Retrofit Mod 5	4.94	45.51	9.22
Retrofit Mod 6	8.65	41.76	4.83

7.3 Analysis of Retrofitted Bridge

This chapter presents the analysis of two types of typical bridges in Mid-America that are commonly retrofitted with cable restrainers. The previous chapter showed that the various connection elements resulted in large differences in the force-displacement relationship for the seismic cable restrainer assemblies. This, in turn, may lead to significant differences in the seismic response of retrofits. Using the results of the experimental test from Section 7.2, the cable restrainers will be modeled. Representative models for each of the cable restrainer retrofits tested in Section 7.2 are developed and the responses of the bridges are compared. The first section will introduce the continuous steel girder bridge and the multi-span simply supported steel girder bridge used for the analytical models. Next, the components of the analytical model created in DRAIN-2DX will be discussed. Two different synthetic ground motions developed for the Mid-America region will be used in the analysis. Finally, the results of the analysis on the two bridges will be presented.

7.3.1 Bridges Used in Analysis

Two different types of typical bridges in Mid-America were chosen for analysis of seismic cable restrainer retrofits. These bridges were modeled after existing bridges that have been considered for cable restrainer retrofits in Tennessee. The following subsections will present the continuous steel girder bridge and the multi-span simply supported steel girder bridge used for analytical models.

7.3.1.1 Multi-Span Simply Supported (MSSS) Steel Girder Bridge

Most MSSS bridges with steel girders consist of 2~5 spans with each span ranging from 30 ft to160 ft and width ranging from 40 ft to100 ft. For long span bridges in general, and longitudinally continuous bridges in particular, a greater economy can be realized by using plate girders in lieu of the predefined rolled beam shapes. Each girder is supported by a elastomeric bearings at their supports.

The typical MSSS bridge used in this study is modeled after a typical MSSS bridge that was retrofitted in Memphis, TN. The layout of the bridge, provided in Figure 7.67, has 3 spans and 2 multi-column bents. Each bent has 4 columns and each span has 11 girders. The span lengths are 40 ft, 80 ft, and 40 ft, respectively, and the width is 64 ft. The height of columns is 15ft. The size of the abutments is 64 ft x 8 ft (WxH), and the number of piles in an abutment is 13. The gap between deck and abutment is 1.5 in. and the gap between decks is 1.0 in. The concrete slabs of the MSSS bridges are supported by steel girders resting on steel bearings. The steel bearings are mounted on the abutments or cap beams. Two adjacent decks are separated by expansion joints above the columns.

One of the primary seismic vulnerabilities in MSSS bridges is unseating at the piers and abutments, which may result in collapse of the superstructure. The objective of the cable restrainer retrofit is to (1) limit relative opening at the abutment and intermediate hinges to reduce the likelihood of unseating, and (2) provide a back-up

safety mechanism should the decks unseat. It is believed that during the event of unseating, the cables would support the deck, thereby preventing collapse.

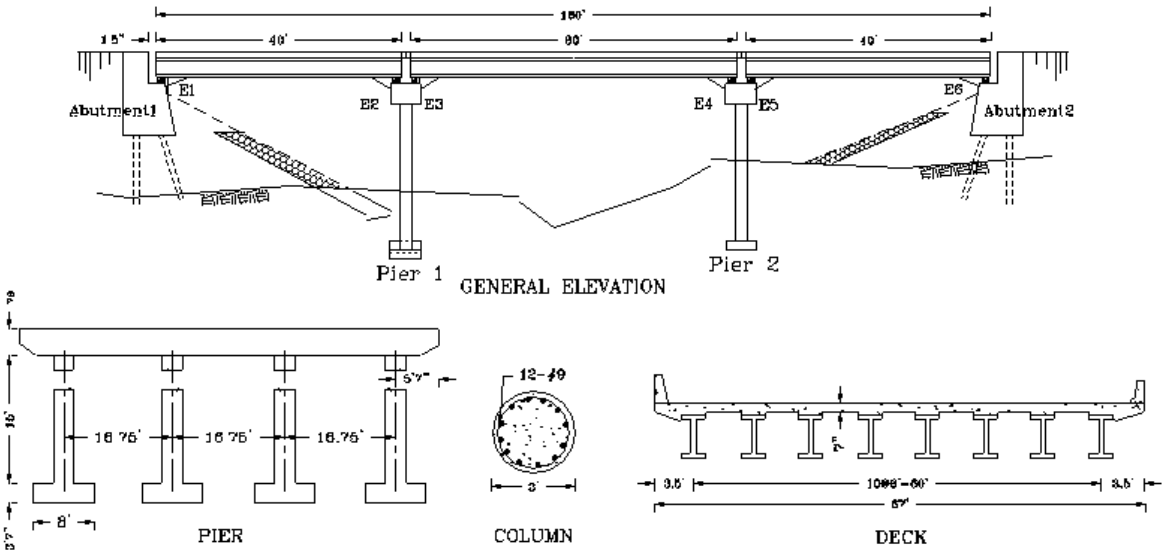

Figure 7.67 Layout of typical multi-span simply supported bridge with steel girders, elastomeric bearings, and restrainers.

7.3.1.2 Continuous Steel Girder Bridge

Figure 7.68 shows a three-span continuous bridge with steel girders located in Shelby, Tennessee. The span lengths of the bridge are 99.5 ft, 124.5 ft, and 107.5 ft, respectively. A 58 ft wide bent cap is supported on four columns of approximate height 16 ft. The bridge decks are a composite system of eight steel girders and a concrete slab. Elastomeric bearings are used at the supports of the bridge.

The continuous bridge has similar vulnerabilities as the MSSS bridge, except that unseating is only a problem at the abutments. Therefore, restrainer cables for continuous bridges are typically only provided at the abutments.

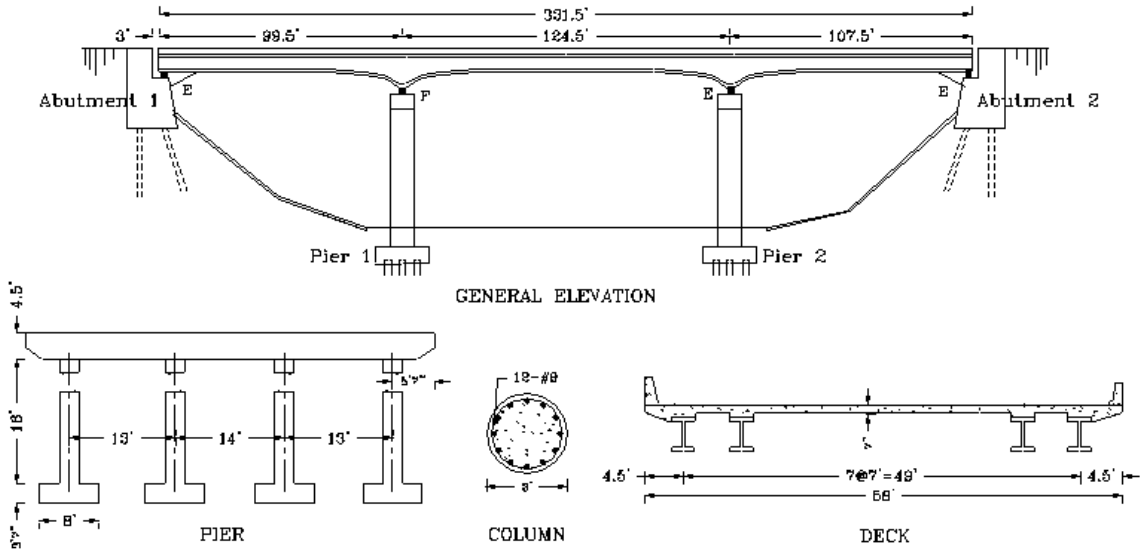

Figure 7.68 Layout of typical continuous bridge with steel girders, elastomeric bearings, and restrainers.

7.3.2 Analytical Bridge Models

Analytical models of the MSSS and continuous bridges are modeled using DRAIN-2DX. DRAIN-2DX is a nonlinear finite element structural analysis program used to perform many types of analyses with many different types of loading: modal analysis, response spectral analysis, and time history analysis (Prakash et al., 1992). Time history analysis using synthetic ground motion developed for Mid-America is used in this study.

In the model of typical MSSS bridge as shown in Figure 7.69, the following types of elements are used: beam-column elements for decks (Type #4); fiber element for columns (Type #15); link elements for fixed steel bearing, abutments, dowels, and impact elements (Type #9); connection elements for elastomeric bearings and foundation springs (Type #6).

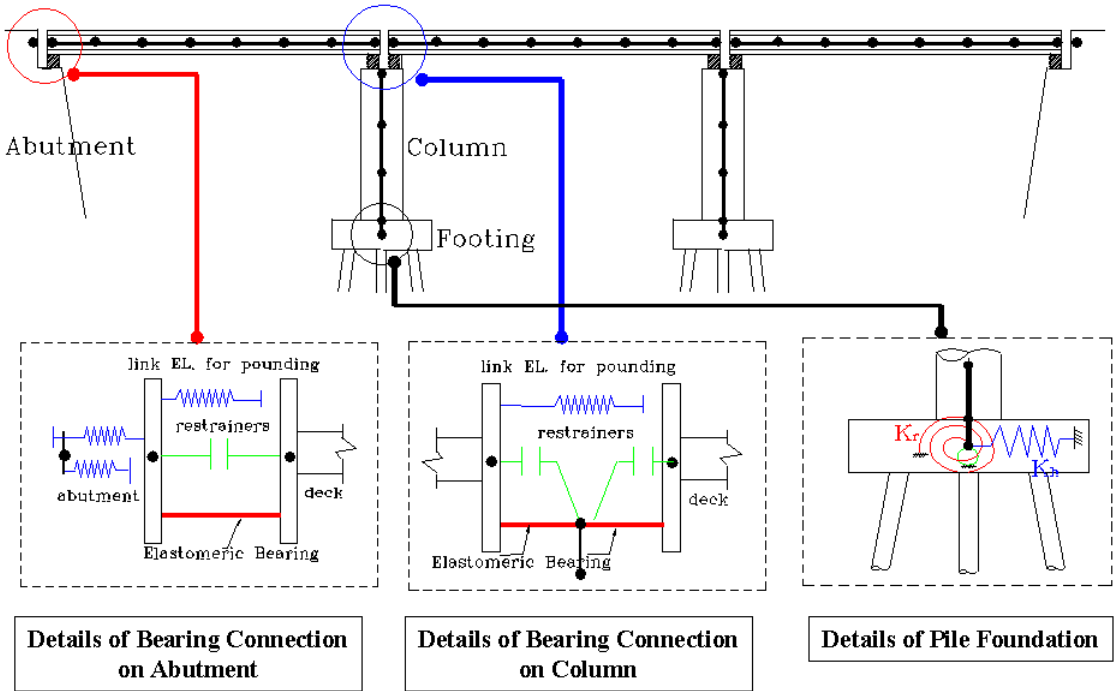

Figure 7.69 Model of MSSS bridge used in DRAIN-2DX.

In the MSSS bridge, there are 10 beam-column elements on the first and the third deck, and 20 elements on the middle deck. The element length of decks is 4 ft. The weight of each column is 64 kips, and the weight of each cap beam is 153 kips. The weight of each footing is 35.8 kips. The cap beams and the footings in the piers are modeled as rigid elements with mass. To obtain more accurate response, the bottom

portion of columns is modeled with more fine fiber elements. Each fiber element has two slices.

7.3.3 Restrainer Elements in Analysis

The two types of analytical bridge models were analyzed with four different seismic cable restrainer configurations. First, the models were analyzed without cable restrainers to obtain the as-built response. Then, the bridges were analyzed with cable restrainers using the force-deformation characteristics of the experimental data (Figure 7.70) in this study. The MSSS steel girder bridge used a total of 22 restrainers (2 per girder) at each abutment and pier, as specified by TDOT. The continuous steel girder bridge used a total of 16 restrainers (2 per girder) and only at the abutments.

The restrainers were modeled as a multi-linear tension only nonlinear inelastic element, as shown in Figure 7.71. Table 7.5 shows the stiffness and deformation values used in the multi-linear element for the different restrainer configurations. These values only represent the characteristics of one cable restrainer and were increased according to the number of restrainers that were used in the analysis of each bridge. The restrainer elements were given 1/2" of slack before they engaged to simulate the required slack specified for ambient temperature shrinkage and expansion of the bridge.

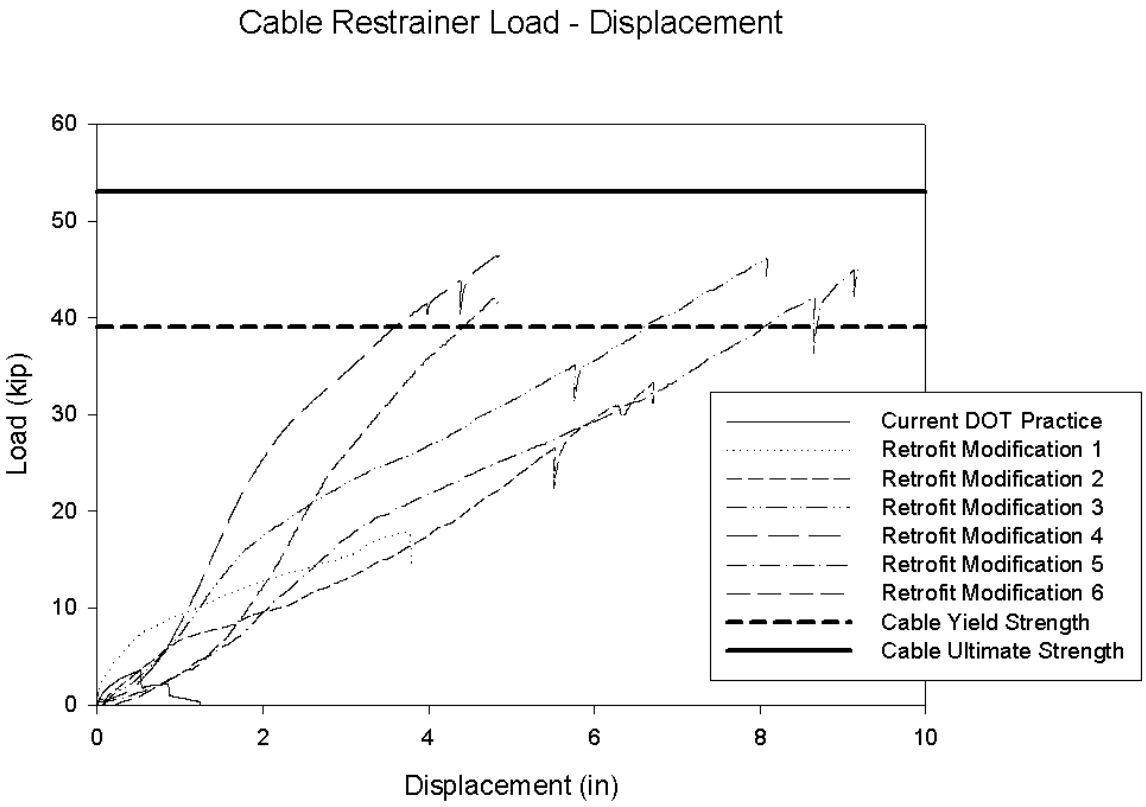

Figure 7.70 Experimental force-displacement behavior of cable restrainers used in analysis.

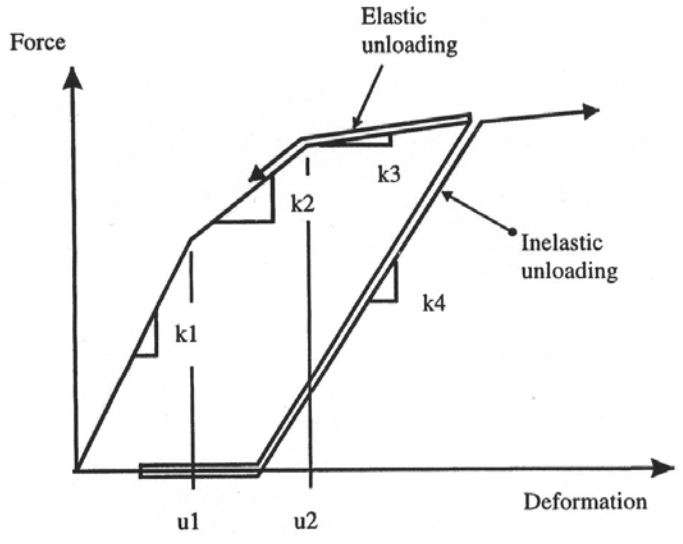

Figure 7.71 Multi-linear tension only nonlinear inelastic element used to model restrainers (Prakash et al., 1992)

Table 7.5 Stiffness and deformation characteristics of single restrainer used in analysis.

Configuration	k1 (k/in)	k2 (k/in)	k3 (k/in)	k4 (k/in)	u1 (in)	u2 (in)
Current DOT	14.42	3.7	0	22.88	0.12	0.58
Retrofit Mod 1	13	3.11	0	62.9	0.59	3.78
Retrofit Mod 2	7.25	4.56	0	46.78	0.97	6.71
Retrofit Mod 3	8.98	4.72	0	46.2	1.76	8.09
Retrofit Mod 4	12.56	6.81	0	49.28	2.28	4.95
Retrofit Mod 5	4.75	4.99	0	63.2	1.99	9.22
Retrofit Mod 6	5.26	10.6	0	50.2	1.35	4.61

7.3.4 Ground Motions

In order to assess the seismic response of these typical bridges in Mid-America, ground motions that are likely to occur in Mid-America must be determined. Since few recorded ground motions exist, synthetic ground motion records are generated. Using the latest regional information and stochastic ground motion models, Wen and Wu (2001) developed a suit of synthetic uniform hazard ground motions for Memphis, TN, and Carbondale, IL. These cities are selected as earthquake sites because they present a cross-section of the Mid-America cities at risk.

One synthetic record from both Memphis, TN and Carbondale, IL, based on a 2% probability of exceedance in 50 years, was selected for the analysis. The characteristics of the two ground motions are shown in Table 7.6, where PGA is the peak ground acceleration and Tg is the characteristic period of the earthquake. The time history plots of the ground motion accelerations are shown in Figure 7.72 and Figure 7.73.

Table 7.6 Characteristics of synthetic ground motions used in analysis.

Location	Moment Magnitude (Ms)	Epicentral Distance (km)	Duration (sec)	PGA (g)	Tg (sec)
Carbondale	8	169.3	27.9	0.673	2.288
Memphis	8	97.6	57.82	0.476	1.631

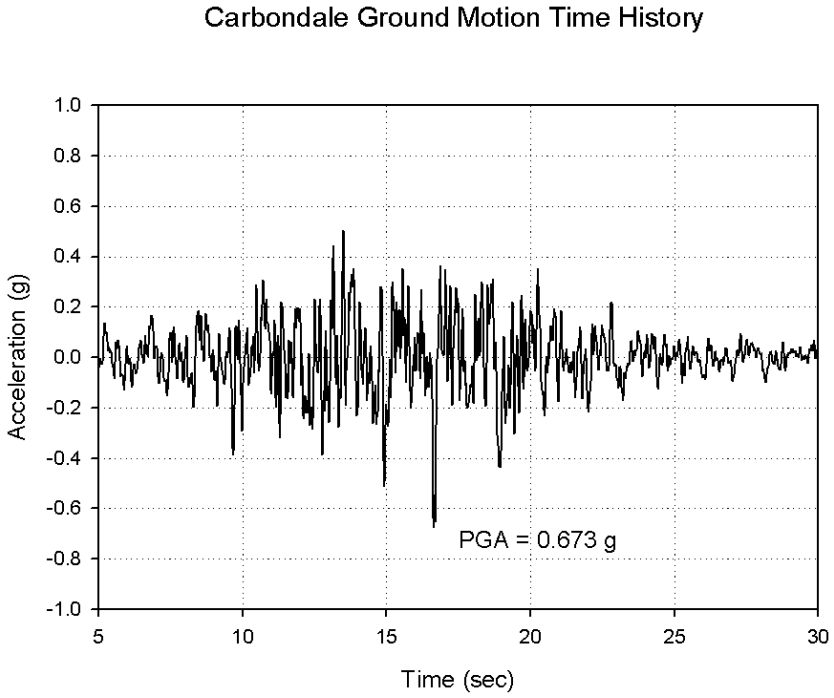

Figure 7.72 Synthetic ground motion time history for Carbondale, IL (2% exceedance in 50 years).

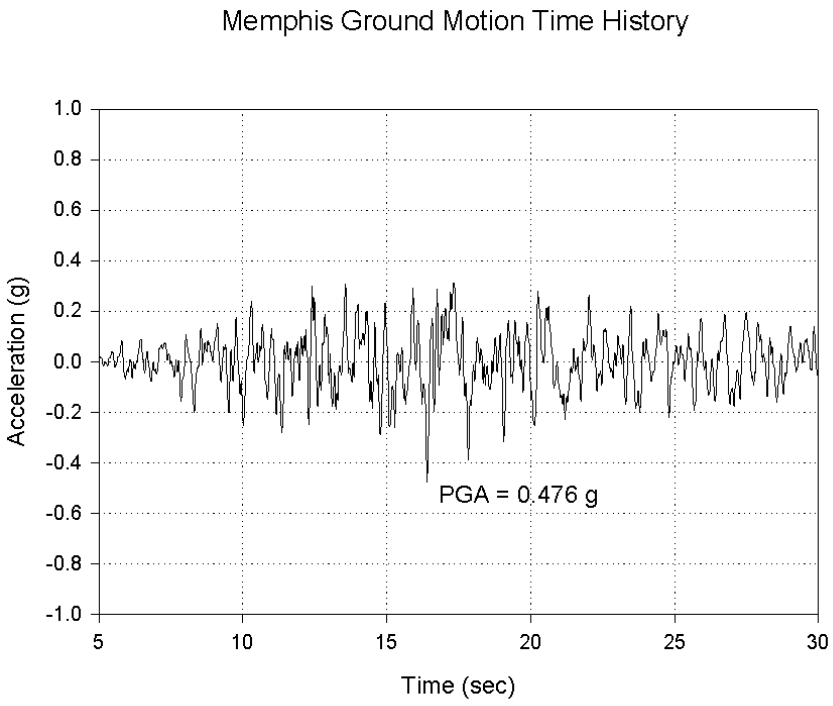

Figure 7.73 Synthetic ground motion time history for Memphis, TN (2% exceedance in 50 years).

7.3.5 Results of Analysis

The two model bridges with different cable restrainers configurations were subjected to the synthetic ground motions in DRAIN-2DX. The relative hinge openings at the abutments and piers were monitored for each of the analyses. For the continuous bridge with a fixed elastomeric bearing over one pier, the column drift was monitored. The hinge openings are important because they can be a good indication to whether or not the bridge superstructure will collapse. If the relative opening is greater than the abutment or pier seat, than collapse of the span is likely. The typical seat width found on existing bridges in Mid-America ranges from about 4" to 16", depending on the type of

bridge, conditions of the bridge, and date of construction. The pier drifts are also important because high drifts can lead to column failure and collapse of the bridge. Previous studies have shown that in typical bridges in the Central and Southern US, lap splice failure begins to occur at approximately 1% drift of the column (Pujol, 1997). The following subsections will present the results from the analysis of the continuous and MSSS bridges with cable restrainers.

7.3.5.1 MSSS Steel Girder Bridge Results

The MSSS as-built response for the Carbondale ground motion results in max opening at the left abutment of 3.58". Using the current DOT cable restrainer configuration results in a reduction of 15%. Since the resistance provided by the restrainers is very small, the effect, as expected, is minimal. Retrofit modifications 1, 2, and 5 have similar results, providing reductions in displacement of approximately 41%. The most effective configurations are retrofit modification 3 and 4 which reduce the displacements by approximately 53% compared to the as-built. Retrofit modification 4 is used a stiffened angle girder connection that is similar to the connection used by IDOT. Retrofit modification 6, similar to NYSDOT configurations, did not work very well on the MSSS bridge because it has a low initial stiffness up to about 2" in displacement. Similar results were obtained for the MSSS bridge subjected to the Memphis ground motion.

Table 7.7 Maximum hinge opening results for MSSS bridge.

Carbondale Ground Motion												
Configuration	Abutment L		Pier 1 L		Pier 1 R		Pier 2 L		Pier 2		Abutment R	
	D	R	D	R	D	R	D	R	D	R	D	R
No Restrainers	3.58	N/A	2.04	N/A	2.12	N/A	1.72	N/A	1.03	N/A	2.26	N/A
Current DOT	3.04	15	1.74	15	2.09	1	1.46	15	1.03	0	2.06	9
Retrofit Mod 1	2.23	38	0.86	58	1.65	22	1.44	16	1.05	--	1.97	13
Retrofit Mod 2	1.91	47	1.01	50	1.42	33	1.34	22	1.08	--	1.88	17
Retrofit Mod 3	1.74	51	1.08	47	1.4	34	1.68	2	0.96	7	1.84	19
Retrofit Mod 4	1.65	54	1.07	48	1.28	40	1.45	16	0.9	13	1.62	28
Retrofit Mod 5	2.23	38	1	51	1.5	29	1.75	--	1.18	--	2.01	11
Retrofit Mod 6	2.36	34	0.98	52	1.52	28	1.55	10	1.06	--	1.93	15
Memphis Ground Motion												
Configuration	Abutment L		Pier 1 L		Pier 1 R		Pier 2 L		Pier 2 R		Abutment R	
	D	R	D	R	D	R	D	R	D	R	D	R
No Restrainers	2.72	N/A	1.63	N/A	1.71	N/A	1.68	N/A	0.9	N/A	2.07	N/A
Current DOT	2.1	23	0.88	46	1.67	2	1.72	--	0.91	--	1.62	22
Retrofit Mod 1	1.55	43	0.91	44	1.06	38	1.75	--	0.83	8	1	52
Retrofit Mod 2	1.71	37	0.92	44	1.27	26	1.43	15	0.8	11	1.25	40
Retrofit Mod 3	1.57	42	1.01	38	1.14	33	1.37	18	0.88	2	1.17	43
Retrofit Mod 4	1.4	49	1	39	1.17	32	1.29	23	1.1	--	1.07	48
Retrofit Mod 5	1.85	32	0.92	44	1.4	18	1.57	7	0.85	6	1.37	34
Retrofit Mod 6	1.8	34	0.93	43	1.38	19	1.55	8	0.83	8	1.42	31

Δ = hinge opening (in); **R** = reduction (%)

7.3.5.2 Continuous Steel Girder Bridge Results

The continuous as-built response for the Carbondale ground motion results in max opening at the left abutment of 4.98". Using the current DOT cable restrainer configuration results in no change at the abutment opening. Since the resistance provided by the restrainers is very small, the effect, as expected, is minimal. Retrofit modifications 1, 2, and 5 have similar results, providing reductions in displacement of approximately 5%. The most effective configurations are retrofit modification 3, 4, and 6 which reduce

the displacements by approximately 18% compared to the as-built. The pier drifts were also reduced by up to 35% with the use of restrainers on the continuous bridge. Similar results were obtained for the continuous bridge subjected to the Memphis ground motion.

Table 7.8 Maximum hinge opening and pier drift results for continuous bridge.

Carbondale Ground Motion								
Configuration	Abutment L		Abutment R		Pier L		Pier R	
	D	R	D	R	D	R	D	R
No Restrainers	4.98	N/A	4.61	N/A	1.91	N/A	0.49	N/A
Current DOT	5	--	4.53	2	1.31	31	0.48	2
Retrofit Mod 1	4.73	5	4.49	3	1.26	34	0.46	6
Retrofit Mod 2	4.72	5	4.41	4	1.24	35	0.45	8
Retrofit Mod 3	4.37	12	4.29	7	1.48	23	0.43	12
Retrofit Mod 4	3.76	24	4	13	1.3	32	0.39	20
Retrofit Mod 5	4.67	6	4.43	4	1.53	20	0.46	6
Retrofit Mod 6	4.1	18	4.25	8	1.53	20	0.44	10
Memphis Ground Motion								
Configuration	Abutment L		Abutment R		Pier L		Pier R	
	D	R	D	R	D	R	D	R
No Restrainers	4.39	N/A	4.8	N/A	1.21	N/A	0.46	N/A
Current DOT	4.37	0	4.77	1	1.19	2	0.46	0
Retrofit Mod 1	4.15	5	4.46	7	1.23	--	0.45	2
Retrofit Mod 2	4.07	7	4.44	7	1.01	17	0.45	2
Retrofit Mod 3	3.91	11	3.86	20	1.43	--	0.46	0
Retrofit Mod 4	3.41	22	4.06	15	0.97	20	0.38	17
Retrofit Mod 5	4.15	5	4.38	9	1.14	6	0.46	0
Retrofit Mod 6	4.04	8	4.18	13	1.01	17	0.45	2

Δ = hinge opening (in); **R** = reduction (%); **D** = drift (%)

7.3.6 Summary of Analytical Results

The results of the analysis show that the type of cable restrainer connection element can have a significant effect on the seismic response of retrofitted bridges.

Using the existing retrofit measures compared with those of retrofit modification 4 results in a difference of 54% in the relative hinge opening at the abutment on the MSSS bridge. Depending on the available seat widths, this may have a significant bearing on whether or not the deck will unseat. Retrofit modification 4 reduced the hinge opening at the abutment by 24% on the continuous bridge. The cable restrainers were not as effective on the continuous bridge because there is more mass and fewer restrainers compared to the MSSS bridge. However, using better connections helped with the response of the bridge. The measured strength, stiffness, and deformation capacity provided by the modified retrofits can significantly improve the behavior of retrofitted bridges.

CHAPTER 8

RETROFIT MEASURES FOR TYPICAL BRIDGES

In chapter 5, it is understood that the primary vulnerabilities in typical Mid-America bridges are damage to steel bearings, instability of rocker bearings, and column damage. Unlike California and other parts of the West Coast, the Mid-America region has s short history of seismic retrofit of bridges. Therefore, it is not clear which methods may be the most effective in improving the seismic response of typical bridges. Retrofit measures which have been commonly used in California for bridges include steel jackets for non-ductile columns, cable restrainers, and isolation bearings (Chai et al., 1991; DesRoches and Fenves, 1997; Hoerner et al., 1986). Additional retrofits, including strengthening of foundations and abutments, have also been performed (Yashinsky, 1991; Kuprenas et al., 1998). The decision to retrofit in Mid-America is further complicated by the infrequent nature of earthquakes in the region. Since the probability of a large earthquake during the life span of a typical bridge is very small, the retrofit measure chosen must be cost-effective (Karshenas and Kaspar, 1997). Therefore, in this study, four cost-effective retrofit strategies have been evaluated. They include replacing steel bearings with elastomeric bearings/lead-rubber bearings, cable restrainers placed at the internal hinges and abutments, and using a combination of cable restrainers and elastomeric bearings. Seismic responses of the typical bridges with the various retrofit measures will be performed to determine the most effective measure.

8.1 Elastomeric Bearings

8.1.1 Overview of Elastomeric Bearings

Elastomeric bearings are now the most commonly used type of device for seismic isolation (Skinner et al., 1993). They are a fully developed commercial product whose main application has been for bridge superstructures which undergo large displacements due to thermal expansion. Within the past three decades the use of bearings made of synthetic, elastomeric material has become increasingly popular.

There are two types of elastomeric bearings as shown in Figure 8.1; plane pads consisting of elastomer only, and reinforced bearings which have alternately layers of elastomer and steel plates. The shape of elastomeric bearings is typically circular or rectangular in design. The steel reinforcement, which is firmly bonded to the elastomer, provides bulging restraint under large compressive loads, as shown in Figure 8.2(a).

In unreinforced pads, bulging restraint is provided by friction between the elastomer and the load surface. The thickness of each laminated pad in reinforced elastomeric bearing should be less than 25.4 mm (1 inch) (TRB, 1977).

Translational movements of the bridge due to creep, shrinkage, or thermal expansion can cause shear deformation of the elastomer as shown in Figure 8.2(b). Rotation of the bearing due to rotation of the bridge girders may cause a nonuniform bulging deformation, as shown in Figure 8.2(c).

Lateral motion of one loaded surface relative to the other is accommodated by both bending and shear. The flexibility in shear is important because this provides isolation to bridges. However, if the lateral deformation of the bearing becomes large, then stability

problems may occur as previously mentioned.

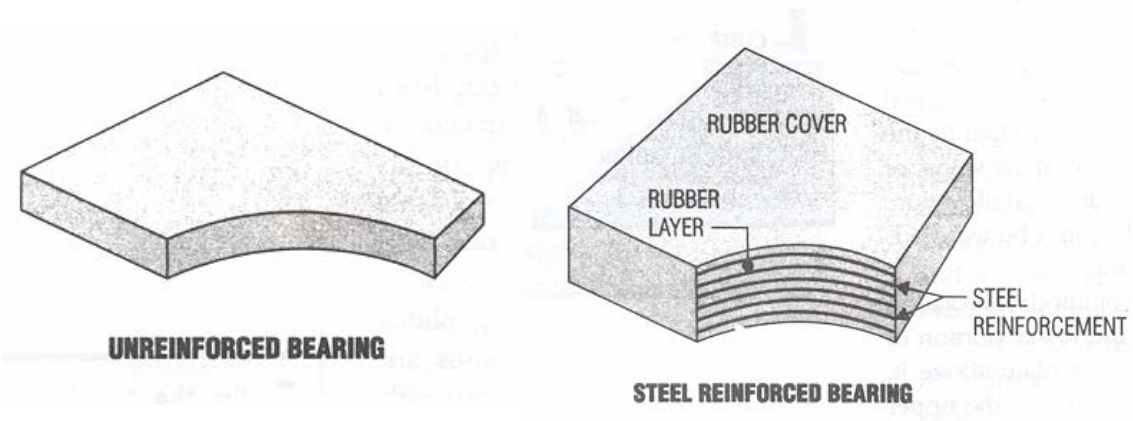

Figure 8.1 Typical Unreinforced and Reinforced Elastomeric Bearings

(Adapted from "State-of-the-Art Elastomeric Bridge Bearing Design", 1991)

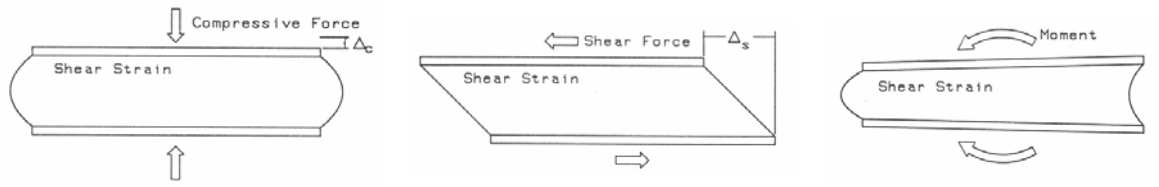

(a) Compression (b) Shear (c) Rotation

Figure 8.2 Strain and Deformation of Elastomeric Bearings

(Adapted from "State-of-the-Art Elastomeric Bridge Bearing Design", 1991)

Since elastomeric bearings are less sensitive to corrosion than steel bearings and provide reliable flexibility, they present an attractive alternative to traditional steel mechanical bearing systems in terms of both functionality and maintenance considerations. The shear stiffness of elastomeric bearings is highly dependent on the thermal change. The stiffness at extreme low temperature (-20°C) is 50~100 times the

room temperature stiffness (Roeder et al., 1990). In extreme cases the elastomer may become brittle and fail. This stiffness increase is a concern for engineers designing bridges in cold regions, thus this effect should be considered in the design of elastomeric bearings.

8.1.2 Analytical Model of Elastomeric Bearings

In the late 1980s, extensive research on elastomeric bearings was conducted by the American Association of State Highway and Transportation Officials (AASHTO) (Roeder et al., 1987). In the study, the basic properties of elastomeric bearings; such as temperature effects, compression loading, rotation, shear and combined loading, stability, and fatigue, were evaluated. The shape of elastomeric bearings was found to be the most important factor in the shear stiffness of the elastomeric bearing. The shear stiffness of elastomeric bearings in low temperature was found to be around 50 times that in normal temperature (20°C). The behavior of elastomeric bearings in compression is almost linear elastic, while the shear stress-strain curve is hysteretic. The shear stiffness of elastomeric bearings is increased with increasing the normal force.

Aiken et al. (1992) carried out an extensive series of tests on three types of seismic isolation bearings; two elastomeric bearings and one lead-rubber bearing, to determine their mechanical characteristics. The effective stiffness and damping ratio of the bearings were calculated as function of the shear strain. Effective stiffness for small shear strain is very large but decreases sharply with increasing shear strain. However, the equivalent viscous damping ratio is nearly constant for a wide range of shear strain values.

Damping ratio for elastomeric bearings is 7% to 10%, but that of lead-rubber bearing is 16% to 20%. In general, it was found that variations in axial load and rate of loading did not significantly affect bearing stiffness and damping properties for moderate shear strain levels. The ultimate-level shear tests achieved bearing shear strains in excess of 500% before failure occurred.

It is indicated by Mizukoshi et al. (1992) that the failure limits and the restoring force characteristics of elastomeric bearings are strongly influenced by their geometric shapes under some loading conditions. That is, as the primary and the secondary shape factors; S1=cross section area of rubber/ free surface area, and S2=diameter of rubber/total thickness of rubber, become smaller, shape deformation capacity under high compression force is drastically reduced due to early occurrence of buckling.

The elastomeric bearings can be modeled with a bilinear element based on the three parameters, K_1, K_2, and Q, where K_1 is the initial stiffness, K_2 is the plastic stiffness, and Q is the characteristic value of an elastomeic bearing (Kelly, 1997). The parameters are a function of the bearing type and size. The stability problem about the axial loading was discussed and formulations of the maximum axial load for some bearing types were suggested.

Following Kelly's model, bilinear elements are used for designing of elastomeric bearings based on the three parameters, K_1, K_2, and Q, as shown in Figure 8.3 (Kelly, 1997). The elastic stiffness, K_1, is estimated from available hysteresis loops from elastomeric bearing tests. The characteristic strength, Q, is estimated from the hysteresis loops for the elastomeric bearings.

The effective stiffness, defined as the secant slope of the peak-to-peak values in a hysteresis loop, is given by

$$K_{eff} = K_2 + Q / D, \quad D \geq D_y \tag{8.1}$$

where D_y is the yield displacement. In terms of the primary parameters,

$$D_y = Q / (K_1 - K_2) \tag{8.2}$$

And the area of the hysteresis loop; the energy dissipated per cycle, W_D, is

$$W_D = 4Q(D - D_y) \tag{8.3}$$

The effective damping, β_{eff}, is defined by

$$\beta_{eff} = 4Q(D - D_y) / 2\pi K_{eff} D^2 \tag{8.4}$$

Two types of elastomeric bearing models, which are rectangular, are used for the analyses in this study. The dimensions of the bearings are 305 mm × 203 mm × 102 mm (12 in. × 8 in. × 4 in., L×W×H,) and 457 mm × 305 mm × 152 mm (18 in.×12 in.×6 in., L×W×H). The second bearing is only for the multi-span continuous steel bridge.

The shear modulus of typical bridge elastomeric bearings, G, is approximately 0.69 Mpa (100 psi) (Skinner et al., 1993). Thus, the effective stiffness of the bearings can be calculated using the following equation.

$$K_{eff} = GA / h_r \tag{8.5}$$

where A is the area of an elastomeric bearing, G is the shear modulus of the elastomer, and h_r is the total height of elastomer.

It is assumed to develop the bilinear model of the small elastomeric bearing that D, which is the maximum design deformation of the elastomeric bearing in the equation

(8.1) is equal to the height of elastomer, 101.6 mm (4 in.), D_y is 10.2 mm (0.4 in.), and K_1 is 3 times of K_2. Then, the effective stiffness of the bearing, K_{eff}, is 0.42 kN/mm (2.4 kips/in.), and the characteristic strength, Q, is 7.1 kN (1.6 kips). From the above information, it can be calculated that K_2 is 0.35 kN/mm (2.0 kips/in.), and K_1 is equal to 1.05 kN/mm (6.0 kips/in.). The damping ratio at 100% shear strain of the elastomeric bearing is 9.5% of the critical from the equation (6.4). When K_1 is equal to $3K_2$, the maximum damping ratio is 17.1% at the bearing deformation of 27.9 mm (1.1 in.).

For the large elastomeric bearing, D and D_y are 152.4 mm (6 in.) and 15.2 mm (0.6 in.), respectively. K_1, K_2, and K_{eff} are 1.58, 0.53, and 0.63 kN/mm (9, 3, and 3.6 kips/in.), respectively. Figure 7.4 shows an experimental result of shear force and transverse displacement relationship of an elastomeric bearing (Roeder et al., 1987). In the graph, the ratio K_1 to K_2 is nearly 3.0.

The rotational stiffness of elastomeric bearing models is assumed to be 6.0e5 kN·mm/rad (5310.5 kips-in./rad) (Mori, et al. 1997) for both elastomeric bearings. The vertical flexibility of the bearings is ignored.

8.2 Lead-Rubber Bearings

8.2.1 Overview of Lead-Rubber Bearings

A common isolation system in recent years is the lead-rubber bearing, which was developed in New Zealand in 1975 by W H Robinson (Skinner, et. al, 1993). The device is a conventional elastomeric bearing modified by inserting a lead-plug in its center as shown in Figure 8.5.

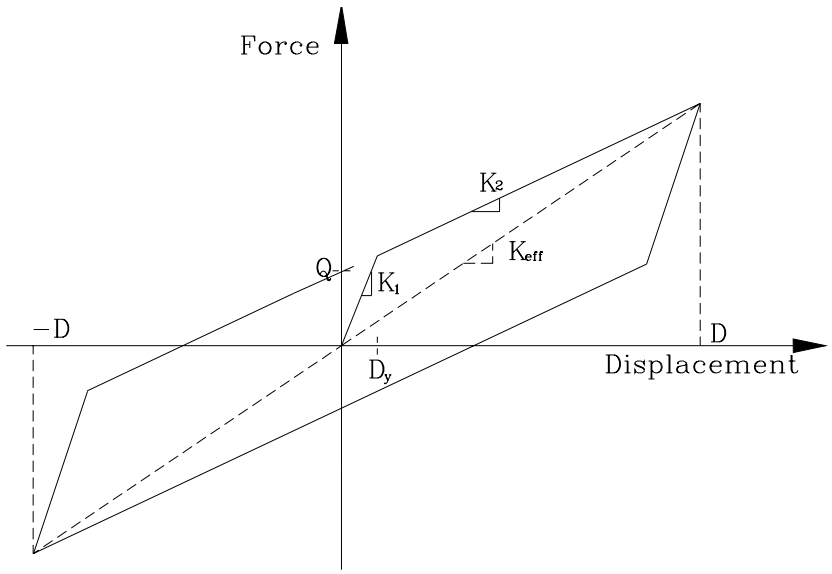

Figure 8.3 Bilinear Modeling of Elastomeric Bearings

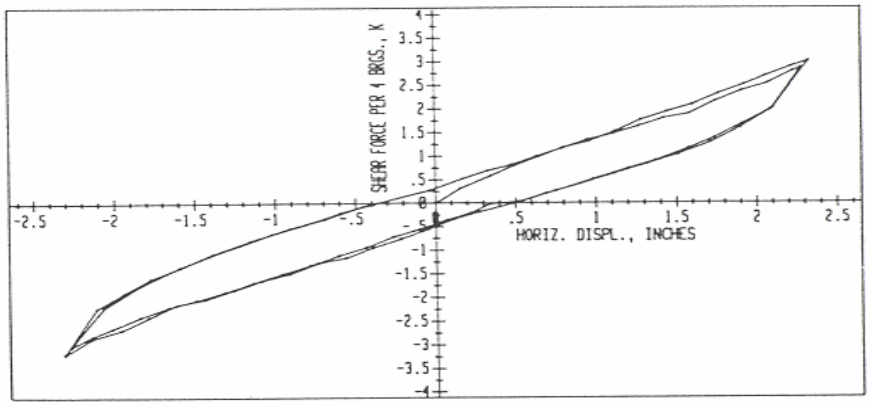

Figure 8.4 Experimental Result of An Elastomeric Bearing of Shear Force vs. Displacement Relationship (Roeder et al., 1987)

The rubber of the bearing changes the natural period of the isolated structure by introducing softening, while the lead contributes vibration damping through energy-

dissipating effects during strong earthquakes and provides required rigidity under service loads. Therefore, the use of lead-rubber bearings between the superstructure and the substructure can result in a significant reduction in forces induced in the bridge structure, as compared to the nonisolated bridges (Ghobarah and Ali, 1988). With base isolation, the piers can be designed to behave elastically, thus avoiding the problems associated with ductile design, and at the same time achieving an economical design. The lead-rubber bearing can be easily replaced after a damaging earthquake. Figure 8.6 shows the force-displacement hysteretic loops of a lead-rubber and an elastomeric bearing with the same dimensions. It is found from the figure that the lead-rubber bearing has a larger yield force and has more energy-dissipation capacity than the elastomeric bearing.

8.2.2 Analytical Model of Lead-Rubber Bearings

The results of several studies (Robinson, 1982; Clark et al., 1993; Mori et al., 1999) have shown that the behavior of lead-rubber bearings is bilinear. Therefore, the behavior can be defined by three parameters; the post-yield stiffness, K_d, the unloading stiffness, K_u, and the yield force, F_y as shown in Figure 8.7.

In this study, to obtain the three parameters for design of a lead-rubber bearing, the procedure described below is used (Skinner et al., 1993):

$$K_d = K_s \tag{8.7a}$$

$$K_u = 10\ K_s \tag{8.7b}$$

where K_s is the same as K_{eff} in the equation (8.5). Since the behavior of a lead plug is assumed to be rigid-plastic and that of an elastomeric bearing is bilinear, the yielding

force of a lead-rubber bearing is the summation of the yield-force of the lead core and the elastomeric bearing. Therefore, the yielding force, F_y, can be calculated by the equation:

$$F_y = \tau(Pb)\, A(Pb) + K_1 D_y \tag{8.8}$$

where the shear stress at which the lead yields $\tau(Pb)$ = 10.5 MPa (1.523 ksi), A(Pb) is the cross-sectional area of the lead plug, K_1 is the initial stiffness of the rubber, and D_y is deformation of the bearing defined in Figure 8.3.

Two types of lead-rubber bearings are used in this study. The dimension of the lead-rubber bearings is the same as those of the elastomeric bearings. The diameter of lead-plug is 63.5 mm (2.5 in.) for both lead-rubber bearings. Following the procedure, the post-yield stiffness, K_d, of the small lead-rubber bearing is equal to 0.42 kN/mm (2.4 kips/in.), and the unloading stiffness, K_u, is 4.20 kN/mm (24.0 kips/in.). The yielding force of the bearing is equal to 42.7 kN (9.6 kips), and the yield deformation is 10.5 mm (0.4 in.). For the large lead-rubber bearing, the unloading and the post-yield stiffness are 0.63 and 6.30 kN/mm (3.6 and 36.0 kips/in.), respectively. The yield force of the bearings is 96.1 kN (21.6 kips) at the yield deformation of 15.2 mm (0.6 in.).

The design method described above is compared with the different methods, the New Zealand MWD. The New Zealand MWD CDP818/A (1981) defines the three parameters as follows:

$$K_d = K_r\,(1 + 12A_p / A_r) \tag{8.9}$$

$$K_r = K_s\,(A_r / A_g) \tag{8.10}$$

$$F_y = 7.06 \times 10^{-3}\, D^2 \tag{8.11}$$

where A_p is the cross-sectional area of a lead plug, A_r is the net area of a bearing without

a lead plug, A_g is the gross bearing area, and D is the diameter of a lead plug. The unloading stiffness, $K_u = 6.5\ K_d$.

The calculated shear stiffnesses for the small lead-rubber bearing designed by the author are listed in Table 8.1. The New Zealand Method predicted post-yield stiffness about 1.5 times more than that of the suggested method. The New Zealand Method includes the hardening of the lead plug to predict the post-yield stiffness, although the suggested method does not. In the shear yield strength, the suggested method considers the strength of the elastomeric bearing, but the New Zealand Method does not. From the Equation (8.11), the shear yield stress can be estimated as 9.0 MPa, which is about 17% less than the value used in the suggested method. Although the two values were predicted differently, the unloading stiffnesses are similar for both design methods. The damping properties of the two models, calculated by the Kelly's equations (Kelly, 1997), is illustrated in Figure 8.8. The maximum damping ratios are 33% of the critical at the displacement of 42.7 mm (1.68 in.) and 28% at 24.0 mm (0.95 in.) for the suggested method and the New Zealand Method, respectively.

Table 8.1 Comparison of NZMWD and the Suggested Method for Designing of Lead-Rubber Bearings

	Shear Stiffness (kN/mm)			Shear yield strength (kN)
	Rubber only	Post-yield	Unloading	
NZ MWD	0.42	0.68	4.27	28.5
Suggested Method	0.42	0.42	4.20	44.0

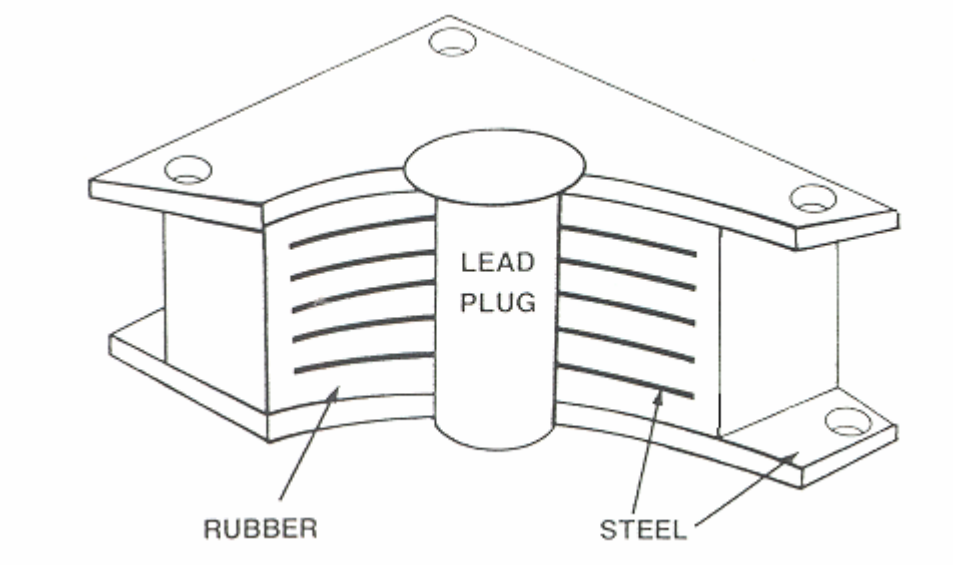

Figure 8.5 Typical Square Lead-Rubber Bearing

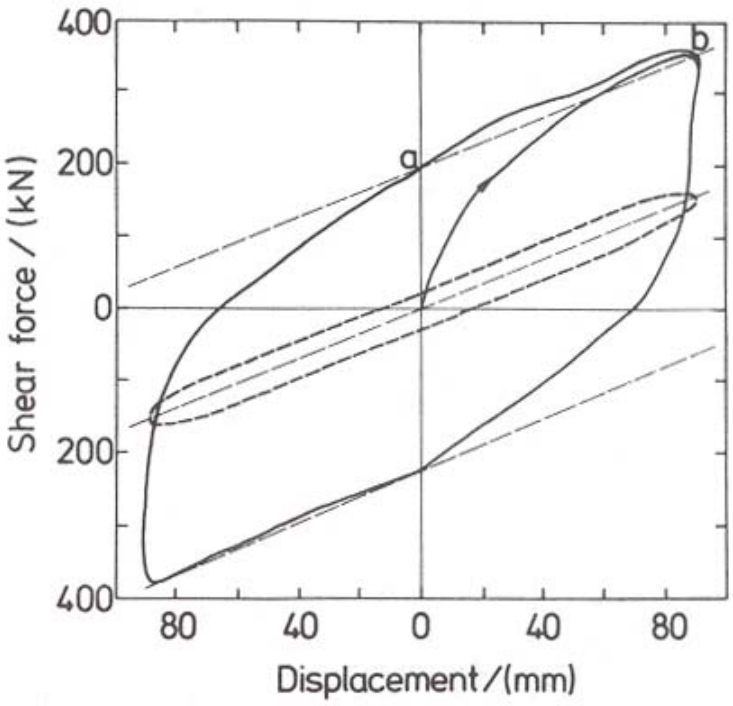

Figure 8.6 Hysteresis Loops of a Lead-Rubber and an Elastomeric Bearing

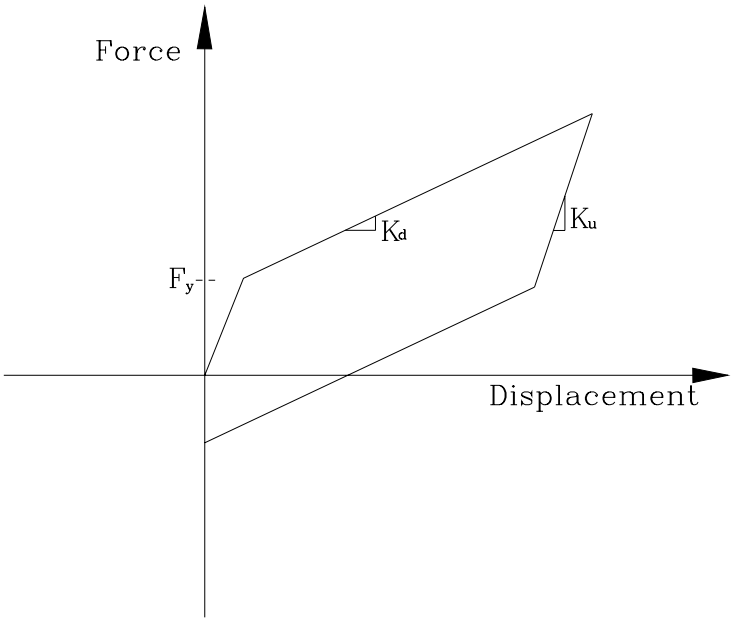

Figure 8.7 Behavior of Lead-Rubber Bearings

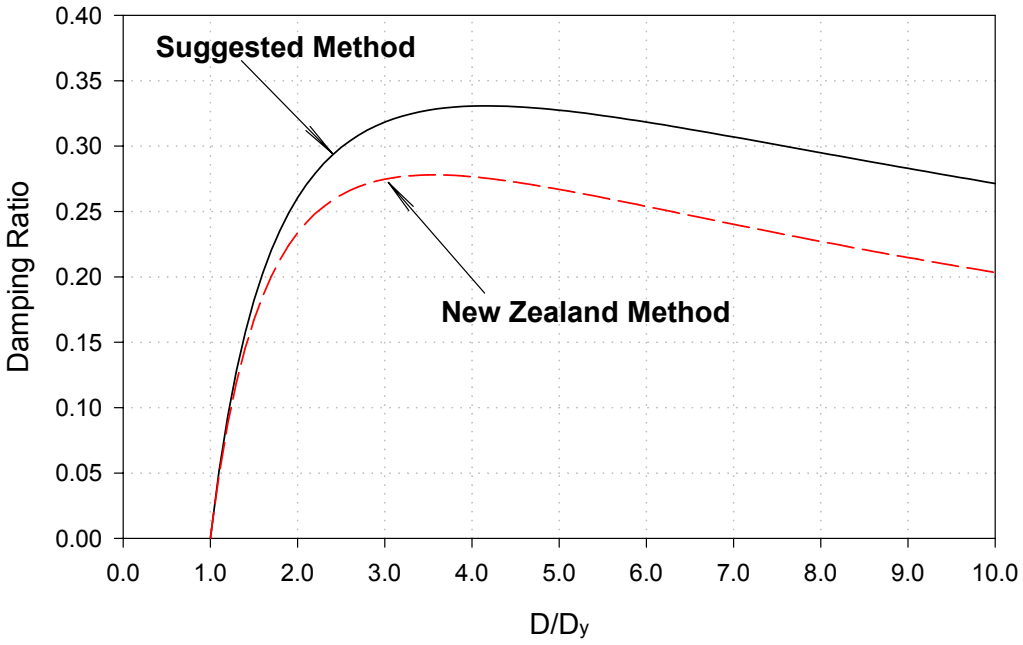

Figure 8.8 Damping Ratio of the Lead-Rubber Bearing

8.3 Restrainer Cables

8.3.1 Overview of Restrainer Cables

Typical restrainer cables used in California is 19.0 mm (3/4 in.) diameter and 143 mm^2 (0.22 $inch^2$) area steel cables as shown in Figure 8.9. The cables have a yield strength of 174 kN (39.1 kips), which corresponds to the yield stress of 1210 MPa (176 ksi). The initial elastic modulus is 69000 MPa (10000 ksi). The post yield strength of the cables increases to an ultimate of about 235 kN (53 kips) per cable. The force-deformation relationship for a typical restrainer cable is shown in Figure 8.10. Figure 8.11 and 8.12 shows various ways of connecting the restrainer cable to the pier or abutment. In some cases, restrainer rods are used instead of cables as shown in Figure 8.13.

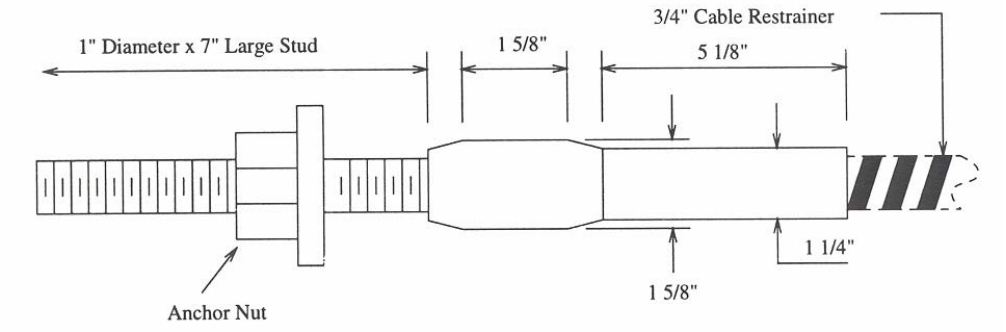

Figure 8.9 Typical Cable Restrainer and Swaged Fitting

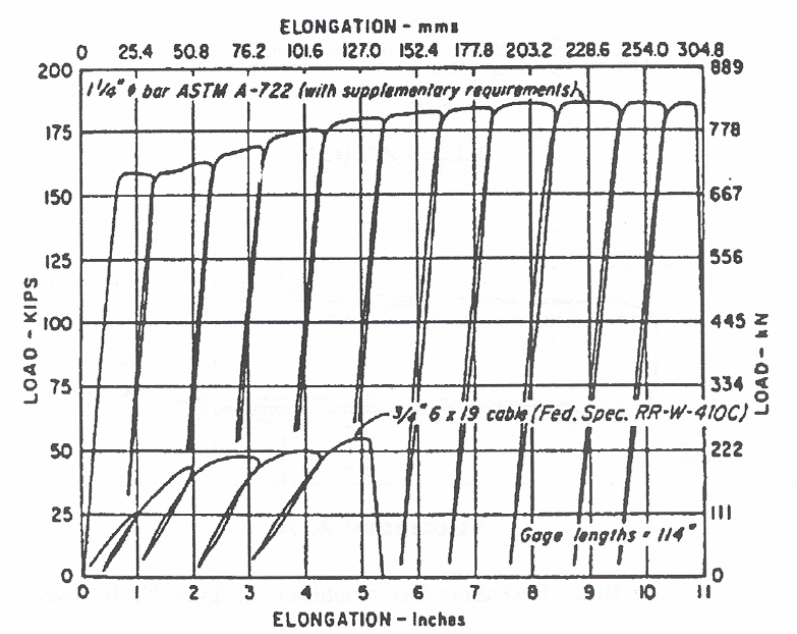

Figure 8.10 Load Deformation Relationship for Restrainers

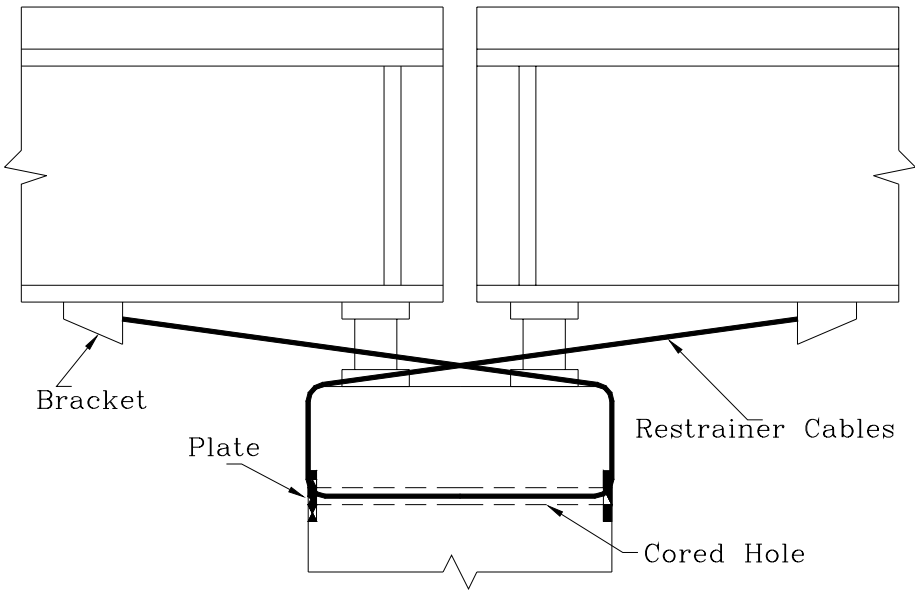

(a) Connection between Decks and Pier

Figure 8.11 Typical Connection of Restrainer Cables for Steel Bridges (Pfeifer, 2001)

(b) Connection between Deck and Abutment or Pier

Figure 8.12 Typical Connection of Restrainer Cables for Steel Bridges (Pfeifer, 2001)

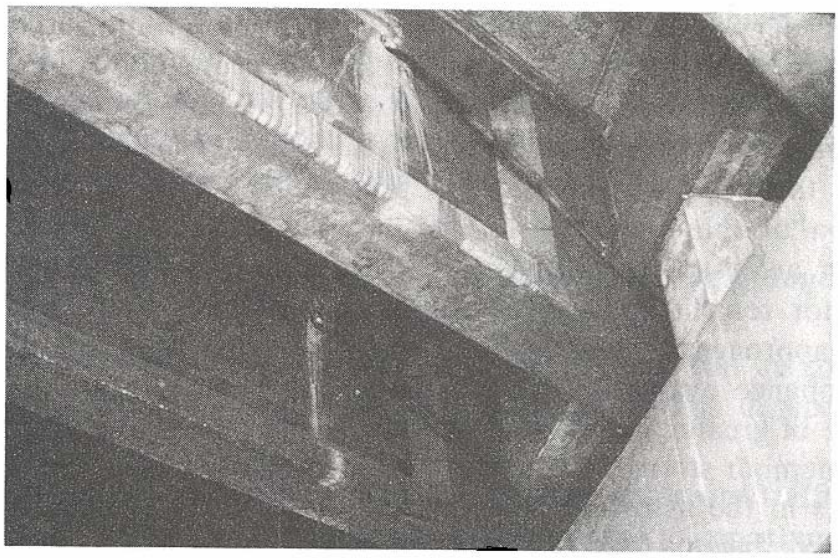

(a) Connection between Deck an Pier

Figure 8.12 Typical Connection of Restrainer Cables for Concrete Bridges

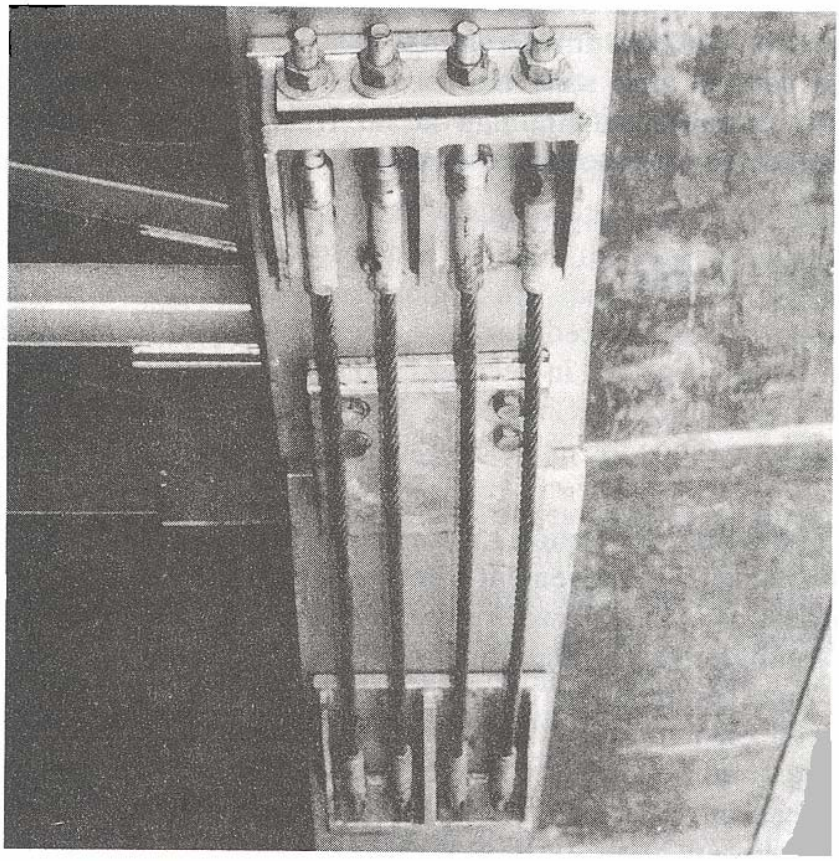

(b) Connection of Deck to Deck

Figure 8.12 Typical Connection of Restrainer Cables for Concrete Bridges

A stopper can be used at an abutment to restrict the relative longitudinal motion between the superstructure and substructure shown in Figure 8.14. A certain amount of travel from thermal expansion effects and allowable earthquake motion can take place before the stopper exerts resistance to motion.

In the transverse direction, shear keys are usually used to restrict the transverse movement. Vertical hold-down devices may be used at bearings to resist the uplift forces. The rotational surfaces in steel bearings are separated from each other

mechanically, and the elastomeric bearings have quite low stiffness in tension. Considering these facts, vertical restrainer devices may be desirable.

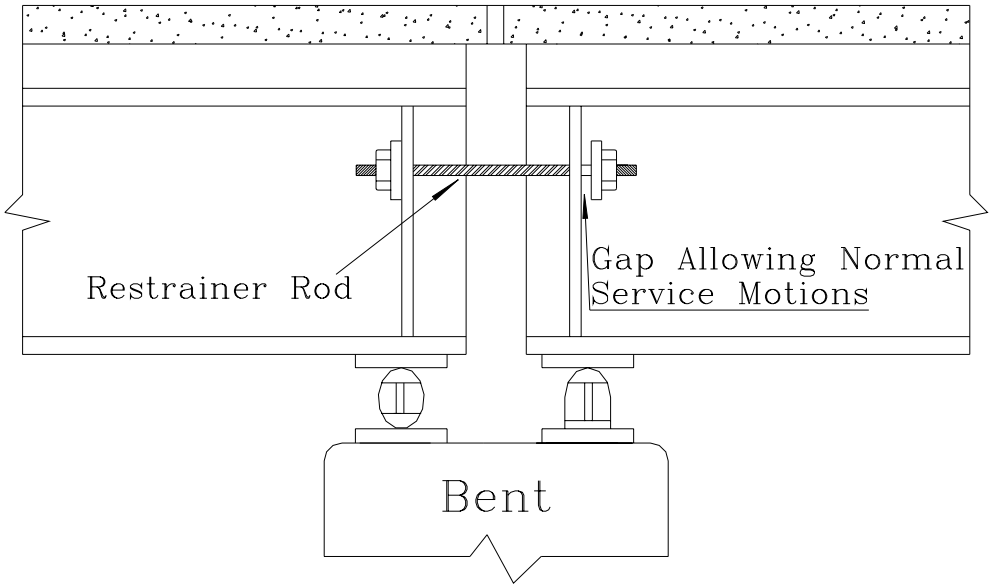

Figure 8.13 Restrainer Connection between Decks for Steel Bridges (Xanthakos, 1996)

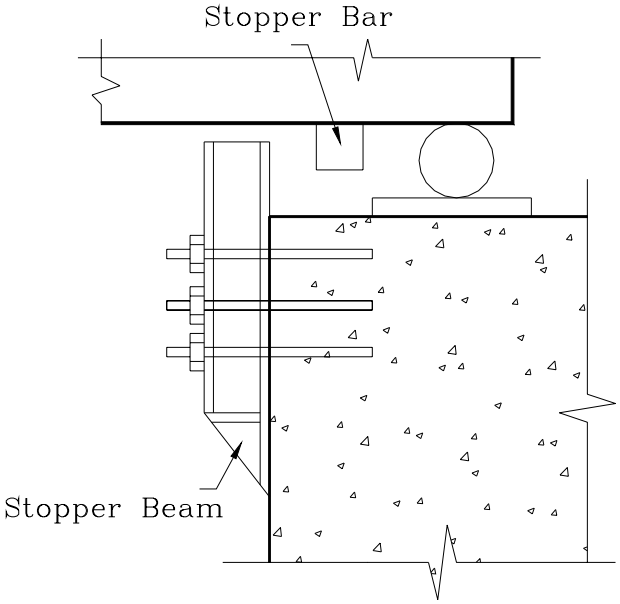

Figure 8.14 Longitudinal Motion Restrainer at Abutments (Xanthakos, 1996)

8.3.2 Analytical Model of Restrainer Cables

The length of restrainer cables used in this study is 1.5 m (5 ft) long. The stiffness (EA/L) of each cable is 6.42 kN/mm (36.7 kips/in.). The hardening ratio is 0.05 for the restrainer cables. The slack of restrainer cables is assumed to be 12.7 mm (0.5 in.), as specified for typical bridges. Restrainer cables are activated only in tension. Therefore, the link element in DRAIN-2DX is suitable for a restrainer cable. The analytical model for the restrainer cables is shown in Figure 8.15.

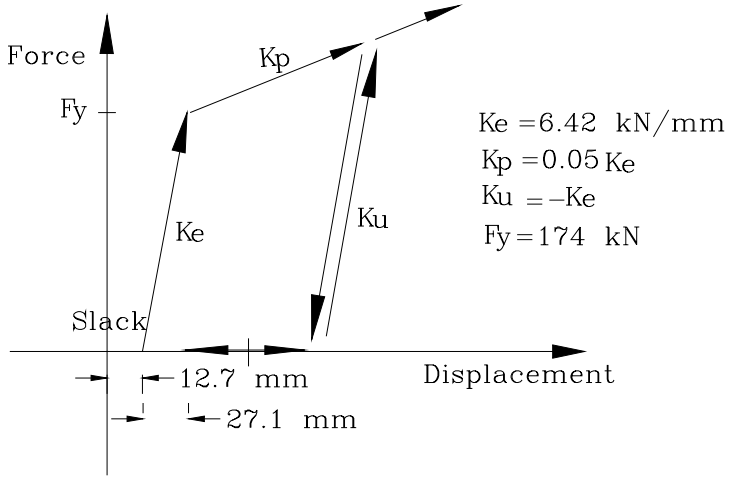

Figure 8.15 Analytical Models for Two Types of Restrainer Cables

8.4 Performance of Retrofit Measures

In this section, the retrofit methods discussed above will be evaluated for the typical bridges. The analytical models previously developed will be modified to account for the effect of the four different retrofit measures; elastomeric bearings (EB), lead-rubber bearings (LRB), restrainer cables (RC), and the combination of restrainer cables and elastomeric bearings (RC-EB).

The revised analytical models will be subjected to the suite of ground motions discussed in chapter 3. The responses of the retrofitted bridges will be compared with those of the as-built bridges to assess the effect of retrofitting.

The four retrofit measures designed in the above sections are installed to modify the response of the typical bridges. Elastomeric bearings/lead-rubber bearings replace the steel bearings and restrainer cables are installed between decks and abutments or between decks and piers as shown in Figure 8.16.

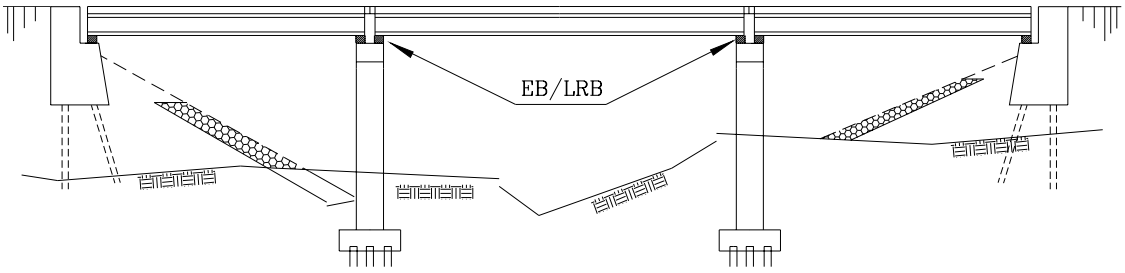

(a) Replacement of Steel Bearings by EB/LRB in MSSS Bridge

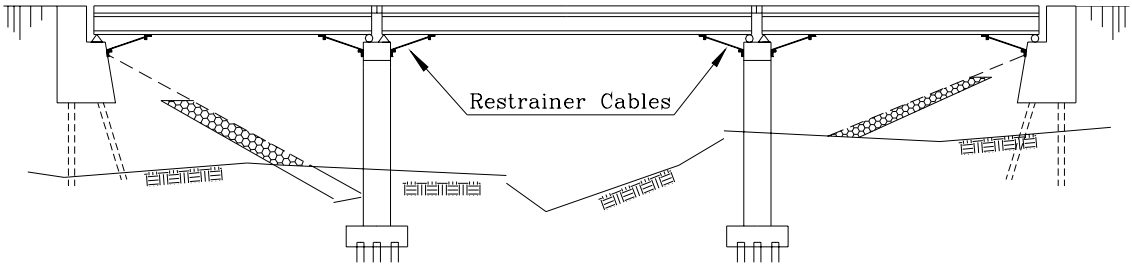

(b) Installation of Restrainer Cables in MSSS Bridge

Figure 8.16 Installation of Retrofit Measures

8.4.1 Performance of Retrofitted MSSS Bridges

The responses of the retrofitted MSSS bridges are listed from Table 8.2. In the table, the ductility and drift of columns and the maximum values of fixed bearings' deformation, relative hinge openings, and abutments' deformation are illustrated. In addition, the retrofitted responses are compared with the response of the as-built bridges.

Elastomeric bearings are understood to have very effective "isolation" function. As expected, the elastomeric bearings reduce the demand of the substructure such as column ductility and drift in the MSSS bridges. For both the steel girder and PSC girder bridge, the elastomeric bearings reduce the column ductility by more than 50%. The bearings, however, are so flexible that they produce large deck displacement and pounding force, which can damage the abutments in passive action. The maximum passive deformation of the abutments is 20.2 mm (0.8 in.) in the MSSS concrete bridge with the elastomeric bearings exceeding the yield deformation, 14.6 mm (0.57 in.). Additionally, the large pounding force can lead to the local damage on the decks.

The effect of lead-rubber bearings on the columns is similar to that of elastomeric bearings. However, the bearings are much stronger and stiffer than elastomeric bearings, thus the bearings do not produce as much isolation as the elastomeric bearings. The ductilities of the columns with lead-rubber bearings exceed the yield point slightly.

However, since lead-rubber bearings have large "energy-dissipation" capacity as shown in Figure 8.6, they can reduce the decks' displacement and hinge openings effectively. Therefore, pounding forces decrease and the deformation of abutments in passive action is reduced sharply compared with the response with elastomeric bearings.

The deformation of the abutments in active action increases slightly compared with elastomeric bearings, but the deformation remains in the elastic range.

The restrainer cables, in general, are moderately effective in reducing the ductility demand on the columns. The restrainer cables reduce the column ductility demand by as much as 24% in the steel girder bridge, and 7% in the concrete bridge. The restrainers are much less effective in limiting the fixed bearing deformation, where there is only 3% reduction in fixed bearing deformation compared with the as-built bridge. The restrainers are effective in limiting the relative hinge opening. The maximum hinge opening in the as-built steel bridge, 59.5 mm (2.33 in.), is reduced to 35.3 mm (1.39 in.) with the restrainer cables. In the concrete bridge, the maximum hinge opening of 49.7 mm (1.96 in.) is reduced to 25.8 mm (1.02 in.). The restrainers have very little effect on the abutment responses.

The negative effect of the restrainer cables is observed on the abutments in the active (pulling) action. The active deformation of the abutments increases with the cables. Especially, the deformation in the concrete bridge exceeds the yield deformation. The restrainer cables increase the interaction between decks. This can help to reduce relative hinge openings and column demand. However, since the increased interaction transfers the inertia forces of the decks to the abutments simultaneously, abutments can be damaged in pulling action.

Although the combination of restrainer cables and elastomeric bearings is not effective to reduce the demand of columns and abutments, it is effective to restrict the hinge opening in the MSSS steel bridge. In the MSSS concrete bridge, it reduces the

demand on the columns and the hinge opening. However, the demand on the abutment with the retrofitting combination is higher than that of as-built bridge. Basically, the characteristics of the two devices in seismic behavior are oppositely different; the elastomeric bearings isolate the substructures in a bridge, however, the restrainer cables connect the superstructure and the substructure more tightly. The combination of these two measures deprives the benefits of each device in the MSSS bridges. Figure 7.17 shows the maximum mean and one standard deviation of the responses for as-built and retrofitted bridges.

Table 8.2 Maximum Values of Critical Responses for Retrofitted MSSS Bridges

MSSS Bridge with Steel Girders								
	Column Ductility		Column Drift		Fixed Bearing	Hinge Opening	Abutment Deformation	
	μc1	μc2	Δc1 (%)	Δc2 (%)	δfb (mm)	Δop (mm)	δa+ (mm)	δa- (mm)
As-Built	1.37	1.02	0.86	0.67	16.1	59.5	5.34	3.52
EB	0.64	0.64	0.43	0.43		66.9	1.58	11.5
LRB	1.01	1.01	0.66	0.66		37.6	2.63	3.21
RC	1.04	0.90	0.69	0.60	15.3	35.3	9.01	3.49
RC-EB	1.34	1.34	0.82	0.82		36.0	7.74	8.62
MSSS Bridge with PSC Girders								
	Column Ductility		Column Drift		Fixed Dowel	Hinge Opening	Abutment Deformation	
	μc1	μc2	Δc1 (%)	Δc2 (%)	δfd (mm)	Δop (mm)	δa+ (mm)	δa- (mm)
As-Built	1.38	1.19	0.86	0.75	55.2	49.7	8.41	5.83
EB	0.62	0.61	0.42	0.42		79.5	1.78	20.2
LRB	1.07	1.07	0.70	0.70		42.9	2.92	7.27
RC	1.29	1.05	0.83	0.69	39.2	25.8	11.7	6.03
RC-EB	1.00	1.00	0.68	0.68		35.2	8.68	8.65

EB : Elastomeric Bearings, LRB : Lead-Rubber Bearings, RC : Restrainer Cables

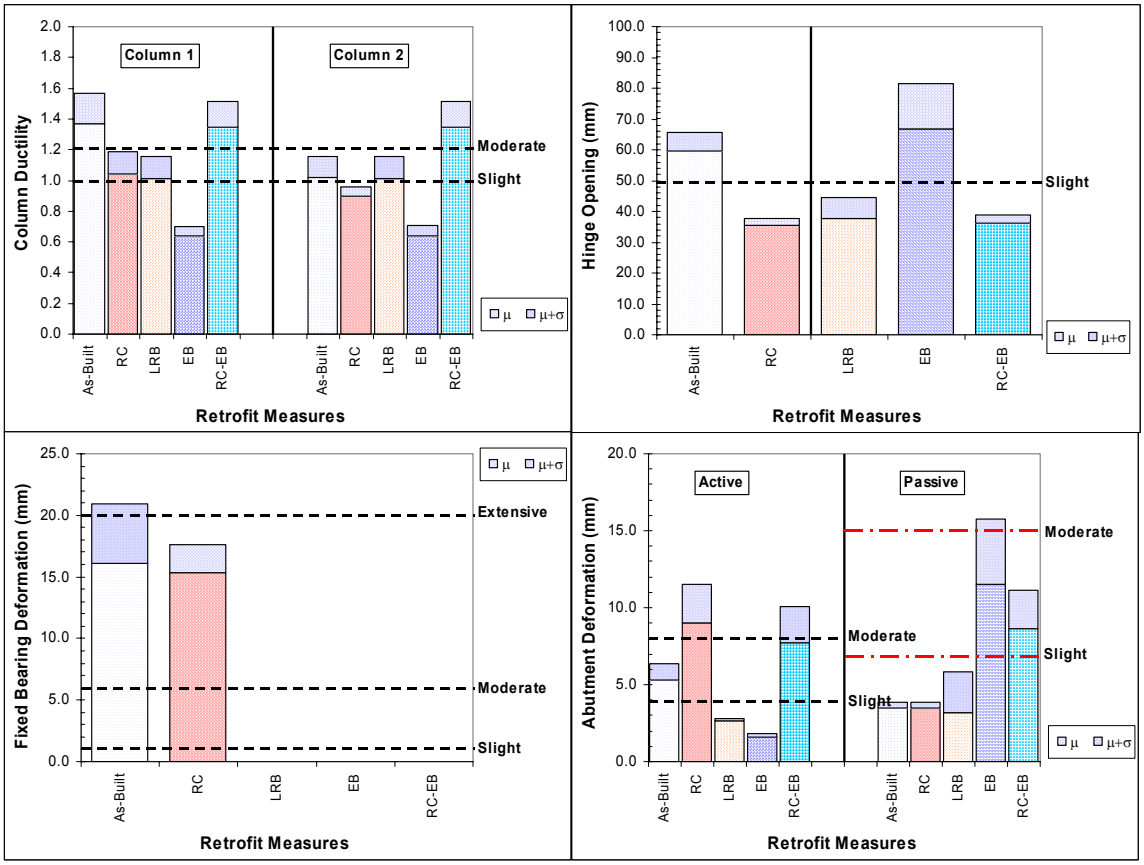

Figure 8.17a Comparison of Responses for As-Built & Retrofitted MSSS Steel Bridges

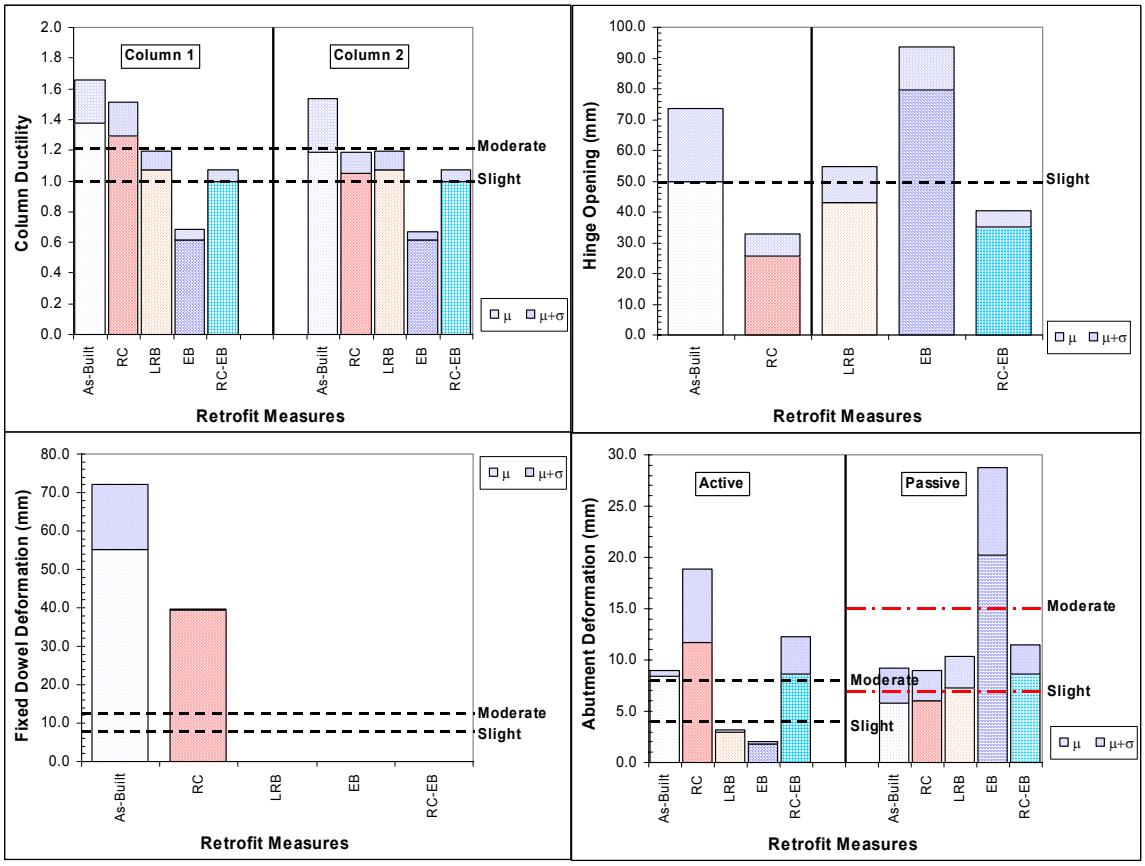

Figure 8.17b Comparison of Responses for As-Built & Retrofitted MSSS Concrete Bridges

8.4.2 Performance of Retrofitted MSC Bridges

Table 8.3 shows the responses of the retrofitted MSC bridges. The second column responses are excluded from the table the response trend of the column is almost same as that of the first column.

- **Steel Girders**

The multi-span continuous steel bridge has a very heavy deck compared with the individual spans of the MSSS bridges. Therefore, when the steel bearings are replaced by elastomeric bearings, the flexibility produces significant pounding forces on the

abutments. The deformations of the abutments in active and passive action exceed the ultimate values. Since the abutments can no longer resist forces, the maximum hinge opening reaches 283 mm (11 in.), which is larger than the usual seat width in the bridge, thus resulting in unseating at the abutments. Although elastomeric bearings generate large responses on the abutments and hinge openings in the bridge, they reduce the demand of the columns compared with that of the as-built bridge.

The lead-rubber bearings reduce the column ductility demand by as much as 67% in the bridge, but they are not effective reducing the hinge openings and the deformation of abutments.

The restrainer cables in the multi-span continuous steel bridge are not very effective in limiting the column demand and the deck movement; they reduce the ductility by 10% and the hinge opening by 12%. In addition, they increase the active deformation of abutments; the maximum value is 6.14 mm (0.24 in.), which is close to the yield point, 7.62 mm (0.3 in.).

Unlike in the MSSS bridges, the combination of restrainer cables and elastomeric bearings in the MSC steel bridge reduces the columns' demand by approximately 20%. However, it is slightly effective to reduce the hinge opening. The cables in the bridge increase the deformation of abutments in active action.

- **PSC Girders**

Elastomeric bearings in the MSC concrete bridge decrease the column ductility by 86%. However, the maximum passive deformation of the abutments (20.0 mm, 0.80 in.) exceeds the yield point (14.6 mm, 0.58 in.). With the elastomeric bearings in the bridge,

about a 100% increase is observed at the hinge opening, but the maximum hinge opening is still less than the typical hinge seat width.

The lead-rubber bearings decrease the column demand by 45% and the active deformation of abutments by 67% comparing with those of the as-built bridge. The maximum hinge opening increases slightly, but it does not exceed the usual seat width.

The restrainer cables are not very effective in the bridge. The maximum responses with the cables are almost the same as those of the as-built bridge. The cables decrease the fixed dowel deformation and the hinge opening slightly. In this bridge, since dowels take the most part of seismic loading to restrict the deck movement, the cables' contribution to modify the response is small.

The combination of RC & EB is very effective to reduce the demand of columns in the bridge. However, it increases the hinge opening and the deformation of abutments.

Table 8.3 Maximum Values of Critical Responses for Retrofitted MSC Bridges

MSC Bridge with Steel Girders						
	Column Ductility	Column Drift	Fixed Bearing	Hinge Opening	Abutment Deformation	
	$\mu c1$	$\Delta c1$ (%)	δfb (mm)	Δop (mm)	$\delta a+$ (mm)	$\delta a-$ (mm)
As-Built	2.32	1.24	8.98	94.4	0.90	13.5
EB	1.32	0.67		283	224	398
LRB	0.76	0.50		84.1	7.30	12.3
RC	2.08	1.15	6.52	82.7	6.14	6.72
RC-EB	1.85	1.16		87.5	6.40	0.41

Table 8.3 Maximum Values of Critical Responses for Retrofitted MSC Bridges

MSC Bridge with PSC Girders						
	Column Ductility	Column Drift	Fixed Dowel	Hinge Opening	Abutment Deformation	
	μc1	Δc1 (%)	δfd (mm)	Δop (mm)	δa+ (mm)	δa- (mm)
As-Built	0.94	0.34	30.4	30.8	8.29	4.06
EB	0.13	0.07		61.1	1.48	20.4
LRB	0.52	0.19		35.5	2.76	3.64
RC	0.94	0.34	27.6	21.5	8.56	3.08
RC-EB	0.17	0.14		40.2	15.5	11.3

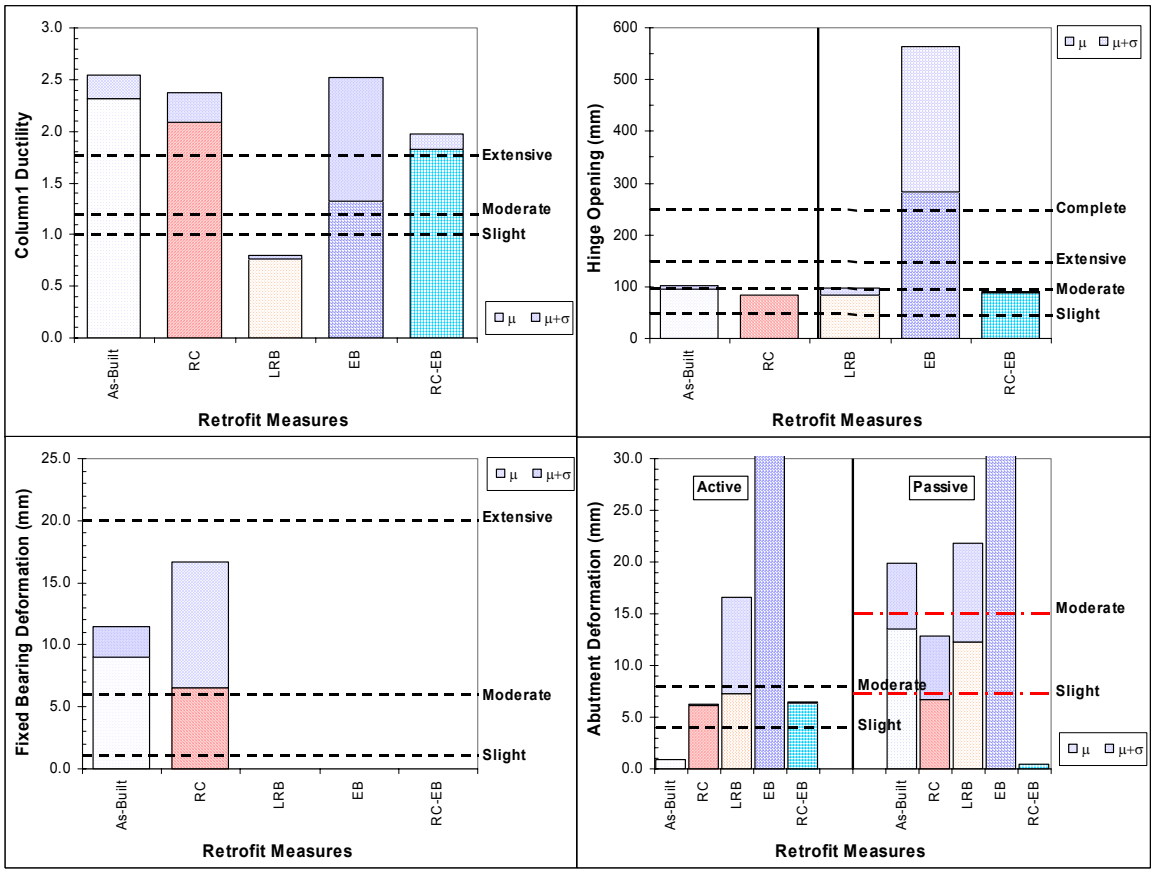

Figure 8.18a Comparison of Responses for As-Built & Retrofitted MSC Steel Bridges

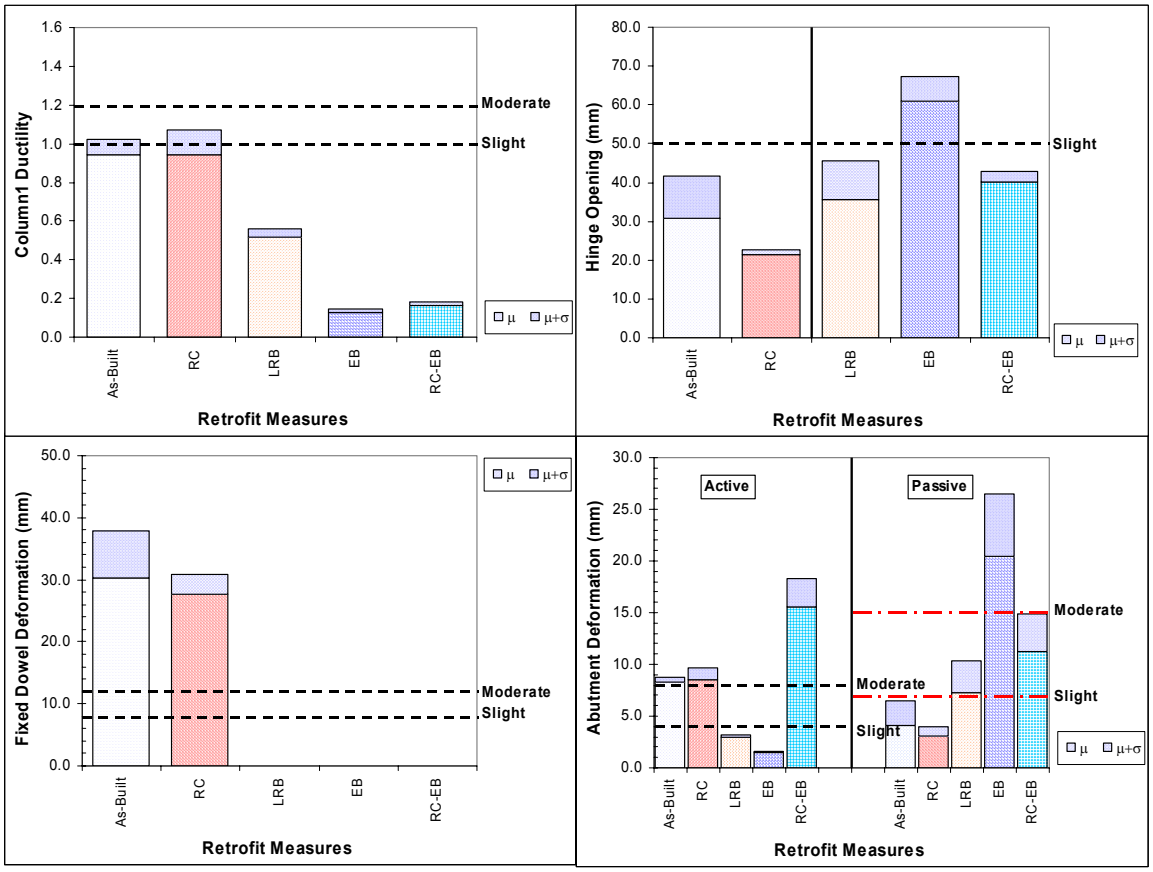

Figure 8.18b Comparison of Responses for As-Built & Retrofitted MSC Concrete Bridges

8.4.3 Performance of Retrofitted SS Bridges

Table 8.4 shows the responses of the retrofitted single span bridges. Elastomeric bearings decrease the abutment deformation in active action but increase the deformation in passive action due to pounding between the deck and abutment compared with that of the as-built bridge. The lead-rubber bearings also reduce the active deformation of the abutments. However, the pounding does not occur with lead-rubber bearings since the lead-rubber bearings govern the displacement of deck effectively. Therefore, the passive

deformation of the abutments is much less than that with elastomeric bearings.

In the single span steel bridge, the maximum deformation of the fixed bearing is 6.6 mm (0.26 in.), which is less than the slack of the restrainer cables, 12.7 mm (0.5 in.). Therefore, the cables are not activated and do not affect anything on the responses.

In the single span concrete bridge, dowels are not strong enough to restrain the deck movement as previously mentioned. Therefore, restrainer cables can help to restrict the deck movement and the pounding. The cables decrease the hinge opening by 43% and the passive deformation of abutments by 35%. However, even though the cables increase the active deformation of abutments by 46%, abutments in the bridges are strong enough to endure the demand from the cables.

The restrainer cables with elastomeric bearings do not reduce neither the hinge opening nor the deformation of abutments. In the SS concrete bridge, since the cables do not restrain the pounding on abutments, the passive deformation on abutments is large.

Table 8.4 Maximum Values of Critical Responses for Retrofitted SS Bridges

SS Bridge with Steel Girders				
	Fixed Bearing	Hinge Opening	Abutment Deformation	
	δfb (mm)	Δop (mm)	δa+ (mm)	δa- (mm)
As-Built	6.60	9.83	1.44	4.12
EB		118	0.47	15.0
LRB		55.8	0.61	1.10
RC	6.60	9.79	1.44	4.11
RC-EB		78.1	9.66	2.26

Table 8.4 Maximum Values of Critical Responses for Retrofitted SS Bridges

SS Bridge with PSC Girders				
	Fixed Dowel	Hinge Opening	Abutment Deformation	
	δfd (mm)	Δop (mm)	δa+ (mm)	δa- (mm)
As-Built	79.5	63.3	1.94	4.34
EB		125.4	0.50	21.9
LRB		77.1	0.7	1.62
RC	40.6	36.4	2.84	2.79
RC-EB		112	10.6	52.8

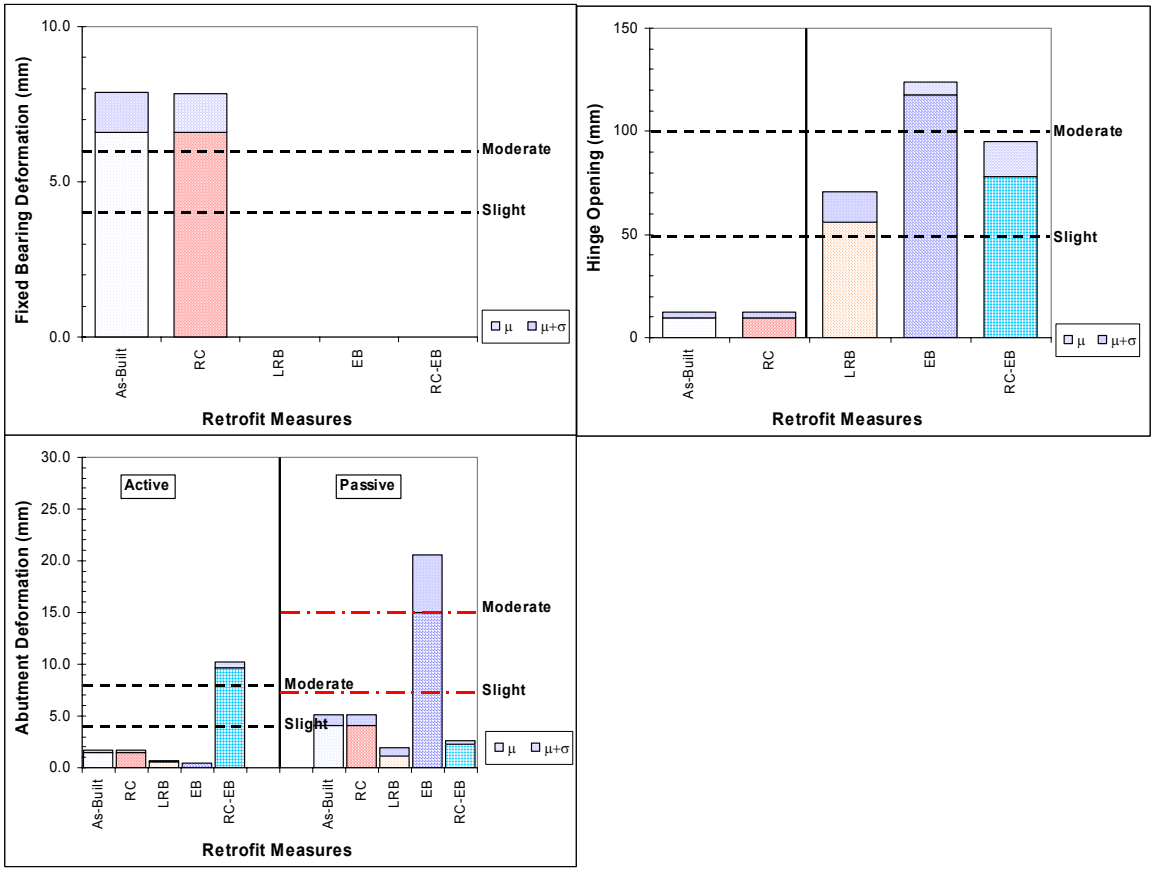

Figure 8.19a Comparison of Responses for As-Built & Retrofitted SS Steel Bridges

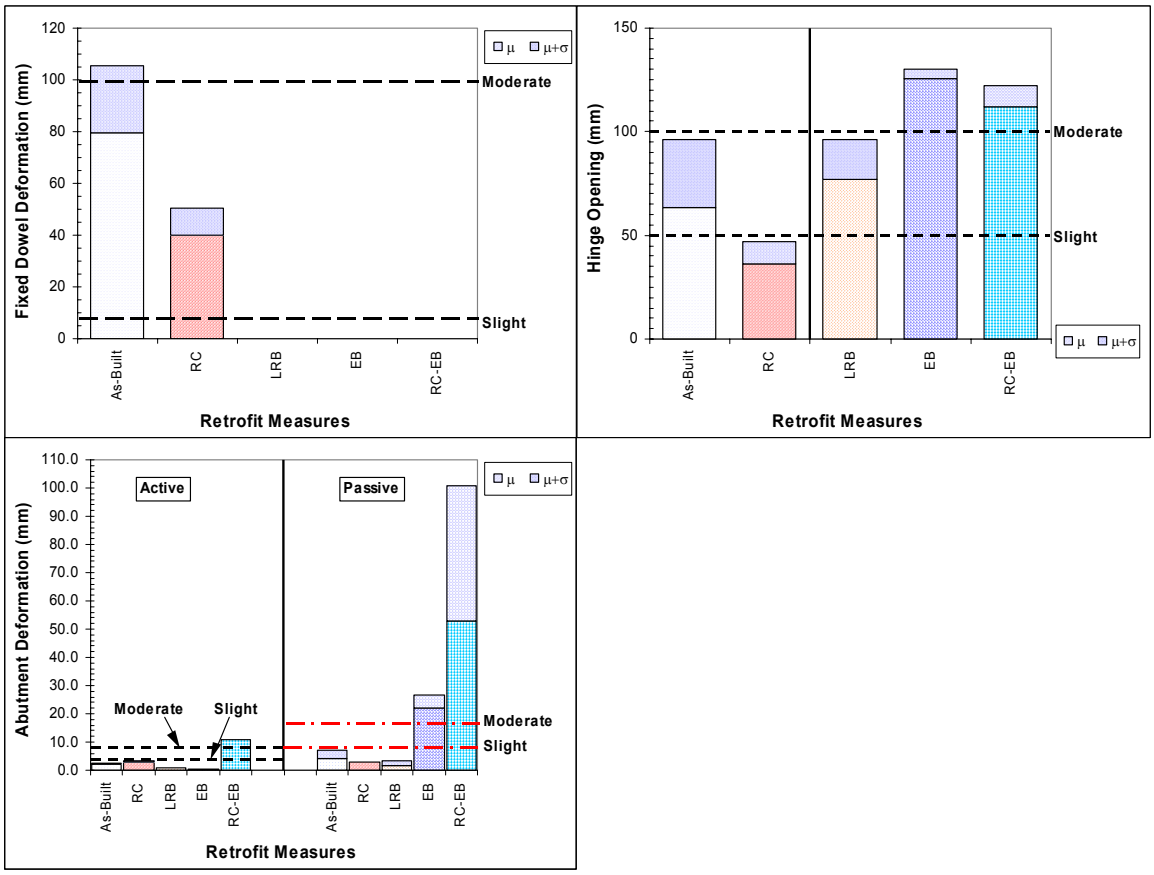

Figure 8.19b Comparison of Responses for As-Built & Retrofitted SS Concrete Bridges

8.5 Summary

In the above section, the four retrofit strategies, elastomeric bearings, lead-rubber bearings, restrainer cables, and elastomeric bearings with restrainer cables are evaluated for modifying the responses of the typical bridges. The three retrofit measures have identical characteristics to modify the seismic response of bridges. The main feature of elastomeric bearings is "isolation". The bearings can cut the inertia forces of superstructures off substructures effectively by increasing the flexibility of the bridges. However, the increased movement of superstructures caused by the flexibility of the

bearings produces problems on abutments and the bearings, such as instability and local damage on the bearings due to large deformation of the bearings. Therefore, it is understood that a great attention is required to use elastomeric bearings as a retrofit device for the typical bridges in Mid-America.

Lead-rubber bearings have large "energy dissipation" capacity comparing to elastomeric bearings. The bearings are assessed as an effective retrofit measure to improve the response of the typical bridges. The bearings can reduce the demand of substructures as well as restrict the deck movement. In addition, the bearings can protect abutments from pounding. In the MSSS steel bridge with the lead-rubber bearings, the ductility of columns is beyond the yield point. The problem can be solved through the optimum design of the bearings.

In general, restrainer cables connect girders to bent caps or abutments in the United States. These cables increase the "interaction" between frames. The developed inertia forces on frames are transferred to abutments through the cables, and thus the demand of columns and the relative displacement decrease. The transferred forces in abutments, however, may damage the abutments in active action. The cables can restrict the hinge opening effectively. Especially, the cables in the single span concrete bridge are effective in restraining the deck movement and the hinge opening. However, the cables have little effect in the single span steel bridge.

The combination of restrainer cables and elastomeric bearings is slightly effective to reduce the demand of columns in the bridges with columns. However, the joint device

increases the demand of abutments in active action. In the SS bridges, the joint device increases the hinge openings.

CHAPTER 9

SUMMARY, CONCLUSIONS, AND IMPACT OF RESEARCH

9.1 Summary and Conclusions

The lack of seismic design practices in the Central and Southeastern United States (Mid-America), coupled with the potential for strong ground motion has led to a significant hazard to the bridge infrastructure in the Mid-America region. This hazard is amplified when one considers the fact that the bridge infrastructure in Mid-America is a key component in the transportation network of the United States. It is estimated that nearly $2.01 trillion in goods originates, goes through, or ends in the Mid-America seismic zone. The economic damage from a major earthquake in the Mid-America region has been estimated at over $26 billion - more than either the 1994 Northridge or 1989 Loma Prieta earthquakes.

The main objective of this research was to evaluate the seismic vulnerability of bridges in the Mid-America region, and determine effective retrofit measures. While previous studies have been performed to evaluate the seismic behavior of specific bridges in Mid-America, there have not been any studies evaluating the seismic vulnerability of a class of bridges which comprise the bridge infrastructure in the Mid-America region. A systematic approach, consisting of deterministic and probabilistic analytical studies is followed.

A profile of the characteristics of typical bridges in Mid-America is developed by

evaluating data from the National Bridge Inventory (NBI) and through surveys sent to Department of Transportation bridge engineers. The results of the NBI and the surveys show that over 95% of bridges can be classified as multi-span simply supported (MSSS), multi-span continuous (MSC), or single span (SS). For each bridge type, the reinforced concrete deck is supported by either steel girders or prestressed concrete girders. The girders are typically supported by multi-column reinforced concrete bents. Using this information, and bridge plans from typical bridges, 6 types of "typical" bridges are developed consisting of MSSS, MSC, and SS – with both steel girder and prestressed concrete girder.

Detailed nonlinear analytical models of each bridge are developed using DRAIN-2DX nonlinear analysis program. The nonlinear models account for nonlinear behavior of the columns, abutments, and bearings. In addition, impact between the decks is represented. Nonlinear translational and rotational springs are used at the footings to represent the flexibility of the foundation.

Nonlinear time history analyses are performed on the 6 bridge types using ground motion developed for a New Madrid seismic event, based on 3 cities: Memphis, TN, Carbondale, IL, and St. Louis, IL. The ground motion records are based on 2 levels of hazard: 10% probability of exceedance in 50 years (G1), and 2% probability of exceedance in 50 years (G2). A suite of 10 ground motions is developed for each hazard level and city. The mean PGA for Suite G1 ranges from 0.08g for Memphis to 0.17g for Carbondale, and the mean PGA for suite G2 ranges from 0.33 for St. Louis to 0.51g for Carbondale.

The results of the time history analysis show that for the 10% in 50 years set of ground motion, the six typical bridge types general perform well. The seismic response of critical components is typically in the elastic range. In a few cases, the fixed bearings experience minor levels of damage, however, these bridges generally perform well.

The deterministic results for the 2% PE in 50 years set of ground motion was considerably different from the results in the 10% PE in 50 years. In general, the analysis using the Memphis and Carbondale set of ground motion records resulted in highly nonlinear behavior, while the response of the bridges during the St. Louis ground motion suite were generally less severe.

The MSSS steel bridge was vulnerable to seismic damage due to failure of the fixed bearings and instability of the rocker bearings. The damage to steel bearings usually resulted from impact between two decks. In addition, the column demands were in the range where slight-to-moderate damage would be expected. Finally, abutment damage would be expected due to significant loading in active action.

The seismic response of the MSSS concrete bridge had similar vulnerabilities as the MSSS steel bridge. The dowel bars were subjected to large forces, resulting in failure of the dowels in most cases. In addition, column yielding and abutment failure would occur in the bridge.

The seismic response of MSC steel bridge was dominated by the inelastic behavior of the columns. Since the MSC steel bridge had a much larger mass that the MSSS Bridges, the demands on the columns were larger than for the MSSS cases. The larger displacement of the MSC steel bridge also resulted in instability problems for the

expansion bearings. However, since pounding was limited in the MSC steel bridge, the response of the fixed bearings was not as critical as in the MSSS bridge.

The response of the MSC concrete bridge was similar to the MSSS concrete bridge. However, both the column response and the fixed dowel response were less severe than that for the MSSS concrete bridge.

Finally, the single span steel and single span concrete bridges were evaluated. The seismic performance of the single span bridge was quite good, with all major components remaining elastic. The single span concrete bridge, however, had slight to moderate damage to the fixed and expansion dowel bars.

Parameter studies were conducted to determine which parameters are most important in determining the seismic response of bridges. The parameters which were evaluated include the deck mass, gap between decks, stiffness/strength of the rocker bearings, and rotational flexibility of the foundation. The results show that the column ductilities increase with increasing deck mass and increasing gap. In addition, the performance of the bearings and the abutments increase significantly with increasing deck mass and gap. The strength and stiffness of the bearings has a moderate effect on the seismic behavior of the bridges.

To improve the seismic resistance of the typical bridges, several retrofit measures are evaluated: (1) replacing steel bearings or elastomeric pads with elastomeric bearings, (2) replacing steel bearings or elastomeric pads with lead rubber bearings, (3) using steel cable restrainers at the intermediate hinges and abutments, and (4) using elastomeric bearings with restrainer cables.

In the MSSS steel & concrete bridges, elastomeric bearings significantly reduce the demands on the columns. However, the increased deck displacements result in large pounding forces and damage at the abutments. The use of restrainer cables with the elastomeric bearings decreases the deck displacements, however, the restrainer cables increase the demands on the columns. The use of restrainer cables alone does not significantly improve the seismic behavior of bridges. The lead-rubber bearings appear to be the most effective retrofit measure for the MSSS bridges. The lead-rubber bearings provided sufficient isolation to reduce the demands on the columns, while having adequate damping to limit the displacement of the decks (thereby limiting pounding at the abutments).

In the MSC steel bridge, the primary vulnerabilities are the large ductility demands on the columns and pounding at the abutments. The most effective retrofit measure for reducing both the demands on the columns and pounding at the abutments is the use of lead-rubber bearings.

The as-built response of the MSC concrete bridge was found to be adequate, except for the response of the dowel bars. The use of lead rubber bearings or restrainer cables improved the seismic performance of the MSC concrete bridge.

For the SS bridges, the as-built bridge experiences slight to moderate damage to the bearings. Replacing the bearings with elastomeric bearings results in large pounding forces at the abutments, and results in worse damage than the as-built bridge. However, using lead-rubber bearings eliminates pounding at the abutments and improves the behavior of the bridge.

Experimental tests of full-scale retrofits typically performed in Mid-America are conducted. The results show that the original TDOT restrainer connections failed in a brittle manner at a load of less than 10% of the yield strength of the cable. Three sets of modifications to existing connections were tested and compared. The first modification consisted of replacing bent plate connections with steel angle connections. The results show that the modified retrofits have much higher strength and stiffness than currently used connections. However, this connection had large displacements before failure. The other modifications evaluated include a (1) stiffened angle, and (2) longitudinally oriented angle. Both connections performed well with much less deformation in the connection element compared with the existing connections. It is recommended that these connections be used in cases where seat widths are very small, and relative displacements need to be limited.

9.2 Impact of Research

A systematic approach is conducted for evaluating the seismic vulnerability of bridges in Mid-America, and determining effective retrofit measures. The contributions for the research in this study are;

(1) The development of a database of characteristics of typical bridges found in Mid-America; (2) The development of detailed analytical models that can be used to simulate the seismic response of bridges to moderate and strong ground motion; (3) The research will lead to an understanding of the types of bridges that are vulnerable to significant damage to bridges, and what factors effect their vulnerability; (4) the research has lead to

recommendations for effective retrofit practices for typical bridges in Mid-America.

The results of the experimental study have led to the replacement of existing deficient restrainer retrofit connections elements with the modified connection developed in this study. Over 150 bridges have had restrainer connections modified in response to the results of this study. In addition, the results of this study will form the basis for future recommended practice for cable restrainer retrofits for simply supported bridges. This is particularly important since several states in the central and southeastern United States are beginning to initiate seismic retrofit programs for simply supported bridges using cable restrainers.

From the analytical study, the most important product of this research study is the development of fragility curves for typical bridges. These curves will be a key tool that can be used for loss estimation, and network vulnerability studies. In particular, the fragility curves developed in this study can form the basis for decision making and prioritization for bridge retrofit in Mid-America.

APPENDIX A

FORMULATION FOR EXPANSION STEEL BEARINGS' CAPACITY

When expansion steel bearing (high type rocker bearing) begins to roll, the configuration is similar to that shown in Figure A.1. In the case, the problem of instability can easily occur. In the figure, there are the vertical load, V, the normal resistance, N, h is the height of expansion bearings, and the frictional force, H_f. The frictional force, H_f, is equal to μV, where μ is the frictional coefficient of steel surface equal to 0.2 (Mander et al., 1996) or 0.15 (Schrage,1981). The rolling moment at the contact point is

$$M_r = V\delta - H_f (h-\eta) \tag{A.1}$$

where:

$$H_f = \mu V$$

$$\delta = (h-r) \sin(\varphi)$$

$$\eta = (h-r) \sin(\varphi) \tan(\varphi/2)$$

If each value is substituted into the equation, the equation is

$$M_r = V(h-r) \sin(\varphi) - \mu V \{h-(h-r) \sin(\varphi) \tan(\varphi/2)\} \tag{A.2}$$

Let M_r=0, and reorganizing. We get

$$\mu h / (h-r) = \sin(\varphi/2) + \mu \sin(\varphi) \tan(\varphi/2) \quad \text{(A.3)}$$

If the solution, φ, does exist in the range, $0< \varphi \leq \psi$, the expansion bearing becomes unstable in the range. In the case, the maximum allowable displacement is:

$$\Delta_{m,all} = a + \delta \quad \text{(A.4)}$$

where:

$$a = r \tan(\varphi)$$

Then, the maximum allowable displacement is

$$\Delta_{m,all} = r \tan(\varphi) + (h-r) \sin(\varphi) \quad \text{(A.5)}$$

If the solution, φ, does not exist in the range, $0< \varphi \leq \psi$, the expansion bearing is stable until the bearing becomes turn over beyond the edge point. In that case, the maximum allowable displacement is:

$$\Delta_{m,all} = r \tan(\psi) + (h-r) \sin(\psi) \quad \text{(A.6)}$$

If the height of the loading point is less than the radius of the rocker shown in Figure A.2, the bearing is not unstable until the contact point goes beyond the edge of the bearing.

When an expansion bearing is stable until the contact point beyond the edge, the maximum allowable displacement of the expansion bearings is independent of the frictional coefficient (μ) but depends on the configuration of the bearings. Therefore, the this case, the maximum allowable displacement is:

$$\Delta_{m,all} = a - \delta \quad (A.7)$$

$$\Delta_{m,all} = r \tan(\psi) - (r-h) \sin(\psi) \quad (A.8)$$

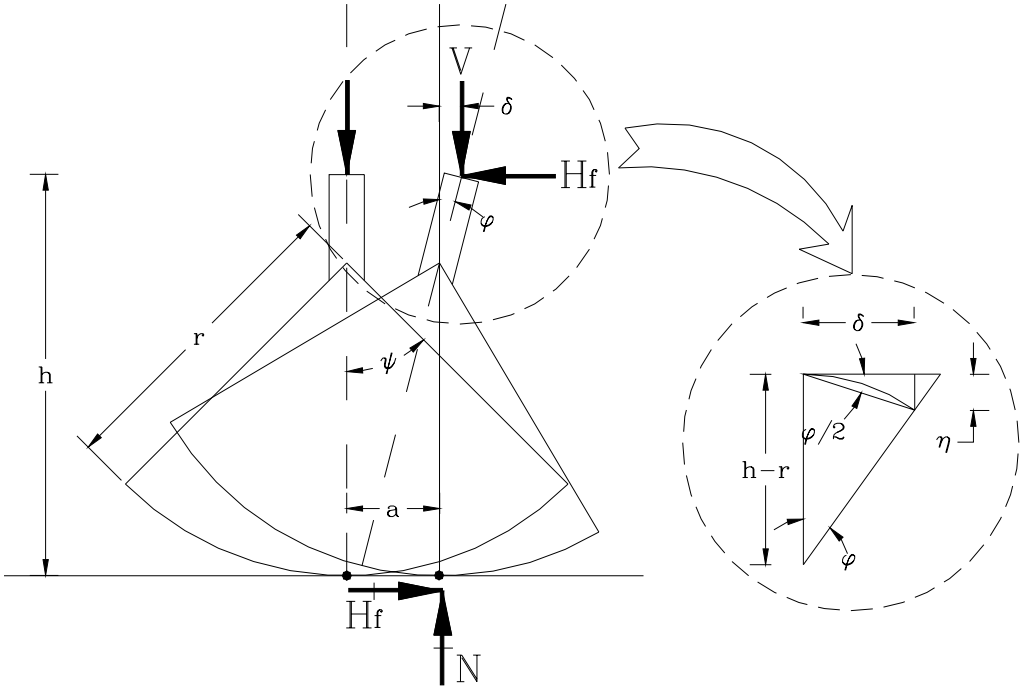

Figure A.1 Stability of Expansion Steel Bearing (h>r)

where:

h = Height of the loading point from the contact surface

r = Radius of the rocker

a = Movement of the contact point from the original

φ = Rolling angle

ψ = Angle of rocker

V = Vertical loading

H_f = Frictional force

N = Normal force

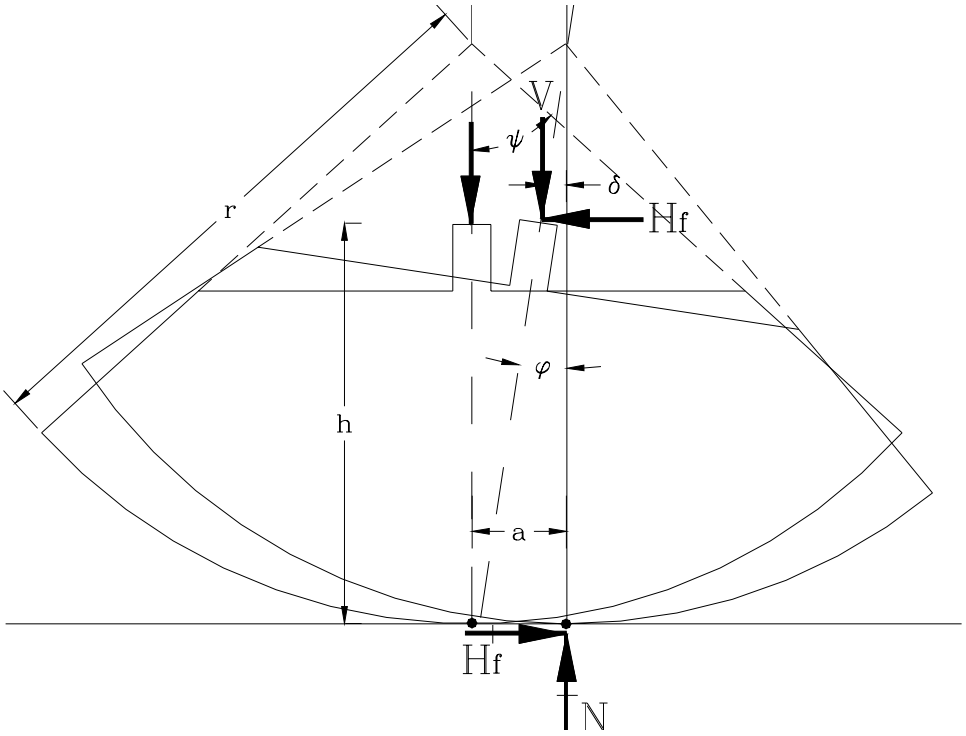

Figure A.2 Stability of Expansion Steel Bearing (h<r)

APPENDIX B

RESULTS OF STATISTICAL ANALYSIS FOR TYPICAL BRIDGES

In this chapter, the results of the statistical analysis have performed in the chapter 5 are shown in Tables B.1 through B.6. Each table shows the mean and the COV (coefficient of variation) of the responses. The figures in the chapter 5.3 to represent the performance of the typical bridges are based on the values in the tables. In the tables, m represents the mean value and σ does the COV for the responses.

Table B.1a Mean and COV of Responses of MSSS Steel Bridge

		Column						Fixed Steel Bearing			Expansion Bearing			Hinge Opening		
		Ductility		*Drift (%)*		*Shear (%)*		*Deformation (mm)*			*Deformation (mm)*			*Displacement (mm)*		
Memphis Ground Motions																
		μc1	μc2	Δc1	Δc2	vc1	vc2	δfx1	δfx2	δfx3	δex1	δex2	δex3	Δop1	Δop2	Δop3
G1	m	0.11	0.10	0.07	0.07	1.62	1.57	0.15	0.05	0.02	5.05	0.37	4.52	4.45	0.32	4.02
	σ(%)	21.8	23.5	21.6	23.2	18.7	19.8	23.4	13.0	9.4	22.0	10.4	23.5	20.6	9.3	20.0
G2	m	**1.19**	0.92	0.76	0.61	16.18	13.89	**12.27**	0.98	0.92	52.73	20.43	39.44	52.73	9.79	38.23
	σ(%)	19.4	11.7	16.3	11.5	13.8	12.2	27.4	63.6	139.7	12.2	33.2	9.6	12.2	15.1	12.6
Carbondale Ground Motions																
		μc1	μc2	Δc1	Δc2	vc1	vc2	δfx1	δfx2	δfx3	δex1	δex2	δex3	Δop1	Δop2	Δop3
G1	m	0.20	0.19	0.13	0.13	3.03	2.92	0.38	0.09	0.03	9.72	0.73	8.32	8.70	0.62	7.60
	σ(%)	9.6	10.0	9.1	9.7	8.1	8.6	21.2	7.2	12.7	9.7	19.8	9.4	9.2	30.3	15.0
G2	m	**1.37**	**1.02**	0.86	0.67	18.31	15.64	**16.13**	1.90	2.84	**59.52**	26.76	43.43	59.52	10.89	42.56
	σ(%)	14.5	13.6	11.9	12.0	13.8	13.3	29.9	69.6	137.4	10.1	16.9	12.0	10.1	16.6	14.6
St. Louis Ground Motions																
		μc1	μc2	Δc1	Δc2	vc1	vc2	δfx1	δfx2	δfx3	δex1	δex2	δex3	Δop1	Δop2	Δop3
G1	m	0.05	0.05	0.03	0.03	0.87	0.82	0.26	0.05	0.02	2.80	0.41	2.03	2.41	0.38	1.72
	σ(%)	9.2	11.7	9.3	11.7	8.6	11.0	33.6	16.8	6.9	11.7	13.9	11.7	10.5	14.0	22.3
G2	m	0.24	0.22	0.16	0.15	3.65	3.51	1.80	0.13	0.05	13.04	1.22	9.81	11.84	1.08	9.02
	σ(%)	30.3	28.9	29.9	28.8	24.7	24.1	47.7	23.4	30.3	22.9	37.9	29.2	20.8	43.8	29.2

Table B.1b Mean and COV of Responses of MSSS Steel Bridge

		Abutment								Pile Foundation			
		Deformation (mm)				*Force (kN)*				*Force(%) Moment(%)*			
Memphis Ground Motions													
		δa1+	δa1-	δa2+	δa2-	Fa1+	Fa1-	Fa2+	Fa2-	Fp1	Mp1	Fp2	Mp2
G1	m	0.94	0.44	0.17	0.06	199.0	296.3	37.0	37.3	1.6	7.6	1.6	7.4
	σ(%)	20.8	23.3	6.1	6.1	20.8	23.3	6.0	6.4	21.5	16.5	19.7	18.6
G2	m	4.01	3.17	0.62	1.14	851.3	2123.9	131.8	763.7	16.7	75.9	14.1	63.1
	σ(%)	17.2	12.2	10.1	104.2	17.2	12.2	10.2	104.1	14.8	15.2	13.4	11.6
Carbondale Ground Motions													
		δa1+	δa1-	δa2+	δa2-	Fa1+	Fa1-	Fa2+	Fa2-	Fp1	Mp1	Fp2	Mp2
G1	m	2.12	1.09	0.22	0.07	450.9	725.9	46.9	47.4	3.1	14.4	3.0	13.8
	σ(%)	20.1	15.1	6.7	4.4	20.1	15.1	6.9	4.4	7.0	8.8	7.5	9.3
G2	m	5.34	3.52	0.68	2.64	1134	2355	143.8	1763.8	19.3	86.8	16.2	72.7
	σ(%)	19.3	10.1	12.0	67.2	19.3	10.1	12.0	67.2	14.6	14.6	15.3	14.9
St. Louis Ground Motions													
		δa1+	δa1-	δa2+	δa2-	Fa1+	Fa1-	Fa2+	Fa2-	Fp1	Mp1	Fp2	Mp2
G1	m	1.50	0.75	0.14	0.05	317.7	504.3	30.6	31.1	1.3	4.4	1.2	4.1
	σ(%)	33.3	30.0	3.6	2.9	33.3	30.0	3.5	2.7	15.0	6.9	14.5	11.5
G2	m	4.41	1.93	0.24	0.08	936.0	1289.9	50.8	51.4	4.8	17.9	4.7	17.3
	σ(%)	14.2	7.5	14.5	14.4	14.2	7.5	14.5	14.5	25.4	21.8	26.2	20.1

Table B.2a Mean and COV of Responses of MSSS Concrete Bridge

		Column						Fixed Dowel			Expansion Dowel			Hinge Opening		
		Ductility		*Drift (%)*		*Shear (%)*		*Deformation (mm)*			*Deformation (mm)*			*Displacement (mm)*		
Memphis Ground Motions																
		μc1	μc2	Δc1	Δc2	vc1	vc2	δfd1	δfd2	δfd3	δed1	δed2	δed3	Δop1	Δop6	
G1	m	0.15	0.14	0.10	0.09	2.43	2.29	3.39	3.40	2.94	4.21	3.71	3.97	3.30	3.58	
	σ(%)	18.8	16.9	18.9	19.8	20.6	18.3	4.7	5.7	8.2	33.5	12.9	19.2	5.7	21.6	
G2	m	**1.00**	0.94	0.66	0.62	15.59	14.96	**37.87**	**13.36**	**4.75**	28.47	17.72	37.20	19.01	31.91	
	σ(%)	18.9	20.0	17.2	18.6	13.7	12.9	37.5	78.1	16.0	4.8	27.5	24.5	111.4	33.1	
Carbondale Ground Motions																
		μc1	μc2	Δc1	Δc2	vc1	vc2	δfd1	δfd2	δfd3	δed1	δed2	δed3	Δop1	Δop6	
G1	m	0.24	0.23	0.16	0.15	4.35	3.73	3.88	3.91	3.41	9.98	5.48	6.98	3.60	6.93	
	σ(%)	9.6	14.1	9.6	14.0	9.3	11.9	3.9	3.9	2.2	28.7	10.8	20.7	3.1	21.9	
G2	m	**1.38**	**1.19**	0.86	0.75	19.68	17.82	**55.17**	**14.10**	**6.19**	32.10	26.76	**47.70**	49.67	44.03	
	σ(%)	20.3	29.3	15.6	21.3	14.8	16.9	30.7	64.4	45.4	18.4	16.7	27.5	47.9	40.1	
St. Louis Ground Motions																
		μc1	μc2	Δc1	Δc2	vc1	vc2	δfd1	δfd2	δfd3	δed1	δed2	δed3	Δop1	Δop6	
G1	m	0.07	0.07	0.05	0.05	1.20	1.20	2.27	2.13	1.84	1.84	2.13	2.27	2.02	2.02	
	σ(%)	11.9	11.9	12.4	12.4	11.1	11.1	8.8	8.9	16.3	16.3	8.9	8.8	9.0	9.0	
G2	m	0.26	0.23	0.17	0.15	4.52	3.97	3.86	3.99	3.48	9.10	5.46	7.59	3.61	6.88	
	σ(%)	20.1	21.3	19.6	20.6	17.5	16.0	3.8	2.4	2.2	25.8	11.4	26.8	4.2	29.3	

Table B.2b Mean and COV of Responses of MSSS Concrete Bridge

		Abutment								Pile Foundation			
		Deformation (mm)				*Force (kN)*				*Force(%) Moment(%)*			
Memphis Ground Motions													
		δa1+	δa1-	δa2+	δa2-	Fa1+	Fa1-	Fa2+	Fa2-	Fp1	Mp1	Fp2	Mp2
G1	m	1.98	0.74	1.33	0.43	421.6	491.9	282.2	290.3	2.6	10.9	2.3	10.5
	σ(%)	37.5	35.0	11.4	9.3	37.5	34.9	11.5	9.2	33.3	23.1	15.5	17.8
G2	m	**7.67**	3.78	7.18	3.35	1564.4	2527.2	1487.9	2242.4	17.4	68.1	14.4	62.2
	σ(%)	11.1	24.9	14.4	52.3	3.4	24.9	11.5	52.4	13.2	14.0	18.6	19.3
Carbondale Ground Motions													
		δa1+	δa1-	δa2+	δa2-	Fa1+	Fa1-	Fa2+	Fa2-	Fp1	Mp1	Fp2	Mp2
G1	m	3.37	1.52	1.49	0.48	716.7	1016.2	317.6	317.6	5.2	20.8	3.6	18.0
	σ(%)	16.9	15.7	0.0	0.0	16.9	15.7	0.0	0.0	13.2	11.5	13.2	11.1
G2	m	**8.41**	5.83	**8.19**	4.64	1645.0	3898.2	1619.0	3101.0	20.1	85.2	17.1	79.6
	σ(%)	6.5	57.6	13.9	70.3	1.9	57.6	3.4	70.3	16.4	23.4	19.2	22.7
St. Louis Ground Motions													
		δa1+	δa1-	δa2+	δa2-	Fa1+	Fa1-	Fa2+	Fa2-	Fp1	Mp1	Fp2	Mp2
G1	m	0.77	0.27	0.77	0.27	163.7	183.0	163.7	183.0	1.4	5.8	1.4	6.0
	σ(%)	9.0	8.8	9.0	8.8	9.0	8.8	9.0	8.8	7.0	13.0	10.5	12.3
G2	m	3.45	1.49	1.49	0.48	732.4	993.9	317.6	317.6	6.1	20.5	4.5	18.7
	σ(%)	22.6	15.8	0.0	0.0	22.6	15.8	0.0	0.0	19.8	20.0	26.4	15.0

Table B.3a Mean and COV of Responses of MSC Steel Bridge

		Column						Fixed Steel Bearing		Expansion Steel Bearing		Hinge Opening	
		Ductility		*Drift (%)*		*Shear (%)*		*Deformation (mm)*		*Deformation (mm)*		*Displacement (mm)*	
Memphis Ground Motions													
		μ_{c1}	μc2	Δc1	Δc2	vc1	vc2	δfx1	δfx2	Δex1	Δex2	Δop1	Δop2
G1	m	0.13	0.13	0.09	0.09	1.80	1.80	0.07	0.07	6.26	6.34	5.70	5.98
	σ(%)	33.7	33.7	32.7	32.7	28.5	28.6	26.8	27.3	33.8	33.7	29.4	28.6
G2	m	**2.02**	**2.02**	**1.12**	**1.12**	18.80	18.74	**6.24**	**6.19**	**84.45**	**84.93**	82.16	83.04
	σ(%)	19.2	19.3	12.7	12.7	11.2	10.9	54.1	53.5	14.8	15.1	14.7	14.8
Carbondale Ground Motions													
		μc1	μc2	Δc1	Δc2	vc1	vc2	δfx1	δfx2	Δex1	Δex2	Δop1	Δop2
G1	m	0.22	0.22	0.15	0.15	2.97	2.97	0.13	0.13	10.52	10.62	9.57	9.83
	σ(%)	14.1	14.2	15.3	15.3	12.8	12.7	11.7	11.6	14.5	14.4	20.1	19.6
G2	m	**2.32**	**2.31**	**1.24**	**1.24**	20.69	20.65	**8.98**	**8.88**	**93.58**	**94.42**	93.58	94.42
	σ(%)	9.6	9.5	7.0	6.6	7.9	7.6	28.1	27.5	7.9	8.1	7.9	8.1
St. Louis Ground Motions													
		μc1	μc2	Δc1	Δc2	vc1	vc2	δfx1	δfx2	Δex1	Δex2	Δop1	Δop2
G1	m	0.06	0.06	0.04	0.04	0.93	0.93	0.05	0.05	2.66	2.72	2.19	2.54
	σ(%)	15.7	15.7	13.1	13.1	13.1	13.1	16.0	16.2	17.0	16.5	28.1	24.0
G2	m	0.30	0.30	0.20	0.20	4.06	4.07	0.21	0.21	14.36	14.47	13.00	13.29
	σ(%)	49.4	49.4	48.5	48.5	38.7	38.7	29.6	29.6	49.9	49.6	47.7	46.5

Table B.3b Mean and COV of Responses of MSC Steel Bridge

		Abutments								Pile Foundation			
		Deformation (mm)				*Force (kN)*				*Force(%) Moment(%)*			
Memphis Ground Motions													
		δ_{a1+}	δa1-	δa2+	δa2-	Fa1+	Fa1-	Fa2+	Fa2-	Fp1	Mp1	Fp2	Mp2
G1	m	0.27	0.12	0.06	0.13	74.2	74.6	81.8	81.4	1.1	6.2	1.1	6.2
	σ(%)	4.6	4.7	4.2	4.2	4.5	4.6	4.2	4.2	22.5	20.5	22.1	20.5
G2	m	0.82	7.83	0.17	7.73	228.3	4606.4	237.2	4709.2	13.6	73.3	13.7	73.2
	σ(%)	10.7	88.4	10.4	87.9	10.7	87.3	10.5	87.9	16.8	15.6	17.4	15.1
Carbondale Ground Motions													
		δa1+	δa1-	δa2+	δa2-	Fa1+	Fa1-	Fa2+	Fa2-	Fp1	Mp1	Fp2	Mp2
G1	m	0.30	0.14	0.07	0.15	81.9	82.4	89.5	89.3	1.9	10.5	1.9	10.5
	σ(%)	4.8	4.7	4.2	4.3	4.7	4.6	4.3	4.4	17.4	19.5	17.4	19.5
G2	m	0.90	**13.48**	0.19	12.78	251.3	7052.9	260.1	7790.7	15.5	83.9	15.9	82.9
	σ(%)	5.9	47.9	5.9	42.1	5.9	32.4	5.9	42.1	11.7	9.4	12.4	9.5
St. Louis Ground Motions													
		δa1+	δa1-	δa2+	δa2-	Fa1+	Fa1-	Fa2+	Fa2-	Fp1	Mp1	Fp2	Mp2
G1	m	0.24	0.11	0.05	0.12	67.0	67.7	74.8	74.5	1.0	3.1	1.0	3.1
	σ(%)	1.9	1.9	1.9	1.7	1.9	1.8	1.6	1.8	22.7	21.7	22.7	21.7
G2	m	0.32	0.15	0.07	0.16	88.8	89.3	96.6	96.3	3.6	14.1	3.6	14.1
	σ(%)	14.1	13.9	13.1	13.0	14.1	14.0	12.9	13.0	28.4	32.5	28.4	32.5

Table B.4a Mean and COV of Responses of MSC Concrete Bridge

		Column						Fixed Dowel			Expansion Dowel			Hinge Opening	
		Ductility		*Drift (%)*		*Shear (%)*		*Deformation (mm)*			*Deformation (mm)*			*Displacement (mm)*	
Memphis Ground Motions															
		μc1	μc2	Δc1	Δc2	vc1	vc2	δfx1	δfx2	δfx3	δex1	δex2	δex3	Δop1	Δop2
G1	m	0.14	0.14	0.05	0.05	6.44	6.47	3.47	1.72	1.74	1.72	1.74	4.12	3.06	3.19
	σ(%)	16.1	16.1	15.5	15.5	15.9	16.1	8.2	16.1	16.2	16.1	16.2	18.8	11.1	15.0
G2	m	0.76	0.76	0.27	0.27	34.16	34.14	**20.76**	**6.74**	**6.75**	6.74	6.75	19.83	13.65	19.23
	σ(%)	8.9	8.7	9.3	9.3	10.7	10.7	20.6	86.0	88.0	86.0	88.0	13.1	44.9	15.0
Carbondale Ground Motions															
		μc1	μc2	Δc1	Δc2	vc1	vc2	δfx1	δfx2	δfx3	δex1	δex2	δex3	Δop1	Δop2
G1	m	0.24	0.24	0.09	0.09	11.71	11.87	**4.64**	3.17	3.17	3.17	3.17	7.45	3.73	5.45
	σ(%)	12.4	12.2	12.2	12.9	13.1	13.1	15.0	4.9	4.7	4.9	4.7	14.9	5.3	11.4
G2	m	0.94	0.96	0.34	0.34	44.14	44.32	**30.37**	**15.86**	**16.15**	15.86	16.15	31.61	26.05	30.75
	σ(%)	8.8	11.0	10.3	11.4	13.0	13.5	24.6	74.9	75.4	74.9	75.4	31.5	35.5	35.0
St. Louis Ground Motions															
		μc1	μc2	Δc1	Δc2	vc1	vc2	δfx1	δfx2	δfx3	δex1	δex2	δex3	Δop1	Δop2
G1	m	0.07	0.07	0.03	0.03	3.47	3.47	2.22	1.14	1.14	1.14	1.14	2.22	1.78	1.78
	σ(%)	13.8	13.8	17.0	17.0	12.2	12.2	10.9	8.8	8.8	8.8	8.8	10.9	11.5	11.5
G2	m	0.20	0.20	0.07	0.07	10.04	10.14	4.07	2.97	3.02	2.97	3.02	6.35	3.56	4.50
	σ(%)	13.3	13.2	6.3	13.8	13.7	14.1	5.2	14.8	15.4	14.8	15.4	13.7	4.0	12.4

Table B.4b Mean and COV of Responses of MSC Concrete Bridge

		Abutment								Pile Foundation			
		Deformation (mm)				*Force (kN)*				*Force(%) Moment(%)*			
Memphis Ground Motions													
		δa1+	δa1-	δa2+	δa2-	Fa1+	Fa1-	Fa2+	Fa2-	Fp1	Mp1	Fp2	Mp2
G1	m	1.50	0.90	1.23	0.45	319.2	605.0	260.8	298.6	6.5	13.3	6.6	13.3
	σ(%)	33.0	40.7	16.0	9.8	33.0	40.7	16.0	9.8	19.6	17.7	19.7	18.1
G2	m	**7.80**	2.85	2.00	0.63	1610.4	1907.4	424.4	420.9	31.1	69.8	31.3	69.5
	σ(%)	5.2	2.3	75.5	73.6	2.0	2.3	75.5	73.6	16.0	15.5	15.7	15.0
Carbondale Ground Motions													
		δa1+	δa1-	δa2+	δa2-	Fa1+	Fa1-	Fa2+	Fa2-	Fp1	Mp1	Fp2	Mp2
G1	m	4.04	2.17	1.49	0.48	858.9	1450.0	317.6	317.6	12.0	21.9	12.3	22.5
	σ(%)	24.2	8.7	0.0	0.0	24.2	8.7	0.0	0.0	18.2	10.8	18.1	11.5
G2	m	**8.29**	4.06	4.36	1.71	1643.8	2713.5	879.5	1145.3	41.2	92.6	41.3	92.9
	σ(%)	5.8	59.7	74.0	111.8	1.3	59.7	71.4	111.8	15.4	17.9	15.7	18.0
St. Louis Ground Motions													
		δa1+	δa1-	δa2+	δa2-	Fa1+	Fa1-	Fa2+	Fa2-	Fp1	Mp1	Fp2	Mp2
G1	m	0.68	0.27	0.68	0.27	144.3	177.4	144.3	177.4	3.8	7.8	3.8	7.8
	σ(%)	11.5	11.5	11.5	11.5	11.4	11.5	11.4	11.5	10.3	9.2	10.6	9.1
G2	m	3.21	1.80	1.49	0.48	681.6	1202.8	317.6	317.6	10.6	19.8	10.7	20.1
	σ(%)	22.1	17.1	0.0	0.0	22.1	17.1	0.0	0.0	17.8	13.6	18.6	13.7

Table B.5 Mean and COV of Responses of SS Steel Bridge

		Fixed Steel Bearing	Expansion Steel Bearing	Hinge Opening	Abutment							
		Deformation (mm)	*Deformation (mm)*	*Displacement (mm)*	*Deformation (mm)*				*Force (kN)*			
Memphis Ground Motions												
		δfx1	δex1	Δop1	δa1+	δa1-	δa2+	δa2-	Fa1+	Fa1-	Fa2+	Fa2-
G1	m	0.33	0.83	0.83	0.28	0.69	0.08	0.11	341.9	261.2	40.0	37.1
	σ(%)	86.8	32.0	32.0	11.0	18.7	2.6	15.4	11.1	18.7	2.8	15.6
G2	m	4.23	6.59	6.57	1.00	2.80	0.09	0.13	1211	1059	47.6	45.9
	σ(%)	22.9	19.3	19.6	21.0	18.9	3.5	3.4	21.0	19.0	3.3	3.4
Carbondale Ground Motions												
		δfx1	δex1	Δop1	δa1+	δa1-	δa2+	δa2-	Fa1+	Fa1-	Fa2+	Fa2-
G1	m	2.78	3.27	1.05	0.52	0.98	0.08	0.13	626.4	370.1	40.6	43.4
	σ(%)	3.3	5.7	17.5	15.3	0.0	0.6	0.5	15.3	0.0	0.4	0.7
G2	m	6.60	9.94	9.83	1.44	4.12	0.10	0.14	1739	1557	51.6	49.1
	σ(%)	19.4	25.2	25.4	17.3	24.3	6.0	3.7	17.2	24.3	6.2	3.7
St. Louis Ground Motions												
		δfx1	δex1	Δop1	δa1+	δa1-	δa2+	δa2-	Fa1+	Fa1-	Fa2+	Fa2-
G1	m	2.36	2.70	0.88	0.39	0.96	0.08	0.12	476.1	362.5	40.4	42.7
	σ(%)	18.5	19.6	8.0	22.9	3.4	0.6	1.8	22.9	3.4	0.3	1.5
G2	m	3.17	3.98	1.85	0.77	1.05	0.08	0.13	934.4	397.8	41.5	44.1
	σ(%)	4.2	5.5	57.9	3.7	20.6	3.3	0.6	3.8	20.6	3.3	0.4

Table B.6 Mean and COV of Responses of SS Concrete Bridge

		Fixed Dowel	Expansion Dowel	Hinge Opening		Abutment							
		Deformation *(mm)*	*Deformation (mm)*	*Displacement (mm)*		*Deformation (mm)*				*Force (kN)*			
Memphis Ground Motions													
		δfd1	δed1	Δop1	Δop2	δa1+	δa1-	δa2+	δa2-	Fa1+	Fa1-	Fa2+	Fa2-
G1	m	**5.72**	5.93	5.72	5.85	0.64	1.79	0.42	0.62	773.7	678.0	215.0	211.2
	σ(%)	12.8	9.1	12.8	7.7	4.0	9.1	7.7	11.8	4.0	9.1	7.7	11.9
G2	m	**71.96**	**70.92**	52.86	46.99	0.87	3.19	1.59	3.21	1050.2	1205.2	807.9	1096.9
	σ(%)	32.3	31.2	54.4	63.8	8.6	55.1	45.2	58.2	8.6	55.1	45.2	58.2
Carbondale Ground Motions													
		δfd1	δed1	Δop1	Δop2	δa1+	δa1-	δa2+	δa2-	Fa1+	Fa1-	Fa2+	Fa2-
G1	m	**13.24**	12.86	13.24	8.36	1.02	2.20	0.57	0.85	1236.0	833.5	289.8	290.5
	σ(%)	33.4	32.0	33.4	14.4	15.2	5.3	2.9	3.2	15.1	5.3	2.9	3.2
G2	m	**79.48**	**78.29**	63.32	58.06	1.01	3.81	1.94	4.34	1219.1	1441.3	984.6	1481.8
	σ(%)	32.7	30.8	52.4	57.0	7.2	58.4	21.9	60.5	7.2	58.4	21.9	60.5
St. Louis Ground Motions													
		δfd1	δed1	Δop1	Δop2	δa1+	δa1-	δa2+	δa2-	Fa1+	Fa1-	Fa2+	Fa2-
G1	m	3.60	3.74	3.59	3.69	0.27	0.63	0.27	0.38	327.4	239.1	135.6	128.3
	σ(%)	10.4	15.4	10.6	17.9	55.1	50.4	17.9	13.7	55.1	50.4	17.8	13.7
G2	m	**11.74**	11.38	11.74	8.50	0.84	2.21	0.58	0.86	1012.2	834.9	292.8	292.0
	σ(%)	36.7	35.7	36.7	18.6	12.7	8.3	0.8	1.6	12.7	8.3	0.8	1.6

APPENDIX C

STRUCTURAL PERIODS OF TYPICAL BRIDGES

As the hazard level, peak ground acceleration (PGA) is being used for a long time. The measure, however, is considered generally as a poor parameter for seismic demand on bridges. Because of the reason, some researchers have tried to use the spectral acceleration (Sa) at the elastic fundamental period of a bridge as the parameter (Shome and Cornell, 1999; Hwang et. al, 2000b). However, the models of bridges in this study are highly nonlinear and the initial stiffness of the fixed and the expansion bearings is very large. Thus, the fundamental periods of the typical bridges with the initial stiffness may not represent the true dynamic characteristic of the bridges.

From this point of view, "structural period", comprehending the plastic deformation of bridge components, is introduced. Actually, structural period depends on the intensity of ground motions and the deformation of bridge components, and furthermore it is even being varied in a seismic analysis. Hence, it is embarrassing to specify the structural period of a bridge system. Up to the present, any method is not suggested for determining structural period for probabilistic seismic demand model. In this study, a simple method is suggested to determine the structural period for a bridge.

In general, abutments are so strong and stiff comparing other components. Thus,

abutments can be considered as rigid elements to specify the structural period of a bridge. In the case, the MSSS bridge can be simplified as a 5 DOFs system in MATLAB (1992) as shown in Figure C.1. In the system, m_1, m_2, and m_3 represent the mass of Deck 1, Deck 2, and Deck 3, respectively. m_4 and m_5 are mass for piers. K_{fx} and K_{ex} are the stiffness of fixed and expansion bearings, respectively. K_c is the stiffness of the unit of columns and foundations.

To determine the effective stiffness of the both types of steel bearings in the system, the average deformation of 100 analyses are calculated, and the effective stiffness is estimated from the analytical models of the bearings. The model of expansion bearings is bilinear, thus the effective stiffness of the bearing can be calculated easily. However, since the model of fixed bearing is complicated, the simple bilinear model is introduced to estimate the effective stiffness as shown in Figure C.2. The initial stiffness of the bilinear model is 135.7 kN/mm (775 kips/in.) and hardening ratio is 5%. The yielding strength is117.4 kN (26.4 kips).

The unit of columns and pile foundations is separated form a bridge model, and push-over analysis is conducted to obtain the effective stiffness of the unit. Then, the stiffness is assumed to be 13.0 kN/mm (74.2 kips/in.) for MSSS bridge as shown in Figure C.3. Then, the mass matrix of the system can be obtained like below:

$$\text{Diag}(M) = [\ m_1 \ \ m_2 \ \ m_3 \ \ m_4 \ \ m_5\ ]$$

and the stiffness matrix of the system is

$$K = \begin{bmatrix} K_{fx}+K_{ex} & 0 & 0 & -K_{ex} & 0 \\ 0 & K_{fx}+K_{ex} & 0 & -K_{fx} & -K_{ex} \\ 0 & 0 & K_{fx}+K_{ex} & 0 & -K_{fx} \\ -K_{ex} & -K_{fx} & 0 & K_{fx}+K_{ex}+K_c & 0 \\ 0 & -K_{ex} & -K_{fx} & 0 & K_{fx}+K_{ex}+K_c \end{bmatrix}$$

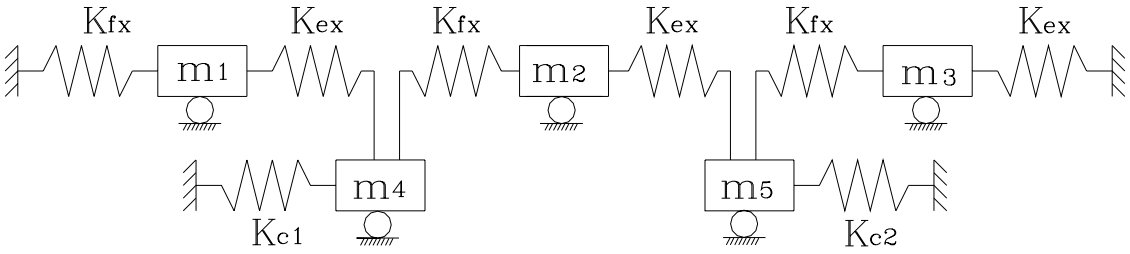

Figure C.1 5 DOFs System of MSSS Steel Bridge in MATLAB

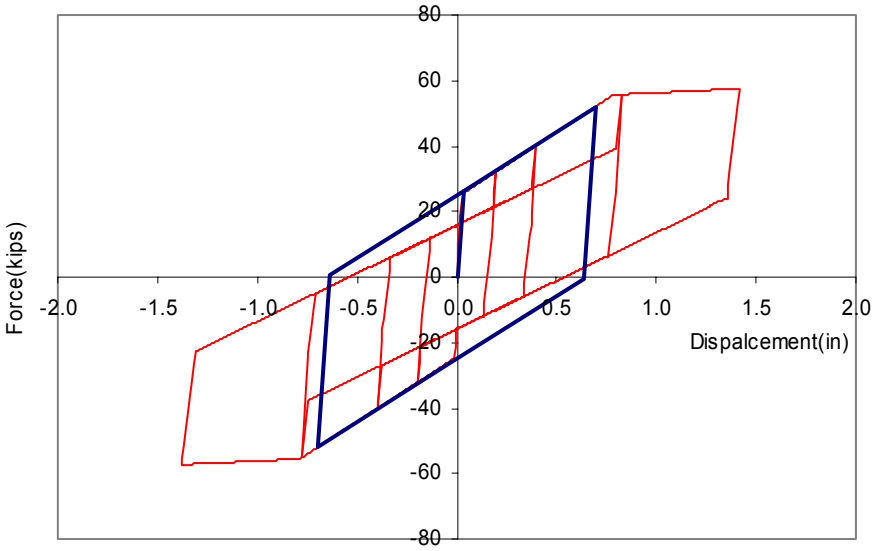

Figure C.2 Simplified Bilinear Model of Fixed Steel Bearing

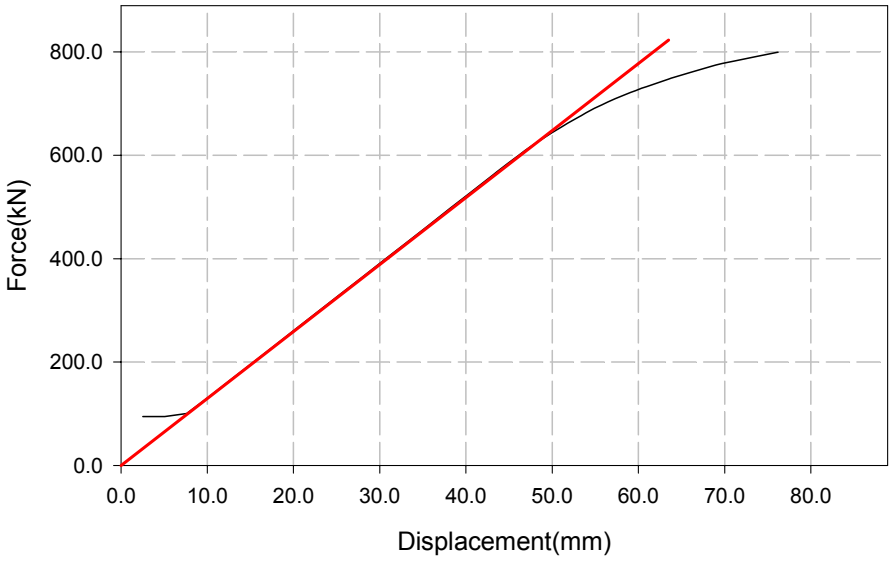

Figure C.3 Linear Model of the Unit of Columns and Pile Foundations of MSSS Bridge

To compare the elastic fundamental periods of the system in MATLAB to the values of the original nonlinear model in DRAIN-2DX, the original initial stiffness is assigned to each component of the system; K_{fx}=1969 (11243), K_{ex}=154 (880), and K_c=13.0 kN/mm (74.2 kips/in.); $m_1=m_3$=134.4 (0.767), m_2=286.8 (1.64), and $m_4=m_5$=49.2 kN sec^2/m (0.281 kips sec^2/in). The natural periods from the two models in the longitudinal direction are compared in the Table C.1. From the result, the system of MSSS steel bridge in MATLAB can represent the original bridge model.

The same procedure can be applied to estimate the structural period of the continuous steel bridge. Figure C.4 shows the linear model of the unit of columns and foundations of the bridge. The 3 DOFs system of the bridge in MATLAB is described in Figure C.5.

Table C.1 Natural Periods of the MSSS Steel Bridge from DRAIN-2DX and MATLAB

Mode	Period (sec)	Effective Modal Mass	Participation Factor
DRAIN-2DX			
1st	0.271	0.81	1.91
2nd	0.147	0.01	0.22
3rd	0.080	0.11	0.70
MATLAB			
1st	0.267	0.81	1.76
2nd	0.141	0.02	0.24
3rd	0.050	0.17	0.81

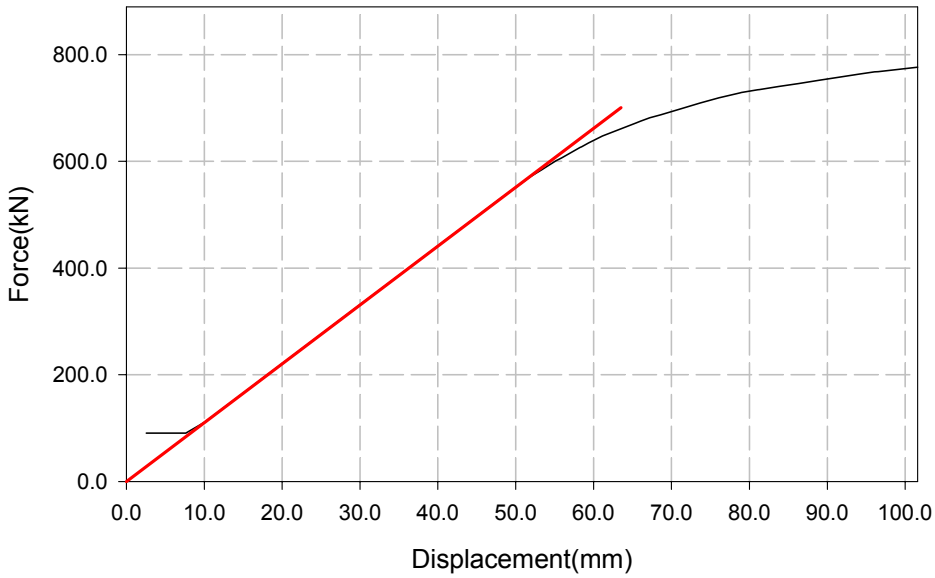

Figure C.4 Linear Model of the Unit of Columns and Pile Foundations of Continuous Steel Bridge

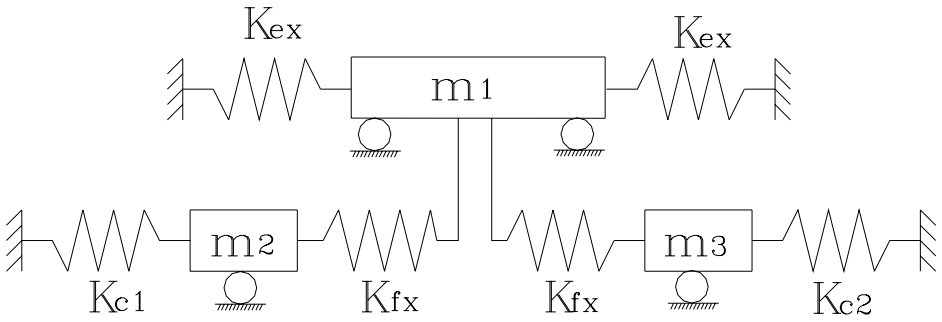

Figure C.5 3 DOFs Model of Continuous Steel Bridge in MATLAB

When the initial stiffness is assigned to each component of the system; K_{fx}=1253.0 (7154.8), K_{ex}=112.0 (639.5), and K_c=11.0 kN/mm (62.8 kips/in.); m_1=1103.7 (6.30) and m_2=m_3=49.6 kN sec^2/m (0.283 kips sec^2/in), the fundamental periods from the two models in the longitudinal direction are compared in the Table C.2.

Table C.2 Natural Periods of MSC Steel Bridge from DRAIN-2DX and MATLAB

Mode	Period (sec)	Effective Modal Mass	Participation Factor
DRAIN-2DX			
1st	0.414	0.95	2.65
MATLAB			
1st	0.439	1.00	2.62

The single span steel bridge is simplified to a system of single DOF as shown in Figure C.6. In the bridge, the fixed bearing type is low type sliding bearing. The behavior of the bearing can be simplified as a linear model shown in Figure C.7. The effective stiffness of low type fixed bearing is assumed to be 59.5 kN/mm (339.7 kips/in.) to estimate structural period. The mass of the deck is 203.7 kN sec^2/m (1.16 kips sec^2/in.).

Figure C.6 Single DOF Model of Single Span Steel Bridge in MATLAB

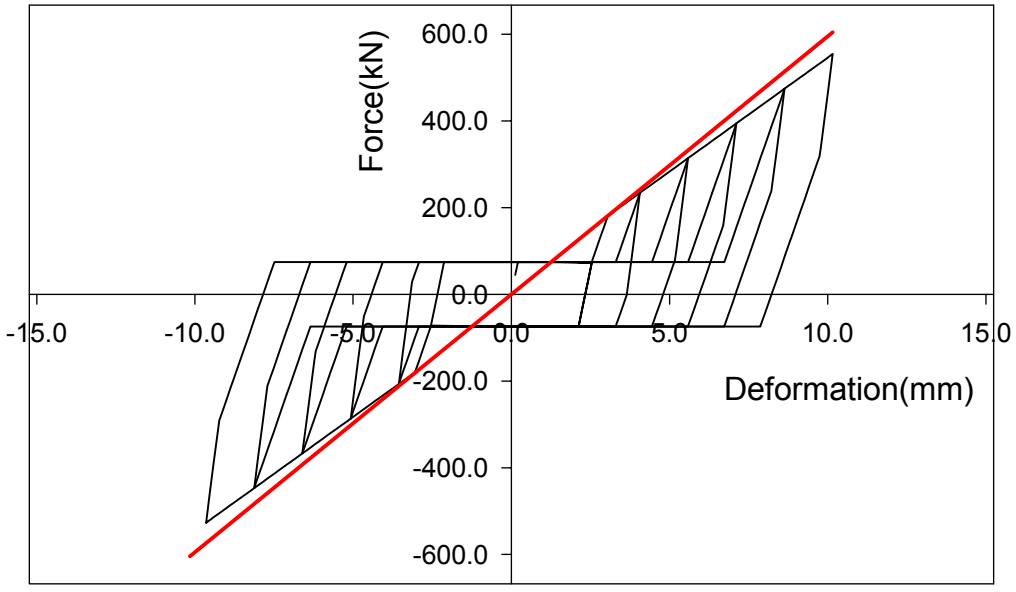

Figure C.7 Linear Model of Low Type Fixed Bearing of Single Span Steel Bridge

When the initial stiffness is assigned to each component of the single DOF system; K_{fx}=1780.0 (10164.0), K_{ex}=5.95 kN/mm (339.8 kips/in.), m_1=203.7 kN sec^2/m (1.163 kips sec^2/in), the first periods from the two models in the longitudinal direction are compared in the Table C.3.

Table C.3 Natural Periods of SS Steel Bridge from DRAIN-2DX and MATLAB

Mode	Period (sec)	Effective Modal Mass	Participation Factor
DRAIN-2DX			
1st	0.098	1.0	1.077
MATLAB			
1st	0.069	1.0	1.078

The same methodology can be utilized to estimate structural periods for concrete bridges , but the mass of decks and columns are different from that of steel bridges.

APPENDIX D

PROBABILISTIC SEISMIC DEMAND MODELS FOR SIMULATED BRIDGES

The probabilistic seismic demand models (PSDM) for bridge components of the simulated bridges in chapter 8 are shown in this chapter. PSDM is obtained using regression analysis and the equation for the regression analysis is like below:

$$\ln(y) = a \ln(x) + b + \varepsilon \quad \text{(D.1)}$$

where y is the response of a bridge, x is the ground motion intensity; PGA or Sa, a and b are the regression coefficient, and ε is a normal random variable with a zero mean and the standard deviation, σ, to represent the variation of the response data.

Figures D.1 and D.2 show the PSDMs in terms of PGA or Sa for the typical bridges on the response data of the bridges.

Tables D.1 to D.6 shows the PSDM for the typical and the retrofitted bridges discussed in chapters 8 and 9. Additionally, the value of R^2 and the logarithmic standard deviation of the ε, σ, are listed. R^2 is the square of the correlation coefficient (R) between tow variables (Chatterjee and Price, 1977). The numerical value of R lies between 1 and –1. This goodness of fit index may be viewed as a measure of the strength

of the linear relationship between two variables. However, a large value of R^2 does not insure that the data has been fitted well (Chatterjee and Price, 1977). Large value of R^2, in general, leads small value of standard deviation, σ. However, in the single span steel bridge, the value of R^2 of deformation of Abutment2 is small (0.49), and the standard deviation is also small (0.05). Since the slops of the fitted lines are almost horizontal, close to zero, although the line fits well the response data, the value of R^2 is small.

The structural periods of the typical and retrofitted bridges are calculated following the method in Appendix C. In the tables for the bridges retrofitted with elastomeric bearings, restrainer cables, or both of them, the * represents the hinge opening used to calculate the probability of exceeding damage states in chapters 8 and 9.

In the tables, the demand notations are like below:

μ : Ductility of Columns

Dr : Drift Ratio of Columns

Fx : Deformation of Fixed Steel Bearings or Fixed Type Dowels

Ex : Deformation of Expansion Steel Beairngs of Expansion Type Dowels

Eb : Deformation of Elastomric Bearings

Lb : Deformation of Lead-Rubber Bearings

Op : Relative Displacement at Expansion Joints

Ab+ : Deformation of Abutments in Active Action

Ab- : Deformation of Abutments in Passive Action

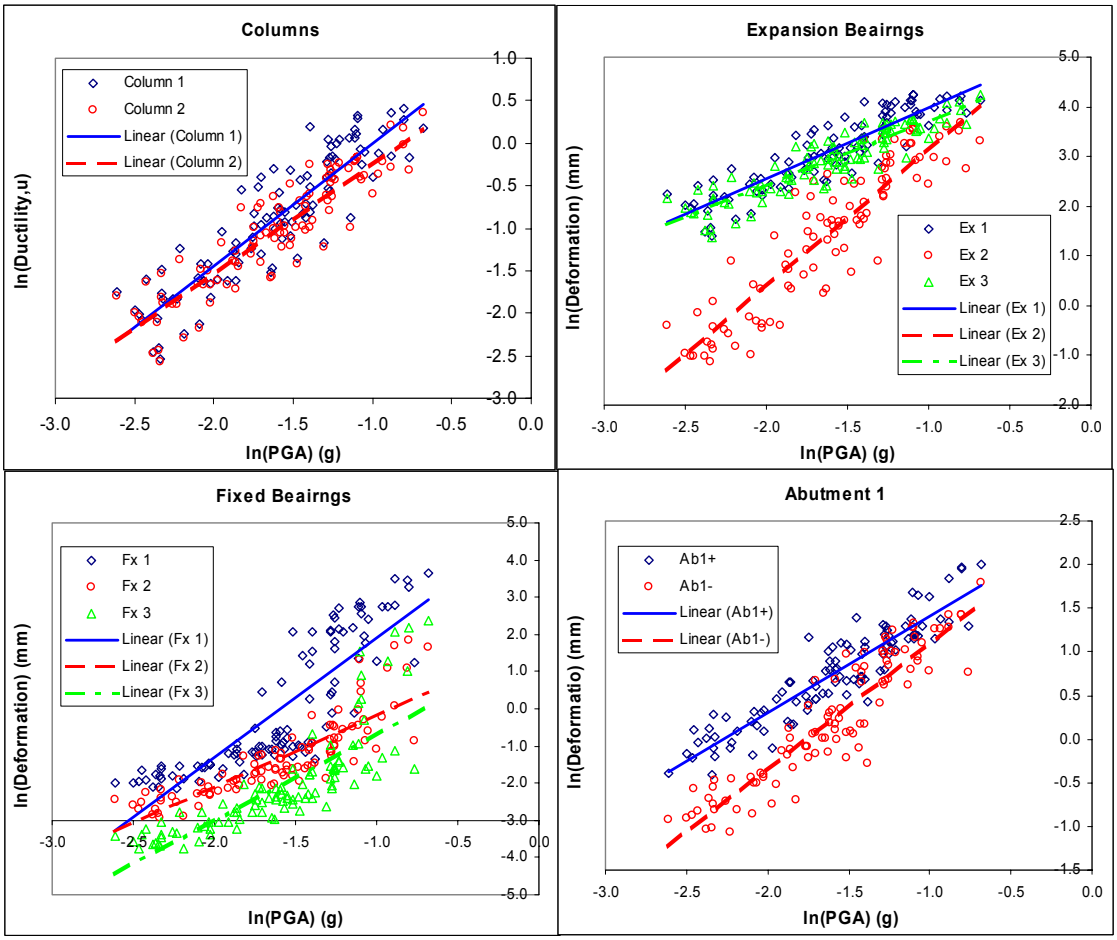

Figure D.1 Regression Analyses of PSDM as A Function of PGA for the MSSS Steel Bridge

Table D.1a PSDM of Components in MSSS Steel Bridge

Response	PGA			Sa (Ts=0.81)		
	PSDM	R^2	σ	PSDM	R^2	σ
Ln(μ1)	1.4405 Ln(x)+1.4419	0.81	0.32	0.9084 Ln(x)+0.1273	0.90	0.24
Ln(μ2)	1.2981 Ln(x)+1.0591	0.83	0.27	0.8117 Ln(x)+0.1332	0.90	0.20
Ln(Dr1)	1.4283 Ln(x)+1.1812	0.80	0.32	0.9017 Ln(x)-0.1212	0.90	0.24
Ln(Dr2)	1.2875 Ln(x)+0.8036	0.82	0.27	0.8040 Ln(x)-0.3802	0.90	0.21
Ln(Fx1)	3.2075 Ln(x)+5.1010	0.72	0.91	1.9479 Ln(x)+2.0917	0.75	0.87
Ln(Fx2)	1.9340 Ln(x)+1.7578	0.73	0.55	1.2168 Ln(x)-0.0103	0.80	0.46
Ln(Fx3)	2.3189Ln(x)+1.6361	0.66	0.77	1.4449 Ln(x)-0.4992	0.71	0.71
Ln(Ex1)	1.4335 Ln(x)+5.4164	0.81	0.32	0.8989 Ln(x)+4.1026	0.89	0.25
Ln(Ex2)	2.7646 Ln(x)+5.9222	0.81	0.61	1.7244 Ln(x)+3.3784	0.88	0.48
Ln(Ex3)	1.2857 Ln(x)+4.9951	0.83	0.27	0.8041 Ln(x)+3.8143	0.91	0.20
Ln(Op1)	1.5223 Ln(x)+5.4937	0.80	0.34	0.9548 Ln(x)+4.0987	0.89	0.27
Ln(Op2)	2.3604 Ln(x)+4.8589	0.74	0.64	1.4906 Ln(x)+2.7070	0.83	0.52
Ln(Op3)	1.2908Ln(x)+4.8921	0.77	0.33	0.8278 Ln(x)+3.7292	0.89	0.23
Ln(Ab1+)	1.1022 Ln(x)+2.5018	0.84	0.22	0.6086 Ln(x)+1.4010	0.72	0.29
Ln(Ab2+)	0.7973 Ln(x)+0.2546	0.77	0.36	0.5087 Ln(x)-0.4665	0.88	0.30
Ln(Ab1-)	1.4470 Ln(x)+2.5581	0.85	0.41	0.8441 Ln(x)+1.1625	0.81	0.41
Ln(Ab2-)	2.0295 Ln(x)+1.5543	0.54	0.87	1.2506 Ln(x)-0.3299	0.57	0.84

Table D.1b PSDM of Components in MSSS Steel Bridge Retrofitted with Elastomeric Bearings

Response	PGA			Sa (Ts=1.16)		
	PSDM	R^2	σ	PSDM	R^2	σ
Ln(μ1)	1.0577 Ln(x)+0.2047	0.76	0.27	0.6412 Ln(x)-0.4473	0.89	0.19
Ln(μ2)	1.0454 Ln(x)+0.1979	0.76	0.27	0.6296 Ln(x)-0.4534	0.87	0.20
Ln(Dr1)	1.0488 Ln(x)-0.0154	0.77	0.27	0.6323 Ln(x)-0.6675	0.88	0.19
Ln(Dr2)	1.0411 Ln(x)-0.0151	0.76	0.27	0.6232 Ln(x)-0.6698	0.87	0.20
Ln(Eb1)	1.2808 Ln(x)+5.2948	0.79	0.31	0.7412 Ln(x)+4.4477	0.83	0.27
Ln(Eb2)	1.1849 Ln(x)+4.8420	0.76	0.31	0.6718 Ln(x)+4.0359	0.78	0.36
Ln(Eb3)	1.0223 Ln(x)+5.0290	0.69	0.32	0.6360 Ln(x)+4.4254	0.85	0.22
Ln(Eb4)	1.0198 Ln(x)+5.0213	0.68	0.32	0.6386 Ln(x)+4.4260	0.85	0.22
Ln(Eb5)	1.1586 Ln(x)+4.8036	0.78	0.29	0.6450 Ln(x)+3.9960	0.77	0.30
Ln(Eb6)	1.2454 Ln(x)+5.2464	0.79	0.30	0.7042 Ln(x)+4.3961	0.80	0.29
Ln(Op4)	1.0676 Ln(x)+5.0202	0.67	0.34	0.6386 Ln(x)+4.4260	0.85	0.22
Ln(Op5)	1.1381 Ln(x)+4.7054	0.75	0.30	0.6450 Ln(x)+3.9960	0.77	0.30
*Ln(Op6)	1.3367 Ln(x)+5.2633	0.76	0.35	0.7042 Ln(x)+4.3961	0.80	0.29
Ln(Ab1+)	0.7416 Ln(x)+0.9975	0.69	0.23	0.4464 Ln(x)+0.5153	0.79	0.19
Ln(Ab2+)	0.7761 Ln(x)+1.0300	0.71	0.23	0.4531 Ln(x)+0.5232	0.77	0.21
Ln(Ab1-)	3.0030 Ln(x)+4.5333	0.60	1.14	1.8712 Ln(x)+2.7649	0.74	0.92
Ln(Ab2-)	2.9970 Ln(x)+4.5957	0.59	1.17	1.8619 Ln(x)+2.8217	0.72	0.96

Table D.1c PSDM of Components in MSSS Steel Bridge Retrofitted with Lead Rubber Bearings

Response	PGA			Sa (Ts=0.77)		
	PSDM	R^2	σ	PSDM	R^2	σ
Ln(μ1)	1.1146 Ln(x)+0.7248	0.82	0.24	0.7056 Ln(x)-0.3352	0.86	0.21
Ln(μ2)	1.1395 Ln(x)+0.7615	0.83	0.24	0.7204 Ln(x)-0.3233	0.87	0.21
Ln(Dr1)	1.1128 Ln(x)+0.4789	0.82	0.24	0.7029 Ln(x)-0.5809	0.85	0.22
Ln(Dr2)	1.1341 Ln(x)+0.5122	0.83	0.23	0.7152 Ln(x)-0.5693	0.86	0.21
Ln(Lb1)	1.3667 Ln(x)+4.8237	0.81	0.30	0.8647 Ln(x)+3.5235	0.85	0.27
Ln(Lb2)	0.8332 Ln(x)+3.2740	0.83	0.17	0.5053 Ln(x)+2.4587	0.80	0.19
Ln(Lb3)	1.1805Ln(x)+4.4236	0.82	0.26	0.7288 Ln(x)+3.2818	0.81	0.26
Ln(Lb4)	1.2153 Ln(x)+4.4866	0.83	0.25	0.7480 Ln(x)+3.3088	0.82	0.26
Ln(Lb5)	0.8516 Ln(x)+3.2980	0.85	0.17	0.5099 Ln(x)+2.4579	0.79	0.20
Ln(Lb6)	1.3922 Ln(x)+4.8536	0.82	0.30	0.8776 Ln(x)+3.5257	0.85	0.27
*Ln(Op1)	1.3110 Ln(x)+4.5862	0.77	0.33	0.7149 Ln(x)+3.1502	0.72	0.33
Ln(Op2)	0.8567 Ln(x)+3.1978	0.81	0.19	0.5448 Ln(x)+2.4107	0.79	0.21
Ln(Op3)	1.1726 Ln(x)+4.2771	0.80	0.27	0.8233 Ln(x)+3.2816	0.82	0.29
Ln(Ab1+)	0.6636 Ln(x)+1.7195	0.70	0.20	0.4215 Ln(x)+1.0898	0.74	0.19
Ln(Ab2+)	0.6793 Ln(x)+1.7248	0.76	0.18	0.4268 Ln(x)+1.0754	0.78	0.17
Ln(Ab1-)	1.0983 Ln(x)+1.4054	0.58	0.43	0.6998 Ln(x)+0.3656	0.61	0.42
Ln(Ab2-)	1.1073 Ln(x)+1.4566	0.57	0.44	0.7196 Ln(x)+0.4226	0.63	0.41

Table D.1d PSDM of Components in MSSS Steel Bridge Retrofitted with Restrainer Cables

Response	PGA			Sa (Ts=0.81)		
	PSDM	R^2	σ	PSDM	R^2	σ
Ln(μ1)	1.2610 Ln(x)+1.0604	0.82	0.28	0.7942 Ln(x)-0.0985	0.90	0.21
Ln(μ2)	1.1946 Ln(x)+0.8392	0.82	0.26	0.7438 Ln(x)-0.2681	0.89	0.21
Ln(Dr1)	1.2728 Ln(x)+0.8486	0.82	0.28	0.8017 Ln(x)-0.3211	0.90	0.21
Ln(Dr2)	1.1866 Ln(x)+0.5886	0.82	0.26	0.7384 Ln(x)-0.5177	0.88	0.21
Ln(Fx1)	3.1759 Ln(x)+5.0677	0.76	0.82	1.9198 Ln(x)+2.0613	0.77	0.80
Ln(Fx2)	2.3950 Ln(x)+2.7659	0.75	0.64	1.4987 Ln(x)+0.5542	0.82	0.55
Ln(Fx3)	1.6520Ln(x)+0.3022	0.75	0.45	1.0209 Ln(x)-1.2373	0.79	0.40
Ln(Ex1)	1.0440 Ln(x)+4.6014	0.78	0.26	0.6544 Ln(x)+3.6385	0.85	0.21
Ln(Ex2)	2.6505 Ln(x)+5.7940	0.79	0.64	1.6298 Ln(x)+3.3150	0.83	0.58
Ln(Ex3)	1.1806 Ln(x)+4.7672	0.81	0.26	0.7375 Ln(x)+3.6756	0.88	0.21
Ln(Op1)	1.1277 Ln(x)+4.6561	0.81	0.25	0.7028 Ln(x)+3.6116	0.87	0.21
Ln(Op2)	2.7675 Ln(x)+5.8689	0.74	0.77	1.7175 Ln(x)+3.2976	0.79	0.69
Ln(Op3)	0.9851Ln(x)+4.2365	0.75	0.26	0.6295 Ln(x)+3.3410	0.85	0.20
Ln(Ab1+)	1.6153 Ln(x)+3.6230	0.83	0.34	0.9668 Ln(x)+2.0834	0.82	0.35
Ln(Ab2+)	2.3645 Ln(x)+3.8231	0.78	0.58	1.4541 Ln(x)+1.6118	0.82	0.53
Ln(Ab1-)	1.4116 Ln(x)+2.4958	0.86	0.26	0.8236 Ln(x)+1.1272	0.82	0.31
Ln(Ab2-)	1.6107 Ln(x)+0.7046	0.52	0.72	1.0216 Ln(x)-0.7679	0.58	0.67

Table D.1e PSDM of Components in MSSS Steel Bridge Retrofitted with Restrainer Cables and Elastomeric Bearings

Response	PGA			Sa (Ts=1.11)		
	PSDM	R^2	σ	PSDM	R^2	σ
Ln(μ1)	1.3635 Ln(x)+1.0127	0.78	0.34	0.8078 Ln(x)+0.0816	0.87	0.26
Ln(μ2)	1.3169 Ln(x)+0.9184	0.76	0.34	0.7860 Ln(x)+0.0281	0.86	0.26
Ln(Dr1)	1.3578 Ln(x)+0.8078	0.78	0.34	0.8032 Ln(x)-0.1214	0.86	0.26
Ln(Dr2)	1.3191 Ln(x)+0.7226	0.76	0.34	0.7845 Ln(x)-0.1734	0.86	0.27
Ln(Eb1)	0.9521 Ln(x)+4.5656	0.80	0.22	0.5392 Ln(x)+3.8767	0.81	0.21
Ln(Eb2)	0.8256 Ln(x)+4.0633	0.79	0.19	0.4356 Ln(x)+3.4483	0.74	0.22
Ln(Eb3)	0.8204Ln(x)+4.4743	0.72	0.24	0.4947 Ln(x)+3.9274	0.83	0.19
Ln(Eb4)	0.8295 Ln(x)+4.5162	0.73	0.23	0.4946 Ln(x)+3.9547	0.82	0.19
Ln(Eb5)	0.8288 Ln(x)+4.1055	0.80	0.19	0.4405 Ln(x)+3.4608	0.72	0.23
Ln(Eb6)	0.9686 Ln(x)+4.5933	0.80	0.22	0.5463 Ln(x)+3.8890	0.81	0.22
Ln(Op4)	0.5930 Ln(x)+3.8427	0.71	0.17	0.3493 Ln(x)+3.4346	0.79	0.15
*Ln(Op5)	0.8582 Ln(x)+4.1378	0.80	0.20	0.4598 Ln(x)+3.4761	0.73	0.23
Ln(Op6)	0.7861Ln(x)+4.0450	0.75	0.21	0.4434 Ln(x)+3.4736	0.76	0.21
Ln(Ab1+)	1.7724 Ln(x)+3.3714	0.80	0.41	0.9835 Ln(x)+2.0575	0.78	0.43
Ln(Ab2+)	1.8045 Ln(x)+3.4712	0.80	0.42	1.0005 Ln(x)+2.1323	0.78	0.44
Ln(Ab1-)	1.5942 Ln(x)+1.4645	0.49	0.75	0.8922 Ln(x)+0.2945	0.49	0.75
Ln(Ab2-)	1.7927 Ln(x)+1.9282	0.51	0.82	1.0565 Ln(x)+0.6954	0.56	0.77

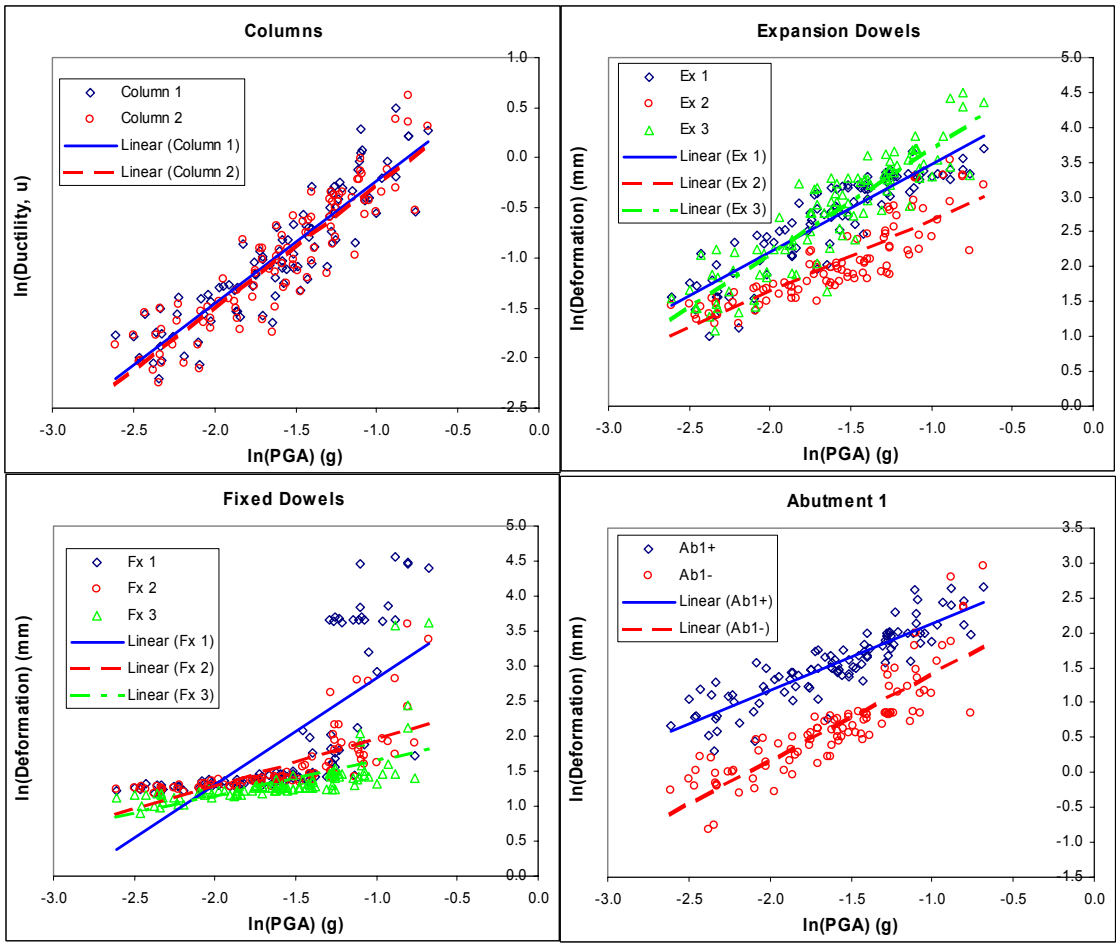

Figure D.2 Regression Analyses of PSDM as A Function of PGA for the MSSS Concrete Bridge

Table D.2a PSDM of Components in MSSS Concrete Bridge

Response	PGA			Sa (Ts=0.81)		
	PSDM	R^2	σ	PSDM	R^2	σ
Ln(μ1)	1.2244 Ln(x)+0.9881	0.82	0.26	0.7335 Ln(x)-0.1717	0.83	0.26
Ln(μ2)	1.2366 Ln(x)+0.9693	0.82	0.27	0.7516 Ln(x)-0.1902	0.85	0.25
Ln(Dr1)	1.2145 Ln(x)+0.7403	0.82	0.26	0.7270 Ln(x)-0.4109	0.82	0.26
Ln(Dr2)	1.2295 Ln(x)+0.7230	0.82	0.26	0.7450 Ln(x)-0.4324	0.84	0.25
Ln(Fx1)	1.5178 Ln(x)+4.3430	0.50	0.71	0.9183 Ln(x)+2.9153	0.51	0.70
Ln(Fx2)	0.6690 Ln(x)+2.6341	0.48	0.32	0.3964 Ln(x)+1.9956	0.47	0.32
Ln(Fx3)	0.5108Ln(x)+2.1673	0.37	0.31	0.3172 Ln(x)+1.6956	0.40	0.30
Ln(Ex1)	1.2598 Ln(x)+4.7293	0.81	0.29	0.7241 Ln(x)+3.5024	0.74	0.33
Ln(Ex2)	1.0436 Ln(x)+3.7291	0.74	0.29	0.6129 Ln(x)+2.7271	0.71	0.30
Ln(Ex3)	1.5265 Ln(x)+5.2262	0.81	0.34	0.9350 Ln(x)+3.8027	0.85	0.30
Ln(Op1)	1.4685 Ln(x)+4.8981	0.76	0.38	0.8584 Ln(x)+3.4838	0.73	0.41
Ln(Op2)	0.9049 Ln(x)+3.3437	0.66	0.30	0.5342 Ln(x)+2.4778	0.65	0.31
Ln(Op3)	1.5913Ln(x)+5.1640	0.79	0.38	0.9639 Ln(x)+3.6683	0.81	0.36
Ln(Ab1+)	0.9538 Ln(x)+3.0788	0.78	0.24	0.5642 Ln(x)+2.1674	0.76	0.24
Ln(Ab2+)	1.0263 Ln(x)+2.4711	0.43	0.54	0.6778 Ln(x)+1.5680	0.53	0.50
Ln(Ab1-)	1.2530 Ln(x)+2.6717	0.74	0.34	0.7509 Ln(x)+1.4852	0.74	0.34
Ln(Ab2-)	1.5314 Ln(x)+2.3287	0.54	0.66	0.9597 Ln(x)+0.9245	0.59	0.62

Table D.2b PSDM of Components in MSSS Concrete Bridge Retrofitted with Elastomeric Bearings

Response	PGA			Sa (Ts=1.46)		
	PSDM	R^2	σ	PSDM	R^2	σ
Ln(μ1)	1.0212 Ln(x)+0.0963	0.74	0.28	0.6468 Ln(x)-0.1891	0.89	0.18
Ln(μ2)	1.0604 Ln(x)+0.1571	0.75	0.28	0.6643 Ln(x)-0.1545	0.89	0.19
Ln(Dr1)	1.0290 Ln(x)-0.0883	0.28	0.28	0.6497 Ln(x)-0.3801	0.89	0.18
Ln(Dr2)	1.0716 Ln(x)-0.0205	0.28	0.28	0.6720 Ln(x)-0.3340	0.89	0.19
Ln(Eb1)	1.1992 Ln(x)+5.3451	0.34	0.34	0.7269 Ln(x)+4.9417	0.81	0.28
Ln(Eb2)	1.1813 Ln(x)+5.0996	0.32	0.32	0.6928 Ln(x)+4.6535	0.77	0.31
Ln(Eb3)	1.0937Ln(x)+5.2792	0.33	0.33	0.6928 Ln(x)+4.9736	0.87	0.22
Ln(Eb4)	1.0937 Ln(x)+5.2792	0.33	0.33	0.6928 Ln(x)+4.9736	0.85	0.23
Ln(Eb5)	1.2234 Ln(x)+5.1805	0.32	0.32	0.6913 Ln(x)+4.5923	0.74	0.33
Ln(Eb6)	1.3521 Ln(x)+5.4690	0.33	0.33	0.7861 Ln(x)+4.9441	0.79	0.26
Ln(Op1)	1.2666 Ln(x)+5.3373	0.68	0.40	0.7179 Ln(x)+4.9468	0.84	0.31
Ln(Op2)	1.2039 Ln(x)+5.0581	0.75	0.33	0.6913 Ln(x)+4.5923	0.76	0.38
*Ln(Op3)	1.1753 Ln(x)+5.3551	0.72	0.34	0.7861 Ln(x)+4.9441	0.74	0.31
Ln(Ab1+)	0.7337 Ln(x)+1.0855	0.26	0.26	0.4562 Ln(x)+0.8628	0.75	0.21
Ln(Ab2+)	0.7824 Ln(x)+1.1644	0.25	0.25	0.4598 Ln(x)+0.8709	0.71	0.24
Ln(Ab1-)	3.3553 Ln(x)+5.5046	0.25	1.25	2.0614 Ln(x)+4.4335	0.69	0.11
Ln(Ab2-)	3.3507 Ln(x)+5.5173	0.26	1.26	2.0589 Ln(x)+4.4483	0.69	0.12

Table D.2c PSDM of Components in MSSS Concrete Bridge Retrofitted with Lead Rubber Bearings

Response	PGA			Sa (Ts=0.87)		
	PSDM	R^2	σ	PSDM	R^2	σ
Ln(μ1)	1.0660 Ln(x)+0.7645	0.77	0.27	0.6700 Ln(x)-0.1472	0.87	0.20
Ln(μ2)	1.1009 Ln(x)+0.8291	0.78	0.27	0.6847 Ln(x)-0.1212	0.86	0.21
Ln(Dr1)	1.0553 Ln(x)+0.5142	0.77	0.27	0.6649 Ln(x)-0.3864	0.87	0.20
Ln(Dr2)	1.0945 Ln(x)+0.5817	0.78	0.27	0.6814 Ln(x)-0.3621	0.86	0.21
Ln(Lb1)	1.3567 Ln(x)+5.0014	0.78	0.33	0.8266 Ln(x)+3.8099	0.83	0.29
Ln(Lb2)	0.7090 Ln(x)+3.2458	0.77	0.18	0.4079 Ln(x)+2.5945	0.73	0.20
Ln(Lb3)	1.1111Ln(x)+4.6478	0.80	0.26	0.6583 Ln(x)+3.6497	0.80	0.26
Ln(Lb4)	1.0940 Ln(x)+4.6132	0.78	0.27	0.6466 Ln(x)+3.6287	0.78	0.27
Ln(Lb5)	0.7005 Ln(x)+3.2332	0.79	0.17	0.3941 Ln(x)+2.5791	0.71	0.20
Ln(Lb6)	1.3641 Ln(x)+5.0143	0.80	0.32	0.8259 Ln(x)+3.8101	0.84	0.28
*Ln(Op1)	1.2783 Ln(x)+4.6955	0.73	0.36	0.8157 Ln(x)+3.6168	0.85	0.27
Ln(Op2)	0.7102 Ln(x)+3.1606	0.76	0.19	0.3913 Ln(x)+2.4876	0.66	0.22
Ln(Op3)	1.1091 Ln(x)+4.5462	0.73	0.31	0..6759Ln(x)+3.5723	0.78	0.28
Ln(Ab1+)	0.5246 Ln(x)+1.5859	0.66	0.17	0.3340 Ln(x)+1.1424	0.77	0.14
Ln(Ab2+)	0.5182 Ln(x)+1.5743	0.71	0.16	0.3133 Ln(x)+1.1163	0.74	0.15
Ln(Ab1-)	1.4273 Ln(x)+2.2396	0.52	0.64	0.9000 Ln(x)+1.0223	0.59	0.59
Ln(Ab2-)	1.6773 Ln(x)+2.7583	0.56	0.68	1.0401 Ln(x)+1.3069	0.62	0.64

Table D.2d PSDM of Components in MSSS Concrete Bridge Retrofitted with Restrainer Cables

Response	PGA			Sa (Ts=0.80)		
	PSDM	R^2	σ	PSDM	R^2	σ
Ln(μ1)	1.2059 Ln(x)+0.9498	0.82	0.26	0.7242 Ln(x)-0.1906	0.83	0.26
Ln(μ2)	1.1725 Ln(x)+0.8409	0.83	0.25	0.7111 Ln(x)-0.2601	0.85	0.23
Ln(Dr1)	1.1997 Ln(x)+0.7092	0.82	0.25	0.7195 Ln(x)-0.4264	0.83	0.26
Ln(Dr2)	1.1774 Ln(x)+0.6175	0.83	0.25	0.7127 Ln(x)-0.4897	0.85	0.23
Ln(Fx1)	1.4162 Ln(x)+4.1725	0.50	0.65	0.8569 Ln(x)+2.8403	0.51	0.65
Ln(Fx2)	0.6837 Ln(x)+2.6605	0.52	0.30	0.3921 Ln(x)+1.9943	0.48	0.32
Ln(Fx3)	0.4977Ln(x)+2.1484	0.44	0.26	0.3071 Ln(x)+1.6868	0.47	0.25
Ln(Ex1)	1.2055 Ln(x)+4.6183	0.79	0.29	0.6921 Ln(x)+3.4434	0.73	0.33
Ln(Ex2)	1.0953 Ln(x)+3.8496	0.77	0.28	0.6496 Ln(x)+2.8050	0.75	0.29
Ln(Ex3)	1.3997 Ln(x)+4.9714	0.80	0.32	0.8569 Ln(x)+3.6658	0.84	0.29
Ln(Op1)	1.4155 Ln(x)+4.7932	0.76	0.37	0.8252 Ln(x)+3.4274	0.72	0.40
Ln(Op2)	1.0147 Ln(x)+3.5638	0.70	0.31	0.6051 Ln(x)+2.5995	0.70	0.31
Ln(Op3)	1.2794Ln(x)+4.5266	0.77	0.33	0.7714 Ln(x)+3.3198	0.78	0.32
Ln(Ab1+)	0.9904 Ln(x)+3.1554	0.79	0.24	0.5888 Ln(x)+2.2124	0.78	0.25
Ln(Ab2+)	1.2770 Ln(x)+3.0419	0.62	0.46	0.8004 Ln(x)+1.8710	0.68	0.42
Ln(Ab1-)	1.2218 Ln(x)+2.6143	0.76	0.32	0.7275 Ln(x)+1.4521	0.75	0.33
Ln(Ab2-)	1.5281 Ln(x)+2.3229	0.55	0.64	0.9490 Ln(x)+0.9123	0.59	0.62

Table D.2e PSDM of Components in MSSS Concrete Bridge Retrofitted with Restrainer Cables and Elastomeric Bearings

Response	PGA			Sa (Ts= 1.40		
	PSDM	R^2	σ	PSDM	R^2	σ
Ln(μ1)	1.4150 Ln(x)+1.1145	0.76	0.37	0.8902 Ln(x)+0.6388	0.88	0.27
Ln(μ2)	1.3437Ln(x)+0.9889	0.71	0.46	0.8712 Ln(x)+0.5892	0.87	0.27
Ln(Dr1)	1.4276 Ln(x)+0.9474	0.76	0.37	0.8958 Ln(x)+0.4627	0.87	0.27
Ln(Dr2)	1.3535 Ln(x)+0.8196	0.72	0.39	0.8727 Ln(x)+0.4072	0.87	0.21
Ln(Eb1)	0.8480 Ln(x)+4.5167	0.77	0.22	0.5059 Ln(x)+4.1759	0.79	0.21
Ln(Eb2)	0.7270 Ln(x)+4.0974	0.78	0.18	0.4165 Ln(x)+3.7706	0.75	0.19
Ln(Eb3)	0.8039 Ln(x)+4.5938	0.68	0.26	0.5282 Ln(x)+4.3687	0.85	0.18
Ln(Eb4)	0.8565 Ln(x)+4.6765	0.72	0.25	0.5379 Ln(x)+4.3867	0.82	0.20
Ln(Eb5)	0.6880 Ln(x)+4.0295	0.74	0.19	0.3970 Ln(x)+3.7260	0.71	0.20
Ln(Eb6)	0.8425 Ln(x)+4.5277	0.75	0.23	0.5149 Ln(x)+4.2139	0.81	0.20
*Ln(Op1)	0.7471 Ln(x)+4.1220	0.77	0.19	0.4315 Ln(x)+3.7931	0.74	0.20
Ln(Op2)	0.7240 Ln(x)+4.0701	0.78	0.18	0.4157 Ln(x)+3.7465	0.74	0.19
Ln(Op3)	0.6439Ln(x)+4.0292	0.72	0.19	0.3973 Ln(x)+3.7970	0.79	0.16
Ln(Ab1+)	1.8216 Ln(x)+3.7801	0.78	0.45	1.0734 Ln(x)+3.0214	0.78	0.45
Ln(Ab2+)	1.8556 Ln(x)+3.8099	0.78	0.46	1.0719 Ln(x)+2.9936	0.75	0.49
Ln(Ab1-)	2.2860 Ln(x)+3.0520	0.54	0.98	1.3528 Ln(x)+2.1114	0.55	0.97
Ln(Ab2-)	2.3631 Ln(x)+3.2682	0.54	1.02	1.4559 Ln(x)+2.4116	0.59	0.95

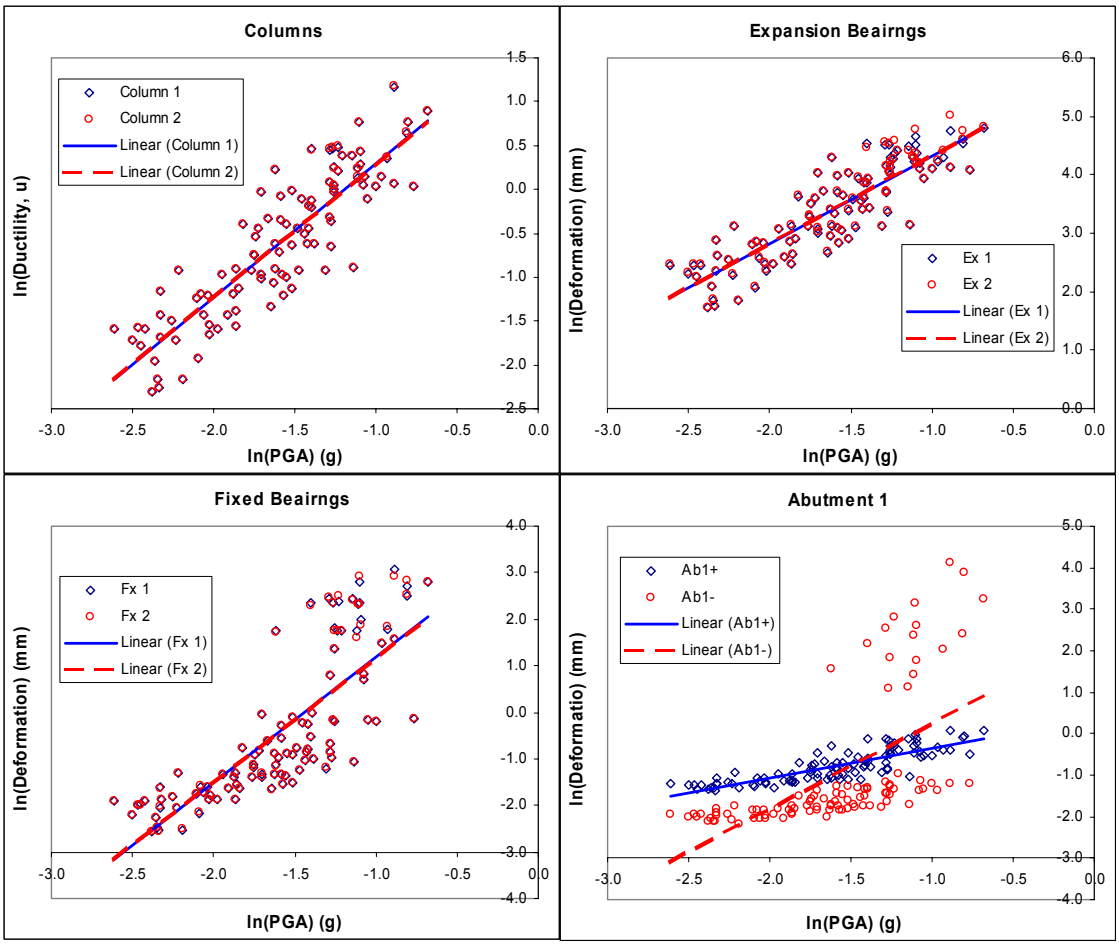

Figure D.3 Regression Analyses of PSDM as A Function of PGA for the MSC Steel Bridge

Table D.3a PSDM of Components in MSC Steel Bridge

Response	PGA			Sa (Ts=1.26)		
	PSDM	R^2	σ	PSDM	R^2	σ
Ln(μ1)	1.5223 Ln(x)+1.8187	0.77	0.39	0.9398 Ln(x)+1.0892	0.89	0.27
Ln(μ2)	1.5236 Ln(x)+1.8210	0.77	0.39	0.9402 Ln(x)+1.0902	0.89	0.27
Ln(Dr1)	1.4704 Ln(x)+1.4784	0.77	0.38	0.9067 Ln(x)+0.7719	0.88	0.26
Ln(Dr2)	1.4711 Ln(x)+1.4796	0.77	0.38	0.9069 Ln(x)+0.7723	0.88	0.26
Ln(Fx1)	2.6907 Ln(x)+3.8702	0.64	0.94	1.7036 Ln(x)+2.6584	0.78	0.74
Ln(Fx2)	2.6895 Ln(x)+3.8673	0.64	0.94	1.7006 Ln(x)+2.6519	0.78	0.74
Ln(Ex1)	1.4988 Ln(x)+5.8105	0.76	0.39	0.9278 Ln(x)+5.0969	0.89	0.27
Ln(Ex2)	1.5153 Ln(x)+5.8479	0.77	0.39	0.9360 Ln(x)+5.1228	0.89	0.27
Ln(Op1)	1.5809 Ln(x)+5.8300	0.74	0.43	0.9910 Ln(x)+5.0997	0.88	0.29
Ln(Op2)	1.5369 Ln(x)+5.8004	0.71	0.45	0.9788 Ln(x)+5.1185	0.88	0.30
Ln(Ab1+)	0.7063 Ln(x)+0.3520	0.70	0.22	0.4508 Ln(x)+0.0403	0.86	0.15
Ln(Ab2+)	0.6790 Ln(x)-1.2146	0.68	0.22	0.4305 Ln(x)-1.5193	0.83	0.16
Ln(Ab1-)	2.0811 Ln(x)+2.3437	0.37	1.26	1.4294 Ln(x)+1.6101	0.53	1.09
Ln(Ab2-)	1.6943 Ln(x)+1.7991	0.31	1.17	1.2081 Ln(x)+1.2826	0.48	1.01

Table D.3b PSDM of Components in MSC Steel Bridge Retrofitted with Elastomeric Bearings

Response	PGA			Sa (Ts=1.44)		
	PSDM	R^2	σ	PSDM	R^2	σ
Ln(μ1)	0.9665 Ln(x)-0.2072	0.71	0.29	0.6193 Ln(x)-0.4784	0.87	0.19
Ln(μ2)	0.9660 Ln(x)-0.2078	0.71	0.29	0.6193 Ln(x)-0.4782	0.87	0.19
Ln(Dr1)	0.9528 Ln(x)-0.4374	0.71	0.29	0.6125 Ln(x)-0.7007	0.87	0.19
Ln(Dr2)	0.9531 Ln(x)-0.4365	0.71	0.29	0.6130 Ln(x)-0.6994	0.87	0.19
Ln(Eb1)	1.2579 Ln(x)+5.7970	0.71	0.37	0.8026 Ln(x)+5.4370	0.87	0.25
Ln(Eb2)	1.3672 Ln(x)+5.8354	0.71	0.41	0.8817 Ln(x)+5.4634	0.87	0.27
Ln(Eb3)	1.3701Ln(x)+5.8408	0.70	0.41	0.8830 Ln(x)+5.4669	0.87	0.27
Ln(Eb4)	1.3368 Ln(x)+5.9635	0.72	0.39	0.8545 Ln(x)+5.5840	0.87	0.26
*Ln(Op1)	1.3097 Ln(x)+5.7953	0.69	0.41	0.8496 Ln(x)+5.4491	0.86	0.27
Ln(Op2)	1.0978 Ln(x)+5.3941	0.67	0.36	0.7153 Ln(x)+5.1105	0.85	0.24
Ln(Ab1+)	0.7514 Ln(x)+1.3089	0.67	0.25	0.4978 Ln(x)+1.1318	0.87	0.25
Ln(Ab2+)	0.9820 Ln(x)+0.1778	0.41	0.54	0.5903 Ln(x)-0.1782	0.44	0.53
Ln(Ab1-)	2.6537 Ln(x)+4.4263	0.44	1.39	1.7914 Ln(x)+3.8694	0.60	1.18
Ln(Ab2-)	2.3891 Ln(x)+3.9001	0.45	1.23	1.6131 Ln(x)+3.3995	0.61	1.04

Table D.3c PSDM of Components in MSC Steel Bridge Retrofitted with Lead Rubber Bearings

Response	PGA			Sa (Ts=1.14)		
	PSDM	R^2	σ	PSDM	R^2	σ
Ln(μ1)	0.9020 Ln(x)+0.2598	0.76	0.24	0.5882 Ln(x)-0.3271	0.86	0.18
Ln(μ2)	0.9033 Ln(x)+0.2626	0.76	0.24	0.5389 Ln(x)-0.3253	0.86	0.18
Ln(Dr1)	0.8998 Ln(x)+0.0246	0.76	0.24	0.5357 Ln(x)-0.5628	0.86	0.18
Ln(Dr2)	0.8978 Ln(x)+0.0220	0.76	0.24	0.5356 Ln(x)-0.5624	0.86	0.18
Ln(Lb1)	1.3374 Ln(x)+5.6066	0.76	0.35	0.8060 Ln(x)+4.7491	0.87	0.24
Ln(Lb2)	1.6962 Ln(x)+5.5145	0.75	0.45	1.0156 Ln(x)+4.4164	0.86	0.34
Ln(Lb3)	1.6968 Ln(x)+5.5155	0.75	0.45	1.0155 Ln(x)+4.4163	0.86	0.34
Ln(Lb4)	1.3556 Ln(x)+5.6710	0.76	0.45	0.8165 Ln(x)+4.8009	0.89	0.24
*Ln(Op1)	1.3438 Ln(x)+5.5088	0.73	0.38	0.8066 Ln(x)+4.6419	0.83	0.30
Ln(Op2)	1.2429 Ln(x)+5.3526	0.73	0.35	0.7411 Ln(x)+4.5429	0.83	0.28
Ln(Ab1+)	0.3835 Ln(x)+1.0252	0.66	0.13	0.2375 Ln(x)+0.7896	0.80	0.10
Ln(Ab2+)	1.4624 Ln(x)+1.8143	0.35	0.92	0.8308 Ln(x)+0.7959	0.36	0.91
Ln(Ab1-)	1.4694 Ln(x)+2.3932	0.34	0.96	0.9643 Ln(x)+1.5770	0.46	0.86
Ln(Ab2-)	1.4940 Ln(x)+2.6597	0.38	0.89	0.8901 Ln(x)+1.6853	0.43	0.85

Table D.3d PSDM of Components in MSC Steel Bridge Retrofitted with Restrainer Cables

Response	PGA			Sa (Ts=1.26)		
	PSDM	R^2	σ	PSDM	R^2	σ
Ln(μ1)	1.4959 Ln(x)+1.7578	0.76	0.39	0.9247 Ln(x)+1.0305	0.88	0.28
Ln(μ2)	1.5000 Ln(x)+1.7656	0.76	0.40	0.9269 Ln(x)+1.0358	0.88	0.28
Ln(Dr1)	1.4422 Ln(x)+1.4113	0.76	0.38	0.8900 Ln(x)+0.7075	0.88	0.227
Ln(Dr2)	1.4440 Ln(x)+1.4140	0.76	0.38	0.8908 Ln(x)+0.7088	0.88	0.27
Ln(Fx1)	2.5294 Ln(x)+3.5059	0.64	0.87	1.5707 Ln(x)+2.2890	0.76	0.72
Ln(Fx2)	2.5395 Ln(x)+3.5269	0.65	0.87	1.5745 Ln(x)+2.3028	0.75	0.73
Ln(Ex1)	1.4259 Ln(x)+5.6395	0.75	0.38	0.8879 Ln(x)+4.9579	0.88	0.26
Ln(Ex2)	1.4665 Ln(x)+5.7342	0.76	0.39	0.9044 Ln(x)+5.0175	0.87	0.28
Ln(Op1)	1.5231 Ln(x)+5.6805	0.76	0.39	0.9338 Ln(x)+4.9261	0.87	0.29
Ln(Op2)	1.4867 Ln(x)+5.6800	0.71	0.44	0.9462 Ln(x)+5.0062	0.87	0.29
Ln(Ab1+)	2.2227 Ln(x)+4.1932	0.76	0.58	1.3153 Ln(x)+3.0065	0.81	0.52
Ln(Ab2+)	2.0821 Ln(x)+2.4512	0.71	0.61	1.2667 Ln(x)+1.4022	0.80	0.51
Ln(Ab1-)	2.0443 Ln(x)+2.2206	0.40	1.17	1.2892 Ln(x)+1.2729	0.48	1.09
Ln(Ab2-)	1.7857 Ln(x)+1.9412	0.37	1.08	1.1368 Ln(x)+1.1328	0.28	1.00

Table D.3e PSDM of Components in MSC Steel Bridge Retrofitted with Restrainer Cables and Elastomeric Bearings

Response	PGA			Sa (Ts=1.40)		
	PSDM	R^2	σ	PSDM	R^2	σ
Ln(μ1)	1.4455 Ln(x)+1.1168	0.71	0.43	0.9286 Ln(x)+0.6694	0.85	0.31
Ln(μ2)	1.4564 Ln(x)+1.1374	0.71	0.43	0.9354 Ln(x)+0.6865	0.85	0.31
Ln(Dr1)	1.4239 Ln(x)+0.8561	0.70	0.43	0.9169 Ln(x)+0.4199	0.85	0.31
Ln(Dr2)	1.4315 Ln(x)+0.0713	0.70	0.43	0.9221 Ln(x)+0.4334	0.85	0.31
Ln(Eb1)	1.0861 Ln(x)+5.4318	0.70	0.33	0.6874 Ln(x)+5.0751	0.82	0.26
Ln(Eb2)	1.0347 Ln(x)+4.9789	0.67	0.34	0.6425 Ln(x)+4.6140	0.74	0.30
Ln(Eb3)	1.0334 Ln(x)+4.9772	0.67	0.34	0.6416 Ln(x)+4.6126	0.75	0.30
Ln(Eb4)	1.2691 Ln(x)+5.7927	0.66	0.43	0.7986 Ln(x)+5.3664	0.75	0.36
Ln(Op1)	1.0449 Ln(x)+5.0351	0.70	0.32	0.6504 Ln(x)+4.6697	0.79	0.27
*Ln(Op2)	0.9943 Ln(x)+5.0203	0.72	0.29	0.6282 Ln(x)+4.6914	0.83	0.22
Ln(Ab1+)	1.3382 Ln(x)+3.2554	0.70	0.40	0.8527 Ln(x)+2.8273	0.83	0.31
Ln(Ab2+)	2.2660 Ln(x)+3.5404	0.35	1.43	1.0801 Ln(x)+2.0823	0.23	1.55
Ln(Ab1-)	2.0363 Ln(x)+3.0608	0.43	1.08	1.1972 Ln(x)+2.2072	0.44	1.08
Ln(Ab2-)	2.0599 Ln(x)+3.7918	0.35	1.32	0.9664 Ln(x)+2.4350	0.22	1.44

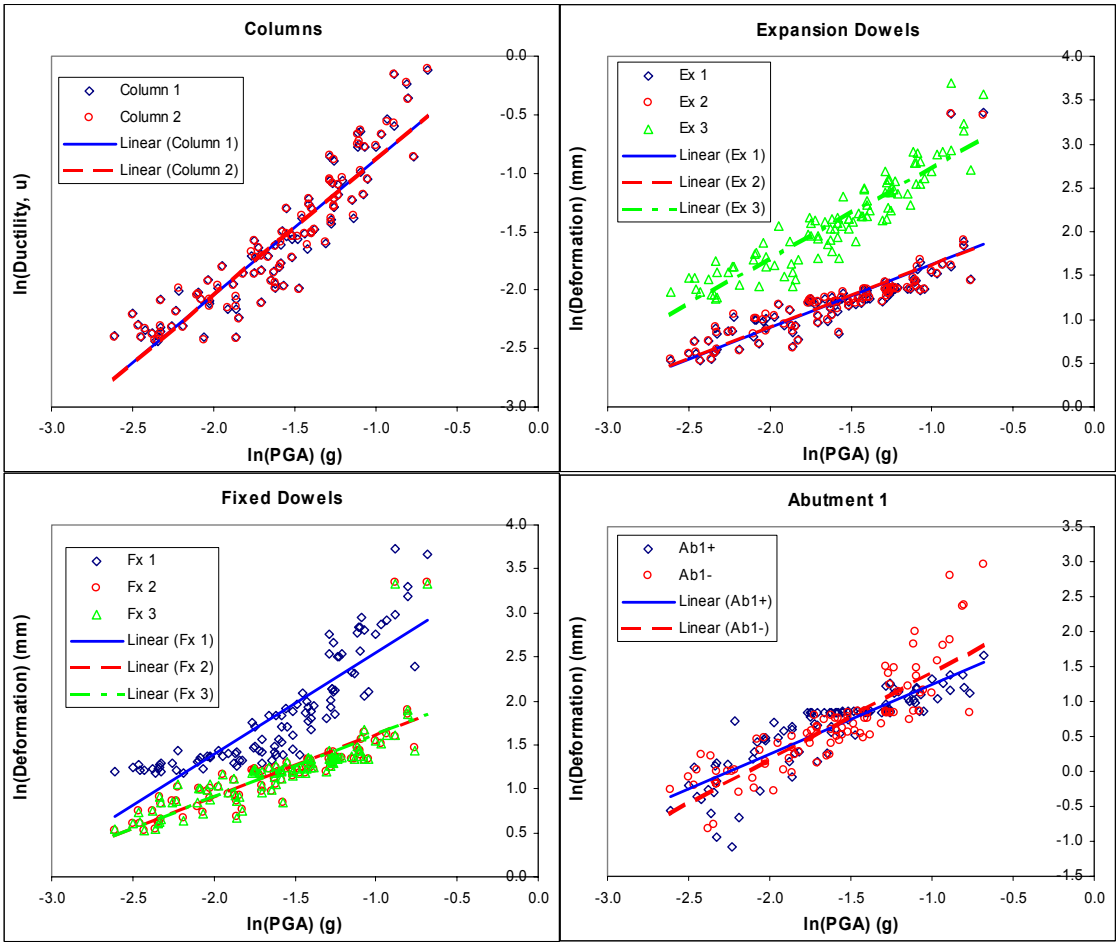

Figure D.4 Regression Analyses of PSDM as A Function of PGA for the MSC Concrete Bridge

Table D.4a PSDM of Components in MSC Concrete Bridge

Response	PGA			Sa (Ts=0.60)		
	PSDM	R^2	σ	PSDM	R^2	σ
Ln(μ1)	1.1586 Ln(x)+0.2765	0.85	0.23	0.8177 Ln(x)-0.8121	0.83	0.24
Ln(μ2)	1.1666 Ln(x)+0.2911	0.85	0.23	0.8234 Ln(x)-0.8050	0.83	0.24
Ln(Dr1)	1.1403 Ln(x)-0.5595	0.84	0.23	0.8020 Ln(x)-1.6336	0.81	0.25
Ln(Dr2)	1.1470 Ln(x)-0.5371	0.84	0.23	0.8088 Ln(x)-1.6156	0.82	0.25
Ln(Fx1)	1.1506 Ln(x)+3.6922	0.74	0.31	0.8113 Ln(x)+2.6105	0.72	0.32
Ln(Fx2)	0.7213 Ln(x)+2.3427	0.63	0.26	0.4979 Ln(x)+1.6546	0.58	0.27
Ln(Fx3)	0.7203Ln(x)+2.3455	0.63	0.26	0.4971 Ln(x)+1.6581	0.59	0.27
Ln(Ex1)	0.7213 Ln(x)+2.3427	0.63	0.26	0.4979 Ln(x)+1.6546	0.58	0.27
Ln(Ex2)	0.7203 Ln(x)+2.3455	0.63	0.26	0.4971 Ln(x)+1.5681	0.59	0.27
Ln(Ex3)	1.0489 Ln(x)+3.7900	0.84	0.21	0.7283 Ln(x)+2.7931	0.80	0.24
Ln(Op1)	0.7228 Ln(x)+2.6411	0.53	0.32	0.5112 Ln(x)+1.9629	0.52	0.32
Ln(Op2)	1.2025 Ln(x)+3.8061	0.82	0.26	0.8414 Ln(x)+2.6694	0.79	0.28
Ln(Ab1+)	1.2628 Ln(x)+3.3749	0.82	0.27	0.8512 Ln(x)+2.1507	0.73	0.34
Ln(Ab2+)	0.2938 Ln(x)+0.8767	0.20	0.27	0.2152 Ln(x)+0.6080	0.22	0.27
Ln(Ab1-)	0.9965 Ln(x)+2.2337	0.75	0.26	0.6750 Ln(x)+1.2708	0.68	0.30
Ln(Ab2-)	0.1446 Ln(x)-0.4915	0.06	0.27	0.1047 Ln(x)-0.6250	0.06	0.27

Table D.4b PSDM of Components in MSC Concrete Bridge Retrofitted with Elastomeric Bearings

Response	PGA			Sa (Ts=1.16)		
	PSDM	R^2	σ	PSDM	R^2	σ
Ln(μ1)	0.8198 Ln(x)-1.8140	0.70	0.25	0.5057 Ln(x)-2.3052	0.84	0.18
Ln(μ2)	0.8186 Ln(x)-1.8156	0.70	0.25	0.5061 Ln(x)-2.3042	0.84	0.18
Ln(Dr1)	0.7413 Ln(x)-2.3154	0.73	0.21	0.4366 Ln(x)-2.7933	0.80	0.18
Ln(Dr2)	0.7441 Ln(x)-2.3080	0.73	0.21	0.4385 Ln(x)-2.7873	0.80	0.18
Ln(Eb1)	0.9346 Ln(x)+5.0125	0.78	0.23	0.5482 Ln(x)+4.4065	0.85	0.19
Ln(Eb2)	0.9693 Ln(x)+5.0481	0.79	0.24	0.5644 Ln(x)+4.4128	0.84	0.20
Ln(Eb3)	0.9693 Ln(x)+5.0481	0.79	0.24	0.5644 Ln(x)+4.4128	0.84	0.20
Ln(Eb4)	0.9685 Ln(x)+5.0462	0.79	0.23	0.5634 Ln(x)+4.4106	0.84	0.20
Ln(Eb5)	0.9685 Ln(x)+5.0462	0.79	0.23	0.5634 Ln(x)+4.4106	0.84	0.20
Ln(Eb6)	0.9183 Ln(x)+4.9632	0.78	0.23	0.5366 Ln(x)+4.3845	0.84	0.19
Ln(Op1)	0.9972 Ln(x)+5.0811	0.78	0.25	0.5775 Ln(x)+4.4225	0.83	0.22
*Ln(Op2)	1.0287 Ln(x)+5.0862	0.77	0.26	0.5926 Ln(x)+4.4016	0.81	0.24
Ln(Ab1+)	0.5948 Ln(x)+0.9427	0.77	0.15	0.3462 Ln(x)+0.5527	0.83	0.13
Ln(Ab2+)	0.6035 Ln(x)+0.9319	0.76	0.16	0.3497 Ln(x)+0.5336	0.81	0.14
Ln(Ab1-)	3.3836 Ln(x)+5.7434	0.64	1.17	1.9709 Ln(x)+3.5268	0.69	1.09
Ln(Ab2-)	3.4231 Ln(x)+5.8790	0.66	1.14	1.9951 Ln(x)+3.6386	0.71	1.05

Table D.4c PSDM of Components in MSC Concrete Bridge Retrofitted with Lead Rubber Bearings

Response	PGA			Sa (Ts=0.66)		
	PSDM	R^2	σ	PSDM	R^2	σ
Ln(μ1)	1.0171 Ln(x)+0.0020	0.84	0.20	0.7151 Ln(x)-0.9493	0.84	0.20
Ln(μ2)	1.0207 Ln(x)+0.0096	0.84	0.21	0.7173 Ln(x)-0.9455	0.84	0.20
Ln(Dr1)	0.9711 Ln(x)-0.8437	0.83	0.21	0.6797 Ln(x)-1.7548	0.82	0.21
Ln(Dr2)	0.9715 Ln(x)-0.8436	0.83	0.20	0.6785 Ln(x)-1.7567	0.82	0.21
Ln(Lb1)	1.1951 Ln(x)+4.5718	0.84	0.24	0.8230 Ln(x)+3.4376	0.81	0.27
Ln(Lb2)	1.2597 Ln(x)+4.3126	0.81	0.28	0.8658 Ln(x)+3.1153	0.78	0.30
Ln(Lb3)	1.2597Ln(x)+4.3126	0.81	0.28	0.8658 Ln(x)+3.1153	0.78	0.30
Ln(Lb4)	1.2603 Ln(x)+4.3136	0.81	0.28	0.8665 Ln(x)+3.1162	0.78	0.30
Ln(Lb5)	1.2603 Ln(x)+4.3136	0.81	0.28	0.8665 Ln(x)+3.1162	0.78	0.30
Ln(Lb6)	1.1884 Ln(x)+4.5491	0.83	0.25	0.8273 Ln(x)+3.4296	0.81	0.26
Ln(Op1)	1.1092 Ln(x)+4.2229	0.78	0.28	0.7608 Ln(x)+3.1672	0.74	0.30
*Ln(Op2)	1.2170 Ln(x)+4.4621	0.82	0.27	0.8454 Ln(x)+3.3139	0.80	0.28
Ln(Ab1+)	0.5443 Ln(x)+1.5476	0.68	0.17	0.3686 Ln(x)+1.0252	0.63	0.19
Ln(Ab2+)	0.5886 Ln(x)+1.6249	0.71	0.18	0.3949 Ln(x)+1.0563	0.65	0.19
Ln(Ab1-)	0.7917 Ln(x)+0.9330	0.46	0.40	0.5540 Ln(x)+0.1899	0.46	0.40
Ln(Ab2-)	0.6662 Ln(x)+0.7066	0.46	0.33	0.4353 Ln(x)+0.0519	0.40	0.35

Table D.4d PSDM of Components in MSC Concrete Bridge Retrofitted with Restrainer Cables

Response	PGA			Sa (Ts=0.60)		
	PSDM	R^2	σ	PSDM	R^2	σ
Ln(μ1)	1.1474 Ln(x)+0.2551	0.85	0.22	0.8115 Ln(x)-0.8206	0.83	0.24
Ln(μ2)	1.1544 Ln(x)+0.2678	0.85	0.22	0.8164 Ln(x)-0.8145	0.83	0.24
Ln(Dr1)	1.1321 Ln(x)-0.5751	0.84	0.23	0.7977 Ln(x)-1.6393	0.81	0.25
Ln(Dr2)	1.1332 Ln(x)-0.5638	0.84	0.23	0.8005 Ln(x)-1.6271	0.82	0.24
Ln(Fx1)	1.1392 Ln(x)+3.6707	0.75	0.31	0.8039 Ln(x)+2.6009	0.72	0.32
Ln(Fx2)	0.7089 Ln(x)+2.3197	0.64	0.25	0.4921 Ln(x)+1.6464	0.60	0.26
Ln(Fx3)	0.7081Ln(x)+2.3225	0.64	0.25	0.4918 Ln(x)+1.6503	0.60	0.26
Ln(Ex1)	0.7089 Ln(x)+2.3197	0.64	0.25	0.4921 Ln(x)+1.6464	0.60	0.26
Ln(Ex2)	0.7081 Ln(x)+2.3225	0.64	0.25	0.4918 Ln(x)+1.6503	0.60	0.26
Ln(Ex3)	1.0152 Ln(x)+3.7254	0.86	0.19	0.7044 Ln(x)+2.7607	0.81	0.22
Ln(Op1)	0.6947 Ln(x)+2.5882	0.55	0.29	0.4640 Ln(x)+1.9394	0.54	0.30
Ln(Op2)	1.1463 Ln(x)+3.6991	0.84	0.23	0.7997 Ln(x)+2.6141	0.80	0.26
Ln(Ab1+)	1.2634 Ln(x)+3.3760	0.82	0.27	0.8556 Ln(x)+2.1558	0.73	0.33
Ln(Ab2+)	0.5031 Ln(x)+1.2802	0.33	0.33	0.3717 Ln(x)+0.8235	0.35	0.39
Ln(Ab1-)	0.9884 Ln(x)+2.2180	0.75	0.27	0.6694 Ln(x)+1.2634	0.67	0.31
Ln(Ab2-)	0.1238 Ln(x)+0.5299	0.06	0.22	0.0920 Ln(x)-0.6417	0.07	0.22

Table D.4e PSDM of Components in MSC Concrete Bridge Retrofitted with Restrainer Cables and Elastomeric Bearings

Response	PGA			Sa (Ts=1.04)		
	PSDM	R^2	σ	PSDM	R^2	σ
Ln(μ1)	1.1497 Ln(x)-1.0061	0.78	0.28	0.6692 Ln(x)-1.8744	0.82	0.26
Ln(μ2)	1.1476 Ln(x)-1.0099	0.78	0.28	0.6684 Ln(x)-1.8760	0.82	0.26
Ln(Dr1)	1.2567 Ln(x)-0.9572	0.81	0.29	0.7052 Ln(x)-1.9447	0.79	0.30
Ln(Dr2)	1.2622 Ln(x)-0.9465	0.81	0.29	0.7093 Ln(x)-1.9368	0.79	0.30
Ln(Eb1)	0.6800 Ln(x)+4.3833	0.77	0.17	0.3891 Ln(x)+3.8600	0.78	0.17
Ln(Eb2)	0.6819 Ln(x)+4.3170	0.80	0.16	0.3898 Ln(x)+3.7917	0.81	0.16
Ln(Eb3)	0.6819 Ln(x)+4.3170	0.80	0.16	0.3898 Ln(x)+3.7917	0.81	0.16
Ln(Eb4)	0.6828 Ln(x)+4.3185	0.80	0.16	0.3904 Ln(x)+3.7927	0.81	0.16
Ln(Eb5)	0.6828 Ln(x)+4.3185	0.80	0.16	0.3904 Ln(x)+3.7927	0.81	0.16
Ln(Eb6)	0.6651 Ln(x)+4.3701	0.77	0.17	0.3770 Ln(x)+3.8529	0.76	0.17
Ln(Op1)	0.6479 Ln(x)+4.2075	0.79	0.15	0.3651 Ln(x)+3.7007	0.78	0.16
*Ln(Op2)	0.6823 Ln(x)+4.2497	0.80	0.16	0.3851 Ln(x)+3.7167	0.79	0.16
Ln(Ab1+)	1.6105 Ln(x)+4.0528	0.78	0.40	0.9203 Ln(x)+2.8114	0.79	0.39
Ln(Ab2+)	1.7366 Ln(x)+4.2126	0.81	0.40	0.9752 Ln(x)+2.8491	0.79	0.42
Ln(Ab1-)	2.3539 Ln(x)+3.3310	0.53	1.02	1.3083 Ln(x)+1.4630	0.51	1.05
Ln(Ab2-)	2.3882 Ln(x)+3.3963	0.57	0.97	1.2843 Ln(x)+1.4382	0.51	1.04

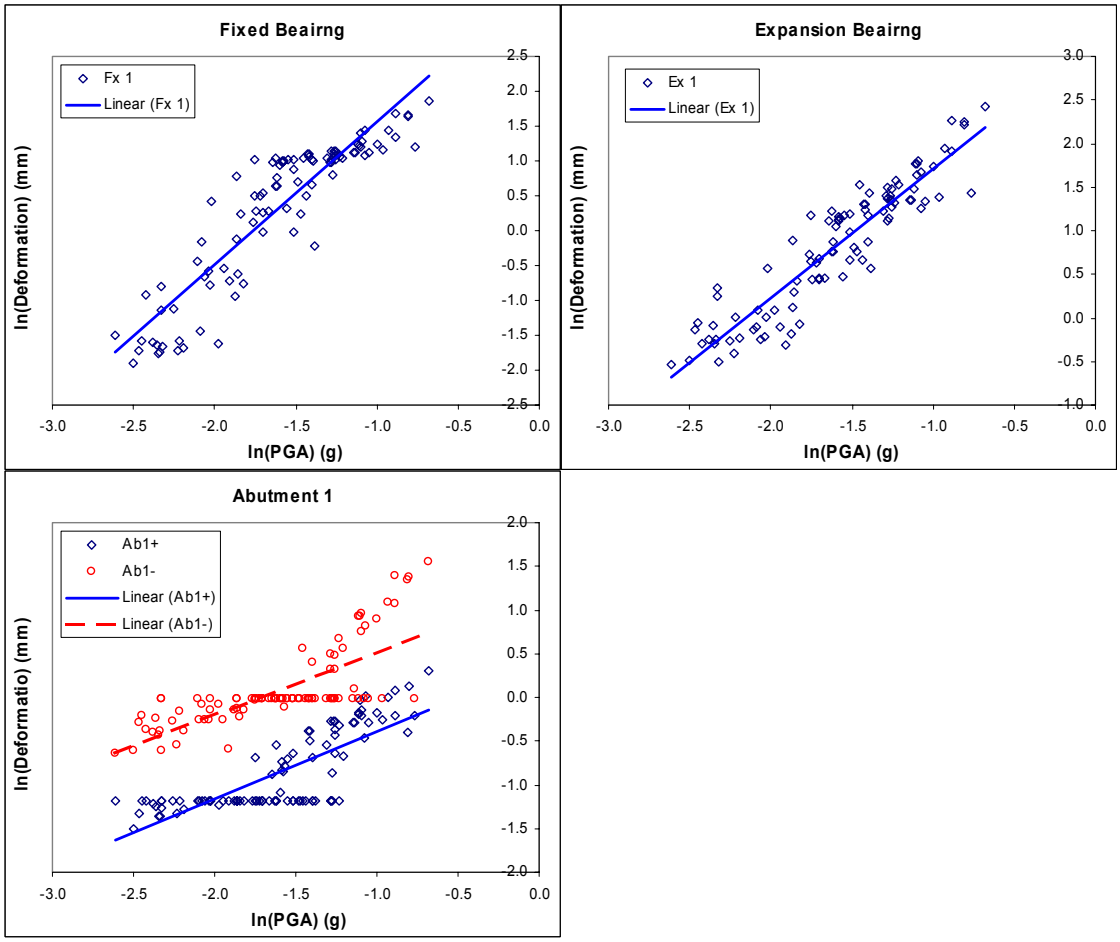

Figure D.5 Regression Analyses of PSDM as A Function of PGA for the SS Steel Bridge

Table D.5a PSDM of Components in SS Steel Bridge

Response	PGA			Sa(Ts=0.33)		
	PSDM	R^2	σ	PSDM	R^2	σ
Ln(Fx1)	2.0505 Ln(x)+3.6097	0.82	0.44	1.6759 Ln(x)+1.8244	0.67	0.60
Ln(Ex1)	1.4814 Ln(x)+3.1967	0.86	0.28	1.2737 Ln(x)+1.9633	0.77	0.35
Ln(Op1)	1.3161 Ln(x)+2.5812	0.62	0.48	1.2216 Ln(x)+1.5662	0.65	0.46
Ln(Ab1+)	0.7698 Ln(x)+0.3753	0.63	0.28	0.7107 Ln(x)-0.2219	0.65	0.27
Ln(Ab2+)	0.0985 Ln(x)-2.3337	0.49	0.05	0.0944 Ln(x)-2.4070	0.55	0.04
Ln(Ab1-)	0.7128 Ln(x)+1.2202	0.55	0.30	0.6531 Ln(x)+0.6628	0.56	0.29
Ln(Ab2-)	0.1312 Ln(x)-1.8933	0.58	0.05	0.1097 Ln(x)-2.0054	0.50	0.06

Table D.5b PSDM of Components in SS Steel Bridge Retrofitted with Elastomeric Bearings

Response	PGA			Sa(Ts=1.30)		
	PSDM	R^2	σ	PSDM	R^2	σ
Ln(Eb1)	1.2778 Ln(x)+5.8483	0.73	0.36	0.8121 Ln(x)+5.3095	0.88	0.24
Ln(Eb2)	1.2719 Ln(x)+5.8341	0.73	0.36	0.8079 Ln(x)+5.2969	0.88	0.24
*Ln(Op1)	1.3140 Ln(x)+5.8278	0.71	0.39	0.8450 Ln(x)+5.2921	0.88	0.26
Ln(Op2)	1.2863 Ln(x)+5.7802	0.70	0.39	0.8287 Ln(x)+5.2587	0.86	0.26
Ln(Ab1+)	0.8618 Ln(x)-0.9793	0.68	0.27	0.5579 Ln(x)-1.3233	0.85	0.19
Ln(Ab2+)	0.8382 Ln(x)-0.1506	0.68	0.27	0.5428 Ln(x)-0.4852	0.85	0.19
Ln(Ab1-)	2.0082 Ln(x)+2.4969	0.39	1.17	1.3966 Ln(x)+1.8742	0.56	0.99
Ln(Ab2-)	2.0995 Ln(x)+2.7900	0.40	1.18	1.4680 Ln(x)+2.1535	0.59	0.98

Table D.5c PSDM of Components in SS Steel Bridge Retrofitted with Lead Rubber Bearings

Response	PGA			Sa(Ts=0.66)		
	PSDM	R^2	σ	PSDM	R^2	σ
Ln(Lb1)	1.2155 Ln(x)+5.0390	0.79	0.29	0.8643 Ln(x)+3.9211	0.82	0.27
Ln(Lb2)	1.2238 Ln(x)+5.0488	0.79	0.29	0.8727 Ln(x)+3.9192	0.82	0.27
Ln(Op1)	1.1352 Ln(x)+4.8132	0.75	0.31	0.7984 Ln(x)+3.7548	0.75	0.30
*Ln(Op2)	1.2077 Ln(x)+4.9014	0.74	0.33	0.8602 Ln(x)+3.7857	0.76	0.32
Ln(Ab1+)	0.3037 Ln(x)-1.1490	0.58	0.12	0.2141 Ln(x)-1.4318	0.58	0.12
Ln(Ab2+)	0.3465 Ln(x)-0.2206	0.58	0.14	0.2408 Ln(x)-0.5464	0.57	0.14
Ln(Ab1-)	0.3498 Ln(x)+0.0747	0.58	0.14	0.2427 Ln(x)-0.2545	0.57	0.14
Ln(Ab2-)	0.3160 Ln(x)+0.1273	0.58	0.12	0.2219 Ln(x)-0.1677	0.58	0.12

Table D.5d PSDM of Components in SS Steel Bridge Retrofitted with Restrainer Cables

Response	PGA			Sa(Ts=0.33)		
	PSDM	R^2	σ	PSDM	R^2	σ
Ln(Fx1)	2.0505 Ln(x)+3.6097	0.82	0.44	1.6759 Ln(x)+1.8244	0.67	0.60
Ln(Ex1)	1.4814 Ln(x)+3.1967	0.86	0.28	1.2737 Ln(x)+1.9633	0.77	0.35
Ln(Op1)	1.3161 Ln(x)+2.5812	0.62	0.48	1.2216 Ln(x)+1.5662	0.65	0.46
Ln(Ab1+)	0.7698 Ln(x)+0.3753	0.63	0.28	0.7107 Ln(x)-0.2219	0.65	0.27
Ln(Ab2+)	0.0985 Ln(x)-2.3337	0.49	0.05	0.0944 Ln(x)-2.4070	0.55	0.04
Ln(Ab1-)	0.7128 Ln(x)+1.2202	0.55	0.30	0.6531 Ln(x)+0.6628	0.56	0.29
Ln(Ab2-)	0.1312 Ln(x)-1.8933	0.58	0.05	0.1097 Ln(x)-2.0054	0.50	0.06

Table D.5e PSDM of Components in SS Steel Bridge Retrofitted with Restrainer Cables and Elastomeric Bearings

Response	PGA			Sa(Ts=0.85)		
	PSDM	R^2	σ	PSDM	R^2	σ
Ln(Eb1)	1.2141 Ln(x)+5.5914	0.78	0.30	0.7315 Ln(x)+4.4987	0.81	0.28
Ln(Eb2)	1.2054 Ln(x)+5.5670	0.78	0.30	0.7266 Ln(x)+4.4825	0.81	0.27
Ln(Op1)	1.1939 Ln(x)+5.5101	0.77	0.31	0.7225 Ln(x)+4.4392	0.80	0.28
*Ln(Op2)	1.2172 Ln(x)+5.5283	0.77	0.31	0.7377 Ln(x)+4.4379	0.81	0.28
Ln(Ab1+)	1.4032 Ln(x)+1.5202	0.66	0.46	0.8872 Ln(x)+0.3061	0.76	0.39
Ln(Ab2+)	1.4811 Ln(x)+2.4749	0.66	0.49	0.9298 Ln(x)+1.1857	0.75	0.43
Ln(Ab1-)	1.5967 Ln(x)+1.5200	0.43	0.85	0.9701 Ln(x)+0.0923	0.45	0.83
Ln(Ab2-)	1.6611 Ln(x)+1.7598	0.42	0.91	1.0209 Ln(x)+0.2882	0.45	0.88

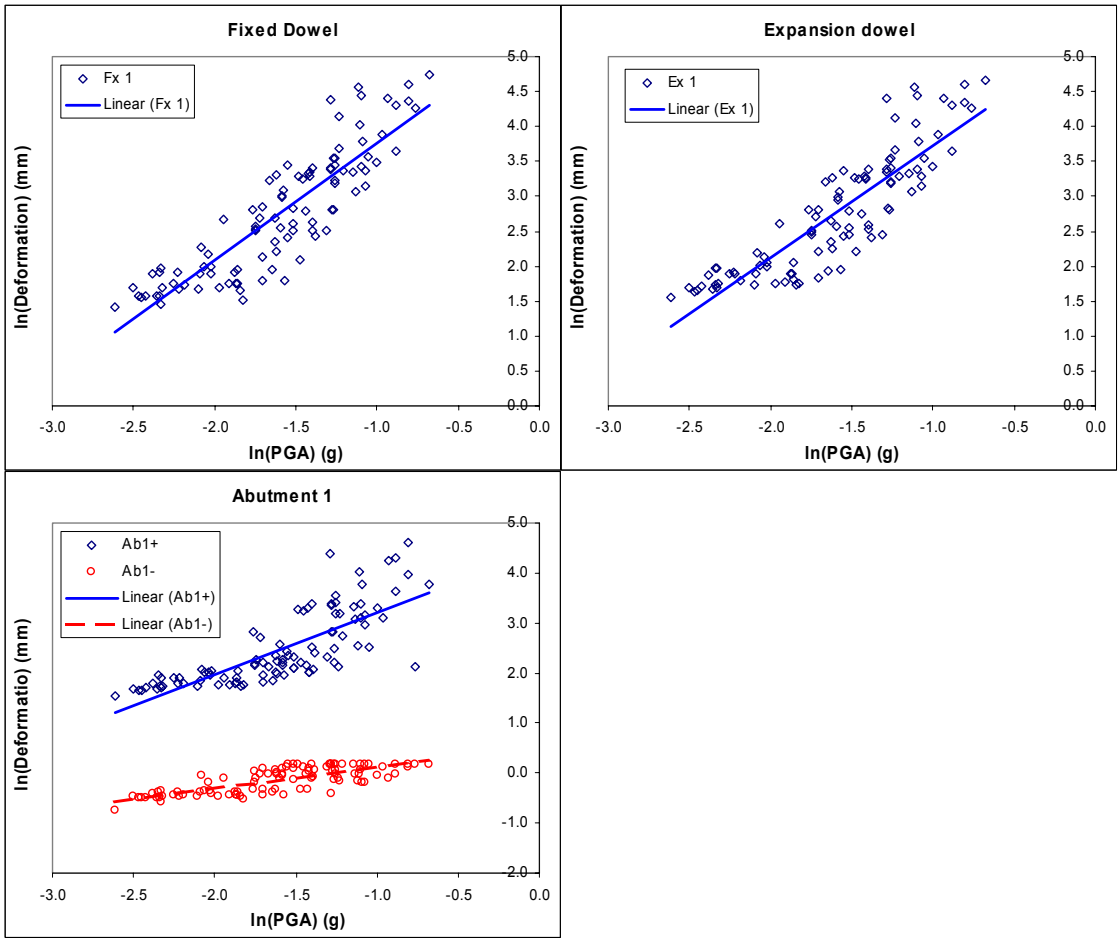

Figure D.6 Regression Analyses of PSDM as A Function of PGA for the SS Concrete Bridge

Table D.6a PSDM of Components in SS Concrete Bridge

Response	PGA			Sa(Ts=0.65)		
	PSDM	R^2	σ	PSDM	R^2	σ
Ln(Fx1)	1.6854 Ln(x)+5.4496	0.77	0.43	1.1642 Ln(x)+3.8534	0.75	0.45
Ln(Ex1)	1.6081 Ln(x)+5.3382	0.77	0.41	1.1173 Ln(x)+3.8214	0.75	0.42
Ln(Op1)	1.4790 Ln(x)+4.9715	0.68	0.47	1.0253 Ln(x)+3.5742	0.66	0.49
Ln(Op2)	1.2409 Ln(x)+4.4611	0.61	0.46	0.8635 Ln(x)+3.2919	0.59	0.47
Ln(Ab1+)	0.4216 Ln(x)+0.5346	0.59	0.16	0.2865 Ln(x)+0.1307	0.55	0.17
Ln(Ab2+)	0.8309 Ln(x)+0.9489	0.45	0.43	0.5947 Ln(x)+0.1816	0.47	0.42
Ln(Ab1-)	0.4451 Ln(x)+1.5907	0.69	0.14	0.2874 Ln(x)+1.1501	0.59	0.16
Ln(Ab2-)	1.0758 Ln(x)+1.7802	0.60	0.41	0.7301 Ln(x)+0.7490	0.56	0.43

Table D.6b PSDM of Components in SS Concrete Bridge Retrofitted with Elastomeric Bearings

Response	PGA			Sa(Ts=1.52)		
	PSDM	R^2	σ	PSDM	R^2	σ
Ln(Eb1)	1.2505 Ln(x)+5.8786	0.72	0.36	0.8053 Ln(x)+5.6003	0.91	0.20
Ln(Eb2)	1.2514 Ln(x)+5.8789	0.72	0.36	0.8051 Ln(x)+5.5988	0.91	0.20
Ln(Op1)	1.2943 Ln(x)+5.8430	0.67	0.42	0.8542 Ln(x)+5.5994	0.89	0.24
*Ln(Op2)	1.3127 Ln(x)+5.8814	0.68	0.42	0.8553 Ln(x)+5.6106	0.89	0.25
Ln(Ab1+)	0.8597 Ln(x)-0.9508	0.65	0.29	0.5691 Ln(x)-1.1089	0.87	0.18
Ln(Ab2+)	0.8645 Ln(x)-0.0659	0.67	0.28	0.5661 Ln(x)-0.2383	0.88	0.17
Ln(Ab1-)	2.2590 Ln(x)+3.0481	0.40	1.28	1.5593 Ln(x)+2.7697	0.58	1.07
Ln(Ab2-)	2.1649 Ln(x)+2.9622	0.39	1.25	1.5241 Ln(x)+2.7592	0.60	1.02

Table D.6c PSDM of Components in SS Concrete Bridge Retrofitted with Lead Rubber Bearings

Response	PGA			Sa(Ts=0.85)		
	PSDM	R^2	σ	PSDM	R^2	σ
Ln(Lb1)	1.2793 Ln(x)+5.4120	0.80	0.30	0.7622 Ln(x)+4.2420	0.81	0.29
Ln(Lb2)	1.2871 Ln(x)+5.4159	0.80	0.30	0.7660 Ln(x)+4.2377	0.81	0.29
Ln(Op1)	1.2624 Ln(x)+5.2524	0.71	0.37	0.7688 Ln(x)+4.1171	0.76	0.34
*Ln(Op2)	1.2794 Ln(x)+5.2414	0.75	0.34	0.7496 Ln(x)+4.0566	0.74	0.35
Ln(Ab1+)	0.3329 Ln(x)-1.0270	0.65	0.11	0.2055 Ln(x)-1.3232	0.71	0.10
Ln(Ab2+)	0.3380 Ln(x)-0.1626	0.67	0.11	0.1987 Ln(x)-0.4748	0.66	0.11
Ln(Ab1-)	0.3990 Ln(x)+0.2492	0.34	0.26	0.2410 Ln(x)-0.1120	0.36	0.25
Ln(Ab2-)	0.4259 Ln(x)+0.4052	0.41	0.24	0.2676 Ln(x)+0.0318	0.46	0.23

Table D.6d PSDM of Components in SS Concrete Bridge Retrofitted with Restrainer Cables

Response	PGA			Sa(Ts=0.56)		
	PSDM	R^2	σ	PSDM	R^2	σ
Ln(Fx1)	1.3636 Ln(x)+4.7866	0.80	0.31	1.0229 Ln(x)+3.5381	0.79	0.32
Ln(Ex1)	1.2759 Ln(x)+4.6559	0.81	0.29	0.9637 Ln(x)+3.4936	0.81	0.29
Ln(Op1)	1.2219 Ln(x)+4.4571	0.73	0.34	0.9261 Ln(x)+3.3470	0.74	0.34
Ln(Op2)	1.1937 Ln(x)+4.3596	0.75	0.32	0.8915 Ln(x)+3.2629	0.73	0.33
Ln(Ab1+)	0.4170 Ln(x)+0.5243	0.59	0.16	0.3074 Ln(x)+0.1375	0.56	0.17
Ln(Ab2+)	1.1133 Ln(x)+1.5179	0.65	0.38	0.8518 Ln(x)+0.5137	0.67	0.36
Ln(Ab1-)	0.4559 Ln(x)+1.6174	0.70	0.14	0.3216 Ln(x)+1.1813	0.61	0.16
Ln(Ab2-)	0.8527 Ln(x)+1.3070	0.59	0.33	0.6233 Ln(x)+0.5113	0.55	0.35

Table D.6e PSDM of Components in SS Concrete Bridge Retrofitted with Restrainer Cables and Elastomeric Bearings

Response	PGA			Sa(Ts=1.01)		
	PSDM	R^2	σ	PSDM	R^2	σ
Ln(Eb1)	1.2531 Ln(x)+5.8090	0.76	0.33	0.7798 Ln(x)+4.9018	0.89	0.22
Ln(Eb2)	1.2472 Ln(x)+5.7896	0.76	0.33	0.7769 Ln(x)+4.8877	0.89	0.22
*Ln(Op1)	1.2897 Ln(x)+5.8187	0.75	0.35	0.8053 Ln(x)+4.8889	0.89	0.23
Ln(Op2)	1.2496 Ln(x)+5.7351	0.74	0.34	0.7791 Ln(x)+4.8326	0.88	0.23
Ln(Ab1+)	1.3410 Ln(x)+1.5211	0.59	0.52	0.8484 Ln(x)+0.5700	0.72	0.43
Ln(Ab2+)	1.3000 Ln(x)+2.3200	0.58	0.51	0.8305 Ln(x)+1.4093	0.72	0.42
Ln(Ab1-)	2.0619 Ln(x)+2.5563	0.44	1.07	1.3106 Ln(x)+1.1024	0.55	0.97
Ln(Ab2-)	2.0585 Ln(x)+2.6455	0.45	1.06	1.3163 Ln(x)+1.2051	0.56	0.95

APPENDIX E

EQUIPMENT SPECIFICATIONS

HCD Series

Hermetically Sealed

HCD series LVDTs are impervious to dirt, water, steam spray and most corrosives. Tungsten inert gas (TIG) welding provides hermetic sealing that is free from oxidation-producing faults that may cause leakage. They have been qualified at pressures up to 1000 psi (70 bars) and are suitable for numerous high-pressure applications. They are terminated with a glass-sealed, MS-type terminal connector. The connector prohibits the core from passing completely through the coil assembly. HCD units have double magnetic shielding that makes them insensitive to external magnetic influences.

Features

- Hermetically sealed by TIG
- CE compliant
- Glass-sealed MS-type connector
- Calibration certificate supplied with all models

Applications

- Harsh industrial environments
- Ideal for pressure installations up to 1,000 psi
- Submersible with appropriate connector

Options

- Captive core option for convenient installation
- Metric thread core
- Guided core
- Small diameter, low mass core
- See accessories section for connector and cable options, page 58.

Specifications

Input Voltage	±15 VDC (nominal), ±25 ma
Operating Temperature Range	32°F to 160°F (0°C to 70°C)
Survival Temperature Range	-65°F to 200°F (-55°C to 95°C)
Null Voltage	0 VDC
Ripple	Less than 25 mV rms
Linearity	0.25% full range
Stability	0.125% full scale
Temperature—Coefficient of Scale Factor	0.04%/°F (0.08%/°C)
Shock Survival	250 g for 11 milliseconds half sine
Vibration Tolerance	10 g up to 2 kHz
Coil Form Material	High density, glass-filled polymer
Housing Material	AISI 400 series stainless steel
Electrical Termination	6-pin connector
Output Impedance	Less than 1 ohm

Performance and Electrical Specifications[1]

HCD Series Model Number	Nominal Linear Range inches	Nominal Linear Range mm	Scale Factor V/inch	Scale Factor V/mm	Response -3 dB Hz
050 HCD	±0.050	±1.25	200.0	8.00	500
125 HCD	±0.125	±3.0	80.0	3.00	500
250 HCD	±0.250	±6.0	40.0	1.60	500
500 HCD	±0.500	±12.5	20.0	0.80	200
1000 HCD	±1.000	±25	10.0	0.40	200
2000 HCD	±2.000	±50	5.0	0.20	200
3000 HCD	±3.000	±75	3.3	0.13	200
5000 HCD	±5.000	±125	2.0	0.08	200
10000 HCD	±10.000	±250	1.0	0.04	200

[1]All calibration is performed at room ambient temperature.

Figure E.1 Schaevitz linear variable differential transformer

DCT Unguided DC LVDT Displacement Transducers

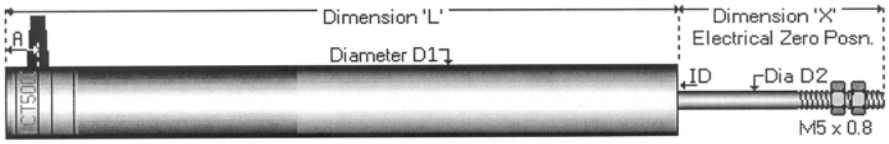

Unit Type	DCT2000
Dim. L	317
Dim. D1	20.6
ID	6.8
Body Weight	361 grms
Over Travel: Inward	15.8

Stroke	±50 mm
Dim. X	81
Dim. D2	Push rod (shown as D2) = 4.75 mm dia. Armature (inside transducer) = 6 mm dia.
Dim. A	9
Armature Weight	37 grms
Over Travel: Outward	NA

The RDP Electronics DCT series are a dc LVDT transducer which makes them probably the most robust position sensor available. The term dc LVDT refers to a position sensor that has all the benefits of the LVDT measurement principle but has built-in dc to dc signal conditioning. Our dc LVDT displacement transducer units have no contact across the position sensor element ensuring very long life. The unguided dc LVDT displacement transducer units have an armature (the moving part of the measurement sensor) that is a completely separate component to the body of the transducer. The armature of the dc displacement transducer should be configured in operation such that it moves in and out of the armature tube, without touching the sides. This type of dc LVDT transducer is appropriate for measurement application where there are many millions of cycles or where there is a very high speed movement.

Electrical Specification	
Supply Single (must be floating w.r.t. output) OR Supply Dual	+20 to +40V dc, 25mA (Output options may change this). ±10 to ±20V, 25mA (Output options may change this).
Standard Output (in/out)	+/-5V and -/+5V (-0%, +5%), selected by connection.
Optional Output (in/out)	0/10V,10/0,4/20mA,20/4mA
Linearity (% error of full scale)	±0.5% standard. 0.25% and 0.1% optional on some models.
Output Load (min) (Ohms)	2k (±10V to ±20V), 20k (+20 to +40V)
Output Ripple	30mV peak to peak
Output Bandwidth (Electrical)	200Hz (flat)
Output Impedance	2 Ohms
Zero Temperature Coefficient	±0.01% F.S./°C
Span Temperature Coefficient	±0.03% F.S./°C
Operating Temperature Range	-50 to +70°C
Electrical Termination	2m screened cable

Figure E.2 RDP linear variable differential transformer.

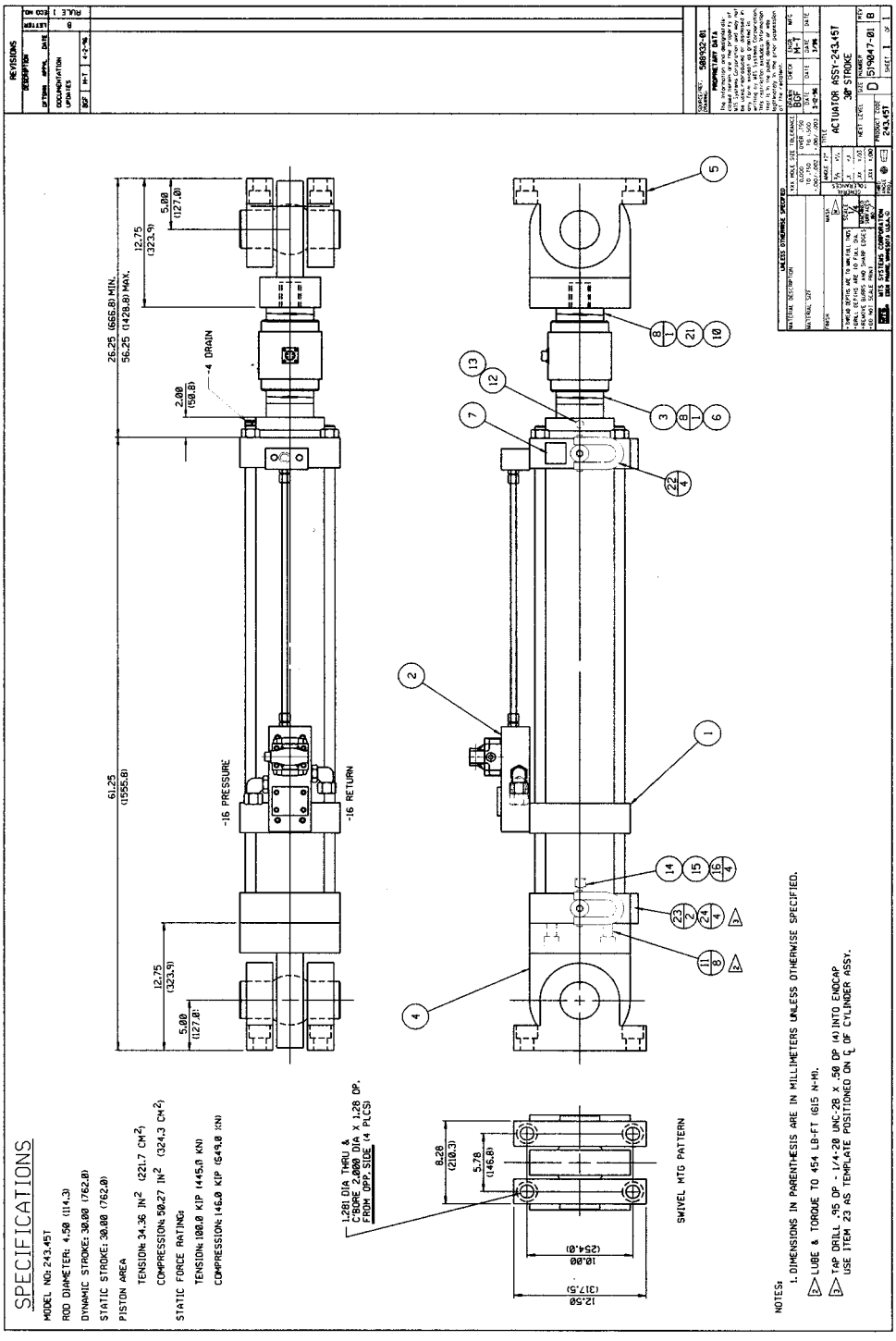

Figure E.3 MTS 243.45T actuator

w i l c o x o n

Model 731A/Model P31 System
Seismic Accelerometer and Power Amplifier

FEATURES:
- Ultra high sensitivity
- Ultra low-noise electronics for clear signals at sub micro-g levels
- Low frequency capable
- Low pass filtered to eliminate high frequencies
- ESD protection
- Miswiring protection

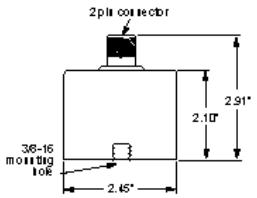

Model 731A

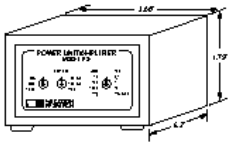

Model P31

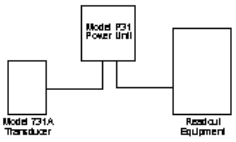

POWERING WITH P31 POWER UNIT

DYNAMIC

Acceleration Sensitivity, selectable			10, 100, 1000 V/g
Velocity Sensitivity, selectable			0.1, 1, 10 V/in/sec
Vibration Range, max.			0.5 g peak
Amplitude Nonlinearity			1%
Frequency Response:			
Filter	100 Hz	450 Hz	Velocity
–10%	0.08 - 70 Hz	0.08 - 300 Hz	– – –
–3dB	0.05 - 100 Hz	0.05 - 450 Hz	0.8 - 150 Hz
Transverse Sensitivity, max.			1% of axial

ELECTRICAL

Output Impedance		2500 Ω
Recommended Load Impedance		> 250 KΩ
Maximum Output Voltage		5 V peak
Noise:		
Spectral	2 Hz	0.03 µg/√Hz
	10 Hz	0.01 µg/√Hz
	100 Hz	0.004 µg/√Hz
Grounding		Case isolated
Output Connector:		
Model 731A		2 pin, MIL-C-5015
Model P31		BNC
Input Connector (P31)		Twin Axial BNC

POWER REQUIREMENTS (P31)

Internal Batteries	Four 9 Volt Alkaline
Battery Life	> 150 hours

ENVIRONMENTAL

Temperature Range	–10 to 65°C
Vibration Limit	10 g peak
Shock Limit	Fragile
Base Strain Sensivitiy	0.0001 g/µstrain

PHYSICAL

Sensing Element Design	PZT ceramic / flexure
Weight:	
Model 731A Seismic Accelerometer	670 grams
Model P31 Power Unit/Amplifier	600 grams
Interconnect Cable, Model 731A to Model P31	R6-2T-J9-10

OUTPUT	CONNECTOR	FUNCTION	CABLE
731A	Shell	case	Shield
	A	power / signal	White
	B	common	Black
P31	Shell	common	Shield
	Pin	signal	Center Conductor
INPUT	**CONNECTOR**	**FUNCTION**	**CABLE**
P31	Shell	ground	Shield
	Pin	power/signal	White
	Socket	common	Black

ACCESSORIES SUPPLIED: SF7 mounting stud; Calibration data (level 3).
NOTE: Special handling required due to sensitivity.

98079 Rev A 5/01

ISO 9001

Due to continual research and development, Wilcoxon Research reserves the right to amend this specification without notice.

WR WILCOXON RESEARCH

21 Firstfield Road, Gaithersburg, MD 20878 • Tel: 301-330-8811 • Fax: 301-330-8873 • 1-800-WILCOXON • Email: sensors@wilcoxon.com • Web: www.wilcoxon.com

Figure E.4 Wilcoxon ultra low frequency seismic accelerometer.

OPTIM Electronics

MEGADAC 3000 Series Specifications

MEGADAC SERIES 3000 STANDARD FEATURES	MEGADAC 3415AC/DC Optim Part NBR - ML1089	MEGADAC 3415AC Optim Part NBR - ML1087	MEGADAC 3407DC Optim Part NBR - ML1085
Maximum Sampling Speed	25,000 Samples/Sec	25,000 Samples/Sec	25,000 Samples/Sec
Sampling Speed Range	0 to 25,000 Samples/Sec	0 to 25,000 Samples/Sec	0 to 25,000 Samples/Sec
ADC Resolution	16 bits	16 bits	16 bits
Memory/RAMDisk Storage	256 Megabytes (Battery Backed)	256 Megabytes	256 Megabytes (Battery Backed)
Maximum Input Channels	512	512	512
Channels/Scan	1 to 512	1 to 512	1 to 512
Channel Sample Order	Any order	Any order	Any order
Max. DAC Output Channels	128	128	128
Scan Synchronization	Internal or External	Internal or External	Internal or External
Available Module Slots	15	15	7
System Gain	1:1 to 4000:1	1:1 to 4000:1	1:1 to 4000:1
Data Alarms	Any/All Channels	Any/All Channels	Any/All Channels
Data Triggers	Any/All Channels	Any/All Channels	Any/All Channels
PC Communication Interfaces	IEEE-488, RS-232, RS-422, RS-485	IEEE-488, RS-232, RS-422, RS-485	IEEE-488, RS-232, RS-422, RS-485
Remote Communication Interfaces	Commercially Available Modems	Commercially Available Modems	Commercially Available Modems
Power Consumption	40 to 80 Watts, (80 to 160 VA)	40 to 80 Watts, (80 to 160 VA)	40 to 80 Watts
AC Power Source (AutoSwitch)	115 VAC 50/60 Hz (105 - 132 VAC) 230 VAC 50/60 Hz (210 - 264 VAC)	115 VAC 50/60 Hz (105 - 132 VAC) 230 VAC 50/60 Hz (210 - 264 VAC)	
DC Power Source (Range)	10.5 - 18 VDC (startup 75 W load) 10.0 - 18 VDC operating		10.5 - 18 VDC (startup 75 W load) 10.0 - 18 VDC operating
Weight	27 to 40 pounds	26 to 39 pounds	19 to 25 pounds
Operating temperature	4 to 50 degrees C	4 to 50 degrees C	4 to 50 degrees C
Relative Humidity	10% to 80% (non-condensing)	10% to 80% (non-condensing)	10% to 80% (non-condensing)
Size	16.62 Inches wide 16.00 Inches deep 6.97 Inches high	16.62 Inches wide 16.00 Inches deep 6.97 Inches high	10.20 Inches wide 16.00 Inches deep 6.97 Inches high

MEGADAC SERIES 3000 MAINFRAME OPTIONS	MEGADAC 3415AC/DC OPTIONS	MEGADAC 3415AC OPTIONS	MEGADAC 3407DC OPTIONS
Memory/RAMDisk Storage - Options	1 Gigabyte (DC=Battery Backed) Optim Part NBR - PL2608	1 Gigabyte Optim Part NBR - PL2608	1 Gigabyte (DC=Battery Backed) Optim Part NBR - PL2608
AC Power Source - Options			External Power Supply (110/220 VAC to 15 VDC) Optim Part NBR - PL2377
DC Power Source - Options	External Power Converter (24 VDC to 12 VDC) Optim Part NBR - 7420045		External Power Converter (24 VDC to 12 VDC) Optim Part NBR - 7420045

Figure E.5 Optim MEGADAC 3415AC.

APPENDIX F

ELASTOMERIC BEARING TEST RESULTS

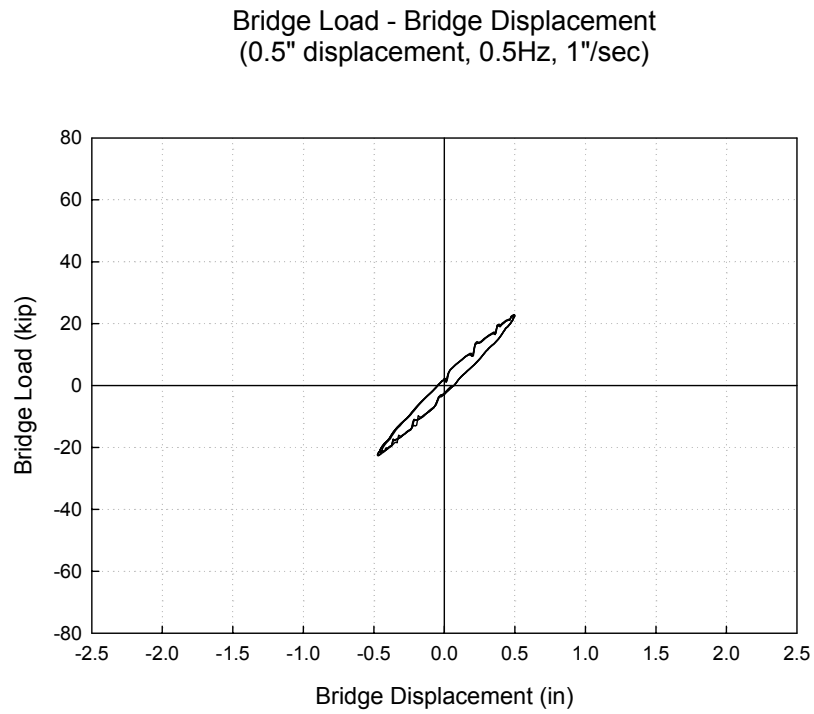

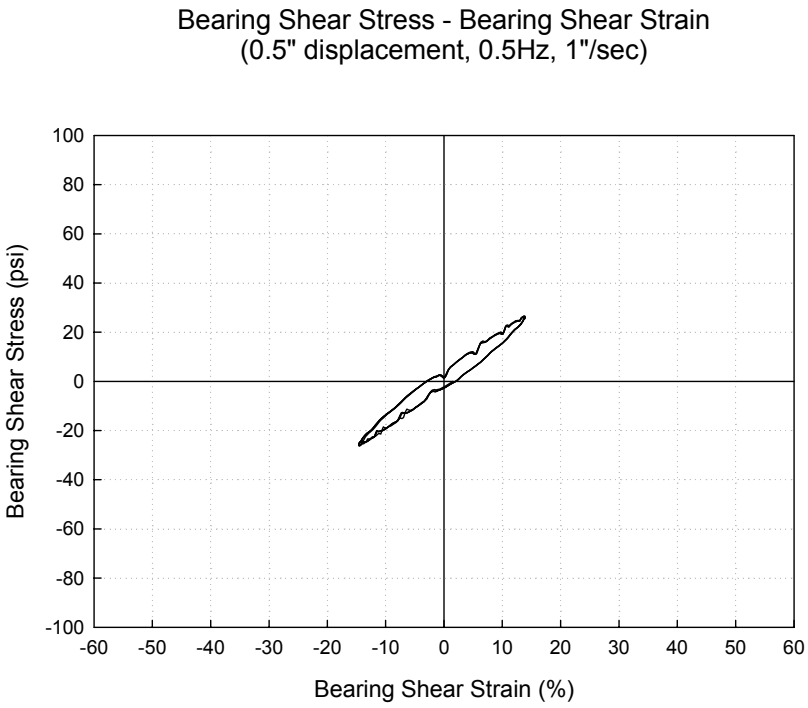

Figure F.1 Plots from Test A.

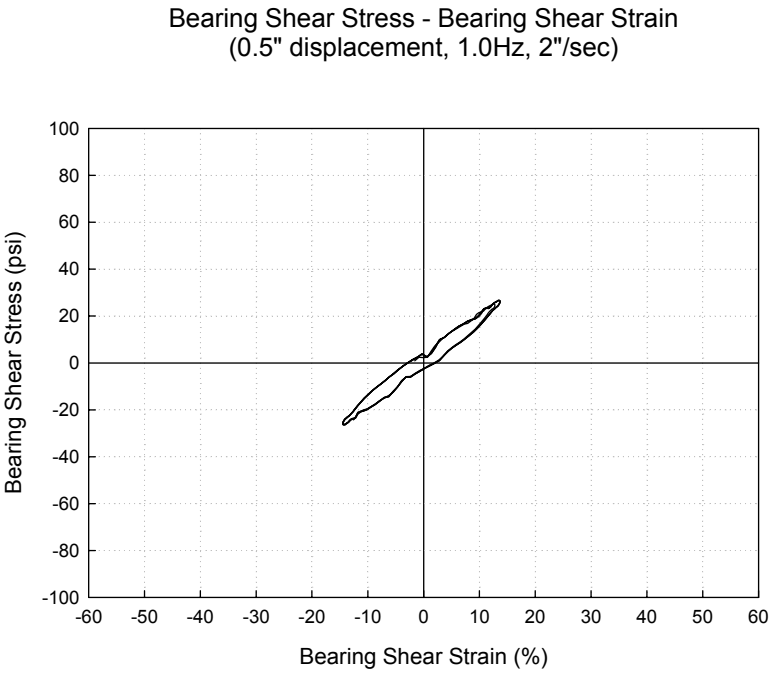

Figure F.2 Plots from Test B.

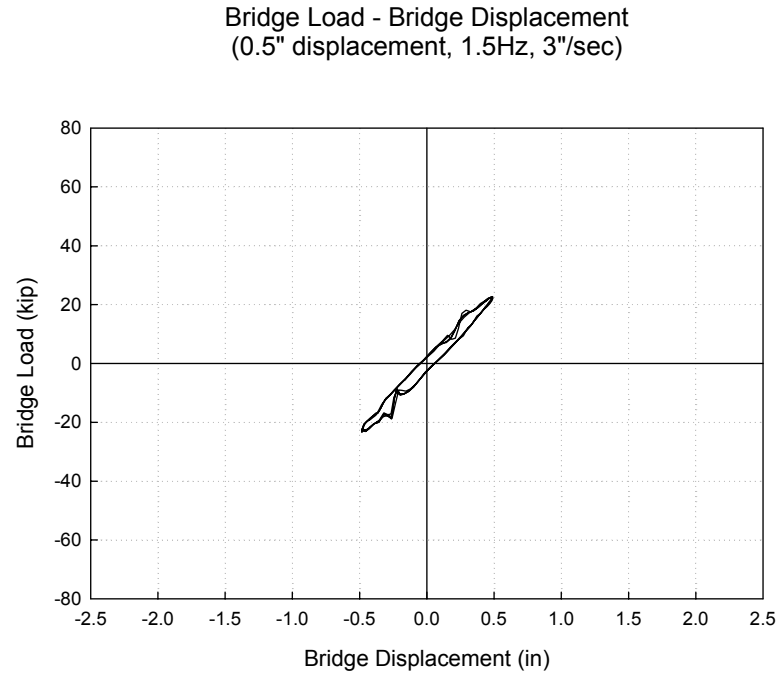

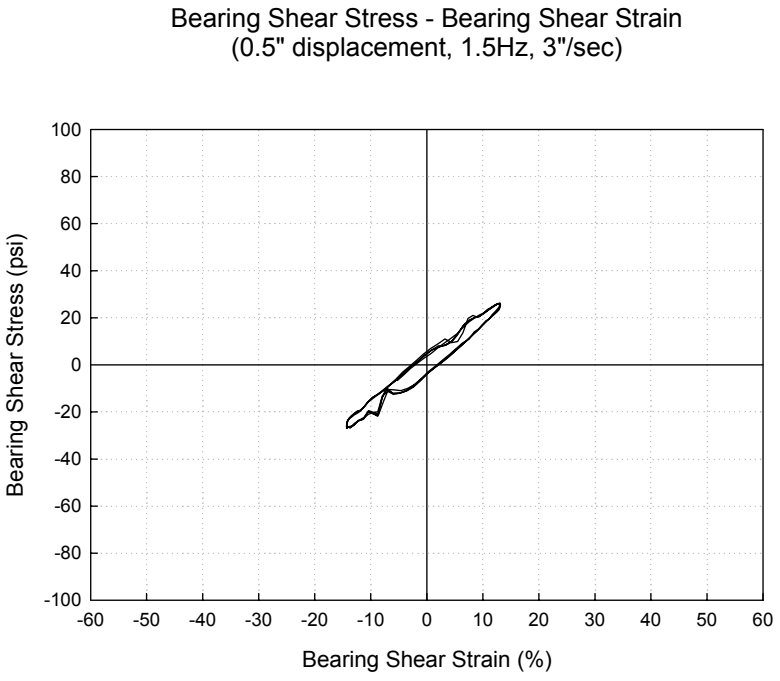

Figure F.3 Plots from Test C.

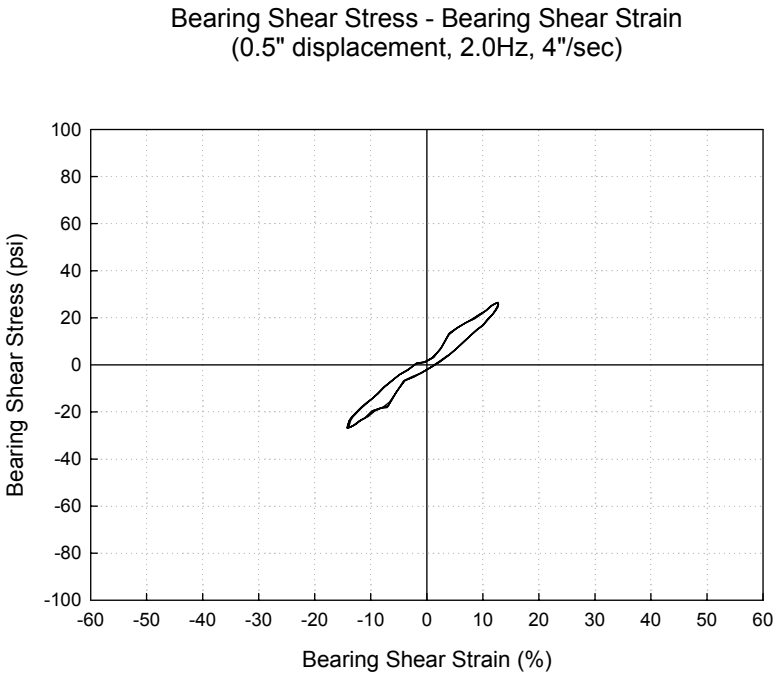

Figure F.4 Plots from Test D.

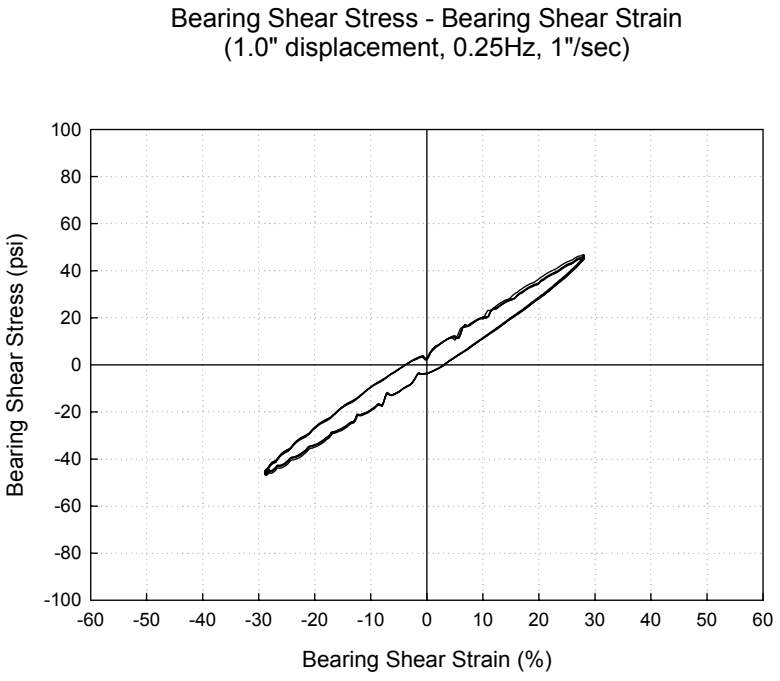

Figure F.5 Plots from Test E.

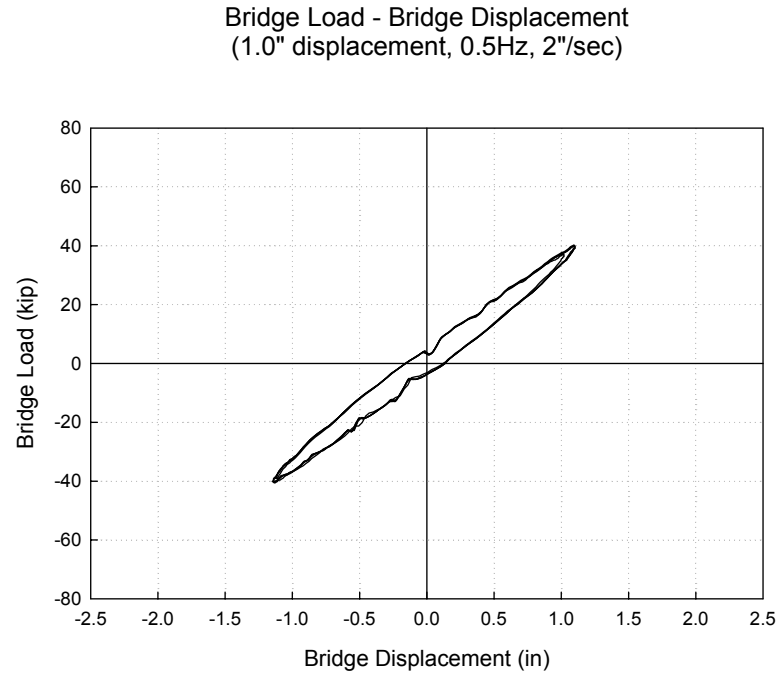

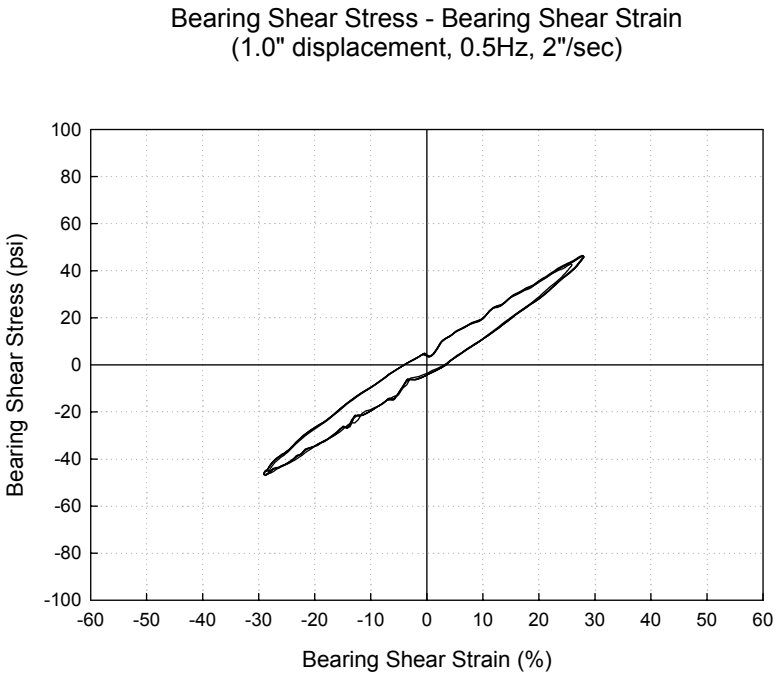

Figure F.6 Plots form Test F.

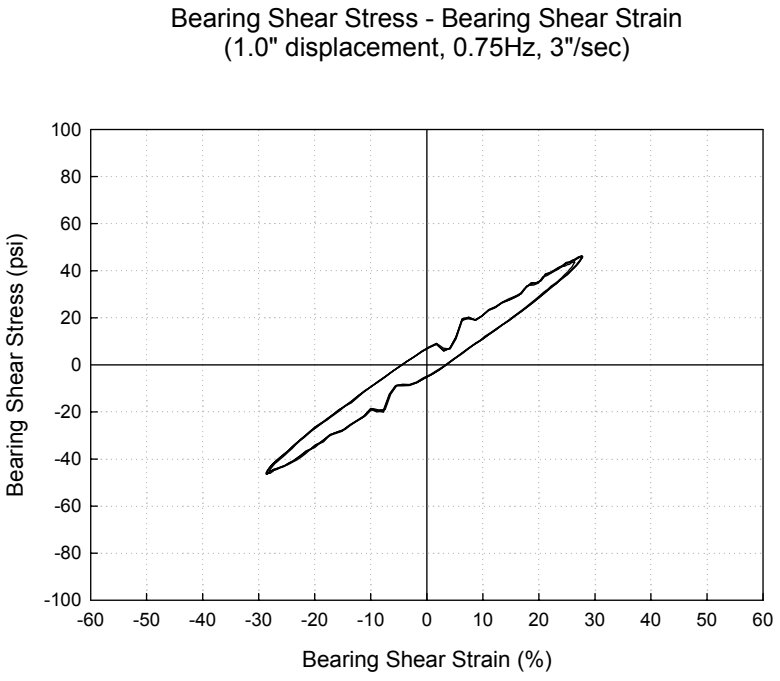

Figure F.7 Plots from Test G.

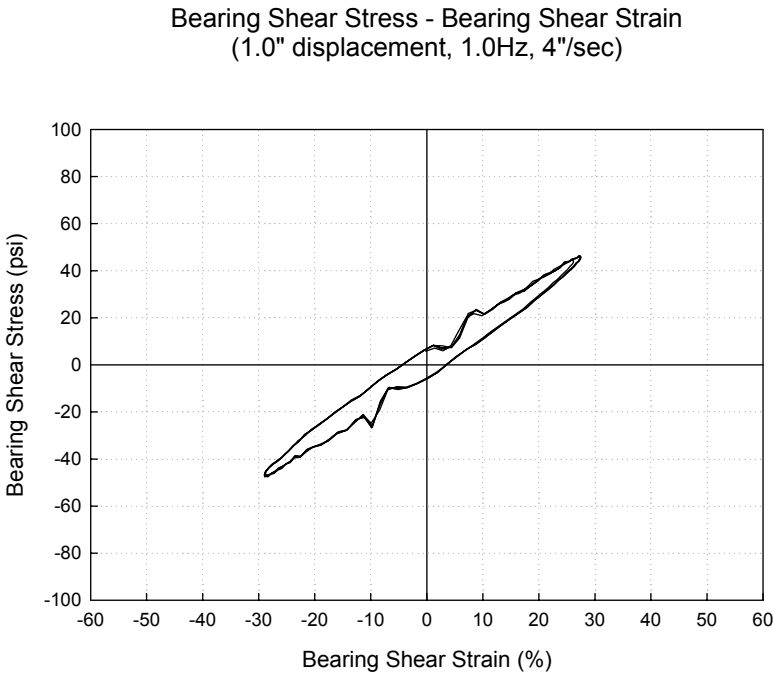

Figure F.8 Plots from Test H.

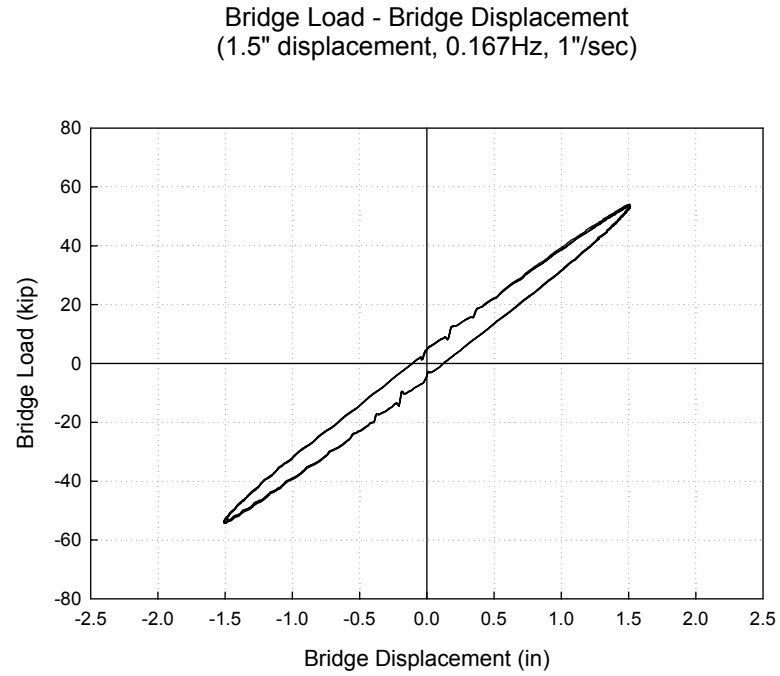

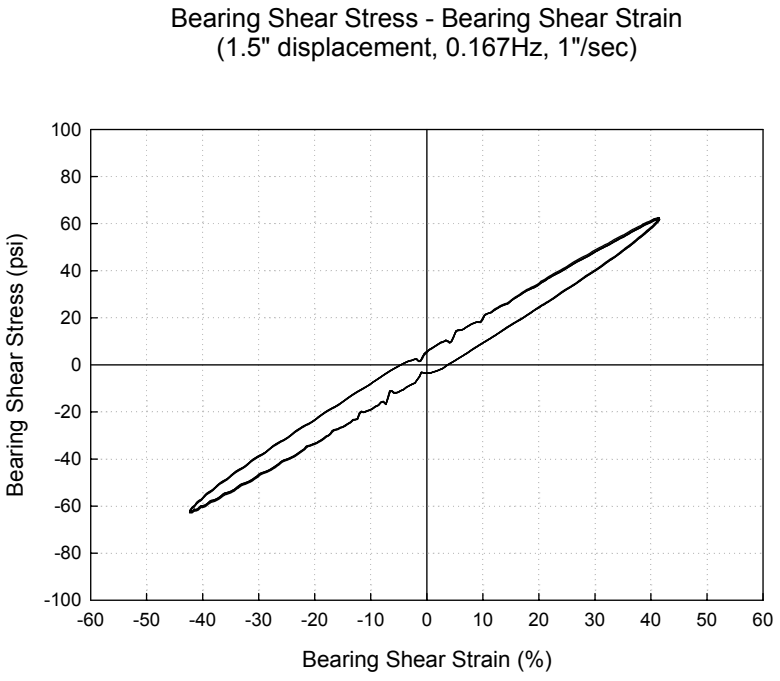

Figure F.9 Plots from Test I.

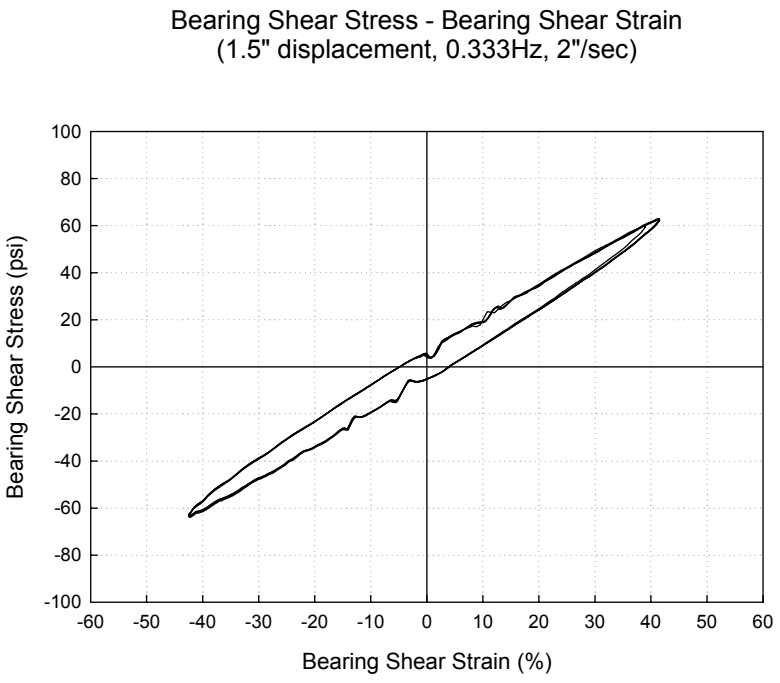

Figure F.10 Plots from Test J.

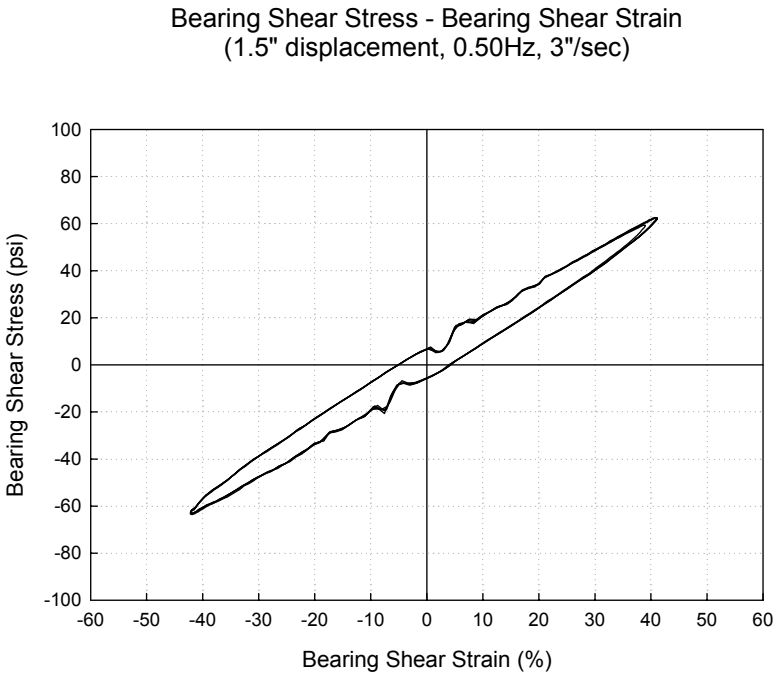

Figure F.11 Plots from Test K.

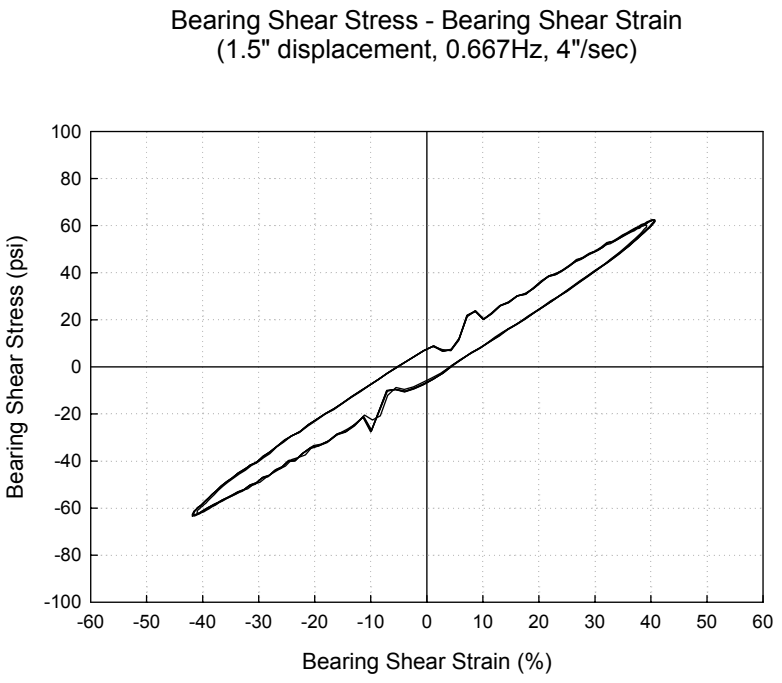

Figure F.12 Plots from Test L.

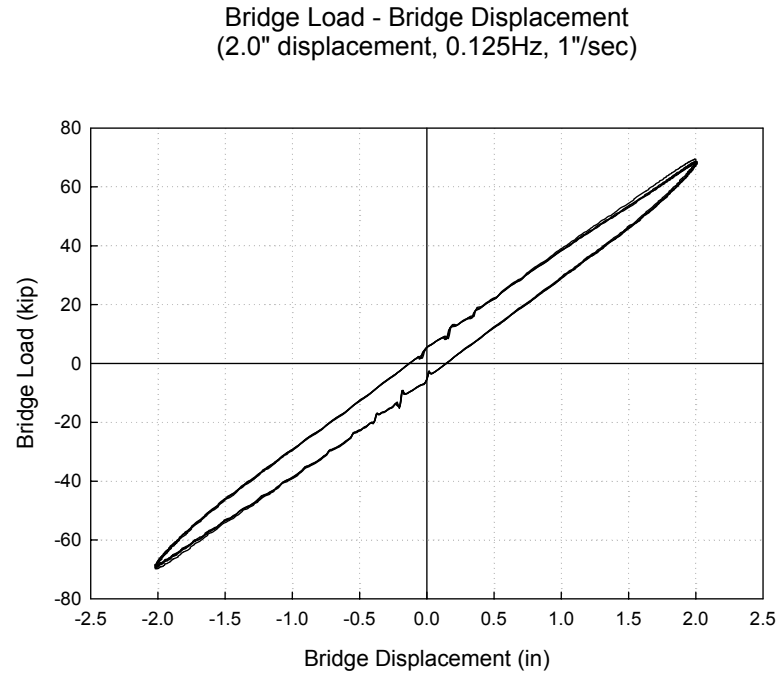

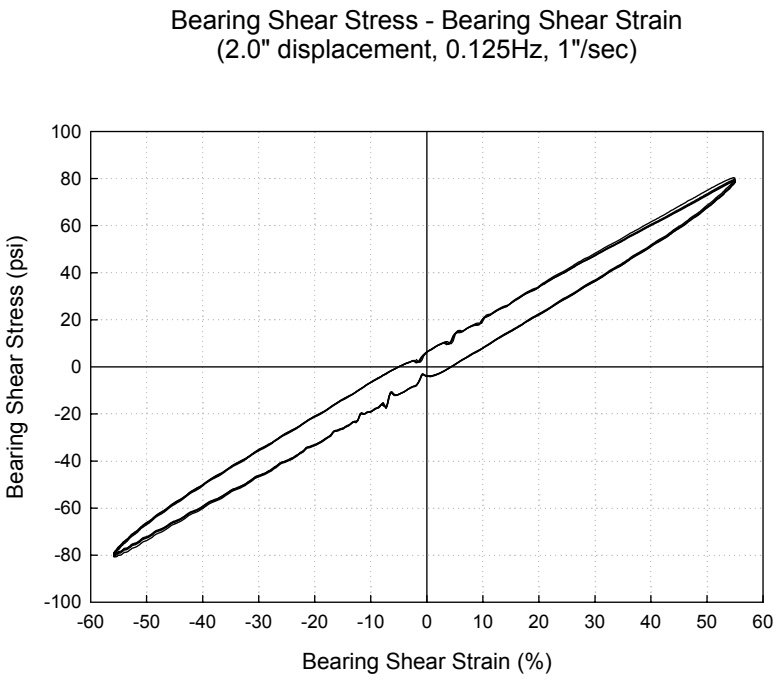

Figure F.13 Plots from Test M.

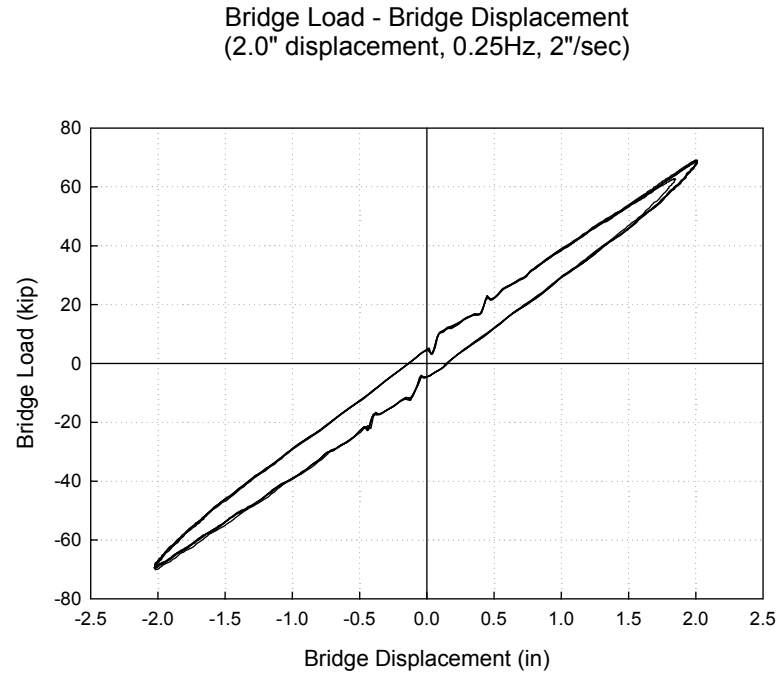

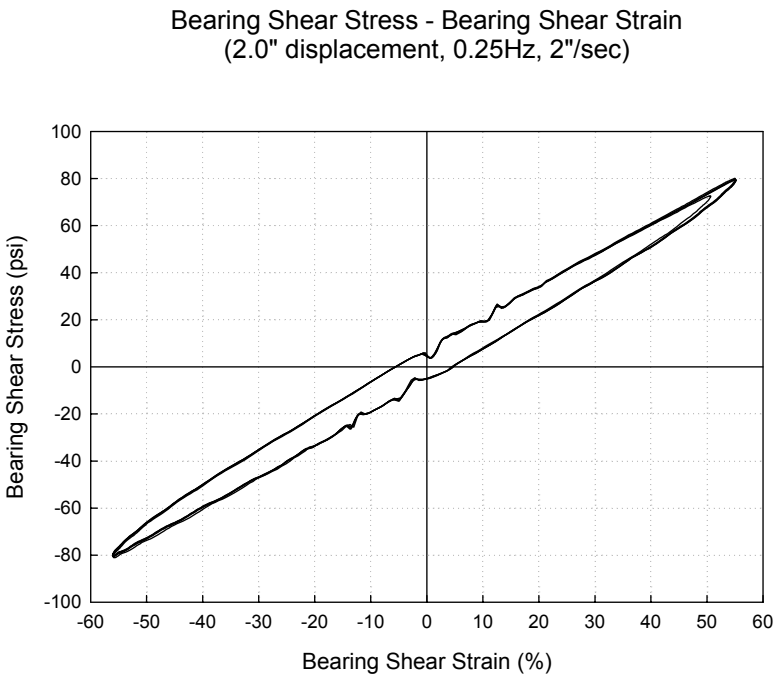

Figure F.14 Plots from Test N.

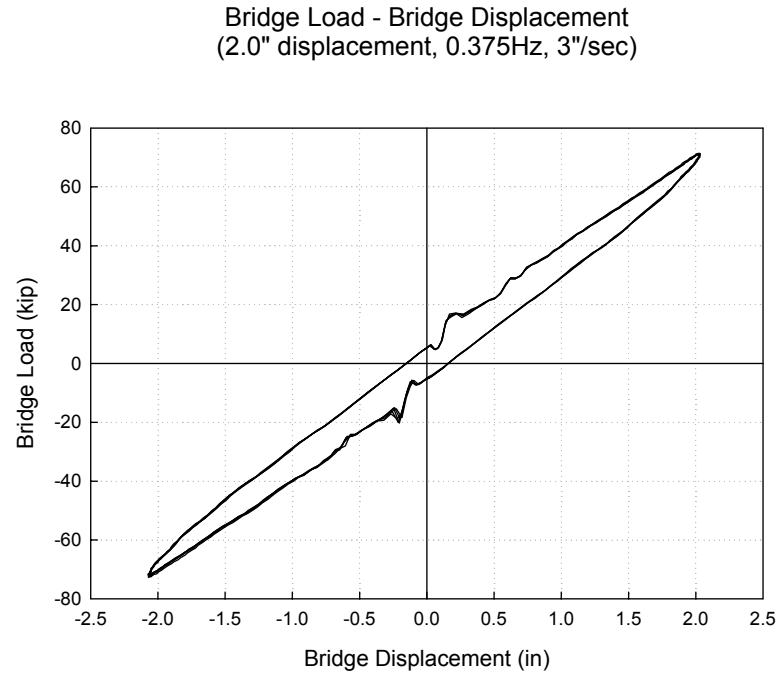

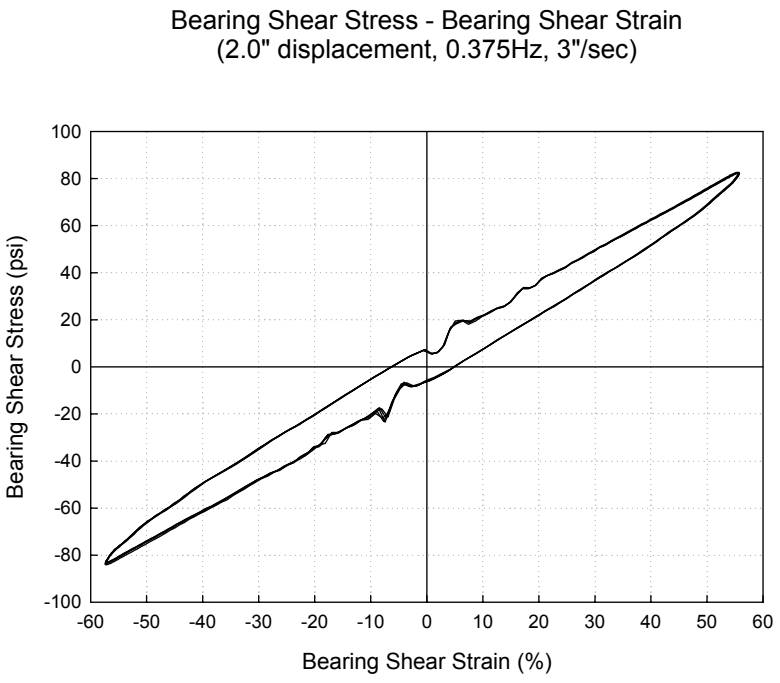

Figure F.15 Plots from Test O.

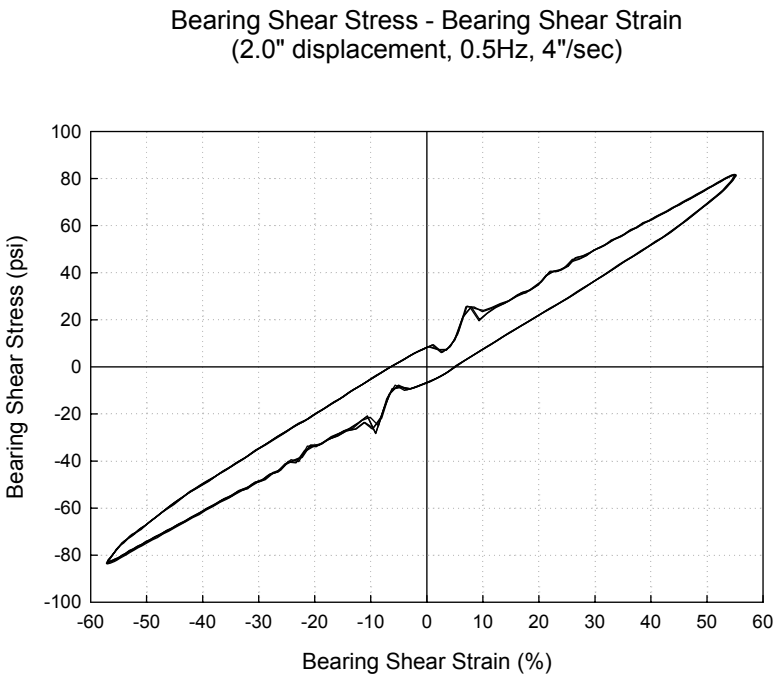

Figure F.16 Plots from Test P.

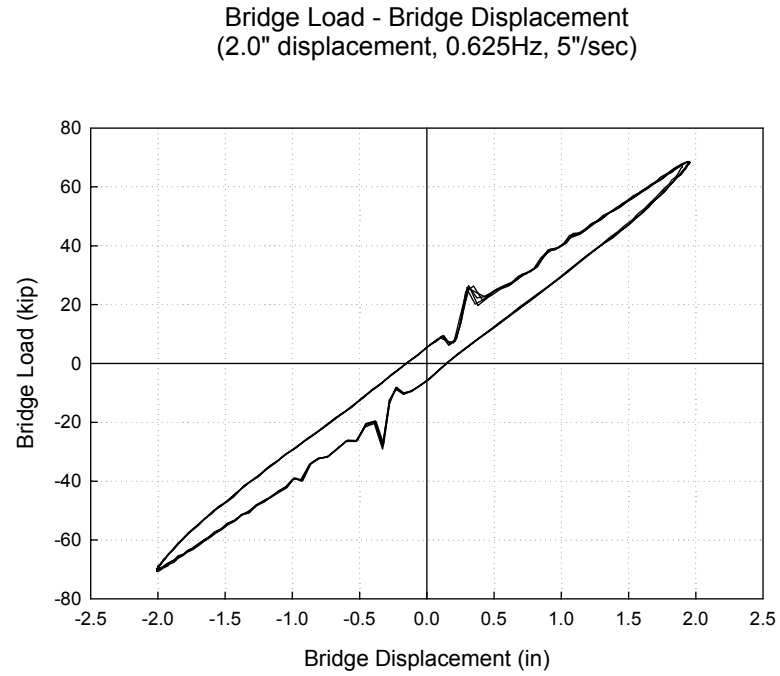

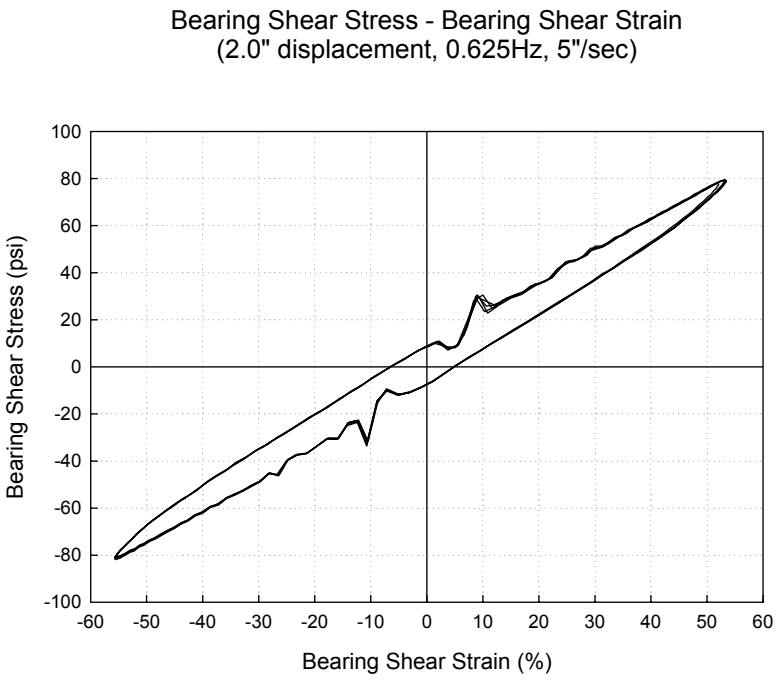

Figure F.17 Plots from Test Q.

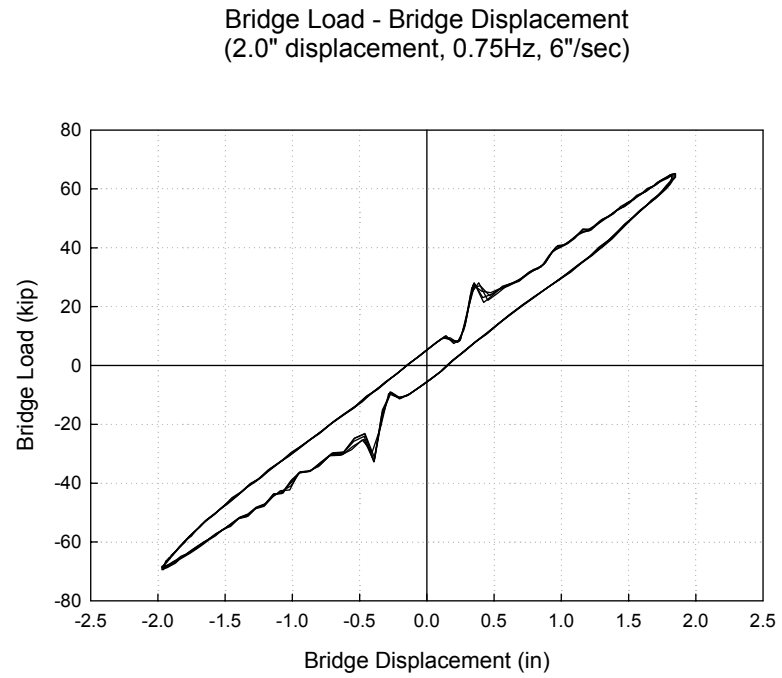

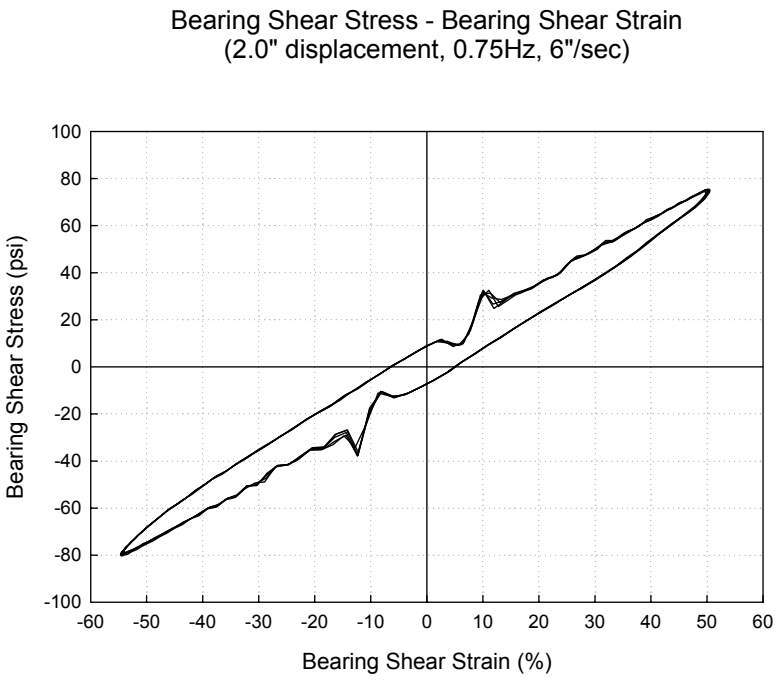

Figure F.18 Plots from Test R.

REFERENCES

AASHTO (1992). *Standard Specification for Highway Bridges*, American Association of State Highway and Transportation Officials, 15th Ed., Washington, D.C.

AASHTO (1996). *Standard Specification for Highway Bridges*, American Association of State Highway and Transportation Officials, 16th Ed., Washington, D.C.

AASHTO-83 (1988). *Guide Specification for Seismic Design of Highway Bridges*, American Association of State Highway and Transportation Officials, Washington, D.C.

Aiken, I. D., Kelly, J. M., Clark, P. W., Tamura, K., Kikuchi, M., and Itoh, T. (1992). "Experimental Studies of The Mechanical Characteristics of Three Types of Seismic Isolation Bearings." *Earthquake Engineering,* Tenth World Conference, Balkema, Rotterdam.

Applied Technology Council (1981). "*Seismic Design Guidelines for Highway Bridges,"* ATC-6, Berkeley, CA, October.

Applied Technology Council (1991). "*Seismic Vulnerability and Impact of Disruption of Lifelines in the Conterminous Untied States*," ATC-25, Redwood City, CA.

Aschheim, M. and Moehle, J.P. (1996). "Seismic Shear Strength of Reinforced Concrete Columns: Discussion," Journal of Structural Engineering, ASCE, Vol. 122, No. 4, April, p461-464.

Ayyub, B.M. and Lai, K. (1989). "Structural Reliability Assessment Using Latin Hypercube Sampling," Proceeding of ICOSSAR '89, the 5th International Conference on Structural safety and Reliability, San Francisco, CA, USA.

Banon, H., Biggs, J.M., and Irvine, H.M. (1981). "Seismic damage in reinforced concrete frames," Journal of Structural Engineering, ASCE, Vol. 107, No. 9, p1713-1729.

Basoz, N.I, Kiremidjian, A.S., King, S.A., and Law, K.H. (1999). "Statistical Analysis of Bridge Damage Data from the 1994 Northridge, CA, Earthquake," *Earthquake Spectra*, EERI, Vol. 15, No. 1, February, 1999, p25-53.

Beresnev, I.A. and Atkinson, G.M. (1997). "Modeling finite-fault radiation from the ω^2 spectrum," *Bulletin of Seismological Society of America*, 87, p67-84.

Beresnev, I.A. and Atkinson, G.M. (1998). " Stochastic finite-fault modeling of ground motions from the 1994 Northridge, California, earthquakes. I. Validation on rock site," *Bulletin of Seismological Society of America*, 88, p1392-1401.

Blakely, R. W. G. (1982). "Application of base isolation to seismic resistant bridges," Comparsion of United States and New Zealand Practices for Highway Bridges, ATC-12, Augus, p77-82.

Blaney, G., W., Kausel, E., and Roesset, J. M. (1976). "Dynamic stiffness of piles," Proc., 2nd Int. Conf. Numerical Methods Geomech., Virginia Polytechnical Institute and State University, Blacksburg, Va., Vol. 2, p1001-1012.

Boore, D.M. (1996). "SMSIM-Fortran programs for simulating ground motions from earthquakes: Version 1.0," *U.S. Geological Survey Open-File Report*, 96-80-A.

Boore, D.M. and Joyner, W.B. (1991). "Estimation of ground motion at deep-soil sites in eastern North America," *Bulletin of Seismological Society of America*, 81, p1402-1410.

Boore, D.M. and Joyner, W.B. (1997). "Site amplifications for generic rock sites," *Bulletin of Seismological Society of America*, 87, p327-341.

Buckle, I., G. (1994). "The Northridge, California earthquake of January 11, 1994: performance of highway bridges," Tech. Rep. NCEER-94-0068,National Center for Earthquake Engineering Research.

Buckle, I., G., and Mayes, R. L. (1989). "The application of seismic isolation to bridges," Seismic Engineering: Research and Practice, *Proceeding of Structures Congress*, p633-642.

CALTRANS (1988). *Memo to Designers 5-1*, California Department of Transportation, Sacramento, CA, September

CALTRANS (1989). *Bridge Design Aids 14-1*, California Department of Transportation, Sacramento, CA, October.

CALTRANS (1990). “Bridge Design Specifications Manual,” California Department of Transportation.

CERI (2001). Center for Earthquake Research and Information, The University of Memphis, http://www.ceri.memphis.edu/public/, Last modified: Sep 18, 2001

Chai, Y, Preistley, M.J. Nigel, and Seible, F. (1991). "Seismic retrofit of circular bridge columns for enhanced flexural performance," ACI Structural Journal, Vol. 88, No. 5 Sep-Oct., 1991, p572-584.

Chadwell, C. (1999). Professional Version Spurred the Development of UCFyber 1999, http://www.zevent.com.

Chatterjee, S., and Price, B. (1977). " Regression Analysis by Example," John Wiley & Sons, Inc.

Chopra, A. K. (1995). "Dynamics of Structures: Theory and Applications to Earthquake Engineering," Prentice Hall, New Jersey.

Clark, P. W., Aiken, I. D., Kelly, J, M. (1993). "Large-Scale Earthquake Simulator Study of the Tohoku University Base-Isolated Building," *Structural Engineering in Natural Hazards Mitigation*, ASCE, New York, NY.

Cook, R. A., and Klingner, R., E. (1992). "Ductile Multiple-Anchor Steel-to-Concrete Connetions", *Journal of Structural Engineering*, Vol. 118, No. 6, June, 1992.

DesRoches, R., and Fenves, G. L. (1997). "New Design and Analysis Procedures for Intermediate Hinges in Multiple-Frames Bridges," *Report No. UCB/EERC-97/12*, Earthquake Engineering Research Center, University of California, Berkeley, CA., December.

Dicleli, M. (1993). "Effects of Extreme Gravity and Seismic Loads on Short to Medium Span Slab-On-Girder Steel Highway Bridges," Ph.D. Thesis, Department of Civil Engineering, University of Ottawa, Ottawa, Canada.

Dicleli, M., and Bruneau, M. (1995a). "Seismic performance of multi-span simply supported slab-on-girder steel highway bridges", *Engineering Structures*, Vol.17, No. 1., p4-14.

Dicleli, M., and Bruneau, M. (1995b). "Seismic performance of single-span simply supported and continuous slab-on-girder steel highway bridges", *Journal of Structural Engineering*, Vol.121, No. 17.

Donlin, C. (1999). URL:http://geopubs.wr.usgs.gov/fact-sheet/fs151-99/Last modified: 11-3-99

Fang, H., Y. (1999). "Foundation Engineering Handbook," Second Edition, Van Nostrand Reinhold, New York.

FEMA-222A 1995, NEHRP Recommend Provisions for Seismic Regulations for New Buildings Part 1-- Provisions, Report No. FEMA-302, Federal Emergency Management Agency, Washington, D.C.

Frankel, A., Mueller, C., Barnhard, T., Perkins, D., Leyendecker, E.V., Dickman, N., Hanson, S., and Hopper, M. (1996). "National seismic-hazard maps: Documentation," *USGS Open-File Report* 96-532.

Gazetas, G. (1984). "Seismic response of end-bearing piles," *Soil Dynamic Earthquake Engrg*., Vol.3(2), p82-93.

Geol, R. K., and Chopra, A. K. (1997), "Evaluation of bridge abutment capacity and stiffness during earthquake." *Earthquake Spectra*, Vol. 13, No. 1, p1-21.

Geol, R. K. (1997), "Earthquake Characteristics of Bridges with Integral Abutments." *Journal of Structural Engineering*. November, 1997.

Ghobarah, A., and Ali, H. M. (1988). "Seismic Performance of Highway Bridges," Journal of Engineering Structures, 10(3), p157-166.

HAZUS *Technical Manual* (1997). Federal Emergency Management Agency, Washington, D.C.

HAZUS99 *User's Manual* (1999). Federal Emergency Management Agency, Washington, D.C.

Herrmann, R.B. and Akinci, A. (1999). Mid-America ground motion models, *URL http://www.eas.slu.edu/People/RBHerrmann/MAEC/maecgnd.html*

Highway Innovative Technology Evaluation Center (1999), *Summary of Evaluation Findings for the Testing of Seismic Isolation and Energy Dissipating Devices*, HITEC, Washington, D.C.

Hoerner, B. J., Snyder, G. M, and Van Orden, R. C. (1986). "Elastomeric Bearings Seismically Retrofit Bridge," Volume 3 published by Earthquake Engineering Research Institute, El Cerroti, CA, p1887-1898.

Hwang, H. and Huo, J.-R. (1998) "Probablistic Seismic Damage Assessment of Highway Bridges," the 6th U.S. National Conference on Earthquake Engineering, Seattle, Washington, June.

Hwang, H., Jernigan, J.B., and Lin, Y. (2000a). "Evaluation of Seismic Damage to Memphis Bridges and Highway Systems," Journal of Bridge Engineering, Vol. 5, No. 4, ASCE, November, 2000, p322-330.

Hwang, H., Liu, J., and Chiu, Y. (2000b). "Seismic Fragility Analysis of Highway Bridges," Center for Earthquake Research and Information, The University of Memphis, Memphis, TN 38152.

Hwang, H. M., Pepper, S. E., and Chokshi, N. C. (1990). "Fragility Assessment of Containment Tangential Shear Failure," *Res Mechanica* 30.

Imbsen, R. A. and Penzien, J. (1986). “Evaluation of energy absorbing characteristic of highway bridges under seismic conditions,” EERC, 86/17

Iwasaki, T., Penzien, J. and Clough, R. (1971), “Literature Survey- Seismic Effects on Highway Bridges,” University of California, Berkeley, EERC Report 71-02.

Jankowski, R., Wild, K., and Fujino, Y. (1998) "Pounding of Superstructure Segments in Isolated Elevated Bridge During Earthquakes" *Earthquake Engineering and Structural Dynamics*, Vol. 27, p487-502.

Jennings, P.C. (1983), “Engineering Seismology,” Reprinted From Earthquakes: Observation, Theory, and Interpretation.

Karshenas, M. and Kasper, I.I. (1997), "Seismic design considerations for steel bridges," Building to Last: Proceeding of Structures Congress XV, Portland, Oregon, American Society of Civil Engineers, New York, Vol. 1, p741-745.

Kelly, J., M. (1981). "Aseismic Base Isolation: Its History and Prospects," Publication SP-American Concrete Institute, Detroit, Michigan, p549-586.

Kelly, J. M. (1997). “Earthquake- Resitance Design with Rubber,” Springer, London, 1997, 2nd.

Kelly, J. M., Buckle, I., G., and Koh, C. –G. (1987) "Mechanical Characteristics of Base Isolation Bearings for A Bridge Deck Model Test" Earthquake Engineering Research Center, Univ. of California, Berkeley, CA, November.

Koh, C. G., and Kelly, J. M. (1989) "Viscoelastic stability model for elastomeric isolation bearings" Journal of Structural Engineering, ASCE, Vol. 115, No. 2, p285-302.

Kottegoda, N.T. and Rosso, R. (1997) "Statistics, Probability, and Reliability for Civil and Environmental Engineers," The McGraw-Hill Companies, Inc.

Kuprenas, J.A, Madjidi, F., Vidaurrazaga, A., and Lim, C.L. (1998). "Seismic Retrofit Program for Los Angeles Bridges," Journal of Infrastructure Systems, Vol.4, No.4, December, p185-191.

Lam, I. P., (1994). "Soil-Structure Interaction Related to Piles and Footings," Proceedings of the Second International Workshop on the Seismic Design of Bridges, Queenstown, News Zealand, August.

Lam, T.T. (2000) "Performance of Steel Laminated Elastomeric Bearings of a Full-Scale Bridge Subjected to Dynamic Loading", A Thesis of. Georgia Institute of Technology, December.

Leyendecker, E. V. and Hunt, R. J. (2000). "Development of Maximum Considered Earthquake Ground Motion Maps," *Earthquake Spectra*, Vol. 16, No. 1, February, 2000.

Lin, Y., Gamble, W.L. and Hawkins, N.M. (1998), "Seismic Behavior of Bridge Column Non-Contact Lap Splices," SRS No. 622, Department of Civil & Environmental Engineering, University of Illinois at Urbana-Champaign, June, 1998.

Maison, B.F., and Kasai, K. (1992), "Dynamics of Pounding when Two Buildings Collide", *Earthquake Engineering and Structural Dynamics*, Vol. 21: p771-786.

Mander, J.B., and Basoz, N. (1999). "Seismic Fragility Curve Theory for Highway Bridges," *Technical Council on Lifeline Earthquake Engineering Monograph*, ASCE, New York, N.Y., No. 16, August, 1999, p31-40.

Mander, J. B, Priestly, M. J, and Park, R. (1988). "Observed Stress-Strain Behavior of Confined Concrete," *Journal of Structural Engineering*, ASCE, Vol. 114 No.8, August., p1827-1849.

Mander, J. B., Kim, D. K., Chen, S. S., and Premus, G. J. (1996). "Response of Steel Bridge Bearings to the Reversed Cyclic Loading", *Technical Report NCEER 96-0014*, Buffalo, NY.

Mander, J. B. and Basoz, N. (1999). "Seismic Fragility Curve Theory for Highway Bridges," *Technical Council on Lifeline Earthquake Engineering monograph*, New York, N.Y. : American Society of Civil Engineers, No. 16.

Maragakis, E., and Saiidi, M., and Hwang, E. (1992) "Analytical Studies on the Seismic Response of Lead Rubber Base Isolated Bridges," Proceeding of Engineering Mechanics, ASCE, New York, NY. p67-70.

Maroney, B., Kutter, B., Romstad, K., Cahi, Y. H., and Vanderbilt, E.(1994). " Interpretation of Large Scale Bridge Abutment Test Results," *Proceedings of 3rd Annual Seismic Research Workshop*, California Department of Transportation, CA, June 27-29.

Maragakis, J.B., Saiidi, M., and Abdel-Ghaffar, S. (1992), "Evaluation of the Response of the Whitewater Bridge During the 1986 Palm Springs Earthquake," Proceedings of the Eighth U.S.-Japan Workshop on Bridge Engineering, Chicago, Illinois, May 1992, p336-350.

Martin, G. R., and Lam, I., P. (1995). "Seismic Design of Pile Foundations: Structural and Geotechnical Issues," Third International Conference on Recent Advances in Geotechnical Earthquake Engineering and Soil Dynamics, April 2-7, Vol. III, St. Louis, Missouri.

Martin, G. R., and Yan, L. (1995). "Modeling Passive Earth Pressure for Bridge Abutments," Geotechnical Special Publication 55, Earthquake-Induced Movements and Seismic Remediation of Existing Foundations and Abutments, ASCE 1995 Annual National Convention, San Diego, October, 1995.

MATLAB. (1992). *MATLAB Reference Guide*, The Math Works, Inc.

Mayes, R. L. (1993). "Response of Isolated Structures to Recent California Earthquakes," *Structural Engineering in Natural Hazards Mitigation*, ASCE, New York, NY.

Mizukoshi, K., Yasaka, A., Iizuka, M., and Takabayashi, K. (1992). "Failure test of laminated rubber bearings with various shapes," Earthquake Engineering, Tenth World Conference, 1992 Balkema, Rotterdam, p2277-2280.

Mori, A., Moss, P. J., Carr, A. J., and Cooke, N. (1997). "Behavior of laminated elastomeric bearings." Structural Engineering and Mechanicx, Vol. 5, No. 4., p451-469.

Mori, A., Moss, P. J., Cooke, N., and Carr, A. J. (1999). "The Behavior of Bearing Used for Seismic Isolation under Shear and Axial Load," *Earthquake Spectra*, Vol. 15, No. 2, May, 1999.

Nagarajaiah, S. and Ferrell, K. (1999) " Stability of Elastomeric Seismic Isolation Bearings" *Journal of Structural Engineering*, Vol.125, No. 9, September, p946-954.

New Zealand Ministry of Works and Development. (1981). "Design of lead-rubber bridge bearings," *Civil Division Publication* 818/A, New Zealand Ministry of Works and Development, Wellington, New Zealand.

Novak, M., (1991), "Piles Under Dynamic Loads," Proceedings, Second International Conference on Recent Advances on Geotechnical Earthquake Engineering and Soil Dynamics, Rolla, Missouri, Vol. 3, p2433-2456.

Park,Y-J., and Ang, A. H-S. (1985). "Mechanistic seismic damage model for reinforced concrete," *Journal of Structural Engineering*, ASCE, Vol. 111, No.4, p722-739.

Park, R, Priestley, J.N, and Gill, D. (1982). "Ductility of Square-Confined Concrete Columns," *Journal of Structural Engineering*, ASCE, Vol. 108, No. ST4, April, p929-950.

Pfeifer, T.A. (2001) "Experimental Tests of Seismic Retrofit Components on A Full-Scale Model of A Typical Steel Bridge in Mid-America," Thesis for master degree, Georgia Institute of Technology, December, 2001.

Poli, S. D., Prisco, M. D. and Gambarova, P. G. (1993) "Shear Response, Deformations, and Subgrade Stiffness of a Dowel Bar Embedded in Concrete," *ACI Structural Journal*, Vol. 89, No. 6, Nov.-Dec.

Prakash, V., Powell, G.H., Campbell, S.D. and Filippou, F.C. (1992) "DRAIN-2DX User Guide," Department of Civil Engineering, University of California at Berkeley.

Priestely, M. J. N., Verma, R., and Xizo, Y. (1994). "Seismic shear Strength of Reinforced Concrete Columns," Journal of Structural Engineering, ASCE, Vol. 120.No. 8: p2310-2329, August, 1994.

Priestely, M. J. N., Verma, R., and Xizo, Y. (1996). "Seismic shear Strength of Reinforced Concrete Columns: Closure by Authors," Structural Engineering Review, Vol. 7.No. 3: p464-467, April, 1996.

Pujol, Santiago (1997). "Drift Capacity of Reinforced Concrete Columns," Master's Thesis, Purdue University.

Randall, M., J. Saiidi, M., S., Maragakis E., M., and Isakovic, T. (1999). "Restrainer Design Procedures for Multi-Span Simply Supported Bridges," Technical Report MCEER-99-0011.

Randolph, M.F. (1981). "Response of Flexible Piles to Lateral Loading," Geotechnique Vol. 31, No. 2, June, 1891, p247-259.

Rashidi, S., and Saadeghvaziri, M. (1997). "Seismic Modeling of Multi-Span Simply Supported Bridges Using ADINA", *Journal of Computers and Structures*, Vol. 64 No. 5/6, p1025-1039.

Robinson, W.H. (1982). "Lead-rubber hyteretic bearings suitable for protecting structures during earthquakes," Earthquake Engineering and Structural Dynamics, Octor, 1982, p593-604.

Roeder, C. W., Stanton, J. F., and Taylor, A. W. (1987). "Performance of Elastomeric Bearings." *National Cooperative Highway Research Progrma Report 298*, Transportation Research Board, National Research Council, Washington, D.C.

Roeder, Charles W., Stanton, John F., and Feller, Troy. (1990). “Low-Temperature Performance of Elastomeric Bearings,” *Journal of Cold Regions Engineering*, Vol. 4, No. 3, September, 1990.

Saadeghvaziri, M., and Rashidi, S. (1997a). “Effect of Steel Bearings on Seismic Response of Bridges in Eastern United States”. 6th U.S. National Conference on Earthquake Engineering.

Saadeghvaziri, M.A. and Rashidi, S. (1997b). “Seismic Design and Retrofit Issues for Bridges in New Jersey,” *Transportation Research Record(1594)*, Transportation Research Board, November, 1997.

Saiidi, M. and Maragakis, E. (1999), "Effect of base isolation on the seismic response of multi-column bridges," *Structural Engineering and Mechanics*, Vol. 8, No. 4, p411-419.

Saiidi, M., Maragakis, E., and Feng, S. (1992), "An Evaluation of the Current Caltrans Seismic Restrainer Design Method," Report No. CCEER-92-8, Civil Engineering Department, University of Nevada, Reno, October 1992.

Saiidi, M., Maragakis, E., and O’Connor, D. (1995). “Seismic Performance of the Madrone Bridge During the 1989 Loma Preita Earthquake,” *Structural Engineering Review,* Vol. 7, No.3. p219-230.

Saiidi, M., Maragakis, E., and Feng, S. (1996). “Parameters in Bridge Restrainer Design for Seismic Retrofit,” *Journal of Structural Engineering, ASCE*, Vol. 122, No.1. January, 1996.

Scharge, I.. (1981). "Anchoring of Bearing by Friction", Publication SP- American Concrete Institute, p197-215.

Selna, L., G., Malvar, L., and Zelinski, R., (1989). “Bridge Retrofit Testing : Hinge Cable Restrainers,” *Journal of Structural Engineering, ASCE*, Vol. 115, No. 4., p920-934.

Shinozuka, M. (1998). "Statistical Analysis of Bridge Fragility Curves", *Proceedings of the US-Italy Workshop on Protective System for Bridges*, New York, N.Y., April 26-28.

Shinozuka, M., Feng, M.Q., Lee, J., and Naganuma, T. (2000a). "Statistical Analysis of Fragility Curves", *Journal of Engineering Mechanics*, ASCE, Vol. 126, No. 12, December 2000, p1224-1231.

Shinozuka, M. and Feng, M.Q., Kim, H., and Kim, S. (2000b). "Nonlinear Static Procedure for Fragility Curve Development, " *Journal of Engineering Mechanics*, Vol., 126, No. 12, ASCE, December, 2000, p1287-1295.

Shome, N. and Cornell, C., A. (1999). "Probabilistic Seismic Demand Analysis of Nonlinear Structures," Reliability of Marine Structures Program, Report No. RMS-35.

Skinner, R. I., Robinson, W. H., and McVerry, G. H. (1993). "An Introduction to Seismic Isolation," JOHN WILEY & SONS, New York.

Stanton, J. F., Scroggins, G., Taylor, A. W., and Roeder, C. W. (1990) "Stability of laminated elastomeric bearings" Journal of Mechanical Engineering, ASCE, Vol. 116, No. 6, p1351-1371.

US Department of Commerce (1993) "1993 Commodity Flow Survey," Report No. TC92-Cf-52, Bureau of the Census.

U.S. Geological Survey (1912). "The New Madrid Earthquake," by Myron L.F., Bull. 494.

U.S. Geological Survey (1996). http://geohazards.cr.usgs.gov/eq/html/ceusmap.html.

Taylor, H. P. J. (1969). "Investigation of the Dowel Shear Forces Carried by the Tensile Steel in Reinforced Concrete Beams," *Technical Report* No. TRA-431, Cement and Concrete Association, London, November, 1969.

Trochalakis, P., Eberhard, M., O., and Stanton, J., F. (1996). "Unseating of Simply Supported Spans During Earthquakes," Technical Report, Research Project T9903, Washington State Transportation Center, University of Washington, Seattle, Washington.

TRANSPORTATIO RESEARCH BOARD. (1977). "Bridge Bearings," Washington: Transportation Research Board, National Research Council, 1977.

Trochanis, A., M., Bielak, J., and Christiano, P. (1991). "Simplified model for analysis of one or two piles." *J. Geotech. Engrg*., Vol. 117(3), p448-466.

Tseng, W. S. and Penzien, J. (1973). "Analytical investigations of the seismic response of long multiple span highway bridges," EERC, 73-12.

Uang, C. M. and Bertero, V. V. (1990). "Evaluation of Seismic Energy and Design of Seismic Restrainers for In-Span Hinges," *Earthquake Engineering and Structural Dynamics*, Vol. 19, No. 1, p77-90.

Vintzeleou, E.N. and Tassios, T.P. (1987). "Behavior of Dowels under Cyclic Deformations," ACI Structural Journal, January-February, 1987, p18-30.

Wald, L. (2000). URL:http://www-socal.wr.usgs.gov/north/Last updated 02/04/00.

Wen, Y. K., and Wu, C. L. (2001). "Uniform Hazard Ground Motions for Mid-America Cities," *Earthquake Spectra*, Vol. 17, No.2, p359-384.

Wiegel, R. L. (1970). “Earthquake Engineering.” Prentice-Hall, Inc., Englewood Cliffs, NJ.

Wolf, J., P. (1985). "Dynamic Soil-Structure Interaction." Prentice-Hall, Inc., Englewood Cliffs, N.J.

Xanthakos, P. P. (1996). “Bridge Strengthening and Rehabilitation,” Prentice Hall, Inc., Upper Saddle River, NJ.

Yang, Yueh-Shiun., Priestely, M.J. Nigel, and Ricles, M. James. (1994). “Longitudinal Seismic Response of Bridge Frames Connected by Restrainers”, Report No. SSRP – 94/09, Structural System Research, University of California, San Diego, California.

Yashinsky, M. (1991). "Seismic retrofit of bridge foundations," 1991 Publication by ASCE, New York, NY, USA, p166-185.

Zimmerman, R., M. and Brittain, R. D. (1979) “Seismic response of multi-span highway bridges,” *Third Canadian Conf. Earthquake Engineering*, p1091-1120.